Control of Type III-mediated Virulence in *Pseudomonas syringae* by Cyclic-di-GMP

Danny Ward

Student ID: 100202750

December 2021

A Thesis Submitted for the Degree of Doctor of Philosophy

Department of Molecular Microbiology, John Innes Centre

School of Biological Sciences, University of East Anglia

Norwich, UK

Word count (excluding appendix): 78 041

Control of Type III-mediated Virulence in *Pseudomonas syringae* by Cyclic-di-GMP

Danny Ward, John Innes Centre, University of East Anglia, UK, PhD, December 2021

Abstract

Pseudomonas syringae is a prominent plant pathogen and disease model organism. These bacteria carry out host infection using the type III secretion system (T3SS), which translocates effector proteins into target cells, altering cellular defence mechanisms and metabolism to promote bacterial colonisation. It was previously shown that the secondary signalling molecule cyclic-di-GMP (CdG) binds to the export ATPase complex at the base of the T3SS (HrcN in *P. syringae*), as well as in closely related homologue proteins. It was hypothesised that this binding interaction plays a role in controlling type III-mediated virulence.

To investigate the CdG:HrcN binding interaction, bacterial strains carrying mutations targeting key predicted CdG binding residues in HrcN were constructed. *In vitro* analyses of purified HrcN confirmed CdG binding and dodecamerisation for the wildtype. However, a G176A point-mutant of HrcN retained CdG binding but appeared to have compromised CdG-induced downstream oligomerisation. The effect of this mutation on virulence was therefore explored *in vivo*. Wildtype and mutant *hrcN P. syringae pathovar* tomato (*Pto*) DC3000 strains were infiltrated into *Arabidopsis thaliana* to evaluate disease phenotypes *in planta*. The *G176A hrcN* point-mutant exhibited a near-asymptomatic disease phenotype despite having a comparable bacterial load to the WT in *A. thaliana* Col-0. Disease symptoms returned in immunocompromised *A. thaliana* lines. The underlying mechanism was then explored. It was shown that a subset of tested effectors (HopAM1, HopAF1, and HopAA1-2) displayed compromised translocation rates for *G176A hrcN* compared to WT using an effector-CyaA reporter system in *Pto*. These effector proteins were shown to be important for disease symptom establishment by way of gene over-expression and gene deletion. Candidate interaction targets in the plant host were identified by co-immunoprecipitation.

From this study, first indication that CdG binding to HrcN in *Pto* may lead to dodecamerisation was shown, and that this interaction is important for full virulence by enabling for efficient translocation of key effector proteins.

Acknowledgements

Live as if you were to die tomorrow. Learn as if you were to live forever.

Table of Contents

Table of Figures

Table of Tables

Table of Abbreviations

Abbreviation	Definition
ADP	Adenosine diphosphate
APS	Ammonium Persulfate
ATP	Adenosine triphosphate
Avr	Avirulence
bbc	*bak1-5/bkk1-1/cerk1*
BSA	Bovine serum albumin
cAMP	Cyclic adenosine monophosphate
CdA	Cyclic-di-adenosine monophosphate
CdG	Bis-(3'-5')-cyclic dimeric guanosine monophosphate
Cfu	Colony forming units
Col-0	Columbia ecotype
Cryo-EM	Cryo-electron microscopy
DGC	Diguanylate cyclase
DRaCALA	Differential radial capillary of ligand assay
DNA	Deoxyribonucleic acid
EDTA	Ethylenediaminetetraacetic acid
ETI	Effector-triggered Immunity
fec	*fls2/efr/cerk1*
FPLC	Fast protein liquid chromatography
His6-tag	polyhistidine-tag (6x)
Hrc	Hypersensitive response conserved
Hrp	Harpin
IPTG	Isopropyl β-D-1-thiogalactopyranoside
ITC	Isothermal titration calorimetry
LB	Lysogeny broth
OD	Optical density
OD_{600}	Optical density (measured at a wavelength of 600 nm)
OE	Over-expression
MDR	Multi-drug resistance
Ni-NTA	Nickel-nitrilotriacetic acid
PAI	Pathogenicity Island
PAMP	Pathogen-associated molecular pattern
PBST	Phosphate-buffered saline, Tween® 20 Detergent
PCR	Polymerase-chain reaction
PDE	Phosphodiesterase
Pi	Inorganic phosphate
PK/LDH	Pyruvate kinase/lactic dehydrogenase
PTI	Pattern-triggered immunity
RNA	Ribonucleic acid
ROS	Reactive oxygen species
Pst	*Pseudomonas syringae* pathovar *tomato*
Pto	*Pseudomonas syringae* pathovar *tomato*
Pv.	Pathovar

SDS-PAGE	Sodium dodecyl sulfate polyacrylamide gel electrophoresis
SPR	Surface plasmon resonance
T3E	Type III Effector
T2SS	Type II secretion system
T3SS	Type III secretion system
T4SS	Type IV secretion system
T6SS	Type VI secretion system
TBE	Tris/boric-acid/EDTA (Ethylenediaminetetraacetic acid)
TEMED	Tetramethylethylenediamine
Tris-HCl	Tris base-hydrochloride
UV	Ultraviolet
WT	Wildtype

Chapter 1: Introduction

1.1. Overview

Pathogenic bacteria infect their hosts through a variety of mechanisms. One such mechanism is called the type III secretion system which exists across a wide variety of bacterial species. While it is a growing area of research interest, many of the details remain unclear regarding this virulence system.

Bacteria use signalling molecules to co-ordinate cellular functionality. One such prominent signalling molecule is cyclic-di-GMP which has previously been documented to regulate a wide variety of aspects relating to cellular function. Recent evidence now suggests a role in the regulation of virulence. Microbial virulence is a tightly regulated system and so by unlocking the details surrounding the interplay between signalling molecules such as cyclic-di-GMP and the type III secretion system machinery, we can begin to form a more complete picture as to how bacteria control their infection processes. *Pseudomonas* has been chosen as a model organism to study the interplay between cyclic-di-GMP and the export ATPase complex, an integral component for type III secretion functionality.

1.2. *Pseudomonas*

The Gram-negative, rod-shaped Gammaproteobacteria *Pseudomonas spp.* is a genus of the 191-member Pseudomonadaceae family. Notable well studied *Pseudomonas spp.* strains include the plant pathogen *Pseudomonas syringae*, the human pathogen *Pseudomonas aeruginosa*, *Pseudomonas fluorescens,* which thrives in the rhizosphere of its plant host, the insect infecting *Pseudomonas entomophila* and *Pseudomonas putida* typically found growing within soil (Nikel et al., 2014). Most *Pseudomonas* species and strains are typically classified as strict aerobes however an anaerobic metabolism does exist as shown in *Pseudomonas aeruginosa* biofilm research (Hassett et al., 2002).

Pseudomonas have been the focus of countless research studies with a wide range of topics including bacterial virulence, host immune responses, biofilm formation, antibiotic resistance, crop-breeding, bio-control, bio-remediation and synthetic biology. The genus includes a wide range of readily-available, biologically important and experimentally tractable strains, which has led to *Pseudomonas*' prominence within scientific research.

1.2.1. *Pseudomonas syringae* (*Pto* DC3000)

1.2.1.1. Significance and Importance

Pseudomonas syringae is a plant pathogen which is well noted for its ability to colonise multiple plant species depending on their pathovar. In the case of *P. syringae* pv. *tomato* DC3000*,* the main host is the tomato plant. However, it also can infect *Arabidopsis thaliana* and *Nicotiana benthamiana* (Whalen et al., 1991, Hann and Rathjen, 2007). *Pseudomonas syringae* can be found on every major continent on earth (with the exception of Antarctica) (Cai et al., 2011). Strain T1 is most prominent within the Americas and Europe while strain JL1065 is most prominent in Africa and Australasia (Cai et al., 2011).

This prominent plant pathogen has led to the devastation of crop yields around the globe leading to weakened food security and increased prices. A high-profile case study highlighting this is the 2010 *Pseudomonas syringae* pv. *actinidiae* outbreak in New Zealand leading to the loss of kiwifruit (Vanneste, 2017). First originating from China and Japan in the 1980s, the disease rapidly spread to Europe, South America and eventually New Zealand from 2008 onwards (Butler et al., 2013).There exist a comprehensive list of over 60 pathovars of *Pseudomonas syringae* which dictate pathogenic specificity towards particular species of plant hosts (Bull et al., 2010).

P. syringae produces a series of effector proteins which help to facilitate plant infection, some of the most notable of which are the ice nucleation active (INA) proteins which promote host freezing (Maki et al., 1974) and HopZ proteins such as HopZ1a which acetylates plant proteins to suppress the host immune response (Ma et al., 2015). Some *P. syringae* effectors however, like the avirulence (Avr) proteins, such as AvrRpm1 are recognised by *Arabidopsis* resistance (R) proteins and trigger a plant immune response highlighting the evolutionary 'arms-race' that has formed between host and microbe (Kim et al., 2009). Within *Pto* DC3000*,* there are approximately 36 well-known effector proteins which are injected via the type III secretion system however many more putative effector proteins are still yet to be fully investigated (Aung et al., 2017)

Pseudomonas syringae lends itself as a model for studying host-pathogen interactions and due to the extensive prior research and genome sequencing and identification. Many previous studies have chosen to investigate plant-microbial interactions and bacterial virulence systems using this model and as such, has led to *P. syringae* becoming a robust tool for allowing us to understand, at the mechanistic and molecular level, exactly how plant-associated micro-organisms function and why.

1.2.1.2.   *P. syringae* Virulence

The virulence of *P. syringae* is driven primarily through flagellar and type IV pili-mediated motility along with secretion of virulence factors and effector proteins through secretion system nanomachinery (Xin et al., 2018). *P. syringae* use three secretion systems: namely type II, type III and type IV however in terms of plant pathogenicity, type III display the greatest importance and as such, are the focus of this study (Xin et al., 2018, Diepold and Armitage, 2015).

1.2.1.2.1. Plant Infection Progression

The molecular disease progression of *P. syringae* bacteria in plant hosts has been well studied. This bacterial species is a common plant pathogen and has been used as a model organism for understanding the molecular mechanisms and intricacies involved with plant infection and plant immunity.

1.2.1.2.1.1.   Bacterial Dispersal and Leaf Attachment

Efficient dispersal of *P. syringae* bacteria is generally achieved via rain and from leaf surface water splashing (Butterworth and McCartney, 1991). While *Pseudomonas* are motile, carriage through rain via the water cycle allows for large numbers of viable bacterial cells to rapidly cover a large area of susceptible plant targets (Butterworth and McCartney, 1991). These bacteria can stimulate bio-precipitation in the atmosphere via InaZ ice-nucleation proteins (Roeters et al., 2021) . This in turn increases the chances of dispersal via rainfall. This is achieved by controlling the initiation of ice nucleation of water in clouds and by affecting the structure of interfacial water (Roeters et al., 2021). These ice-nucleation proteins also cause frost damage in plants, and so serve as a virulence factor (Lindow et al., 1982).

P. syringae thrives when humidity and temperature are all at optimal levels and microbiome composition is suitable. These three factors have been dubbed the 'disease triangle' (Xin et al., 2018). In the case of many *P. syringae* strains, a higher average humidity and a higher temperature (between 21 °C and 30 °C) are seen as more favourable for bacterial colonisation due to a weaker immune response from the plant, and greater bacterial proliferation rates (Menna et al., 2015).

Following bacterial dispersal, *P. syringae* will attach to the plant surface. This has been shown to be achieved by the fimbriae attachment pili, production of exopolysaccharides and adhesins, the flagella, and curli fibres (Pilla et al., 2021, Romantschuk et al., 1994, Romantschuk et al., 1997). In the case of *P. syringae* it has been modelled that these bacteria will typically favour attachment in cluster

formations across a leaf surface, and likely will partake in re-attachment elsewhere on the leaf to aid bacterial exploration of the phyllosphere (van der Wal et al., 2013). *P. syringae* can live on the surface of the plant as an epiphyte, most typically in an avirulent phase, however the bacteria also have the ability to enter the plant via open stomata or wounds to colonise the leaf apoplast as part of a virulent phase of plant colonisation (Arnold and Preston, 2019, Pilla et al., 2021).

1.2.1.2.1.2.   Stomatal Entry

A stoma is a pore accompanied with a pair of parenchyma guard cells located predominantly on the underside of a leaf used for gas exchange. These stomatal openings vary in density and size on the leaf surface depending on the plant species. It is through these pores, that *P. syringae* can gain entry into the leaf apoplast (Hockett et al., 2013). *P. syringae* uses polar-located flagella, along with surfactant production for motility to gain entry into the leaf apoplast through these open stomata via swimming, swarming and twitching (Burch et al., 2012). Coronatine is a phytotoxin released by *P. syringae Pto* which impairs a stomatal closure response in response to PAMP-detection (Toum et al., 2016). This occurs because coronatine inhibits NADPH oxidase-dependent ROS production in the plant guard cells, leading to a loss of turgor pressure caused by solute extrusion through ion channels (Toum et al., 2016). This is particularly essential for *P. syringae* infection at night when leaf stomata close regardless of pathogen-detection in *Arabidopsis* (Panchal et al., 2016). Attachment, motility, and eventual bacterial colonisation are highly influenced by changes in the external environment including with fluctuations in temperature and light (Río-Álvarez et al., 2014, Hockett et al., 2013).

1.2.1.2.1.3.   Activation of Virulence Factors Including the T3SS

Once in the apoplast, the *Pseudomonas* bacteria use a variety of virulence factors to aid bacterial proliferation and survival. Production and release of plant hormones, cell wall-degrading enzymes, phytotoxins, and exopolysaccharides from the plant are typically observed during this stage of infection (Ichinose et al., 2013). This also includes the dynamic formation and activation of the type III secretion system to deliver effector proteins into nearby plant cells. Collectively this will result in changes to the host cell including dampening of plant defence responses, nutrient re-distribution, changes to hormone signalling, metabolic alterations, altered cell structure, changes to organelle function, and other cellular manipulation, ultimately aiding bacterial colonisation and multiplication (Pfeilmeier et al., 2016).

1.2.1.2.1.4.   Chlorosis, Necrosis and Water Soaking

Downstream physical disease symptoms on the infected leaves will begin to emerge as the infection progresses, as bacteria multiply, and as the hypersensitive response (HR) continues. HR is an immune-dependent localised cell death defence response triggered by the plant to restrict the growth of invading bacteria (Balint-Kurti, 2019). In the case of *P. syringae*, disease symptoms are primarily localised to the leaves, fruits, and stems of infected plants.

Chlorosis is a yellowing of the leaf tissue which occurs due to lack of chlorophyll. It is known that release of chlorosis-inducing phytotoxins such as coronatine, phaseolotoxin, and tabtoxin leads to the formation of chlorosis symptoms (Bender, 1999). Additionally, the translocation of T3SS effector proteins is known to be implicated in the formation of this disease symptom (Chakravarthy et al., 2018). Necrosis of leaf tissue is characterised by the formation of brown or black specks across the leaf both at the marginal edge, and within the centre of the leaf (Mikiciński et al., 2020). Necrosis is cell death of leaf tissue and is caused by restricted water and nutrient flow into affected regions. While chlorosis and necrosis are closely linked and have similar visual disease symptoms, it should be noted

that they are two separate and distinct manifestations of disease progression and feature different molecular mechanisms involved in their formation.

There is growing evidence to suggest that both leaf chlorosis and necrosis is in part driven by translocation of a few key T3SS effector proteins rather than with a larger portion of the effector protein repertoire, however the finer molecular details remain incomplete. Unpicking the full molecular mechanism of each known (and putative) effector protein and linking this to disease progression is a large area of ongoing active research.

Water soaking or hydrosis is another typically observed disease symptom characteristic of *P. syringae* infection. Extracellular polysaccharide production from *Pseudomonads* play an important role in the establishment of this symptom (El-Banoby and Rudolph, 1979). It has been shown that the increase of aqueous conditions in the apoplast create a more favourable colonisation environment for *P. syringae* (Xin et al., 2016). Additionally, it was demonstrated that T3SS effectors HopM1 and AvrE play an important role in this water soaking process (Xin et al., 2016).

1.3. Type III Secretion System

Type III secretion systems are needle-like nanomachines used by various Gram-negative bacteria to deliver bacterial effector proteins in to target cells (Galan and Collmer, 1999). There are two types of T3SS, non-flagellar (often called the injectisome or T3SSa) and the flagella (T3SSb) (Diepold and Armitage, 2015). These systems share a high level of structural conservation and a close evolutionary lineage with each other (Diepold and Armitage, 2015). For flagellar T3SS, this system aids cellular motility, while with non-flagellar T3SS, this system facilitates bacterial virulence (Diepold and Armitage, 2015). The non-flagellar injectisome (T3SSa) is the main focus of this thesis.

The Yop type III virulon system of *Yersinia pestis* is a well-studied early example of such a system whereby 25 Ysc proteins allow for the injection of effector proteins into eukaryotic cytosol of the host target cell via a needle and body structure (Cornelis, 2002). Shown in Table 1.1 are some examples of clinically or agriculturally important, or otherwise impactful type III secretion systems within a variety of organisms.

Table 1.1. Examples of type III secretion systems found within bacteria (Coburn et al., 2007, Puhar and Sansonetti, 2014).

Species	System	Hosts	Role
Bordetella bronchiseptica	Bop	Humans, dogs, pigs	Virulence
Burkholderia pseudomallei	Bsa/Bop	Humans	Virulence
Chlamydia trachomatis	Inc	Humans, birds	Virulence
Dickeya dadantii	Dsp/ hrp	Plants	Virulence
Escherichia coli	Ces/Esc/Esp/Sep/Tir	Humans, cows	Virulence
Ralstonia solanacearum	Hrp/hrc	Plants	Virulence
Bradyrhizobium elkanii	Rhc/Nop	Legumes	Nodulation
Pseudomonas aeuruginosa	Psc/Pop	Humans	Virulence
Pseudomonas syringae	Hrc/Hrp	Plants	Virulence
salmonella typhimurium	Iag/Inv/Prg/Sic/Sic/Spa/Ssp/Org	Humans, rodents, chickens, cows, pigs	Virulence
Shigella flexneri	Ipa/Ipg/ Mxi/ Spa/ Osp	Humans	Virulence

Vibrio parahaemolyticus	Vop	Humans	Virulence
Xanthomonas campestris	Xop	Plants	Virulence
Yersinia enterocolitica	Yop/Ysc/Ypk	Humans, cattle, rodents, fleas	Virulence

1.3.1.   The Type III Secretion System General Structure, Assembly and Function

The general structure of type III secretion system machinery is shown in Figure 1.1 while Figure 1.2 shows the detailed structure of the T3SS in *P. syringae*. Present across all type III secretion systems is a basal body structure comprised of membrane-spanning type III secretion system rings and an ATPase protein located in the cytoplasm (Tampakaki et al., 2004, Eichelberg et al., 1994, Fan and Macnab, 1996, Deng et al., 2017). Also present among all type III enabled species is a pilus and translocon that, along with the basal body, form the needle complex (Tampakaki et al., 2004, Lombardi et al., 2019). Various effector proteins, chaperones and assembly components are also essential for proper function however the quantity and type vary considerably between species (Tampakaki et al., 2004, LeBlanc et al., 2021).
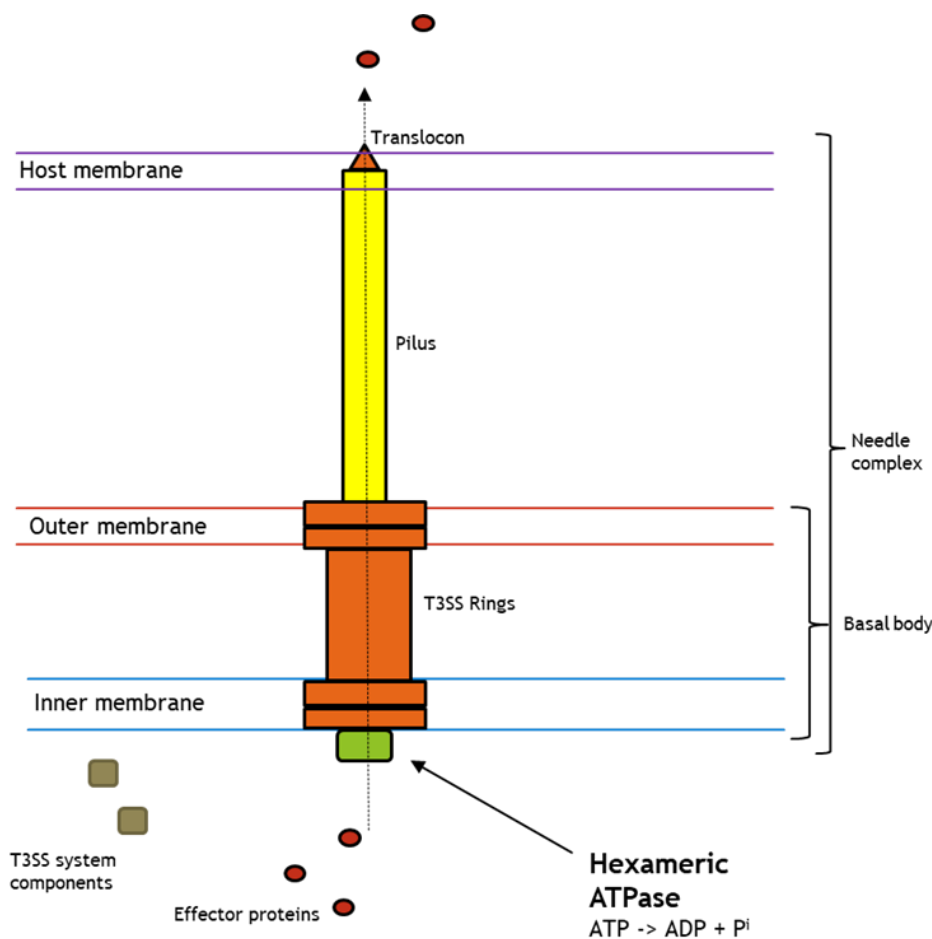
Figure 1.1. Cartoon representation of the bacterial type III secretion system machinery.
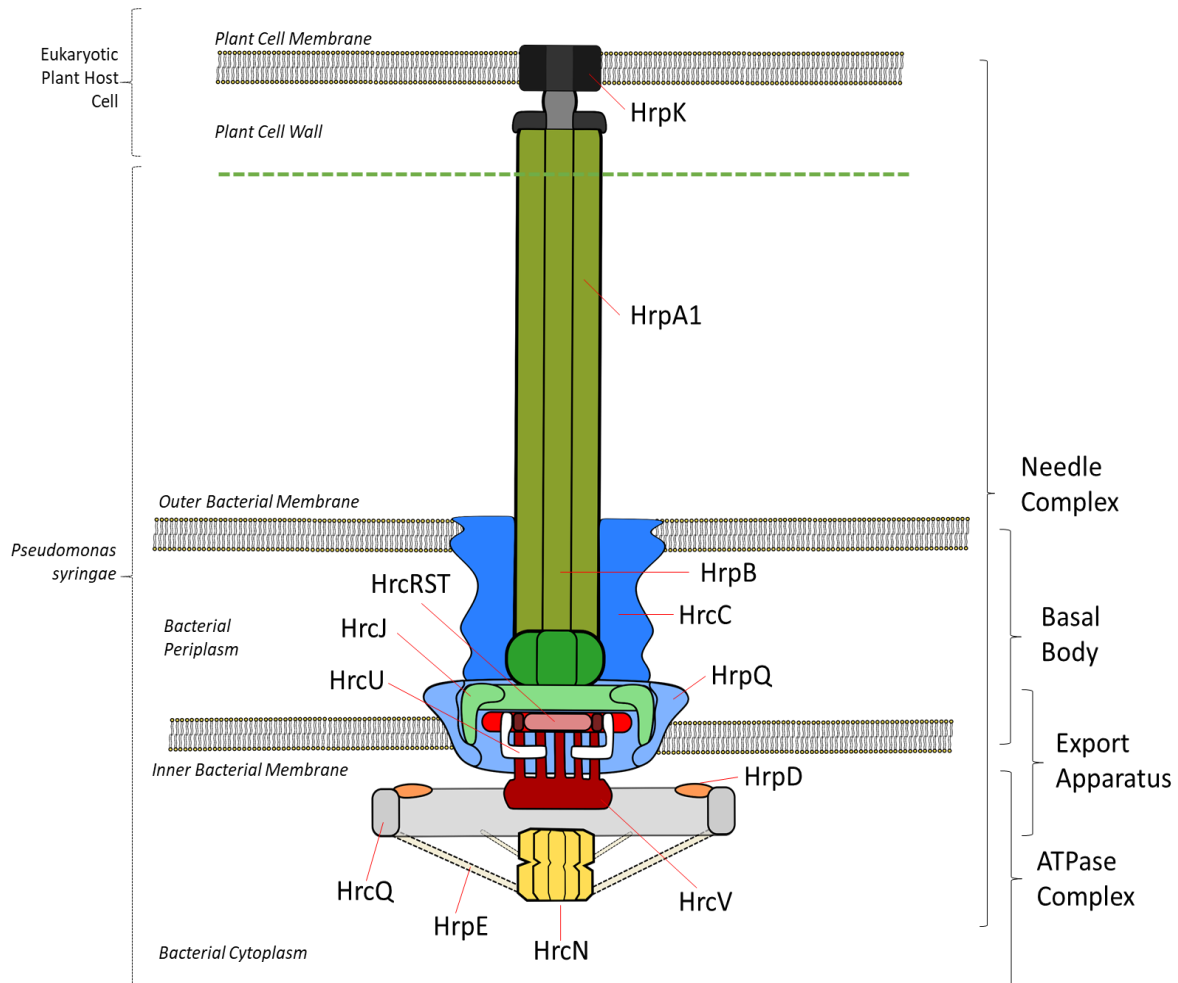
Figure 1.2. Cartoon representation of the *Pseudomonas syringae* type III secretion system (adapted from Diepold and Armitage, 2015, Trampari, 2016).

As an example, with the type III secretion system from *salmonella typhimurium*, typical basal body lengths have been shown to range from 29 to 34 nm while needle length has been shown to be around 60-80 nm (Nans et al., 2015, Coburn et al., 2007). The needle-like injectisome must first be assembled and then following this an export apparatus that enables for the export of effector proteins and pore-formation proteins when contact has been made with the host cell is assembled (Notti and Stebbins, 2016).

The injectisome assembly process involves the use of approximately 25-30 different proteins (Table 1.2), however many of these are not present in the final structure with most only having involvement in the assembly process after which these assembly proteins are discarded or are stored in the cytosol (Diepold and Wagner, 2014). It is estimated that 15 of these proteins are present in the final functional injectisome complex (Buttner, 2012). Recent evidence shows that mobile pilotins may be important components for the assembly of the T3SS and for substrate specificity (Wimmi et al., 2022).

Table 1.2. Key Type III Secretion System Proteins for *P. syringae* (Bergeron et al., 2016, Sato and Frank, 2011, Naito et al., 2017, Quinaud et al., 2005, Feltman et al., 2001, Crabill et al., 2012, Collmer et al., 2000, Ha et al., 2004, Sawa, 2014, Pastor et al., 2005, Lin and Martin, 2005, Dijk et al., 2002, Wu et al., 2004, Morello and Collmer, 2009, Moscoso et al., 2011).

Function	*P. syringae*
ATPase	HrcN
Chaperone	AvrF, PphF, ShcA, ShcM
Effector Proteins	AvrB, AvrE, AvrPphB, AvrRpt2, AvrPto, AvrPtoB, HopA1, HopAI1, HopF2, HopG1, HopI1, HopM1, HopU1, Hopz1, Hopz2, Hopz3
Export protein	HrpJ
Pilin/needle monomer	HrpA1, HrpB
Needle-tip	HrpA
Outer ring	HrcC
Inner rings	HrcRST, RrpQ, HrcJ, HrcU
Secretion Proteins	HrpE, HrpJ, HrpO, HrpP, HrpQ, HrcT, HrpT, HrcV, HrcU
Sigma factors	HrpL
Switch protein	HrpP
Translocator	HrpK1, HrpJ, HrpU
Transcriptional regulator	HrpR, HrpS, HrpV
Harpins	HrpZ, HrpZ1, HrpW1, HopAK1, HopP1

The T3SS assembles in a co-ordinated and ordered hierarchal sequence following assembly activation, where the final complex is anchored into the peptidoglycan layer on the bacterial membrane (Diepold, 2020, Deng et al., 2017). The final complex consists of three key regions: the transmembrane region, the cytoplasmic region, and the extra-cellular region (Rahmatelahi et al., 2021). The inner-membrane spanning basal body structure is first assembled (Diepold, 2020, Deng et al., 2017). This comprises of membrane-spanning rings which consist of multiple proteins, the assembly order of which will follow the inside-out model or the outside-in model dependent on the bacterial species (Deng et al., 2017). This is determined by protein-protein interaction kinetics (Deng et al., 2017). Assembly of the export apparatus will occur at the base of the basal body (Diepold, 2020). The needle complex will then begin assembly following completion of the cytoplasmic membrane region, where pilus monomers will stack on top of each other guided by a ruler protein (Diepold, 2020, Shaulov et al., 2017). This forms a channel between bacteria and target cell consisting of a hollow polymerised filament of helical needle proteins (Hu et al., 2018). Needle formation leads to structural rearrangements in the membrane rings (Diepold, 2020). The fully assembled virulence complex is known as the type III injectisome (T3SSa); however, a similar assembly process will occur for the bacterial type III flagellum (T3SSb) with some differences seen in structure and assembly order (Halte and Erhardt, 2021). Despite some differences observed, the assembly and architecture of the export gate is well conserved between flagellar and virulence type III secretion systems (Johnson et al., 2019). Assembly of the T3SS is aided by various accessory proteins, chaperones, and scaffold proteins which do not remain in the final complex (Kato et al., 2018). The exact order of individual T3SS component assembly varies between species, usually dependent on the timing of tightly controlled gene expression (Diepold, 2020, Charova et al., 2018).

At the end of the needle tip is a scaffold protein that allows for translocon pore formation where the translocon is then able to facilitate the passage of effector proteins into the target cell (Dortet et al., 2018). This has been shown to be achieved by lipid bilayer binding, pore-formation produced through

molecular hydrophobicity led by the translocon C-terminal domain and more recently, by modification of the host epigenome (Dortet et al., 2018, Buttner et al., 2002).

The injection of effector proteins directly into the host cell leads to a variety of effects that facilitate the survival and colonisation of the pathogen by allowing for evasion of an immune response. Bacterial infection of plants which triggers pattern recognition receptors (PRRs) leads to PAMP-triggered immunity (PTI) which resists colonisation by way of callose deposition, alteration of cellular signalling and impacts tissue vascularisation (Nicaise et al., 2009). Many injected effector proteins inhibit activation of many of these immune response pathways (Kumar et al., 2021).

One example to illustrate such a phenomenon would be the effector protein HopAF1 from *Pseudomonas syringae* which has been shown to supress plant immunity by blocking ethylene induction, a molecule which plays an important role in plant immunity cellular signalling (Washington et al., 2016). This is achieved by HopAF1 which targets methionine recycling through MTN1 and MTN2 methylthioadenosine nucleosidase protein activity manipulation (Washington et al., 2016). These are key proteins involved in the Yang cycle responsible for ethylene biosynthesis (Washington et al., 2016).

1.3.1.1. Substrate Secretion

The recruitment and secretion of T3SS substrates is an area which is not fully understood. There are still areas relating to the regulation of effector protein and chaperone expression and recruitment that still require investigation. What is known is that effector proteins contain a secretion signal, and this is required for recruitment and subsequent translocation through the needle complex (Samudrala et al., 2009). Recent protein modelling studies have indicated that T3SS effector proteins are often mechanically labile, and this may help explain secretion compatibility through the system (LeBlanc et al., 2021).

The secretion signal motif lacks homology across species, but it is agreed that the highly-variable secretion signal is found in the N-termini of effector proteins (Niemann et al., 2013, Buchko et al., 2010). However, this area is one of controversy as there is also evidence for mRNA-based secretion signals. It has been shown that some of these secretion signals are in the form of, or may collaborate with, Hfq-regulated RNA (Niemann et al., 2013, Habyarimana and Ahmer, 2013). There is no evidence to suggest that any type of secretion signal associated with type III secreted substrates are cleaved as part of the secretion process. This is in contrast with many other signal sequences seen in other systems. Recent structural data shows that effector protein loading can be achieved in a side chain-independent manner, helping to explain the plasticity and structural disorder often observed with N-terminal signal sequences (Miletic et al., 2021).

This secretion signal is recognised by chaperones (chaperone-dependent effectors) or by T3SS components independent of chaperones (Ghosh, 2004). Effector proteins are then recruited to a sorting platform at the base of the type III secretion system (Samudrala et al., 2009, Ghosh, 2004). Chaperones are proteins which aid with protein folding or assembly of macromolecular complexes. In the case of the T3SS, many chaperones are critical for system assembly and effector protein recruitment and translocation (Job et al., 2010). There are III main classes of T3SS chaperone grouped by their molecule of recognition. Class I chaperones recognise effector proteins, class II chaperones recognise translocator molecules, while class III chaperones recognise needle-forming proteins (Job et al., 2010). It has been recently demonstrated that an N-terminal secretor domain may be important for proper T3SS chaperone function in some cases, as demonstrated with the T3SS of *Y. pseudotuberculosis* (Gurung et al., 2022).

Alongside the chaperone proteins, secretion regulator proteins also carry out functions, little of which are known about. Some of these proteins are important for the secretion process itself, others are important for proper needle assembly and pore formation, but many secretion proteins and their functions still remain unclear (Schoehn et al., 2003, Zarivach et al., 2008, Lohou et al., 2013, Manera et al., 2021).

This sorting platform often consists of a C-ring, the export apparatus, and the ATPase complex (Lara-Tejero et al., 2011, Bernal et al., 2019). In the case of *Pseudomonas syringae*, based on structural evidence, these proteins are likely to be HrcQ, HrpD (C-ring), HrcRST, HrcU, HrcV (export apparatus) and HrcN, HrpE (ATPase complex) however further confirmation by experimentation is necessary (Trampari, 2016).

This sorting platform allows for the selection of effector proteins along with structural and functional components (Bernal et al., 2019, Hu et al., 2015). Effector proteins and other relevant components necessary for establishing infection are sorted into early, middle, and late substrates, and are secreted accordingly (Takaya et al., 2019, Riordan et al., 2008). There is strong evidence to suggest that the functionality of the sorting platform is dependent on chaperone switching activity of phases and stabilisation of substrates (Takaya et al., 2019). As demonstrated in *S. flexneri*, this sorting platform is critical for substrate selection and for energising secretion (Tachiyama et al., 2021). This sorting platform assembles from Spa33 monomers which oligomerise and associate with the basal body to connect to the Spa47 T3SS export ATPase in *S. flexneri* (Tachiyama et al., 2021).

The proteins are secreted in an unfolded state. It has been shown by Dohlich *et al*., 2014, that fusion proteins which prevent protein-unfolding cannot be secreted by the system. The wildtype variant of the protein used in this study, which could unfold, was secreted as expected (Dohlich et al., 2014).

Effector proteins will travel through the entry portal at the base of the needle (a funnel starting at approximately 15 Å in diameter, decreasing to 10Å) before moving into an atrium with a diameter of approximately 40 Å (Radics et al., 2013). It is not fully understood what the importance is of the atrium as little investigation has been undertaken on this feature. It has been suggested that this structural feature may allow for the polarisation of effector substrates so that they travel through N-terminal first (Radics et al., 2013). The mechanism for this has not been demonstrated.

Following the atrium is the narrow inner needle channel (approximately 20 Å diameter) which extends approximately 25 to 150 nm depending on the species of bacteria (Nans et al., 2015). This needle is made up from an estimated 100 subunits each around 10 kDa each, which are guided by a ruler-protein which determines the final length. This process is dependent on proton motive force. This is generated by bacterial metabolic processes (i.e. respiration) which drive unfolded proteins toward the host end of the needle in contact with the host cell membrane. It is thought that the unfolding of proteins by the ATPase releases potential energy which, coupled with electrostatic repulsion, moves proteins through the inner needle channel (Akeda and Galan, 2005, Rathinavelan et al., 2010). It has been shown that an aromatic tryptophan groove in the needle channel may be an important feature for maintaining electrostatic repulsion which guides effector proteins in a screw-like rotation motion up the needle channel (Rathinavelan et al., 2010).

1.3.1.2. The Type III Machinery of *P. syringae*: Hrp and Hrc

In *P. syringae*, this type III secretion system is produced from the expression of *hrp and hrc genes*. The *hrp and hrc* genes present within the *hrp* pathogenicity island display three mosaic-like loci. The first of these loci, based on deletion-mutant analyses suggest dedication to effector proteins (the exchangeable effector loci), the second loci to type III secretion genes (the *hrp/hrc* gene cluster), and

the latter loci demonstrating a contribution to parasitic fitness and tomato pathogenicity within *Pseudomonas syringae* (*Pto*) (conserved effector loci) (Alfano and Collmer, 1997). One of these loci, the *hrp/hrc* gene cluster is shown within Figure 1.3 (Alfano and Collmer, 1997). It has been shown that strains lacking the *hrp/hrc* gene cluster loci can grow and survive on host plants, however, despite this, they unable to cause disease (or showed significantly diminished disease-associated symptoms) highlighting the importance of this cluster for proper type III functionality (Clarke et al., 2010, Fouts et al., 2003). These *hrp/hrc* genes encode for 3 major protein groups: the Hrp type III secretion system, avirulence proteins (*avr)*, and Hrp-dependent outer proteins (Hop) (Collmer et al., 2000). It has been shown that there exists hypervariability within amino acid residues across bacterial species which utilise the Hrp pili which suggests and allows for speculation, from a broader perspective, that the Hrp operon is subject to extensive adaptive pressure to evolve in order to better that of the evolutionary defence mechanisms employed by plant hosts (Weber and Koebnik, 2006).
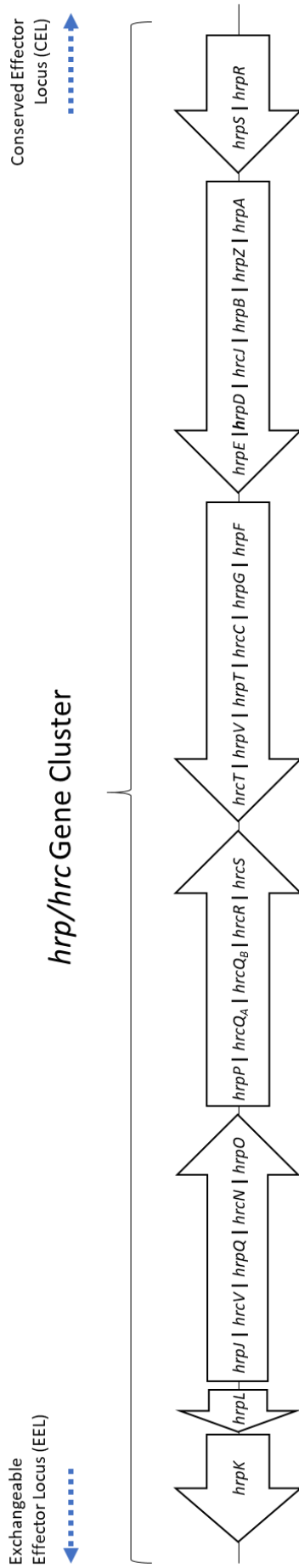
Figure 1.3. Graphical representation depicting the *hrp/hrc* gene cluster from *Pseudomonas syringae* (Alfano et al., 2000, Alfano and Collmer, 1997, Rezzonico et al., 2004)

1.3.1.2.1. HrcN

In *Pseudomonas syringae,* the hypersensitive response conserved plant injectisome protein (HrcN) is an ATPase protein translocase that drives the main type III secretion system machinery (Muller et al., 2006). HrcN exists as a dodecamer ring which is 11.5 ± 1 nm in diameter with a height of 12.0 ± 2 nm (Muller et al., 2006). Within the ring is a 2.0-3.8 nm channel (Muller et al., 2006). It has been shown via structural analyses that HrcN has four known forms; these include a 48 kDa monomer, a 300 kDa hexamer, a 575 kDa dodecamer and a 3500 kDa membrane-bound form which has been shown to hydrolyse ATP in to ADP and phosphate (Pozidis et al., 2003).

In terms of mechanism, HrcN has been shown to undergo homo-oligomerisation which in turn drives ATP hydrolysis (ATP + H_2O <=> ADP + inorganic phosphate (Pi)) which powers the basal secretion pump that drives the type III needle pilus (Pozidis et al., 2003). It has been shown that HrcN interacts with HrpE (a secretion component protein) enabling type III effector recruitment and secretion however the mechanism behind this still remains inconclusive (Fang, 2010). Despite this however, it is known that this HrcN-HrpE interaction is involved in colonisation as Δ*hrcN* and Δ*hrcE* mutants showed reduced colonisation ability in regard to type III-mediated infection (Schmidt et al., 2012)*.* HrcN appears to be hyperactivated once dodecamerisation has been achieved (i.e. formation of the 575 kDa variant of the HrcN protein) (Pozidis et al., 2003). This was shown in a study where isolated monomeric His6-HrcN was used to demonstrate the natural favouring of 575 kDa HrcN dodecamer assembly *in vivo* which then led to ATP turnover (Pozidis et al., 2003). Much like *P. aeruginosa,* it is hypothesised that cyclic-di-GMP acts as a regulator of the type III secretion system in *P. syringae* by binding to HrcN however, current evidence supporting this is limited (Trampari et al., 2015).

From an evolutionary standpoint, HrcN shares significant homology to other type III secretion system ATPase proteins including YscN (*Yersinia spp.)*, PscN (*Pseudomonas aeruginosa*), InvC (*Salmonella* SPI-1), Spa47 (*Shigella flexneri*), EscN (Enteropathogenic *E. coli*) and FliI (flagellar T3SSb in *Salmonella typhimurium* and *Pseudomonas fluorescens).* Interestingly, the ATPase protein also shares sequence similarity with the mitochondrial F1 and V1 ATPases which, while it contains an additional α sub-unit not found in type III secretion systems, does have a similar catalytic β subunit (Abrahams et al., 1994). While the F1 and V1 ATPases are more adapted towards eukaryotic function, the evolutionary link can still be inferred.

1.3.1.3.   Regulation

1.3.1.3.1. Transcriptional Regulation

Assembly of the type III secretion system is an energy and resource expensive process for bacteria and thus, the environmentally-dependent control of this apparatus is an evolutionary advantage. One method that bacteria regulate type III assembly is at the transcriptional level. Often these regulatory pathways are complex that depend on intracellular and extracellular signalling networks. Examples of key transcriptional regulation systems within *Pseudomonas* are described in Table 1.3.

Table 1.3*.* Example Systems of Type III Secretion System Transcriptional Regulation in *Pseudomonas* (Brutinel and Yahr, 2008, Marsden et al., 2016, Wu and Jin, 2005, Wu et al., 2004).

System	Regulated Gene(s)	Effect	Species
algD operon	*algU*	Type III expression at low Ca^{2+} levels and with host cell contact	*Pseudomonas aeruginosa*
cAMP-Vfr system	*vfr*	Vfr, in the presence of cAMP, activates *exsA*	*Pseudomonas aeruginosa*

		transcription leading to type III gene expression	
CvsSR two-component system	*hrpR, hrpS, algU*	High Ca^{2+} leads to expression of type III components and repression of *algU* sigma factor.	*Pseudomonas syringae Pto*
ExsDCE cascade	*exsA*	high Ca^{2+} prevents type III gene expression	*Pseudomonas aeruginosa*
Ptr system	*exsA*	Suppression of type III secretion system during copper stress or DNA damage	*Pseudomonas aeruginosa*

1.3.1.3.2. Cyclic-di-GMP and Post-translational Regulation

For many bacteria, control of the type III secretion system at a post-translational level will also confer a significant evolutionary advantage as it allows for fine-tuning of the system operation ensuring that type III function is efficiently used on when necessary for survival. There exists evidence to show that the secondary signalling molecule, cyclic-di-GMP regulates type III secretion systems however the very nature and extent of this remains unclear (Trampari, 2016, Moscoso et al., 2014, Moscoso et al., 2011). Moscoso et al (2011) demonstrated that cyclic-di-GMP along with a diguanylate cyclase WspR, are involved in small-RNA RsmY/RsmZ-dependent type III secretion system regulation in *P. aeruginosa* as part of the RetS/GacS signalling cascade. Further evidence to support cyclic-di-GMP as a type III regulatory molecule by Trampari (2016) showed CdG-dependent allosteric control over a FliI export ATPase protein (in *P. fluorescens*) at the base of the T3SS complex. Additionally, it was shown that HrcN of *P. syringae* binds to CdG, however the downstream effect this has on virulence and function was not determined (Trampari et al., 2015).

CdG is known to have direct control over bacterial virulence however, with the finer details there is still uncertainty (Hall and Lee, 2018). CdG binding appears to show universality across highly conserved T3SS-associated ATPases, with indication that such binding may be more widespread across other types of secretion systems and type IV pili (Roelofs et al., 2015, Trampari et al., 2015, McCarthy et al., 2019, McCarthy et al., 2017). It is not clear whether the downstream responses to CdG-binding vary significantly between bacterial species.

This growing evidence does begin to suggest that CdG may have a direct influence over secretion system functionality and that this may be a conserved system across a broad spectrum of bacterial species however extensive additional research would be necessary to support this. It could also be proposed that secretion system-associated ATPase complexes which have been shown to bind to cyclic-di-GMP, could also be integral to this conserved system. However, again, this would require significantly more testing to reach any conclusions surrounding this.

1.3.1.3.2.1. Structure

Bis-(3'-5')-cyclic dimeric guanosine monophosphate, more commonly known as cyclic-di-GMP was first discovered in the late 1980s where it was shown to act as an allosteric regulator of cellulose biosynthesis in *Gluconacetobacter xylinus* (Ross et al., 1987). This laid the foundation for numerous future studies that unveiled the broad spectrum of functions that cyclic-di-GMP fills. The role of cyclic-di-GMP has been well studied across bacterial function but particularly within *Pseudomonas spp.*

where it exists as a secondary messenger involved in signal transduction where under high concentrations, it most notably plays a leading role in the formation of biofilms, induction of low cellular motility and is involved in the modulation of virulence (Cole and Lee, 2016, Hall and Lee, 2018).

With a molecular mass of 690.4 g/mol, Cyclic-di-GMP is a large secondary messenger molecule, the structure of which is shown in Figure 1.4 (PubChem, 2018). It is found within most known bacteria and curiously also within Dictyostelium eukaryotes, however this acquisition has probably been achieved via horizontal gene transfer. The role of cyclic-di-GMP in Dictyostelium, as a secreted molecule, leads to stalk cell differentiation (Chen and Schaap, 2012). This is different to that of bacteria and will not be covered in further detail here.
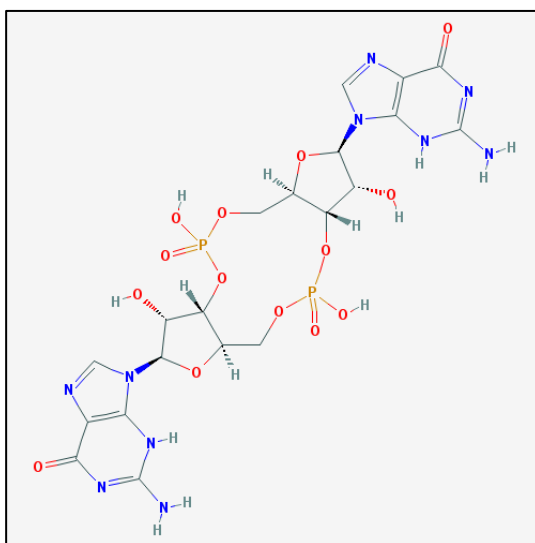
Figure 1.4. Chemical two-dimensional structure of cyclic-di-GMP (PubChem, 2018).

1.3.1.3.2.2. Function

Cyclic-di-GMP is synthesised by approximately 29 to 40 enzymes in a typical *Pseudomonas* cell which vary depending on the species (Sarenko et al., 2017). These enzymes are forms of diguanylate cyclases (containing a GGDEF domain) which synthesise cyclic-di-GMP from two GTP molecules. Degradation of cyclic-di-GMP occurs via phosphodiesterases (containing an EAL domain) where the molecule is converted in to 5'-phosphoguanylyl-(3'-5')-guanosine (pGpG) and/or guanosine monophosphate (GMP) (Orr et al., 2015, Cohen et al., 2015).

Some would suggest that varying levels of cyclic-di-GMP can exist in "localised pools" within a bacterial cell allowing for micro-control of specific environments using a common signalling molecule however this is a controversial statement that many would disagree with (Ross et al., 1987, Huang et al., 2003, Kulasakara et al., 2006). Due to a rapid diffusion rate within the bacteria, it is unlikely that this would be the case.

While much of the early work surround cyclic-di-GMP was carried out in *Caulobacter crescentus* and *Xanthomonas campestris*, much of the current detailed understanding arose from work within *Pseudomonas.* Cyclic-di-GMP signalling is involved the regulation of biofilm formation, motility, virulence among other characteristic phenotypical alterations across *Pseudomonas* species. In

general, it has been shown that increased levels of cyclic-di-GMP in *Pseudomonas* lead to the production of biofilm, decreased cellular motility and metabolic change (Valentini and Filloux, 2016).

The Wsp (wrinkly spreader phenotype) chemosensory system (found in *P. aeruginosa* an *P. fluorescens*) is one of the most well studied cyclic-di-GMP regulated pathways. Cyclic-di-GMP regulates environmentally-dependent adhesion factors (such as those encoded for by the *psl and pel* operons) which give rise to a distinct wrinkly spreader (WS) phenotype as opposed to a smooth phenotype (SM) (Malone et al., 2007). The operon consists of genes: *wspA, wspB, wspc, wspD, wspE, wspF and wspR* (Hickman et al., 2005). WspR is an important part of this operon. WspR is a GGDEF-domain-containing diguanylate cyclase which catalyses the synthesis of cyclic-di-GMP leading to altered phenotypical changes (Malone et al., 2007). WspF also seems to play a large role with transcriptome analysis showing 560 genes which were affected in response to deletion of the *wspF* gene highlighting the complex nature of many of these regulatory systems (Hickman et al., 2005).

Strong phenotypic differences have been observed in *Pseudomonas* regarding cyclic-di-GMP levels however the impact of cyclic-di-GMP can also be seen across a wide range of other bacteria too. Knock-out mutants of key enzymes responsible for cyclic-di-GMP synthesis have been constructed to study the impact of cyclic-di-GMP on cellular function. An example study produced a diguanylate cyclase null mutant *Acidithiobacillus caldus* strain that, while was able to survive, it led to dramatic effects on motility and adherence (Castro et al., 2015). Another similar study demonstrated how cyclic-di-GMP knock-out mutants displayed defective biofilm formation and altered cell surface phenotypes within *Mycobacterium smegmatis* (Gupta et al., 2015).

This begins to highlight the importance of cyclic-di-GMP within bacterial regulation and how it underpins a large proportion of critical cellular functionality. While this is still a relatively emerging concept regarding global bacterial regulation, evidence continues to grow to show the large impact of this secondary messenger molecule across a wide variety of bacterial species (Valentini and Filloux, 2016).

1.3.1.3.3. Cyclic-di-GMP Binding Proteins

Certain cyclic-di-GMP binding proteins have been identified. These include a certain class of PilZ proteins along with Clp, PelD, FleQ, and VpsT (Xu et al., 2016, Leduc and Roberts, 2009, Lee et al., 2007, Matsuyama et al., 2016, Hickman and Harwood, 2008, Srivastava et al., 2011). Arginine, asparagine and glutamate residues are frequently seen in the binding sites of Cyclic-di-GMP-interacting proteins as they bind to specific atoms on the guanine base, however, the similarity across binding sites for non-GGDEF, EAL, HD-GYP (cyclic-di-GMP synthases and hydrolases) and PilZ proteins ends here (Chou and Galperin, 2016). In the case of cyclic-di-GMP synthesising GGDEF-domains a characteristic RXXD motif is present five residues upstream of the cyclic-di-GMP binding active site while with cyclic-di-GMP hydrolysing EAL-domains, a characteristic EXLXR motif that wraps around the cyclic-di-GMP ribose-phosphate ring can often be observed (Chan et al., 2004, Barends et al., 2009). GGDEF and EAL domains, along with HD-GYP domains are conserved polypeptide regions featuring distinct amino acid residues involved in CdG signalling and regulation, and can be used for CdG binding protein identification (Simm et al., 2004, Chou and Galperin, 2016). There can be minor variations to these examples however such as EVLRR replacing EXLXR in EAL-containing FimX from *P. aeruginosa* (Navarro et al., 2009). PilZ-domains (type IV pilus control) also possess characteristic cyclic-di-GMP binding motifs; these are RXXXR and DXSXXG which both bind to a guanine base each (Benach et al., 2007).

One prominent cyclic-di-GMP binding protein would be RimK, a post-translational ribosomal modification protein in *Pseudomonas* (Little et al., 2016). RimK has been shown to interact with cyclic-di-GMP and disrupting proper RimK function leads to altered motility and surface attachment phenotypes, along with decreased rhizosphere and plant colonisation (Little et al., 2016). RimK, when activated by cyclic-di-GMP, acts as an ATP-dependent glutamyl ligase (Little et al., 2016). This enzyme adds glutamate residues to the C-terminus of RpsF, a ribosomal protein (Little et al., 2016). This glutamate affects ribosomal function and thus, remodels the bacterial proteome in relation to environmental pressures (Little et al., 2016). The interaction is subject to regulation through small regulatory RimA and RimB proteins along with cyclic-di-GMP itself (Little et al., 2016). This example highlights how precise control of a cyclic-di-GMP binding protein allows for *Pseudomonas to* respond to its environment. One should note that RimK is not present in just *Pseudomonas;* RimK homologs are present across a wide range of prokaryotes and eukaryotes and so this system gives us a broad insight into how bacteria regulate function through cyclic-di-GMP.

Another example shows that, along with post-translational ribosomal modification, cyclic-di-GMP also has implications in controlling flagella synthesis for host immunity evasion (specifically, flg22-triggered immunity). Pathogen/microbe-associated molecular patterns such as that of the bacterial flagellum are recognised by plant pattern recognition sensors (PPRs). FLS2 (FLAGELLIN SENSING 2) is an example of a PPR which recognises a flg22 PAMP on *Pseudomonas* flagella, and then subsequently triggers flg22-triggered immunity (Pfeilmeier et al., 2016). FLS2 activation was shown to be reduced with decreased expression of *wspR19* which correlates with reduced flagellin accumulation and increased cyclic-di-GMP production (Pfeilmeier et al., 2016).

Alongside these examples, CdG is also known to repress flagella activity and assembly across multiple organisms, leading to regulation of motility (Wolfe and Visick, 2008). A good example of this is with the MorA protein of *P. putida* (Choy et al., 2004). This is a GGDEF/EAL flagellar protein which when knocked-out, gave rise to altered motility phenotypes and delayed flagellar development in planktonic cells (Choy et al., 2004). It was found that *morA* restricted the expression of key flagella genes including *fliC* (Choy et al., 2004).

1.3.1.3.4. Limitations and Future of the Research

There currently exists no bioinformatic-based methods to easily and reliably screen for all cyclic-di-GMP binding sites and so a more carefully measured and strategic approach must be employed by targeting suspect proteins. While GGDEF, EAL and HD-GYP proteins show characteristic binding motifs, cyclic-di-GMP receptors do not. Cyclic-di-GMP receptor sites often display no common patterns which can be used for computational identification methods and so traditional wet laboratory methods must instead be used. In order to fully understand the effects of cyclic-di-GMP and all of its roles, we must begin to identify more cyclic-di-GMP binding proteins and study how they function.

A key practical screening method used to detect cyclic-di-GMP binding is differential radial capillary action of ligand assay (DRaCALA) which is able to detect protein binding to low molecular weight ligands in whole-cell lysates (Orr and Lee, 2017, Roelofs et al., 2011). This can often be combined with further biochemical assays, isothermal titration calorimetry and peptide arrays to identify new cyclic-di-GMP binding proteins. This screening cascade is usually based off cyclic-di-GMP affinity pulldown assays or associated cyclic-di-GMP homologue proteins.

1.4. Effector Proteins

For *P. syringae,* there are a range of known type III effector proteins per strain, the majority of which facilitate bacterial colonisation while repressing the host immune response (Studholme et al., 2009). This is achieved in various ways including the targeting of plant resistance proteins, the blocking of immune-receptor signalling, RNA pathway interaction, organelle function disruption and alteration of cellular trafficking (Guo et al., 2009). Examples of key *P. syringae* effector proteins and their mechanisms of action are illustrated in Figure 1.5.

Typically, across *P. syringae* strains, a range of 15-35 well-expressed effector proteins can be expected drawing from at least 58 effector protein families, however this figure is variable (Baltrus et al., 2011). Some strains appear to have a relatively small effector protein repertoire, such as *Pseudomonas syringae* pv. japonica. (Pja), a pathogen of barley (*Hordeum vulgare*) which is believed to only have approximately 10 known effector proteins (Baltrus et al., 2011). In contrast, others strains such as *Pto* DC3000 have a much more extensive effector protein repertoire, with estimates of approximately 35-40 known effector proteins alongside other putative proteins.

In most cases, despite many strains having a range of different effector proteins in their repertoire, often only a few are shared among other strains (Alfano and Collmer, 2004). This suggests that a strains given effector protein repertoire is highly specialised towards colonisation of their target host organism, and these differences are one of the main factors in defining a strain and its pathovar (Alfano and Collmer, 2004) . An example of this is with *P. syringae Pto* DC3000, B728a *Psy*, and 1448a *Pph* strains which only share 13 common effectors despite have a much larger effector protein repertoire each (approximately 40 more in each pathovar) (Vinatzer et al., 2006).
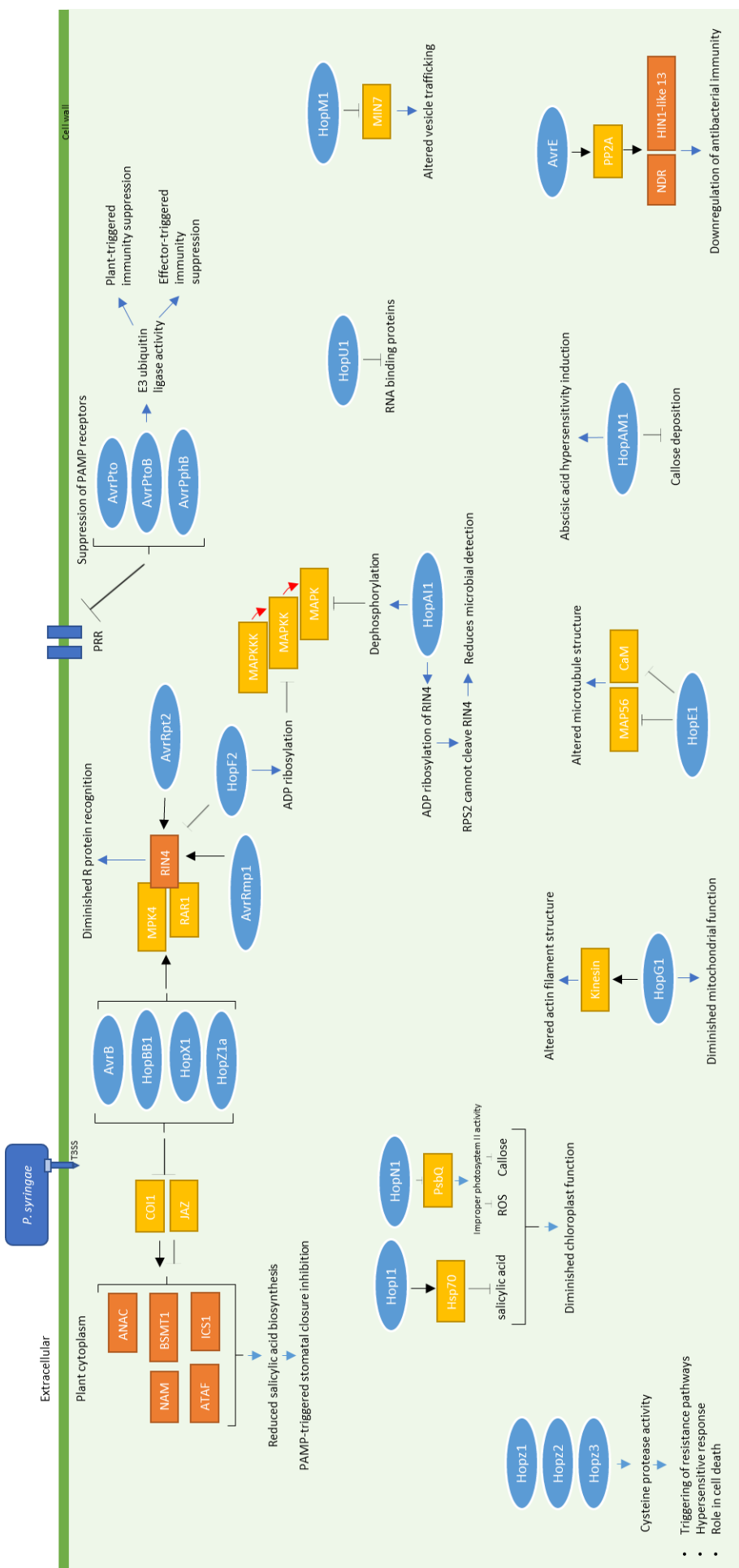
Figure 1.5. Examples of key *P. syringae* effector proteins and their known or proposed mechanisms of action. Effector proteins are represented as blue ovals. (Adapted from Block and Alfano, 2011, Xin et al., 2018, Xin et al., 2015, Zheng et al., 2012, Xin and He, 2013, Zhou et al., 2009).

1.4.1. Effector Translocation Control

1.4.1.1. *hrp/hrc* Regulon

The *hrp* (hypersensitive response and pathogenicity)/*hrc* (hypersensitive response and conserved) regulon is subject to tightly orchestrated genetic regulation for finely-tuned T3SS control at a transcriptional level. The regulatory control of the *hrp* regulon in turn will lead to downstream control of effector proteins and their translocation.

The *hrp* pathogenicity cluster consists of T3SS-system components, regulatory elements, effector-related elements, and translocation-components and is located in a tripartite pathogenicity island (T-PAI) (Alfano et al., 2000). Precise control of all these elements is necessary for dynamic activation and deactivation of the T3SS. This is necessary as the T3SS is highly energy-dependent, and so well-regulated control provides a fitness advantage for bacterial survival and pathogenicity (Alfano et al., 2000). Strains naturally lacking a classic *hrp/hrc* locus in *P. syringae* exhibit an atypical T3SS, with altered downstream host infection phenotypes (Clarke et al., 2010).

There are a variety of global regulatory networks that have been shown to exert control on the *hrp/hrc* regulon. It was previously predicted by way of a boolean computer model that simulated knock-out experiments of key genes that the *hrp/hrc* regulon in *P. syringae Pto* DC3000 is a tightly regulated system driven predominantly by the GacS/GacA two-component system (MacLean and Studholme, 2010). This is part of the Gac/Rsm regulatory pathway, a signal transduction pathway that is well known for regulating a variety of processes in *Pseudomonas* bacteria. These include control of virulence, biofilm formation, motility, and response to external stress (Grenga et al., 2017).

This Gac/Rsm system is itself subject to various layers of regulation. For example, it has been shown that the PagR and PagI quorum-sensing regulators upregulate its expression (Panijel et al., 2013). The Gac/Rsm regulatory cascade is closely linked with CdG. This pathway leads to control of downstream CdG levels and related bacterial phenotypes in *P. aeruginosa* (Moscoso et al., 2014).

1.4.1.1.1. HrpL

HrpL is a sigma factor of the *hrp/hrc* regulon that functions as a master T3SS regulator through negative autogenous control (Waite et al., 2017). This has been well characterised in *Pseudomonas syringae*, where HrpL co-ordinates expression of most genes associated with the T3SS (Waite et al., 2017). Promotion of *hrpL* is associated with enhancer binding proteins HrpR and HrpS (forming a hetero-hexamer), along with sigma-54 (Waite et al., 2017). Control of T3SS genes is achieved by HrpL binding to the conserved *hrp* box cis-element of T3SS gene promoters (Wang et al., 2018). This follows *hrpL* activation from HrpRS operon oligomer binding with a RpoN alternative sigma factor to the *hrpL* promoter (O'Malley and Anderson, 2021). HrpL binding to the *hrp box* of T3SS genes allows for their transcription. This includes effector proteins and so HrpL is considered to be a highly important regulator of effector proteins (Collmer et al., 2000). Additionally, HrpL represses its own transcription as a form of negative autogenous regulation. This allows for the fine-tuning of T3SS gene expression (Waite et al., 2017).

1.4.1.2. *hop* Genes

Effector proteins are typically encoded outside the *hrp/hrc* pathogenicity cluster, and instead exist elsewhere on the *Pseudomonas* chromosome. In *Pseudomonas syringae*, it was previously thought that there were approximately 35 known T3SS effector-encoding genes (Guo et al., 2009). These T3SS effector-encoding genes are typically known as *hop* genes. Ongoing research continues to add to this list where the number of putative effector proteins could be over 75 (Lee et al., 2019). These proteins

exhibit high diversity with a variety of different sizes, potential mechanisms and evolutionary lineages (Lee et al., 2019). Expression regulation of *hop* effector genes is primarily driven by HrpL activation along with other members of the *hrp/hrc* regulon (Schechter et al., 2006, O'Malley and Anderson, 2021). Additional layers of transcriptional regulation are likely present; however, the full regulatory system is still not fully understood.

Newly identified *hop* genes and novel effector protein candidates must currently meet strict assessment criteria and follow a pre-defined nomenclature before acceptance within the field. New candidates must have phylogenetic *hop*-family membership, show HrpL-dependence, evidence of T3SS-dependent secretion, and a downstream avirulence or HR phenotype (Lindeberg et al., 2005). Despite these strict criteria, there have been past examples of putative effector genes being declassified due to emerging evidence (Lindeberg et al., 2005).

There are many putative effector genes with new type III-associated genes frequently being discovered. Depending on the species, it is often the case that putative effector genes may be very weakly expressed or may be pseudogenes. Many effector genes are organised into distinct clusters. Shown in Table 1.4 is a list of known effector gene clusters in *Pto* DC3000.

Table 1.4. Known *Pto* DC3000 *hop* T3SS effector gene clusters. Weakly expressed genes or potential pseudogenes have been denoted with '*'. (Wei et al., 2015, Kvitko et al., 2009, Wei et al., 2007, Wei and Collmer, 2018).

Gene Cluster	Effector Gene	Locus ORF
	hopK1	44
	hopY1	61
I	*hopU1*	501
	hopF2	502
II	*hopH1*	588
	hopC1	589
IV	*hopD1*	876
	hopQ1-1	877
	hopR1	883
	hopAM1-1	1022
Conserved Effector Locus (CEL) (VI)	*hopN1*	1370
	hopAA1-1	1372
	hopM1	1375
	avrE	1377
	hopB1	1406
	hopAF1	1568
	avrPtoB	3087
	avrPto	4001
	hopE1	4331
VIII	**hopS2*	4588
	*hopT2	4590
	*hopO1-3'	4592
	*hopT1-2	4593
	*hopO1-2	4594
	*hopS1'	4597
	*hopAD1	4691
IX	*hopAA1-2*	4718

	hopV1	4720
	hopAO1	4722
	*hopD'	4724
	hopG1	4727
	*hopQ1-2	4732
	hopI1	4776
	hopA1	5354
	*hopBM1	5633
pDC3000A (X)	*hopAM1-2*	A0005
	hopX1	A0012
	HopO1-1	A0018
	hopT1-1	A0019

1.4.1.3.   CdG Control of Effector Proteins

The role of CdG on control of effector protein translocation remains understudied. There exists only limited investigation into any direct potential relationships between CdG and effector control. CdG-dependent control of effector proteins predominantly operate at the transcriptional level (Martinez-Gil and Ramos, 2018). CdG is believed to impact the transcription of genes in the *hrp/hrc* operon. It has been shown that *hrpA, hrpN, dspE* and *hrpL* genes had altered transcription levels in environments where CdG levels were altered in the plant pathogen *Dickeya dadantii* (Yi et al., 2010). A similar transcriptional response was observed in *Erwinia amylovora* where high CdG levels led to inhibited *hrpA* expression (Edmunds et al., 2013). These *hrp/hrc* cluster components are important for proper T3SS assembly and function, and therefore for T3SS effector translocation. Related to these previous studies, it was shown that increased levels of CdG in *P. syringae* pv. tomato (and pv. phaseolicola) led to a 2-fold decrease in *hrpL* and *hrpA* gene expression, although no effect on bacterial virulence was observed (Pérez-Mendoza et al., 2014). Outside of these examples however, further evidence remains limited, particularly so in *P. syringae*. It is likely the case that complex regulatory networks exist to control *hrp/hrc* cluster transcription in a CdG-dependent manner, with well-choreographed crosstalk between regulatory RNAs and cyclic-di-GMP binding proteins (Yuan et al., 2015). This in turn leads to downstream control of effector proteins and their translocation.

To date, no evidence of direct CdG binding to T3SS-translocated effector proteins has been identified. Similarly, there is no evidence of direct CdG binding to the T3SS for post-translational control of effector protein translocation. It was previously shown that CdG binds to HrcN of the T3SS however it was not identified what the downstream implications of this was in relation to effector control (Trampari et al., 2015).

1.4.2.   Known Effectors and Their Targets

The effector proteins in *P. syringae* DC3000 have been studied numerous times over the past few decades with many host cell targets being described. Shown below in Table 1.5 is a list of known *P. syringae* effector proteins, some examples of their known targets, and accompanying citations referencing the previous studies supporting these findings. It should be noted that other known effector protein interactions have been previously shown, and that many effectors have multiple plant targets. Only a limited selection has been included in this table for brevity. Furthermore, several effector proteins have been omitted from this table due to lack of published data. Effector and plant protein interactions continue to be discovered over time, and so the list is subject to continual expansion.

Table 1.5. A List of Selected *P. syringae* Effector Proteins and Examples of their Plant Cellular Targets (Adapted from Büttner, 2016, Wei and Collmer, 2018, Xin et al., 2016).

Effector Protein	Effector Targets	Effector Function	Plant Species	Reference
AvrE	PP2A	ROS signalling disruption and downregulation of NHL13, induction of water soaking phenotype	*A. thaliana*	(Jin et al., 2016, Xin et al., 2016)
AvrPto	EFR kinase domain	EFR autophosphorylation inhibition	*A. thaliana*	(Xiang et al., 2008)
AvrPtoB	EFR	E3 ubiquitin ligase which ubiquinates EFR	*A. thaliana*	(Göhre et al., 2008)
HopA1	EDS1	EDS1:RPS4 complex disruption	*A. thaliana*	(Bhattacharjee et al., 2011)
HopAA1-2	EDS1 and PBS3	Proteasome-mediated degradation protection disruption	*A. thaliana*	(Palmer, 2018)
HopAD1	NTL9	NTL9-regulated gene expression suppression during ETI	*A. thaliana*	(Block et al., 2014)
HopAF1	MTN1 and MTN2	Inhibits methionine recycling limiting PAMP-induced ethylene production	*A. thaliana*	(Washington et al., 2016)
HopAM1	EDS1, HSP90.2, and SGT1B	Cell death disruption	*A. thaliana*	(Iakovidis et al., 2016)
HopD1	NTL9 Transcription Factor	NTL9-regulation ETI gene expression suppression	*A. thaliana*	(Block et al., 2014)
HopE1	Calmodulin	MAP65 dissociation from microtubules	*A. thaliana*	(Guo et al., 2016)
HopF2	MKK5	ADP ribosylation of MKK5 at R313	*A. thaliana*	(Wang et al., 2010)
HopG1	Mitochondrial-localized kinesin motor protein	Induces actin filament bundling	*A. thaliana*	(Shimono et al., 2016)
HopH1	EXO70B1	PTI disruption	*A. thaliana*	(Wang et al., 2019)
HopI1	Hsp70	Increased Hsp70 ATPase activity and	*A. thaliana*	(Jelenska et al., 2010)

		recruitment to chloroplasts		
HopM1	MIN7	Vesicle trafficking inhibition through MIN7 degradation, induction of water soaking phenotype	*A. thaliana*	(Nomura et al., 2006, Xin et al., 2016)
HopN1	PsbQ	Reduced PSII activity and ROS suppression	*S. lycopersicum*	(Rodríguez-Herva et al., 2012)
HopQ1-1	TFT1 and TFT5 14-3-3 proteins	Phosphorylation-dependent cell signalling interference	*S. lycopersicum*	(Li et al., 2013)
HopU1	GRP7	ADP-Ribosylation and reduced PRR transcript binding to GRP7	*A. thaliana*	(Fu et al., 2007, Nicaise et al., 2013)
HopX1	JAZ proteins	Cysteine protease which degrades JAZ-proteins	*A. thaliana*	(Gimenez-Ibanez et al., 2014)

1.5. Plant Immunity

Plants lack what we would recognise as an adaptive immune system. As such, plants have developed a complex series of immune pathways dependent on receptor recognition of elicitors, and downstream signalling. Plants have evolved two main immune strategies to defend against potential pathogens. These are PAMP-triggered immunity (PTI) and effector-triggered immunity (ETI). It is generally considered that the former is more effective for defending against non-adapted pathogens due to non-host resistance while the latter is more effective against adapted pathogens. This two-branched immune system concept has previously been described by a four-phased 'zigzag' model which proposed a back-and-forth-like interaction between microbial elicitor and plant defences in an evolutionary arms-race. However, more recently this model has been challenged as new developments in the field have emerged (Jones and Dangl, 2006, Pritchard and Birch, 2014)

It has recently been shown that these two types of immunity likely work together, and that one type of plant immunity may boost the response in the other (Ngou et al., 2021). It was demonstrated that ETI enhanced PTI defence responses, suggesting that the two types of immunity are complementary and that both are required for a stronger overall immune response (Ngou et al., 2021). Together, these two types of immunity provide plants with robust and tightly-controlled defence mechanisms against a wide variety of potential microbial pathogens.

A general overview of plant immunity is shown as an illustrative cartoon in Figure 1.6, where both PTI and ETI function are presented.
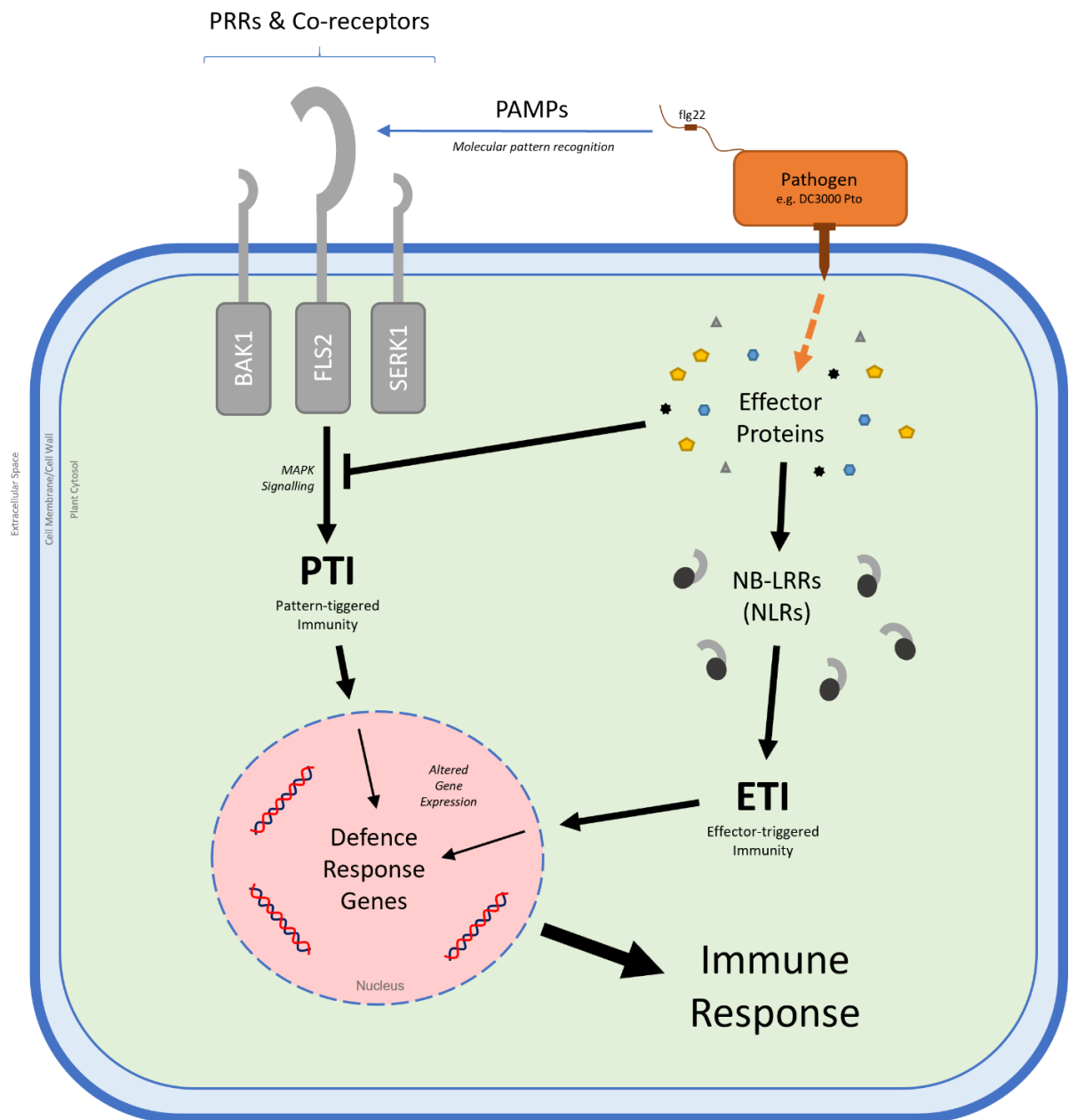
Figure 1.6. An illustrative cartoon representing a general overview of plant immunity. The plant system consists of two main immune response pathways. The first is pattern-triggered immunity (PTI) where molecular pathogen-associated molecular patterns (PAMPs) are recognised by pattern recognition receptors (PRRs). In this example, bacterial flagellin flg22 is recognised by FLS2, along with relevant co-receptors. This leads to a downstream immune response. The second is effector-triggered immunity (ETI) where translocated effector proteins are recognised by intracellular nucleotide-binding leucine-rich repeat proteins (NB-LRRs or NLRs), leading to a downstream immune response. (Adapted from Dodds and Rathjen, 2010, Dangl et al., 2013, Kumar and Verma, 2013).

1.5.1. Immune Recognition

1.5.1.1. PRRs

On the surface of invading microbial elicitors are pathogen-associated molecular patterns or PAMPS. These highly conserved microbial epitopes are recognised by plant immune receptors called pattern recognition receptors or PRRs. One notable example of this is the leucine-rich FLS2 (FLAGELLIN

SENSITIVE 2) receptor kinase, which recognises and binds to the flg22 PAMP from bacterial flagellin leading to a ROS burst and downstream immune signalling cascades (Chinchilla et al., 2006). Another notable example is elongation factor thermo unstable (EF-Tu). This is a highly-abundant G protein involved in the catalysis of aminoacyl-tRNA binding to the ribosomal A-site widely present across prokaryotic life (Harvey et al., 2019). EF-Tu is a common epitope that triggers PTI after recognition from the PAMP-receptor EFR (EF-Tu Receptor) (Furukawa et al., 2014, Zipfel et al., 2006).

Brassinosteroid insensitive 1-associated receptor kinase (BAK1) is a key component of this PRR-mediated recognition of PAMPs (Chinchilla et al., 2007, Li et al., 2002). BAK1 is a leucine-rich repeat receptor kinase (LRR-RK) and is part of the somatic embryogenesis receptor kinase (SERK) sub-group. BAK1 was shown to be critical for plant immunity, and plants lacking BAK1 display a high susceptibility towards invading microbial pathogens, with a minimal downstream immune response (Chinchilla et al., 2007). Absence of BAK1 consequently leads to a severely compromised downstream phosphorylation cascade and reduced gene expression changes typically seen with plant immunity (Chinchilla et al., 2007).

1.5.1.2. NB-LRRs (NLRs)

R proteins provide resistance against plant pathogens and are encoded for by *R* (resistance) genes. These will facilitate the recognition of effector proteins from microbial pathogens. Many of these effector receptor R proteins contain characteristic nucleotide binding (NB) domains and leucin-rich repeats (LRRs), often with either an N-terminal TIR (Toll, interleukin-1 receptor) domain or a coiled-coil (CC) domain, and are associated with ETI (Knepper and Day, 2010). These effector receptors are known as nucleotide-binding domain and leucine-rich repeats (NB-LRRs or NLRs). These receptors can recognise pathogen effectors via direct or indirect molecular mechanisms. Direct recognition will usually see an effector protein physically binding to the NB-LRR, while indirect recognition is often mediated by an associated accessory protein (Cesari, 2018). Other forms of pathogen recognition include wall associated kinases (WAKs) and members of the EDS1 family which lead to downstream MAPK kinase cascades following binding.

1.5.1.3. *R* Genes and Avirulence Genes

R genes in plants mainly encode for R proteins typically consisting of NB-LRR-like proteins. These R proteins usually convey resistance against microbial pathogens through a variety of mechanisms. The most common and most well studied mechanism is with direct binding of R proteins to microbial avirulent (Avr) proteins. This has long been described by the gene-for-gene hypothesis after its original discovery by Harold Henry Flor in the mid-1900s (Flor, 1947, Flor, 1942). This was originally shown using the fungal pathogen *Melampsora lini* of flax *Linum usitatissimumi* where pairs of matching genes in the host and pathogen were inherited allowing for disease establishment (Flor, 1947, Flor, 1942). This concept linking *R* gene products and *avr* genes remains true in many examples of plant immunity today. Other pathogen resistance mechanisms include guarding guardee proteins against Avr proteins (the guard hypothesis), pathogen toxin degradation, and PAMP detection (Van Der Biezen and Jones, 1998).

1.5.1.4. Signalling Pathways and Downstream Responses

The downstream signalling and responses for both PTI and ETI are complex and vary depending on the plant species. Some key examples are briefly covered here to illustrate the type of downstream, cellular events typically observed and relevant to this study.

1.5.1.4.1. MAPKs

A characteristic downstream response in innate plant immunity is a series of MAP kinase cascades. These are plant mitogen-activated protein kinases (MAPKs) which are triggered in response to PAMP detection and phytohormone signalling (Rasmussen et al., 2012). MAPK signalling cascades have been linked to both PTI and ETI, and in the case of *Arabidopsis,* there is likely to be a degree of functional redundancy present (Rasmussen et al., 2012).

A signalling MAPK cascade that has been well studied in *A. thaliana* is the MAPK3 pathway. MAP3K is a MAP kinase kinase kinase. Direct or indirect stimulation by a PRR leads to phosphorylation and activation of a MAPK3 such as MEKKα (del Pozo et al., 2004, Rasmussen et al., 2012). This in turn leads to downstream phosphorylation and activation of a MAP2K, a MAP kinase kinase, by MAPK3 (Rasmussen et al., 2012). This MAPK phosphorylation repeats downstream leading to a signalling cascade that influences transcriptional control, altering gene expression and cellular function (Zhang and Klessig, 2001). In *Arabidopsis* there are at least 60 MAP3Ks, 10 MAP2KS, and 20 MAPKs highlighting the complexity of signalling present across the genus (Ichimura et al., 2002).

1.5.1.4.2. Hypersensitive Response

The hypersensitive response (HR) is a key downstream mechanism used widely by plants to stop microbial pathogen spread following immune system activation (Atkinson et al., 1985). This response is a controlled induction of rapid cell death localised at the site of pathogen presence, restricting microbial growth and proliferation in the plant (Atkinson et al., 1985).

The activation of HR occurs via direct or indirect activation. Most commonly this is achieved with cellular protein modification in the plant cell by virulence factors, which is then detected by NLRs, or less commonly by direct binding of virulence factors to NLRs (Bonardi and Dangl, 2012). One NLR may recognise multiple virulence factors or virulence factor-induced protein modifications (Bonardi and Dangl, 2012). It has been hypothesised that this can lead to functional NLR pairs (with a sensor NLR and a helper NLR) or NLR networks, where NLRs work cooperatively or through negative regulation to mediate plant immunity via HR induction (Wu et al., 2017).

HR is typically a multiphase process. The first phase consists of an ion flux (hydroxide and potassium efflux, calcium and hydrogen influx) following *R* gene activation (Baker et al., 1993, Atkinson et al., 1985). The second phase is an oxidative burst leading to the production of ROS species (Baker et al., 1993). Alongside this, research over the past few years indicates that a resistome complex with high affinity for the cell membrane may form following sensing by the NLRs leading to pore formation and cell death as part of HR (Adachi et al., 2019).

1.5.1.4.3. ROS Burst

As part of the second phase of HR following PAMP-perception, a rapid burst of reactive oxygen species (ROS) is triggered by NADPH oxidases located around the plasma membrane (Baker et al., 1993). Typical ROS chemistry includes superoxide radicals, hydrogen peroxide, and hydroxyl radicals (Scandalios, 1993). These are free radicals that easily react with other molecules including invading potential pathogens, leading to damage of DNA, RNA, and proteins, eventually leading to cell death (Sharma et al., 2012). A recent example demonstrating this defence mechanism is with RBOHD NADH oxidase, which undergoes phosphorylation and ubiquitination to produce ROS in the presence of Ca^{2+} during innate PTI (Lee et al., 2020). Measurement of ROS bursts is a conventional assay for detecting a reactive plant immune response when challenged with an immune elicitor.

1.5.1.4.4. Phytohormone Signalling Pathways

Phytohormones such as salicylic acid (SA), jasmonic acid (JA), and ethylene (ET) have been shown to play an important role in plant defence, in particular with ETI (Liu et al., 2016, Checker et al., 2018). These phytohormones are low-molecular weight signalling molecules typically involved in a variety of non-defence-related processes including plant growth and development, but also lend themselves to pathogen resistance by being major components of well-orchestrated signalling networks (Checker et al., 2018). These networks are tightly co-ordinated and controlled, and often feature signalling cross-talk for fine-tuning of regulation (Derksen et al., 2013, Checker et al., 2018). These signalling networks have been shown to lead to rapid downstream changes in gene expression and cellular function, most notably during ETI. This was shown via RNA sequencing with transcriptional reprogramming observed in *A. thaliana* during the ETI stage of plant defence during *P. syringae* infection (Mine et al., 2018).

1.5.1.4.5. Other Known Responses

Alongside these key examples described above, there are a myriad of other cellular events associated with PTI and ETI. Other known cellular events include altered gene expression, callose deposition, phytoalexin production, damage-associated molecular patterns (DAMPs), closure of stomata, and CA^{2+} signalling (Li et al., 2016). These collectively all play an important role in the defence against invading microbial pathogens. This is a large area of ongoing research where many research groups are working to describe the complex downstream plant immune responses across a range of plant species.

1.6. Previous Key Work Relevant to this Project

Prior to this work, CdG binding to FliI, a HrcN homologous type III ATPase protein in *P. fluorescens* of the bacterial flagella (T3SSb) was identified and characterised (Trampari et al., 2015, Trampari, 2016). This enabled identification of key residues involved in CdG binding as shown below in Figure 1.7 (Trampari et al., 2015). This homology model was produced from information derived from site-specific mutagenesis, mass spectrometry and subsequent *in silico* analysis (Trampari et al., 2015, Trampari, 2016). Using this information, predicted binding residues for HrcN in *P. syringae* of the T3SS injectisome (T3SSa) were derived using further bioinformatic analysis. It was demonstrated that CdG binds to HrcN (along with other related homologue proteins), however, the downstream implications of this interaction on virulence remain unclear (Trampari et al., 2015).
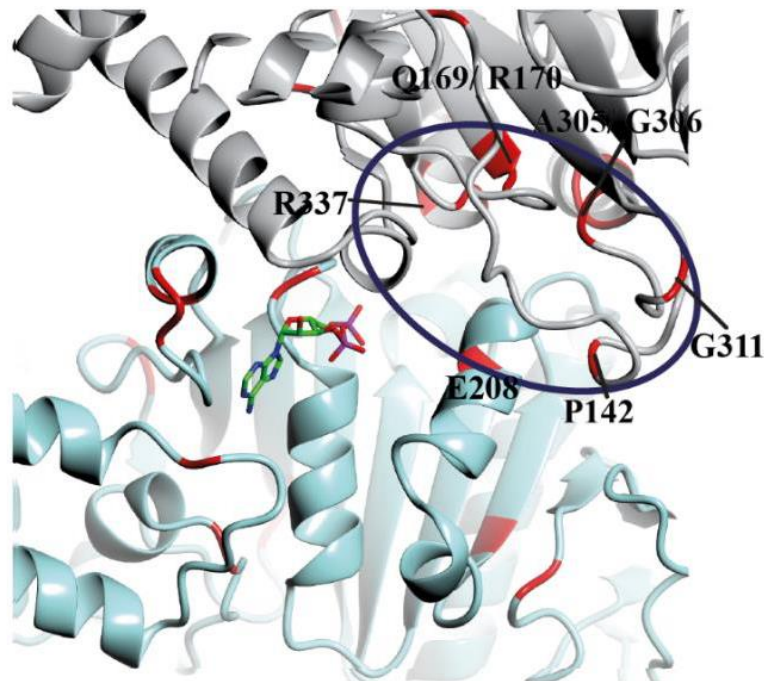
Figure 1.7. Identified cyclic-di-GMP binding residues within FliI (Trampari, 2016)

1.7. Main Thesis Aim

In this thesis, the following fundamental biological question shall be explored. What impact does the binding interaction between CdG and the HrcN T3SS ATPase of *P. syringae Pto* DC3000 have on virulence?

Chapter 2: Materials and Methods

2.1. Materials

2.1.1. Reagents

All reagents and chemicals were purchased and supplied from Merck, ThermoFisher Scientific, and Promega (and their associated brands) unless stated otherwise.

2.1.2. Growth Media

The different growth media used across various experiments in this study are described in Table 2.1.

Table 2.1. List of growth media used in this study.

Media	Recipe
L	Tryptone 10 g, yeast extract 5 g, NaCl 5 g, glucose 1 g, ddH$_2$O to 1 litre
LB	Tryptone 10 g, yeast extract 5 g, NaCl 10 g, ddH$_2$O to 1 litre
Kings	Proteose peptone 20 g, glycerol 10 mL, K$_2$HPO$_4$ 1.6 g, 1M HCl up to 1 litre at pH 7.2
hrp-Inducing Media	5.5 g KH$_2$PO$_4$, 1.5 g K$_2$HPO$_4$, 1 g (NH$_4$)SO$_4$, 0.34 g MgCl$_2$, 0.1 g NaCl, 2.9 g fructose up to 1 litre at pH 5.5
Terrific Broth	Tryptone 12 g, yeast extract 24 g, glycerol, 4 mL, 0.17 M KH$_2$PO$_4$. 0.72 M K$_2$HPO$_4$, ddH$_2$O up to 1 litre
SOC (Super optimal broth with catabolite repression)	Tryptone 20 g, yeast extract 5 g, NaCl 0.5 g, 20 mM glucose, ddH$_2$O to 1 litre

2.1.3. Oligonucleotide Primers

Shown in Table 2.2 are the oligonucleotide primers used within this study across experimental work.

Table 2.2. List of oligonucleotide primers used within this study.

Oligonucleotide	Sequence	Target	Purpose
DC3000-1-HrcN-FWD	CCGCTCGAGCCAGGAATGCACGCTGC	*hrcN*	Site directed mutagenesis
DC3000-1-HrcN-REV	GCGGATCCCAGCGGTTCGCCCGATG	*hrcN*	Site directed mutagenesis

DC3000-2-HrcN-FWD	CCGCTCGAGACGTCATCGTCTTCGGG	*hrcN*	Site directed mutagenesis
DC3000-2-HrcN-REV	GGTACTCGAGCGTTCAGTTGCACCG	*hrcN*	Site directed mutagenesis
P142Q-FWD-DC3000-HrcN	CCTTGCCGCAAACCCAGCGGG	*hrcN*	Site directed mutagenesis
P142Q-REV-DC3000-HrcN	GCCGCTGGGTTTGCGGCAAGG	*hrcN*	Site directed mutagenesis
Q169P-FWD-DC3000-HrcN	GTGAAGGCCCGCGGGTCGG	*hrcN*	Site directed mutagenesis
Q169P-REV-DC3000-HrcN	CCGACCCGCGGGCCTTCAC	*hrcN*	Site directed mutagenesis
R170Q-FWD-DC3000-HrcN	TGAAGGCCAGCAGGTCGGGCTG	*hrcN*	Site directed mutagenesis
R170Q-REV-DC3000-HrcN	CAGCCCGACCTGCTGGCCTTCA	*hrcN*	Site directed mutagenesis
E208D-FWD-DC3000-HrcN	GGCCGCGACCTGCGCGA	*hrcN*	Site directed mutagenesis
E208D-REV-DC3000-HrcN	CGCGCAGGTCGCGGCCC	*hrcN*	Site directed mutagenesis
G306A-FWDDC3000-HrcN	AACGTGCCGCGATGAGCGA	*hrcN*	Site directed mutagenesis
G306A-REV-DC3000-HrcN	TCGCTCATCGCGGCACGTT	*hrcN*	Site directed mutagenesis
G311A-FWD-DC3000-HrcN	TGAGCGAAAACGCTTCGATCACCG	*hrcN*	Site directed mutagenesis
G311A-REV-DC3000-HrcN	CGGTGATCGAAGCGTTTTCGCTCA	*hrcN*	Site directed mutagenesis
R335P-FWD-DC3000-HrcN	ATGAAGTACGCTCTTTGCTCGACGGC	*hrcN*	Site directed mutagenesis
R335P-FWD-DC3000-HrcN	GCCGTCGAGCAAAGAGCGTACTTCAT	*hrcN*	Site directed mutagenesis
L338V-FWD-DC3000-HrcN	GCTCGTTGGTCGACGGCCA	*hrcN*	Site directed mutagenesis
L338V-REV-DC3000-HrcN	TGGCCGTCGACCAACGAGC	*hrcN*	Site directed mutagenesis
OE_DC3000_FWD	CAGAAGCCATATGGTGAACGCCGCACTGAAC	*hrcN*	Site directed mutagenesis
OE_DC3000_REV	GGTACTCGAGTTACTCCGGCAGTTGCGA	*hrcN*	Site directed mutagenesis
R346H FWD (HrcN)	CGCTGCAGACCACGCTGATGG	*hrcN*	Site directed mutagenesis
R346H REV (HrcN)	CGCATATGCCTGGTCCAGTGACG	*hrcN*	Site directed mutagenesis
F174H FWD (HrcN)	CGCTGCAGGACACCCACG	*hrcN*	Site directed mutagenesis
F174H REV (HrcN)	CGCATATGGAGCAACGAGCGTACT	*hrcN*	Site directed mutagenesis
FWD P142G HrcN 2019	CTTGCCGGGAACCCAGCGG	*hrcN*	Site directed mutagenesis

REV P142G HrcN 2019	GCCGCTGGGTTCCCGGCAAGG	*hrcN*	Site directed mutagenesis
FWD Q169N HrcN 2019	GTGAAGGCAACCGGGTCGG	*hrcN*	Site directed mutagenesis
REV Q169N HrcN 2019	CCGACCCGGTTGCCTTCAC	*hrcN*	Site directed mutagenesis
FWD R170Q HrcN 2019	TGAAGGCCAGCAAGTCGGGCTG	*hrcN*	Site directed mutagenesis
REV R170Q HrcN 2019	CAGCCCGACTTGCTGGCCTTCA	*hrcN*	Site directed mutagenesis
FWD R335Q HrcN 2019	ATGAAGTACGCTGAATGCTCGACCGGC	*hrcN*	Site directed mutagenesis
REV R335Q HrcN 2019	CCGTCGAGCATTCAGCGTACTTCA	*hrcN*	Site directed mutagenesis
FWDExternalHrcN	CAGCAGGACCTGGCGCTG	External *hrcN* Region	Sequencing
REVExternalHrcN	TCGCGGCGGGCAAAGCC	External *hrcN* Region	Sequencing
FWD Cya 'P3' Reporter Plasmid Primer	TGAGCATGCTACCGAGTAACGCAGCT	Gateway cloning LR inserted Type III *Pto* DC3000 effector-encoding gene lacking stop codon + Cya fusion	Sequencing
REV Cya 'P4' Reporter Plasmid Primer	AGTGGTACCGATATCGAATTCTTAGCTGT	Gateway cloning LR inserted Type III *Pto* DC3000 effector-encoding gene lacking stop codon + Cya fusion	Sequencing
HrcNCompFWD	GTCAAGCTTGCGTTTCAAGGACC	*hrcN*	Other
HrcNCompREVPstl	GACACTAGTTTACTCCGGCAGTT	*hrcN*	Other
HrcNCompExtFWD	TCTCAAGGAAGAGTCGCTGGT	*hrcN*	Sequencing
HrcNCompExtREV	CTCATGCCATCGGTCGACAT	*hrcN*	Sequencing
HrcCCompFWD	GCTAAGCTTCCATCGATCCGCAG	*HrcC*	Other

HrcCCompREV	ATCGGATCCTCATGGTTTCGCTC	*HrcC*	Other
HrcCCompExtFWD	GGCTGGCGGTCGTCG	*HrcC*	Sequencing
HrcCCompExtREV	AACTGCACGACAGTGTAATC	*HrcC*	Sequencing
pTN7R (Schweizer 2006)	CACAGCATAACTGGACTGATTTC	*Tn7T* inserted at *glmS* site	Genetic Complementation
pGlmS-Down (Schweizer 2006)	GCACATCGGCGACGTGCTCTC	*Tn7T* inserted at *glmS* site	Genetic Complementation
OvExp HopAM1 FWD	GAAGCGGTACCATGCACGCAAATCCT	*hopAM1*	Expression
OvExp HopAM1 REV	TGGTACTCGAGTTAGTCGCCTAGGAA	*hopAM1*	Expression
Del HopAM1 OutFWD	CGCATATGGGTATCGATGATGCC	*hopAM1*	Gene deletion
Del HopAM1 InnREV	CGTCTAGAAGGATTTGCGTGCAT	*hopAM1*	Gene deletion
Del HopAM1 InnFWD	CGCTCTAGATTCCTAGGCGACTAA	*hopAM1*	Gene deletion
Del HopAM1 OutREV	CGGGATCCGTCGCTAATGGAGCT	*hopAM1*	Gene deletion
EXTFWDHopAM1	GCGAAATCTGCATAGGCAA	*hopAM1*	Sequencing
EXTREVHopAM1	AGGAGCCCTATACGTGG	*hopAM1*	Sequencing
OvExp HopAA12 FWD	GAAGCGGTACCATGCACATCAACCAA	*hopAA1-2*	Expression
OvExp HopAA12 REV	TGGTACTCGAGTTACAAACGCCTGAG	*hopAA1-2*	Expression
Del HopAA12 OutFWD	CTCATATGACCCACGCTTTTGCG	*hopAA1-2*	Gene deletion
Del HopAA12 InnREV	CGCTCTAGAGGAAATTCTATCTCG	*hopAA1-2*	Gene deletion
Del HopAA12 InnFWD	CGTCTAGAGCGGCCTGTGGGTTG	*hopAA1-2*	Gene deletion
Del HopAA12 OutREV	CGGGATCCTGTGGTGTGGTGTCG	*hopAA1-2*	Gene deletion
EXTFWDHopAA12	GGGAGGACCTGCTGATGC	*hopAA1-2*	Sequencing
EXTREVHopAA12	AAGGCAATCGTGACCATT	*hopAA1-2*	Sequencing
OvExp HopAF1 FWD	GAAGCGGTACCATGGGGCTATGTATT	*hopAF1*	Expression
OvExp HopAF1 REV	TGGTACTCGAGTTATTGTGCGACCAG	*hopAF1*	Expression
Del HopAF1 OutFWD	CTCATATGTGCAGTATGTAGGCT	*hopAF1*	Gene deletion
Del HopAF1 InnREV	CGCTCTAGAAATACATAGCCCCAT	*hopAF1*	Gene deletion
Del HopAF1 InnFWD	CGCTCTAGACTGGTCGCACAATAA	*hopAF1*	Gene deletion

Del HopAF1 OutREV	ATGGATCCGCGCTGAAAACGCAA	*hopAF1*	Gene deletion
EXTFWDHopAF1	TTTGAAATCAGCCCACCTT	*hopAF1*	Sequencing
EXTREVHopAF1	CAACACTCATGAAAGCGA	*hopAF1*	Sequencing
OvExp HopQ1 FWD	GAAGCGGTACCATGCATCGTCCTATC	*hopQ1-1*	Expression
OvExp HopQ1 REV	TGGTACTCGAGTCAATCTGGGGCTAC	*hopQ1-1*	Expression
Del HopQ1 OutFWD	CTCATATGATCAGCGCAATTTTC	*hopQ1-1*	Gene deletion
Del HopQ1 InnREV	CGTCTAGAGATAGGACGATGCAT	*hopQ1-1*	Gene deletion
Del HopQ1 InnFWD	CGCTCTAGAGTAGCCCCAGATTGA	*hopQ1-1*	Gene deletion
Del HopQ1 OutREV	GCGGATCCTATTTTCCGGAGCGC	*hopQ1-1*	Gene deletion
EXTFWDHopQ1	CTGCGCTCGATCAAAATG	*hopQ1-1*	Sequencing
EXTREVHopQ1	GTCCATGAGCGATCTACT	*hopQ1-1*	Sequencing
AF1DelOutFWD V2 PstI`	CGCTGCAGTGCAGTATGTAGGCT	*hopAF1*	Gene deletion
Q1DelOutFWD V2 PstI	CGCTGCAGATCAGCGCAATTTTC	*hopQ1-1*	Gene deletion
HopH1 OvExp FWD KpnI	GAAGCGGTACCATGATCACTCCGTCT	*hopH1*	Expression
HopH1 OvExp REV XhoI	TGGTACTCGAGCTATTGATGTGCCCT	*hopH1*	Expression
HopH1 del OutFWD NdeI	CTCATATGTTTGCGCATCTGCGC	*hopH1*	Gene deletion
HopH1 del InnREV XbaI	CGTCTAGAAGACGGAGTGATCAT	*hopH1*	Gene deletion
HopH1 del InnFWD XbaI	CGCTCTAGAAGGGCACATCAATAG	*hopH1*	Gene deletion
HopH1 del OutREV BamHI	CTGGATCCACCAAGCTGGCG	*hopH1*	Gene deletion
EXT HopH1 FWD	GCGCTAAGCTCCTTATGT	*hopH1*	Sequencing

2.1.4.   Plasmids

The plasmids used in this study are described in Table 2.3.

Table 2.3. List of plasmids used in this study

Plasmid	Basic Vector	Insert	Insert Genotype	Promoter	Purpose	Source/Reference	Resistance	Tag	Other Plasmid Features
pTS-1	pTS-1	-	-	-	Chromosomal Integration	(Campilongo et al., 2017)	Tetracycline	-	*sacB*
pTS-1- WT *hrcN*	pTS-1	*hrcN*	WT	-	Chromosomal Integration	Malone Lab, John Innes Centre (Trampari et al., 2015)	Tetracycline	-	*sacB*
pTS-1- G176A *hrcN*	pTS-1	*hrcN*	G176A	-	Chromosomal Integration	Malone Lab, John Innes Centre	Tetracycline	-	*sacB*
pTS-1- E208D *hrcN*	pTS-1	*hrcN*	E208D	-	Chromosomal Integration	This study	Tetracycline	-	*sacB*
pTS-1- R170Q *hrcN*	pTS-1	*hrcN*	R170Q	-	Chromosomal Integration	This study	Tetracycline	-	*sacB*

pTS-1-G311A-hrcN	pTS-1	hrcN	G311A	-	Chromosomal Integration	This study	Tetracycline	-	sacB
pTS-1-L338V-hrcN	pTS-1	hrcN	L338V	-	Chromosomal Integration	This study	Tetracycline	-	sacB
pTS-1-F174Y-hrcN	pTS-1	hrcN	F174Y	-	Chromosomal Integration	This study	Tetracycline	-	sacB
pTS-1-R356H-hrcN	pTS-1	hrcN	R356H	-	Chromosomal Integration	This study	Tetracycline	-	sacB
pTS-1-P142G-hrcN	pTS-1	hrcN	P142G	-	Chromosomal Integration	This study	Tetracycline	-	sacB
pTS1-1-WT pscN	pTS-1	pscN	WT	-	Chromosomal Integration	This study	Tetracycline	-	sacB
pTS1-1-P137Q pscN	pTS-1	pscN	P137Q	-	Chromosomal Integration	This study	Tetracycline	-	sacB
pTS1-1-Q164P pscN	pTS-1	pscN	Q164P	-	Chromosomal Integration	This study	Tetracycline	-	sacB
pTS1-1-E203D pscN	pTS-1	pscN	E203D	-	Chromosomal Integration	This study	Tetracycline	-	sacB
pTS1-1-G301D pscN	pTS-1	pscN	G301D	-	Chromosomal Integration	This study	Tetracycline	-	sacB
pTS1-1-G306D pscN	pTS-1	pscN	G306D	-	Chromosomal Integration	This study	Tetracycline	-	sacB
pTS1-1-R335Q pscN	pTS-1	pscN	R335Q	-	Chromosomal Integration	This study	Tetracycline	-	sacB
pTS-1-ΔhrcC	pTS-1	ΔhrcC	-	-	Gene Deletion	Malone Lab, John Innes Centre	Tetracycline	-	sacB
pTS-1-ΔhrcN	pTS-1	ΔhrcN	-	-	Gene Deletion	This study	Tetracycline	-	sacB
pTS-1-ΔhopAA1-2	pTS-1	ΔhopAA1-2	WT	-	Gene Deletion	This study	Tetracycline	-	sacB
pTS-1-ΔhopAM1	pTS-1	ΔhopAM1	WT	-	Gene Deletion	This study	Tetracycline	-	sacB
pTS-1-ΔhopAF1	pTS-1	ΔhopAF1	WT	-	Gene Deletion	This study	Tetracycline	-	sacB
pETM11	pETM11	-	-	lacI	Over-expression	(Dümmler et al., 2005)	Kanamycin	N-terminal His6-tag	-
pETM11-WT hrcN	pETM11	hrcN	WT	lacI	Over-expression	This study	Kanamycin	N-terminal His6-tag	-
pETM11-P142Q hrcN	pETM11	hrcN	P142Q	lacI	Over-expression	This study	Kanamycin	N-terminal His6-tag	-
pETM11-G176A hrcN	pETM11	hrcN	G176A	lacI	Over-expression	This study	Kanamycin	N-terminal His6-tag	-
pETM11-E208D hrcN	pETM11	hrcN	E208D	lacI	Over-expression	This study	Kanamycin	N-terminal His6-tag	-
pETM11-G311A-hrcN	pETM11	hrcN	G311A	lacI	Over-expression	This study	Kanamycin	N-terminal His6-tag	-
pETM11-R335P-hrcN	pETM11	hrcN	R335P	lacI	Over-expression	This study	Kanamycin	N-terminal His6-tag	-
pETM11-L338V-hrcN	pETM11	hrcN	L338V	lacI	Over-expression	This study	Kanamycin	N-terminal His6-tag	-
pETM11-L338V-hrcN	pETM11	pscN	WT	lacI	Over-expression	This study	Kanamycin	N-terminal His6-tag	-
pETM11-P137Q-pscN	pETM11	pscN	P137Q	lacI	Over-expression	This study	Kanamycin	N-terminal His6-tag	-
pETM11-E208D-pscN	pETM11	pscN	E203D	lacI	Over-expression	This study	Kanamycin	N-terminal His6-tag	-
pETM11-G301D-pscN	pETM11	pscN	G301D	lacI	Over-expression	This study	Kanamycin	N-terminal His6-tag	-
pETM11-G306D-pscN	pETM11	pscN	G306D	lacI	Over-expression	This study	Kanamycin	N-terminal His6-tag	-
pETM11-R335Q-pscN	pETM11	pscN	R335Q	lacI	Over-expression	This study	Kanamycin	N-terminal His6-tag	-
pETM11-WT hrcN (Δ1-18)	pETM11	hrcN	Δ1-18 (N-terminal truncation)	lacI	Over-expression	This study	Kanamycin	N-terminal His6-tag	-

pETM11-G176A hrcN (Δ1-18)	pETM11	hrcN	G176A Δ1-18 (N-terminal truncation)	lacI	Over-expression	This study	Kanamycin	N-terminal His6-tag	-
pETM11-E208D hrcN (Δ1-18)	pETM11	hrcN	E208D Δ1-18 (N-terminal truncation)	lacI	Over-expression	This study	Kanamycin	N-terminal His6-tag	-
pETM11-G311A hrcN (Δ1-18)	pETM11	hrcN	G311A Δ1-18 (N-terminal truncation)	lacI	Over-expression	This study	Kanamycin	N-terminal His6-tag	-
pETM11-L338V hrcN (Δ1-18)	pETM11	hrcN	L338V Δ1-18 (N-terminal truncation)	lacI	Over-expression	This study	Kanamycin	N-terminal His6-tag	-
pETM11-F174Y hrcN (Δ1-18)	pETM11	hrcN	F174Y Δ1-18 (N-terminal truncation)	lacI	Over-expression	This study	Kanamycin	N-terminal His6-tag	-
pETM11-P142G hrcN (Δ1-18)	pETM11	hrcN	P142G Δ1-18 (N-terminal truncation)	lacI	Over-expression	This study	Kanamycin	N-terminal His6-tag	-
pBBR4	pBBR4	-	-	tac	Over-expression	(Malone et al., 2010)	Carbenicillin	-	-
pBBR4-wspR19	pBBR4	wspR19	WT	tac	Diguanylate cyclase expression	This study	Carbenicillin	-	-
pBBR4-bifA	pBBR4	BifA	WT	tac	Phosphodiesterase expression	This study	Carbenicillin	-	-
pCPP5371 (Empty CyaA backbone)	pCPP5371	-	-	hrp (avrPto)	CyaA:T3SS effector protein fusions	(Oh et al., 2007)	Gentamicin, Chloramphenicol	C-terminal CyaA tag	ccdB
pENTR-SD/D-TOPO	pENTR-SD/D-TOPO	-	-	T7	Gateway Cloning	(Schechter et al., 2004)	Kanamycin	-	ccdB
pENTR-SD/D-TOPO-shcE-avrE1	pENTR-SD/D-TOPO	shcE-avrE1	Lacking stop codon	T7	Gateway cloning of T3SS effector-encoding genes lacking stop codons	(Kvitko et al., 2009)	Kanamycin	-	ccdB
pENTR-SD/D-TOPO-hopB1	pENTR-SD/D-TOPO	hopB1	Lacking stop codon	T7	Gateway cloning of T3SS effector-encoding genes lacking stop codons	(Munkvold et al., 2009)	Kanamycin	-	ccdB
pENTR-SD/D-TOPO -hopE1	pENTR-SD/D-TOPO	hopE1	Lacking stop codon	T7	Gateway cloning of T3SS effector-encoding genes lacking stop codons	(Munkvold et al., 2009)	Kanamycin	-	ccdB
pENTR-SD/D-TOPO-shcF-hopF2	pENTR-SD/D-TOPO	shcF-hopF2	Lacking stop codon	T7	Gateway cloning of T3SS effector-encoding genes lacking stop codons	(Wei et al., 2018)	Kanamycin	-	ccdB
pENTR-SD/D-TOPO-hopG1	pENTR-SD/D-TOPO	hopG1	Lacking stop codon	T7	Gateway cloning of T3SS effector-encoding genes lacking stop codons	(Munkvold et al., 2009)	Kanamycin	-	ccdB
pENTR-SD/D-TOPO-hopH1	pENTR-SD/D-TOPO	hopH1	Lacking stop codon	T7	Gateway cloning of T3SS effector-encoding genes lacking stop codons	(Munkvold et al., 2009)	Kanamycin	-	ccdB
pENTR-SD/D-TOPO-hopI1	pENTR-SD/D-TOPO	hopI1	Lacking stop codon	T7	Gateway cloning of T3SS effector-encoding genes lacking stop codons	(Munkvold et al., 2009)	Kanamycin	-	ccdB
pENTR-SD/D-TOPO-hopK1	pENTR-SD/D-TOPO	hopK1	Lacking stop codon	T7	Gateway cloning of T3SS effector-encoding genes lacking stop codons	(Wei et al., 2018)	Kanamycin	-	ccdB
pENTR-SD/D-TOPO-shcO-hopO1-1	pENTR-SD/D-TOPO	shcO-hopO1-1	Lacking stop codon	T7	Gateway cloning of T3SS effector-encoding genes lacking stop codons	(Kvitko et al., 2009)	Kanamycin	-	ccdB
pENTR-SD/D-TOPO-hopQ1-1	pENTR-SD/D-TOPO	hopQ1-1	Lacking stop codon	T7	Gateway cloning of T3SS effector-encoding genes lacking stop codons	(Munkvold et al., 2009)	Kanamycin	-	ccdB
pENTR-SD/D-TOPO-hopR1	pENTR-SD/D-TOPO	hopR1	Lacking stop codon	T7	Gateway cloning of T3SS effector-encoding genes lacking stop codons	(Kvitko et al., 2009)	Kanamycin	-	ccdB
pENTR-SD/D-TOPO-hopT1-1	pENTR-SD/D-TOPO	hopT1-1	Lacking stop codon	T7	Gateway cloning of T3SS effector-encoding genes lacking stop codons	(Munkvold et al., 2009)	Kanamycin	-	ccdB
pENTR-SD/D-TOPO-hopU1	pENTR-SD/D-TOPO	hopU1	Lacking stop codon	T7	Gateway cloning of T3SS effector-encoding genes lacking stop codons	(Munkvold et al., 2009)	Kanamycin	-	ccdB
pENTR-SD/D-TOPO-	pENTR-SD/D-TOPO	hopX1	Lacking stop codon	T7	Gateway cloning of T3SS effector-	(Munkvold et al., 2009)	Kanamycin	-	ccdB

TOPO-*hopX1*					encoding genes lacking stop codons				
pENTR-SD/D-TOPO-*hopY1*	pENTR-SD/D-TOPO	*hopY1*	Lacking stop codon	T7	Gateway cloning of T3SS effector-encoding genes lacking stop codons	(Munkvold et al., 2009)	Kanamycin	-	*ccdB*
pENTR-SD/D-TOPO-*hopAA1-1*	pENTR-SD/D-TOPO	*hopAA1-1*	Lacking stop codon	T7	Gateway cloning of T3SS effector-encoding genes lacking stop codons	(Munkvold et al., 2009)	Kanamycin	-	*ccdB*
pENTR-SD/D-TOPO-*hopAA1-2*	pENTR-SD/D-TOPO	*hopAA1-2*	Lacking stop codon	T7	Gateway cloning of T3SS effector-encoding genes lacking stop codons	(Munkvold et al., 2009)	Kanamycin	-	*ccdB*
pENTR-SD/D-TOPO-*hopAF1*	pENTR-SD/D-TOPO	*hopAF1*	Lacking stop codon	T7	Gateway cloning of T3SS effector-encoding genes lacking stop codons	(Munkvold et al., 2009)	Kanamycin	-	*ccdB*
pENTR-SD/D-TOPO-*hopAM1*	pENTR-SD/D-TOPO	*hopAM1*	Lacking stop codon	T7	Gateway cloning of T3SS effector-encoding genes lacking stop codons	(Munkvold et al., 2009)	Kanamycin	-	*ccdB*
pENTR-SD/D-TOPO-*hopA1*	pENTR-SD/D-TOPO	*hopA1*	Lacking stop codon	T7	Gateway cloning of T3SS effector-encoding genes lacking stop codons	(Kvitko et al., 2009)	Kanamycin	-	*ccdB*
pENTR-SD/D-TOPO-*schM-hopM1*	pENTR-SD/D-TOPO	*shcM-hopM1*	Lacking stop codon	T7	Gateway cloning of T3SS effector-encoding genes lacking stop codons	(Kvitko et al., 2009)	Kanamycin	-	*ccdB*
pENTR-SD/D-TOPO-*avrPto*	pENTR-SD/D-TOPO	*avrPto*	Lacking stop codon	T7	Gateway cloning of T3SS effector-encoding genes lacking stop codons	(Kvitko et al., 2009)	Kanamycin	-	*ccdB*
pENTR-SD/D-TOPO-*avrPtoB*	pENTR-SD/D-TOPO	*avrPtoB*	Lacking stop codon	T7	Gateway cloning of T3SS effector-encoding genes lacking stop codons	(Kvitko et al., 2009)	Kanamycin	-	*ccdB*
pDEST pCPP5371-*shcE-avrE1*-CyaA	pDEST pCPP5371	*shcE-avrE1*	Lacking stop codon	*hrp* (*avrPto*)	*In planta* cAMP analyses of effector-CyaA T3SS translocation	This study	Gentamycin	C-terminal CyaA tag	-
pDEST pCPP5371-*hopB1*-CyaA	pDEST pCPP5371	*hopB1*	Lacking stop codon	*hrp* (*avrPto*)	*In planta* cAMP analyses of effector-CyaA T3SS translocation	This study	Gentamycin	C-terminal CyaA tag	-
pDEST pCPP5371-*hopE1*-CyaA	pDEST pCPP5371	*hopE1*	Lacking stop codon	*hrp* (*avrPto*)	*In planta* cAMP analyses of effector-CyaA T3SS translocation	This study	Gentamycin	C-terminal CyaA tag	-
pDEST pCPP5371-*shcF-hopF2*-CyaA	pDEST pCPP5371	*shcF-hopF2*	Lacking stop codon	*hrp* (*avrPto*)	*In planta* cAMP analyses of effector-CyaA T3SS translocation	This study	Gentamycin	C-terminal CyaA tag	-
pDEST pCPP5371-*hopG1*-CyaA	pDEST pCPP5371	*hopG1*	Lacking stop codon	*hrp* (*avrPto*)	*In planta* cAMP analyses of effector-CyaA T3SS translocation	This study	Gentamycin	C-terminal CyaA tag	-
pDEST pCPP5371-*hopH1*-CyaA	pDEST pCPP5371	*hopH1*	Lacking stop codon	*hrp* (*avrPto*)	*In planta* cAMP analyses of effector-CyaA T3SS translocation	This study	Gentamycin	C-terminal CyaA tag	-
pDEST pCPP5371-*hopI1*-CyaA	pDEST pCPP5371	*hopI1*	Lacking stop codon	*hrp* (*avrPto*)	*In planta* cAMP analyses of effector-CyaA T3SS translocation	This study	Gentamycin	C-terminal CyaA tag	-
pDEST pCPP5371-*hopK1*-CyaA	pDEST pCPP5371	*hopK1*	Lacking stop codon	*hrp* (*avrPto*)	*In planta* cAMP analyses of effector-CyaA T3SS translocation	This study	Gentamycin	C-terminal CyaA tag	-
pDEST pCPP5371-*shcO-hopO1-1*-CyaA	pDEST pCPP5371	*shcO-hopO1-1*	Lacking stop codon	*hrp* (*avrPto*)	*In planta* cAMP analyses of effector-CyaA T3SS translocation	This study	Gentamycin	C-terminal CyaA tag	-
pDEST pCPP5371-*hopQ1-1*-CyaA	pDEST pCPP5371	*hopQ1-1*	Lacking stop codon	*hrp* (*avrPto*)	*In planta* cAMP analyses of effector-CyaA T3SS translocation	This study	Gentamycin	C-terminal CyaA tag	-
pDEST pCPP5371-*hopR1*-CyaA	pDEST pCPP5371	*hopR1*	Lacking stop codon	*hrp* (*avrPto*)	*In planta* cAMP analyses of effector-CyaA T3SS translocation	This study	Gentamycin	C-terminal CyaA tag	-
pDEST pCPP5371-*hopT1-1*-CyaA	pDEST pCPP5371	*hopT1-1*	Lacking stop codon	*hrp* (*avrPto*)	*In planta* cAMP analyses of effector-CyaA T3SS translocation	This study	Gentamycin	C-terminal CyaA tag	-
pDEST pCPP5371-	pDEST pCPP5371	*hopU1*	Lacking stop codon	*hrp* (*avrPto*)	*In planta* cAMP analyses of effector-	This study	Gentamycin	C-terminal	-

*hopU1-*CyaA					CyaA T3SS translocation			CyaA tag	
pDEST pCPP5371-*hopX1-*CyaA	pDEST pCPP5371	*hopX1*	Lacking stop codon	*hrp* (*avrPto*)	*In planta* cAMP analyses of effector-CyaA T3SS translocation	This study	Gentamycin	C-terminal CyaA tag	-
pDEST pCPP5371-*hopY1-*CyaA	pDEST pCPP5371	*hopY1*	Lacking stop codon	*hrp* (*avrPto*)	*In planta* cAMP analyses of effector-CyaA T3SS translocation	This study	Gentamycin	C-terminal CyaA tag	-
pDEST pCPP5371-*hopAA1-1-*CyaA	pDEST pCPP5371	*hopAA1-1*	Lacking stop codon	*hrp* (*avrPto*)	*In planta* cAMP analyses of effector-CyaA T3SS translocation	This study	Gentamycin	C-terminal CyaA tag	-
pDEST pCPP5371-*hopAA1-2-*CyaA	pDEST pCPP5371	*hopAA1-2*	Lacking stop codon	*hrp* (*avrPto*)	*In planta* cAMP analyses of effector-CyaA T3SS translocation	This study	Gentamycin	C-terminal CyaA tag	-
pDEST pCPP5371-*hopAF1-*CyaA	pDEST pCPP5371	*hopAF1*	Lacking stop codon	*hrp* (*avrPto*)	*In planta* cAMP analyses of effector-CyaA T3SS translocation	This study	Gentamycin	C-terminal CyaA tag	-
pDEST pCPP5371-*hopAM1-*CyaA	pDEST pCPP5371	*hopAM1*	Lacking stop codon	*hrp* (*avrPto*)	*In planta* cAMP analyses of effector-CyaA T3SS translocation	This study	Gentamycin	C-terminal CyaA tag	-
pDEST pCPP5371-*hopA1-*CyaA	pDEST pCPP5371	*hopA1*	Lacking stop codon	*hrp* (*avrPto*)	*In planta* cAMP analyses of effector-CyaA T3SS translocation	This study	Gentamycin	C-terminal CyaA tag	-
pDEST pCPP5371-*shcM-hopM1-*CyaA	pDEST pCPP5371	*shcM-hopM1*	Lacking stop codon	*hrp* (*avrPto*)	*In planta* cAMP analyses of effector-CyaA T3SS translocation	This study	Gentamycin	C-terminal CyaA tag	-
pDEST pCPP5371-*avrPto-*CyaA	pDEST pCPP5371	*avrPto*	Lacking stop codon	*hrp* (*avrPto*)	*In planta* cAMP analyses of effector-CyaA T3SS translocation	This study	Gentamycin	C-terminal CyaA tag	-
pDEST pCPP5371-*avrPtoB-*CyaA	pDEST pCPP5371	*avrPtoB*	Lacking stop codon	*hrp* (*avrPto*)	*In planta* cAMP analyses of effector-CyaA T3SS translocation	This study	Gentamycin	C-terminal CyaA tag	-
pUC18T-MiniTn7T	pUC18T-MiniTn7T	-	-	-	Genetic complementation	(Choi et al., 2005)	Gentamycin	-	-
pUC18T-MiniTn7T-WT *hrcN*	pUC18T-MiniTn7T	*hrcN*	WT	Native *hrcN* promoter region (200 bp upstream of gene)	Genetic complementation	This study	Gentamycin	-	-
pUC18T-MiniTn7T-WT *hrcC*	pUC18T-MiniTn7T	*hrcC*	WT	Native *hrcC* promoter region (200 bp upstream of gene)	Genetic complementation	This study	Gentamycin	-	-
pTNS2	pTNS2	*tnsABCD*	WT	T7	Helper plasmid for genetic complementation	(Choi et al., 2005)	Carbenicillin	-	-
pBBR2	pBBR2	-	-	*tac*	Stable over-expression in DC3000	(Pfeilmeier et al., 2016)	Kanamycin	-	-
pBBR2-HopAA1-2	pBBR2	*hopAA1-2*	WT	*tac*	Stable over-expression in DC3000	This study	Kanamycin	-	-
pBBR2-HopAM1	pBBR2	*hopAM1*	WT	*tac*	Stable over-expression in DC3000	This study	Kanamycin	-	-
pBBR2-HopAF1	pBBR2	*hopAF1*	WT	*tac*	Stable over-expression in DC3000	This study	Kanamycin	-	-

2.1.5.   Kits

Described in Table 2.4 are the various experimental kits used in this study.

Table 2.4. List of experimental kits used within this study

Kit	Supplier	Use
Macherey-Nagel Nucleospin Extract 740609.50	Fisher Scientific	Gel extraction and PCR purification
Macherey-Nagel Nucleospin Plasmid 740588.50	Fisher Scientific	Plasmid purification

| Direct cAMP ELISA kit | Enzo Life Sciences | cAMP-based ELISAs for CyaA reporter assays |

2.1.6.   Antibodies

Various antibodies were used in experimental work throughout this study. These antibodies are described in Table 2.5.

Table 2.5. List of antibodies used in this study

Antibody	Source	Type	Production Organism
Anti-HrcN	Minotech Biotechnology	Polyclonal IgG	Rabbit
Anti-HrcC	Minotech Biotechnology	Polyclonal IgG	Rabbit
Anti-HrpA	Minotech Biotechnology	Polyclonal IgG	Rabbit
Anti-Adenylate Cyclase Toxin Antibody, B. pertussis Antibody, clone 3D1	Merck Millipore	Monoclonal IgG1	Mouse
Anti-rabbit HRP-conjugate	Sigma-Aldrich	Polyclonal IgG	Goat
Anti-mouse HRP-conjugate	Merck Millipore	Polyclonal IgG	Goat

2.1.7.   Organisms

Various strains and species of living organisms were used in this study. An overview of parental bacterial strains used in this study are described in Table 2.6. An expanded table showing all bacterial strains used can be found in the appendix section in Table 8.1.

Table 2.6. An overview of parental bacterial strains used in this study

Name	Organism	Genotype	Purpose	Source/Refence
DH5α	*Escherichia coli*	F- Φ80lacZΔM15 Δ(lacZYA-argF) U169 recA1 endA1 hsdR17(rk-, mk+) phoA supE44 thi-1 gyrA96 relA1 λ-	Molecular cloning	Invitrogen/ThermoFisher
DB3.1	*Escherichia coli*	F- gyrA462 endA1 Δ(sr1-recA) mcrB mrr hsdS20(r_B-, m_B-) supE44ara-14 galK2 lacY1 proA2 rpsL20(Sm^R) xyl-5 λ- leu mtl1	Plasmid purification	(Oh et al., 2007)
BL21 (DE3) pLysS	*Escherichia coli*	F-ompT hsdSB(r_B- m_B-) gal dcm (DE3) pLysS (Cam^R)	Over-expression	Malone Lab, John Innes Centre
Pto DC3000	*Pseudomonas syringae*	WT *hrcN*	*In vivo* analyses	Malone Lab, John Innes Centre

The plant-lines used in this study are described in Table 2.7.

Table 2.7. List of plants used in this study

Name	Organism	Parental Plant-line	Genotype	Purpose	Features	Source/Reference
Col-0	*Arabidopsis thaliana*	Col-0	Col-0	*In planta experiments*	-	John Innes Centre

fec	*Arabidopsis thaliana*	Col-0	fec	*In planta experiments*	Lacking fls2, efr and cerk1 immune pathways	(Yuan et al., 2021)
bbc	*Arabidopsis thaliana*	Col-0	bbc	*In planta experiments*	Lacking bak1-5, bkk-1 and cerk1 immune pathways	(Yuan et al., 2021)
Money maker	*Solanum lycopersicum*	Moneymaker	Moneymaker	*In planta experiments*	-	John Innes Centre

2.2. Methods

2.2.1. *Pseudomonas* Genome Purification

The required *Pseudomonas* stocks were streaked out from glycerol stock on to the appropriate agar (L-agar (1.5 % agar) for *P. syringae*) and left to incubate overnight at 28 °C. A single colony from the overnight plates were then used to inoculate 10 mL of suitable liquid media (L-media for *P. syringae*) which was incubated overnight at 28 °C at 220 rpm.

2 mL of the overnight culture underwent centrifugation at 13.2 rpm for 2 minutes and the supernatant was subsequently removed. 600 µL of 3 M guanidinium thiocyanate 10 mM EDTA (pH 7.0) was then used to re-suspend the pellet. After an 85 °C incubation for 5 minutes, 1 mg of RNase solution (1 µL of RNAase with 60 µL of 10 x Buffer (Promega)) was added. After tube inversion, the samples were heated for 15 minutes at 37 °C. 200 µL of 10 M ammonium acetate (pH 7) was added and gently mixed. The samples underwent centrifugation for 3 minutes at 13.2 rpm. 600 µL of supernatant was removed and the pellet was mixed with 600 µL of isopropanol. The tubes were gently mixed by repeat inversion before undergoing centrifugation at 13.2 rpm for 1 minute. The supernatant was removed and approximately 400 µL of 70 % ethanol was added to cover the pellet. After tube inversion to wash the pellet, the supernatant was removed. This ethanol step was repeated and left to air dry until the ethanol had evaporated. The dry pellet was re-suspended in 300 µL of 10 mM tris (pH 8.0) with gentle agitation. The re-suspension was left to incubate at 65 °C for 5 hours and then aliquoted in to 30 µL volumes and stored at -20 °C.

2.2.2. Overlap Extension Mutagenesis Polymerase-chain Reaction

To sterile PCR tubes 10 µL of 10 x Phusion Buffer (New England Biolabs), 5 µL of DNTPs (2mM), 0.25 µL purified DC3000 genome template DNA or PCR product template, 1-2 µL of a forward primer (10 pmol), 1-2 µL of a reverse primer (10 pmol) and 0.5 µL of Phusion polymerase® were added in the described order to sterile Millipore water (variable volume) to reach a total of 50 µL. The following conditions were used as shown in Table 2.8. PCR product success was determined by agarose gel electrophoresis (3 µL of PCR product + 0.6 µL loading dye).

PCR reactions were conducted in two rounds (denoted as PCR 1 and PCR 2). For PCR 1, in one reaction, a forward primer with a reverse primer (containing a sequence leading to a desired residue mutation)

gave the first section of the *hrcN* gene (approximately 350-750 bp for chromosomal integration, 300-1000 bp for over-expression). In a separate PCR 1 reaction, a reverse primer with a forward primer (containing a sequence leading to a desired residue mutation) gave the second section of the *hrcN* gene (approximately 350-750 bp for chromosomal integration, 300-1000 bp for over-expression). PCR 2, then utilised both reactions from PCR 1 to join the two fragments together. This has been visualised in Figure 2.1.

Table 2.8. PCR conditions used for overlap-extension mutagenesis.

Step	Temperature (°C)	Time (s)	Cycles
Denaturation	98	300	1
Denaturation	98	10	35
Extension	72	30 (per Kb)	
Extension	72	420	1
Hold	4	∞	1
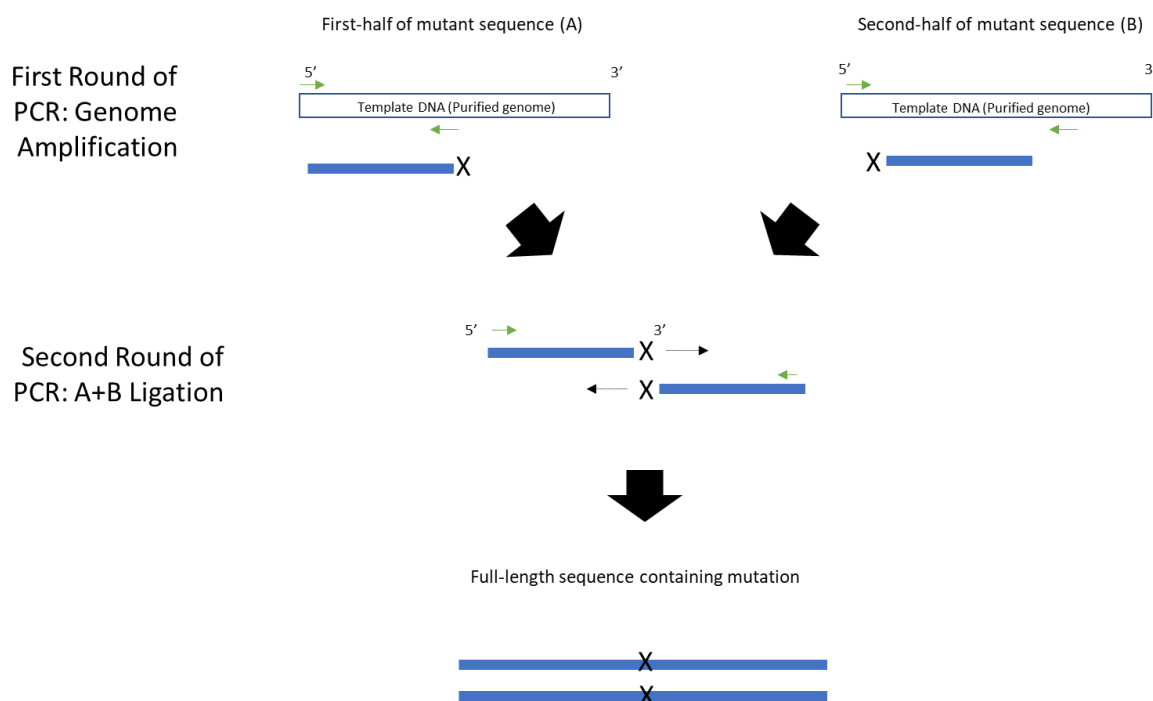
Figure 2.1. Overlap extension mutagenesis polymerase-chain reaction. Primers are represented with green arrows while the PCR products are depicted in blue. "X" indicates the presence of the desired mutation. Thin black arrows show the direction of extension.

2.2.3.   Restriction Digest

30-50 µL of plasmid DNA, 6 µL of CutSmart® buffer (New England Biolabs), 2 µL (40 U) of enzyme 1 (New England Biolabs), 2 µL (40 U) of enzyme 2 (New England Biolabs), and sterile water were added to sterile PCR tubes (to a total reaction volume of 60 µL). This double-digestion utilised New England Biolabs High-Fidelity (HF) enzymes. The tubes were incubated for 2 hours at 37 °C. Following this, the digested samples were cleaned-up with a NucleoSpin® Gel and PCR Clean-up kit – 740609.50 (Macherey-Nagel) to remove the restriction enzymes so that the samples were suitable for future ligation reactions.

2.2.4.   T4 Ligation

5 µL of appropriately restricted and purified plasmid, 8 µL of appropriately restricted genetic insert, 3 µL of 10 x T4 ligase buffer (New England Biolabs), 1 µL of T4 ligase (New England Biolabs) and sterile water (up to a total volume of 30 µL) were added to a sterile PCR tube. The tube was incubated overnight at 16 °C.

2.2.5.   Agarose Gel Electrophoresis

A 1 % agarose gel was prepared which consisted of 70 mL TBE (1 x) and 0.7 g agarose dissolved by microwave heating for approximately 2 minutes (volumes were scaled up or down appropriately depending on gel size required). After cooling slightly, 10 µL of ethidium bromide was added and mixed gently. This was then poured into a gel mould with a well comb and left to set for 30-60 minutes.

The set gel was then transferred to an agarose gel electrophoresis tank after removing from the mould, the well comb was removed, and the tank was filled with 1 x TBE covering the gel surface by approximately 1 mm. Samples were loaded in to wells at a 5:1 ratio of sample to loading dye (3 µL sample with 0.6 µL loading dye). The gel was run at 120 v for 25 – 40 minutes. The DNA within the gel was then visualised using UV light.

2.2.6.   Gel Extraction

Samples were run on a gel using the gel electrophoresis protocol however wells were loaded fully (~ 25 µL) and run. Following this, the gel was placed on a UV transilluminator, and the desired bands were physically extracted using a razor blade ensuring UV exposure was kept to a minimum and stored in micro-centrifuge tubes where the weight of the gel slice was determined. Following this, the excised bands were purified using a NucleoSpin® Gel and PCR Clean-up kit – 740609.50 (Macherey-Nagel) following the gel extraction protocol.

2.2.7.   DH5α Chemically Competent *E. coli* Transformation with DNA by Heat-shock

70 µL DH5α chemically competent *E. coli* (Life Technologies Ltd/Invitrogen) were thawed on ice in a sterile micro-centrifuge tube. To the cells, 10 µL of plasmid were added and flicked gently to mix. The tube was incubated on ice for 15 minutes. The tube then was incubated for 45 seconds in a 37 °C water bath and was immediately incubated for 2 minutes on ice following this. 1 mL of SOC media was then added to the tube and the cells were allowed to recover at 37 °C with agitation (220 rpm). 20 µL was removed from the tube following this. A cell pellet was formed (3 minutes, 13 000 rpm) and the supernatant was discarded. The cell pellet was then re-suspended with the previously removed 20 µL to make a concentrated sample. This re-suspension was then plated on to LB with a suitable antibiotic for plasmid selection. The plates were incubated overnight at 37 °C.

2.2.8.   BigDye™ Sequencing Reaction

For DNA sequencing, 5.5 µL H20, 1 µL of Big Dye v3.1 5x sequencing buffer (Thermo Fisher), 1 µL of appropriate sequencing primer (at a minimum of 3.2 pmol/µl), 1 µL of Big Dye v3.1 and 2.5 µL of prepared plasmid were combined into a PCR tube. The sequencing reaction as shown in Table 2.9 was then followed.

Table 2.9. Big Dye v3.1 Sequencing Reaction

Step	Temperature (°C)	Time (s)	Cycles
Initial denaturation	96	60	1
Denaturation	96	10	25
Annealing	50	5	
Extension	60	240	
Final Step	4	600	1
Hold	10	∞	1

2.2.9. Plant Growth

Arabidopsis thaliana and *Solanum lycopersium* plants were grown in controlled environment horticultural facilities under fixed conditions.

Arabidopisis thaliana growth conditions were:

- Short day 10-hour lighting conditions [120-180 µmol m^{-2} s^{-2} light intensity]
- 70 percent relative humidity
- 22°C growth temperature
- 4-5 week old saplings + 1 week 4°C seed vernalisation
- Grown in mixed *Arabidopsis* peat (Levington F2 600 ITS Peat, 100 ITS 4mm grit, 196g Exemptor Chloronicotinyl Insecticide).
- Plants stored in containment level 2 controlled environment rooms under appropriate licenses.

Tomato plant (*Solanum lycopersicum* - Moneymaker variety) growth conditions were:

- Short day 10-hour lighting conditions [120-180 µmol m^{-2} s^{-2} light intensity]
- 80 percent relative humidity
- 22°C growth temperature
- 4-5 week old saplings in mixed *Arabidopsis* peat (Levington F2 600 ITS Peat, 100 ITS 4mm grit, 196g Exemptor Chloronicotinyl Insecticide).
- Plants stored in containment level 2 controlled environment rooms under appropriate licenses.

2.2.10. Plant Infection Assay with *Pseudomonas Syringae Pto* DC3000

Wildtype *Pseudomonas syringae Pto* DC3000 was streaked out from glycerol stock on to l-agar and left to incubate for 3 days at 28 °C. Single colonies from these plates were then used to inoculate L-media (10 mL for leaf infiltration) with 50 µg/mL rifampicin. These were incubated overnight at 28 °C until an OD_{600} of 0.8-1.0 had been reached. Once grown, the bacteria were washed twice in 10 mM $MgCl_2$ (4000 x g, 10 minutes to pellet. Supernatant removed, resuspension in 50 mL 10 mM $MgCl_2$) and the final OD_{600} adjusted to 0.0002.

6-week-old (5-week growth, 1-week vernalisation) *Arabidopsis thaliana* (or *Solanum lycopersium*) then had a sufficient number of leaves marked for infection of multiple plant replicates. The plants were covered with a plastic dome to raise humidity and thus cause the stomata to open prior to infiltration for 1-2 hours. Using sterile flat-tipped syringes, the bacteria was applied to the underside of the targeted leaves to fully inoculate the leaf. Any excess liquid was wiped away.

Leaf disc samples were collected at 0, 2 and 3-days post-infection and a serial dilution series was prepared to evaluate bacteria growth. A cork-borer was used to collect 2 discs (radius of 0.384 cm) per plant for each time-point. Each set of 2 leaf discs were added to a 2 mL centrifuge tube containing 200 μL 10 mM $MgCL_2$ and 2 glass beads. The leaf discs were lysed using a tissue lysis machine (Qiagen Retsch) via a 45 second lysis cycle at 30 Hz. This was repeated for another 45 seconds after a 1-minute cool-down period. A 10^{-1} to 10^{-5} dilution series was prepared with the cell lysate which was then subsequently plated onto room-temperature L-media (with 50 μg/mL rifampicin and 25 μL/mL nystatin anti-fungal agent) square plates. This was carried out via multi-channel pipette spotting 20 μL of each dilution for each plant on to the plate. The plates were incubated overnight at 28 °C followed by 2 further days at 4 °C before colony counting.

2.2.11. PCR Purification

PCR products were purified using a NucleoSpin® Gel and PCR Clean-up kit – 740609.50 (Macherey-Nagel) following the PCR clean-up protocol.

2.2.12. Chromosomal Integration of pTS1-based Mutant Gene Constructs into *Pseudomonas* via Allelic Exchange

2.2.12.1. Transformation via Electroporation

Pseudomonas syringae Pto DC3000 was streaked onto L-agar from a glycerol stock and was incubated for 2 days at 28 °C. A single colony was then used to inoculate 50 mL of L medium which was incubated overnight at 28 °C, 220 rpm until an OD_{600} of 0.8-1.2 had been reached.

With the overnight culture, it was ensured that the OD_{600}. was 0.8, then 5 ml of culture underwent centrifugation at 4000 rpm for 8 minutes to form a pellet. The supernatant was removed and the pellet was resuspended in 2 mL 300 mM sucrose. This supernatant was divided equally in to two micro-centrifuge tubes and underwent centrifugation at 11 000 g for 2 minutes. The supernatant was removed and the sucrose wash was repeated 4 further times. The final cell pellets were resuspended in to 200 μL of 300 mM sucrose. 7 μL of DNA (approximately 300 ng) was added. The cells were then transformed via electroporation (2500 v, 2.5 milli-seconds) using an Eppendorf Eporator. 1 ml of L-medium was immediately added. After transferring to a 15 mL falcon tube, 2 mL of additional L-medium was added prior to a 4-5 hour shaking incubation at 28 °C. The samples underwent centrifugation (3000 g, 5 minutes) and subsequently, the supernatant was removed except for the final 100 μL which was used for resuspension. This was plated on to L-agar + tetracycline (12.5 μL/mL) which were incubated for two days at 28 °C to select for single-crossover candidates. Following growth, selected colonies were re-streaked on to new L-agar + tetracycline (12.5 μL/mL) plates to reduce wildtype background, which were then incubated overnight at 28 °C.

2.2.12.2. Double-crossover Screen via SacB-based Sucrose Selection

From the re-streaked transformation plates, 50 mL of Kings B medium was inoculated using well-separated single colonies, and incubated overnight at 28 °C, 200 rpm. To then begin selection for double-crossover mutants, tetracycline enrichment followed by sucrose selection was then followed.

From the overnight culture, 30 µL was added to 3 mL Kings B medium (1:100 dilution) which was then incubated for 4 hours, 28 °C, 200 rpm. At 4 hours. 3 µL of 5 mg/ml tetracycline was added and incubated for 2 further hours. At 6 hours total incubation, the samples underwent centrifugation at 4000 rpm for 8 minutes. Following this, the supernatant was removed, and the pellet resuspended in 5 mL Kings B medium with 5 µg/ml tetracycline, 2 mg/ml phosphomycin and 2 mg/ml piperacillin. The cultures were then incubated for 5 further hours with vortexing each hour to break apart cell-growth vessel adhesion to minimise antibiotic shielding. After 11 hours total incubation time, the samples underwent centrifugation at 4000 rpm for 8 minutes, the supernatant was removed, and the pellet was resuspended in 3 mL of Kings B medium. 100 µL was then plated on to L-agar + sucrose (10%) and a dilution series (10-1 to 10-3, 100 µL each) on to L-agar. These plates were grown for 2 days at 28 °C.

To screen for mutant double-crossovers against a background of wildtype revertants, a pick and patch procedure was followed where colonies were taken from the previous tetracycline enrichment and sucrose selection stage and patched (50 sample streaks per plate) on to L-agar + tetracycline (12.5 mg/ml) and L-agar + rifampicin (50 mg/ml). These were incubated for 2 days at 28 °C. To confirm double-crossover candidates, the colonies present on the L-agar + rifampicin but not on the corresponding L-agar + tetracycline were re-streaked on to fresh L-agar + tetracycline (12.5 mg/ml) and L-agar + rifampicin (50 mg/ml) which were incubated for 2 days at 28 °C. Colonies which grew L-agar + rifampicin but not on the corresponding L-agar + tetracycline were used for a colony PCR reaction (Bergkessel and Guthrie, 2013). This reaction product was then purified (PCR Clean-up kit – 740609.50 (Machery-Nagel)) and sequenced to verify successful chromosomal integration of the mutant gene. Glycerol stocks (500 µL culture + 500 µL 50 % glycerol) were prepared and stored at -80 °C for successful mutants.

A graphical representation depicting the double-crossover tetracycline-SacB selection methodology can be seen in Figure 2.2.
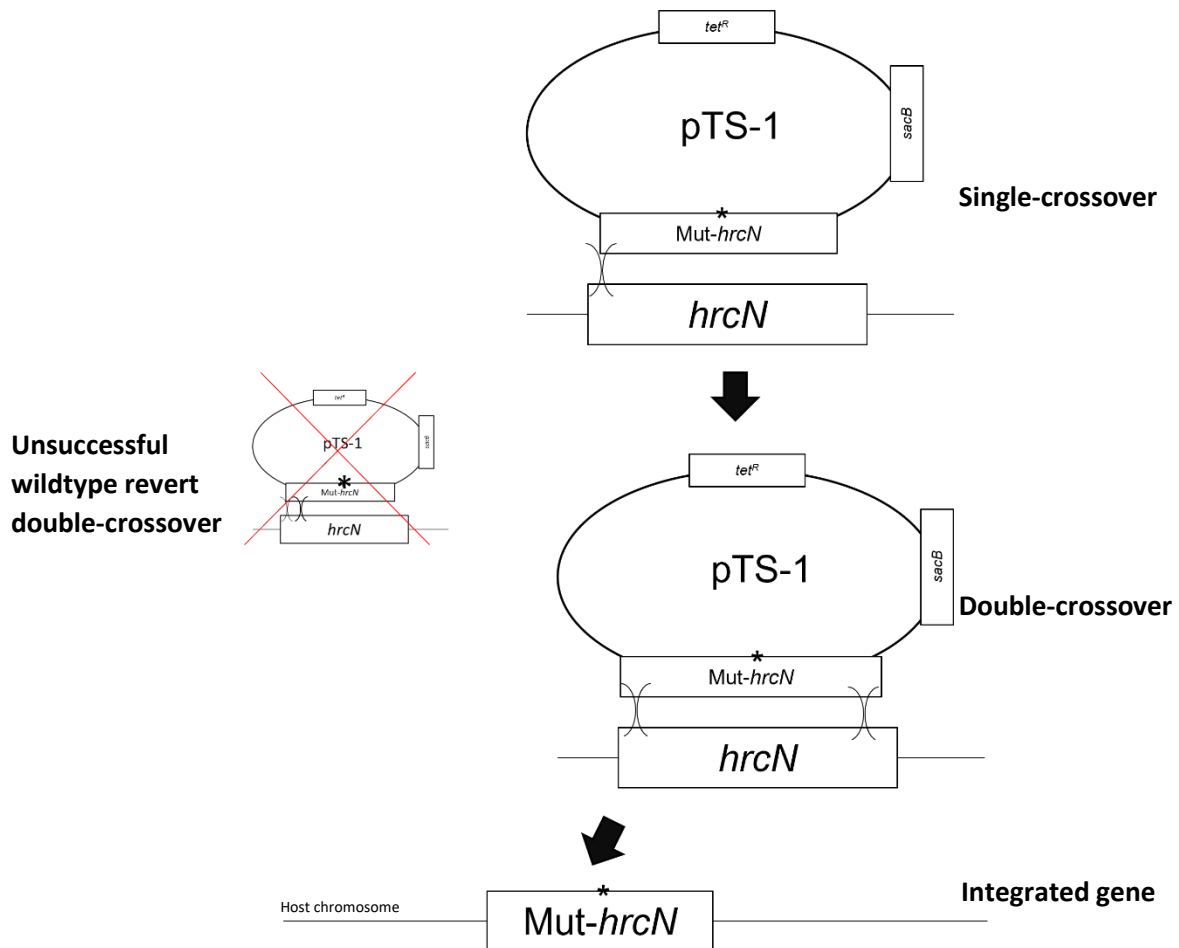
Figure 2.2. Chromosomal integration via allelic exchange demonstrated using *hrcN* as an example gene. Shown are the three stages (single-cross over, double-crossover and gene integration). Also shown is the unsuccessful wildtype revert double-crossover indicated by the red cross-through. "*" shows the presence of the desired mutation.

2.2.13.   Protein Over-production

Protein production was achieved using transformed BL21(DE3) PlysS *E. coli* which grew in L-media + kanamycin (50 µg/mL) and chloramphenicol (25 µg/mL). These bacteria were transformed with a pETM11 inducible expression vector which contains a kanamycin resistance cassette, and which contained an expressible protein with a His6-tag. From a 5 mL overnight culture, 1 litre of terrific broth with kanamycin (50 µg/mL) and chloramphenicol (25 µg/mL) was inoculated and grown at 37 °C, 220 rpm until an OD_{600} of 0.4 was reached. After this point, IPTG was added to a final concentration of 1 mM. The induced cultures were allowed to produce protein overnight at 18 °C, 220 rpm. Following expression, cultures underwent centrifugation at 5000 x g for 30 minutes to form a pellet. The supernatant was removed and the pellets from 2 x 1 litre cultures were re-suspended in 30 mL of chromatography equilibration buffer A (20 mM HEPES, 250 mM NaCl, 2 mM $MgCl_2$, 3 % glycerol pH 7.8). The cell pellets were not frozen, purification continued immediately after resuspension.

2.2.14.   Protein Purification via Fast Liquid Protein Chromatography

Induced BL21(DE3) PlysS cell pellets were lysed using an MSE Soniprep 150 ultrasonic disintegrator. 5 x 1-minute ultrasonication steps on ice (full power, 50 Hz) with 1 minute cool-down between stages. The lysed cells were then loaded into a 50 mL centrifuge tube and underwent centrifugation at 16,000

rpm for 30 minutes to form a pellet. The supernatant (soluble fraction) was separated from the pellet (insoluble fraction). This supernatant was held on ice while loading into an Amersham Biosciences AKTA FPLC system.

Prior to loading, the AKTA FPLC was fitted with a fresh HisTrap™ Excel 1 mL Ni-NTA affinity column (GE Healthcare). This column was washed with chromatography equilibrium buffer (buffer A) for 10 minutes at a 1 mL/min flowrate. The inbuilt UV spectrophotometer unit was calibrated to zero following this. The lysed cells were injected into the column at a flow rate of 1 mL/min. The column was washed with 10 % buffer B (20 mM HEPES, 250 mM NaCl, 2 mM $MgCl_2$, 3 % glycerol, 500 mM imidazole pH 7.8) for around 15 minutes at 1 mL/min until the UV curve releveled to baseline. A 100 % buffer A to 100 % buffer B gradient was then run at 1 mL/min for 10 minutes, collecting 1 mL elutions in microcentrifuge tubes or a 96 deep-well plate. Tubes were stored on ice in a 4 °C refrigerator, and fractions were used immediately for *in vitro* assay work. Protein concentration was calculated by way of a standard Bradford assay with Coomassie Brilliant Blue G-250 dye (Bradford, 1976).

2.2.15.   SDS-PAGE

Protein samples were mixed 1:2 with SDS loading buffer and boiled at 100 °C for 10 minutes. These were loaded on to a RunBlue™ SDS-PAGE precast mini gel (Expedeon) in an SDS-PAGE running chamber filled with 1 x Tris/Tricine/SDS buffer (Expedeon). The gel was run at 200 v for 1 hour. The run gel was stained for 1 hour in InstantBlue™ protein stain (Expedeon) and left to de-stain overnight in water. The protein bands were visualised in a G:BOX Chemi XRQ with GeneSys software (Syngene).

2.2.16.   Pyruvate Kinase/Lactic Dehydrogenase ATPase Assay

ATPase (enzyme coupled) assays were used to evaluate the ATPase activity of the purified protein. This is done by measuring the A_{340} absorbance change as NADH is oxidised via LDH using pyruvate produced from pyruvate kinase from ATPase activity. This was read from a 96-well plate, over 90 minutes (1 read per minute) in a FLUOstar Omega or a SPECTROstar Nano plate reader (BMG Labtech) at 25 °C. 8 wells were used of varying ATP concentrations, 2 replicates for each: 0, 0.125, 0.25, 0.5, 0.75, 1.0, 1.5, 2.0 mM ATP. Wells had 90 µL of reaction master mix and had 10 µL of the appropriate ATP solution added directly prior to plate reading as this initiates the reaction. In each well, prior to ATP addition were the following: 8 µL of 5 mM NADH, 1 µL of 80 mM PEP, 1.5 µL of PK/LDH enzyme (Sigma), 1 µM final concentration of protein, made up to 90 µL with 100 mM Tris, pH 9.0. This was prepared as a master mix for all wells.

2.2.17.   Differential Radial Capillary Action of Ligand Assay (DRaCALA)

In 1.5 mL microcentrifuge tubes, increasing concentrations of purified protein (0.325 µM to 40 µM) and 0.6 µM 2'-Fluo-AHC-c-diGMP (BioLog Life Science) were added up to a total volume of 15 µL with protein buffer. The tubes were left to incubate on ice for 10 minutes at room temperature in a dark environment. 5 µL of the reaction was dropped onto Hybond-C extra (Fisher Scientific) or Amersham™ Protran™ (GE Healthcare) supported nitrocellulose membrane (0.45 µM pore size). Alongside, a positive and negative control were also included. The droplets were left to briefly dry and were then visualised using the UV fluorescence mode on a G:Box F3 Imager (Syngene).

2.2.18.   Analytical Gel Filtration

To analyse protein sample oligomerisation with CdG, a 10/300 GL Superdex™ Increase column (GE Healthcare) was used (30 mL column volume). The column was washed with 4 column lengths (30 mL

x 4) of Millipore water followed by 5 column lengths (30 mL x 5) of gel filtration buffer (50 mM HEPES, 150 mM NaCl, 5 % glycerol).

Affinity-purified protein samples (+/- CdG) were loaded onto the column for analysis via size exclusion. For +CdG samples, 50 µM CdG was added 5 minutes prior to loading, samples were kept on ice. All samples were crosslinked on-ice via UV-crosslinking (1 minute, 150 mJ/cm^2 at 254 nm with a Stratalinker). Samples underwent centrifugation at 13 000 rpm for 10 minutes at 4 °C prior to loading onto the analytical gel filtration column to separate out any large aggregates and precipitates. Purified protein sample (500 µL) was injected through a loop onto the column and passed through at a fixed flow rate (0.75 mL/min) not exceeding column pressure limits. Loaded sample was separated out by size, detected by an ultraviolet sensor. The column was then washed and stored in 20 % ethanol.

2.2.19. Mass Photometry

A Refeyn mass photometry instrument (Refeyn TwoMP) was used to analyse the oligomeric response of purified HrcN protein to CdG following analytical gel filtration. The predicted dodecamer fraction was immediately collected following elution (+/- CdG) and loaded onto a prepared glass slide (1 µL in 10 µL PBS) in a ring well following autofocus with buffer only. The samples were analysed, where visual light signals were used to estimate oligomeric species present in the sample calibrated against previously analysed known standard samples (BSA phosphate and urease).

2.2.20. Western Blotting

SDS-PAGE was performed with the samples of interest which had been heated to 100 °C for 10 minutes in 1x loading dye as described previously. These proteins were then blotted on to a PVDF membrane (pre-washed in methanol for 15 seconds followed by water for 2 minutes) using a Fisher Western blotting apparatus filled with 1 x transfer buffer (diluted from 10x – 250 mM TRIS, 1.9 M glycine with 20 % v/v methanol) and run at 80 v for 45 minutes with ice cooling. This membrane was then blocked overnight at 8 °C in PBS buffer (137 mM NaCl, 2.7 mM KCl, 10 mM Na_2HPO_4, 1.8 mM KH_2PO_4) with 0.01 % Tween-20 and 5 % milk powder.

The blocked membrane incubated with the primary antibody (1:10 000 in PBST + 5 % milk) for 1-2 hours in a 50 mL falcon tube on a tube roller at 8 °C. The incubated membrane was washed in PBST for 15 minutes, then for 5 minutes followed by a further 5 minutes, each time using fresh PBST.

The washed membrane was then incubated with the detection anti-rabbit horseradish peroxidase antibody (1:3000 in PBST + 5 % milk) for 1-2 hours in a 50 mL falcon tube on a tube roller at 8 °C. The previously described PBST wash steps were then performed again.

The membrane was the visualised using ECL Prime Western blotting detection reagent (GE Healthcare) where chemiluminescence was detected using an ImageQuant LAS-500 (GE Healthcare).

2.2.21. ROS Burst Assay

Eight 4 mm *A. thaliana* Col-0 leaf discs (per sample) from 4-week-old plants were floated overnight in 200 µL sterile H_2O in a 96-well plate. This was replaced with a solution of 17 mg/ml luminol (L-012) and 200 µg/mL horseradish peroxidase. Boiled (10 minutes, 100°C) or un-boiled *Pto* DC3000 bacterial extracts (50 ng/mL protein concentration) or pure positive control 100 nM flg22 peptide were added. Luminescence was captured using a Varioskan Flash multiplate reader over a 4-hour time window (Albert and Fürst, 2017).

2.2.22.   CyaA T3SS Effector Fusion Reporter Assay

Molecular gateway cloning of effectors and plasmids, as well as running of assays were performed as previously described (Chakravarthy et al., 2017b).

pCPP5371-CyaA backbone vectors were Gateway cloned with T3E (lacking stop-codons)-pENTR-SD/D-TOPO vectors via an LR reaction to create pCPP5371::T3E + C-terminal CyaA vectors (pDEST). The LR reaction was carried out at 25 °C for 1 hour (150 ng pCPP5371, 150 ng T3E-pENTR-SD/D-TOPO, up to 8 uL with TE buffer, 2 uL LR Clonase II). The reaction was inactivated using proteinase K (1 uL, 10 minutes, 37 °C). DH5α *E. coli* were transformed with the constructs and were subsequently verified using colony PCR and sequencing. Relevant *Pto* DC3000 strains were transformed with these verified plasmids using electroporation.

Pseudomonas syringae Pto DC3000 transformed with the T3E-CyaA reporter plasmid (pCPP5371::T3SS effector-encoding gene lacking stop codon) was grown overnight in L media + 25 µg gentamycin at 28°C. The optical density of cultures was adjusted to an OD_{600} of 0.05 (5 x 10^7 cfu/mL) in 10 mM $MgCl_2$. This solution was infiltrated into 4-week-old *Arabidopsis thaliana* leaves using a 1 mL flat-end syringe. 8 leaves were infiltrated per plant, 3 plants per sample. For multiple time-points, a separate triplicate of plants were used for each timepoint due to leaf quantity limitations. Plastic humidity domes covered the plants throughout the experiment. Plants were left for 6 hours (or for their respective timepoint). Following this infection window, sample collection then took place. Using a leaf corer (4 mm diameter), leaf discs from the infected leaves were collected and placed into 2 mL microcentrifuge tubes with 2 glass beads. Each tube contained 1 cm^2 total of leaf tissue from the 8 infiltrated leaves. The tubes were immediately flash frozen in liquid nitrogen. The frozen samples were ground using a Qiagen Tissue Lyser II (30 hz, 45 seconds x 2) and then were returned to liquid nitrogen. The tubes were then stored at -80 °C.

The cAMP levels in the infiltrated leaf tissue were then tested by ELISA. The quantity of cAMP directly correlates to the level of effector protein translocation from bacteria to plant due to the fused CyaA adenylate cyclase. 300 µL of 0.1 M HCl was added to each tube of frozen ground leaf tissue and vortexed vigorously. The tubes underwent centrifugation at 13 000 rpm for 10 minutes. The sample was vortexed to resuspend the pellet. The tubes underwent centrifugation again at 13 000 rpm for 10 minutes. The supernatant was collected and used to create dilutions of 1:5 and 1:50 in 0.1 M HCl.

A direct cAMP ELISA kit (Enzo) was used to quantify the cAMP. 50 µL of neutralising reagent was added to each antibody-coated well. 100 µL of each 1:50 diluted sample was added to their respective wells. cAMP samples were prepared and loaded in a set of control wells (200 pmol/mL, 50 pmol/mL, 12.5 pmol/mL, 3.13 pmol/mL, 0.78 pmol/mL and 0 pmol/mL). An empty blank well and a non-specific binding well were also included. 50 µL of the kit conjugate solution was added to the wells followed by 50 µL of kit antibody. The plate was sealed and shook at 200 rpm at room temperature for 2 hours. A Bradford assay was performed alongside this in a regular 96-well plate using the 1:5 diluted samples and a set of BSA standards (1.4 mg/mL, 1.0 mg/mL, 0.5 mg/mL, 0.25 mg/mL and 0 mg/mL).

Following the ELISA plate incubation, the wells were emptied and washed 3 times with 400 µL of 1 x wash buffer. 200 µL of the kit substrate solution was added to the wells. The plate was covered and left to incubate for 1 hour in the dark without shaking. Following this 50 µL of stop solution was added to each well and the absorbance was measured at 405 nm using a plate reader. A well with a more intense yellow colour and thus, a greater absorbance reading had a lower cAMP concentration. Data was analysed by comparing each well against the logarithmic curve generated from the cAMP

standards. This value was then divided by the calculated sample protein concentration to give pmol cAMP/μg protein.

2.2.23. Bacterial Growth Assay

Overnight cultures of bacteria were prepared from solid growth medium single colonies. A 96-well flat bottom clear assay plate was used. 150 μL media with any necessary antibiotics was added to the wells. The wells around the edge of the plate were omitted to increase reliability. The overnight culture was added in triplicate to the relevant wells with a final OD_{600} of 0.01. A film lid was added to the plate. The plate was loaded into a plate reader with hourly measurements collected at the appropriate temperature and for the appropriate growth period length. For *Pseudomonas syringae Pto* DC3000, this was 28 °C for 48-72 hours.

2.2.24. Mass Spectrometry

Protein samples were prepared via trypsin digest and were then run on an Orbitrap Fusion™ Tribrid™ Mass Spectrometer by Dr. Gerhard Saalbach and Dr. Carlo de-Oliveira-Martins. For trypsin digestion, protein bands of interest were run and cut out from a standard SDS-PAGE gel. In LoBind® 1.5 mL tubes (Eppendorf), the gel slice was added along with 1 mL 30 % ethanol for 30 minutes at 65 °C. This was repeated with fresh ethanol until the gel slice was clear. The liquid was removed and 1 mL of TEAB with 50 % acetonitrile was added for 15 minutes at room temperature. This was removed and 1 mL of 10 mM DTT was added to the tube for 30 minutes at 55 °C. This was removed and 1 mL of 30 mM iodoacetamide (IAA) was added for 30 minutes and kept in the dark. This was removed and 1 mL TEAB with 50 % acetonitrile was added for 15 minutes at room temperature. This was removed and 1 mL of TEAB was added for 15 minutes at room temperature. This was removed and the gel slice was cut into small fragments and added to 1 mL TEAB with 50 % acetonitrile in a fresh tube. 1 mL acetonitrile was added causing the gel fragments to become white and hardened. The liquid was removed, and the fragments were dried in a speed vac for 30 minutes. The samples were then analysed with mass spectrometry.

2.2.25. Co-immunoprecipitation of CyaA-fused effector proteins from *Pto* DC3000-infected *Arabidopsis thaliana* Col-0

Pseudomonas syringae Pto DC3000 strains with effector-CyaA fusions (in a pCPP5295 stable expression vector driven by a *hrp*-promoter) were infiltrated (OD_{600} 0.05) into *Arabidopsis thaliana* Col-0 leaves (30 per plant). The infection was allowed to proceed for 2 days where leaves were then harvested. Leaf discs (radius of 0.384 mm) were collected from the leaves (1 per leaf) using a sterile cork-borer. Infected leaf discs were put into microcentrifuge tubes and frozen immediately with liquid nitrogen. The contents of the tubes were then homogenised using a Qiagen TissueLyser II by shaking with two glass beads in 600 μL sample buffer (20 mM Tris-HCl pH 8, 150 mM NaCl, 1 mM EDTA, 1% Triton X-100, 1 tablet/100 mL cOmplete™ ULTRA protease inhibitor cocktail) at 30 hertz for 45 seconds, twice with a 1-minute cool-down period in-between. Alongside effector-CyaA infected tissue, negative controls were also included. These were non-CyaA WT *P. syringae Pto* DC3000 infected *A. thaliana* Col-0 tissue, and uninfected *A. thaliana* tissue.

This co-immunoprecipitation protocol used Protein A Dynabeads™ (ThermoFisher Scientific) and an anti-CyaA antibody (Merck Millipore) for effector interaction target pull-down. Dynabeads™ were resuspended via vortexing for 2 minutes. 50 μL (1.5 mg) of Dynabeads™ were transferred to 1.5 mL microcentrifuge tubes, with each tube containing a different sample or technical replicate. The tubes were places onto a magnetic tube rack for 1 minute to separate the Dynabeads™ from the storage

solution and the supernatant was discarded. The beads were removed from the magnet and had 5 µg anti-CyaA antibody added per tube, diluted in 200 µL wash buffer (PBS + 0.02 % Tween-20, pH 7.4). The tubes were left to rotate for 2 hours at 4 °C on a tube rotator to allow the antibody to bind to the protein A Dynabeads™. Tubes were placed on the magnetic rack for 1 minute to separate beads from solution. The supernatant was discarded, and the beads were resuspended in fresh wash buffer. The antibody-bead complexes were crosslinked on-ice via UV-crosslinking (1 minute, 150 mJ/cm^2 at 254 nm with a Stratalinker).

The beads were returned to the magnetic rack for 1 minute, and the separated supernatant was discarded. 600 µL of the homogenised plant tissue was added to the beads after removal from the magnetic rack. The tubes were rotated for 2 hours at 4 °C on a tube rotator to allow the crosslinked anti-CyaA antibody-protein A Dynabeads™ complexes to bind to effector-CyaA plant cell component interaction complexes. The tubes were returned to the magnetic rack following this and washed 3 times with 200 µL wash buffer accompanied with gentle pipetting. The beads were resuspended, and the wash buffer was discarded each wash. Following the final wash and discarding of the final supernatant, 100 µL of washing buffer was added to the beads. They were then transferred to clean 1.5 mL microcentrifuge tubes.

The tubes were returned to the magnetic rack for 1 minute and the supernatant removed. 15 µL of elution buffer (50 mM glycine, pH 2.8) was added to the beads, along with 15 µL of 2 x SDS sample loading buffer (with trace bromophenol blue). The tubes were heated for 10 minutes at 70 °C. The tubes were places onto the magnetic rack for 1 minute and the supernatant was loaded onto an SDS protein gel, ensuring adequate separation between lanes to allow for gel slice extraction for mass spectrometry analysis. A different gel was used for each sample to minimise cross-contamination. 10 % SDS gels were poured and allowed to polymerase for 24 hours prior to running, using a full separating gel only with no stacking gel top-portion. The gels were allowed to run for 2-5 minutes so the sample moved 2-5 mm into the top of the gel. After washing the gels with water, the samples bands were cut out. From here the previously described mass spectrometry protocol was followed.

Chapter 3: *In vitro* Characterisation of HrcN and CdG-Binding Mutants

3.1. Introduction

3.1.1. General Overview

HrcN is an export ATPase protein located at the base of the type III secretion system in *Pseudomonas syringae* where it localises as a peripheral membrane protein (Pozidis et al., 2003). Part of this protein's functionality is known. However, the detailed mechanism of action along with its regulation are still areas of active research. Current knowledge of type III secretion system associated ATPases states that the ATPase enzyme catalyses the hydrolysis of ATP into ADP and free phosphate, often accompanied by a structural conformational change of the ATPase (Gao et al., 2018). The breakdown of the phosphate bond in this reaction releases energy. This has been shown to be important for proper substrate unfolding and translocation, and is therefore important for establishment of full virulence (Yoshida et al., 2014). The HrcN protein, and its ATPase activity, is important for the proper function of the type III secretion system and associated virulence (Trampari et al., 2015, Lorenz and Büttner, 2009).

HrcN has been shown to be highly conserved among certain bacterial species. Some examples of closely related proteins can be found in other *Pseudomonas* species such as the plant growth promoting bacteria *Pseudomonas fluorescens* (FliI, bacterial flagella ATPase) and the human pathogen *Pseudomonas aeruginosa* (PscN, T3SS ATPase). Examples in non-*Pseudomonas* bacteria include the plant pathogens *Brennaria* and *Erwinia*, as well as the human foodborne pathogen *Vibrio* (Diepold and Armitage, 2015).

Previous work has functionally characterised the homologue protein FliI from *Pseudomonas fluorescens*, which is found at the base of the bacterial flagellum (Trampari, 2016). It was shown that purified wildtype FliI bound to CdG, but some mutant variants that targeted key predicted residues in the CdG binding interface had altered binding affinities and ATPase activity (Trampari et al., 2015, Trampari, 2016). It was further shown that CdG binds to highly conserved residues in a binding pocket at the interface of two FliI subunits. Certain biophysical aspects of HrcN were also tested. It was shown that HrcN can bind to CdG and that the addition of CdG may reduce ATPase activity (Trampari et al., 2015, Trampari, 2016). Pairwise sequence alignment shows a percentage identity of 67.84 % across a 34 % query cover indicating a reasonable level of sequence conservation between *fliI* and *hrcN*. This suggests that there may be some degree of functional similarity between these two systems.

3.1.2. ATPase Function

ATPases are enzymes which catalyse ATP hydrolysis to form ADP. This hydrolysis process releases energy from breakdown of the phosphate bond in ATP. Walker motifs (Walker A and Walker B) are commonly found in ATPases (Walker et al., 1982). The Walker A motif (G-x(4)-GK-[TS]) is the main phosphate binding loop, with the Walker B motif ([RK]-x(3)-G-x(3)-LhhhD) located downstream (Walker et al., 1982). This facilitates binding of phosphate to the ATPase leading to energy-producing dephosphorylation.

The export ATPase has been shown to be necessary for proper substrate export through the T3SS across the bacterial membrane, although it is possible to bypass ATPase function in certain circumstances. An example of an ATPase-independent type III secretion system from *Salmonella enterica* was created by generating T3SS mutations which increased proton motive force for substrate export (Erhardt et al., 2014). Export of particular substrates was still possible however the efficiency of localisation and effector unfolding seemed to be greatly decreased (Erhardt et al., 2014). This infers that the ATPase protein, while possibly dispensable under certain controlled conditions, is necessary for full efficient system function.

Confirmational changes associated with the T3SS ATPase have been shown to be important for secretion function and the separation of chaperones from effector proteins (Gao et al., 2018). It was shown that the Spa47 T3SS-associated ATPase from *Shigella flexneri* underwent a confirmational change upon binding of ATP in a conserved luminal loop which allowed for ATP hydrolysis (Gao et al., 2018).

3.1.3.   CdG-dependent Regulation of ATPases

ATPases are known to be regulated in a variety of ways including both transcriptional and post-translational control. Post-translational control by way of direct CdG binding is explored in this chapter in relation to HrcN. CdG has been shown to be important for various other regulation mechanisms of bacterial virulence and cellular function. This is particularly notable across the *Pseudomonas* genus where research has highlighted the widespread role of CdG-dependent regulation throughout the bacterial lifecycle. There is detailed evidence that CdG has regulatory roles regarding cell motility, formation of biofilm, the cell cycle, cell differentiation as well as with virulence (Römling et al., 2013). There is evidence to indicate that CdG is important for the function and regulation of the T3SS ATPase (Trampari et al., 2015). Additionally, there is evidence to suggest that this mechanism is widespread across secretion system-associated ATPases including the type II, IV, and VI secretion systems, as well as the type IV pili (Roelofs et al., 2015, McCarthy et al., 2019, McCarthy et al., 2017, Trampari et al., 2015). Little is currently known about the effect of CdG on the HrcN ATPase and what possible implications this has on bacterial virulence.

3.1.4.   ATPase Oligomerisation

Many ATPases oligomerise, whereby monomeric subunits form a higher-order structure in a homo-oligomeric or hetero-oligomeric manner. HrcN has been shown to have interesting oligomerisation properties, where the protein is able to exist in various distinct oligomerisation states: a 48 kDa monomer, a 300 kDa hexamer, a 575 kDa dodecamer and a higher order 3.5 MDa state (Pozidis et al., 2003). Each of these oligomeric states are homo-oligomers that feature repeating monomeric subunits. The native conditions required for induction of these oligomerisation states and their biological importance remain unclear. T3SS ATPase oligomerisation appears across multiple systems in bacteria; however, it is not clear as to whether mechanistic control is different in each case. An example which illustrates a similar system is with HrcN homologue ATPase Spa47 in *S. flexneri*. Spa47 has been shown to oligomerise, and this oligomerisation is necessary for T3SS function (Burgess et al., 2016b). Formation of the Spa47 oligomeric-complex led to significantly increased ATPase activity, and this activity was necessary for cellular invasion (Burgess et al., 2016b). It is not clear the role of CdG on this system.

3.1.5.   Summary

This chapter focuses on furthering our understanding of the functional biochemistry of the purified HrcN ATPase and deciphering the role and importance of CdG on this protein's structure and function. This was performed with a focus on construct generation, protein purification and testing of *in vitro* HrcN to determine its interactions with CdG, and to provide functional context for subsequent *in vivo* work described in following chapters.

3.1.6.   Chapter Aims

1. To generate point mutations in *hrcN* of *P. syringae* that target residues predicted to be a part of the cyclic-di-GMP binding interface.

2. To over-express and purify mutant HrcN proteins in an *E. coli* expression system. Then to perform *In vitro* characterisation of purified HrcN to understand CdG binding and its effects on protein function.

3.2. Results

3.2.1. Construction of *hrcN* and *pscN* Expression Vectors Was Successful

Mutant T3SS ATPase constructs were generated that targeted key residues of the predicted CdG binding interface. Key CdG binding residues were identified in HrcN based on previous published work with its homologue FliI (Trampari et al., 2015). These residues were systematically mutated with conservative substitutions to evaluate the impact on functionality. These mutations were expected to introduce possible altered CdG binding, or downstream responses should these residues play an important role in protein regulation. Production of mutant HrcN constructs allowed for protein expression, purification, and downstream experimental work to better understand the function of the T3SS HrcN ATPase and to observe the effect of CdG on function, if any.

For *in vitro* over-expression work, mutant gene fragments were synthesised by overlap-extension PCR and cloned into *E. coli* in a pETM11 protein expression vector. HrcN, the type III ATPase from *Pseudomonas syringae* was the main focus of this project. Early work also included PscN, a closely related type III ATPase from the opportunistic human pathogen *Pseudomonas aeruginosa.* Due to suboptimal cloning feasibility and poor protein solubility, work on *pscN* did not continue past the protein purification stage. Shown in Table 3.1 is a list of point-mutations targeting key predicted CdG-binding residues in both HrcN and PscN, constructed and expressed in *E. coli*.

Table 3.1. Constructed HrcN and PscN mutat variants which were used for *in vitro* protein studies.

HrcN	PscN
WT	WT
P142Q	P137Q
G176A	E203D
E208D	G301D
G311A	G306D
R335P	R330Q
L338V	

3.2.1.1. Mutagenesis

Mutant gene fragments (targeting key residues of the predicted HrcN:CdG binding site) for over-expression were produced using two-round overlap extension PCRs. The first round of this overlap extension PCR produced two fragments with primers binding to the very start and end of the *hrcN* gene. Fragment A represents the first half up to the mutation, and fragment B represents the latter half after the mutation. The two fragments each contained an overlapping sequence at their 'internal' end, incorporating the point mutant in question. As indicated in Figure 3.1, A band was present for a selection of mutants in the appropriate range of 300 to 1000 bp (which varied depending on the mutation position).
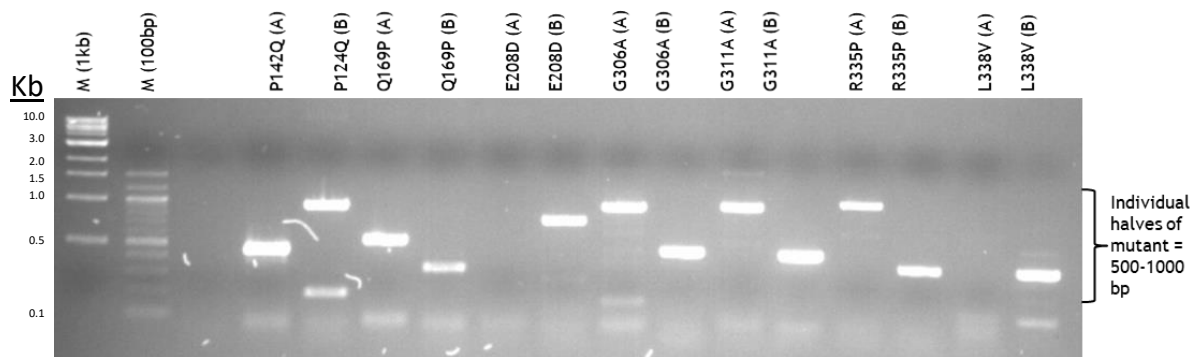
Figure 3.1. First-round PCR products for generation of mutant *hrcN* alleles for HrcN over-expression construct generation. A selection of key point mutation fragments have been shown in this agarose gel as an example. Successful amplification reactions saw a 500 to 1000 bp band present in each case.

The first-round overlap extension PCR products were then used to amplify the full length *hrcN* gene with the desired mutation present in a second-round reaction. As indicated in Figure 3.2, this was seen to be successful with an expected full length *hrcN* fragment of 1350 bp visible on the gel.
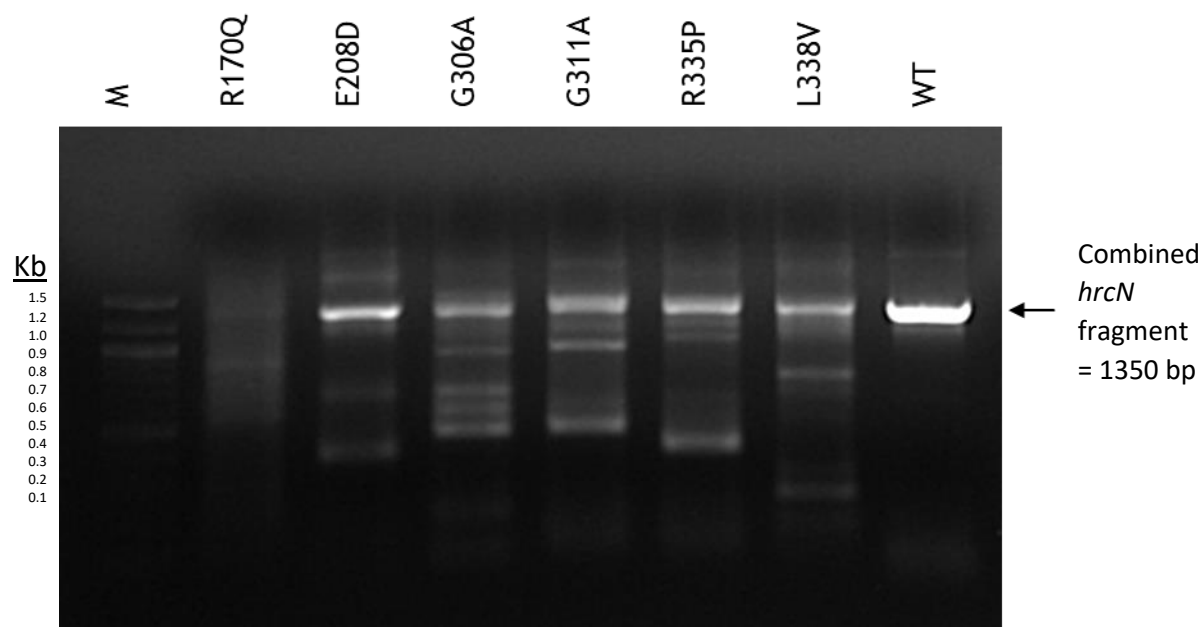
Figure 3.2. Second-round PCR products for generation of mutant *hrcN* alleles for HrcN over-expression construct generation. Shown are a selection of example constructs where a positive 1350 bp was successfully generated.

3.2.1.2.   Cloning

Colony PCR, restriction digests and sequencing were conducted to verify the accuracy and success of the cloned over-expression mutant *hrcN* constructs. A positive band at 1350 bp is shown in Figure 3.3 from a colony PCR of example cloned DNA. This band indicated the successful recombination of *hrcN* into a pETM11 protein expression vector.
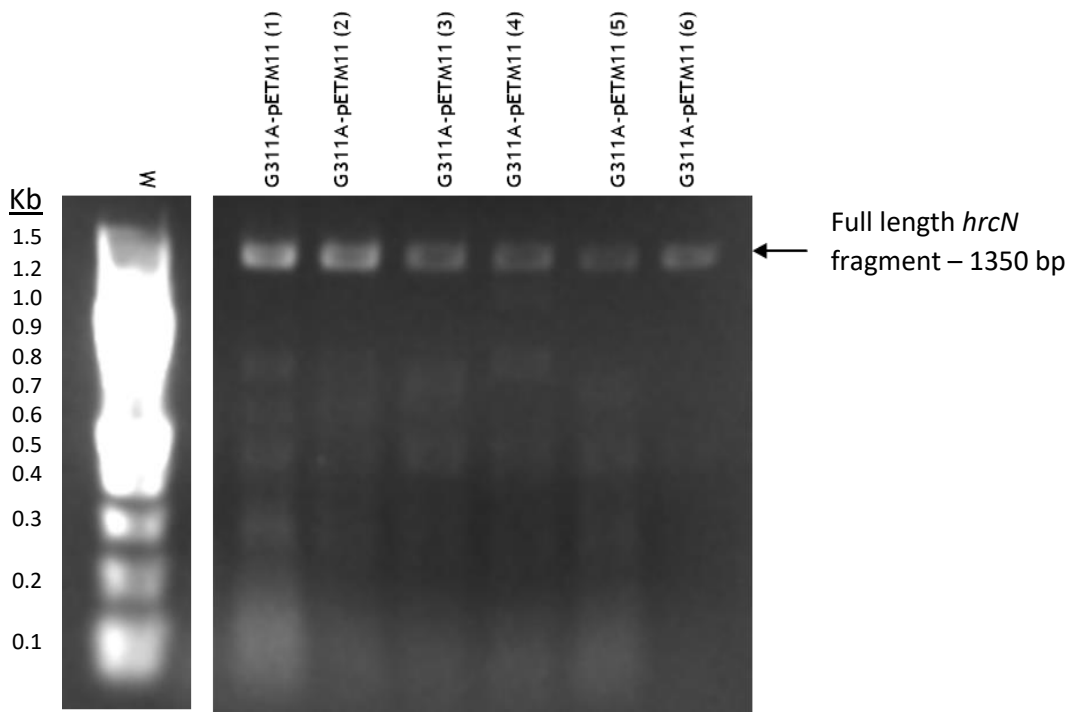
Figure 3.3. Colony PCR showing successful colony PCR amplification of a cloned mutant *hrcN* construct in a pETM11 protein expression vector. The amplified *hrcN* band visible for all colonies has been highlighted at 1350 bp.

Restriction digest was used for verification of successful cloning. An example of this is shown in Figure 3.4 where a full length 1350 bp mutant *hrcN* band was cut out of its pETM11 vector via restriction digest using specific NdeI and XhoI restriction enzymes.
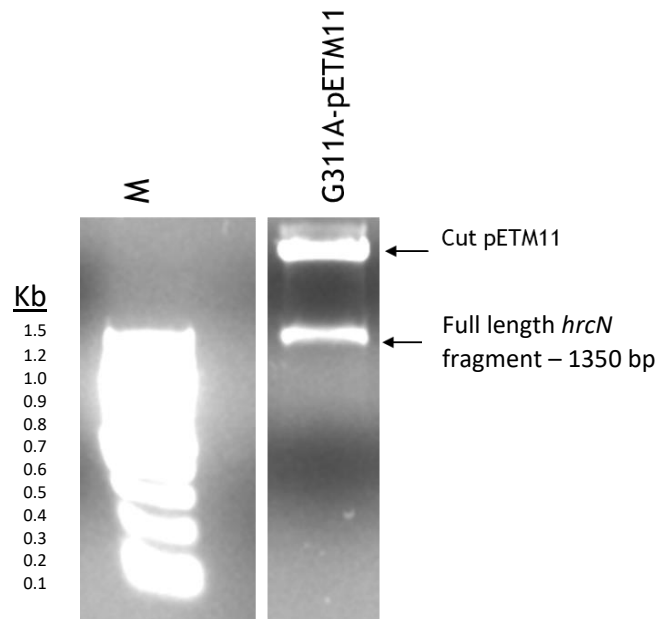
Figure 3.4. Restriction digest with NdeI and XhoI showing successfully ligated mutant *hrcN* fragment for an example construct in a pETM11 protein expression vector. The digested positive band is indicated at 1350 bp.

All generated mutant *hrcN* expression constructs were sequenced and confirmed to be correct. An example of this is shown in Figure 3.5. The upper aligned row shows the original WT sequence while the bottom aligned row shows the sequenced mutant *hrcN* construct. In this example, the intended point mutation is shown highlighted in yellow where a guanine has been mutated to an adenine (for a glycine to aspartate amino acid change).

```
 800  GGGCCCAGCGCGAAATCGGCCTGGCGGCCGGTGAACCGCCCACACGCCGC   849
      ||||||||||||||||||||||||||||||||||||||||||||||||||
  90  GGGCCCAGCGCGAAATCGGCCTGGCGGCCGGTGAACCGCCCACACGCCGC   139

 850  GGCTATCCGCCATCGGTGTTCGCCGCGCTGCCACGCCTGATGGAGCGTGC   899
      ||||||||||||||||||||||||||||||||||||||||||||||||||
 140  GGCTATCCGCCATCGGTGTTCGCCGCGCTGCCACGCCTGATGGAGCGTGC   189

 900  CGGGCAATCCGAGCGGGGCTCGATCACCGCGCTCTACACCGTACTGGTGG   949
      |||.||||||||||||||||||||||||||||||||||||||||||||||
 190  CGGACAATCCGAGCGGGGCTCGATCACCGCGCTCTACACCGTACTGGTGG   239

 950  AAGGCGACGACATGAGCGAGCCGGTGGCCGACGAGACCCGCTCGATTCTC   999
      ||||||||||||||||||||||||||||||||||||||||||||||||||
 240  AAGGCGACGACATGAGCGAGCCGGTGGCCGACGAGACCCGCTCGATTCTC   289

1000  DACGGGCACATCGTGCTGTCGCGCAAGCTGGCCGCCGCCAACCACTATCC  1049
      ||||||||||||||||||||||||||||||||||||||||||||||||||
 290  GACGGGCACATCGTGCTGTCGCGCAAGCTGGCCGCCGCCAACCACTATCC   339

1050  GGCCATCGACGTGCTGCACTCGGTGAGCCGGGTCATGAACCAGATCGTCG  1099
      ||||||||||||||||||||||||||||||||||||||||||||||||||
 340  GGCCATCGACGTGCTGCACTCGGTGAGCCGGGTCATGAACCAGATCGTCG   389

1100  ACGACGATCAGCGCCATGCGGCCGGACGCTTGCGCGAATGGCTGGCGAAG  1149
      ||||||||||||||||||||||||||||||||||||||||||||||||||
 390  ACGACGATCAGCGCCATGCGGCCGGACGCTTGCGCGAATGGCTGGCGAAG   439

1150  TACGAGGAAGTCGAGTTGCTGCTGAAGATCGGCGAATACCAGAAAGGCCA  1199
      |||||||||||||||||||||||||||||||||||||||||||||||||
 440  TACGAGGAAGTCGAGTTGCTGCTGAAGATCGGCGAATACCAGAAAGGCC-   488
```

Figure 3.5. Example pairwise alignment showing successful *hrcN* mutant generation. The top aligned row shows the WT sequence while the bottom shows the sequenced mutant *hrcN* fragment. The point mutation has been highlighted in yellow.

3.2.2.   Protein Production and Purification Was Achieved for HrcN

Protein production and purification was performed to allow for *in vitro* characterisation of the T3SS ATPase to better understand functionality and response to CdG. Mutant full length N-terminal His6-tagged HrcN protein production and purification from an IPTG-inducible expression vector in BL21(DE3) plysS *E. coli* was successful. As shown in Figure 3.6, the 48.4 kDa HrcN protein band is present once protein production has been induced by IPTG. WT HrcN protein over-expression was confirmed by Orbitrap mass spectrometry of the induced band, and Western blotting with an anti-HrcN antibody. As with the molecular cloning above, this project initially included work with the PscN ATPase from PA01 *P. aeruginosa.* Evidence of successful expression is shown in this figure alongside HrcN. However, due to consistently poor protein purification results and difficulty generating further constructs, work with PscN did not continue beyond this point.
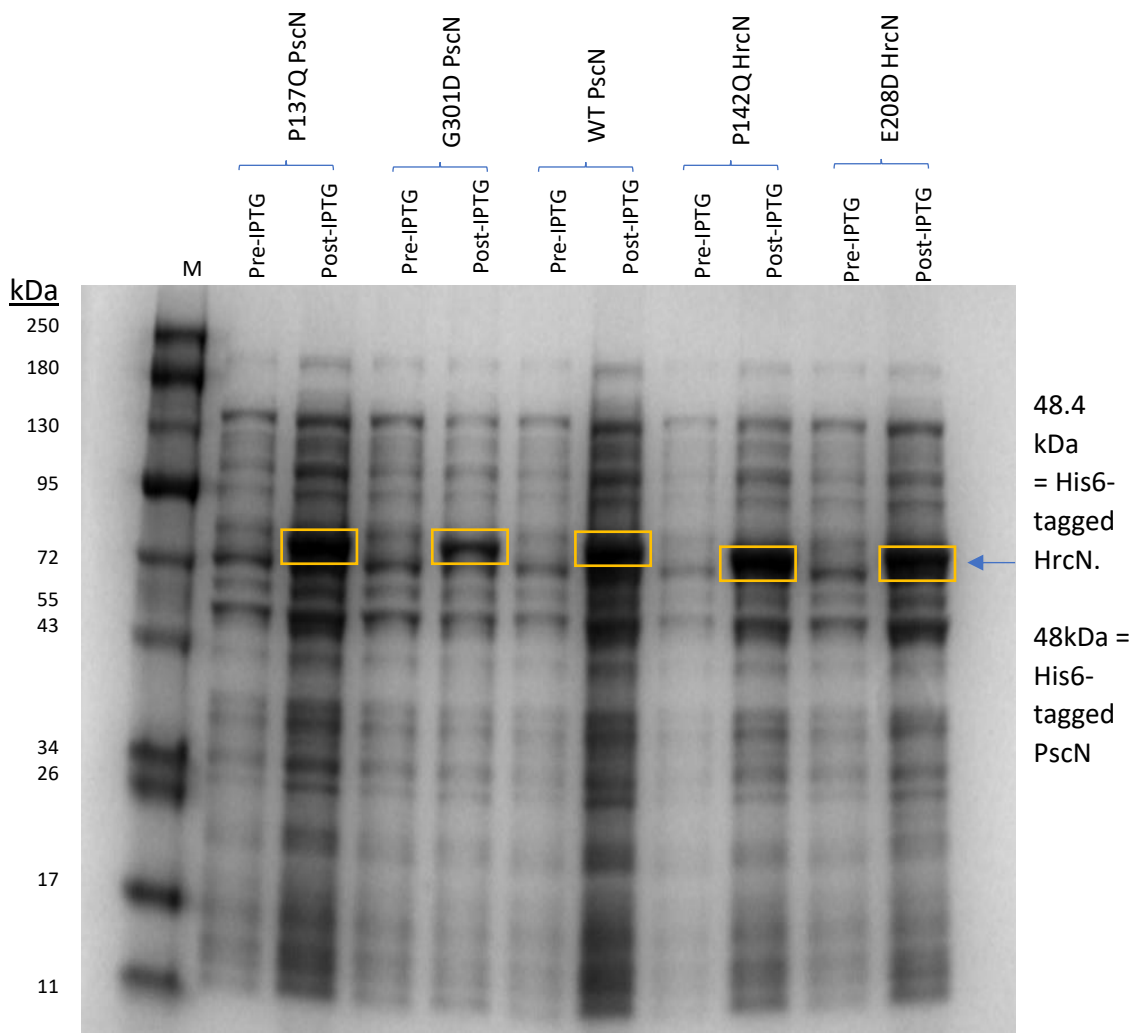
Figure 3.6. Expression of full-length His6-tagged HrcN and PscN proteins in BL21(DE3) E. coli using a pETM11 expression vector. Shown are bacterial cells before the addition of IPTG, and after the addition of IPTG following overnight protein expression at 18 °C.

His6-tagged HrcN proteins were successfully purified using Ni-NTA affinity-based FPLC. An example of this is shown in Figure 3.7. Here, the 48.4 kDa HrcN protein containing an L338V point mutation has been purified from its bacterial host. Eluted fraction concentrations containing workable HrcN protein typically ranged from 0.5 to 7 mg/mL. Over-expressed PscN protein had poor solubility and could not be purified well. As such, work with PscN ended here.
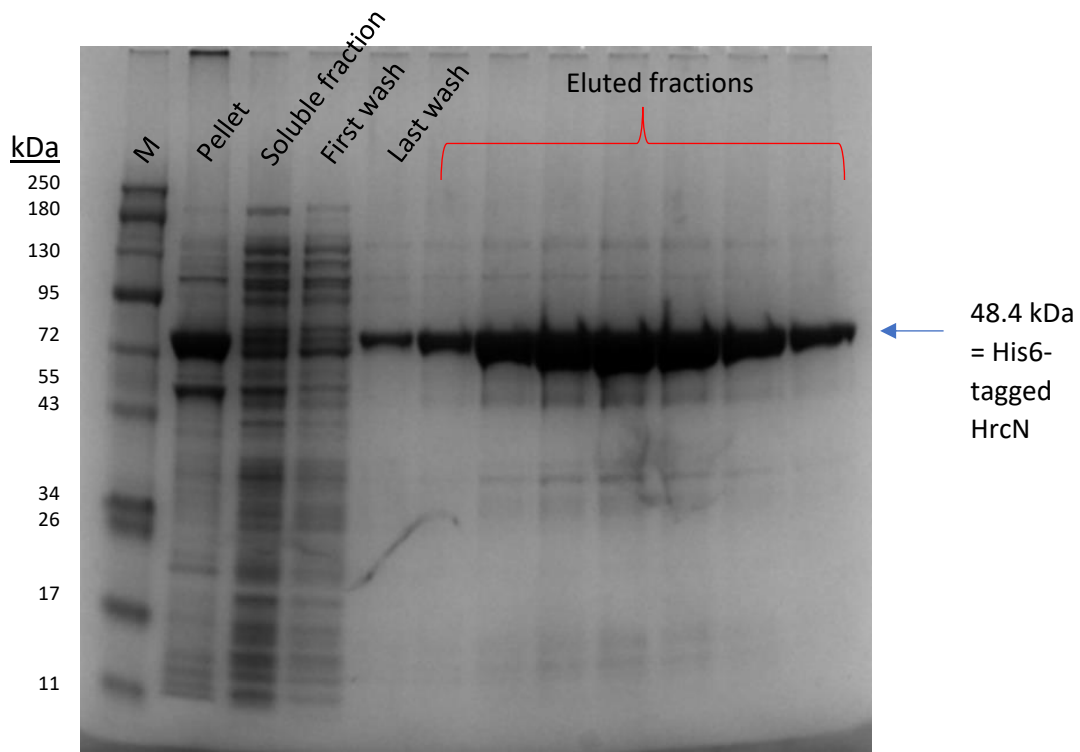
Figure 3.7. HrcN proteins were successfully purified by fast protein liquid chromatography. This example shows the purification of His6-tagged L338V HrcN. The purified HrcN protein band is present at the 48.4 kDa gel region.

The purity of HrcN was further increased by running eluted fractions through a Superdex 200 10/300 GL Increase gel filtration column. Shown in Figure 3.8 is an example gel where the 48.4 kDa HrcN band can be seen. The use of additional gel filtration allowed for increased purity by removing trace contaminating bands of a higher or lower molecular weight than HrcN.
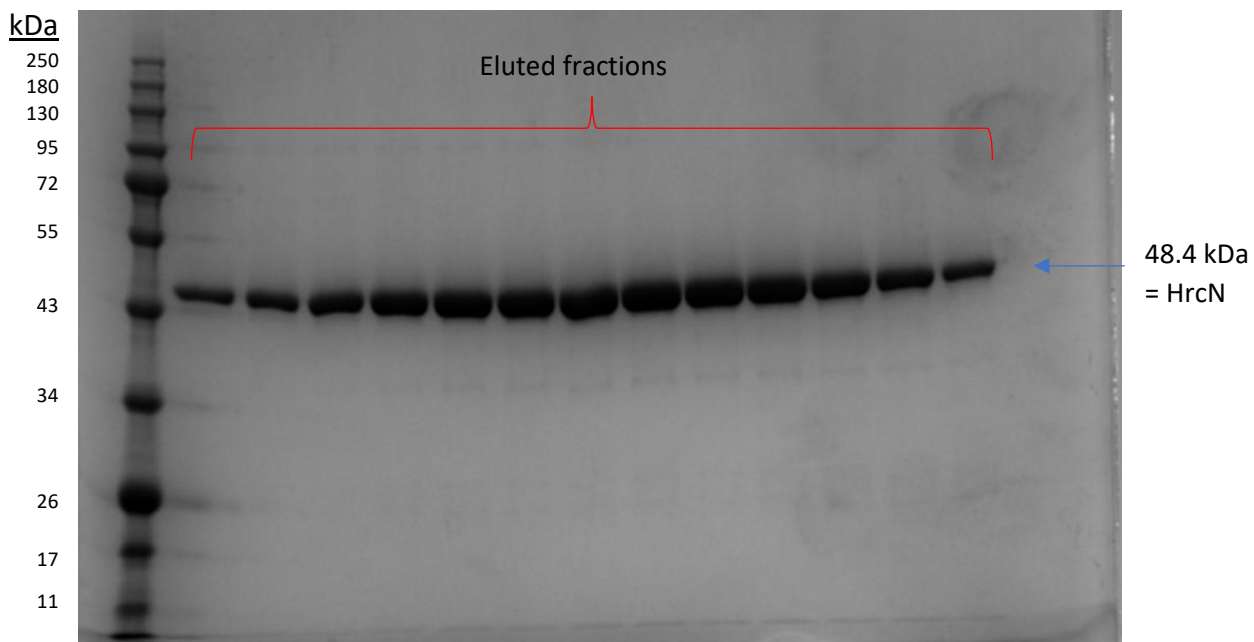
Figure 3.8. Eluted HrcN fractions purified via gel filtration following Ni-NTA affinity chromatography.

3.2.3. N-terminal Truncated Expression Vectors Were Successfully Created

Full-length HrcN exhibited poor protein stability where it would degrade and aggregate rapidly. Freezing the protein post-purification also appeared to affect its biochemical behaviour and so protein work had to be performed with fresh samples each time. To try to circumvent these stability issues, a truncated form of HrcN lacking the first 18 residues of the N-terminal was constructed. This removed the predicted multimerization domain to discourage spontaneous multimerization and aggregation. This was cloned and purified in a similar manner to the full-length HrcN constructs (above).

N-terminal truncated HrcN proteins were over-expressed and purified using the same approach as with full-length HrcN. In the case of WT and G176A N-terminal truncated HrcN, these were successfully constructed, over-expressed, and purified. An example gel showing cloning of N-terminal truncated *hrcN* is shown in Figure 3.9, while an example gel showing N-terminal truncated HrcN purification is shown in Figure 3.10. While these proteins offered increased stability compared to full-length HrcN, stability was still low and so assay work still proceeded immediately following column-based purification.

Other N-terminal truncated HrcN mutants were also constructed. However, these proteins were generally insoluble and unstable. As such, too low of a protein concentration was attainable for downstream assay work and so work with these mutants did not continue past initial purification and preliminary testing. Work with N-terminal truncated HrcN focused on WT and G176A HrcN going forward.
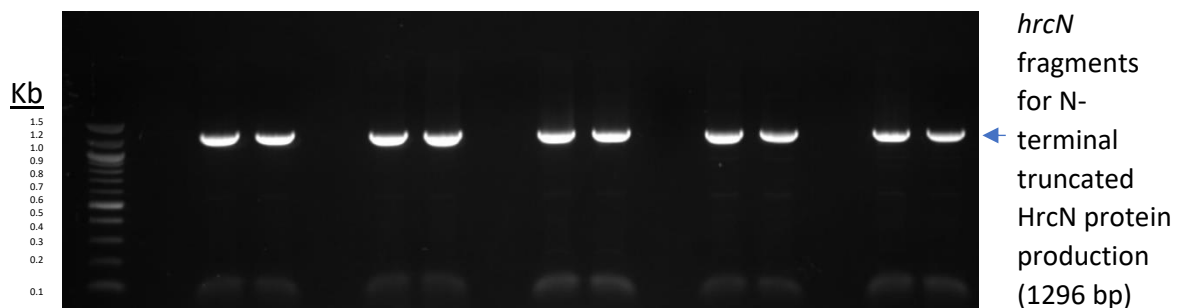
Figure 3.9. Example gel highlighting *hrcN* bands for N-terminal truncated HrcN protein production that were cloned into a pETM11a vector for protein over-expression and subsequent nickel affinity chromatography-based purification.
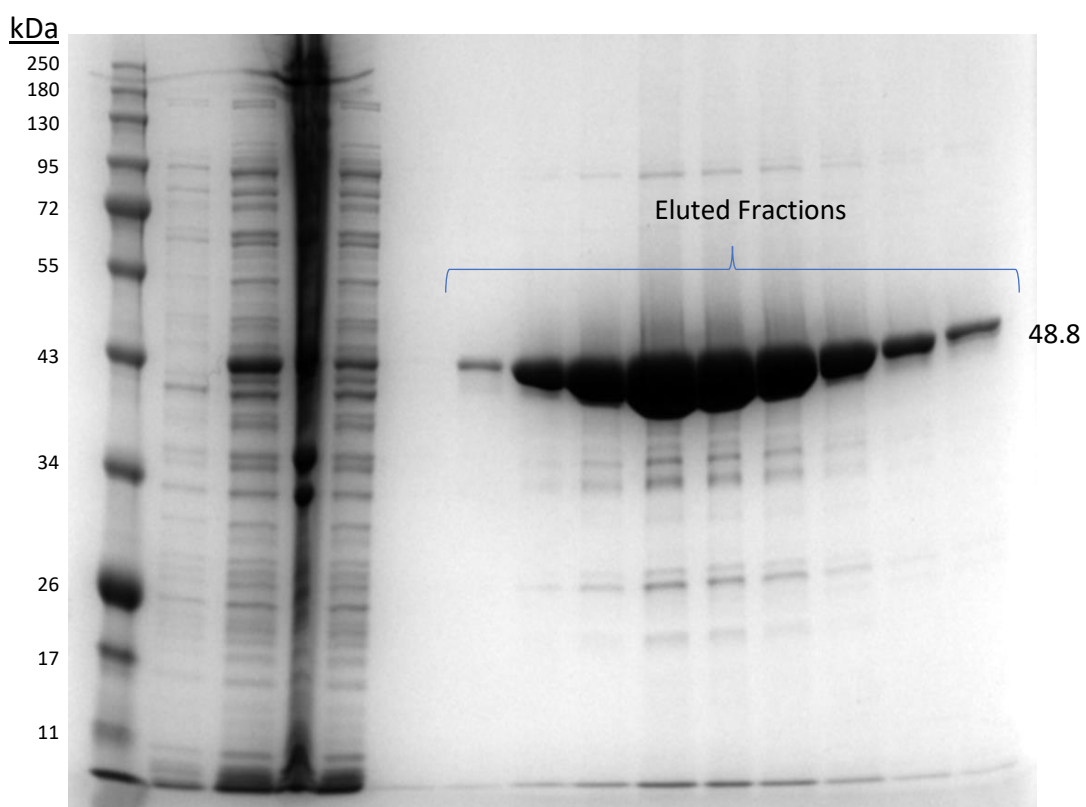
Figure 3.10. Purification of over-expressed N-terminal truncated (Δ1-18) HrcN (WT)

3.2.4. Most Purified HrcN Proteins Retain ATPase Function but CdG Has No Effect

HrcN is an ATPase, and so enzymatic functionality was tested upon protein purification. This was to ensure that the protein was still active and to identify any possible differences that may help to give insight into the mechanistic function of HrcN. CdG is known to impact ATPase activity in some HrcN homologues, and so CdG was included to evaluate the effect of this molecule on protein functionality.

3.2.4.1. Initial ATPase Activity Screen Shows ATPase Activity Across Most HrcN Proteins

Following protein purification, the ATPase activity of HrcN was tested to evaluate whether enzyme functionality was retained. A wider range of mutants were first purified and evaluated for ATPase

function. Shown in Table 3.2 is full-length ATPase activity confirmation for the initial screen of purified HrcN proteins. A threshold value of 5 nmol/min/mg was chosen as the cut-off for determining whether a protein retained ATPase activity. This value was chosen to account for background ATPase levels. All purified HrcN proteins retained ATPase activity except for HrcN containing a P142Q mutation. This mutation was predicted to be quite disruptive and so this lack of ATPase activity was not entirely unexpected.

Table 3.2. ATPase activity of purified HrcN proteins determined by LK/PDH ATPase assays.

Protein	ATPase Function	Response to CdG
WT HrcN	✔	X
G176A HrcN	✔	X
E208D HrcN	✔	X
G311A HrcN	✔	X
R335P HrcN	✔	X
L338V HrcN	✔	X
P142Q HrcN	X	X

While most HrcN mutant proteins retained ATPase activity, there was variation in activity levels. Due to inherent differences in protein preparations and protein stabilities, it was not possible to draw further conclusions from this. What was found was that CdG appeared to have no significant effect on ATPase activity across any of the purified HrcN proteins. Following this initial screen, a key G176A HrcN mutant was selected as the main mutant of focus alongside WT HrcN. This mutant was chosen due to it having interesting downstream responses to CdG (as described later in this chapter), and presented an altered *in vivo* phenotype compared to WT as shown in the following chapter. Focusing on this mutant, allowed for more detailed investigation into the underlying mechanism of HrcN.

3.2.4.2.   WT HrcN in a Low CdG Background Shows No Response to CdG or CdA

The previous assays with HrcN showed some degree of variance between experimental repeats. To help reduce this, the assay was repeated with a co-expression protein preparation. Wildtype HrcN was co-expressed with a non-tagged BifA phosphodiesterase to reduce any background CdG from the over-expressing bacteria for more consistent purified protein. In Figure 3.11, the ATPase activity has been shown for the low background CdG wildtype HrcN protein. No significant differences in ATPase activity were observed with or without the addition in CdG. At 2 mM ATP without CdG, an ATPase activity of 885.1 nmol/min/mg was observed. With 50 μM CdG no significant changes were observed with 881.7 nmol/min/mg (p = 0.9). With 50 μM CdA, ATPase activity remained consistent at 834.8 nmol/min/mg (p = 0.74). This confirms that the addition of these cyclic di-nucleotides does not appear to affect ATPase function of purified WT HrcN under these experimental conditions.
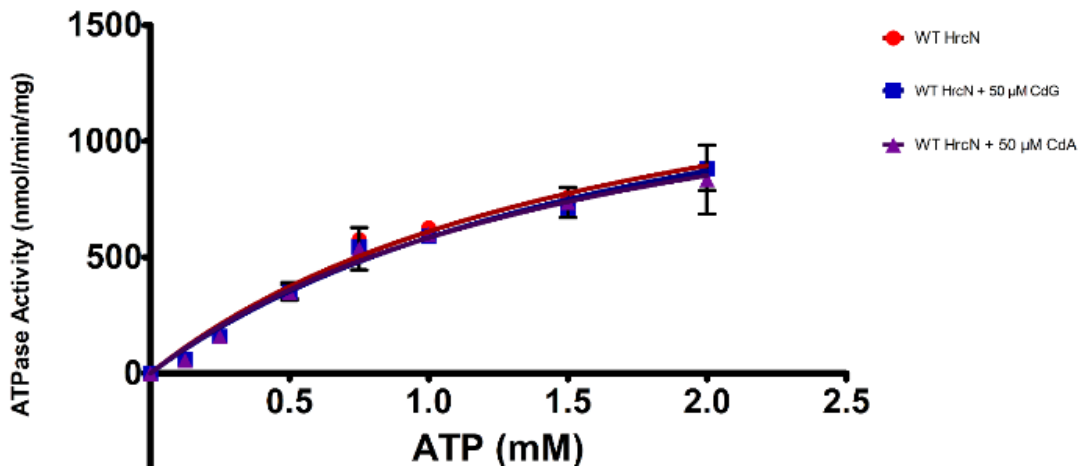
Figure 3.11. ATPase activity of purified WT HrcN co-expressed with a non-purified BifA PDE (for low background CdG) +/- 50μM CdG or CdA. ATPase activity measured via a PK/LDH ATPase assay. This reaction has been plotted as a Michaelis-Menten saturation curve where HrcN is present at 1 μM. Error bars show standard error of the mean (n = 2).

3.2.4.3. WT and G176A HrcN: Full-length and N-terminal Truncations Retain ATPase Activity, but CdG Has No Effect

WT HrcN and G176A HrcN were selected for further study following on from the initial purification and ATPase analyses. Full-length and N-terminal truncated proteins were used across a variety of assays. This G176A HrcN mutant was chosen as it showed consistent and repeatable altered downstream responses to CdG in preliminary assays (data not shown). This allowed for comparison with WT HrcN to better understand the impact of CdG binding to HrcN. Additionally, the altered downstream responses for G176A HrcN linked up with data in subsequent chapters.

Additionally, the other HrcN variants frequently suffered from very poor solubility and stability and so required extensive optimisation for much of the assay work. G176A HrcN however appeared to have a more acceptable level of solubility and as such required much less optimisation. It was decided to focus on this mutant in order to draw meaningful conclusions, rather than focusing on optimising other proteins for extended periods of time.

Full-length and N-terminal truncated HrcN proteins were subjected to oligomerisation analyses. The N-terminal region is the predicted multimerization domain and is believed to be necessary for proper dodecamerisation of HrcN. This served as a negative control for oligomeric study, while also allowing for CdG binding assays due to its increased stability. HrcN frequently self-aggregated in the full-length construct. However, this behaviour was limited with the N-terminal truncation allowing for more robust conclusions to be drawn from appropriate assays.

Shown in Figure 3.12 are ATPase assays from purified HrcN for both full-length and N-terminal truncated WT and G176A. In all cases, ATPase activity was retained. The ATPase activity was much greater for full-length WT HrcN compared to the other mutants. This could be due to differences in protein stability, protein preparation variation, or due to differences in oligomerisation and protein function. From these assays alone, it is not possible to compare across experiments due to stability issues, as the proteins were each purified and tested on different days. Possible differences in oligomerisation ability are explored in further detail in subsequent experiments in this chapter.

In Figure 3.12 A, full-length WT HrcN had an ATPase activity of 885 nmol/min/mg at 2 mM without CdG, and 882 nmol/min/mg with 50 µM CdG (non-statistically significant difference, p = 0.9). In Figure 3.12 B N-terminal truncated WT HrcN had an ATPase activity of 94.6 nmol/min/mg at 2 mM without CdG, and 103.0 nmol/min/mg with 50 µM CdG (non-statistically significant difference, p = 0.5). Full-length G176A HrcN had an ATPase activity of 57.7 nmol/min/mg at 2 mM without CdG, and 68.7 nmol/min/mg with 50 µM CdG (non-statistically significant difference, p = 0.7) in Figure 3.12 C. Lastly, Figure 3.12 D shows N-terminal truncated G176A HrcN with an ATPase activity of 109.7 nmol/min/mg at 2 mM without CdG, and 103.0 nmol/min/mg with 50 µM CdG (non-statistically significant difference, p = 0.4).
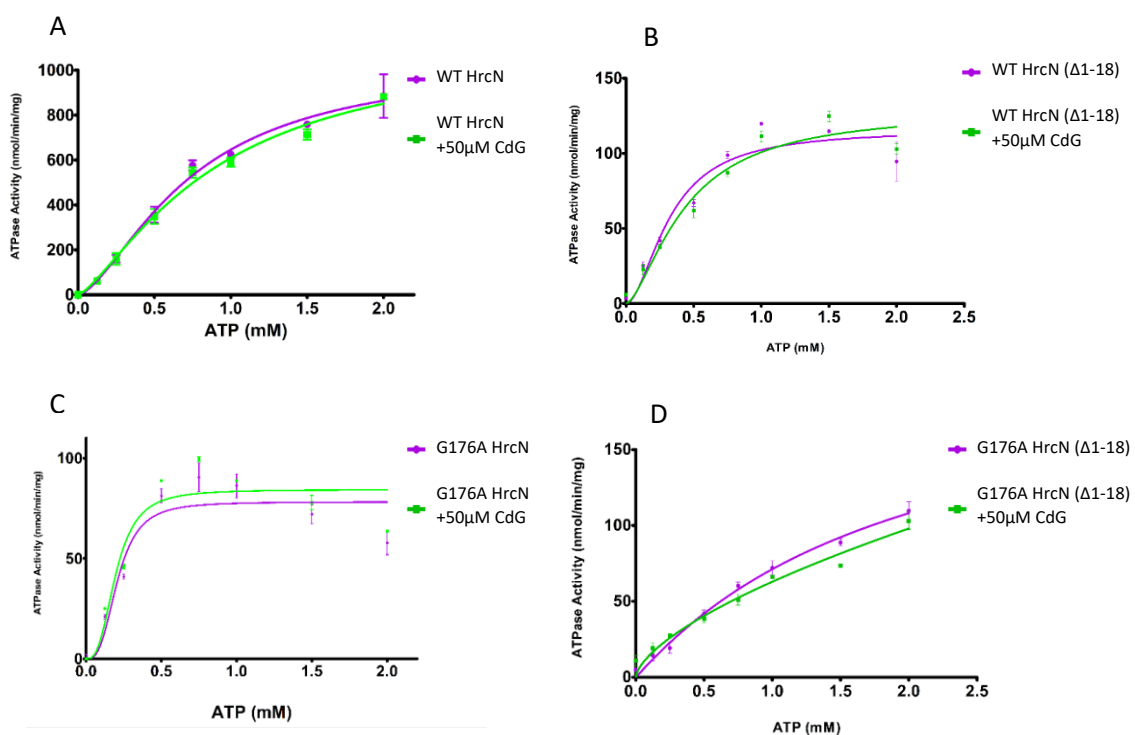
Figure 3.12. ATPase activity demonstrated for purified HrcN via PK/LDH ATPase assay. This reaction has been plotted as a Michaelis-Menten saturation curve where HrcN is 1 µM. CdG was added at 50 µM concentrations. A) is full length WT HrcN, B) is N-terminal truncated WT HrcN, C) is full-length G176A HrcN, D) is N-terminal truncated G176A HrcN. Error bars show standard error of the mean (n = 2)

3.2.5.   DRaCALAs Show Evidence of CdG Binding for WT and G176A HrcN

HrcN was identified as a CdG-binding protein based on a previously performed CdG capture compound screen (Trampari et al., 2015, Nesper et al., 2012), although the *in vivo* and *in vitro* consequences of this binding were not thoroughly investigated. Binding of CdG to HrcN was investigated to first confirm binding to WT HrcN, and to then compare this to the G176A HrcN variant to identify whether there were any differences with CdG binding. N-terminal truncated HrcN was tested due to its increased stability, providing a more robust and reliable indication of CdG-binding. Full-length HrcN was subject to rapid degradation and aggregation, and so was not amenable to DRaCALA analysis.

3.2.5.1. WT HrcN Δ1-18

Fluorescent-CdG was used in a DRaCALA assay with purified HrcN Δ1-18 (Figure 3.13). An increasing concentration of HrcN causes central localisation of the fluorescent-CdG molecule on a nitrocellulose membrane. This is indicative of protein binding and retardation of the fluorescent molecule. In comparison, no central fluorescent-CdG localisation was observed with H_2O or BSA negative control samples.
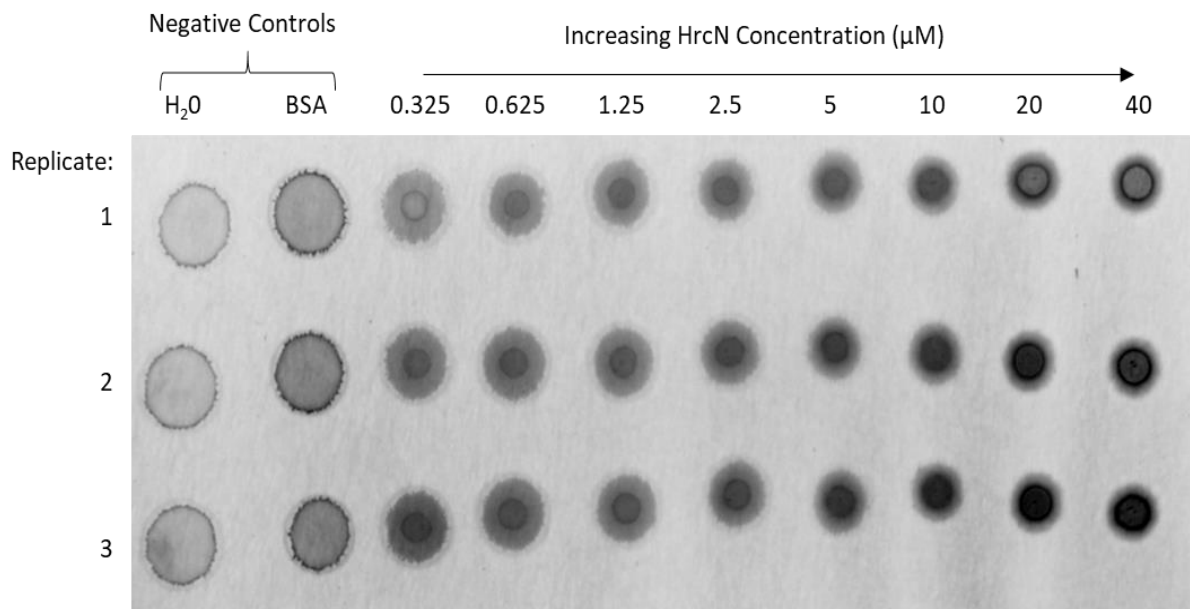
Figure 3.13. Fluorescent-CdG DRaCALA with increasing concentrations of purified Δ1-18 WT HrcN. Fluorescent-CdG is included at a fixed 0.6 µM final concentration.

This indication of CdG-binding with HrcN was explored further by investigating the specificity to CdG. This was done with a competition assay where an excess of non-fluorescently labelled nucleotides was added to test for competition for the HrcN binding site against 0.6 µM of fluorescent-CdG (Figure 3.14).

Fluorescent-CdG was displaced and outcompeted for the HrcN binding site by an excess of non-fluorescently labelled CdG. In comparison, the same is not seen for other non-CdG competing nucleotides. This was the case for non-fluorescently labelled CdA, ATP, ADP, NADH, cAMP, GTP, CTP, TTP, PgPg, and cXMP. Central localisation was observed for a fluorescent-CdG-only positive control with no competing non-labelled nucleotides. No central localisation was observed for the H_2O and BSA fluorescent-CdG negative controls which lack the HrcN protein. This confirms that binding to HrcN is specific for CdG.
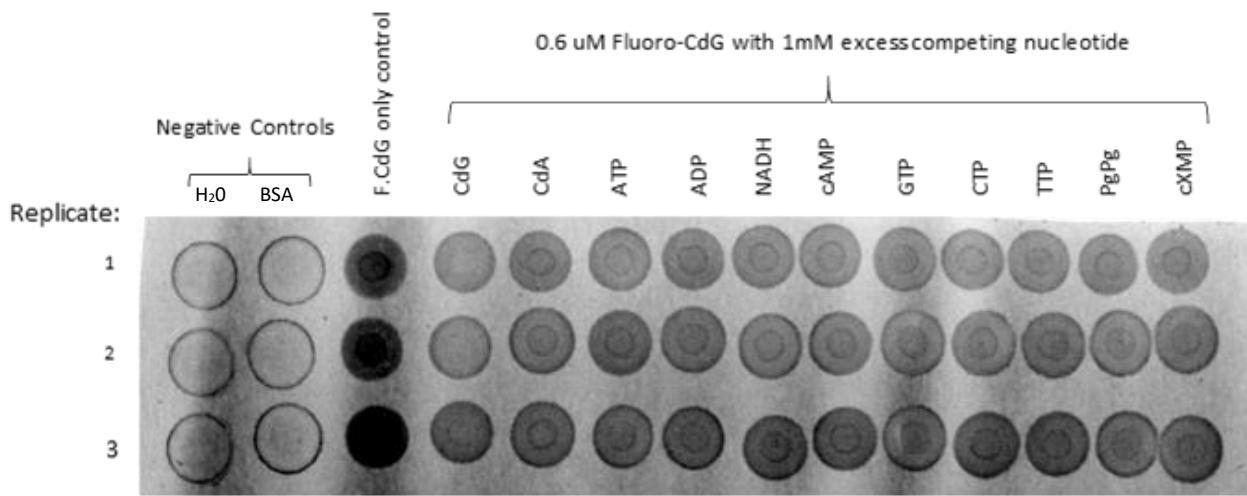
Figure 3.14. Δ1-18 WT HrcN fluorescent-CdG competition DRaCALA with excess unlabelled nucleotides. Fluorescent-CdG is at a fixed 0.6 µM final concentration, non-labelled nucleotides at 1mM.

This binding specificity was explored further with a fluorescent-CdA nucleotide. A DRaCALA was performed with a fixed concentration of fluorescent-CdA mixed with an increasing concentration of purified WT HrcN Δ1-18 (Figure 3.15). No clear central localisation was observed with fluorescent-CdA, despite an increasing concentration of HrcN. There is evidence of small amounts of localisation at high concentrations (40 µM) however the effect of this is minimal. There is no central localisation for the H_2O and BSA negative controls. This confirms that the interaction indicated by DRaCALA central localisation between purified HrcN and fluorescent-CdG is not due to non-specific interaction, and that CdA does not bind to purified HrcN.
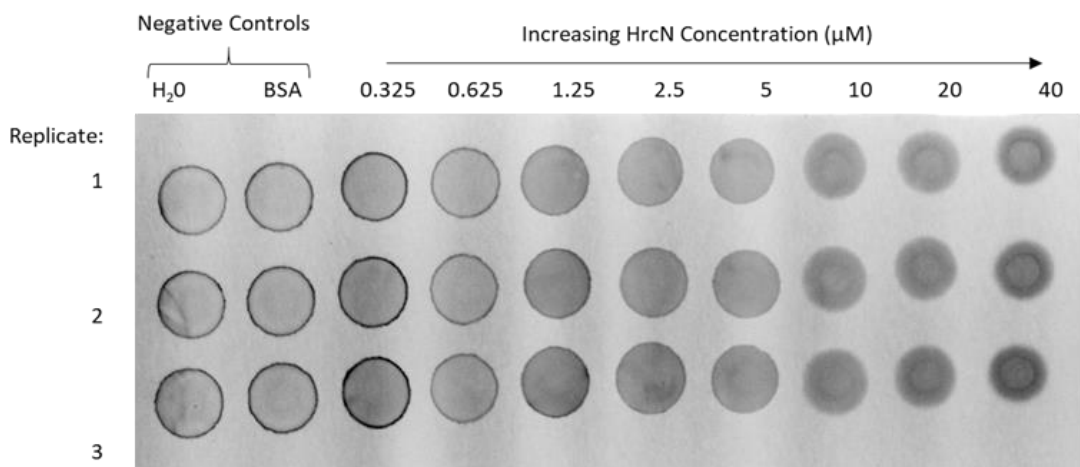
Figure 3.15. Δ1-18 WT HrcN fluorescent-CdA DRaCALA. Fluorescent-CdA is included at a fixed 0.6 µM final concentration.

3.2.5.2.   G176A HrcN Δ1-18

DRaCALA assays were then performed for purified G176A HrcN with fluorescent-CdG (Figure 3.16). Increasing concentrations of G176A HrcN causes a central localisation of fluorescent-CdG on a nitrocellulose membrane, indicative of CdG binding. No such central localisation binding-response of fluorescent-CdG was observed for negative H_2O and BSA controls which lacked the addition of G176A HrcN.
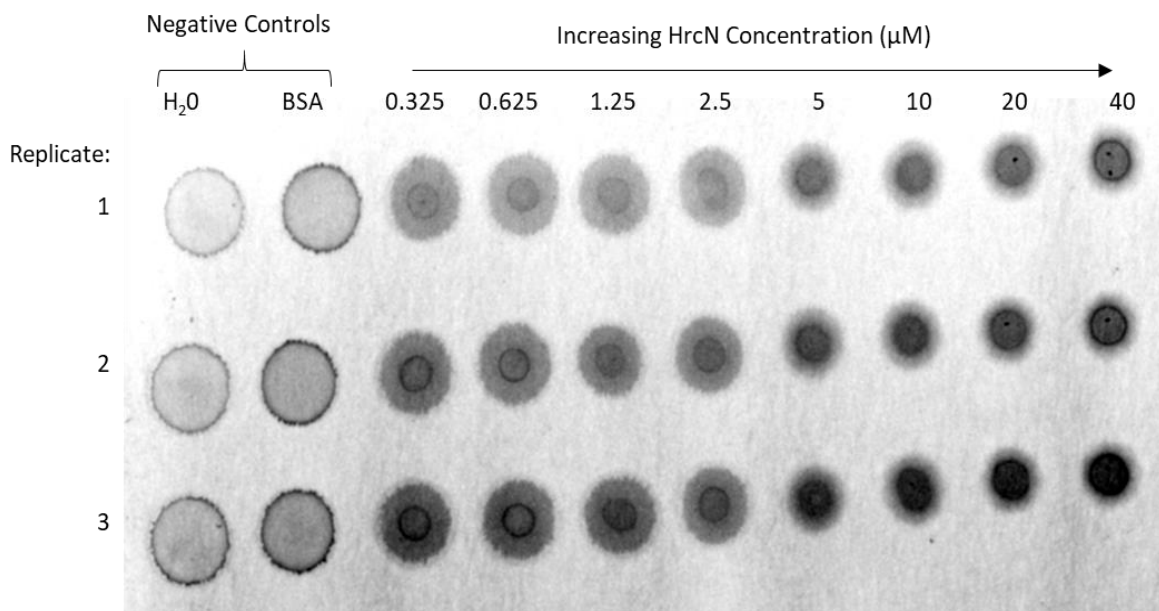
Figure 3.16. Fluorescent-CdG DRaCALA with increasing concentrations of purified Δ1-18 G176A HrcN. Fluorescent-CdG is included at a fixed 0.6 µM final concentration.

Specificity to fluorescent-CdG with G176A HrcN was investigated with a competition DRaCALA where an excess of non-fluorescently labelled nucleotides competed for the HrcN binding site with 0.6 µM fluorescent-CdG (Figure 3.17). 0.6 µM fluorescent-CdG was displaced from the G176A HrcN binding site when mixed with an excess of non-labelled CdG. This was not the case for non-CdG competing nucleotides. An excess of CdA, ATP, NADH, cAMP, GTP, CTP, TTP, PgPg, and cXMP did not displace fluorescent-CdG from the binding site, indicating that the binding interaction for CdG is specific. The fluorescent-CdG-only positive control with no competing non-labelled nucleotides shows expected central localisation. The negative H_2O and BSA controls show no central localisation as expected, confirming that HrcN is binding to CdG rather than due to non-specific interactions.

The excess non-labelled CdG was not able to fully displace all fluorescent-CdG, and a very small amount of localisation remained with these samples. It is likely that this is due to HrcN protein instability, and that the HrcN binding site does not remain fully accessible upon protein degradation. As such, non-labelled CdG may not be able to access all HrcN binding sites, leaving very small quantities of fluorescent-CdG present in a sample leading to subtle signs of central localisation.
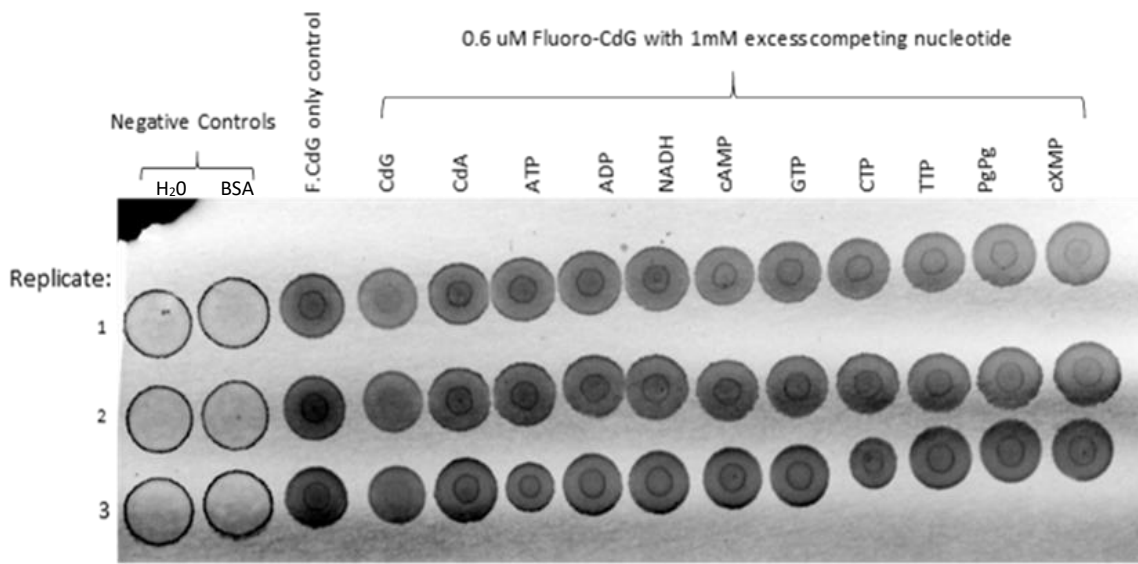
Figure 3.17. Δ1-18 G176A HrcN fluorescent-CdG competition DRaCALA with excess unlabelled nucleotides. Fluorescent-CdG is at a fixed 0.6 µM final concentration, non-labelled nucleotides at 1mM.

The specificity of CdG binding to G176A HrcN was further investigated with a fluorescent-CdA DRaCALA. Increasing concentrations of purified G176A HrcN were mixed with 0.6 µM fluorescent-CdA and spotted onto a nitrocellulose membrane (Figure 3.18). No indication of central fluorescent-CdA localisation was seen when mixed with G176A HrcN other than subtle non-specific interaction at high concentrations. Negative H_2O and BSA controls also do not show any central localisation. This confirms that G176A HrcN does not bind specifically to CdA, and that the interaction between G176A HrcN and CdG is a specific interaction.
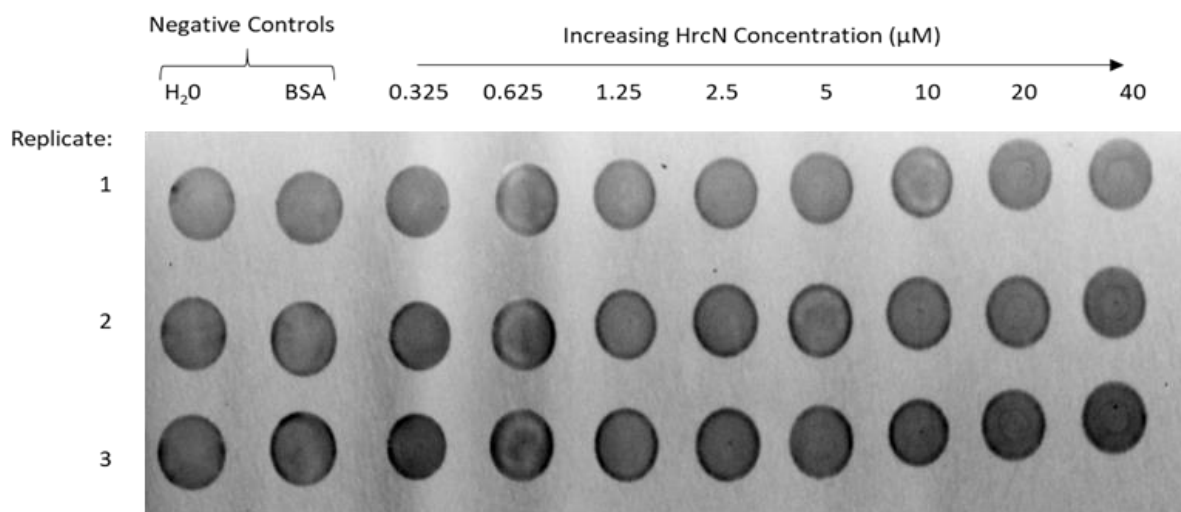
Figure 3.18. Δ1-18 G176A HrcN fluorescent-CdA DRaCALA. Fluorescent-CdA is included at a fixed 0.6 µM final concentration.

3.2.6. Analytical Gel Filtration Shows Differences in CdG-induced Oligomerisation for Full-length G176A HrcN

Oligomerisation of WT vs G176A HrcN purified proteins was tested using gel filtration to analyse any differences present upon CdG addition. Both full-length and N-terminal truncated HrcN proteins were tested. Full-length HrcN retains the predicted multimerization domain and should show some degree of oligomerisation, while N-terminal truncations lack this domain and so will not be able to oligomerise.

3.2.6.1. WT HrcN (Full-length) Shows Evidence of Dodecamer Formation with CdG Addition

Full-length WT HrcN was purified and loaded immediately onto an analytical gel filtration column (GE Healthcare Superdex 200 10/300 GL Increase) in the absence or presence of 50 µM CdG. The WT HrcN was co-expressed with a non-purified BifA phosphodiesterase to ensure low background CdG-levels and minimise the impact of cellular cdG on protein behaviour. The analytical gel filtration runs (+/- CdG) are shown in Figure 3.19.

A series of peaks were observed when run without prior incubation with CdG. A very small peak can be seen at approximately 7 mL. It is probable that this is a void peak of aggregate proteins. At 13 mL, a large peak can be seen which is likely to be monomeric HrcN (48.4 kDa). Any peaks following this are likely to be small contaminating proteins and components of the buffer.

Upon addition with 50 µM CdG, two new peaks are seen. The single peak at 7 mL, forms a secondary double peak. This is likely to be separation between the void aggregate peak and a small dodecamer peak forming (580 - 800 kDa). A large peak at 21 mL forms, which is likely the added CdG (690 Da) due to its small size.
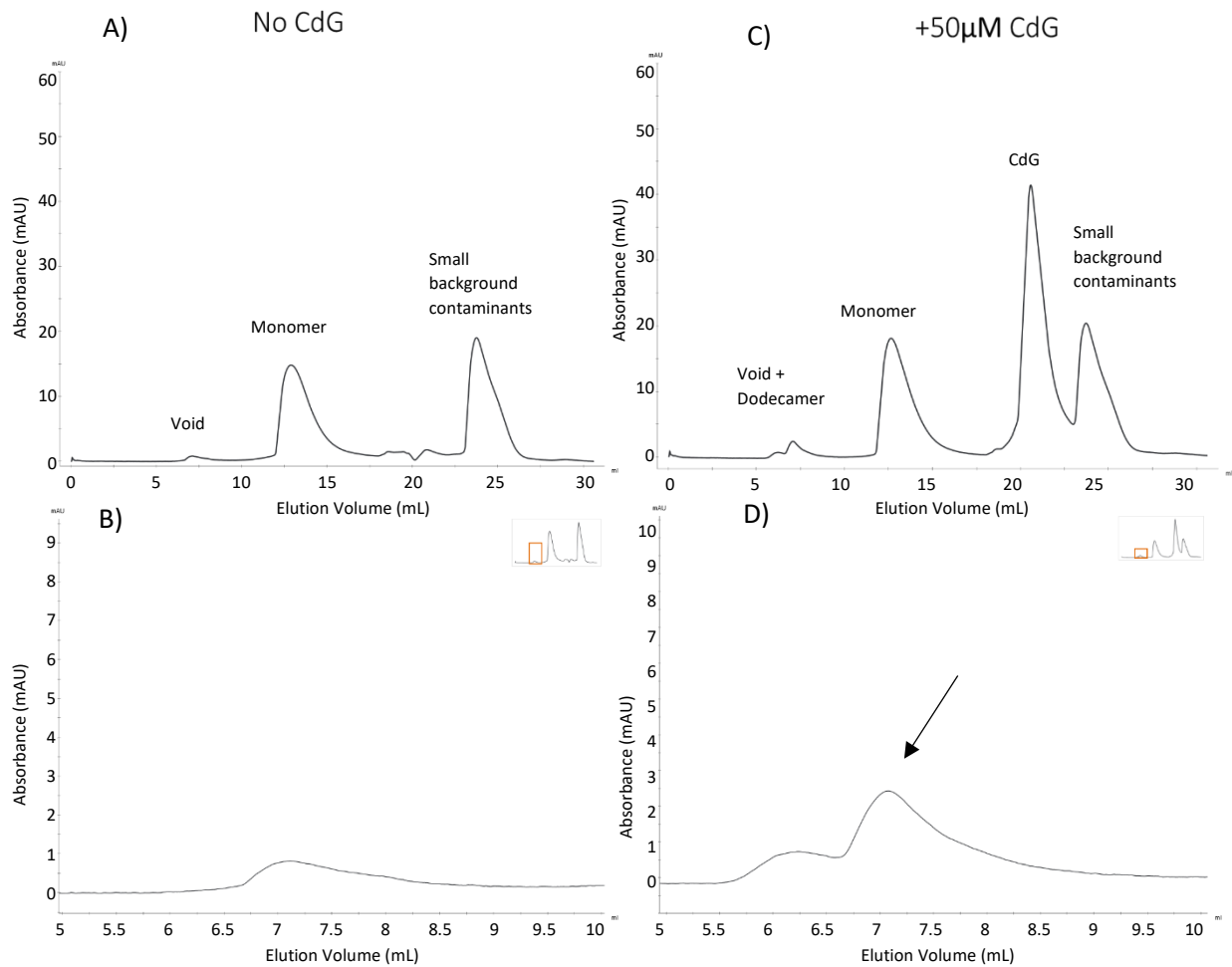
Figure 3.19. Analytical gel filtration run for purified full-length WT HrcN on a Superdex 200 10/300 GL Increase analytical gel filtration column. 500 µL of sample loaded at 1 mg/ml (approximately 30 µM). A) shows a run without the addition of CdG where B) is a close-up of the expected dodecamer retention region from the same run. C) shows a run with the addition of 50 µM CdG (incubated prior to column-loading) where D) is a close-up of the expected dodecamer retention region from the same run. The proposed dodecamer peak has been highlighted with a black arrow. Purified proteins were co-expressed with a non-purified BifA phosphodiesterase for a low CdG background.

3.2.6.2. G176A HrcN (Full-length) Does Not Show Evidence of Dodecamer Formation with CdG Addition

Next, full-length G176A HrcN was purified and loaded immediately onto an analytical gel filtration column (GE Healthcare Superdex 200 10/300 GL Increase) in the absence or presence of 50 µM CdG. As before, G176A HrcN was co-expressed with a non-purified BifA phosphodiesterase for low background CdG-levels. These analytical gel filtration runs (+/- CdG) are shown in Figure 3.20.

Similar to the full-length WT HrcN, a series of peaks can be seen in the absence of CdG. These include a possible void peak at 7mL, and a possible monomer peak at 13 mL. Smaller peaks can be seen comparable to the WT which are likely to be small contaminating proteins and buffer components.

With the addition of CdG, unlike with WT HrcN, full-length G176A HrcN does not show formation of a double peak around 7 mL. It is possible that only protein aggregates are forming, and that efficient

formation of a dodecamer is not possible or is too unstable. A large peak at 21 mL forms as seen with the WT, which is likely to be the added CdG.
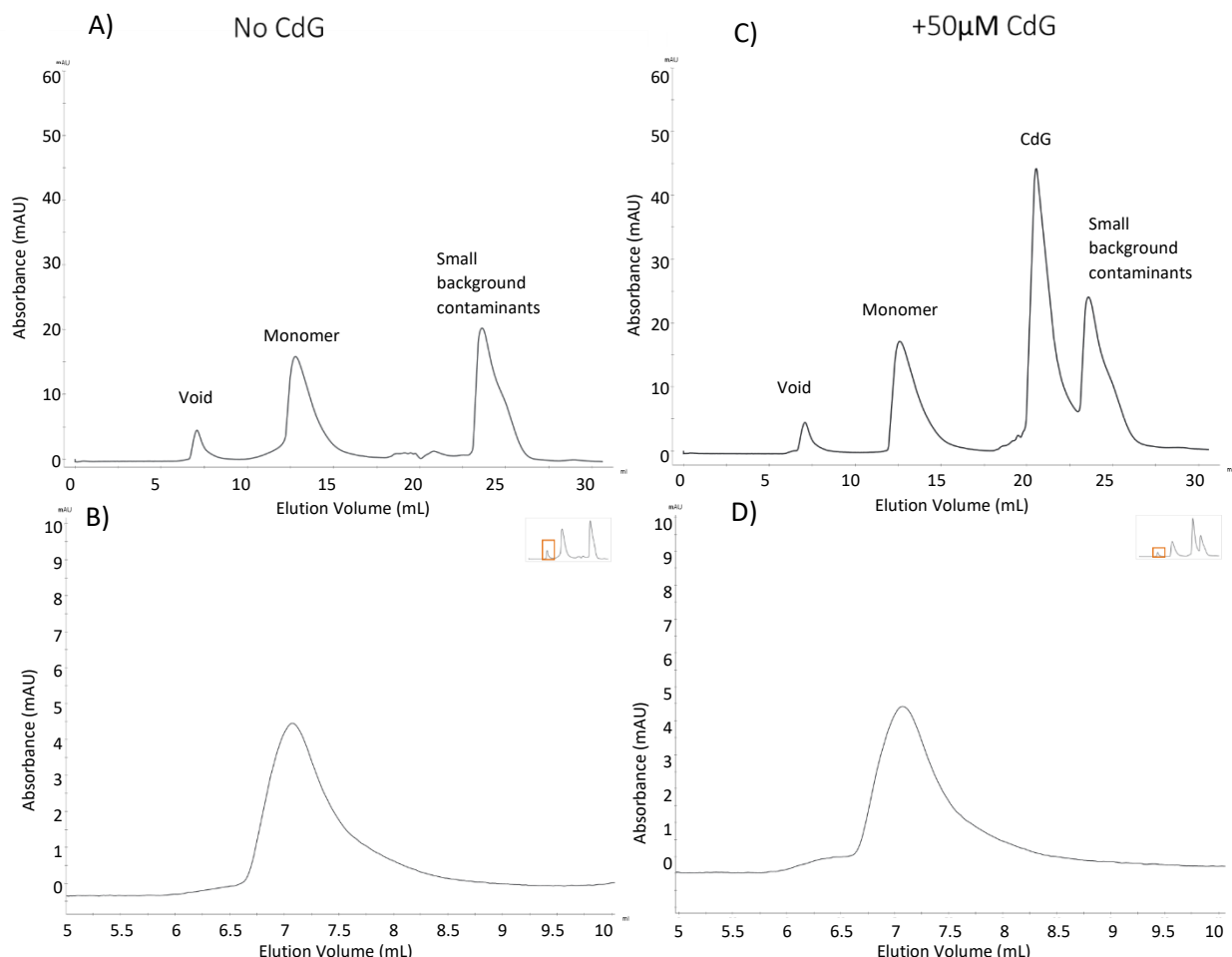
Figure 3.20. Analytical gel filtration run for purified full-length G176A HrcN on a Superdex 200 10/300 GL Increase analytical gel filtration column. 500 µL of sample loaded at 1 mg/ml (approximately 30 µM). A) shows a run without the addition of CdG where B) is a close-up of the expected dodecamer retention region from the same run. C) shows a run with the addition of 50 µM CdG (incubated prior to column-loading) where D) is a close-up of the expected dodecamer retention region from the same run. Purified proteins were co-expressed with a non-purified BifA phosphodiesterase for a low CdG background.

3.2.6.3. WT HrcN (N-terminal Truncation Δ1-18) Does Not Show Evidence of Dodecamer Formation with CdG Addition

N-terminal truncated (Δ1-18) WT HrcN was purified and loaded immediately onto an analytical gel filtration column (GE Healthcare Superdex 200 10/300 GL Increase) in the absence or presence of 50 µM CdG. The truncated WT HrcN was co-expressed with a non-purified BifA phosphodiesterase for low background CdG-levels. These analytical gel filtration runs (+/- CdG) are shown in Figure 3.21.

The N-terminus is believed to be the predicted multimerization domain for HrcN, and it is necessary for proper oligomerisation (monomers into dodecamers). Upon truncation of this domain, there was no evidence for dodecamer formation compared to the full-length WT HrcN.

Without CdG, a single possible void peak can be seen at 7 mL, and a possible monomer peak at 13 mL. Smaller contaminating proteins and buffer components can be seen, comparable to previous sample

runs. With 50 µM CdG incubation prior to loading on the column, N-terminal truncated WT HrcN does not appear to show a double peak forming at 7 mL in contrast to the full-length WT, suggesting that dodecamers are unable to form. The single peak for CdG is present at 21 mL as previously seen.
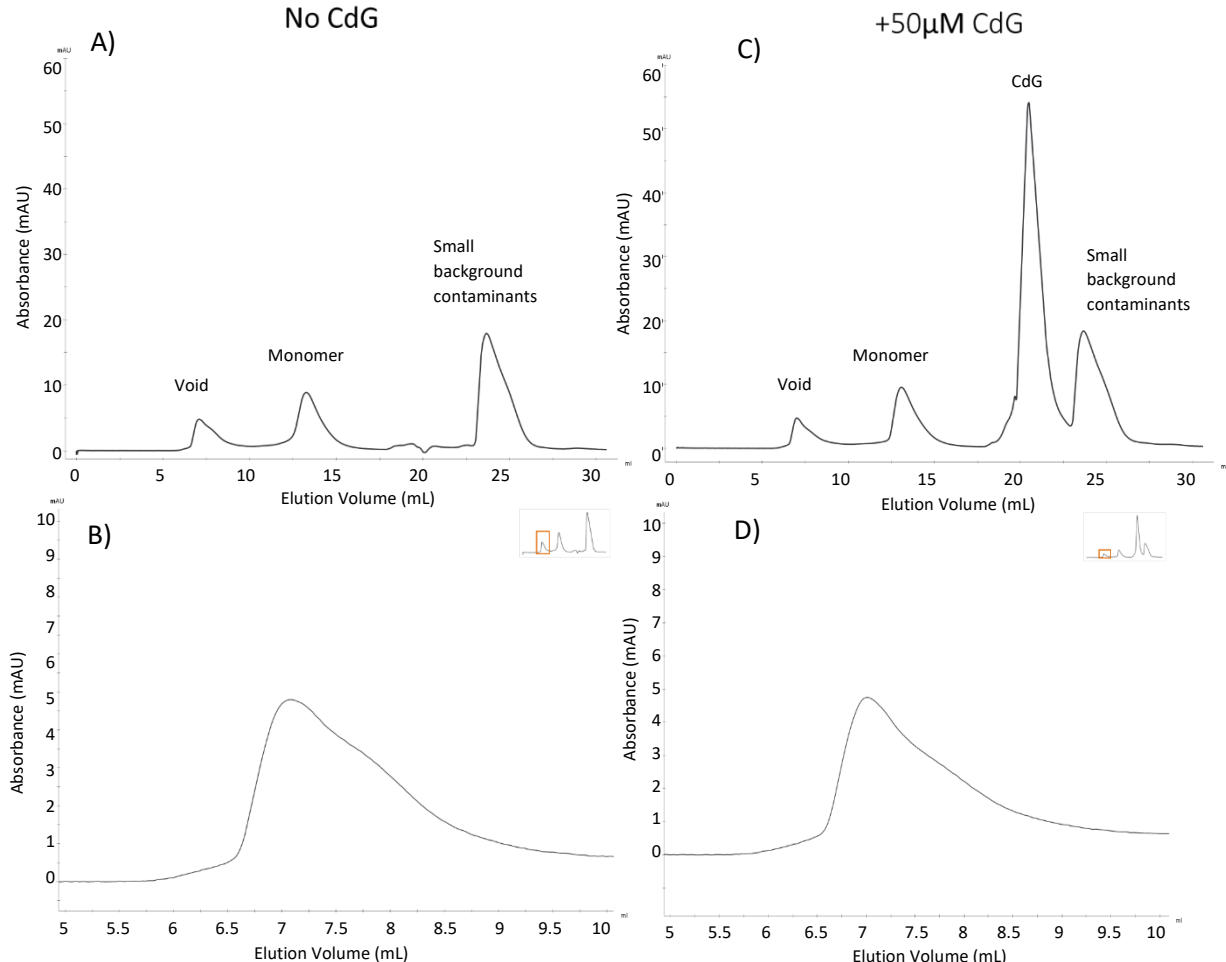
Figure 3.21. Analytical gel filtration run for purified Δ1-18 WT HrcN on a Superdex 200 10/300 GL Increase analytical gel filtration column. 500 µL of sample loaded at 1 mg/ml (approximately 30 µM). A) shows a run without the addition of CdG where B) is a close-up of the expected dodecamer retention region from the same run. C) shows a run with the addition of 50 µM CdG (incubated prior to column-loading) where D) is a close-up of the expected dodecamer retention region from the same run. Purified proteins were co-expressed with a non-purified BifA phosphodiesterase for a low CdG background.

3.2.6.4.   G176A HrcN (N-terminal Truncation Δ1-18) Does Not Show Evidence of Dodecamer Formation with CdG Addition

N-terminal truncated G176A HrcN Δ1-18 was purified and loaded immediately onto an analytical gel filtration column (GE Healthcare Superdex 200 10/300 GL Increase) in the absence or presence of 50 µM CdG. Truncated G176A HrcN was co-expressed with a non-purified BifA phosphodiesterase for low background CdG-levels. These analytical gel filtration runs (+/- CdG) are shown in Figure 3.22.

A comparable result is seen for both N-terminal truncated WT and full length G176A HrcN. There is no evidence of dodecamer formation. A possible void peak is present at 7 mL, with a possible monomer peak present at 13 mL without the addition of CdG. As previously observed in all other HrcN samples, smaller contaminating background proteins and buffer components are present. With the addition of

CdG, no double peak is evident at 7 mL. A single possible CdG peak forms at 21 mL as previously seen in other described HrcN samples.
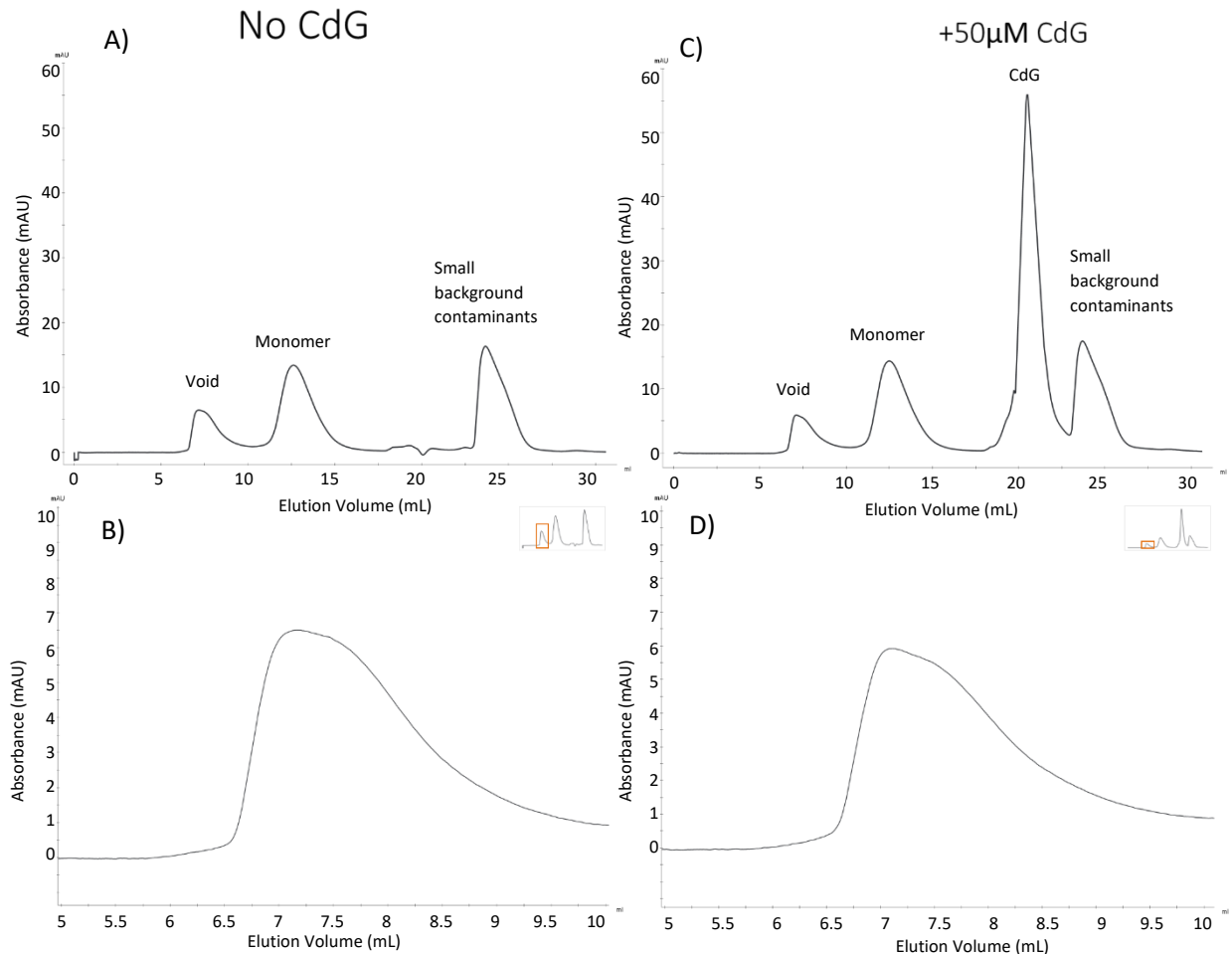
Figure 3.22. Analytical gel filtration run for purified Δ1-18 G176A HrcN on a Superdex 200 10/300 GL Increase analytical gel filtration column. 500 µL of sample loaded at 1 mg/ml (approximately 30 µM). A) shows a run without the addition of CdG where B) is a close-up of the expected dodecamer retention region from the same run. C) shows a run with the addition of 50 µM CdG (incubated prior to column-loading) where D) is a close-up of the expected dodecamer retention region from the same run. Purified proteins were co-expressed with a non-purified BifA phosphodiesterase for a low CdG background.

3.2.7. Mass Photometry (Refeyn) Supports Compromised CdG-induced Dodecamerisation Ability for G176A HrcN

3.2.7.1. WT HrcN (Full-length) Shows a Dodecamer-like Peak with CdG

The isolated suspected dodecamer fraction from analytical gel filtration HrcN runs were further analysed using mass photometry to gain a more solid understanding of whether dodecamer formation was indeed impaired in G176A HrcN or not. Purified HrcN proteins were immediately loaded onto an analytical gel filtration column (GE Healthcare Superdex 200 10/300 GL Increase) in the absence or presence of 50 µM CdG. The isolated suspected dodecamer fraction at 7 mL was immediately collected and loaded onto a Refeyn mass photometry machine.

The mass photometry analyses for full-length WT HrcN isolated dodecamer fractions (+/- CdG) can be seen in Figure 3.23. Without CdG, most of the sample exists in a monomeric state. It is likely that this is either due to unstable higher-order complexes dissociating, or due to monomeric contamination pulled from the high-concentration monomeric fraction. There is some evidence for higher-order aggregates spread across the sample demonstrated by a noisy baseline, however no single clearly defined peak is present. This is likely due to there being low concentrations of aggregates of varying sizes present as opposed to a high-concentration aggregate of a single fixed size.

With the addition of 50 µM CdG, a small peak can be seen around 600 kDa. This is the approximate size of a dodecamer. It is possible that any HrcN dodecamer that forms is relatively unstable, hence the small peak, with much of the dodecamer falling back into a monomeric state after coming off the column.
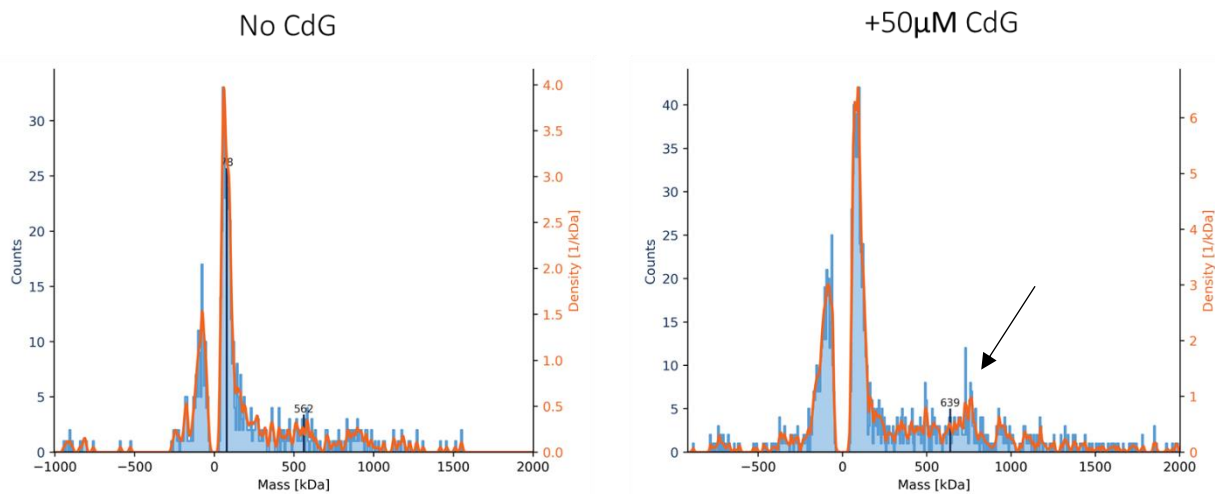
Figure 3.23. Oligomeric analysis of purified full-length WT HrcN (isolated dodecamer fraction only) using Refeyn mass photometry. Left panel shows run without the addition of CdG, right panel shows sample incubation with 50 µM CdG prior to column run. Purified proteins co-expressed with a non-purified BifA phosphodiesterase for a low CdG background. The predicted dodecamer peak is highlighted with an arrow.

3.2.7.2.   G176A HrcN (Full-length) Does Not Show a Dodecamer-like Peak with CdG

The mass photometry analyses for full-length G176A HrcN isolated dodecamer fractions (+/- CdG) can be seen in Figure 3.24. Without the addition of CdG, only background monomeric protein can be detected with no indication of any other clearly defined peaks. With 50 µM CdG, in contrast to the full-length WT HrcN which showed some evidence of a dodecamer around 600 kDa, no such small peak is observed for full-length G176A HrcN. From this, it could be suggested that full-length G176A is unable to form dodecamers, can only form dodecamers very inefficiently, or that these dodecamers are highly unstable and rapidly revert to a monomeric state.
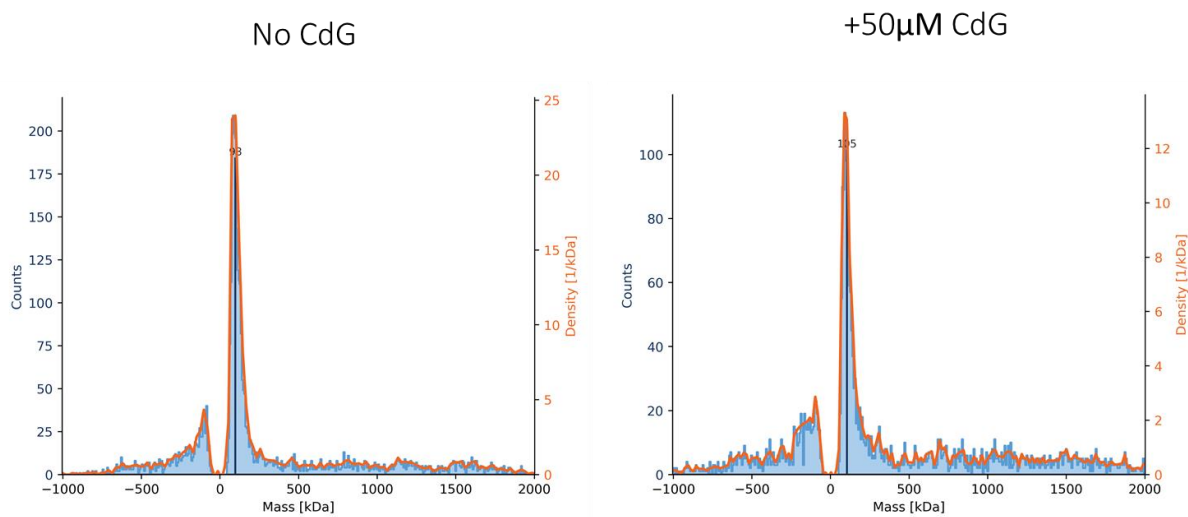
Figure 3.24. Oligomeric analysis of purified full-length G176A HrcN (isolated dodecamer fraction only) using Refeyn mass photometry. Left panel shows run without the addition of CdG, right panel shows sample incubation with 50 μM CdG prior to column run. Purified proteins co-expressed with a non-purified BifA phosphodiesterase for a low CdG background.

3.2.8. Structural Predictions of the HrcN Protein Give Insights into Oligomerisation and CdG Binding

3.2.8.1. AlphaFold Structural Prediction Was Performed

Finally, structural prediction and modelling of HrcN were performed. Experimental structural work was started but due to the unstable nature of the HrcN purified protein, *in silico* structural prediction was deemed to be the more appropriate technique. AlphaFold (DeepMind) artificial intelligence-driven protein structure prediction software was used to model the HrcN protein using deep learning algorithms (Jumper et al., 2021).

Shown in Figure 3.25 is the predicted structure for HrcN produced using AlphaFold version 2.1.0 where the HrcN amino acid sequence was submitted A rainbow-coloured ribbon model is shown in Figure 3.25 A where blue represents the N-terminus, and red represents the C-terminus. In Figure 3.25 B is a Coulombic electrostatic potential space-fill model where red are regions of negative predicted electrostatic potential, and in blue are regions of positive predicted electrostatic potential. A close-up view of HrcN showing the predicted CdG binding residues that were mutated as part of this study are shown in Figure 3.25 C.
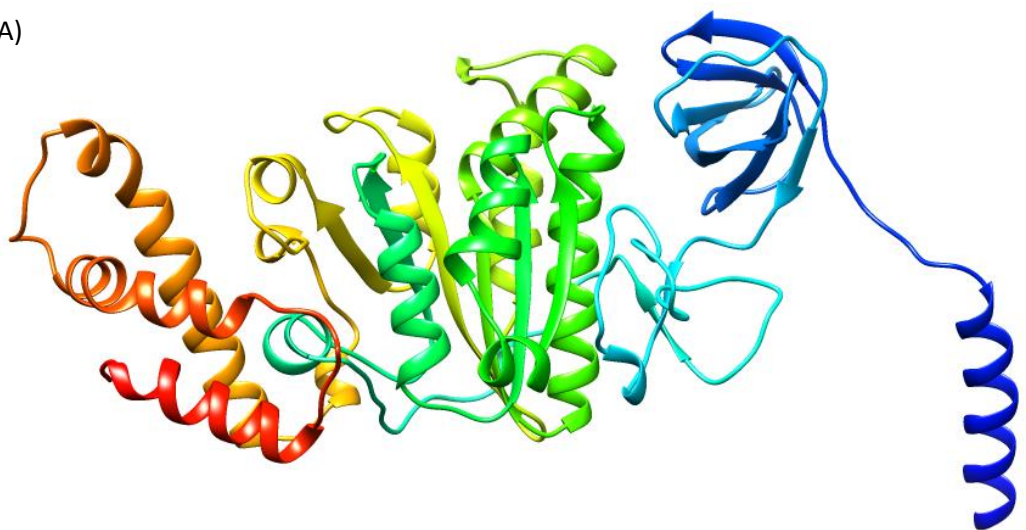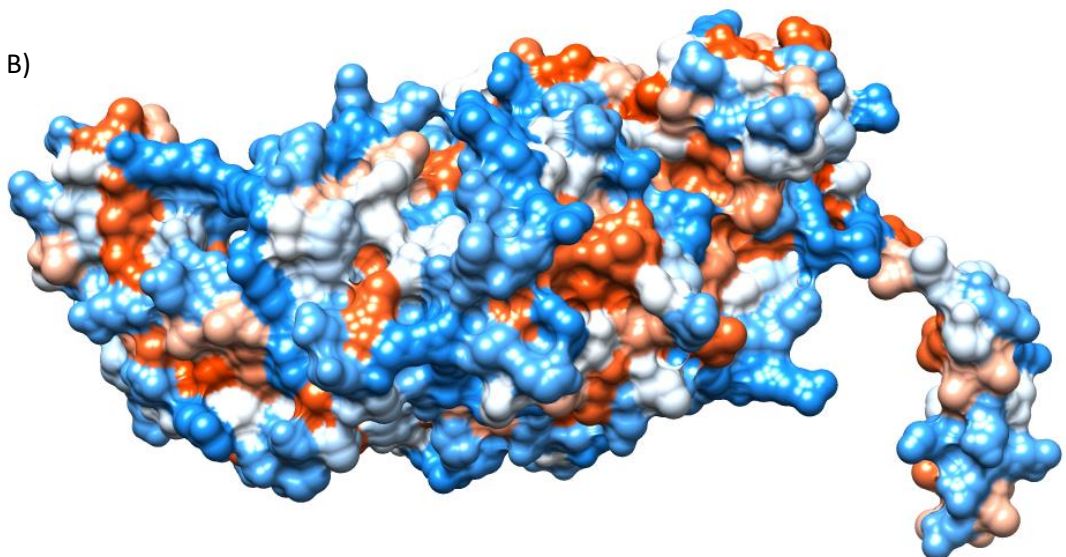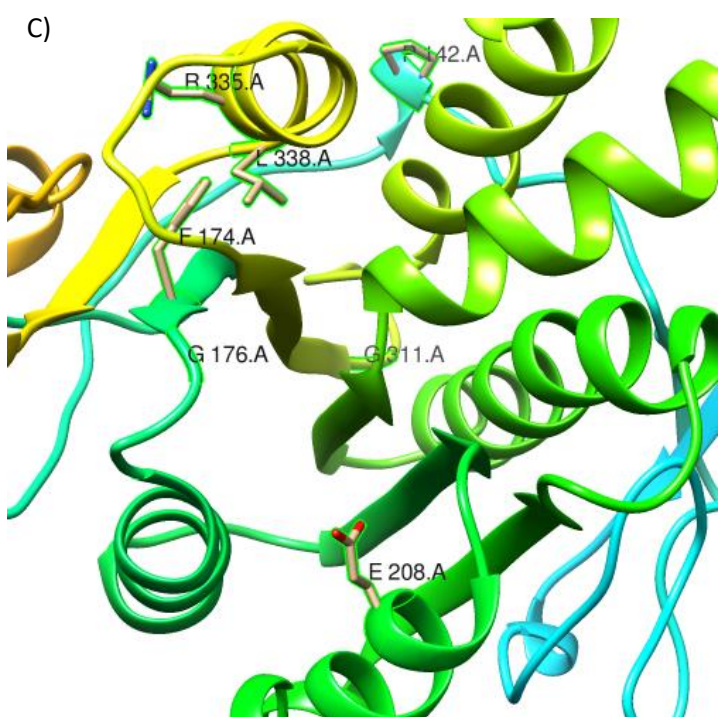
Figure 3.25. Predicted AlphaFold monomeric structure for WT HrcN T3SS ATPase from *P. syringae Pto* DC3000, visualised via UCSF Chimera. A) shows a ribbon-model representation of secondary structure features with rainbow colouration where blue represents the N-terminus, and red represents the C-terminus. B) shows a Coulombic electrostatic potential space-fill model where red are regions of negative predicted electrostatic potential, and in blue are regions of positive predicted electrostatic potential. C) shows labelled key predicted CdG binding interface residues mutated as part of this study (First letter denotes the residue, numbers denote residue position, final

3.2.8.2. Comparison to SWISS-MODEL and Phyre2 Structural Predictions Shows Similar Physical Features

The AlphaFold structural prediction from the previous section was compared against other structural prediction software. SWISS-MODEL and Phyre2 homology modelling structural prediction software use a different algorithmic methodology compared to AlphaFold, which draws upon artificial intelligence. SWISS-MODEL and Phyre2 are rapidly being viewed as older approaches, and are being superseded by AlphaFold due to its technological advancement. Despite this, these are well-established structural prediction tools, the results of which can be complementary to AI-derived structural predictions. Comparing the more current AlphaFold software to existing well-established tools for HrcN structural prediction helps to add validity to the findings and offers additional insights into the structure of HrcN.

Shown in Figure 3.26 is a comparison between the predicted structure for HrcN using AlphaFold compared to SWISS-MODEL (Figure 3.26 A), and AlphaFold compared to Phyre2 (Figure 3.26 B). Alignments were performed using the inbuilt match align superposition function in UCSF Chimera software version 1.15. The rainbow-coloured structure is the AlphaFold model while the light blue structure is the model being compared. In both cases, models produced by SWISS-MODEL and Phyre2 both show a high level of similarity to the AlphaFold model. There was some variation in the position and angle of structural elements between models, however overall, there were no large differences observed. This helps to add further supporting evidence that the predicted structure generated for HrcN is reliable. To fully confirm the structure of HrcN, experimental structural work would be needed.

A)
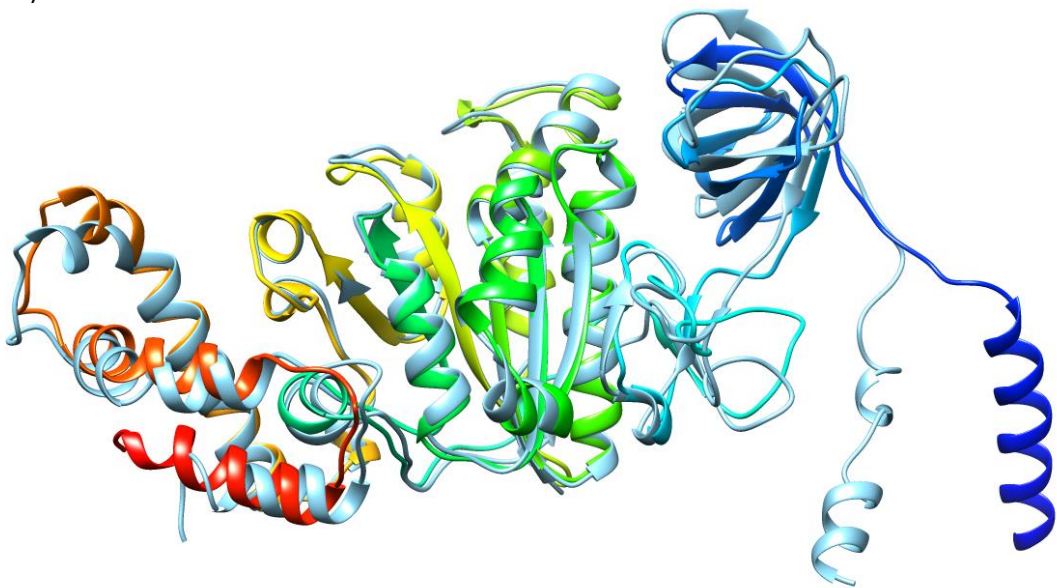
B)
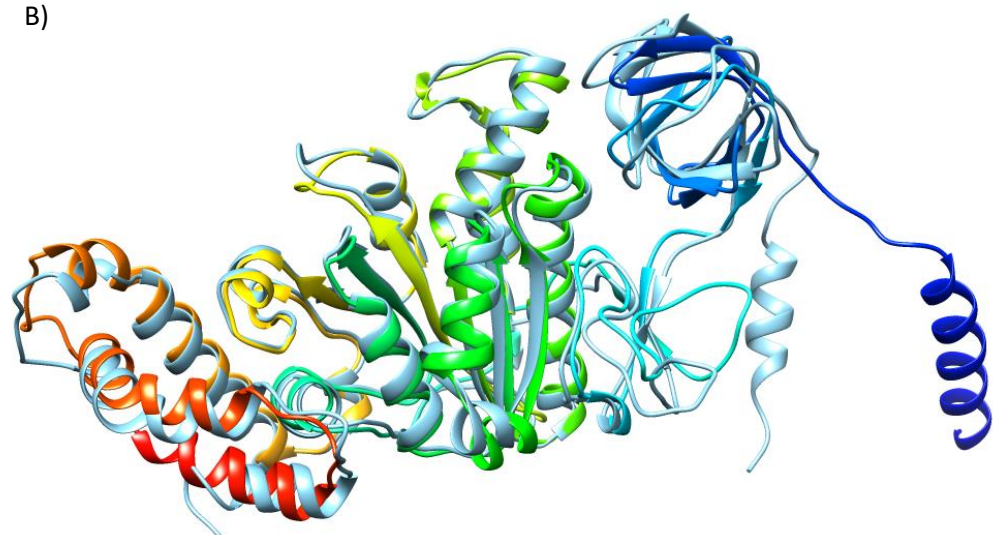
Figure 3.26. Comparison of AlphaFold WT HrcN predicted structure to structural predictions using alternative software. The AlphaFold predicted structure is shown in rainbow-colours, while the structure being compared is in full light blue. A) shows HrcN AlphaFold predicted structure compared to HrcN SWISS-MODEL predicted structure, B) shows HrcN AlphaFold predicted structure compared to HrcN Phyre2 predicted structure.

3.2.8.3. Comparing WT HrcN and G176A HrcN Monomeric Structural Predictions Reveal No Clear Structural Differences

In Figure 3.27, visualisations of G176A HrcN monomeric structural prediction using AlphaFold can be seen. A rainbow-coloured ribbon model is shown in Figure 3.27 A where blue represents the N-terminus, and red represents the C-terminus. This G176A HrcN AlphaFold monomeric structural prediction was compared with the WT HrcN AlphaFold monomeric structural prediction (from Figure 3.26). This comparison can be seen in Figure 3.27 B and C. A very high level of structural similarity overall was observed with only some very minor differences present. Around the glycine to alanine point-substitution at residue position 176, no clear differences in structural prediction were evident. This could be due to potential limitations of the structural prediction software and so further experimental work would be necessary to investigate possible structural differences in more detail. Given the conservative nature of the substitution, it is unlikely that major structural differences would be present.
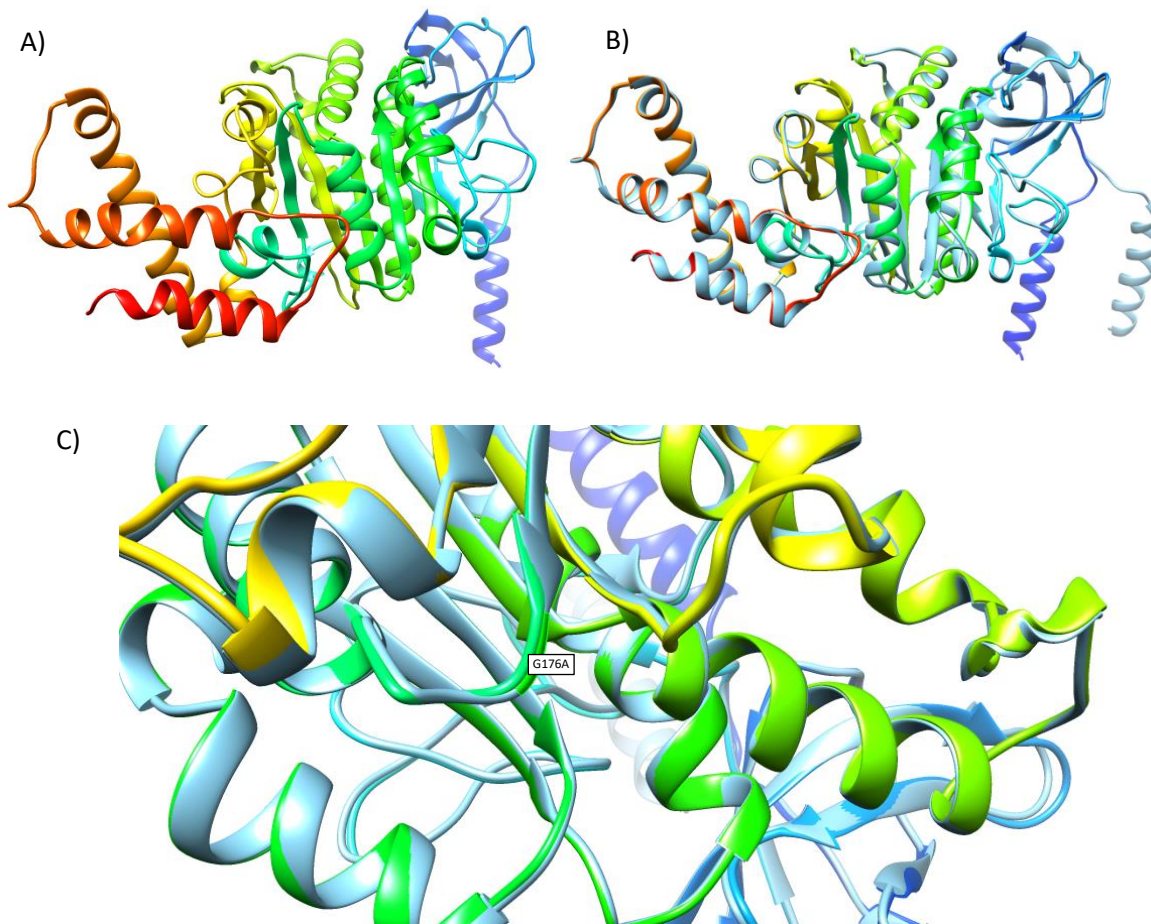
Figure 3.27. Predicted AlphaFold monomeric structure for G176A HrcN, visualised via UCSF Chimera. G176A HrcN is presented as a ribbon-model representation of secondary structure features with rainbow colouration where blue represents the N-terminus, and red represents the C-terminus. A) Shows the predicted G176A HrcN AlphaFold monomer. B) shows a comparison of the AlphaFold predicted G176A HrcN monomer (rainbow-coloured) to the predicted WT HrcN monomer (light blue). C) shows a close-up view of this same comparison centred around the G176A point-substitution.

3.2.8.4. WT HrcN Dodecamer Structural Prediction

Shown in Figure 3.28 is the predicted dodecamer structure for WT HrcN. This was generated using a GalaxyHomomer homo-oligomer prediction tool (Baek et al., 2017). The amino acid sequence was input into the software, and the server automatically predicted the oligomeric state. 12 WT HrcN monomers are predicted to homo-oligomerise to form a dodecamer. This dodecamer structure appeared to consist of two distinct hexameric oligomers joined along the central plane with opposing symmetry.

A)

B)
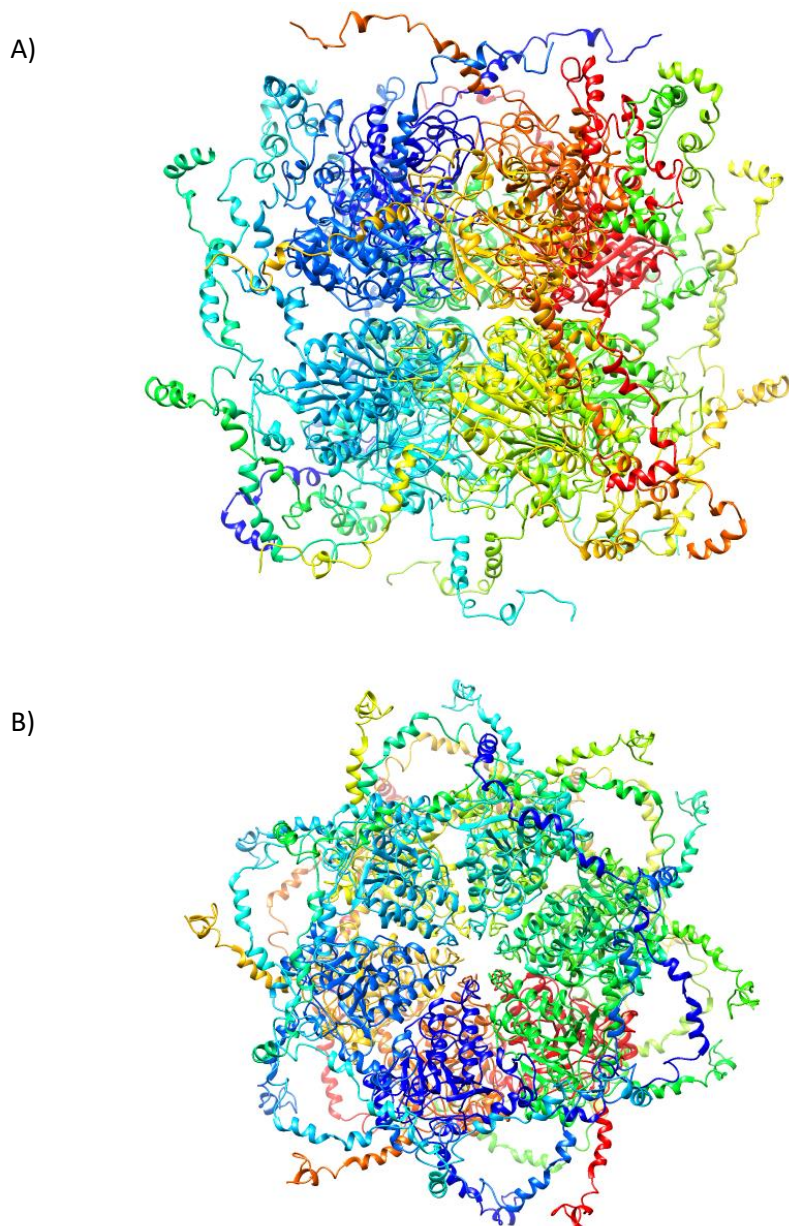
Figure 3.28. Dodecamer homo-oligomer structural prediction for WT HrcN. Structure generated using a GalaxyHomomer online server. The structure is presented as a ribbon-model representation of secondary structure features with rainbow colouration. Each monomer is shown as a different colour. A) Shows a side view of the predicted structure. B) Shows a top-down view of the predicted structure.

3.2.8.5. Comparing WT and G176A HrcN Dodecamer Structural Predictions Show Different Oligomeric Structures

A dodecamer structural prediction for G176A HrcN was generated using an identical approach as with WT HrcN. This was generated using the GalaxyHomomer homo-oligomer prediction tool as before (Baek et al., 2017). Shown in Figure 3.29 A and B is the dodecamer prediction for G176A HrcN. In Figure 3.29 C and D are comparisons between WT and G176A HrcN predicted dodecamers. For G176A HrcN, the predicted dodecamer varies considerably in structure compared to the WT. It could be that this altered G176A version of the dodecamer may be less stable or may form less readily, if at all. This would benefit from further experimental work to explore this hypothesis in greater detail.
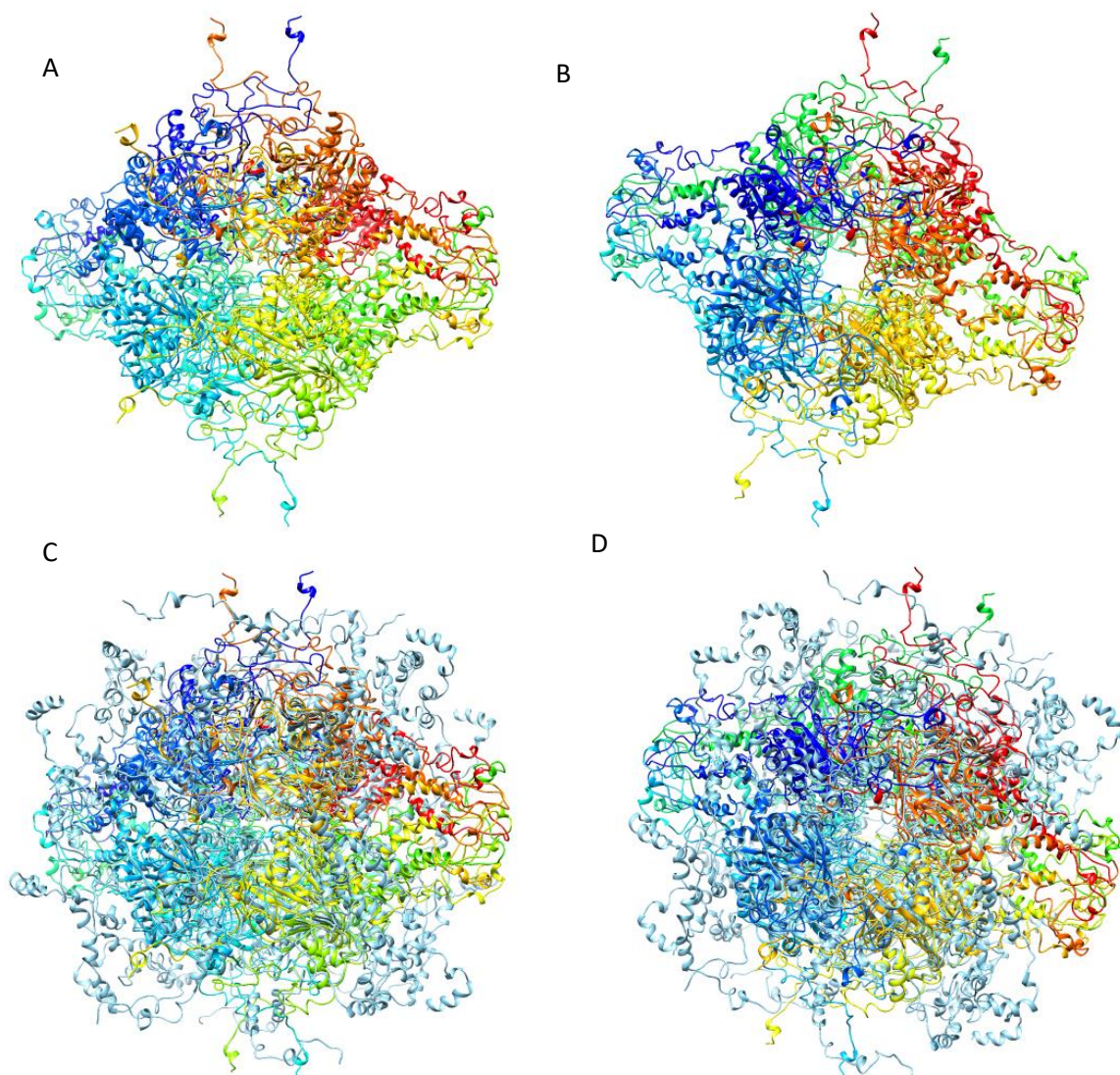
Figure 3.29. Predicted dodecamer structure for G176A HrcN T3SS ATPase generated using GalaxyHomomer. Structures are presented as a ribbon-model representation of secondary structure features with rainbow colouration for G176A where each monomer is a different colour. A) shows a side view of the predicted dodecamer for G176A. B) Shows a top-down view of this same structure. C) Shows a side view comparison of the predicted G176A HrcN dodecamer (rainbow-coloured) against the WT HrcN predicted dodecamer (light blue). D) shows a top-down view of this same comparison.

3.3. Discussion

3.3.1. General Overview

In this section, WT HrcN and point-mutant derivatives were successfully cloned, over-expressed and purified. Upon purification, HrcN was seen to be highly unstable, with rapid precipitation and degradation observed. This is likely due to HrcN being expressed and purified outside of its native host environment. It may be that HrcN requires other neighbouring T3SS-associated proteins and co-factors to provide structural stability. Due to the unstable nature of purified HrcN, *in vitro* work proved challenging. HrcN required fresh purification each day and was loaded immediately into experimental assays to minimise the impact of degradation. Even with these precautions, HrcN was too unstable to conduct a variety of assays, with unreliable and non-robust results emerging. Fortunately, certain assays allowed for demonstration of some key aspects of HrcN function that have been included in this thesis.

Several mutated proteins targeting key residues in the predicted CdG binding site of HrcN were constructed, expressed, purified and screened for ATPase activity. Following this, G176A HrcN was chosen as the main mutant of focus due to interesting downstream responses to CdG. A full-length version and a N-terminal truncated version (which lacked the predicted multimerization domain and so could not oligomerise) were tested in a series of downstream assays following purification. CdG binding for HrcN was confirmed by way of a DRaCALA assay which indicated similar levels of CdG binding for WT compared to G176A.

Full-length WT HrcN showed indication of some dodecamerisation in response to CdG. The response here was lower than expected, however this was likely due to stability issues or due to lack of necessary accessory components removed during the purification process. In comparison however, data for G176A HrcN gave first indication of possible compromised dodecamerisation ability in response to CdG. Across analytical gel filtration and mass photometry experiments, there was no indication of CdG-induced dodecamerisation for this mutant in contrast to the WT. Both WT and G176A lacking their N-terminus as truncated constructs were not able to oligomerise in response to CdG as expected, as this region is the predicted multimerization domain.

Based on the results from this chapter, it can be concluded that while the binding capacity for WT and G176A HrcN remains consistent, downstream CdG-induced oligomeric effects may possibly be disrupted for the G176A HrcN variant. This provides a potential mechanistic insight helping to explain some of the results observed in the chapters that follow. CdG binding seems to play an important role in the correct oligomerisation of HrcN, and this oligomerisation may be necessary for full bacterial type III-mediated virulence. This is explored further in chapters 4 and 5, which investigate type III function *in vivo* in relation to HrcN.

Alongside these new findings, a predicted structure of HrcN was generated using AlphaFold AI-driven structural prediction software. Future work can investigate and verify this structure in more detail with experimental structural work. This is elaborated on further in the discussion chapter. Additionally, in future work, structural prediction confidence can be investigated to better assess the reliability and accuracy of any generated models.

3.3.2. CdG-binding to Similar ATPases

There are some examples of CdG binding to ATPases in the published literature. The best example similar to HrcN is FliI on which this study is based (Trampari et al., 2015). In that study, the addition of CdG led to inhibited ATPase activity *in vitro* (Trampari et al., 2015). A similar CdG binding response

was seen with the distantly related type IV secretion system export ClpB2 rotary ATPase (Trampari et al., 2015). This is contrary to what was observed with purified HrcN in this chapter, where CdG did not significantly alter ATPase activity. This discrepancy could be due to altered mechanistic function with HrcN, differences in protein stability, or due to another unaccounted factor.

In *P. aeruginosa*, CdG was shown to bind to FleQ, an AAA+ ATPase enhancer binding protein transcriptional regulator (Matsuyama et al., 2016). It was shown that the CdG binding site is distinct from the ATPase domain shown with a crystal structure bound to CdG (Matsuyama et al., 2016). CdG was shown to be responsible for oligomeric re-organisation in solution for FleQ, shifting the structure from a dimeric to hexameric state (Matsuyama et al., 2016). This is comparable to HrcN, albeit here a monomeric to dodecamer oligomeric state change is thought to occur.

Another key type of CdG-binding ATPase are those possessing a MshEN domain, which are associated with the type II secretion system. A crystal structure of MshE from *Vibrio cholerae* bound to CdG was produced where two tandem 24-residue highly-conserved nucleotide binding motifs were identified (RLGxx(L/V/I)(L/V/I)xxG(L/V/I)(L/V/I)xxxxLxxxLxxQ) (Wang et al., 2016). Mutating these highly conserved CdG binding residues led to reduced CdG binding and biofilm formation (Wang et al., 2016). As with HrcN, the addition of CdG did not affect ATPase activity (Wang et al., 2016).

A later study investigated type IV pilus-associated PilB ATPase protein subunits from *Geobacter sulfurreducens* where evidence of probable CdG-binding motifs were identified in the N-terminus region (Solanki et al., 2018). No changes to PilB secondary structure was observed with the addition of CdG, suggesting that dodecamerisation inducing ability of CdG may not be universally conserved among all ATPase:CdG binding interactions (Solanki et al., 2018). This PilB assembly ATPase has been shown to regulate exopolysaccharide production in *Myxococcus xanthus* through CdG binding where motility and biofilm formation are closely regulated (Black et al., 2017). CdG binding to the closely related type IV pilin PilB2 ATPase in *Clostridium perfringens* was also confirmed by way of DRaCALA (Hendrick et al., 2017). No change in ATPase activity was seen for PilB2 in response to CdG, similar to that seen with HrcN in this chapter (Hendrick et al., 2017).

These examples highlight that ATPase:CdG binding is seen across multiple systems, and this binding typically results in control of function. Based on current literature, it is thought that CdG binding is linked to ATPase oligomerisation in some instances, and this leads to a form of post-translational regulation. In other cases however, there is no clear link with CdG binding and oligomerisation. There is still uncertainty regarding how widespread this type of regulation is, and the mechanistic details regarding each system.

3.3.3. CdG-induced Oligomerisation

HrcN is a homo-oligomer where 12 monomeric units self-oligomerise to form a dodecamer structure. There was originally uncertainty in the field as to whether HrcN (and similarly related proteins) formed dimers and hexamers instead of dodecamers. As research continued, it seems more likely that HrcN forms dodecamer structures, at least *in vitro* following protein purification. It may be possible that hexamers and dimers are able to form under the right conditions such as with necessary accessory proteins or type III structural components. Based on the data collected in this chapter, there was no indication of any dimer or hexamer formation, however. To better understand the oligomerisation properties of secretion system export ATPases in a more native context, additional techniques may be appropriate. This could include purifying the type III secretion system as a complex so that any necessary accessory proteins are present.

If technology allows, the most optimal experimental approach would be to visualise HrcN oligomerisation *in vivo* throughout infection in relation to CdG:HrcN binding mutants. This could possibly be achieved with fluorescent tags. However, due to the large size of a tag such as green fluorescent protein, this is itself likely to affect oligomerisation ability of HrcN. Despite this however, this approach would allow for fluorescent microscopy where HrcN monomer localisation could be identified in the bacterial cell and may allow for the visualisation of dodecamer formation. This approach faces many technical challenges and distinguishing between monomer and dodecamer states would be difficult. More optimal labelling techniques could be explored such as with quantum dots, chemical probes or smaller fluorescent tags which may help minimise any steric hindrance and may allow for more accurate visualisation of oligomeric state changes.

Alongside HrcN, other similarly related proteins and complexes within bacteria show evidence of CdG-dependent regulation of oligomerisation. The bacterial flagellum shares a high level of structural similarity to the type III secretion system. CdG has been shown to bind FliI of the bacterial flagellum which has been shown to form oligomers, and these oligomers are necessary for flagellum assembly and function (Claret et al., 2003, Trampari et al., 2015). There is evidence that CdG binding to FliI leads to the formation of dodecamer and hexamer structures from monomers and dimers in the case of *P. fluorescens* (Trampari, 2016, Trampari et al., 2015). The multimerization domain of FliI is located in the N-terminal region, similar to HrcN (Minamino et al., 2006).

Other components of the bacterial flagellum have been shown to oligomerise such as the MS-ring (Johnson et al., 2020, Kawamoto et al., 2021). Concentric rings are formed through monomer multimerization resulting in a final structure consisting of 33 or 34 subunits (Johnson et al., 2020, Kawamoto et al., 2021). The flagella MS-ring shares a high level of similarity to T3SS basal body concentric rings. No direct link related to CdG-binding and the oligomerisation of these concentric ring structures has been shown in either the T3SS or the bacterial flagellum. This suggests that CdG-controlled oligomerisation may potentially occur solely at the export ATPase apparatus in relation to the T3SS. Further experimental testing is required to better understand this.

There are also examples of oligomerisation for systems involving substrate transport across membranes where there is no evidence that CdG plays a role. An example is with the formation of hexameric and pentameric oligomeric complexes in the Ton ABC transporter system with ExbBD inner membrane proteins (Maki-Yonekura et al., 2018). While this system binds ATP and forms oligomeric complexes, there is currently no proven link with CdG. This suggests that CdG binding may not be conserved across all forms of ATP-dependent membrane transport or secretion systems. CdG post-translational-dependent regulation of protein secretion may be limited to certain systems such as the type III injectisome.

3.3.4.   Concluding Remarks

To conclude, in this chapter, HrcN was purified and tested *in vitro* to analyse the response to CdG. It was demonstrated that CdG binds to HrcN and that this leads to dodecamerisation. A G176A HrcN point-substitution mutant, which targeted a key binding residue in the predicted CdG binding site, retained CdG binding. However, downstream oligomerisation may possibly be disrupted based on initial evidence. The function of HrcN *in vivo*, is explored in the following chapter.

Chapter 4: Investigating the *in planta* Importance of the
CdG:HrcN Binding Interaction in *P. syringae*

4.1. Introduction

4.1.1. General Overview

In the previous chapter, it was shown that purified HrcN binds to CdG, and that most of the purified protein variants still retain functional enzymatic activity despite mutagenesis. It was also demonstrated that downstream oligomeric differences may be present in response to CdG in relation to a *G176A* mutant. This chapter aims to add biological context to these *in vitro* findings by constructing and testing *in vivo Pseudomonas syringae Pto* chromosomal mutants. These strains will be predominantly tested *in planta* with the well-characterised model organism *Arabidopsis thaliana*, to better understand the underlying plant-pathogen interactions.

4.1.2. Previous CdG-linked Plant Pathogenesis Research Examples

Type III-mediated virulence of *Pseudomonas syringae* has previously been investigated *in planta*, however there is a lack of research that focuses on modification to the T3SS structure in this organism, and less so in relation to CdG-dependent regulation. Despite this, there are varying levels of evidence confirming that CdG is important in the regulation of virulence across a variety of bacterial phytopathogens. One example was a study which investigated the impact of CdG on biosynthesis of T3SS components (Yuan et al., 2018). This study demonstrated that GcpA, a diguanylate cyclase altered levels of H-NS and RsmB, which in turn led to altered T3SS gene expression and virulence in *Dickeya dadantii* infection of *Bactis campestris* (Yuan et al., 2018). Another example looked at the impact of CdG on *Erwinia amylovora (Edmunds et al., 2013)*. The predicted *Edc* diguanylate cyclase was deleted resulting in lower levels of cellular CdG, which in turn led to reduced disease severity on an immature-pear and apple shoot infection model by affecting motility and biofilm formation (Edmunds et al., 2013).

It has predominantly been shown that CdG-dependent regulation occurs at the transcriptional-level. There are some investigative examples looking at post-translational T3SS-regulation with CdG however, so such regulation is not without precedent. In *Pseudomonas aeruginosa* it has been shown that dimeric CdG regulates alginate production in a post-translational manner (Whitney et al., 2015). CdG directly binds to the PilZ domain of Alg44, a protein shown to be necessary for *in vitro* and *in vivo* production of alginate, a component of the *Pseudomonas* biofilm (Whitney et al., 2015). Alginate is important for biofilm formation in some strains of *P. aeruginosa* aiding virulence and antibiotic resistance (Hentzer et al., 2001). CdG was shown to be important for alginate regulation via polymer modification and expression of extracellular alginate epimerases (Martínez-Ortiz et al., 2020). This highlights a previously established link between CdG and post-translational regulation of pathogenicity in *Pseudomonas*. This can then be linked to *Pseudomonas syringae* where an older study previously described how alginate is important for *in planta* virulence and epiphytic fitness (Yu et al., 1999). Related to this, in *Pseudomonas syringae Pto* DC3000, it was shown that high levels of CdG were associated with altered plant colonisation ability and altered immune evasion (Pfeilmeier et al., 2016). Additionally, cyclic-di-GMP has been shown to be important for cyst formation in plant-colonising nitrogen-fixing *Azotobacter vinelandii*, a bacterial species which shares close relation to *Pseudomonas*, belonging to the same *Pseudomonadaceae* family (Martínez-Ortiz et al., 2020). Cyst formation has been shown to be important for bacterial colonisation (Martínez-Ortiz et al., 2020). Collectively, this highlights the important role that CdG plays in regulating aspects of virulence and plant colonisation in a post-translational manner in *Pseudomonas* spp. and closely related organisms.

4.1.3.   The Type III Injectisome and Infection

The T3SS is important for infection in a wide variety of bacteria. This is particularly well studied in species of *Pseudomonas.* It has been shown that in many cases, bacterial colonisation is severely hindered with compromised T3SS function. Examples that highlight this are studies where T3SS function was abolished with deletion of *hrcC* (Deng et al., 1998, Yuan and He, 1996, Roine et al., 1997). This *hrcC* gene encodes a major structural component of the T3SS basal body that is necessary for proper system assembly and function. It was shown that Δ*hrcC P. syringae* was unable to cause disease, bacterial type III substrate secretion was compromised, and that full bacterial colonisation of plant hosts could not be achieved.

Regulation of the T3SS is tightly regulated by HrpRS of the *hrp/hrc* gene cluster in *P. syringae*. A Chp8 diguanylate cyclase in *Pto,* expressed in response to HrpRS, led to PAMP suppression and increases in extracellular polysaccharides, promoting *Pto* DC3000 pathogenicity (Engl et al., 2014). CdG levels were significantly increased upon expression of *chp8* indicating that high CdG levels play an important role in type III-mediated virulence (Engl et al., 2014).

It has been shown that the T3SS ATPase is important for full efficiency substrate translocation from the T3SS in *Salmonella enterica* (Erhardt et al., 2014). However, this study was able to recover protein secretion through the type III secretion system by introducing mutations that increased proton motive force and flagellar substrate levels, despite the presence of a poorly functioning ATPase (Erhardt et al., 2014). The HrcN T3SS ATPase from *P. syringae* is important for T3SS function, however, it is not fully clear the impact this has on virulence. It was previously shown that deletion of *hrcN* abolished type III effector translocation into plant cells (Tian, 2010). Deletion of a closely related HrcN protein from plant pathogen *Xanthomonas campestris* pv. vesicatoria showed that this protein was essential for effector delivery, and as such, for type III-mediated bacterial pathogenicity (Lorenz and Büttner, 2009).

4.1.4.   Immuno-compromised *A. thaliana* (fec and bbc)

Two mutant lines of *A. thaliana* are used in this chapter (fec and bbc) to investigate the *in vivo* disease progression of key *P. syringae* mutants. These plant lines lack a functional immune system due to targeted gene deletions. With the fec *A. thaliana* line, genes *fls2, efr,* and *cerk1* have been knocked-out. In the case of bbc *A. thaliana*, *bak1-5, bkk1-1,* and *cerk1* genes have been knocked-out. These genes are major pattern recognition receptor (PRR) genes, the loss of which compromise downstream immune signalling in the plant.

These lines were developed in the lab of Cyril Zipfel at The Sainsbury Laboratory, UK as part of a study which investigated BAK-1 dependent immune signalling pathways in plants (Schwessinger et al., 2011). These mutant lines originate from a Col-0 ecotype background, where the genes of interest were knocked-out using a combination of mutagenesis, plant crossing, and genotype verification (Schwessinger et al., 2011). This approach builds on an earlier study where various *bak1* mutations were made in *A. thaliana* plants to show that the FLS2 receptor and BAK1 forms a flagellin-induced complex that initiates plant defence (Chinchilla et al., 2007). It was shown that these BAK1 immune-compromised *A. thaliana* plant lines show compromised ROS burst responses to immune elicitors (Schwessinger et al., 2011). A subsequent study used these immune-suppressed *A. thaliana* lines to investigate *P. syringae* pv. tomato disease progression in relation to water-soaking effector proteins (Xin et al., 2016). A more recent study published in 2021 used these immunocompromised *A. thaliana* plant lines to show distinct activation mechanisms of pattern-triggered immunity (PTI) and effector-triggered immunity (ETI) in response to *P. syringae* (Yuan et al., 2021)

4.1.5. Summary

To understand the *in vivo* biological implications of the CdG:HrcN interaction and how this may connect to the biochemistry discussed in the previous chapter, the work in this chapter uses mutant *Pseudomonas syringae* strains to examine the T3SS system operating inside the living organism. Plant host models are used for infection assays to explore the importance of the CdG interaction with the T3SS HrcN ATPase. A variety of hypotheses are tested to try to unpick some of the virulence-associated phenotypes that arise from the results in this chapter.

4.1.6. Chapter Aims

1. To generate mutant *hrcN* constructs (point mutations of key residues in the predicted CdG binding site) to integrate into the *P. syringae Pto* DC3000 genome via allelic exchange.
2. To test these mutants in a selection of *in vivo* assays to understand the importance of the CdG:HrcN interaction in plant infection.

4.2. Results

4.2.1. *hrcN* Site-specific Mutants in *P. syringae* Were Successfully Created

4.2.1.1. Mutagenesis

Pseudomonas syringae strains suitable for *in vivo* analyses were created. Like the *in vitro* constructs generated in the previous chapter, these *in vivo* mutants forced substitutions of key residues in the predicted CdG-binding site in HrcN. The *in vivo* mutants were constructed to have the same point-mutations as the *in vitro* constructs to allow for comparison between experiments, and to make links between *in vivo* and *in vitro* HrcN function.

Construction of these *in vivo* mutant strains was achieved by producing mutant *hrcN* fragments via overlap extension PCR that were then ligated into a pTS-1 vector. This allowed for *sacB*-based sucrose counterselection and subsequent chromosomal integration via allelic exchange. In this process, a modified gene fragment homologous to *hrcN* in the *Pto* DC3000 chromosome was inserted into pTS1. This modified *hrcN* fragment was constructed with genetic mutations that encode for key amino acid residue substitutions in the HrcN:CdG predicted binding site. This mutagenesis was performed using multi-stage overlap-extension PCR which allowed for precise and targeted base changes. These mutated *hrcN* fragments were then integrated into the *Pto* DC3000 chromosome via allelic exchange by homologous recombination. Double-crossover events at the region of interest were screened for using a multi-step tetracycline selection and *sacB*-counterselection screening process. Double-crossover candidates were verified by colony PCR and Sanger sequencing.

The first round of overlap extension PCR for *hrcN* chromosomal integration mutant constructs is shown in Figure 4.1. Here two fragments of around 250 bp to 400 bp can be observed for each of the constructs where A represents the front half of the mutated sequence and B represents the back half. These two halves were subsequently annealed at their overlapping sequence sites in the second round of overlap extension PCR. This was ultimately successful for all *hrcN* chromosomal integration primary-PCR reactions.
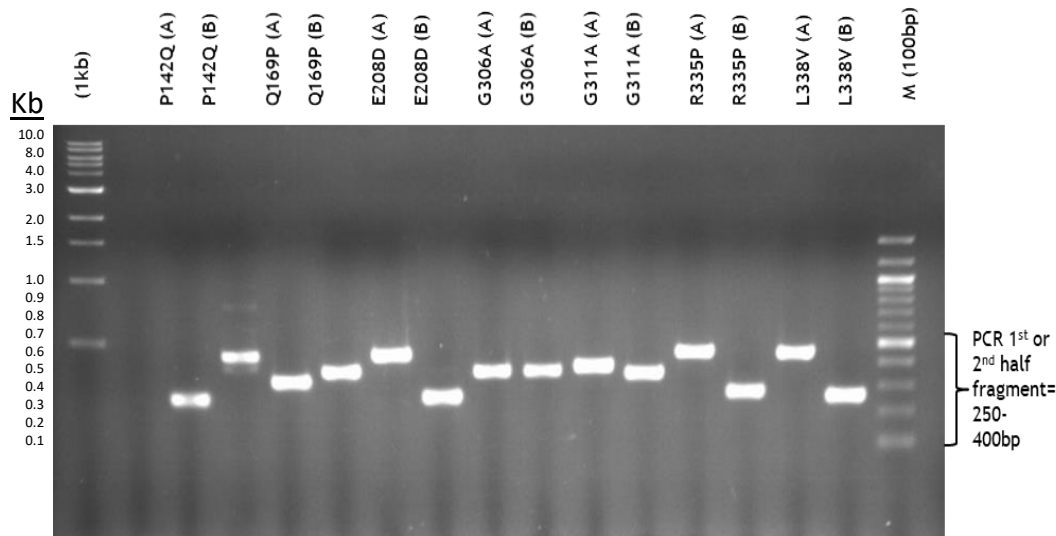
Figure 4.1. First round of over-lap extension PCR for *hrcN* chromosomal integration mutant constructs. A 250 to 400 bp fragment was created for generation of a selection of *hrcN* mutagenesis of key residues in the predicted HrcN:CdG binding site. The letter A indicates the first half of a mutant fragment, the letter B indicates the latter half.

As shown in Figure 4.2, the front (A) and back (B) halves of the primary overlap extension PCR products for each mutation have been used to amplify a full length mutant *hrcN* construct. This can be seen at the expected region of 700 bp.
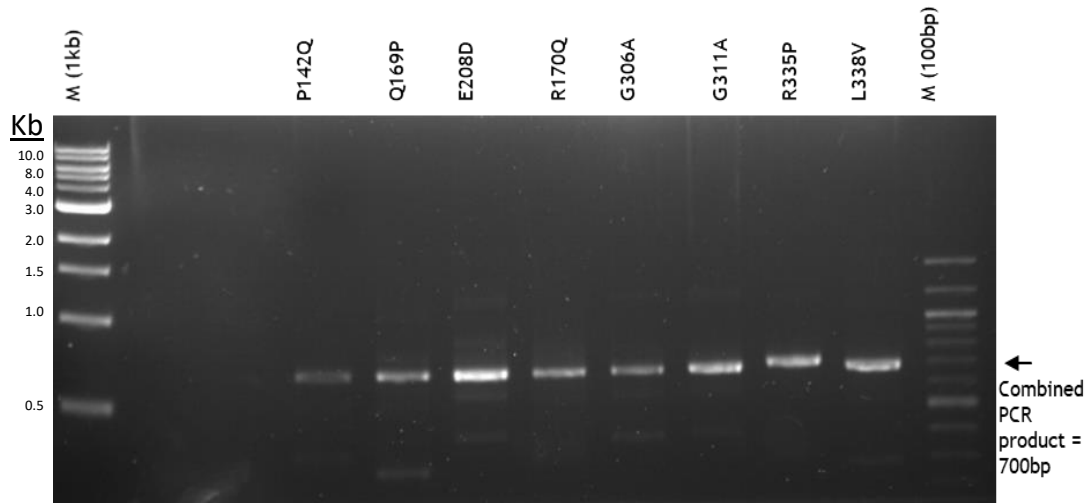
Figure 4.2. Second round of overlap extension PCR for *hrcN* chromosomal integration mutant constructs. Combined PCR fragments of approximately 700 bp were generated in each case.

4.2.1.2. Cloning

Successful ligation of mutant *hrcN* into the pTS-1 chromosomal integration vector was verified with colony PCR on transformed colonies. Restriction digest of the plasmids extracted from those colonies followed by Sanger sequencing was used to ensure the mutated gene sequence was correct and contained the desired mutation at the expected position in each case.

Shown in Figure 4.3, is an example colony PCR reaction demonstrating successful amplification of the cloned *hrcN* gene into DH5α *E. coli*. The chromosomal integration *hrcN* mutant gene construct can be observed at the expected length of 700 bp. Not shown are the other *hrcN* mutants, however these showed similar positive results with the expected 700 bp *hrcN* mutant amplified in each case.
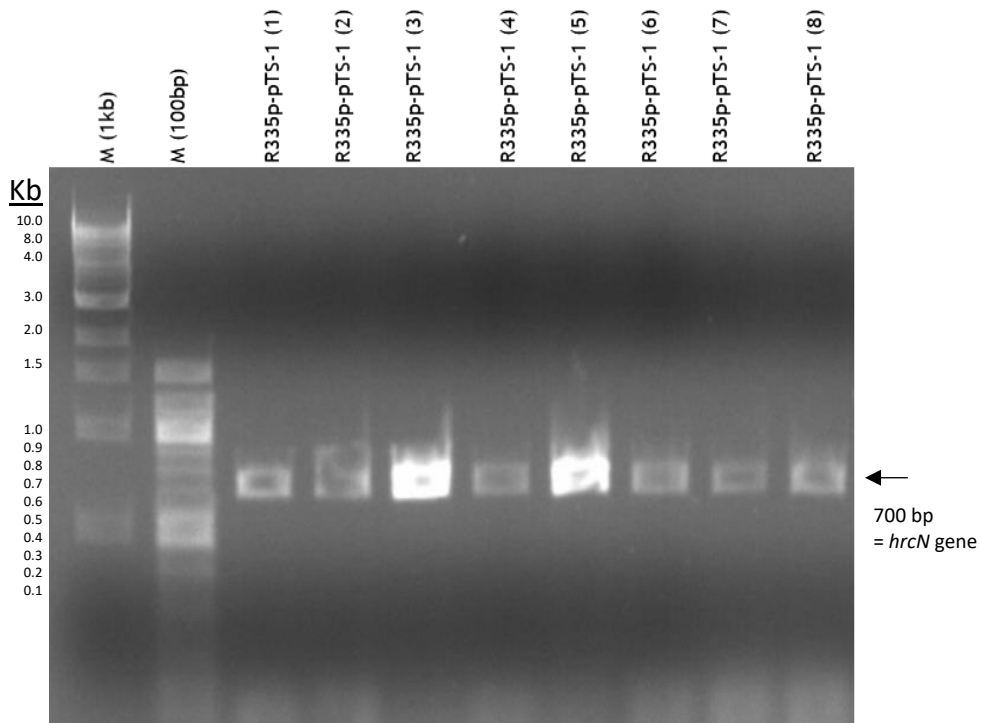
Figure 4.3. Colony PCR showing successful ligation of an *hrcN* mutant construct into a pTS-1 chromosomal integration vector.

To minimise the risk of false-positive results, this cloning verification was then strengthened with restriction digestion to show the cut empty pTS1 vector and the cut *hrcN* gene insert. This is shown in Figure 4.4 where for a selection of mutants, a positive result shows the cut empty pTS-1 plasmid at around 3900 bp and the cut *hrcN* fragment at 700 bp. All mutants were ultimately successful in showing both expected bands for the restriction digest (not shown).
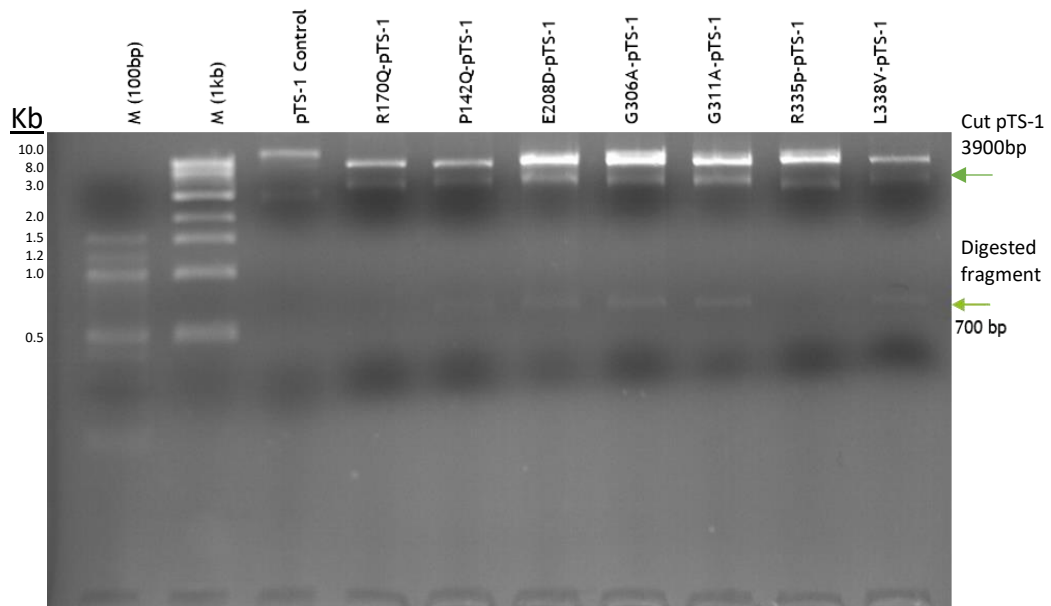
Figure 4.4. Restriction digest (using BamHI and XhoI restriction enzymes) of mutant *hrcN* pTS-1 chromosomal integration constructs. The digested mutant fragment can be seen at 700 bp. The upper fragments in each sample lane are uncut pTS-1 plasmids (top), and digested pTS-1 plasmids (lower).

Figure 4.5 shows an example sequencing reaction pairwise alignment for *E208D hrcN* against the wildtype *hrcN* gene. Present is the expected base pair change giving rise to an aspartate residue in place of a glutamate. The start of the sequences display ambiguity due to the sequencing reaction displaying lower accuracy at the primer binding sites. Colony PCR and sequencing was performed for all mutant constructs. This was successful for all mutant *hrcN* chromosomal integration constructs (not shown).

```
         hrcN  201 CCAGGAATGCACGCTGCTCAGCGCCCTCGGTGCGCCGG----ACGGCATT
                   |..|||||..|.||..||    |.||.|||
Mutant hrcN (E208D)  1 --------------------GATCCCTCTTTCCGGGGGGGGGAAAGGGATT

              247 CAGGTCGGTGCGCCGATCCGCCCGCTCGGCATCGCCCATCGAATAGGCGT
                   ..||||..|.|.||||||||||||||||||||||||||||||||
               31 -TTGTCGCGGGGGCGATCCGCCCGCTCGGCATCGCCCATCGAATAGGCGT

              297 GGACGACACGTTGCTGGGCTGCGTGCTGGACGGTTTCGGACGGCCGCTGC
                   ||||||||||||||||||||||||||||||||||||||||||||||||||
               80 GGACGACACGTTGCTGGGCTGCGTGCTGGACGGTTTCGGACGGCCGCTGC

              347 TCGGTGATTGCCTGGGGGCCTTTGCCGGGCCGGATGATCGCCGCGACACG
                   ||||||||||||||||||||||||||||||||||||||||||||||||||
              130 TCGGTGATTGCCTGGGGGCCTTTGCCGGGCCGGATGATCGCCGCGACACG

              397 CTGCCGGTGATTGCCGACGCCTTGCCGCCAACCCAGCGGCCGCGCATCAC
                   ||||||||||||||||||||||||||||||||||||||||||||||||||
              180 CTGCCGGTGATTGCCGACGCCTTGCCGCCAACCCAGCGGCCGCGCATCAC

              447 CCGGTCTTTGCCTACCGGCATACGGGCCATCGACAGCGCCATTCTGCTCG
                   ||||||||||||||||||||||||||||||||||||||||||||||||||
              230 CCGGTCTTTGCCTACCGGCATACGGGCCATCGACAGCGCCATTCTGCTCG

              497 GTGAAGGCCAGCGGGTCGGGCTGTTCGCCGGTGCCGGTTGCGGCAAGACC
                   ||||||||||||||||||||||||||||||||||||||||||||||||||
              280 GTGAAGGCCAGCGGGTCGGGCTGTTCGCCGGTGCCGGTTGCGGCAAGACC

              547 ACGCTGATGGCCGAACTGGCCCGCAACATGGACTGCGACGTCATCGTCTT
                   ||||||||||||||||||||||||||||||||||||||||||||||||||
              330 ACGCTGATGGCCGAACTGGCCCGCAACATGGACTGCGACGTCATCGTCTT

              597 CGGGCTGATCGGTGAGCGGGGCCGCGAACTGCGCGAGTTTCTCGACCATG
                   |||||||||||||||||||||||||||.||||||||||||||||||||||
              380 CGGGCTGATCGGTGAGCGGGGCCGCGACTGCGCGAGTTTCTCGACCATG

              647 AACTGGACGAAACCCTGCGCGCTCGCTCGGTACTGGTTTGTGCCACGTCC
                   ||||||||||||||||||||||||||||||||||||||||||||||||||
              430 AACTGGACGAAACCCTGCGCGCTCGCTCGGTACTGGTTTGTGCCACGTCC

              697 GATCGATCCAGTATGGAACGCGCCCGCGCCGCTTTCACGGCAACCGCCAT
                   ||||||||||||||||||||||||||||||||||||||||||||||||||
              480 GATCGATCCAGTATGGAACGCGCCCGCGCCGCTTTCACGGCAACCGCCAT

              747 CGCCGAAGCCTTTCGCGCGCGGGGCCAGAAGGTCTTGCTGCTGCTCGACT
                   ||||||||||||||||||||||||||||||||||||||||||||||||||
              530 CGCCGAAGCCTTTCGCGCGCGGGGCCAGAAGGTCTTGCTGCTGCTCGACT

              797 CCCTGACCCGATTTGCCCGTGCGCAACGGGAAATCGGCATTGCATCGGGC
                   ||||||||||||||||||||||||||||||||||||||||||||||||||
              580 CCCTGACCCGATTTGCCCGTGCGCAACGGGAAATCGGCATTGCATCGGGC

              847 GAACCGCTGGGCCGCGGCGGTCTGCCACCCTCGGTGTACACCCTGCTGCC
                   |||||||||||               |.||.||| ||||
              630 GAACCGCTGGG---------------ATCCCCGG-GTAC-----------
```

Figure 4.5. Example pairwise sequencing alignment between wildtype *hrcN* and sequenced *E208D* mutant *hrcN*

4.2.1.3.   Mutant *hrcN* Strains Show No Growth Defects

Following generation and verification of plasmid constructs, chromosomal integration into the *Pto* DC3000 genome proceeded by way of allelic exchange via homologous recombination. Double-crossover candidates were screened for using a counter selection method as previously described. Screened candidate strains were verified using colony PCR and Sanger sequencing to amplify and confirm successful integration of the mutated gene sequence into the *Pto* DC3000 genome. The verified *Pto* DC3000 strains (carrying mutant *hrcN* alleles) were stored for future use as glycerol stocks and were re-streaked out fresh for experimental work.

Shown in Figure 4.6 is a bacterial growth assay in L media of the mutant *hrcN P. syringae Pto* DC3000 strains constructed using allelic exchange. This was performed to verify that all constructed strains grew at comparable rates, and that mutagenesis had not introduced any growth defects. This enabled for easier interpretation of the results in subsequent *in vivo* infection experiments.

All strains started with an OD$_{600}$ of 0.01. No major differences in growth patterns, or growth defects were seen between strains. All strains enter the logarithmic growth phase at approximately 9 hours. For all strains, there is a transition into the stationary growth phase at approximately 45-50 hours with a final OD$_{600}$ reading of 0.45-0.5.
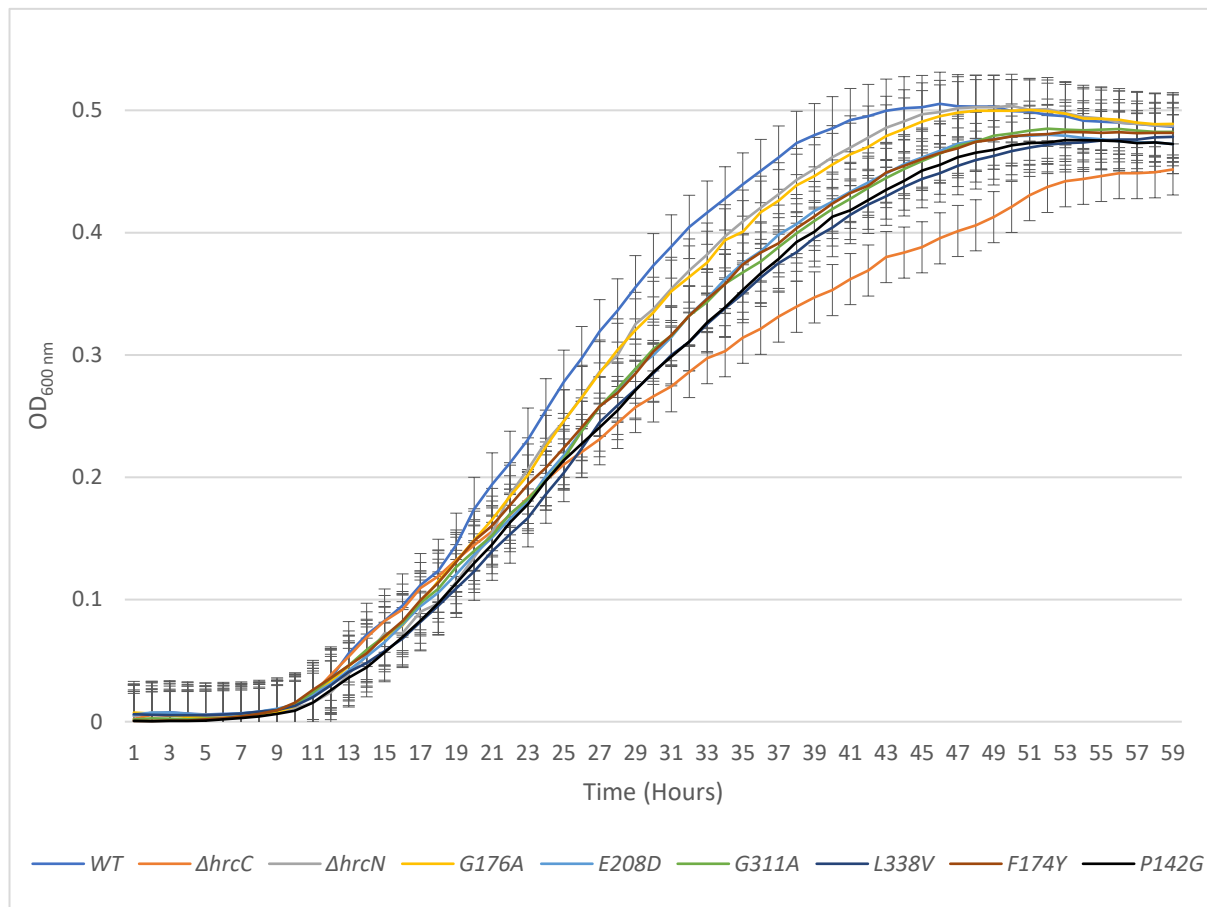
Figure 4.6. Allelic exchange WT and mutant *hrcN P. syringae Pto* DC3000 strains grown in L media at 28 °C across an incubation period of 60 hours from a starting 0.01 OD$_{600}$. Δ*hrcN* and Δ*hrcC Pto* DC3000 have key T3SS components deleted. *G176A, E208D, G311A, L338V, F174Y* and *P142G Pto* DC3000 contain point-mutations in *hrcN* targeting key predicted CdG-binding site residues. Error bars show standard error of the mean (n = 3).

4.2.2. *Pto* DC3000 Strains Carrying Mutant *hrcN* Alleles Show Asymptomatic Disease Phenotypes for *G176A* and *G311A hrcN* in *Arabidopsis thaliana*

4.2.2.1. Leaf Phenotypes

Virulence assays were performed using the mutant *hrcN P. syringae* strains. *A. thaliana* Col-0 was used as a model infection system to evaluate disease phenotypes. Shown in Figure 4.7 are the various disease phenotypes that were commonly observed on day 6 post bacterial infiltration infection.

The WT *P. syringae* strain shows normal disease symptoms, where chlorosis and necrosis can be observed spread evenly across the leaves. The uninfected control on the last row shows uninoculated healthy leaves from the same batch of plants grown under the same conditions for comparison. Δ*hrcC* and Δ*hrcN* are negative controls and lack a functioning type III secretion system and HrcN ATPase respectively.

As expected, for these Δ*hrcC* and Δ*hrcN* negative control strains, colonisation has not been possible and disease symptoms are not present. Interestingly, for *G176A* and *G311A hrcN* point-mutant strains, minimal disease symptoms were observed, and extensive chlorosis and necrosis were not evident. There are subtle traces of disease symptoms on some leaves, however the overall severity of the disease phenotypes were greatly reduced with these mutants.

The disease symptoms for *E208D*, *L338V* and *F174Y* seem comparable to WT. In some leaves, it could be argued that the disease severity is increased, and they show more extensive leaf chlorosis and necrosis. However, this phenotype was inconsistent and difficult to repeat.
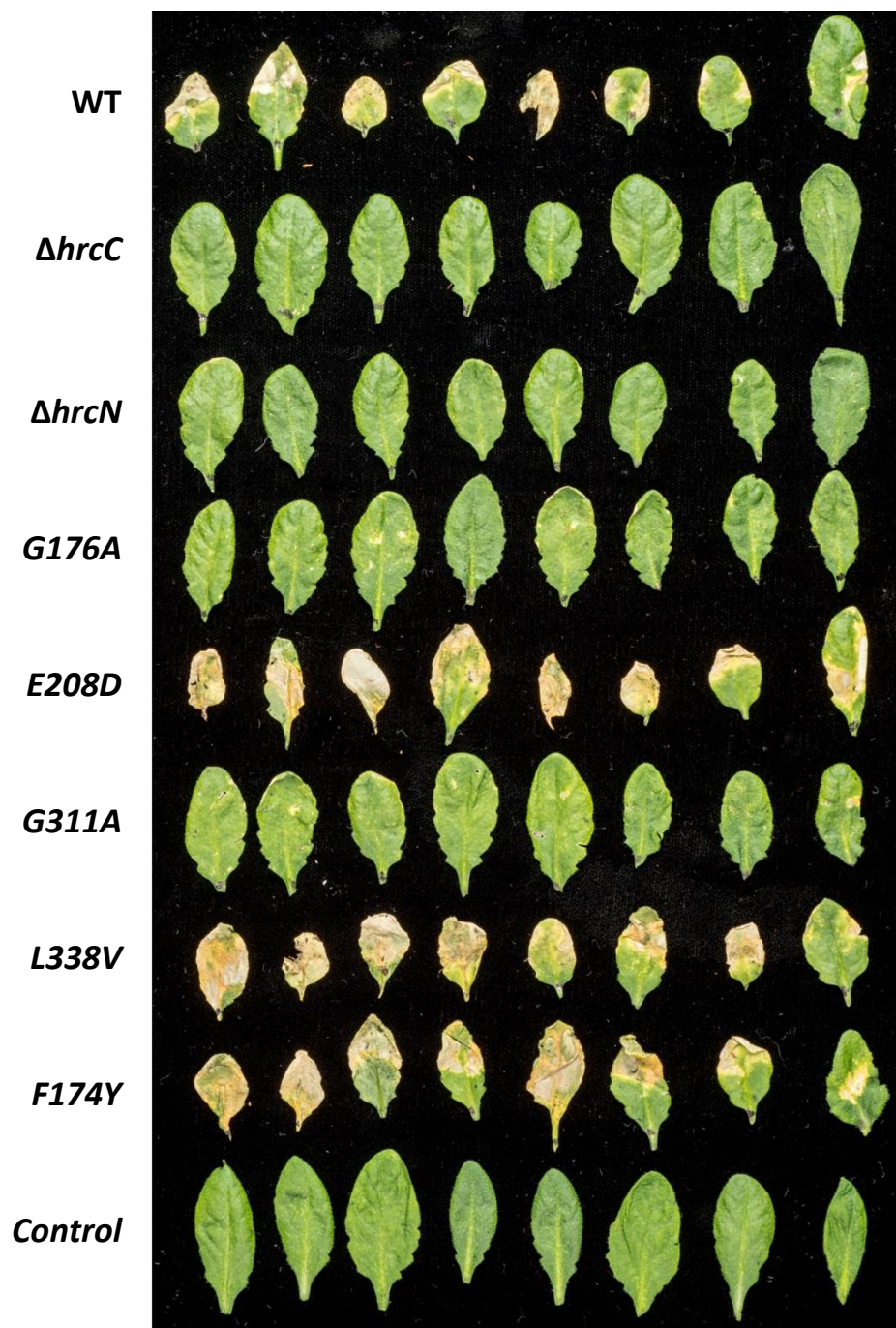
Figure 4.7. Infiltration infection disease phenotypes across *A. thaliana* Col-0 with *P. syringae Pto* DC3000 mutant strains containing point mutations in the predicted CdG binding site of the HrcN T3SS ATPase. Leaves photographed 6 days post-infection (n = 3 plants).

4.2.2.2.   Quantified Visual Disease Severity

The varying levels of leaf yellowing seen in the plant infection assays were quantified using an average pixel intensity calculation applied to the leaf image using ImageJ (version 1.52a). This calculated the abundance of yellow pixels in a given area on a scale of 1 to 255. A greater average pixel intensity

shows a higher degree of leaf yellowing, and thus visual disease symptom severity by way of chlorosis. Shown in Figure 4.8 are the quantified values for the infected leaves shown in Figure 4.7. Quantification of visual disease severity was calculated in order to draw more robust conclusions from leaf phenotypes, and to allow for statistical analyses to be performed.

No statistically significant differences were observed when comparing WT to *E208D* (p = 0.4), *L338V* (p = 0.79) and *F174Y* (p = 0.14) *hrcN* infected leaves. Statistically significant differences were observed when comparing the average pixel intensity values for WT compared to the *G176A* (p = 0.0006) and the *G311A* (p = 0.00001) *hrcN* point-mutant strains.

There are also statistically significant differences from WT for Δ*hrcC* (p = 0.0002), Δ*hrcN* (p = 0.0006), and the uninfected leaf controls (p= 0.00001).

This is supported with an ANOVA across all samples which confirms that the mean values of the columns are not the same, and there are statistically significant differences present (p = < 0.0001).
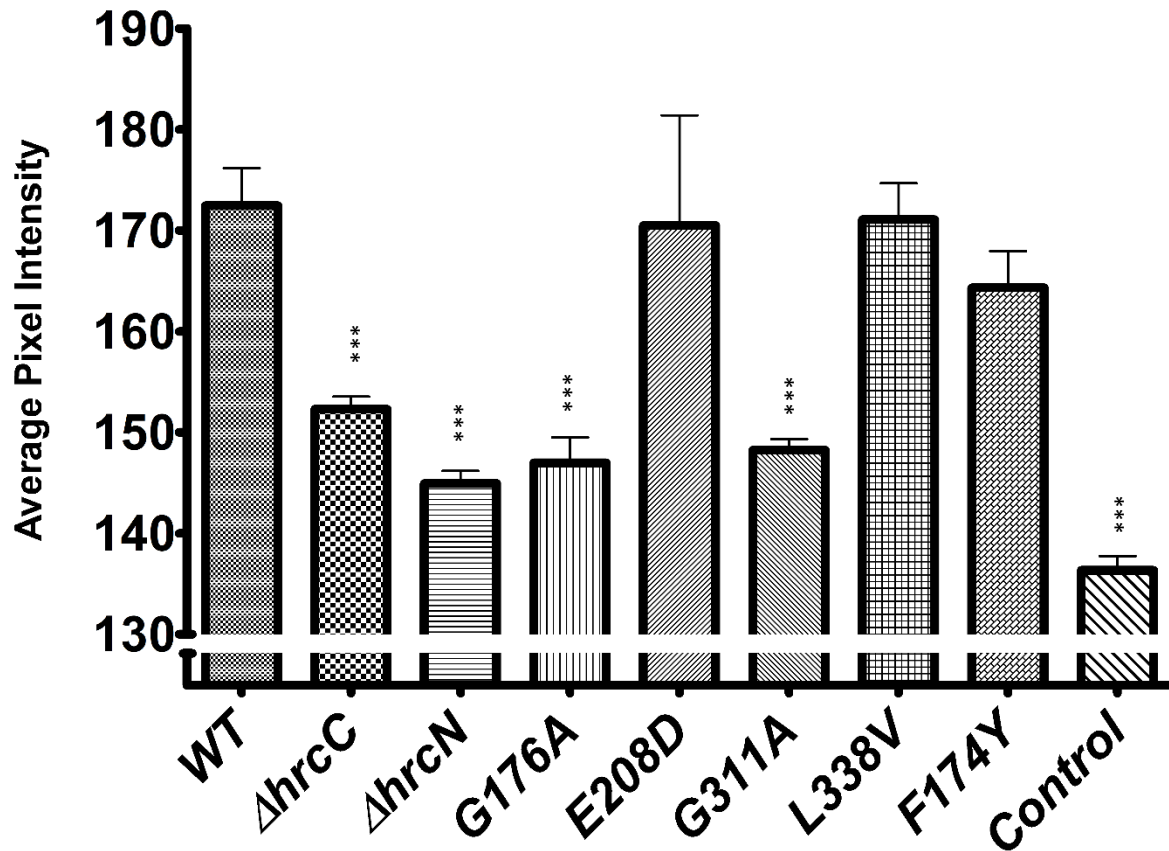
Figure 4.8. Average pixel intensity analysis across representing levels of leaf yellowing for *A. thaliana* Col-0 leaves infiltrated with *Pto* DC3000 (carrying mutant *hrcN* alleles) strains 6 days post-infection. Average pixel intensity calculation was performed using ImageJ software (version 1.52a). Error bars show standard error of the mean. Asterisks represent a statistically significant difference for a given sample compared to the WT (2 sample t-test) where '***' shows p = ≤ 0.001. (n = 8 leaves)

4.2.2.3.   Bacterial Load

Bacterial load was calculated for each infection in order to monitor the success of leaf colonisation for the various *hrcN* mutants shown in Figure 4.7. The cfu counts for each strain across this infection are shown in Figure 4.9. At day 0, the bacteria have been infiltrated into the leaves and bacterial load appears consistent across all mutant strains with no significant differences, as expected. As the infection proceeds over day 2 and day 3, differences become evident. Bacterial colonisation was established for all mutants where a significant difference was observed between day 0 and day 3, with the exception for Δ*hrcC* and Δ*hrcN*, the negative controls. The negative controls started similarly at 3 log(cfu/cm^2) but did not reach cell densities higher than 4 log(cfu/cm^2). There is a statistically significant difference on day 3 between WT and Δ*hrcC* (2-sample t-test p = < 0.001), showing that colonisation was not possible for those strains lacking type III functionality.

Bacterial loads at day 3 reached between 6 and 7 log(cfu/cm^2) for WT *hrcN*, *G176A*, *E208D*, *G311A*, *L338V* and *F174Y*; a significant increase (p = <0.001) compared to day 0 where bacterial load started at around 3 log(cfu/cm^2). All constructed mutant *hrcN* strains (excluding the negative controls) were able to colonise *Arabidopsis thaliana* Col-0 effectively. Despite this however, markedly different leaf disease phenotypes were present across the mutants.
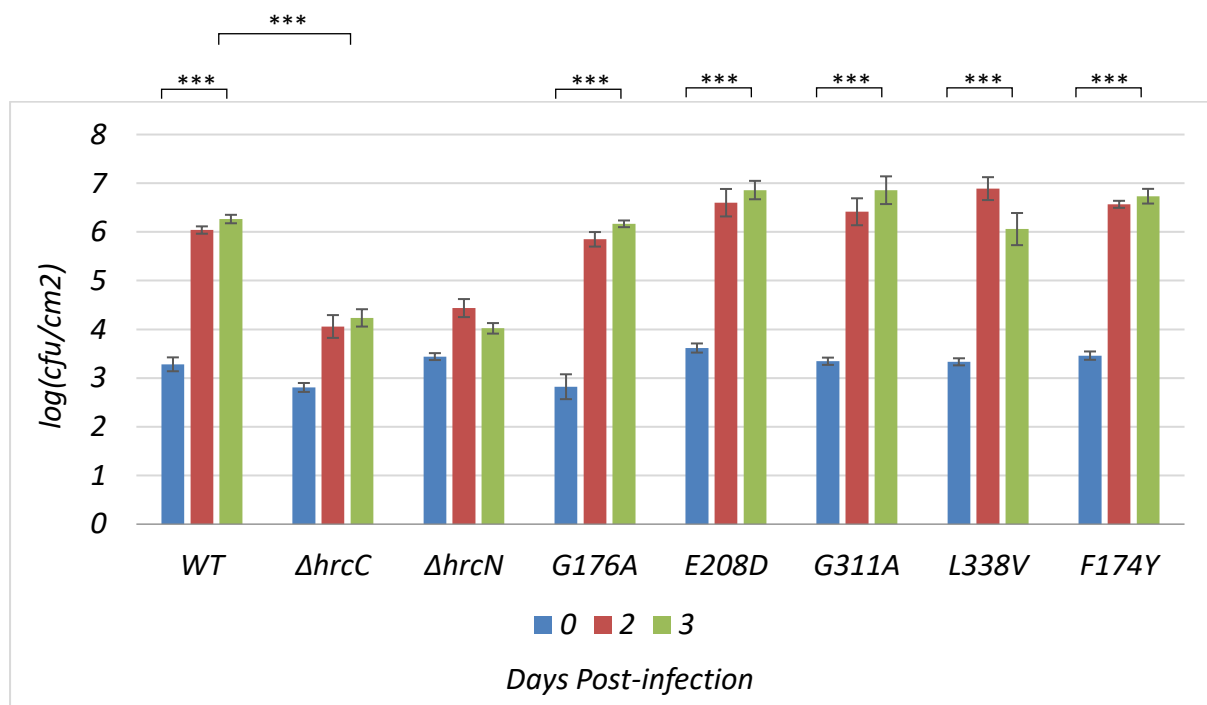
Figure 4.9. Infiltration of *A. thaliana* Col-0 plants with *P. syringae Pto* DC3000 *hrcN* strains. Colony forming units were determined using 4 mm diameter leaf disc sampling across a 3-day infection window. Error bars show standard error of the mean. Asterisks represent a statistical significance difference of a given sample compared to the WT (2 sample t-test) where '***' denotes p = ≤ 0.001 (n = 4 plants).

4.2.3. *G176A* and *G311A hrcN* Show Different Disease Phenotypes in Tomato (*Solanum lycopersicum*) Infections Compared to WT

4.2.3.1. Leaf Phenotypes

With the mutant *hrcN P. syringae Pto* DC3000 strains, *Solanum lycopersicum* 'Moneymaker' tomato plants were infected to evaluate disease severity (Figure 4.10). This was performed to compare differences in disease phenotypes present between the infection in the model host *A. thaliana* and the native host *S. lycopersicum*. These plant systems have many differences in their cellular architecture and immune systems, and so the infection process will likely differ between them.

The WT *hrcN* showed standard infection phenotype traits. There is an even distribution of chlorosis across the leaf with signs of necrosis and leaf wilting. The negative controls Δ*hrcC* and Δ*hrcN* that lack a functional type III secretion system do not show signs of bacterial proliferation and disease. There is some slight yellowing and wounding around the infiltration sites, however this is to be expected as part of the plant wounding-response and immune defence response.

G176A and *G311A* appear different in comparison to the other mutants, similar but not identical to what was observed with infection of *A. thaliana* Col-0 in Figure 4.7. Symptoms are less severe, especially in the case of *G311A* where there are minimal traces of chlorosis, necrosis, and leaf wilting. The *G176A* leaves do show minor levels of disease symptoms, most notably a high wilting response but otherwise appear less severe when compared to *E208D*, *L338V*, *F174Y* and *P142G*.

With the *E208D*, *L338V*, *F174Y* and *P142G* mutations, the disease symptoms appeared to a similar disease severity or greater than for the wildtype. Potential hypervirulence is best illustrated with *P142G* which show heavily wilted leaves that have undergone extensive necrosis.

The uninfected control shows healthy leaves as expected. This shows that any disease symptoms present within this batch of plants are highly likely to be caused solely from infiltrated *P. syringae* as opposed to any external variables.
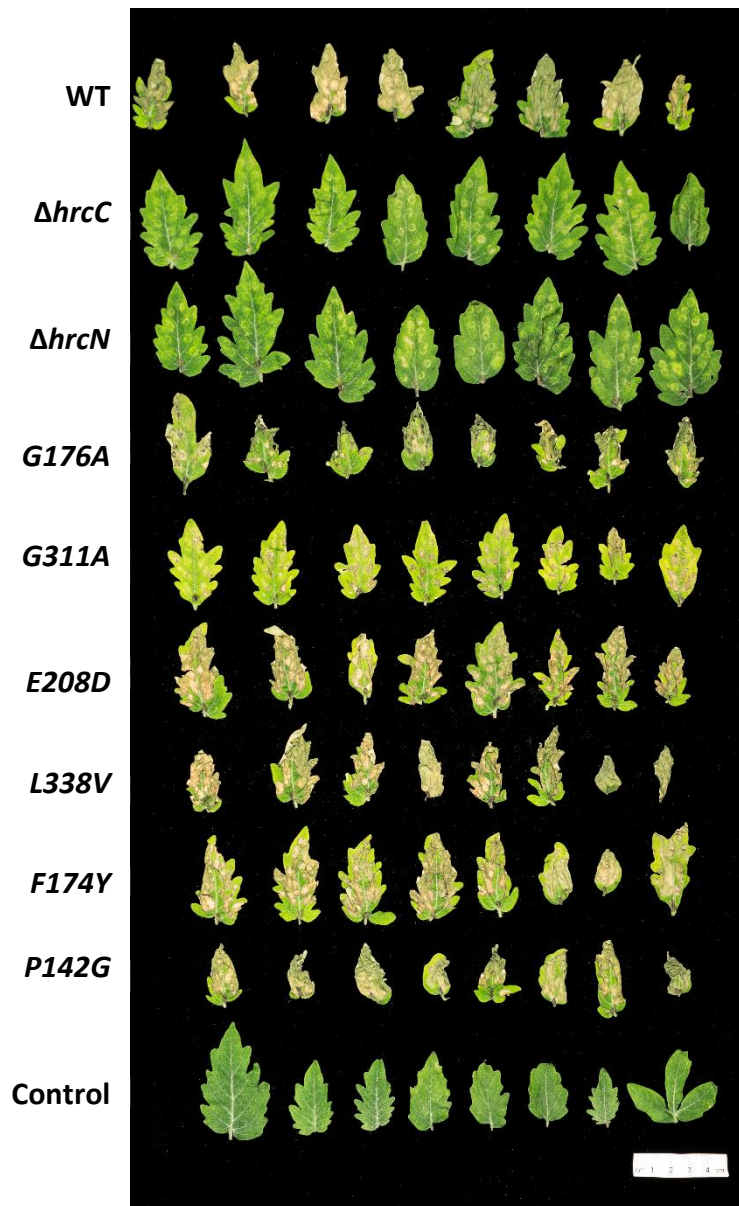
Figure 4.10. Infiltration infection disease phenotypes across *Solanum lycopersicum* 'Moneymaker' tomato plants with *Pto* mutant strains containing point mutations in the predicted CdG binding site of the HrcN T3SS ATPase. Leaves photographed 6 days post-infection (n = 3 plants).

4.2.3.2.   Quantified Visual Disease Severity

The leaves in Figure 4.10 were analysed with ImageJ software to calculate the average yellow pixel intensity across the sampled leaves to give a relative measure of leaf yellowing. The quantified leaf infection values are shown in Figure 4.11.

Compared to the WT, only the Δ*hrcC* (p = 0.0014), Δ*hrcN* (p = 0.001) and uninfected leaf controls (p = 0.007) showed statistically significant differences in average pixel intensity. *G176A* and *G311A* did not show statistically significant differences compared to the WT. The same is true for the *E208D*, *L338V*, *F174Y* and *P142G* mutants.

An ANOVA statistical test across all of the columns confirms that there are statistically significant differences between the mean averages of the column values (p = < 0.0001).
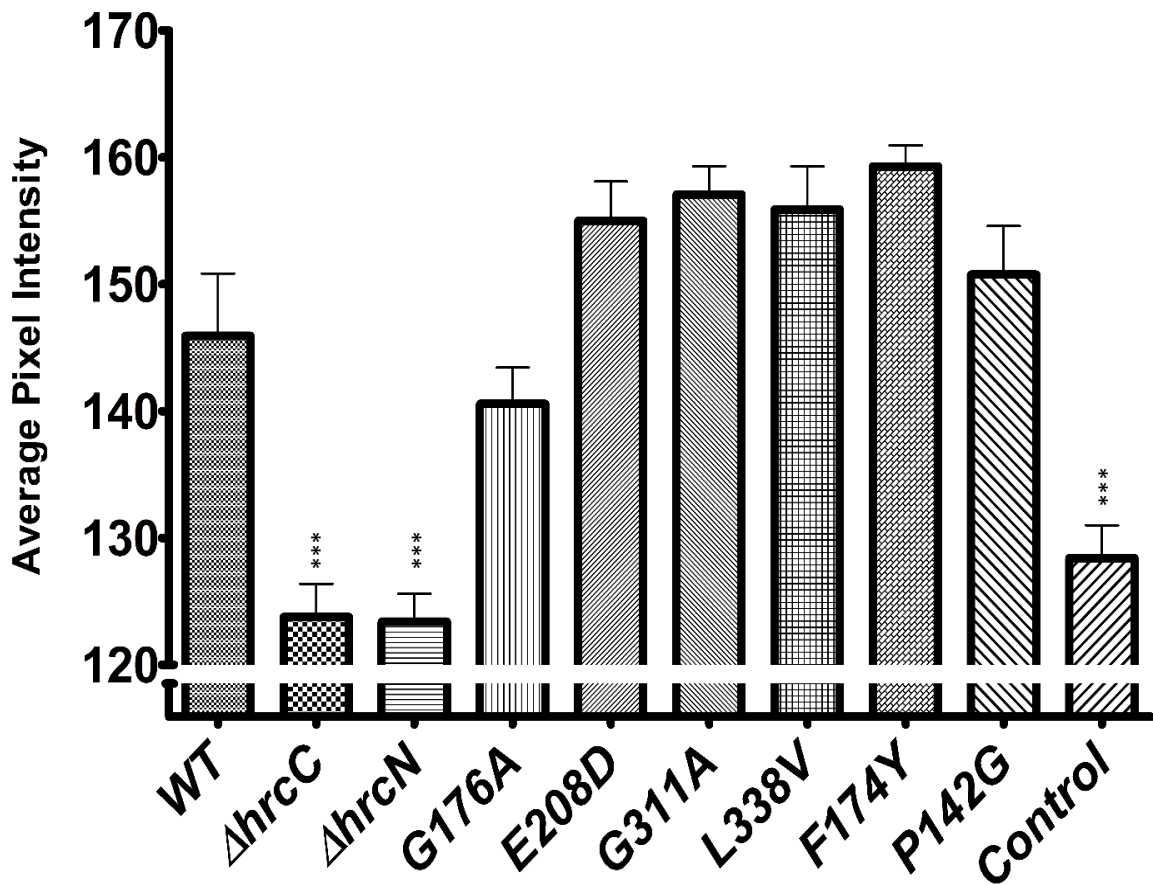
Figure 4.11. Average pixel intensity analysis across representing levels of leaf yellowing for tomato leaves infiltrated with mutant *Pto* strains 6 days post-infection. Average pixel intensity calculation was performed using ImageJ software (version 1.52a). Error bars show standard error of the mean. Asterisks represent a statistically significant difference of a given sample compared to the WT (2 sample t-test) where '***' denotes p = ≤ 0.001 (n = 8 leaves).

4.2.3.3.   Bacterial Load

By counting the colony forming units across the infected leaves from Figure 4.10, similar bacterial leaf colonisation characteristics can be observed (Figure 4.12).

At day 0, the bacteria have been infiltrated into the leaves and bacterial load appears consistent across all mutant strains with no significant differences as expected. As the infection proceeds over day 2 and day 3, differences emerge between some strains, similar to what was observed in Figure 4.9. Bacterial colonisation was established for all mutants, where a significant difference (p = <0.001) was observed between day 0 and day 3 with the exception for Δ*hrcC* and Δ*hrcN*, the negative controls. There is a statistically significant difference between the day 3 value of the WT and day 3 of the negative Δ*hrcC* control (p = <0.001).

The bacterial load at day 3 reached between 7 and 8 log(cfu/cm^2) for WT *hrcN*, *G176A*, *E208D*, *G311A*, *L338V*, *F174Y* and *P142G*, which is a significant increase compared to day 0 where bacterial load started at around 3 to 4 log(cfu/cm^2). The negative controls started similarly at 3 to 4 log(cfu/cm^2) but

could not colonise greater than around 5 log(cfu/cm^2) showing that full colonisation was not possible for these strains lacking full type III functionality.

This demonstrates that all constructed mutant *hrcN* strains (excluding the negative controls) are able to colonise their native host *Solanum lycopersicum* to a similar level. Despite this however, differences in visible leaf disease phenotypes are present for certain mutants.
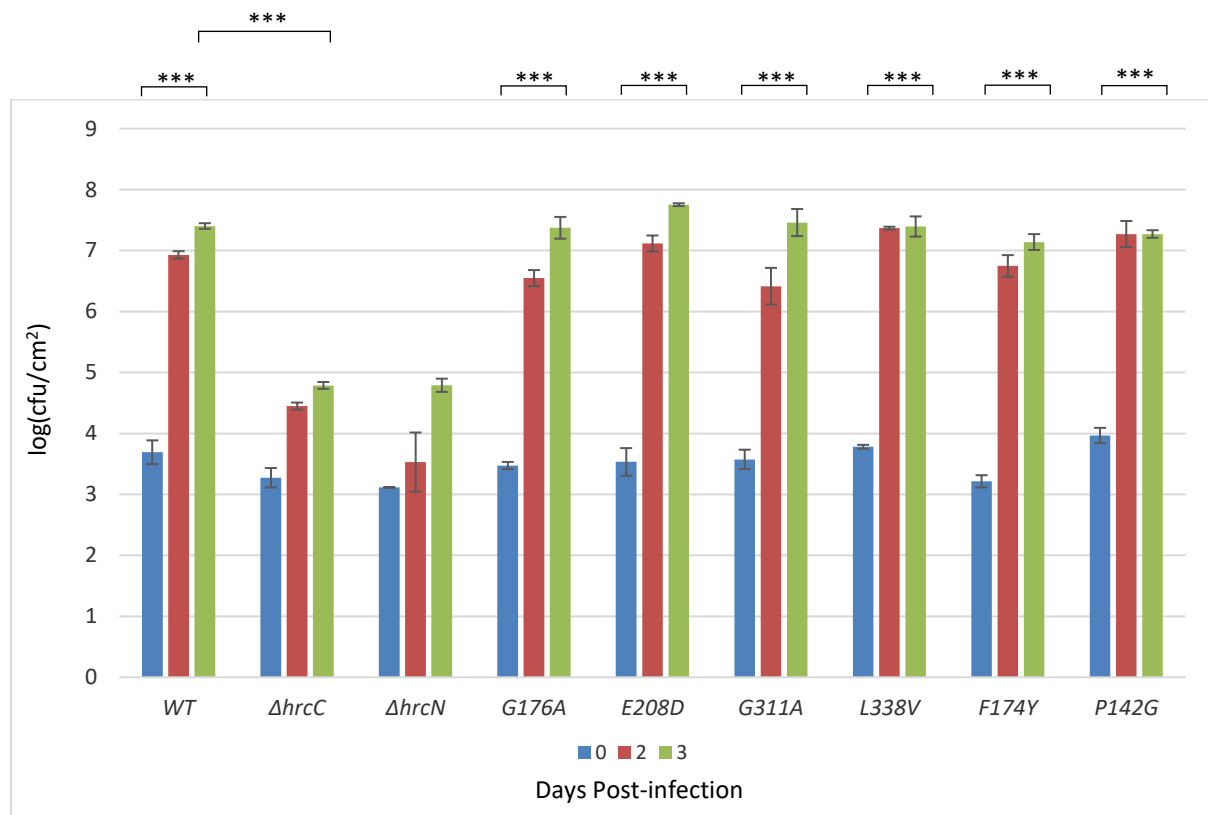
Figure 4.12. Infiltration of tomato plants with *hrcN mutant Pto* strains. Colony forming units were determined using 4 mm diameter leaf disc sampling across a 3-day infection window. Error bars show standard error of the mean. Asterisks represent a statistical significance difference of a given sample compared to the WT (2 sample t-test) where '***' denotes p = ≤ 0.001 (n = 3 plants).

4.2.4.   Western Blotting Confirms the T3SS Is Present Throughout Infection with the *hrcN* Point Mutant Strains

Western blotting was carried out to test whether mutagenesis of *hrcN* altered the expression of *hrcN* and the presence of associated type III system components. Specific antibodies were used to detect the presence of HrcN and HrpQ system components in infected samples. HrpQ is a major structural component of the type III basal body and is necessary for dynamic assembly of the T3SS. The location of HrcN and HrpQ system components on the T3SS are illustrated in Figure 4.13. Verification of the presence of these key T3SS system components was necessary to identify whether visible disease phenotypes observed in *hrcN* mutants was due to lack of the T3SS during part of the infection process.
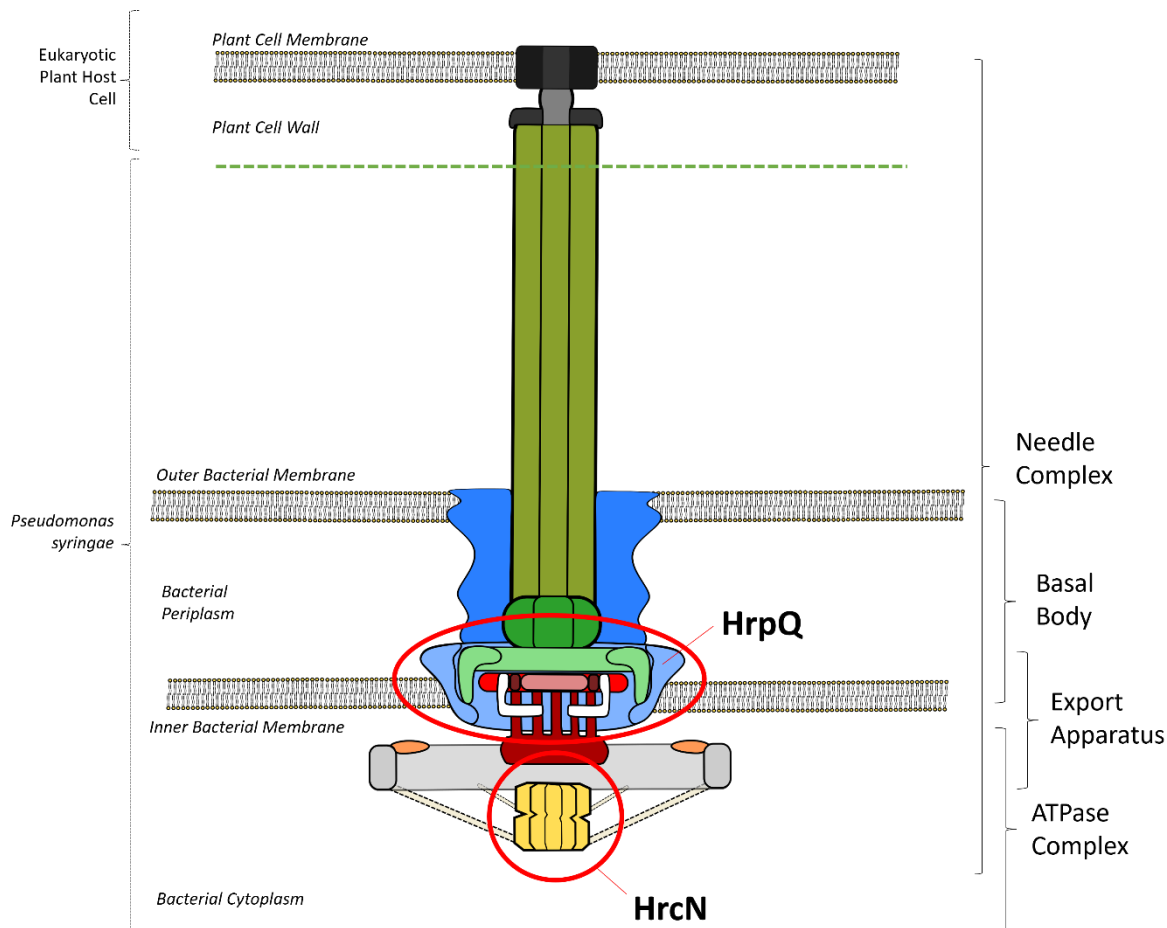
Figure 4.13. Illustrative cartoon indicating the location of HrcN and HrpQ structural components of the T3SS targeted in Western blotting experiments.

4.2.4.1.   Anti-HrcN

In Figure 4.14, a western blot of *A. thaliana* Col-0 leaf tissue infected with *Pto hrcN* mutant infected leaf tissue at day 3 post-infection is shown. An anti-HrcN antibody was used to detect the presence of HrcN in these samples. Indicated at 48.4 kDa is the HrcN band. HrcN was detected for all strains except for Δ*hrcC*, Δ*hrcN* and the uninfected plant tissue control. This is expected as Δ*hrcC* cannot build the type III secretion system (and so HrcN is likely being turned over when it fails to properly assemble), Δ*hrcN* lacks the HrcN protein entirely and the uninfected *A. thaliana* tissue does not naturally contain the HrcN ATPase.

For WT, *G176A*, *E208D*, *G311A*, *L338V* and *F174Y*, a distinct HrcN band can be seen. A *P142G* band can also be seen but is much more pronounced. Above the HrcN band, a non-specific band can be seen at 48.6 kDa. This was subsequently identified as the closely related protein FliI by Orbitrap mass spectrometry (not shown).
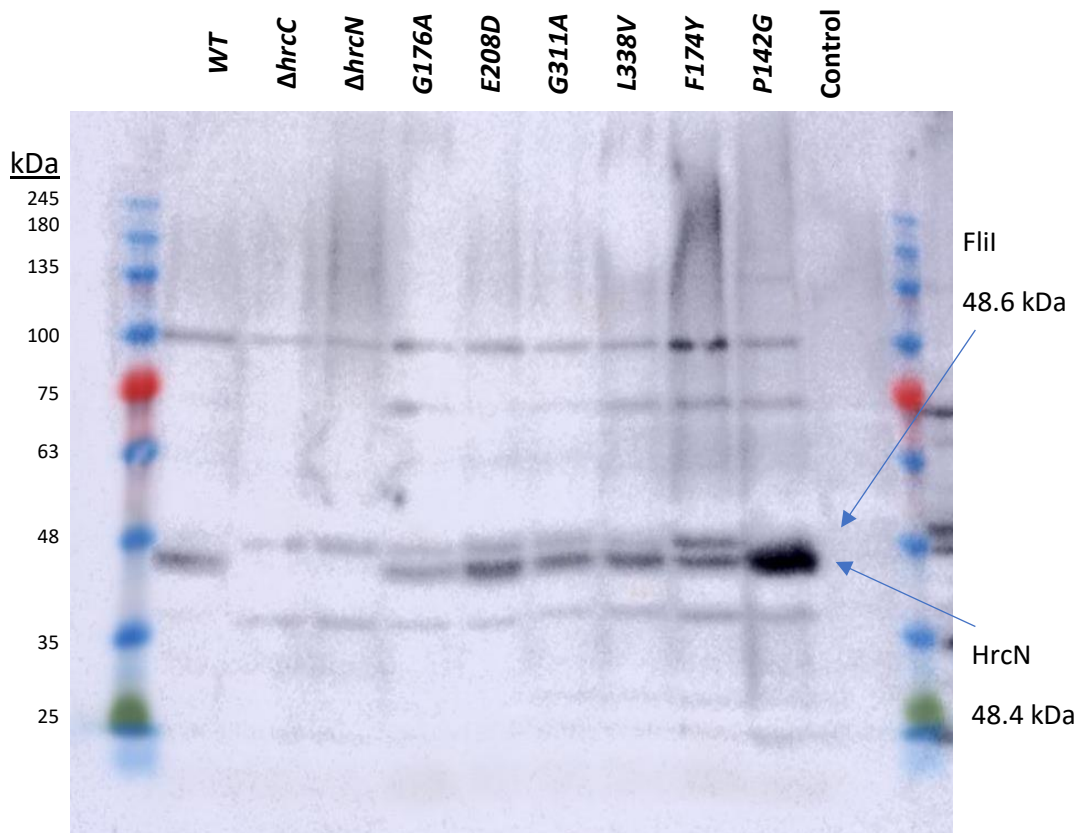
Figure 4.14. Anti-HrcN Western blot of *A. thaliana* Col-0 leaf tissue infected with *Pto hrcN* mutants. Infected leaf tissue was collected at day 3 post-infection. The identified proteins (indicated with arrows) were confirmed with Orbitrap mass spectrometry. The negative control contains uninfected leaf tissue.

Infected leaf tissue at day 9 post-infection is shown in Figure 4.15. The HrcN band is visible and well-defined for WT, *G176A*, *E208D* and *L338V*. A fainter band can be seen for *G311A*. A band cannot be seen for *F174Y*. This may be a blotting issue, or the protein may have degraded due to poorer stability. The Δ*hrcC*, Δ*hrcN* and the uninfected plant tissue lanes do not show a HrcN band as expected.

This confirms that HrcN is present throughout infection with the *Pto hrcN* point mutant strains and any phenotypic differences in infection are not due to HrcN absence. This also confirms that Δ*hrcC* and Δ*hrcN* are appropriate negative controls where the HrcN protein is absent.
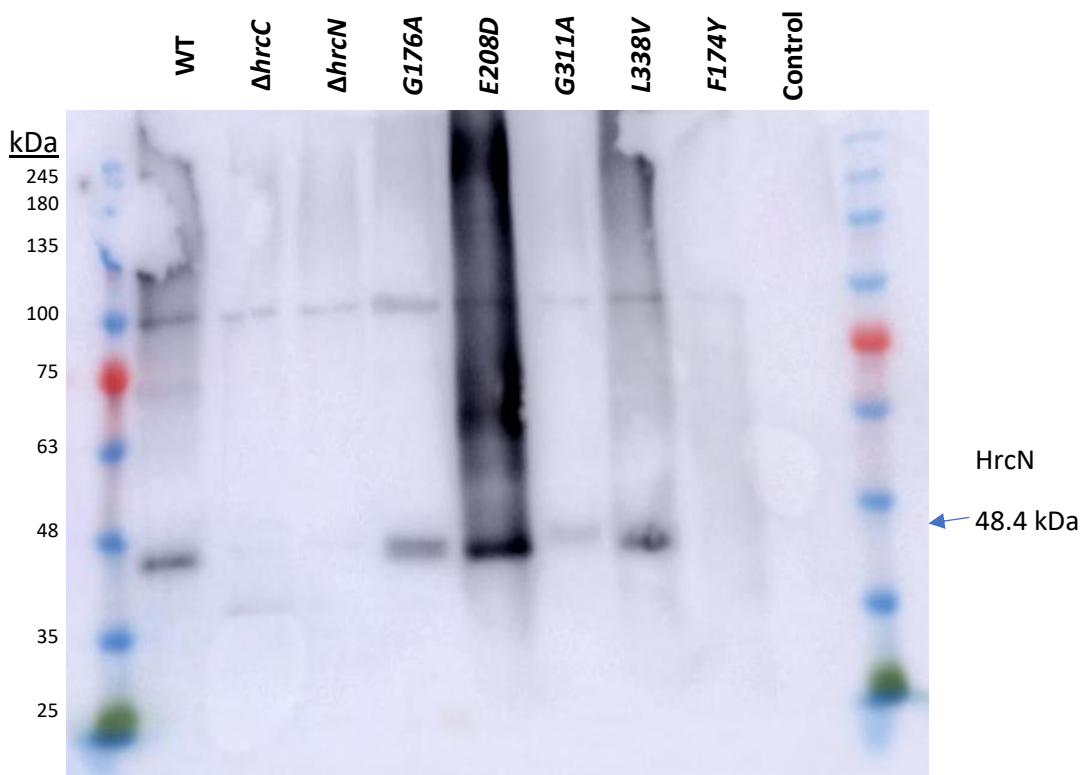
Figure 4.15. Anti-HrcN Western blot of *A. thaliana* Col-0 leaf tissue infected with *Pto hrcN* mutants. Infected leaf tissue was collected at day 9 post-infection. The negative control contains uninfected leaf tissue.

4.2.4.2.   Anti-HrpQ

HrpQ is a major structural component of the type III secretion system. In Figure 4.16, a Western blot with anti-HrpQ is shown on day 3 post-infection. *A. thaliana* Col-0 leaf tissue infected with mutant *hrcN P. syringae*. HrpQ is indicated at the expected 35.9 kDa region and is present for all lanes except for the uninfected plant tissue negative control as expected. A HrpQ band is seen for all other strains. This confirms that the point-mutations introduced into HrcN do not impact the deployment of HrpQ.
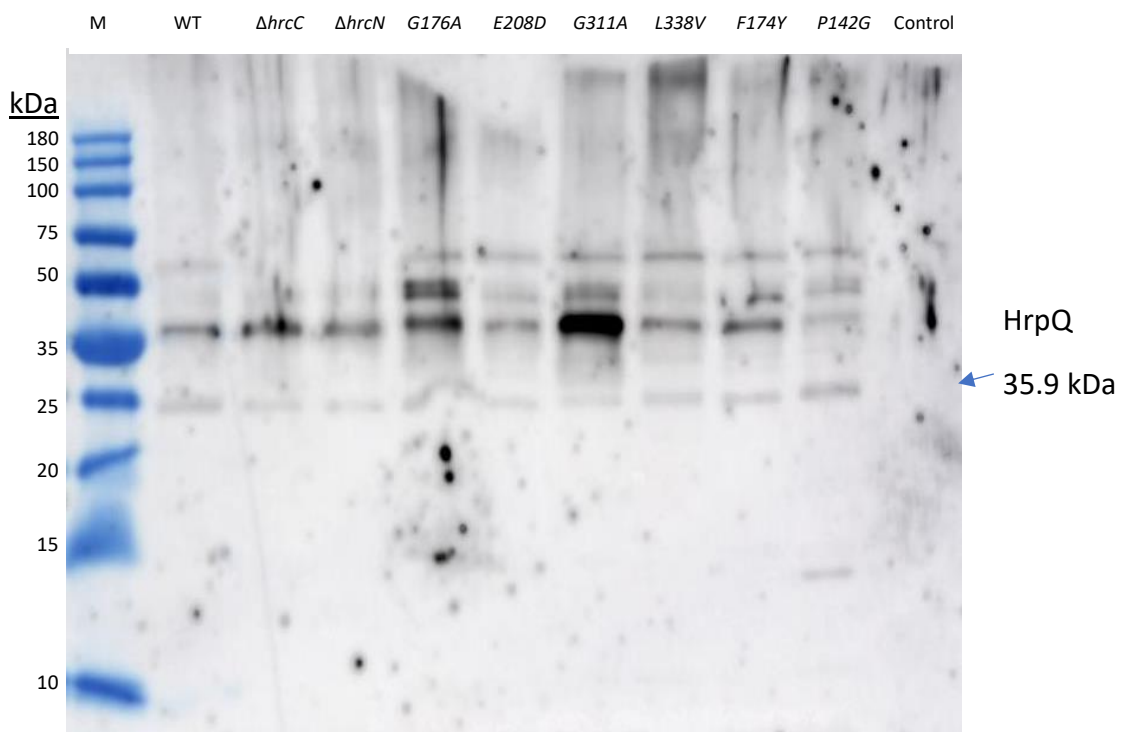
Figure 4.16. Anti-HrpQ Western blot of *A. thaliana* Col-0 leaf tissue infected with mutant *hrcN P. syringae Pto* DC3000 Infected leaf tissue was collected at day 3 post-infection. The negative control contains uninfected leaf tissue.

In Figure 4.17, a Western blot with anti-HrpQ is shown on day 9 post-infection *A. thaliana* Col-0 leaf tissue infected with mutant *hrcN P. syringae*. HrpQ is indicated at the expected 35.9 kDa region and is present for all lanes expect for the uninfected plant tissue negative control as expected. This suggests that the type III HrpQ component remains present throughout infection up to day 9 post-infection in all strains and is not subject to significant amounts of degradation or expression limitation.
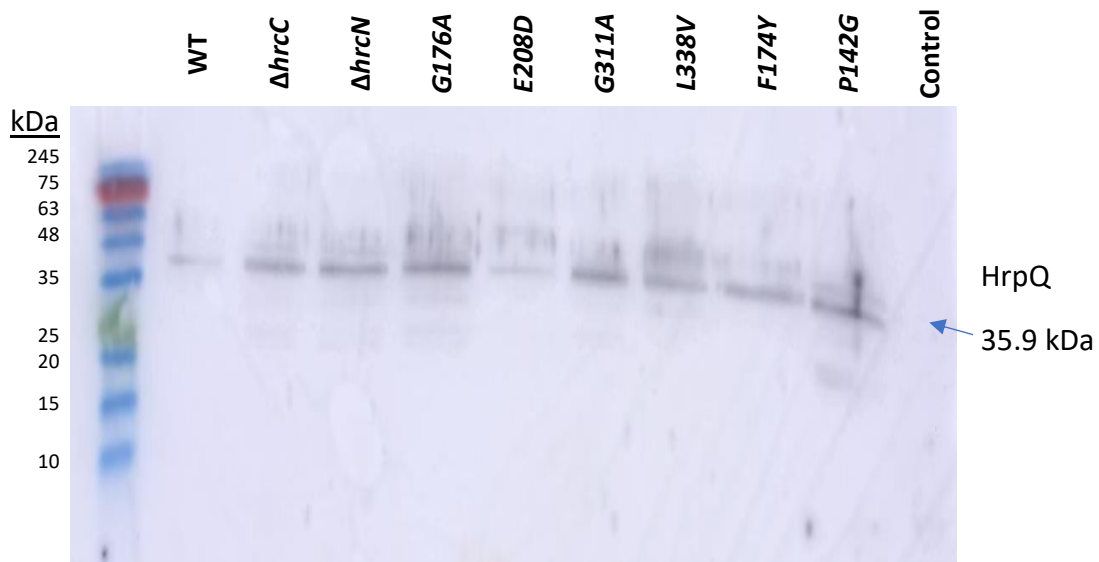
Figure 4.17. Anti-HrpQ Western blot of *A. thaliana* Col-0 leaf tissue infected with mutant *hrcN P. syringae Pto* DC3000. Infected leaf tissue was collected at day 9 post-infection. The negative control is uninfected leaf tissue blotted against anti-HrpQ.

4.2.5. Key Genotypes Were Successfully Complemented

4.2.5.1. Leaf Phenotypes

Genetically complemented *Pto* DC3000 strains (carrying mutant *hrcN* alleles) were constructed by integrating a WT copy of *hrcN* under the control of its native promoter and 200 bp upstream regulation elements into the chromosome at the *att::*Tn*7* site using a pUC18-mini-Tn7T plasmid. Additionally, a WT copy of *hrcC* was expressed in the Δ*hrcC* background alongside a WT control. This technique confirmed successful targeted mutagenesis of *hrcN* was achieved and that any phenotypical effects observed were not produced as a result of secondary, off-target mutations.

These strains were used in an infiltration assay with *A. thaliana* Col-0 plants. Day 6 post-infection disease phenotype leaves are shown in Figure 4.18 while the colony forming unit counts for day 0, 2 and 3 post-infection are shown in Figure 4.20.

The day 6 post-infection leaf phenotypes are shown in Figure 4.18. What can be seen is that by complementing the mutant *hrcN* strains, a phenotype recovery has been achieved where previously near asymptomatic mutants (*G176A* and *G311A*) show WT-levels of chlorosis and necrosis. The *Pto* DC3000 strain carrying a *E208D hrcN* allele that previously showed symptoms in prior assays, remains unaffected by an additional copy of WT *hrcN* being expressed.

In addition to this, Δ*hrcC* and Δ*hrcN* also show a recovery of phenotypes as expected when complemented.

WT *Pto* with an additional copy of WT *hrcN* did not show any phenotypic defects or other unusual results. The same is true for WT *Pto* with an additional copy of WT *hrcC*.

The uninfected leaf control shows no disease symptoms, as expected.
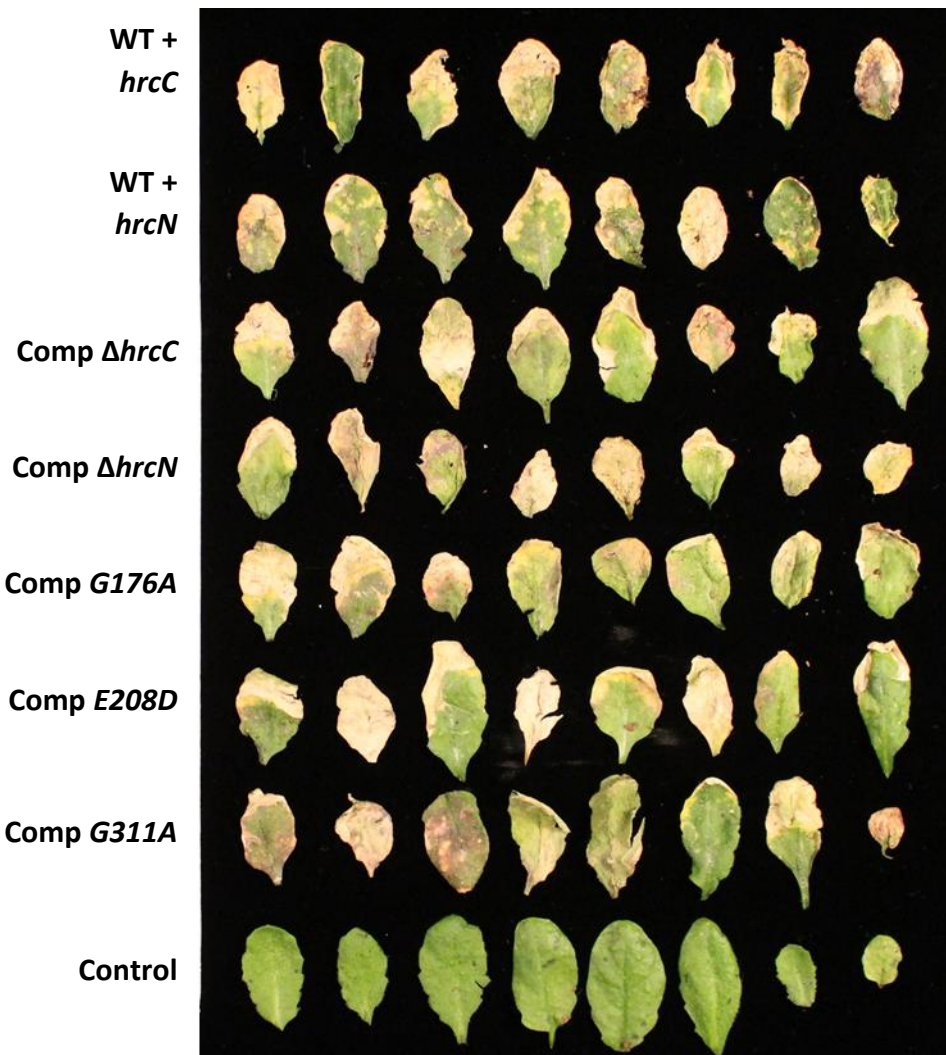
Figure 4.18. Infiltration infection disease phenotypes across *A. thaliana* Col-0 with genetically complemented *Pto* mutant strains expressing a WT chromosomal copy of *hrcN*/*C*. Leaves photographed 6 days post-infection (n = 3 plants).

4.2.5.2. Quantified Visual Disease Severity

The visual disease symptoms in Figure 4.18 were quantified using average pixel intensity analyses with ImageJ software. These data are shown in Figure 4.19.

An ANOVA when excluding the negative uninfected control shows there are no statistically significant differences (p = 0.1) between complemented strains; they all achieve a similar level of disease severity. When comparing the mean average pixel intensity value of the uninfected control with the other samples, a statistically significant difference is observed for all (p = <0.0001). No other statistically significant differences are present for strains compared to their respective *hrcN* or *hrcC* WT.
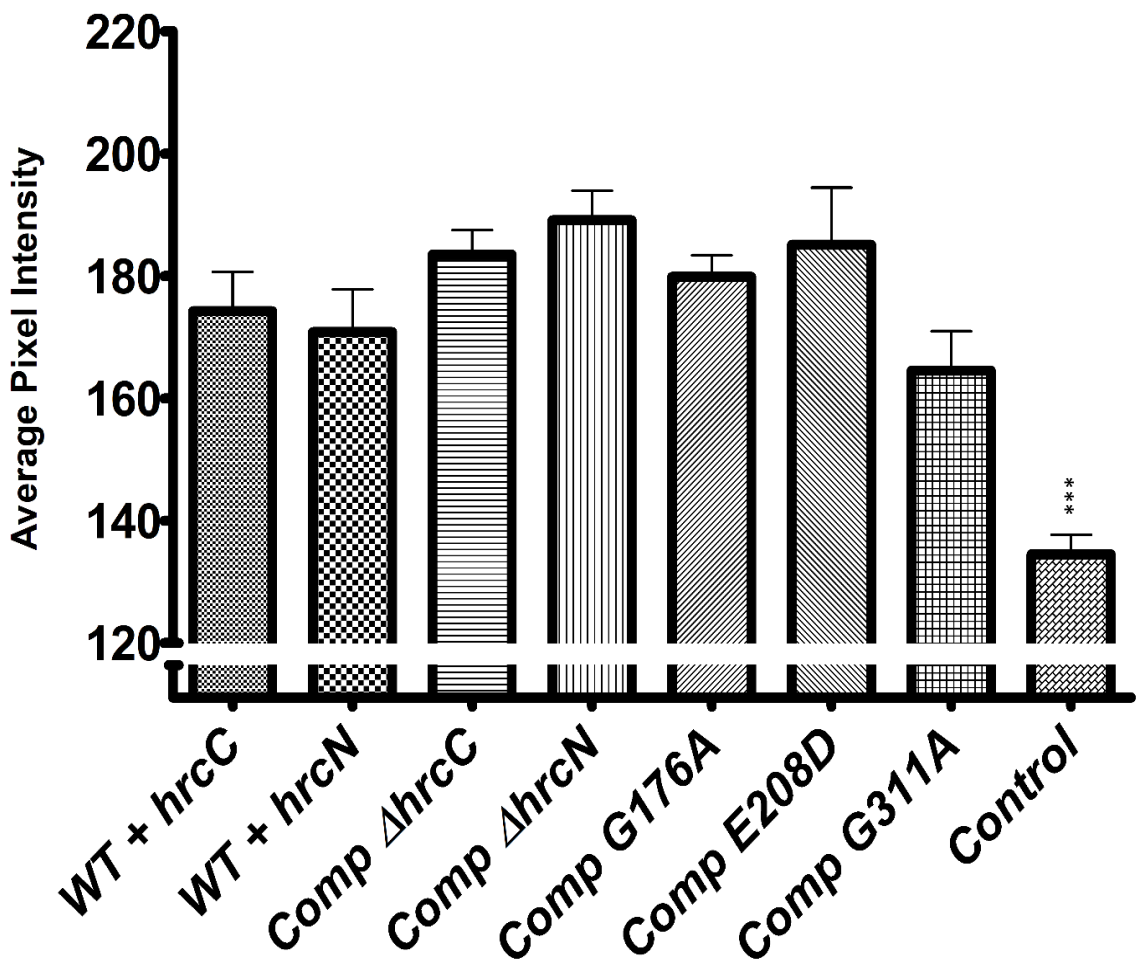
Figure 4.19. Average pixel intensity analysis across representing levels of leaf yellowing for *A. thaliana* Col-0 leaves infiltrated with genetically complemented *Pto hrcN* mutant strains 6 days post-infection. Average pixel intensity calculation was performed using ImageJ software (version 1.52a). Error bars show standard error of the mean. Asterisks represent a statistically significant difference of a given sample compared to the WT (2 sample t-test) where '***' denotes p ≤ 0.001 (n = 8 leaves).

4.2.5.3. Bacterial Load

The cfu data shown in Figure 4.20 confirms the phenotype recovery seen in the day 6 post-infection leaf image. All mutants were able to infect to levels comparable (and not statistically significantly different to) the WT values by day 3 post-infection. An ANOVA of the day 3 post-infection values confirms there are no statistically significant differences present (p = 0.2). Δ*hrcC* and Δ*hrcN*, which were unable to establish full colonisation in previous experiments (acting as negative controls) also showed a recovery of colonisation. These results confirm that targeted point-mutant generation and gene deletion of *hrcN* and *hrcC* was successful, and that disease phenotypes observed were due to these mutations and not any off-target effects.
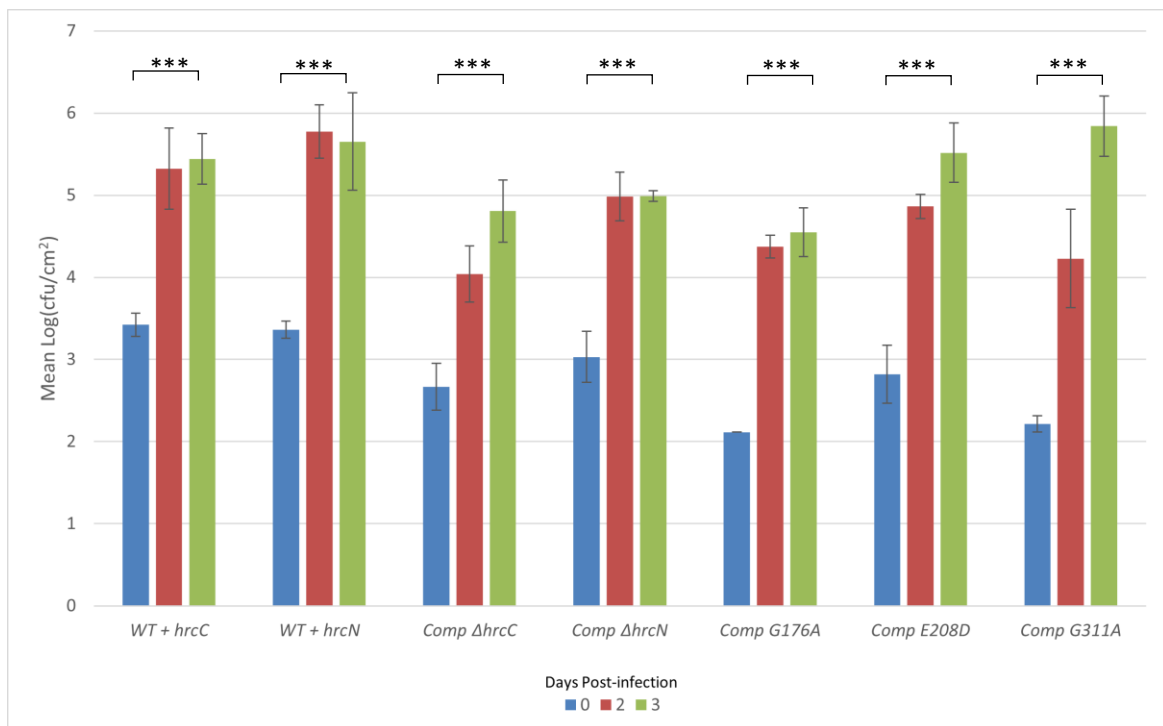
Figure 4.20. Infiltration of *A. thaliana* Col-0 plants with genetically complemented *Pto hrcN* mutant strains. Colony forming units were determined using 4 mm diameter leaf disc sampling across a 3-day infection window. Error bars show standard error of the mean. Asterisks represent a statistically significant difference of a given sample compared to the WT (2 sample t-test) where '***' denotes $p \leq 0.001$ (n = 3 plants)

4.2.6. ROS Burst Assays Detect No Change in Cellular Immunogenicity to the *Pto hrcN* Mutants

One possible explanation for the phenotypic differences described above was that mutating the *hrcN:*CdG binding site may give rise to different immune responses in the infected plant hosts. A straightforward measure of plant immune responses is through measurement of ROS bursts. In Figure 4.21, is an example of a positive ROS immune burst curve from WT *P. syringae* (left) compared to a negative ROS immune response (right). The area under the curve was calculated in each case and then compared to see whether mutagenesis of *hrcN* led to any changes in immune system recognition.
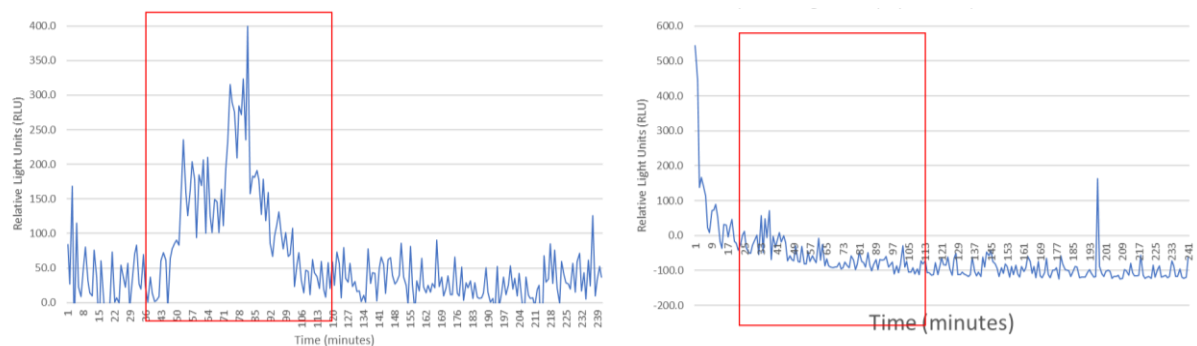
Figure 4.21. An example of a positive and negative ROS burst assay from *A. thaliana* Col-0 leaf discs in response to *Pto* exposure. The left image shows a ROS burst (highlighted in red) in response to WT *Pto.* The right image shows the response to a H$_2$0 negative control (the expected region has been highlighted red).

Shown in Figure 4.22 are the average ROS burst values observed when washed whole cell *Pto hrcN* mutants were applied to *A. thaliana* Col-0 leaf discs. These cells have not been ruptured and so immunogenicity will be induced only from external cellular features, including the T3SS pilus. The area under the curve of the ROS burst peaks was calculated for each ROS burst peak allowing for comparison of plant immune response between *hrcN* mutants.

Flg22 was used as a positive control to demonstrate an FLS2-dependent ROS burst. This is a pure peptide and so gave rise to a very high relative luminescence value for the peak area of 185 350. The negative control was H$_2$O and ellicited a minimal baseline luminescence value.

The whole cell bacteria added for the *hrcN* mutants produced a much lower luminescence value than Flg22. This was because the immunogenic agents are not pure, are not found in such a concentrated quantity on the cell surface, are subject to steric hindrance and may have immuno-suppresive agents present.

Whole cell wildtype *hrcN P. syringae Pto* DC3000 produced a relative luminescence peak area value of 10 407. *E208D hrcN* was the lowest value in comparison to the WT with a relative luminescence value of 3690 (a -64.54% change) however this was not a statistically significant difference (p = 0.3). *F174Y hrcN* had the greatest relative luminescence peak area under curve value at 14 965 compared to the WT peak (a 43.8% change), however this too was not statistically significant (p = 0.6).

With the other *hrcN* values, while differences in luminescence values were observed, none were significant. Δ*hrcC* was measured to be 9261 (a -11 % change compared to WT, p = 0.9), Δ*hrcN* was 7903 (a -24 % change compared to WT, p = 0.7), *G176A* was 3782 (a -64 % change compared to WT, p = 0.3), *G311A* was 10 942 (a 5.1 % change compared to WT, p = 0.9), *L338V* was 14 349 (a 38 % change compared to WT, p = 0.7), and *P142G* was calculated to be 11 489 (a 10.4 % change compared to WT, p = 0.9).

It can be concluded from this experiment that mutating *hrcN* has little or no effect on immunogenicity and plant ROS defence responses against whole *P. syringae* cells. This is the form that the bacteria would be in during plant infiltration and infection and so these results suggest that differences in immune responses are not the reason behind the differences in leaf disease phenotypes that were observed for the *Pto hrcN* mutants.
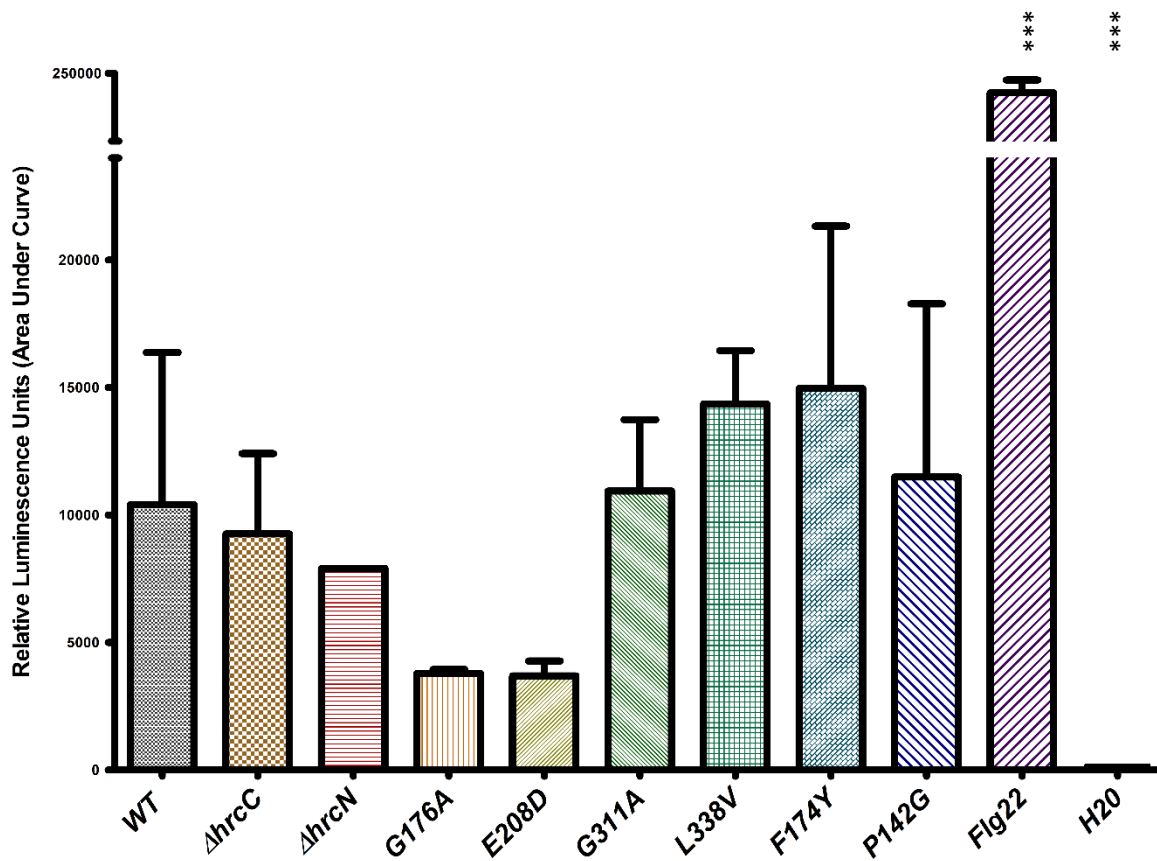
Figure 4.22. Area under curve relative luminescence unit values observed for ROS burst plant immune responses for washed whole cell *Pto hrcN* mutants applied to *A. thaliana* Col-0 discs over a 2-hour period. Error bars show standard error of the mean. Asterisks represent a statistical significance difference of a given sample compared to the WT (2 sample t-test) where '***' denotes p ≤ 0.001 (n = 3)

Shown in Figure 4.23 are the average ROS burst values observed when washed and boiled *Pto hrcN* mutant lystates were applied to *A. thaliana* Col-0 leaf discs. These cells were ruptured, revealing the immunogenicity of all cellular components, not just external features. It is possible that during the infiltration infection process a proportion of bacterial cells are ruptured and so any internal immunogenic differences are also important to note. Because the cells have been ruptured, there is a greater concentration of immunogenic cellular material and so the relative luminescence ROS peaks observed were much greater than with unboiled cells, as expected.

A high relative luminescence value for the positive pure Flg22 peptide and a minimal value for the negative H_2O controls confirm that luminescence values are indeed the result of a plant ROS burst in response to an immunogenic agent, rather than by chance or background contamination.

Boiled WT *hrcN* cellular lysate led to a calculated relative luminescence peak curve area of 10 8098. *E208D hrcN* was the test sample that gave the lowest measurement of 8616. This was a percentage change of -92 %, however this difference was not statistically significant (p = 0.2). No *hrcN* samples led to a luminenscence value greater than that measured with the WT.

As seen in the previous experiment, while differences were observed between *hrcN* samples, none of these differences were statistically significant. The relative luminescence peak area for Δ*hrcC* was calculated to be 96 220 (a -11 % change compared to WT, p = 0.9), Δ*hrcN* was 47 015 (a -57 % change compared to WT, p = 0.4), *G176A* was 44 988 (a -58 % change compared to WT, p = 0.4), *G311A* was 10 197 (a -90.6 % change compared to WT, p = 0.2), *L338V* was 48310 (a -55 % change compared to WT, p = 0.4), *F174Y* was 26 948 (a -75 % change compared to WT, p = 0.2), and the relative luminescence ROS burst curve area for *P142G* was calculated to be 21 120 (a -80.5 % change compared to WT, p = 0.2).

This experiment confirms that similar levels of immunogenicity exist between lysed *hrcN P. syringae* samples. While small differences between strains may be present, these are not statistically significant. The ROS burst experiments shown in Figure 4.22 and Figure 4.23 suggest that the leaf disease phenotype differences observed between mutant *hrcN* strains are not caused by a variations in immunogenicity towards the plant defence responses, even if a portion of bacterial cells are ruptured during the infiltration process.
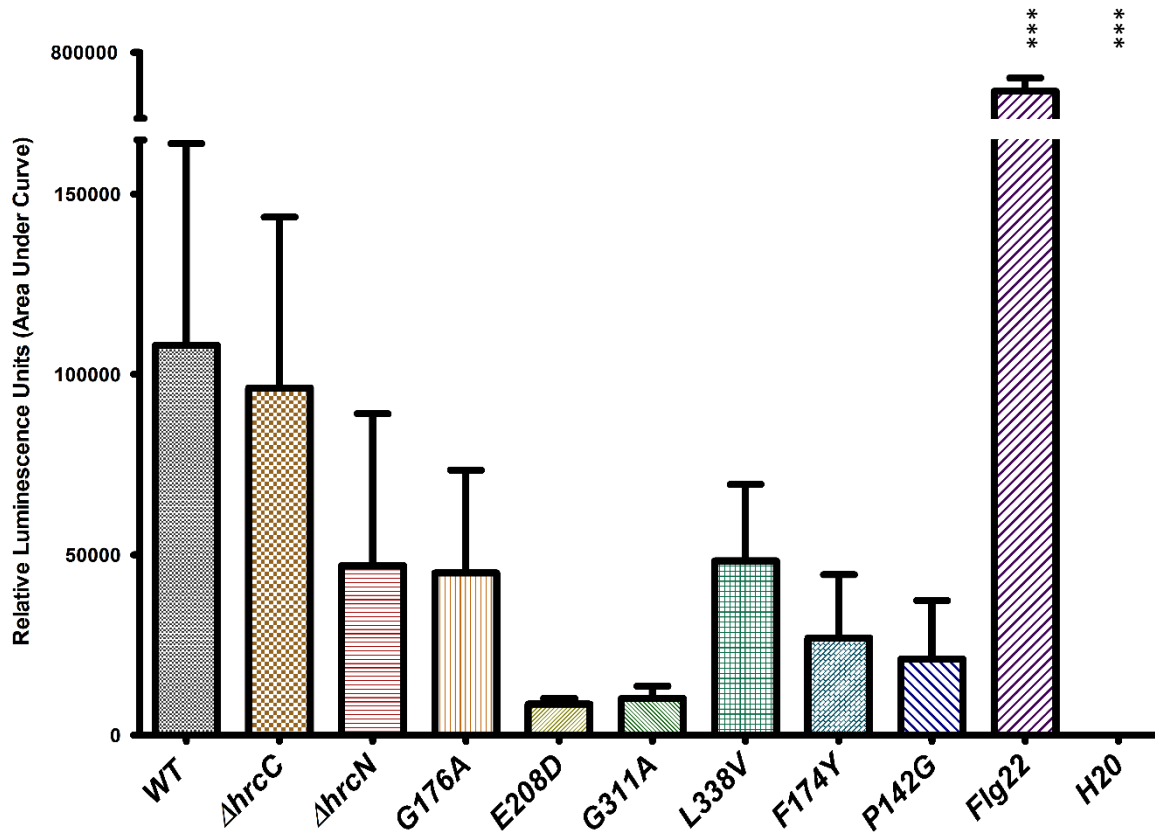
Figure 4.23. Relative luminescence values observed for ROS burst plant immune responses for washed and boiled *Pto hrcN* mutant lysates applied to *A. thaliana* Col-0 discs over a 2-hour period. Error bars show standard error of the mean. Asterisks represent a statistically significant difference of a given sample compared to the WT (2 sample t-test) where '***' denotes p ≤ 0.001 (n = 3).

4.2.7.   Long-term Infection Assays Show No Late-stage Failure to Thrive in *G176A* or *G311A hrcN* Mutants

The next hypothesis tested was that mutating the predicted CdG:HrcN binding interface impacted the success of late-stage infection. While cell densities for infection assays are generally measured at 3 days post-infection, leaf phenotypes are only measured after 5-7 days. If the *hrcN* mutants were rapidly cleared following the initial stages of an infection, this time window could explain why certain mutations showed different phenotypes when compared to WT *hrcN*. An *A. thaliana* infiltration experiment with *Pto hrcN* mutant strains over an extended infection window of 8 days is shown in Figure 4.24.

No significant increase in bacterial load was observed for the negative controls Δ*hrcC* and Δ*hrcN* over the course of the experiment, as expected. At day 1 post-infection, the strains are 3.5 and 3.2 log(cfu/cm^2) respectively. Across the entire infection up to day 8, these two strains were able to colonise to cell densities no greater than 4.5 log(cfu/cm^2). This was not a statistically significant difference confirming that strains lacking a functional T3SS were not able to achieve bacterial plant colonisation.

The WT, *G176A*, *E208D*, *G311A*, *L338V*, *F174Y* and *P142G* strains were able to achieve complete bacterial colonisation, however, with no statistically significant differences present between any of the mutant strains. At day 1 post-infection, the strains had reached densities of between 4 and 5 log(cfu/cm^2). By day 2, all of these strains reached a bacterial load of between 7 and 8 log(cfu/cm^2). This represents a statistically significant increase for all strains (p = <0.001).

As the infection proceeded beyond the standard 3-day infection window, bacterial load began to decrease as the bacterial death phase was reached; leaf tissue began to die, and nutrients ultimately began to run out. From day 4, the WT, *G176A*, *E208D*, *G311A*, *L338V*, *F174Y* and *P142G* strains are at a comparable level to day 2 and day 3 post infection, with cell densities between 7 and 8 log(cfu/cm^2). As the infection window progresses towards day 8, a steady decrease of bacterial load was observed for all these strains to values between 5.7 and 6.7 log(cfu/cm^2). Some minor variations were observed during this decline, which can most likely be attributed to the poor condition of individual leaves during this period.

This experiment suggests that differences in disease phenotypes between the *Pto hrcN* mutants are unlikely caused by variations in cell density in the later stages of infection. The WT, *G176A*, *E208D*, *G311A*, *L338V*, *F174Y* and *P142G* mutant *hrcN* strains are all able to infect to a similar level from day 1 post-infection to day 8 post-infection.
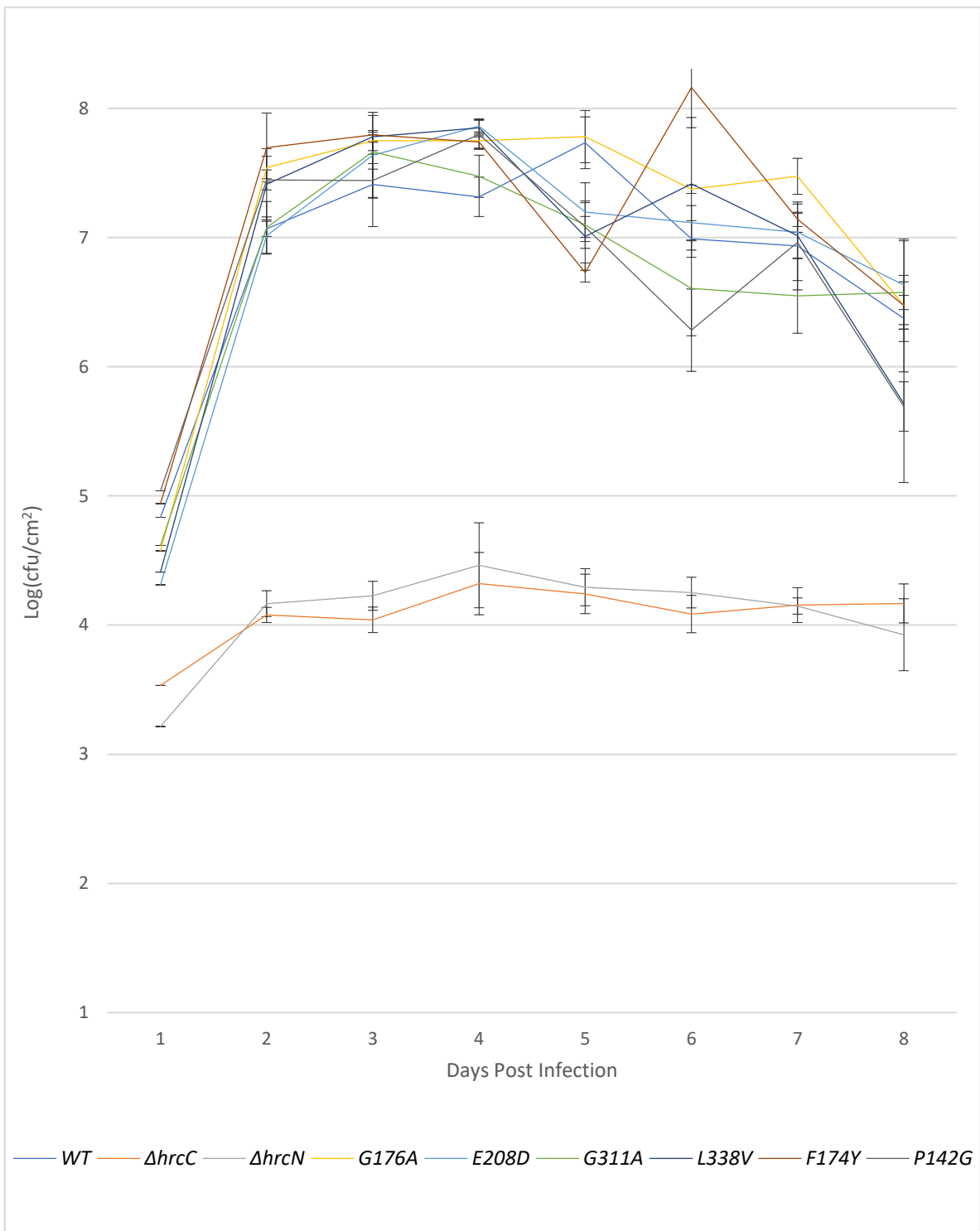
Figure 4.24. Extended infection window infiltration assays, using *A. thaliana* Col-0 plants with *Pto hrcN* mutant strains. Colony forming units were enumerated from 4 mm diameter leaf disc sampling across an 8-day infection window. Error bars show standard error of the mean (n = 3 plants).

4.2.8. A Recovery of Disease Severity Was Observed for *Pto* DC3000 Carrying *G176A* and *G311A hrcN* Mutant Alleles in Infections of Immune-compromised *A. thaliana*

4.2.8.1. Immunocompromised fec Plants

4.2.8.1.1. Leaf Phenotypes

A variety of potential hypotheses that seek to explain the differences in leaf phenotypes seen between mutant *hrcN P. syringae* strains have been tested within this chapter. The strongest hypothesis that remains is whether mutating the T3SS *hrcN*:CdG binding site affects the correct translocation of effector proteins from *P. syringae* to host.

In Figure 4.25, immunocompromised *A. thaliana* plants have been infiltrated with *Pto hrcN* mutant strains. These are fec mutant plants, which have *fls2*, *efr* and *cerk1*-dependent immunity genes deleted and so lack a functional immune system. Many effector proteins are directly involved in host immune manipulation, so if mutation of the T3SS HrcN:CdG binding site affects effector protein translocation, then different disease symptoms may arise compared to non-immunocompromised plants.

WT *hrcN* displays characteristic *P. syringae* disease symptoms with no visible variation with WT Col-0 *A. thaliana* infection (Figure 4.25). Chlorosis, necrosis, and leaf wilting were all observed as before. Infection with the negative control Δ*hrcC* showed healthy leaves with no indication of any disease symptoms as expected.

However, *G176A* and *G311A*, which displayed minimal symptoms in WT Col-0 now display extensive disease symptoms in fec *A. thaliana.* There is even chlorosis spread across the leaves with signs of necrosis and wilting.

E208D shows disease symptoms similar to that of the WT. It could be argued that any visual hints of hypervirulence seen in this strain are now not present in this immunocompromised infection.
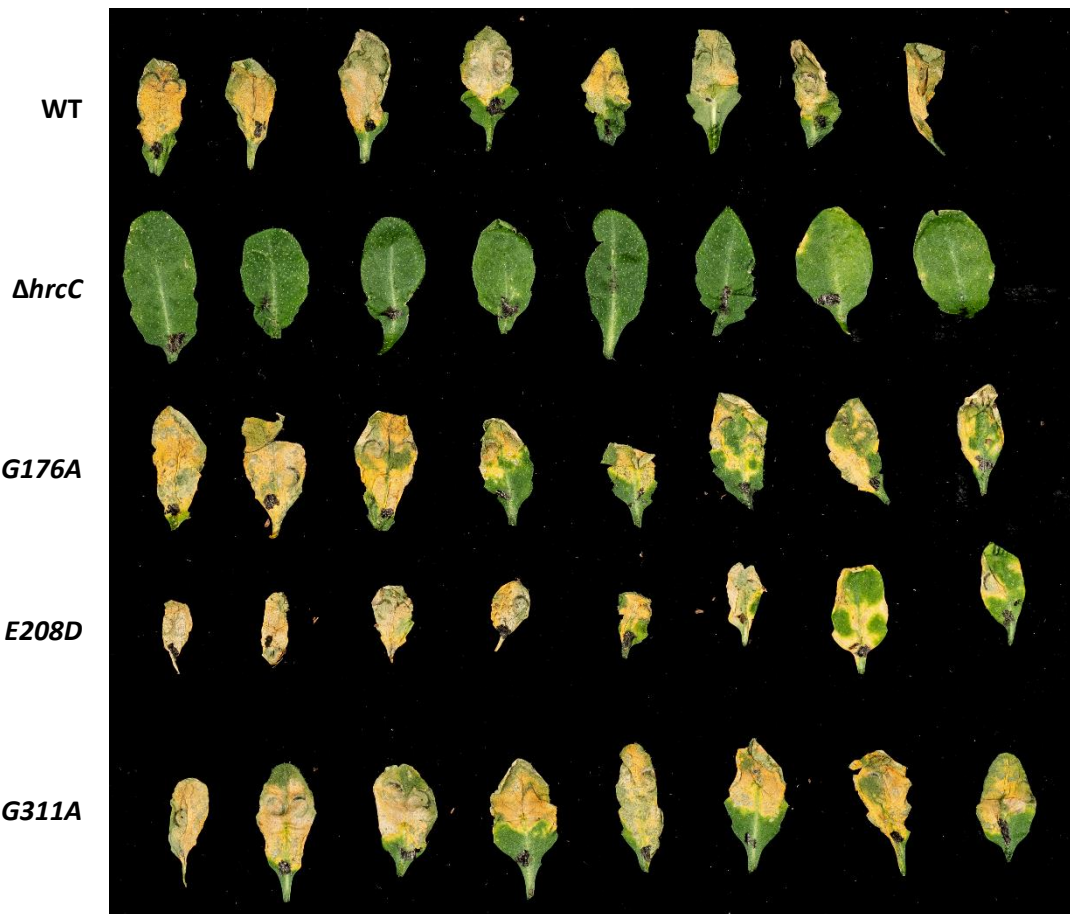
Figure 4.25. Mutant *Pto hrcN* infiltration infections of immunocompromised fec *A. thaliana*. Photos taken 6 days post-infection (n= 3 plants).

4.2.8.1.2. Quantified Visual Disease Severity

The visual disease severity represented by leaf yellowing was quantified by calculation of the average pixel intensity across the sampled leaves using ImageJ software. This has been shown in Figure 4.26.

Comparing WT to the *G176A*, *E208D* and *G311A hrcN* mutants, no significant differences were observed. There was a statistically significant difference with the Δ*hrcC* (p= 0.00001) negative control as expected.

An ANOVA across the columns confirms that statistically significant differences are present (p = < 0.0001).
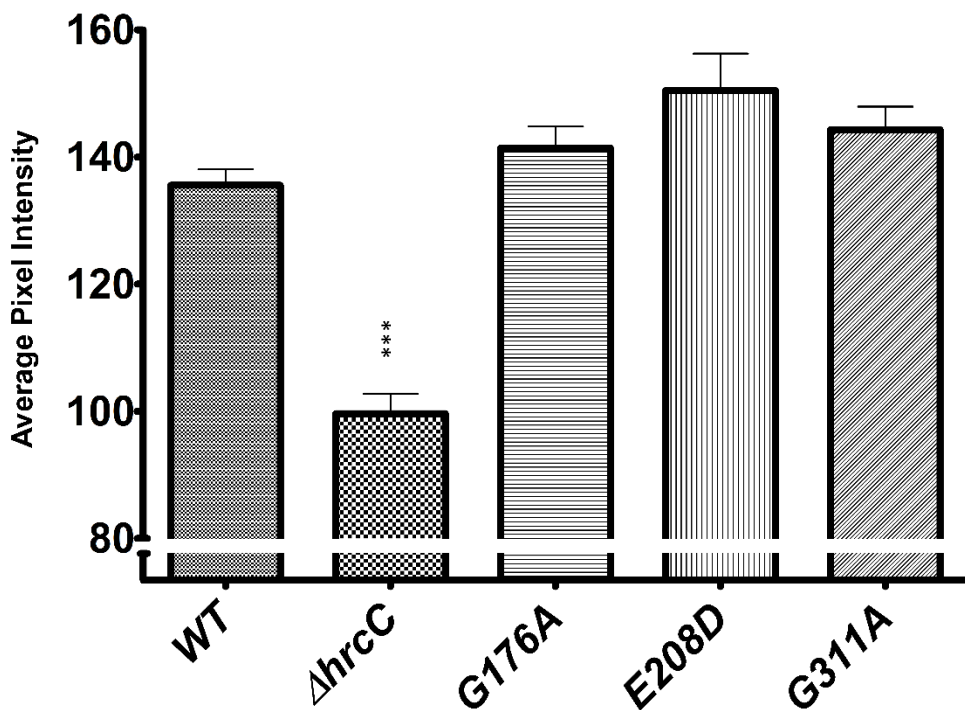
Figure 4.26. Average pixel intensity analysis representing levels of leaf yellowing for *A. thaliana* immuno-compromised fec leaves infiltrated with *Pto hrcN* mutant strains 6 days post-infection. Average pixel intensity calculation was performed using ImageJ software (version 1.52a). Error bars show standard error of the mean. Asterisks represent a statistical significance difference of a given sample compared to the WT (2 sample t-test) where '***' denotes $p \leq 0.001$. (n = 8 leaves)

4.2.8.1.3. Bacterial Load

The bacterial load for this fec infiltration is shown in Figure 4.27. The WT, *G176A*, *E208D* and *G311A* strains all infect well and are not significantly different from each other when comparing individual days. At day 0 post-infection, these strains grow to densities between 3 and 4 log(cfu/cm^2). By day 2 and 3, these strains have been able to establish a complete bacterial colonisation. By day 3, all these strains reached cell densities between 7.5 and 8 log(cfu/cm^2). This is a statistically significant increase for WT, *G176A*, *E208D* and *G311A* between day 0 and day 3 (p = <0.001).

At day 0 post-infection, Δ*hrcC* reaches 3.2 log(cfu/cm^2) similar to the other strains in this infection. By day 2 and 3, Δ*hrcC* was only able to reach 4.6 log(cfu/cm^2). There is a significant difference between day 3 of the WT and day 3 of Δ*hrcC* (p = <0.001). The Δ*hrcC* negative control was unable to achieve a significant increase in bacterial load across the infection window and as such, it was confirmed that bacterial colonisation did not occur for this mutant, even in the fec background.
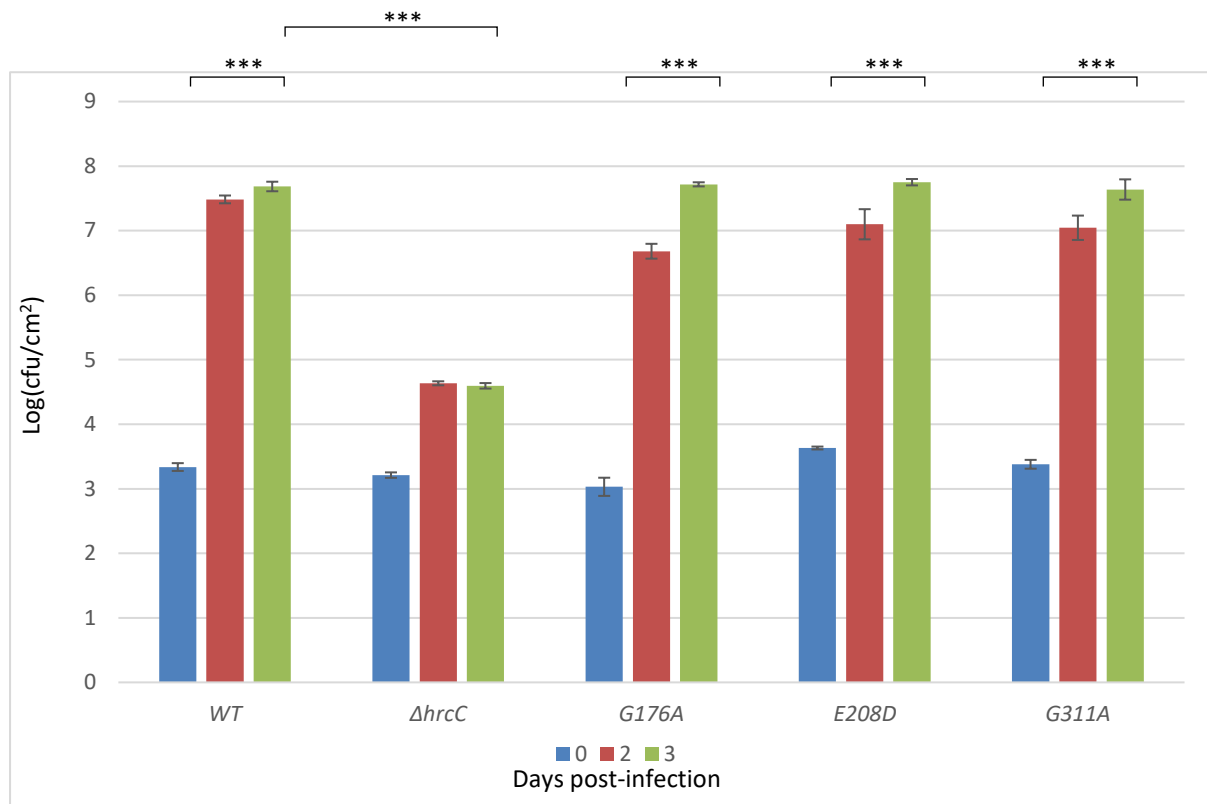
Figure 4.27. Mutant *Pto hrcN* mutant infiltration infections of immunocompromised fec *A. thaliana*. These plants have *fls2*, *efr* and *cerk1*-dependent immunity deleted. Error bars show standard error of the mean. Asterisks represent a statistical significance difference of a given sample compared to the WT (2 sample t-test) where '***' denotes $p \leq 0.001$ (n = 3 plants)

4.2.8.2.   Immunocompromised *Arabidopsis thaliana* bbc Plants

4.2.8.2.1. Leaf Phenotypes

Next, a second immunocompromised *A. thaliana* mutant was infiltrated with mutant *hrcN P. syringae Pto* DC3000 (Figure 4.28). This is bbc *A. thaliana* which has *bak1-5, bkk-1, cerk1*-dependent immunity deleted. Like the fec *A. thaliana* mutant, this variety lacks a functioning immune system, however this has been achieved through mutagenesis of different key pathways.

What is seen with the infection in bbc immunocompromised *A. thaliana* is that the WT infects as expected. Chlorosis was evenly distributed across the leaves with evidence of necrosis and wilting, commonly observed with *P. syringae* infections.

The negative controls Δ*hrcC* and Δ*hrcN* do not show evidence of full bacterial colonisation being established with no prominent disease symptoms. There were some minor traces of leaf wounding around the infiltration sites, however no leaf chlorosis or necrosis symptoms were visible across the leaves.

G176A and *G311A* previously displayed minimal or no disease symptoms in standard non-immunocompromised *A. thaliana* Col-0 (Figure 4.7). However, in the bbc infection shown in Figure 4.28, characteristic disease symptoms were restored. There is evidence of extensive chlorosis that is evenly spread across the leaves, visible necrosis and a high degree of leaf wilting.

E208D, *L338V*, *F174Y* and *P142G* all show similar levels of disease severity. Any previous traces of potential hyper-virulence are not present within this bbc infection. All strains are consistent with observations of the WT. There is evidence of evenly-spread chlorosis, leaf necrosis and leaf wilting that is characteristic of WT *P. syringae* infections.

The uninfected control bbc leaves remain healthy. They show no evidence of chlorosis or necrosis. This confirms that the symptoms observed from mutant *hrcN* strain infiltration are highly likely to be caused by the bacterial infiltration as opposed to any external factors.
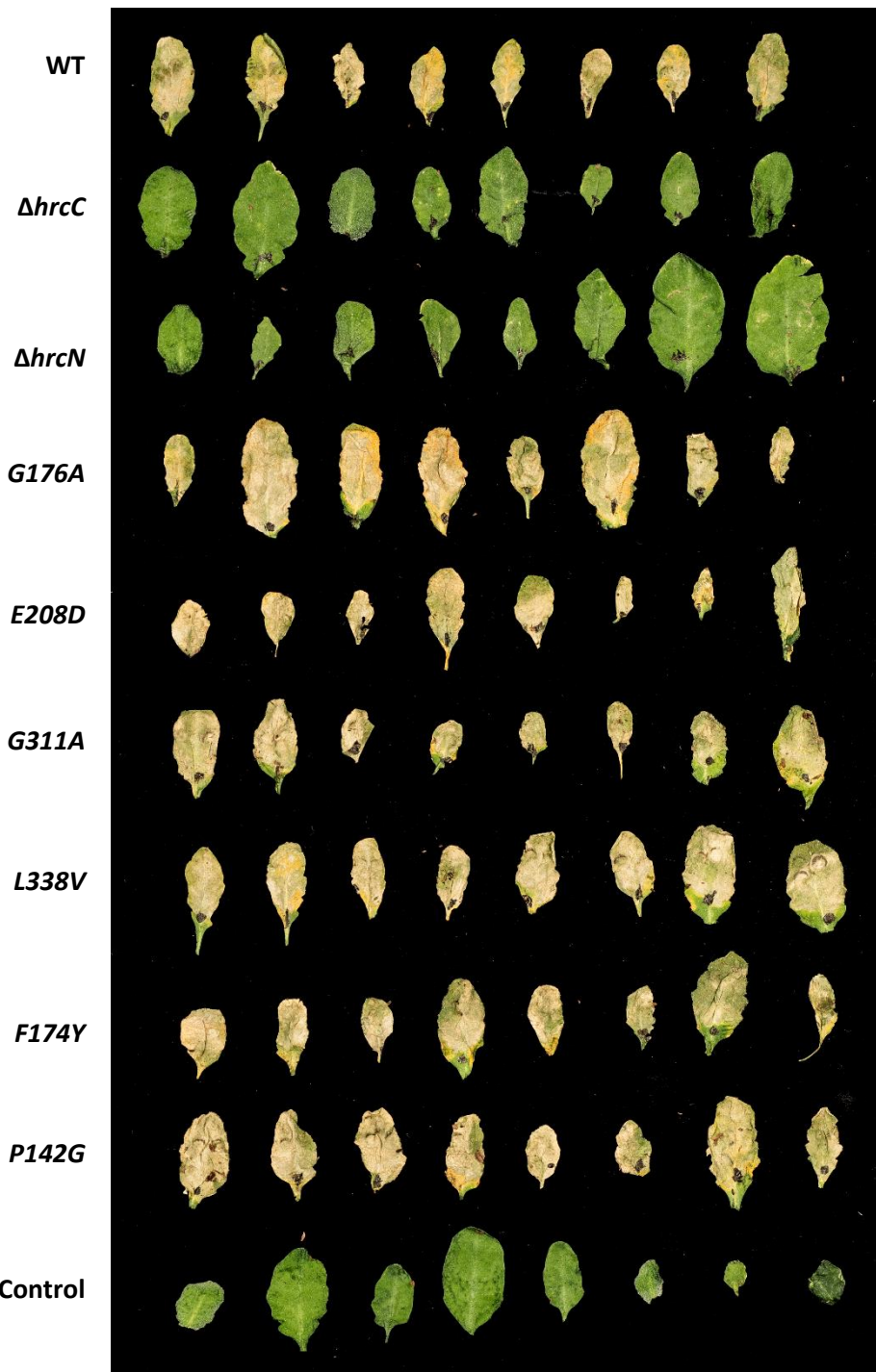
Figure 4.28. Mutant *Pto hrcN* infiltration infections of immunocompromised bbc *A. thaliana*. These plants have *bak1-5,bkk-1,cerk1*-dependent immunity deleted. Photos taken 6 days post-infection (n = 3 plants)

4.2.8.2.2. Quantified Visual Disease Severity

Visual disease severity by way of leaf yellowing was calculated using ImageJ to perform average pixel intensity analyses. This is shown in Figure 4.29.

Comparing WT to Δ*hrcC* (p = 0.00001), Δ*hrcN* (p = 0.00001), and the uninfected leaf control (p = 0.00001) shows statistically significant differences as expected. There are no statistically significant differences between the WT and any of the other *hrcN* point-mutants.

An ANOVA statistical test across the columns confirms that the mean averages of the columns are not identical and that statistically significant differences are present (p = < 0.0001).
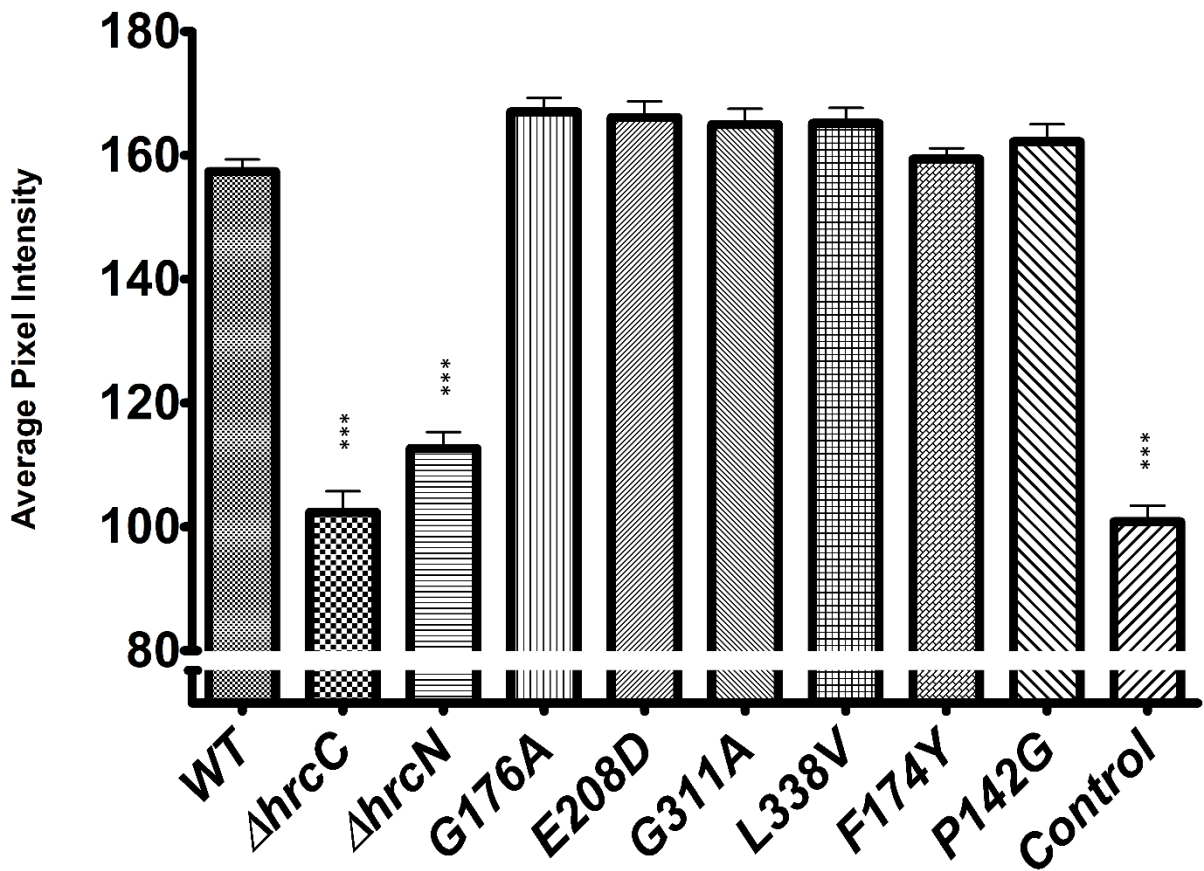
Figure 4.29. Average pixel intensity analysis across representing levels of leaf yellowing for *A. thaliana* immuno-compromised bbc leaves infiltrated with mutant *Pto* strains (carrying mutant *hrcN* alleles) 6 days post-infection. Average pixel intensity calculation was performed using ImageJ software (version 1.52a). Error bars show standard error of the mean. Asterisks represent a statistically significant difference of a given sample compared to the WT (2 sample t-test) where '***' denotes p = ≤ 0.001. (n = 8 leaves)

4.2.8.2.3. Bacterial Load

Shown in Figure 4.30 are the bacterial load values for the bbc *A. thaliana* infiltration with mutant *hrcN P. syringae Pto* DC3000. Similar trends are observed comparable to previous infections discussed in this chapter.

The WT, *G176A*, *E208D*, *G311A*, *L338V*, *F174Y* and *P142G hrcN* strains all display comparable levels of bacterial colonisation with no significant differences present when comparing between strains for the same days. All of these strains reach cell densities of approximately 4 $log(cfu/cm^2)$ at day 0 post-infection. By day 2 and day 3, these values are all between 7 and 8 $log(cfu/cm^2)$. This is a statistically significant increase for all strains when comparing day 0 with day 3 of the infection process (p = <0.001).

The negative controls Δ*hrcC* and Δ*hrcN* show minimal increases in bacterial load confirming that complete bacterial colonisation was not possible for these strains. Like the other strains in the experiment, these controls reached cell densities of approximately 4 log(cfu/cm^2) at day 0 post-infection. By day 2 and 3, these strains could reach no higher than 5.5 log(cfu/cm^2). There is a significant difference between day 3 for the WT and for Δ*hrcC* (p = <0.001). This confirms that strains lacking a fully functional type III secretion system were not able to achieve complete leaf infection.
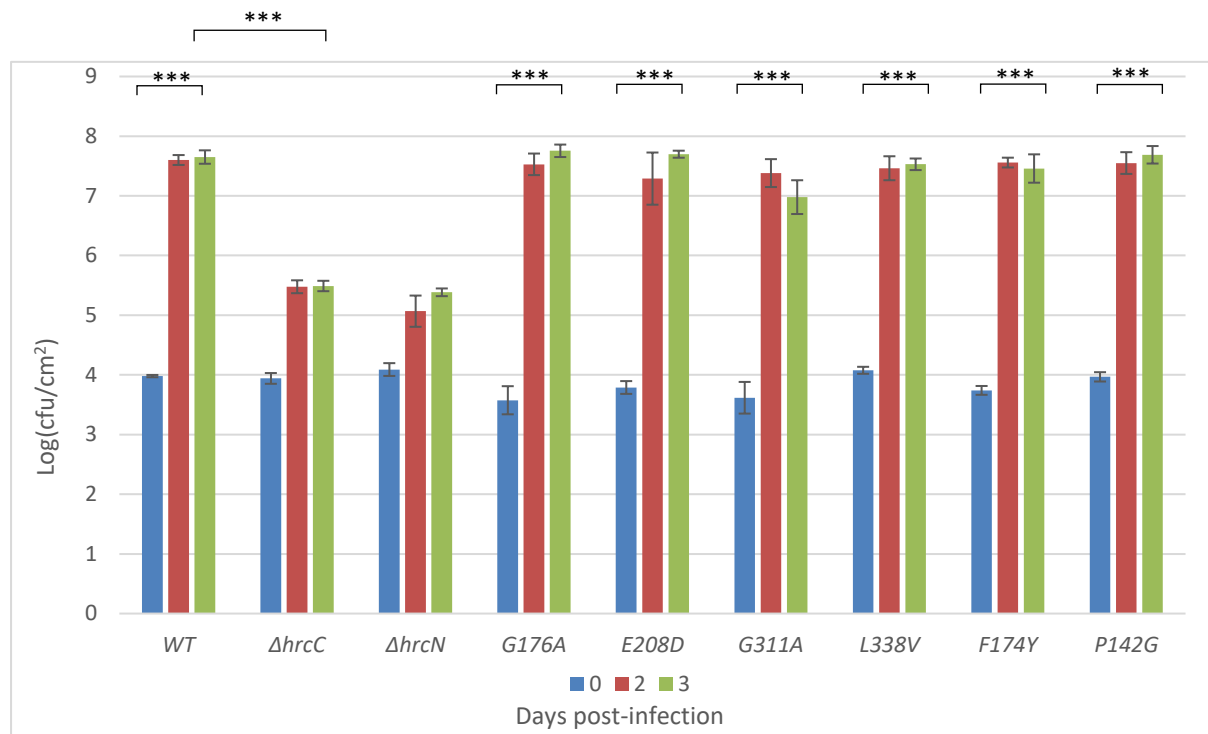
Figure 4.30. *Pto* DC3000 (carrying mutant *hrcN* alleles) infiltration infections of immunocompromised bbc *A. thaliana*. These plants have bak1-5,bkk-1,cerk1-dependent immunity deleted. Error bars show standard error of the mean. Asterisks represent a statistically significant difference of a given sample compared to the WT (2 sample t-test) where '***' denotes p = ≤ 0.001. (n = 3 plants)

4.2.9. Overexpression of the Phosphodiesterase (PDE) *bifA* (Low Background CdG) Levels) Induces Altered Disease Phenotypes with Strains Carrying *G176A* and *G311A hrcN* Mutations in Col-0 Leaf Infiltrations Compared to WT *Pto*

4.2.9.1. Leaf Phenotypes

To examine the effect of cdG on plant infection by *Pto hrcN* mutants, *Pto* infection strains were produced containing a pBBR4-*tac-bifA* plasmid, which expressed the *bifA* phosphodiesterase gene. BifA breaks down CdG resulting in very low levels of background CdG. This experiment was performed to probe the link between CdG and virulence through type III-mediated infection. Infiltration infections are shown in Figure 4.31.

When comparing sample rows , some interesting differences can be noted. The Δ*hrcC*, Δ*hrcN* and the uninfected leaf control show no visible signs of chlorosis or necrosis as expected. In comparison, WT, *G176A*, *E208D*, *G311A*, *L338V*, *F174Y* and *P142G* all show varying levels of disease severity. In this experiment overall disease severity appears to be lower with the addition of *bifA* when compared to

a standard WT infection without *bifA*. The level of disease severity in *G176A* also appears lower (with less chlorosis and necrosis) when compared to other infection strains.
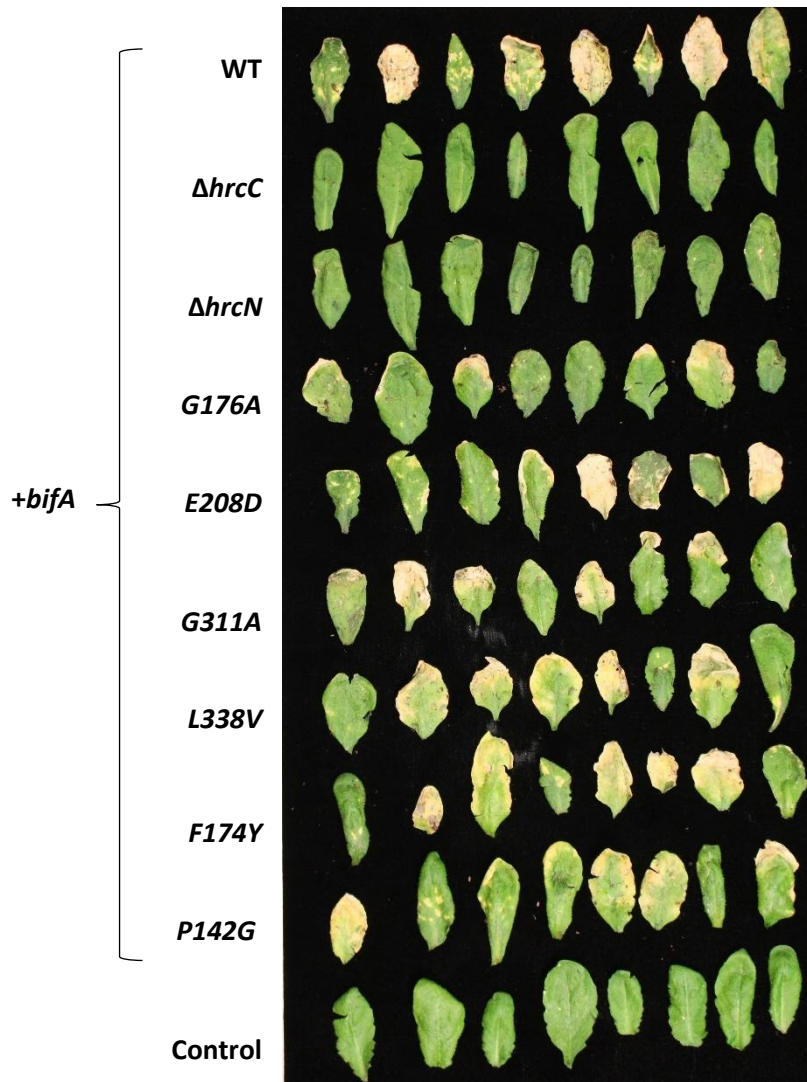
Figure 4.31. Infiltrated *A. thaliana* Col-0 plants with *Pto* DC3000 strains (carrying mutant *hrcN* alleles) expressing a *bifA* phosphodiesterase on a pBBR4-*tac* plasmid for a low CdG background. Visual disease phenotype leaf images were taken at day 6 post-infection (n = 3 plants).

4.2.9.2.   Quantified Visual Disease Severity

In Figure 4.32, *hrcN Pto* strains + pBBR4-*tac-bifA* (in a low CdG background) infiltrated into *A. thaliana* Col-0 plants has been quantified via ImageJ. What was observed were comparable average pixel intensity values for WT, *E208D*, *G311A*, *L338V*, *F174Y* and *P142G* with *bifA*. *G176A* was measured to have a lower average pixel intensity across the leaves. The negative controls (Δ*hrcC*, Δ*hrcN* and the uninfected control leaves) all had the lowest average pixel intensity values as expected.

An ANOVA across all of the columns show that statistically significant differences are present and that the mean averages of the samples are not identical (p = <0.0001). Comparing any of the negative

controls to the WT *hrcN* or point-mutant *hrcN* columns shows a statistically significant difference (p = < 0.0001) in all cases. When comparing the WT to the point-mutants there are no statistically significant differences except for *G176A* which did have a statistically significant difference (p = < 0.03).
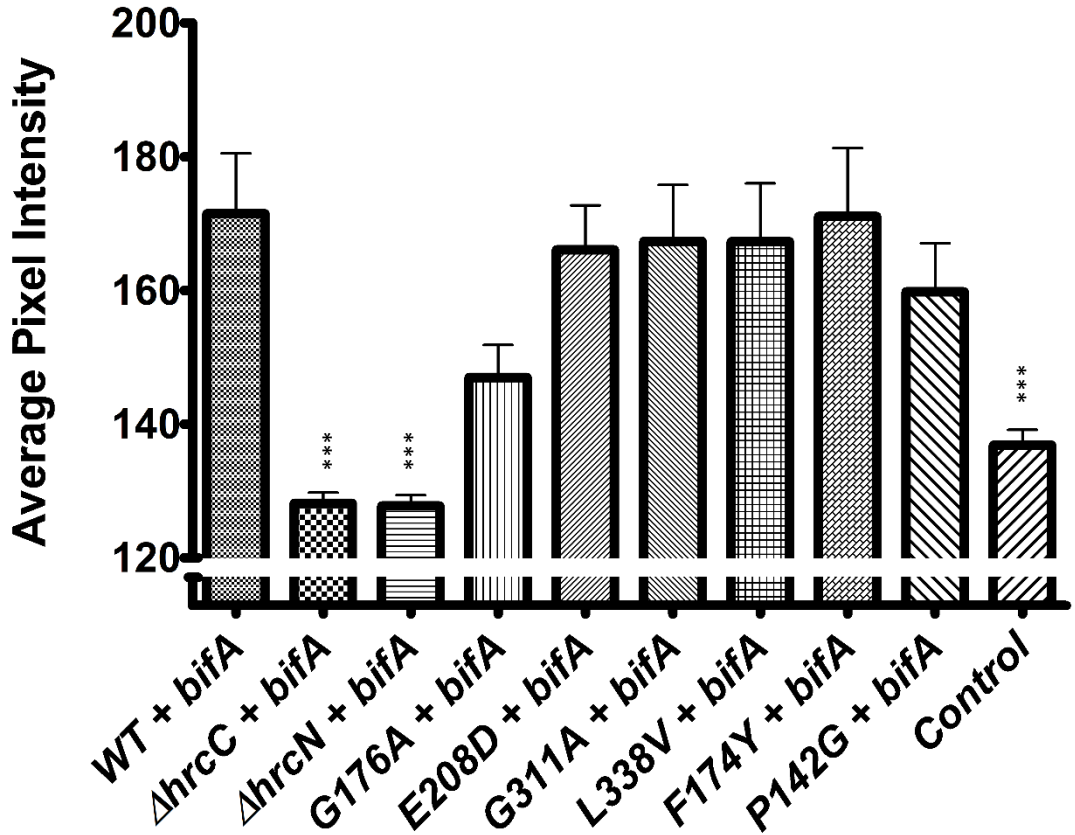
Figure 4.32. ImageJ pixel intensity analysis quantifying chlorosis disease phenotypes present for *A. thaliana* Col-0 infiltrated with *Pto hrcN* + pBBR4-*tac-bifA* (low background CdG) strains at day 6 post-infection. The average pixel intensity (0 to 255) was measured across the area of each infected leaf which was then subsequently averaged for each sample. A greater average pixel intensity correlates with an increase in disease severity by way of leaf chlorosis. Error bars show standard error of the mean. Asterisks represent a statistically significant difference of a given sample compared to the WT (2 sample t-test) where '***' denotes p = ≤ 0.001. (n = 8 leaves)

4.2.9.3.   Bacterial Load

In Figure 4.33, what can be seen is that the cfu values for WT, *G176A*, *E208D*, *G311A*, *L338V*, *F174Y* and *P142G* are all comparable by day 3 post-infection reaching around 7 mean log(cfu/cm^2). In comparison, the negative Δ*hrcC* and Δ*hrcN* were not able to establish leaf colonisation with a much lower day 3 post-infection value of below 4 mean log(cfu/cm^2).

Comparing day 3 post-infection for WT against the negative controls Δ*hrcC* and Δ*hrcN* shows a statistically significant difference (p = 0.0001 for both). No statistically significant differences are observed among the WT and point-mutant columns.
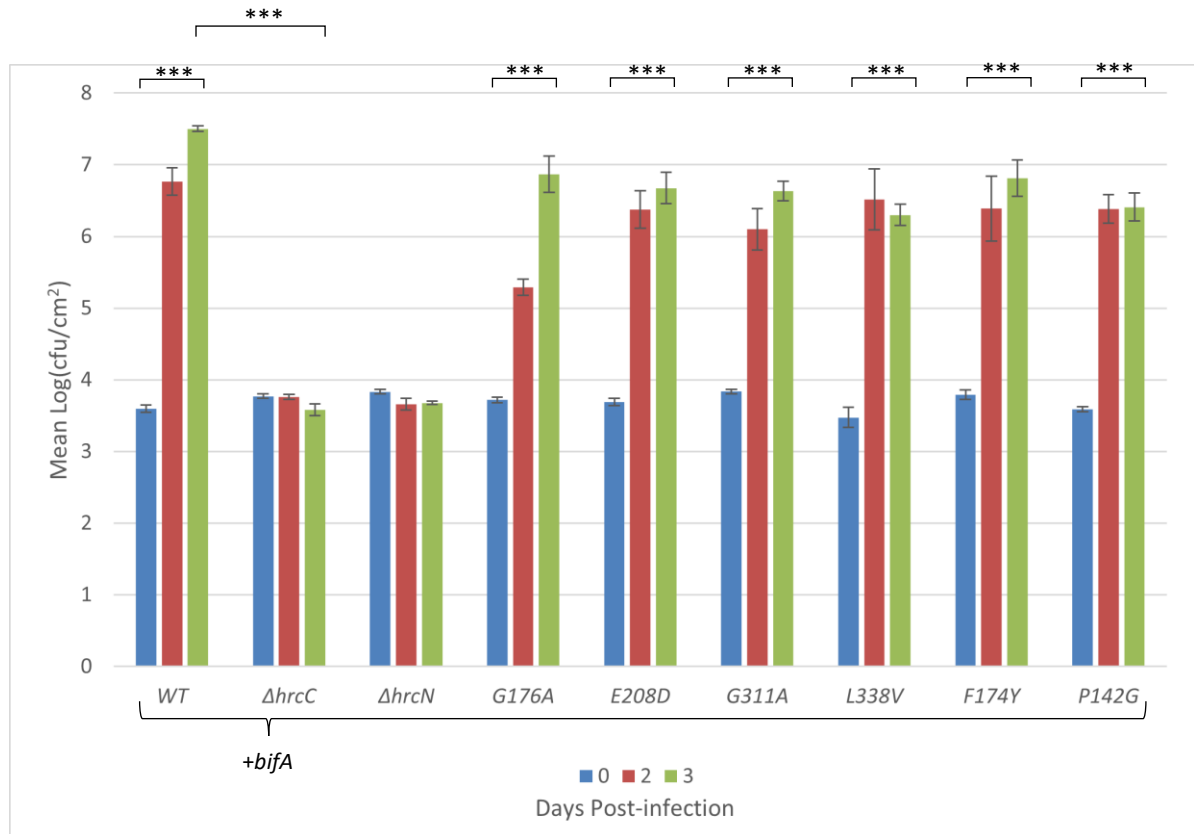
Figure 4.33. Infiltrated *A. thaliana* Col-0 plants with *Pto* DC3000 strains (carrying mutant *hrcN* alleles) expressing a *bifA* phosphodiesterase on a pBBR4-*tac* plasmid for a low CdG background. Leaves were sampled for cfu counts at day 0, 2 and 3 post-infection. Error bars show standard error of the mean. Asterisks represent a statistically significant difference of a given sample compared to the WT (2 sample t-test) where '***' denotes p = ≤ 0.001. (n = 3 plants).

4.2.10. Over-expression of Diguanylate Cyclase (DGC) *wspR19* (High Background CdG Levels) Shows an Altered Disease Phenotype with Strains Carrying *G176A* and *G311A hrcN* Mutations in Col-0 Leaf Infiltrations Compared to WT *Pto*

4.2.10.1. Leaf Phenotypes

In Figure 4.34, visual disease phenotypes from an *A. thaliana* Col-0 infiltration assay in a high CdG environment are shown. These *Pto* DC3000 infection strains had a pBBR4-*tac*-*wspR19* plasmid which expressed a *wspR19* diguanylate cyclase which leads to the synthesis of CdG resulting in higher levels of background CdG (an estimated 15 times than that of a WT background) (Pfeilmeier et al., 2016). This was performed to confirm a link between CdG and virulence through type III-mediated infection by evaluating the resulting infection phenotypes across *hrcN* mutants.

Day 6 post-infection leaves are shown allowing for visual comparison of disease phenotypes. Δ*hrcC*, Δ*hrcN* and the uninfected control show no evidence of chlorosis or necrosis as expected. In comparison, WT, *G176A*, *E208D*, *G311A*, *L338V*, *F174Y* and *P142G* all show a high level of chlorosis and necrosis. This level of disease severity seems comparable across these mutants in general.
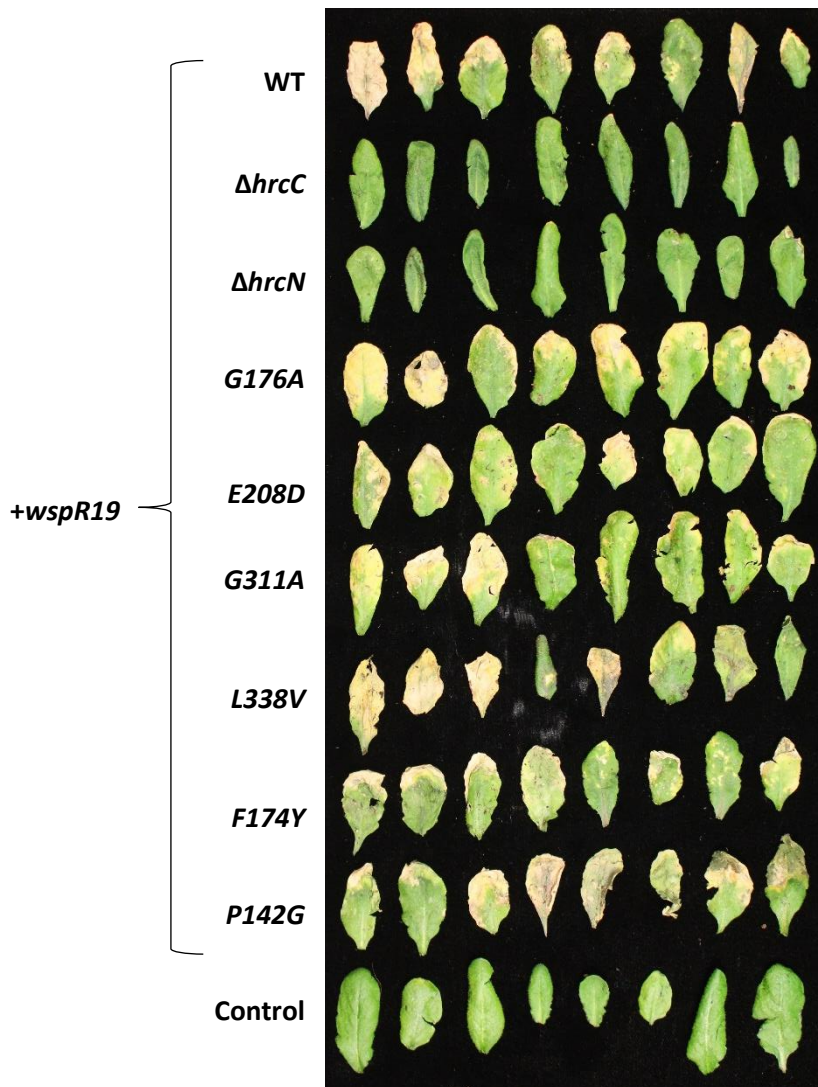
Figure 4.34. Infiltrated *A. thaliana* Col-0 plants with *Pto* DC3000 strains (carrying mutant *hrcN* alleles) expressing a *wspR19* diguanylate cyclase on a pBBR4-*tac* plasmid for a high CdG background (15x that of WT). Visual disease phenotype leaf images were taken at day 6 post-infection (n = 3 plants).

4.2.10.2. Quantified Visual Disease Severity

In Figure 4.35, *hrcN Pto* DC3000 strains + pBBR4-*tac-wspR19* (in a high CdG background) infiltrated into *A. thaliana* Col-0 plants has been quantified via ImageJ. In this analysis, the negative Δ*hrcC*, Δ*hrcN* and uninfected controls had the lowest average pixel intensity values. When compared to the other samples, this difference was statistically significant. WT, *G176A*, *E208D*, *G311A*, *L338V*, *F174Y* and *P142G* with *wspR19* had comparable greater average pixel intensity values.

An ANOVA across all the columns show that statistically significant differences are present and that the mean averages of the samples are not identical (p = <0.0001). Comparing any of the negative controls to the WT *hrcN* or point-mutant *hrcN* columns shows a statistically significant difference (p = < 0.0001) in all cases.
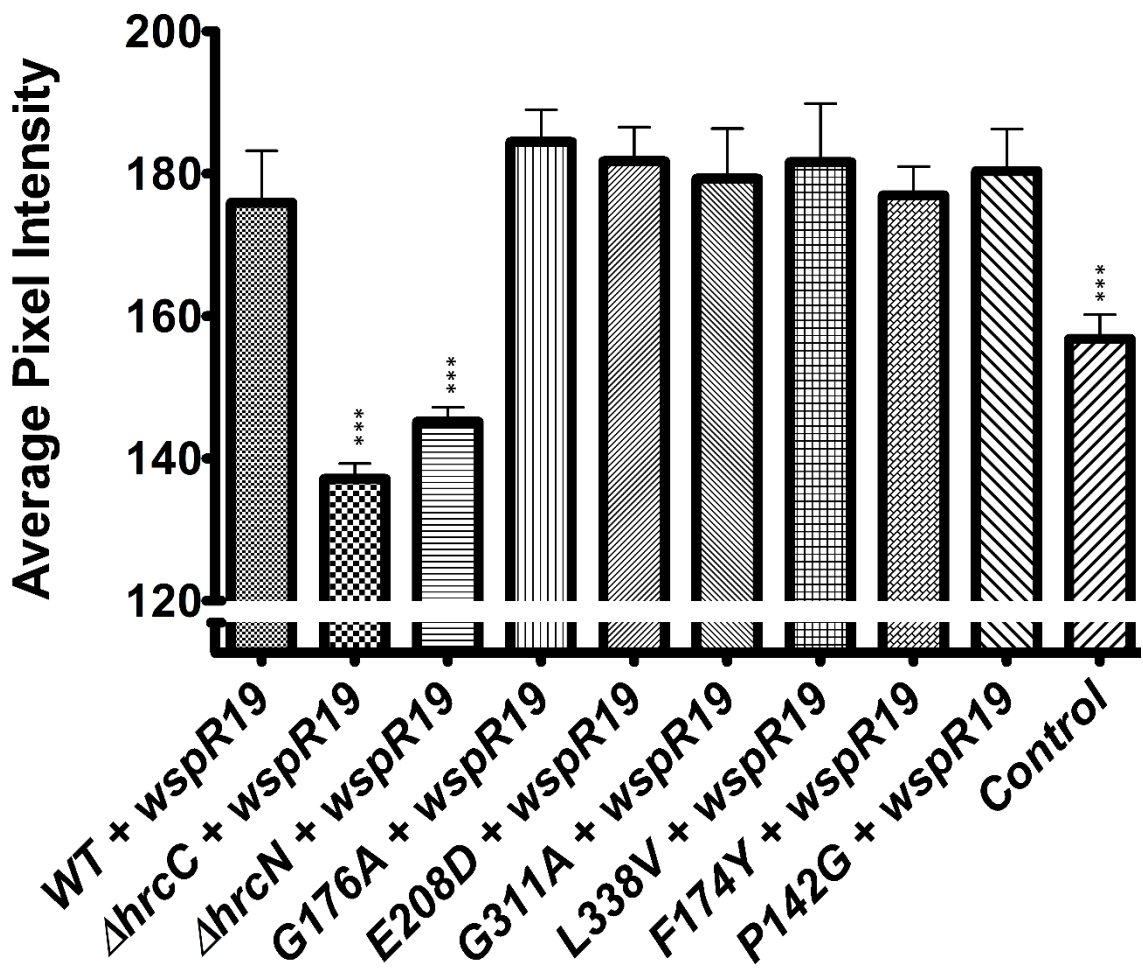
Figure 4.35. ImageJ pixel intensity analysis quantifying chlorosis disease phenotypes present for *A. thaliana* Col-0 infiltrated with *Pto hrcN* + pBBR4-*tac-wsprR19* (high background CdG) strains at day 6 post-infection. The average pixel intensity (0 to 255) was measured across the area of each infected leaf which was then subsequently averaged for each sample. A greater average pixel intensity correlates with an increase in disease severity by way of leaf chlorosis. Error bars show standard error of the mean. Asterisks represent a statistically significant difference of a given sample compared to the WT (2 sample t-test) where '***' denotes P = ≤ 0.001. (n = 8 leaves)

4.2.10.3.   Bacterial Load

In Figure 4.36, what can be seen is that the cfu values for WT, *G176A*, *E208D*, *G311A*, *L338V*, *F174Y* and *P142G* are all comparable by day 3 post-infection reaching around 7 mean log(cfu/cm^2). The value for *F174Y* is slightly lower but this is a non-significant difference. In comparison, the negative Δ*hrcC* and Δ*hrcN* were not able to establish leaf colonisation with a much lower day 3 post-infection value of below 4 mean log(cfu/cm^2).

Comparing day 3 post-infection for WT against the negative controls Δ*hrcC* and Δ*hrcN* shows a statistically significant difference (p = 0.0001 for both). No statistically significant differences are observed among the WT and point-mutant columns themselves.
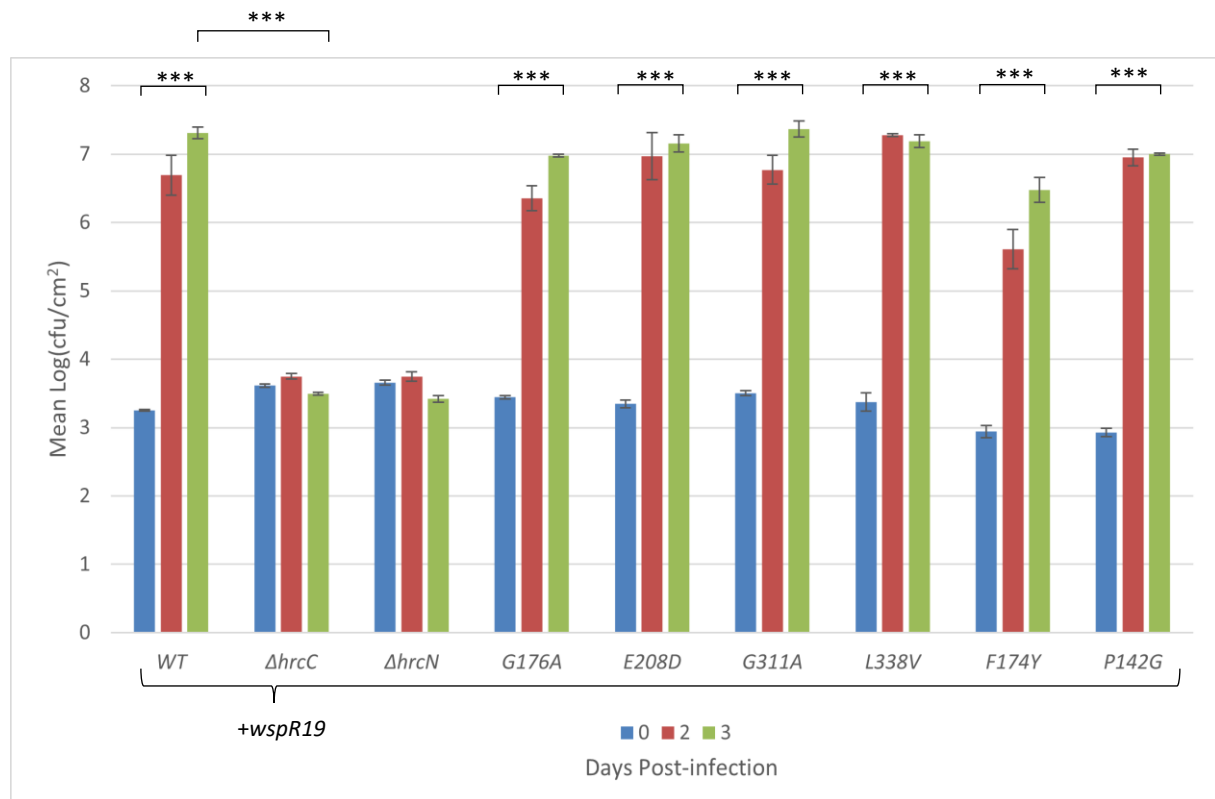
Figure 4.36. Infiltrated *A. thaliana* Col-0 plants with *Pto* DC3000 strains (carrying mutant *hrcN* alleles) expressing a *wspR19* diguanylate cyclase on a pBBR4-*tac* plasmid for a high CdG background. Leaves were sampled for cfu counts at day 0, 2 and 3 post-infection. Error bars show standard error of the mean. Asterisks represent a statistically significant difference of a given sample compared to the WT (2 sample t-test) where '***' denotes p = ≤ 0.001. (n = 3 plants).

4.2.11. T3SS System Components Are Still Present in a Low or High CdG Infection Background

4.2.11.1. Anti-HrcN

hrcN Pto DC3000 strains were used to infect *Arabidopsis thaliana* Col-0 leaf tissue. These bacterial strains had a low or high cellular CdG background environment. This was achieved by constitutive over-expression of phosphodiesterase *bifA* (low CdG levels, trace amounts) or diguanylate cyclase *wspR19* (high CdG levels, approximately 15 time greater than WT) on a stable pBBR4 plasmid throughout infection. At 3 days post-infection, infected leaves were collected and T3SS components were analysed by way of Western blot. Blotting with an anti-HrcN antibody has been shown in Figure 4.37. A HrcN band is present as expected at 48.4 kDa for all samples with exception for the negative Δ*hrcN* control. This indicates that HrcN is still present and expressed despite the increase or decrease of CdG levels throughout plant infection.
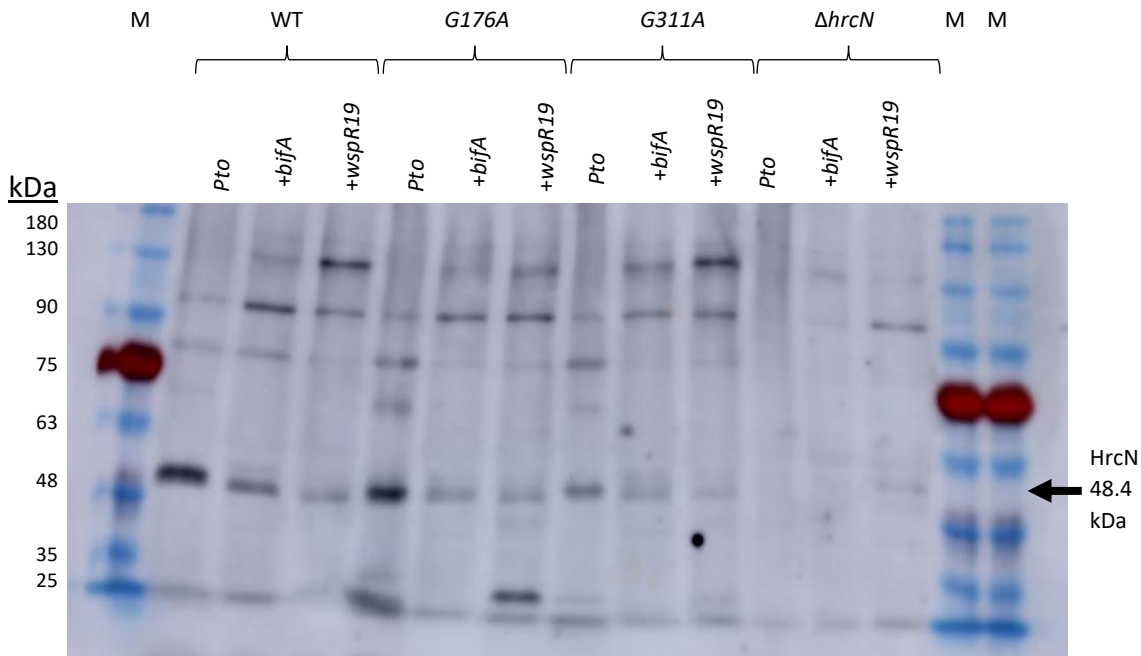
Figure 4.37. Anti-HrcN Western blot of *A. thaliana* Col-0 leaf tissue infected with *Pto* DC3000 *hrcN mutants*. Infected leaf tissue in a low or high CdG background was collected at day 3 post-infection. A *bifA* phosphodiesterase was over-expressed on a stable pBBR4 vector throughout infection for low CdG levels (trace quantities). A *wspR19* diguanylate cyclase was over-expressed on a stable pBBR4 vector throughout infection for high CdG levels (approximately 15 times greater than WT CdG background).

4.2.11.2. Anti-HrpQ

Infected *Arabidopsis thaliana* Col-0 plant tissue infected with *Pto* DC3000 *hrcN* mutant strains in a low or high CdG background environment were blot with an anti-HrpQ antibody. This has been shown in Figure 4.38. Similar to with anti-HrcN, there is no indication that presence and expression of HrpQ has been impacted in anyway as it can still be detected by way of Western blot from infected tissue. This suggests that altering background CdG levels does not impact the presence of major T3SS components throughout infection, and that phenotypic differences in disease severity are likely due to another cause.
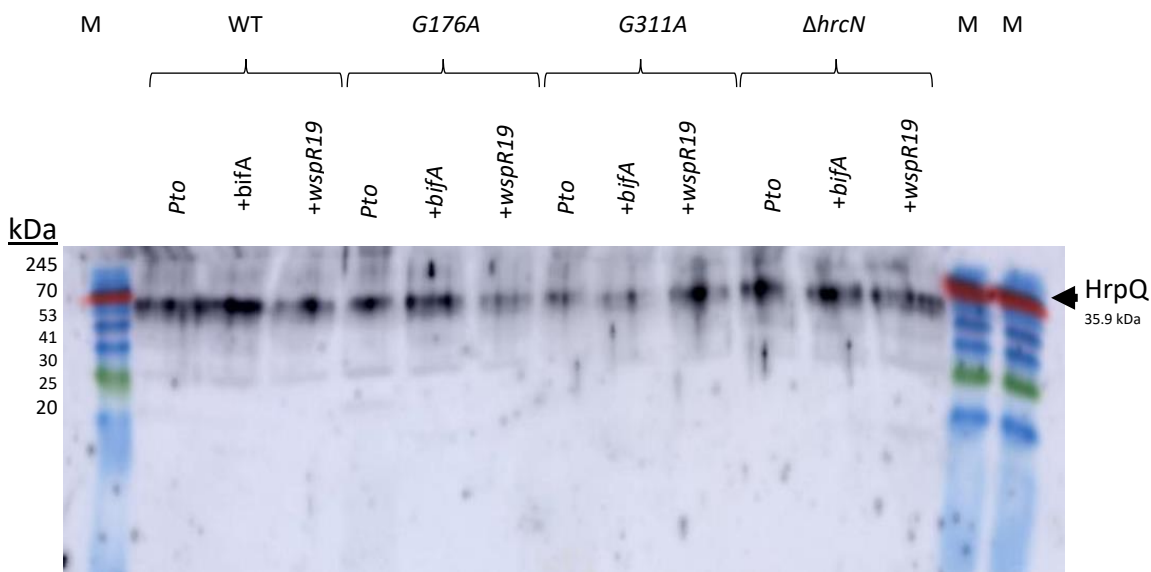
Figure 4.38. Anti-HrpQ Western blot of *A. thaliana* Col-0 leaf tissue infected with *Pto* DC3000 *hrcN* mutants. Infected leaf tissue in a low or high CdG background was collected at day 3 post-infection. A *bifA* phosphodiesterase was over-expressed on a stable pBBR4 vector throughout infection for low CdG levels (trace quantities). A *wspR19* diguanylate cyclase was over-expressed on a stable pBBR4 vector throughout infection for high CdG levels (approximately 15 times greater than WT CdG background).

4.3. Discussion

4.3.1. General Overview

It was shown in this chapter that various *in vivo* analyses were performed to help unpick what potential implications mutating key residues of the predicted CdG binding site of HrcN has on *P. syringae* type III-mediated virulence. It was shown by way of plant infection assays that point-mutations of particular key residues in the CdG:HrcN binding interface led to altered virulence phenotypes. Mutations *G176A* and *G311A* were able to achieve full bacterial colonisation comparable to the wildtype and other mutants however visual disease symptoms on the leaves were considerably different across both *A. thaliana* Col-0 and the native host *Solanum lycopersicum*. These mutants consistently showed near asymptomatic disease symptoms in *A. thaliana* Col-0. In *Solanum lycopersicum, G311A* showed similar minimal symptoms while *G176A* showed some albeit notably different and less severe symptoms compared to the WT and the other mutants. The subtle differences seen between the two plant hosts could be explained due to the differences in internal molecular defence complexity between *A. thaliana* and the native host *Solanum lycopersicum* in response to *P. syringae* infection. *E208D*, *L338V*, *F174Y* and *P142G* mutations led to symptoms comparable to or arguably greater than that of the wildtype in both *A. thaliana* and *Solanum lycopersicum*.

The chapter went on to show testing of a selection of hypotheses to try to explain why these differences in disease phenotypes were seen despite a consistent bacterial load across the mutant *hrcN P. syringae* strains. This included evaluating type III components via Western blotting, looking at the later stages of infection, measuring leaf immune response to *P. syringae* strains, and infecting immunocompromised plants.

HrcN and HrpQ were shown to be present throughout infection revealing that the components are present as expected despite mutation of *hrcN*. Evidence showed that the later stages of plant infection are unaffected between mutants in comparison to the wildtype and so differences in plant disease symptoms are not related to this. By way of ROS burst assay, it was shown that there were no major differences between immune responses to live *P. syringae hrcN* mutants showing that mutagenesis of *hrcN* did not lead to altered plant disease symptoms from altered immune responses. Lastly, immunocompromised bbc and fec plants were infected with mutant *hrcN P. syringae*. It was thought that if the differences in disease symptoms between mutants were driven by effector proteins interacting with plant defence components, then a plant lacking a functional immune system may give rise to different visual disease phenotypes. In these immunocompromised plants, this was indeed the case where the *G176A* and *G311A* mutants that showed minimal disease symptoms in Col-0, saw a return of characteristic wildtype-like infection symptoms. With *E208D*, *L338V*, *F174Y* and *P142G hrcN* mutants, any traces of hypervirulence were no longer present.

This evidence strongly suggested that mutating key residues in the predicted CdG binding site in the *P. syringae* T3SS HrcN ATPase leads to different leaf disease phenotypes potentially due to altered effector protein translocation and function. This is explored in more detail in the next chapter.

There is limited previous evidence showing other examples of the decoupling of leaf disease symptoms to bacterial load. What is often seen is that any changes to leaf disease symptom severity are accompanied by an increase or decrease in bacterial colonisation success. A good example of this is with a study that knocked out the catabolite repression control (Crc) protein in *P. syringae* and found a decrease in necrotic lesions alongside a decrease in bacterial load (Chakravarthy et al., 2017a).

The effect of CdG abundance was explored in relation to the observed disease phenotypes. A diguanylate cyclase (*wspR19*) for increased CdG levels (approximately 15 times greater than WT), and a phosphodiesterase (*bifA*) for reduced CdG levels (trace levels only compared to WT) was constitutively over-expressed in a stable expression vector throughout plant infection across *hrcN Pto* DC3000 mutants. It was shown that a possible compensatory effect may be seen with modulation of CdG levels in relation to the previously asymptomatic *G176A* and *G311A* mutants. It was shown via Western blotting that HrcN and HrpQ type III secretion system components were still present throughout plant infection without major changes in their relative abundance compared to the WT. No changes in plant colony forming units were seen in both low and high CdG environments. In the case of high CdG, this is consistent with previous infiltration experiments with *Pto* DC3000 where no changes in plant colonisation were seen (Pfeilmeier et al., 2016).

It is not immediately clear as to why a reduced CdG background sees a return of disease symptoms for the previously asymptomatic mutants. It is possible that low CdG is triggering a feedback loop leading to the upregulation of associated genes and regulatory networks. This in turn may be causing an indirect compensatory effect. It was previously shown that reduced CdG levels led to increased expression of quorum sensing regulated genes in *Pseudomonas aeruginosa* (Lin Chua et al., 2017).

In the case of increased CdG abundance, it is possible that this is providing a more direct compensatory effect. Having more CdG present around the binding site may lessen the effects caused by impaired mechanistic function of HrcN. This may be true if CdG binding stability to HrcN was impacted, or if the downstream CdG-induced oligomerisation of HrcN was compromised due to mutagenesis. By having a greater chance of binding to CdG, any stability issues related to CdG binding may be partially circumvented.

Based on these data, it can be concluded that effector translocation may be impacted in some way in the case of the *G176A* and *G311A hrcN* mutants and may be the underlying mechanism behind phenotypic differences in disease severity despite consistent bacterial leaf colonisation. Other possible hypotheses including immunogenic differences, long-term infection viability, and T3SS component absence were explored. It was concluded that based on the data collected, it was likely that these alternative hypotheses were likely to not be true. The use of immunocompromised bbc and fec *A. thaliana* plants showed a return of disease severity for *G176A* and *G311A*. This inferred that an interaction with the immune system was impacted in some way and that absence of a functioning immune system allowed for visual symptoms to be restored. This suggests that effector proteins which may interact with components of the plant immune system may be compromised in their translocation or function due to mutagenesis of *hrcN*. The following chapter will explore the potential underlying mechanism driving the phenotypic differences in more detail and will investigate the hypothesis that effector proteins may be implicated in some manner.

4.3.2. An Asymptomatic Disease Response

Observed for *G176A and G311A hrcN Pto* infections was an asymptomatic-like disease response. While there were very subtle signs of minimal visual disease severity, in comparison to the WT, there were significantly reduced chlorosis and necrosis-like symptoms present in Col-0 infection. Accompanying these phenotypes were consistent bacterial loads not statistically significant from the WT. This indicated that these bacterial strains were still able to colonise the leaf over the infection window sampled, however full visual disease symptoms were not able to be established. Typically seen within the literature is a coupled response where a reduction in visual disease severity led to a drop in leaf colonisation. Cases where bacterial load and visual disease severity are decoupled are rare in published works however there are examples which have found a similar phenomenon before.

It was previously shown that *Pto* strains lacking syringolin A (a secreted virulence factor) exhibited a similar response whereby bacterial colonisation was relatively unaffected however infected wheat plants appeared asymptomatic (Dudnik and Dudler, 2014). It was determined that secretion of this molecule was important for lesion formation however was not essential for bacterial colonisation (Dudnik and Dudler, 2014). A similar response was seen with the lack of secreted toxin coronatine albeit with a slight drop in bacterial colonisation ability (Uppalapati et al., 2008). Strains lacking the coronatine gene produced reduced necrotic lesions on tomato seedlings while still able to establish a reasonable level of bacterial colonisation, although compromised to a small extent compared to the WT (Uppalapati et al., 2008). These examples highlight that a decoupling of disease severity and bacterial colonisation is possible under certain circumstances, and that secreted molecules play an important role in the proper establishment of disease symptoms.

Based on the data presented in this chapter, it is hypothesised that effector protein translocation is important for visual disease establishment in *Pto*. Differential translocation of effectors is known to modulate visual disease severity however this is most typically associated with a drop in bacterial colonisation. Effector translocation modulation is usually achieved by complete cluster or individual gene deletion leading to the complete abolition of a given effector. A good example of this was a study which systematically deleted key effector clusters and evaluated *Pto* infection phenotypes (Kvitko et al., 2009). It was found that disease severity was compromised in some instances, however, so was bacterial colonisation (Kvitko et al., 2009). Additionally, it is often the case that deletion of some effectors leads to an unaltered infection phenotype due to functional redundancy making experimentation challenging, and so investigation remains limited.

Creating a strain which has compromised effector protein translocation, but not complete abolition is not common in the literature. It could be that with complete abolition of an effector, bacterial colonisation may begin to decrease but when small amounts of that effector are allowed to be translocated, bacterial colonisation can be established but not enough for visual disease severity to form. This could infer that there is a threshold of effector translocation which may need to be met for each effector protein which is distinct for colonisation and for visual disease establishment.

Symptomless *P. syringae* strains have previously been found where there was no induction of HR in non-host plants (Klement et al., 1997). It was found that these strains induced host responses during an early stage of pathogenesis. This led to development of early induced resistance (EIR) in the infected plants, suppressing a HR response. As such, no visual disease symptoms could form. It was hypothesised that both higher temperatures and HR delay caused by certain pathovars or mutants, led to EIR developing more quickly (Klement et al., 1997). Early induction of plant-induced systemic resistance has been shown to provide enhanced resistance to pathogens leading to altered disease severity. It could be that with *G176A* and *G311A hrcN* strains, EIR is triggered due to altered secretion profiles leading to a slower or suppressed HR response.

It could be a combination of altered secretion profiles of key T3SS virulence factors including effector proteins, along with an altered EIR and HR response in the plant that is leading to the asymptomatic-like infection phenotype seen with *G176A* and *G311A hrcN Pto*. The underlying mechanism driving this phenotype is likely complex with various different factors involved from both bacterial and plant perspectives. By understanding this asymptomatic-like phenotype in more detail at a mechanistic level, this helps further our understanding of type III-mediated virulence and plant health.

4.3.3.   Concluding Remarks

In this chapter, the function of HrcN was tested *in vivo*. Conservative chromosomal point-substitutions were constructed in *Pto* DC3000 which targeted residues in the predicted CdG-binding site of HrcN. *G176A and G311A* mutants could not establish visual disease severity but maintained effective bacterial colonisation of the leaf in *A. thaliana*. Testing of a variety of possible hypotheses followed and it was deduced that T3SS effector proteins may play an important role in the underlying mechanism behind this phenotype. The following chapter investigates the role of effector proteins in disease establishment to help understand the underlying mechanism in more detail.

Chapter 5: Understanding How T3SS Effector Delivery is Affected by CdG:HrcN Binding in *P. syringae*

5.1. Introduction

5.1.1. General Overview

The previous chapter considered a variety of possible hypotheses that might explain the different virulence phenotypes associated with certain mutations in the predicted CdG binding site of HrcN. This chapter builds on this previous work by investigating in more detail the translocation of T3SS effector proteins and how the CdG:HrcN binding interaction may regulate this process during infection.

Effector proteins are translocated through the T3SS into host cells, facilitating a more favourable environment for bacterial colonisation. Commonly observed effector protein mechanisms in the host cell include disruption of the host immune system, cell signalling, autophagy, cellular vesicle trafficking and the cell cytoskeleton (Abe et al., 2005, Choi et al., 2017, Gimenez-Ibanez et al., 2018). The suppression of these host defences and cellular functions allow for bacterial colonisation (Collmer et al., 2000). These effector proteins typically have a variety of targets and effects inside the host organism.

These effector proteins are deployed throughout infection and contribute to bacterial colonisation success and disease phenotype establishment. A *Pto* DC3000 strain has previously been produced which lacked 28 well-expressed effector protein genes and thus a fully functional effector protein repertoire (Cunnac et al., 2011). Full deletion of these effector proteins led to a mutant which showed very poor colonisation ability with minimal plant cell death (Cunnac et al., 2011). However, with re-introduction of certain effector proteins, a recovery of bacterial virulence was achieved confirming the importance of proper effector protein translocation for colonisation and full disease establishment (Cunnac et al., 2011).

The regulation of effector translocation via the type III secretion system is an area that is not yet fully understood. In the literature, there are examples that demonstrate an understanding of particular T3SS regulation mechanisms but due to the complexity of the overall system, there is still a great deal that is unknown or lacking detail.

5.1.2. Effector Reporter Assays

Measuring and quantifying the translocation of effector proteins through the T3SS into host organisms has been attempted with a variety of tools and techniques. Reporter systems are viewed as one of the most popular current options across multiple different bacterial systems for measuring effector translocation into eukaryotic cells. A reporter system that has shown promise in the past uses fluorescence resonance energy transfer (FRET) detection, achieved with direct fluorescent labelling, or via a FRET-substrate based system. An example of this was a study that investigated the translocation of EspF, EspG, EspH, EspZ, Map, and Tir T3SS effector proteins from *E. coli* using the *blaM* reporter gene and a CCF2-AM FRET substrate (Mills et al., 2008). This system was adapted from a system first described in 2004 where the *E. coli* Cif effector was investigated using a TEM-1 beta-lactamase fusion with FRET (Charpentier and Oswald, 2004). Both systems worked on a similar principle where successful translocation of fused effector proteins through the T3SS would lead to a change in FRET-detectable fluorescence emission due to TEM-induced catalytic cleavage of the CCF2 β-lactam ring found on an CCF2-AM FRET substrate present in the eukaryotic host cell (Charpentier and Oswald, 2004). This system was a useful steppingstone. However, it would have been subject to many issues associated with FRET-imaging, most notably a low signal-to-noise ratio and sensitivity to external local environment changes. An alternative system called LOV (light-oxygen-voltage) attempted to overcome these technical limitations using *E. coli* and *S. flexneri* (Gawthorne et al.,

2016). The LOV domain binds flavin mononucleotide (FMN) and when irradiated with ultraviolet light, will emit measurable green fluorescence (Gawthorne et al., 2016). Despite the promising results described with this technique, such a reporter system has yet to be adapted for *Pseudomonas* species and as such, was not chosen to investigate the effector proteins in this study.

Another technique used in the past is an ELK-tag, which uses a small bipartite phosphorylatable peptide tag fused to an effector protein of interest (Day et al., 2003). This tag will undergo host cell protein kinase-dependent phosphorylation if successfully translocated, where it can then be detected by the appropriate phosphospecific antibody (Day et al., 2003). This is a 35-residue tag consisting of a SV40 large tumour antigen NLS, fused to part of the eukaryotic transcription factor Elk-1 (Day et al., 2003). This system was adapted where *Yersinia pestis* T3SS tagged effector proteins YopE, YopH, LcrQ, YopK, YopN, and YopJ were fused to a glycogen synthase kinase (GSK) tag, which consisted of a 13-residue phosphorylatable region (Garcia et al., 2006). This GSK tag allowed for simple detection of translocated effector proteins in HeLa cells with phosphospecific GSK-3β antibodies. Quantification of delivery timing and protein abundance was not possible with this system (Garcia et al., 2006).

With many of the earlier techniques used to investigate effector protein translocation, issues were often encountered relating to toxicity to eukaryotic host cells, improper folding due to steric hindrance and impaired translocation through the T3SS. Additionally, many early techniques were too simple to allow for quantitative investigation into the timing and protein abundance of effector delivery. As such, smaller and more refined reporter systems are now preferred. One such effective method for quantitatively measuring effector translocation is with the fusion of an adenylate cyclase 'CyaA' domain to the C-terminus of a given effector-encoding gene lacking a stop codon, driven by a *hrp* promoter (Chakravarthy et al., 2017b). This CyaA domain is the catalytic cya_{2-400} region of the *Bordetella pertussis* CyaA adenylate cyclase toxin. The CyaA domain leads to calmodulin-dependent conversion of adenosine triphosphate (ATP) to cyclic adenosine monophosphate (cAMP). This reporter system leads to the increase of cAMP levels in infected plant tissue upon successful translocation and folding of an effector-fusion through the T3SS (Chakravarthy et al., 2017b). This conversion of ATP to cAMP cannot occur in bacteria due to lack of calmodulin, hence, is a specific reaction dependent on effector translocation into eukaryotic plant cells where calmodulin is present. Additionally, the CyaA domain cannot exit from bacteria alone without the effector-fusion due to it lacking the necessary signal sequence required to pass through the T3SS. This reporter system underpins much of the research in this chapter and has been used to measure effector protein translocation between *hrcN Pto* DC3000 strains described previously throughout this thesis.

The CyaA fusion effector reporter system has previously been demonstrated in a selection of published works over the past few decades. One of the earliest uses of a Cya-based reporter strategy was in *Yersinia enterocolitica* studying the Yop virulon (Boland et al., 1996). The translocation of T3SS effector proteins YopM and YopN into PU5-1.8 macrophages was quantified using this Cya-fusion strategy, where it was found that various other type III Yop proteins were needed for proper effector translocation (Boland et al., 1996).

5.1.2.1. C-terminal CyaA Effector-fusion in *P. syringae*

Eventually, this system became adapted for plant pathology-related studies. CyaA-fused effector proteins from *P. syringae Pto* DC3000 were constructed and tested to better understand their role in virulence (Schechter et al., 2004). The *Pto* DC3000 effector AvrPto was the main effector protein used to optimise the system, with *Nicotiana benthamiana* serving as the model host plant (Schechter et al., 2004). Since this original study, the CyaA effector fusion reporter system in *P. syringae Pto* has been used in a wide variety of studies. Some notable examples have been described below. The CyaA

reporter system was used to study *Pto* DC3000 effector proteins HopB1 and HrpK (Petnicki-Ocwieja et al., 2005). Domain deletions were constructed on these effector proteins to show their importance and role in effector function (Petnicki-Ocwieja et al., 2005). It was shown that deletion of different domains present in HrpK led to different levels of protein translocation and stability, indicated by varying levels of cAMP in infected plant tissue (Petnicki-Ocwieja et al., 2005). In a subsequent study, it was shown that cAMP levels increased over time in infected *A. thaliana* tissue with a HopM1-CyaA *P. syringae Pto* DC3000 strain, and that effector-triggered immunity did not appear to affect this translocation in a study focused on plant immunity (Nomura et al., 2011). Another study used CyaA-fusions with effectors AvrPto and HopY1 to investigate the effect of low temperature on *P. syringae Pto* virulence (Li et al., 2020). It was seen that translocation rates (reflective of cAMP accumulation) of these effectors remained consistent at both 16 °C and 22 °C in a selection of *A. thaliana* ecotypes (Li et al., 2020).

This CyaA system has been used to study the mechanism of chaperones alongside effector proteins highlighting the reporter systems versatility. The role of effector chaperones ShcO1, ShcS1 and ShcS2 were investigated using CyaA-fused effector proteins (Guo et al., 2005). It was shown by way of cAMP accumulation in infected *Nicotiana benthamiana* leaves that all chaperones of interest were important for CyaA-fused-effector translocation, and that ShcS1 and ShcS2 were able to substitute for ShcO1 when this protein was absent (Guo et al., 2005). Interaction between these chaperone proteins and their associated effector protein was confirmed by means of co-immunoprecipitation (Guo et al., 2005).

5.1.3. Chapter Aims

1. To construct a reporter assay that will allow the quantification of T3SS effector translocation from bacteria to plant host.
2. This system will be used to understand how effector delivery is affected by altering the predicted CdG binding site in HrcN.
3. To investigate differentially secreted effectors using molecular biology and computational techniques, in order to understand the disease phenotypes observed for various *hrcN* mutants targeting key residues in the predicted CdG binding site.

5.2. Results

5.2.1. CyaA T3SS Effector C-terminal Fusion Expression Vectors Were Successfully Constructed

Based on the results in Chapter 4, it was hypothesised that differences in visual disease phenotypes present across key *P. syringae Pto* mutants may be due to altered effector translocation. Measurement of effector translocation was performed by creating effector reporter constructs based on the CyaA-fusion system (Chakravarthy et al., 2017b).

Effector-CyaA fusions were constructed and cloned for expression via a pCPP5371 vector driven by a *hrp*-promoter. Effector-encoding genes lacking a stop codon were cloned into the pCPP5371 via Gateway™ cloning. Effector proteins were present on a pCPP Gateway™ entry vector (pENTR/SD/D-TOPO). These underwent a recombination event with a pCPP5371 Gateway™ destination vector at *att* sites as part of an LR-reaction catalysed by a Gateway™ LR Clonase™ II enzyme to create a final expression clone. This fused the catalytic *cya*$_{2\text{-}400}$ domain of *Bordetella pertussis* to the C-terminal of the cloned effector protein. This allowed for *hrp* promoter-driven expression of effector proteins fused

to a functional CyaA reporter tag. Non-cloned by-products contained a toxic *ccdB* gene and so these colonies did not grow, leading to a very high cloning efficiency.

Confirmation of successful effector cloning was confirmed by PCR using universal primers. Shown in Figure 5.1 is an example DNA agarose gel featuring a variety of successful effector clone bands.
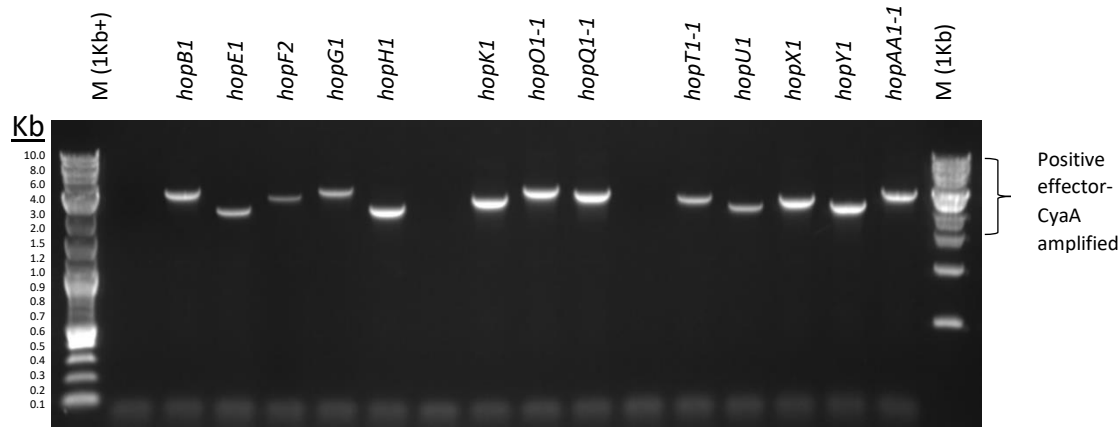
Figure 5.1. Representative DNA agarose gel showing selected successful example effector-CyaA constructs generated by Gateway™ cloning, verified by colony PCR using universal primers. Bands present for each sample were the correct molecular size indicating a positive clone.

Construction of this reporter assay included a wide range of effector proteins. The effector protein-CyaA fusion expression vectors generated and ultimately tested in this screen, along with any necessary chaperones (for proper protein translocation and folding), are shown below in Table 5.1.

Table 5.1. List of C-terminal CyaA-fused effector proteins and associated chaperones necessary for proper folding used as part of this study.

C-terminal CyaA-fused Effector Protein	Associated chaperone
AvrPto	N/A
AvrPtoB	N/A
HopA1	N/A
AvrE	ShcE
HopM1	ShcM
HopB1	N/A
HopE1	N/A
HopF2	ShcF
HopG1	N/A
HopH1	N/A
HopI1	N/A
HopK1	N/A
HopO1-1	ShcO
HopQ1-1	N/A
HopR1	N/A
HopT1-1	N/A
HopU1	N/A
HopX1	N/A
HopY1	N/A

HopAA1-1	N/A
HopAA1-2	N/A
HopAF1	N/A

5.2.2. CyaA T3SS Effector C-terminal Fusion Translocation Reporter Assays

5.2.2.1. CyaA Reporter Assays Show Effector Protein Translocation Over Time

5.2.2.1.1. Col-0 *A. thaliana*

The CyaA effector fusions were then used to quantify effector translocation from mutant *hrcN* *P. syringae Pto* DC3000 strains into *A. thaliana* leaves. An initial screen with a few selected effector proteins was performed across a broad range of *hrcN* mutants to test reporter system functionality, and to identify any potential differences in translocation on a macro-scale. These experiments were broadly successful, but initially displayed high variability and took time to optimise (data not shown). Based on these initial experiments, the selected effectors were robustly tested for a few key *hrcN* mutants to screen for differences in translocation

To verify the CyaA system was functional and to determine an appropriate infection time window, effector translocation was measured over time. This was first tested in *A. thaliana* Col-0, then immune-compromised bbc plants to see the effect of the immune system on CyaA-system function.

The translocation of the AvrE effector over time into *A. thaliana* Col-0 across the *hrcN P. syringae* mutants is shown in Figure 5.2. The cAMP/µg protein value from the CyaA-fused AvrE translocation from each mutant was measured at 3 hours, 6 hours, and 9 hours post-infection. In all cases except the Δ*hrcN* negative control, there was a distinct increase in cAMP/µg protein across all *hrcN* mutants over time. The cAMP/µg protein values and statistical data are shown in Table 5.2.
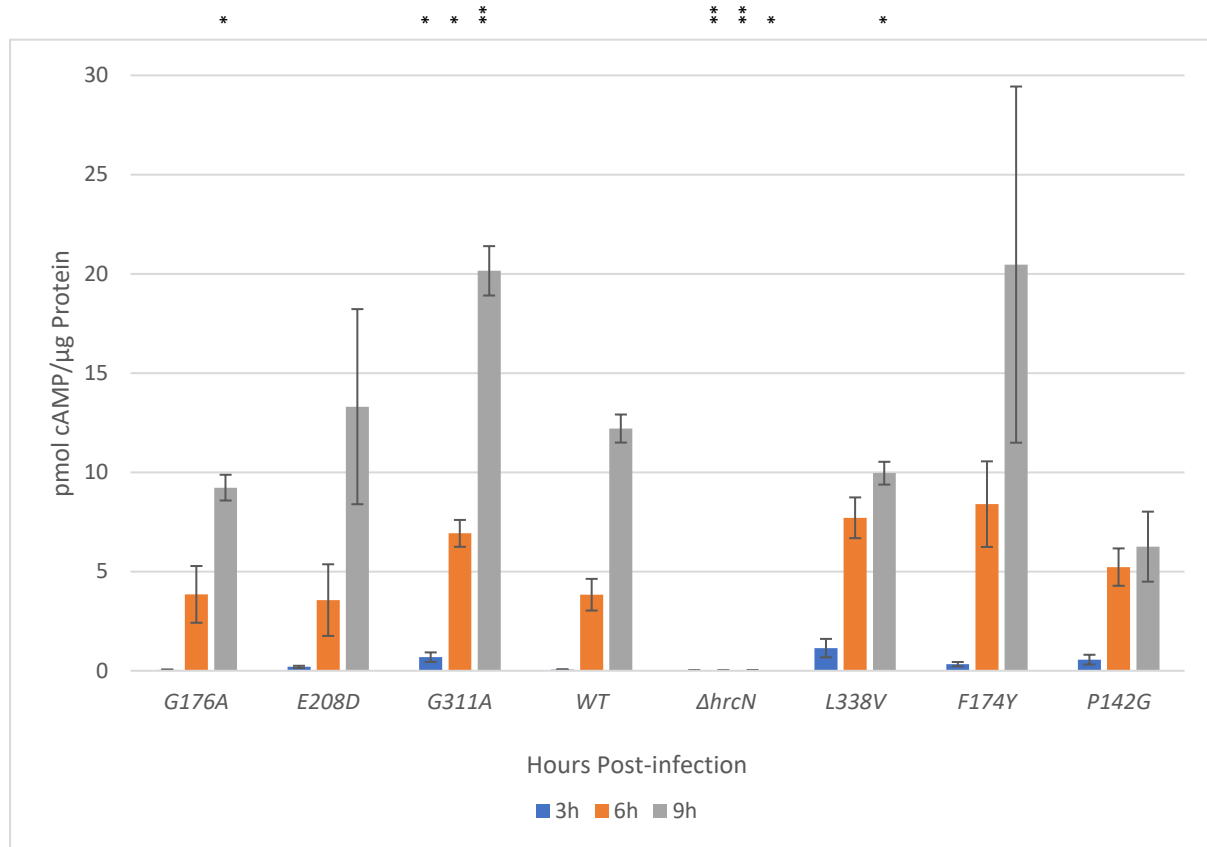
Figure 5.2. CyaA-T3SS effector fusion reporter time-course assay quantifying AvrE effector translocation at 3 hours, 6 hours, and 9 hours post-infection from mutant *hrcN P. syringae Pto* DC3000 infiltrated into *A. thaliana* Col-0. cAMP levels directly correlate to effector translocation rate. Asterix symbols (*) represent statistical significance (2-sample t test) compared to the mean WT cAMP value of a like-timepoint where '*' = $p \leq 0.05$, '**' = $p \leq 0.01$, and '***' = $p \leq 0.001$. Error bars show standard error of the mean (n = 3).

Table 5.2. Average cAMP/µg protein values over time for *hrcN Pto* DC3000 AvrE effector-CyaA fusion strains infected Col-0 *A. thaliana* tissue. p values show significance of a mutant cAMP/µg value compared to WT, calculated using a 2-sample t-test.

AvrE CyaA-fusion *hrcN Pto* DC3000 strain	3 hours		6 hours		9 hours	
	cAMP/µg protein	p value	cAMP/µg protein	p value	cAMP/µg protein	p value
WT	0.06	N/A	3.8	N/A	12.2	N/A
G176A	0.05	0.8	3.8	1.0	9.2	0.03
E208D	0.2	0.1	3.6	0.9	13.3	0.8
G311A	0.7	0.05	6.9	0.04	20.2	0.005
L338V	1.1	0.09	7.7	0.04	10.0	0.07
F174Y	0.3	0.1	8.4	0.1	20.5	0.4
P142G	0.6	0.08	5.2	0.3	6.3	0.03
ΔhrcN	0.0112	0.04	0.0107	0.039	0.0122	0.04

This experiment confirmed that effector translocation does increase over time (represented by increasing cAMP levels). This was observed in all *hrcN* mutants except for the Δ*hrcN* control, indicating that a functional type III-injectisome was essential for significant increases in cAMP.

5.2.2.1.2. bbc *A. thaliana*

Next, immunocompromised bbc *A. thaliana* plants were infected as part of a time-course translocation quantification experiment of CyaA-fused AvrE across selected *hrcN* strains, as shown in Figure 5.3. This was to evaluate any possible immune-system limitations on effector-CyaA translocation and determine the most appropriate plant host for wider effector protein screening. A smaller sub-set of mutants were chosen. *G176A* and *G311A hrcN* were chosen due to these mutants displaying an asymptomatic *in planta* visual disease response (as shown in the previous chapter) while *P142G hrcN* was included to compare against a symptomatic mutant. The cAMP/µg protein values and statistical data are shown in Table 5.3.
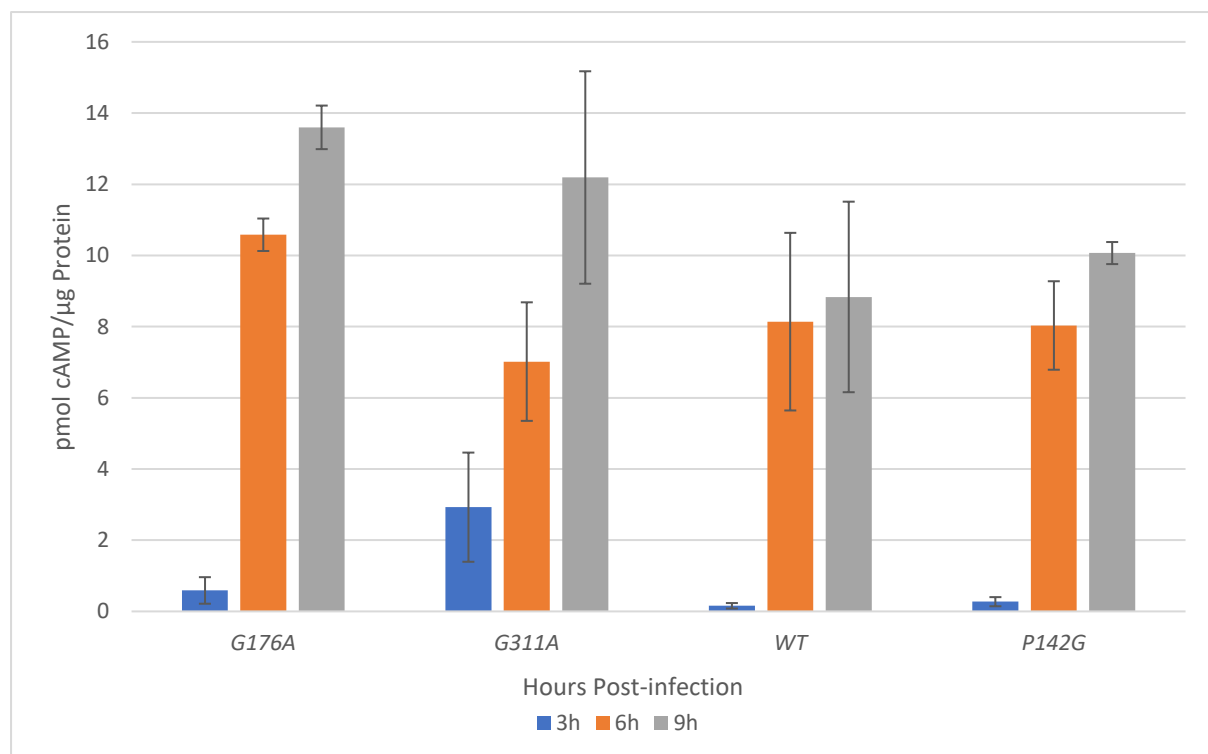
Figure 5.3. CyaA-T3SS effector fusion reporter time-course assay quantifying AvrE effector translocation at 3 hours, 6 hours, and 9 hours post-infection from mutant *hrcN P. syringae Pto* DC3000 infiltrated into immunocompromised bbc *A. thaliana*. cAMP levels directly correlate to effector translocation rate. Error bars show standard error of the mean (n = 3).

Table 5.3. Average cAMP/µg protein values over time for *hrcN Pto* DC3000 AvrE effector-CyaA fusion strains infected bbc immunocompromised *A. thaliana* tissue. p values show significance of a mutant cAMP/µg value compared to WT, calculated using a 2-sample t-test.

AvrE CyaA-fusion *hrcN Pto* DC3000 strain	3 hours		6 hours		9 hours	
	cAMP/µg protein	p value	cAMP/µg protein	p value	cAMP/µg protein	p value
WT	0.16	N/A	8.1	N/A	8.8	N/A
G176A	0.6	0.3	10.6	0.4	13.6	0.2

G311A	2.9	0.15	7.0	0.7	12.2	0.4
P142G	0.3	0.3	8.0	0.97	10	0.7

From these time-course experiments, it was shown that the CyaA-reporter system is fully functional, and that cAMP activity increases over time, as function of increased effector protein translocation. A negative Δ*hrcN* control saw no effector translocation in a Col-0 background, indicating that background cAMP levels would not rise without the presence of a functioning T3SS and proper translocation of a CyaA-fused effector protein. An infection window of 6 hours was chosen for the full effector protein screen for experimental practicality. Col-0 was chosen as the model for the full effector reporter screen. While both Col-0 and bbc plants generated strong cAMP signals, the lack of a fully functional immune system may mask any differences in effector translocation if immune system interaction plays an important role. As such, a native Col-0 background was chosen to increase the biological relevance of these assays.

5.2.2.2. CyaA Reporter Screening of Effector Proteins Shows Differential Translocation in Infections with *Pto* Carrying Mutant *hrcN* Alleles

Following confirmation of CyaA system function, the translocation of a wider effector set across selected *hrcN Pto* mutants was explored. A large effector screen was conducted to identify any evidence of differential translocation of effector proteins. Across the screen, differential translocation of some type III effector proteins was observed across a range of *hrcN Pto* DC3000 mutants. This is shown across Figure 5.4 to Figure 5.8.

Shown in Figure 5.4 are five tested effectors in WT, Δ*hrcN*, *G176A*, *E208D*, and *G311A hrcN Pto* DC3000 strains. Tested effectors were HopB1-CyaA, HopE1-CyaA, HopF2-CyaA, HopG1-CyaA, and HopH1-CyaA. Relative T3SS effector translocation was determined via direct cAMP-ELISA from a pre-determined quantity of infected Col-0 *A. thaliana* tissue after a 6-hour infection time-point for each strain tested. ANOVAs were used to determine whether variance was present between sample columns, with further statistical analysis conducted by way of 2-way t-tests comparing mutant *hrcN* values to WT. The cAMP/µg protein values and statistical ANOVA p values are shown in Table 5.4.

ANOVAs (excluding the negative control Δ*hrcN*) showed that there were no statistically significant differences between the mean cAMP/µg protein values of sample columns for HopB1, HopE1, HopF2, and HopH1. Statistically significant differences for HopG1 (p = 0.035) were observed between strains.

When comparing mutant *hrcN* strains to their respective WT mean cAMP/µg protein values for a given effector using 2-way t-tests, statistically significant differences were observed for some samples. The statistical p values are shown in Table 5.5. In all cases, Δ*hrcN* infections were statistically different to the WT as expected. Statistically significant differences were observed for HopB1 (*G176A*), HopE1 (*G176A, E208D*), and HopF2 (*E208D*).
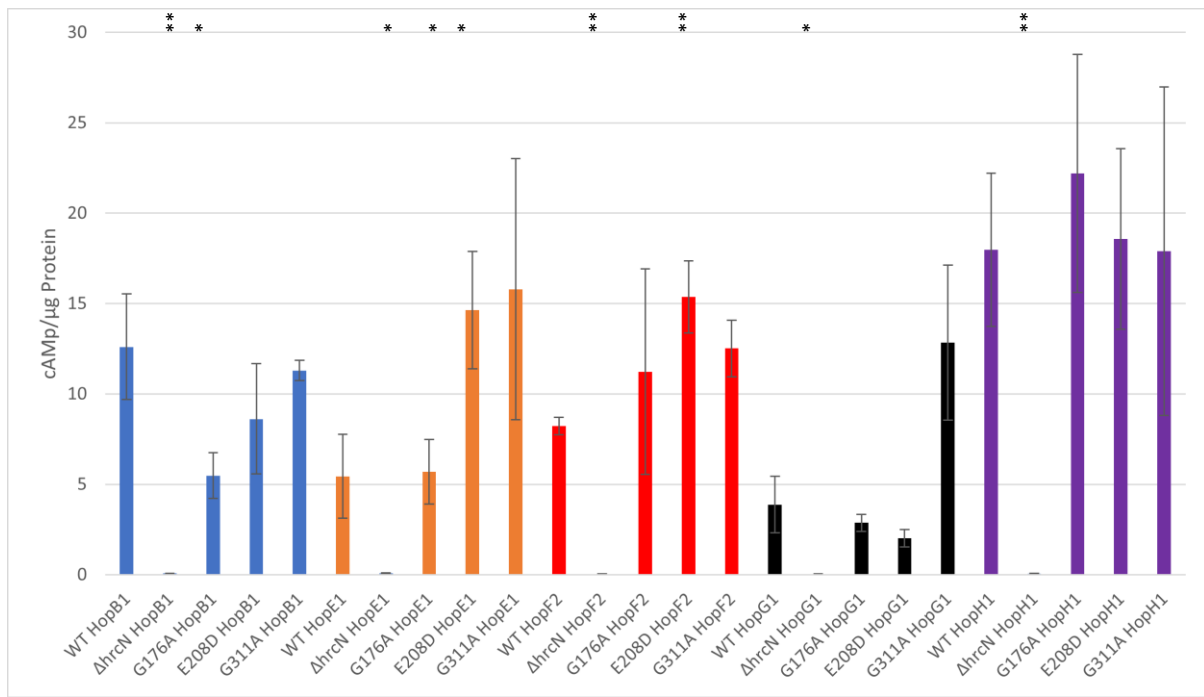
Figure 5.4. CyaA-T3SS effector fusion reporter assay quantifying effector translocation from mutant *hrcN P. syringae Pto* DC3000 infiltrated into *A. thaliana* Col-0. cAMP levels directly correlate to effector translocation rate. HopB1, HopE1, HopF2, HopG1 and HopH1 CyaA fused effectors analysed in WT *hrcN*, Δ*hrcN*, *G176A hrcN, E208D hrcN and G311A hrcN Pto* DC3000 strains. Leaf tissue collected at 6 hours post-infection. Asterix symbols (*) represent statistical significance (2-sample t test) compared to WT cAMP value where '*' = p ≤ 0.05, '**' = p ≤ 0.01, and '***' = p ≤ 0.001 (n = 3).

Shown in Figure 5.5 are five tested effectors in WT, Δ*hrcN*, *G176A*, *E208D*, and *G311A hrcN Pto* DC3000 strains. Tested effectors were HopI1-CyaA, HopK1-CyaA, HopO1-1-CyaA, HopQ1-CyaA, and HopR1-CyaA. Relative T3SS effector translocation was determined via direct cAMP-ELISA from a pre-determined quantity of infected Col-0 *A. thaliana* tissue after a 6-hour infection time-point for each strain tested. The cAMP/µg protein values and statistical ANOVA p values are shown in Table 5.4.

ANOVAs (excluding the negative control Δ*hrcN*) showed that there were no statistically significant differences between the mean cAMP/µg protein values of sample columns for HopI1, HopK1, HopO1-1, and HopR1. Statistically significant differences were observed for HopQ1 (p = <0.001).

When comparing mutant *hrcN* strains to their respective WT mean cAMP/µg protein values for a given effector using 2-way t-tests, statistically significant differences were observed for some samples. The statistical p values are shown in Table 5.5. In all cases, Δ*hrcN* infections were statistically different to the WT as expected. Statistically significant differences were observed for HopI1 (*G176A*), HopR1 (*G176A*), and HopQ1 (*G311A*).
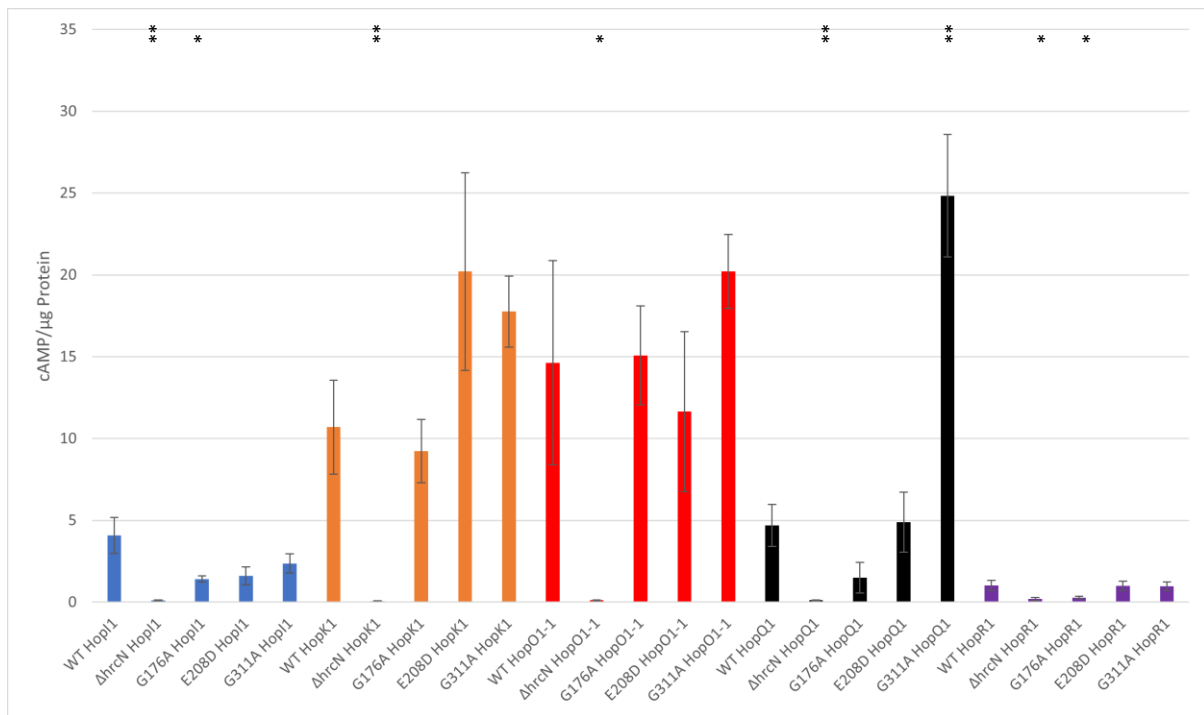
Figure 5.5. CyaA-T3SS effector fusion reporter assay quantifying effector translocation from mutant *hrcN P. syringae Pto* DC3000 infiltrated into *A. thaliana* Col-0. cAMP levels directly correlate to effector translocation rate. HopI1, HopK1, HopO1-1, HopQ1 and HopR1 CyaA fused effectors analysed in WT *hrcN*, *ΔhrcN*, *G176A hrcN*, *E208D hrcN* and *G311A hrcN Pto* DC3000 strains. Leaf tissue collected at 6 hours post-infection. Asterix symbols (*) represent statistical significance (2-sample t test) compared to WT cAMP value '*' = p ≤ 0.05, and '**' = p ≤ 0.01 (n = 3).

Shown in Figure 5.6 are four tested effectors in WT, Δ*hrcN*, *G176A*, *E208D*, and *G311A hrcN Pto* DC3000 strains. Tested effectors were HopT1-1-CyaA, HopU1-CyaA, HopX1-CyaA, and HopY1-CyaA. The cAMP/μg protein values and statistical ANOVA p values are shown in Table 5.4.

ANOVAs (excluding the negative control Δ*hrcN*) showed that there were no statistically significant differences between the mean cAMP/μg protein values of sample columns for HopT1-1, HopU1, HopX1, and HopY1.

When comparing mutant *hrcN* strains to their respective WT mean cAMP/μg protein values for a given effector using 2-way t-tests, no statistically significant differences were observed across samples with exception for all the Δ*hrcN* negative controls. This was due to high variance observed in both WT and Δ*hrcN* strains with this particular effector, as such strong conclusions cannot be drawn from this individual sample. The statistical p values are shown in Table 5.5.
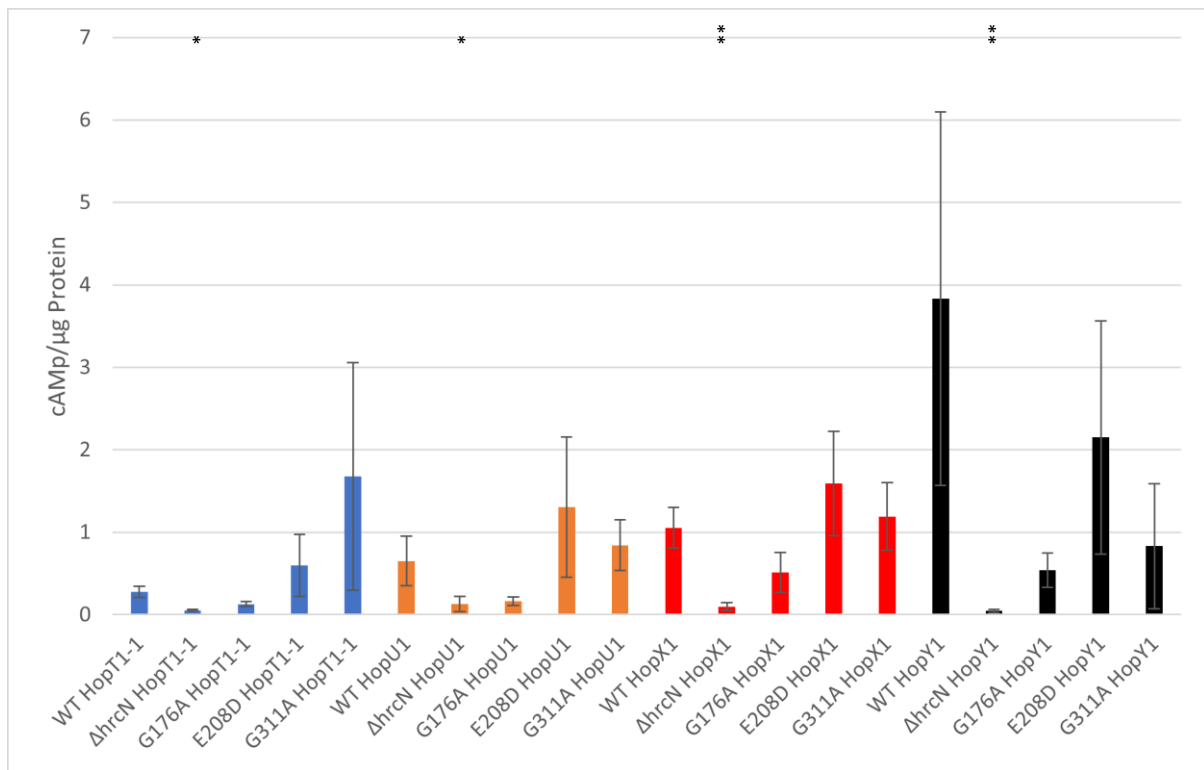
Figure 5.6. CyaA-T3SS effector fusion reporter assay quantifying effector translocation from mutant *hrcN P. syringae Pto* DC3000 infiltrated into *A. thaliana* Col-0. cAMP levels directly correlate to effector translocation rate. HopT1-1, HopU1, HopX1 and HopY1 CyaA fused effectors analysed in WT *hrcN*, Δ*hrcN*, *G176A hrcN*, *E208D hrcN* and *G311A hrcN* DC3000 strains. Leaf tissue collected at 6 hours post-infection. Asterix symbols (*) represent statistical significance (2-sample t test) compared to WT cAMP value where '*' = $p \leq 0.05$, and '**' = $p \leq 0.01$ (n = 3).

Shown in Figure 5.7 are four tested effectors in WT, Δ*hrcN*, *G176A*, *E208D*, and *G311A hrcN Pto* DC3000 strains. Tested effectors were HopAA1-1-CyaA, HopAA1-2-CyaA, HopAF1-CyaA, and HopAM1-CyaA. The cAMP/µg protein values and statistical ANOVA p values are shown in Table 5.4.

ANOVAs (excluding the negative control Δ*hrcN*) showed that there were no statistically significant differences between the mean cAMP/µg protein values of sample columns for HopAA1-1 and HopAA1-2. Statistically significant differences were observed for HopAF1 (p = 0.035) and HopAM1 (p = 0.027).

When comparing mutant *hrcN* strains to their respective WT mean cAMP/µg protein values for a given effector using 2-way t-tests, statistically significant differences were observed for some samples. The statistical p values are shown in Table 5.5. In all cases, Δ*hrcN* infections were statistically different to the WT as expected. Statistically significant differences were observed for HopAA1-2 (*G176A*), HopAF1 (*E208D, G311A*), and HopAM1 (*G176A. G311A*). This is shown in Table 5.5.

166
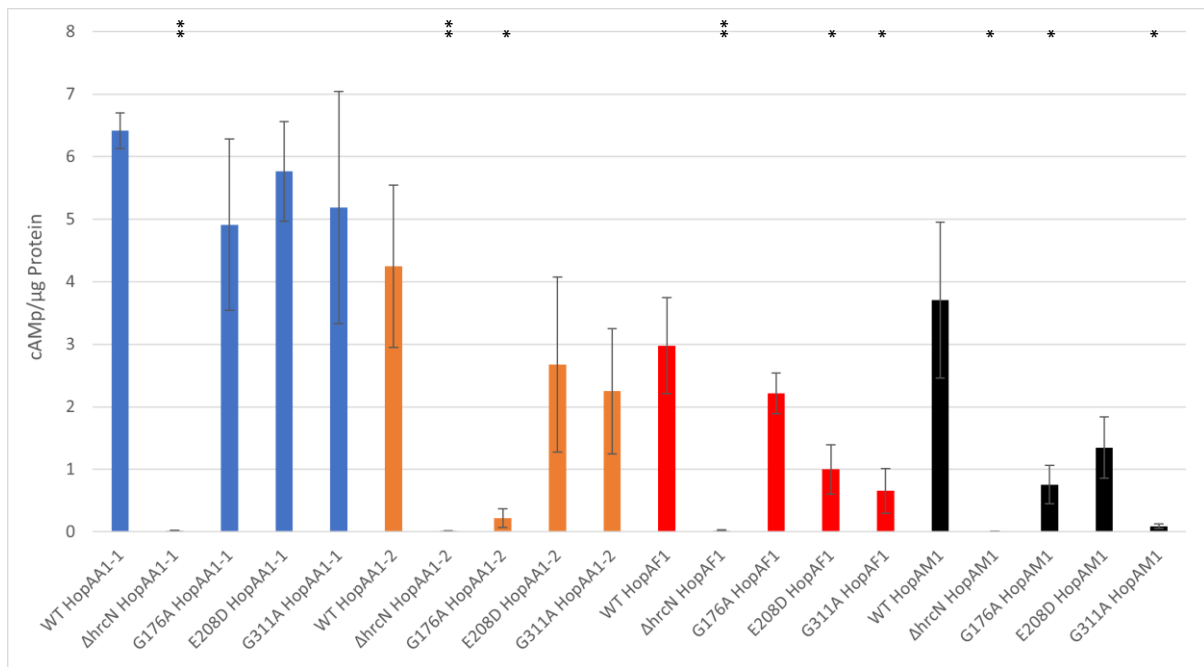
Figure 5.7. CyaA-T3SS effector fusion reporter assay quantifying effector translocation from mutant *hrcN P. syringae Pto* DC3000 infiltrated into *A. thaliana* Col-0. cAMP levels directly correlate to effector translocation rate. HopAA1-1, HopAA1-2, HopAF1 and HopAM1 CyaA fused effectors analysed in WT *hrcN*, Δ*hrcN*, *G176A hrcN*, *E208D hrcN* and *G311A hrcN Pto* DC3000 strains. Leaf tissue collected at 6 hours post-infection. Asterix symbols (*) represent statistical significance (2-sample t test) compared to WT cAMP value where '*' = p ≤ 0.05, and '**' = p ≤ 0.01 (n = 3).

Shown in Figure 5.8 are five tested effectors in WT, Δ*hrcN*, *G176A*, *E208D*, and *G311A hrcN Pto* DC3000 strains. Tested effectors were AvrPto-CyaA, AvrPtoB-CyaA, HopA1-CyaA, AvrE-CyaA, and HopM1-CyaA. The cAMP/μg protein values and statistical ANOVA p values are shown in Table 5.4.

ANOVAs (excluding the negative control Δ*hrcN*) showed that there were no statistically significant differences between the mean cAMP/μg protein values of sample columns for AvrPto. AvrPtoB and AvrE. Statistically significant differences were observed for HopA1 (p = 0.02).

When comparing mutant *hrcN* strains to their respective WT mean cAMP/μg protein values for a given effector using 2-way t-tests, statistically significant differences were observed for some samples. The statistical p values are shown in Table 5.5. In all cases, Δ*hrcN* infections were statistically different to the WT as expected. Statistically significant differences were observed for AvrPto (*G311A*), HopA1 (*G311A*) and AvrE (*G176A, E208D*).
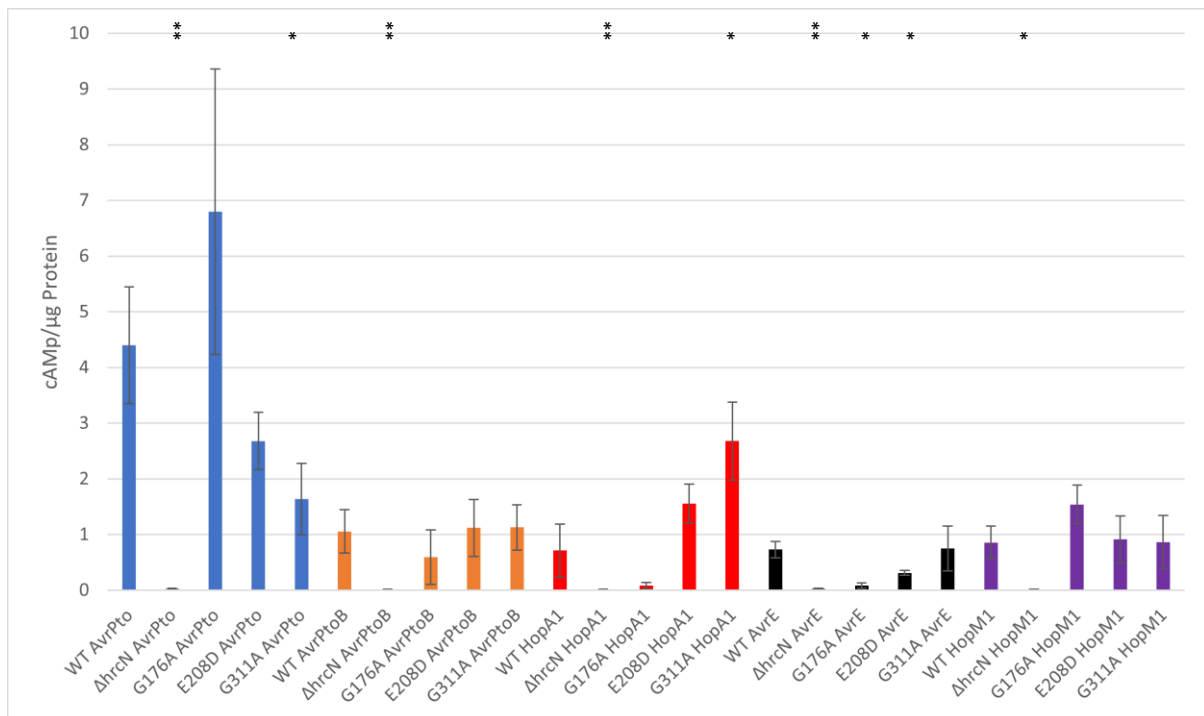
Figure 5.8. CyaA-T3SS effector fusion reporter assay quantifying effector translocation from mutant *hrcN P. syringae Pto* DC3000 infiltrated into *A. thaliana* Col-0. cAMP levels directly correlate to effector translocation rate. AvrPto, AvrPtoB, HopA1, AvrE and HopM1 CyaA fused effectors analysed in WT *hrcN*, *ΔhrcN*, *G176A hrcN*, *E208D hrcN* and *G311A hrcN Pto* DC3000 strains. Leaf tissue collected at 6 hours post-infection. Asterix symbols (*) represent statistical significance (2-sample t test) compared to WT cAMP value where '*' = $p \leq 0.05$, and '**' = $p \leq 0.01$ (n = 3).

Table 5.4. Average cAMP/μg protein values at a 6-hour timepoint for *hrcN Pto* DC3000 effector-CyaA fusion strains infected Col-0 *A. thaliana* tissue. p values show significance between tested strains for a given effector (excluding the negative *ΔhrcN* control), calculated using an ANOVA.

| T3E | Pto DC3000 hrcN strain | | | | | ANOVA p Value |
	WT	ΔhrcN	G176A	E208D	G311A	
HopB1	12.61	0.07	5.48	8.62	11.29	0.192
HopE1	5.44	0.08	5.69	14.64	15.78	0.234
HopF2	8.22	0.04	11.23	15.37	12.52	0.482
HopG1	3.87	0.03	2.86	2.02	12.84	0.035
HopH1	17.98	0.05	22.20	18.58	17.89	0.958
HopI1	4.08	0.10	1.42	1.61	2.37	0.087
HopK1	10.69	0.07	9.23	20.20	17.76	0.173
HopO1-1	14.63	0.11	15.08	11.65	20.21	0.602
HopQ1	4.70	0.11	1.49	4.89	24.83	0.001
HopR1	1.03	0.20	0.28	1.00	0.98	0.185
HopT1-1	0.28	0.05	0.13	0.60	1.68	0.461
HopU1	0.65	0.13	0.16	1.31	0.84	0.447
HopX1	1.05	0.10	0.51	1.59	1.19	0.479
HopY1	3.83	0.04	0.54	2.15	0.83	0.381
HopAA1-1	6.41	0.02	4.91	5.76	5.19	0.830
HopAA1-2	4.24	0.02	0.22	2.68	2.25	0.148
HopAF1	2.98	0.02	2.22	1.00	0.66	0.035

HopAM1	3.70	0.01	0.75	1.35	0.09	0.027
AvrPto	4.40	0.03	6.80	2.68	1.64	0.140
AvrPtoB	1.05	0.02	0.59	1.12	1.13	0.811
HopA1	0.71	0.01	0.08	1.55	2.68	0.02
AvrE	0.73	0.02	0.08	0.31	0.75	0.158
HopM1	0.86	0.01	1.54	0.91	0.86	0.567

Table 5.5. 2 sample t-test p values comparing WT to respective *hrcN* mutant for a given CyaA-fused effector protein. Calculated from cAMP/µg protein values at a 6-hour timepoint for *hrcN Pto* DC3000 effector-CyaA fusion strains infected Col-0 *A. thaliana* tissue.

CyaA-fused Effector Protein	Effector-CyaA fusion *hrcN Pto* DC3000 strain			
	Δ*hrcN*	G176A	E208D	G311A
HopB1	0.01	0.05	0.2	0.3
HopE1	0.04	0.47	0.04	0.12
HopF2	< 0.01	0.31	0.01	0.3
HopG1	0.04	0.29	0.16	0.06
HopH1	0.01	0.31	0.47	0.5
HopI1	0.01	0.04	0.06	0.12
HopK1	0.01	0.35	0.11	0.06
HopO1-1	0.04	0.48	0.36	0.22
HopQ1	0.01	0.06	0.47	< 0.01
HopR1	0.03	0.04	0.47	0.45
HopT1-1	0.02	0.06	0.23	0.18
HopU1	0.09	0.09	0.25	0.34
HopX1	0.01	0.09	0.24	0.4
HopY1	0.01	0.11	0.28	0.14
HopAA1-1	< 0.01	0.17	0.24	0.27
HopAA1-2	0.02	0.02	0.23	0.15
HopAF1	0.01	0.21	0.04	0.03
HopAM1	0.02	0.04	0.08	0.02
AvrPto	0.01	0.22	0.11	0.04
AvrPtoB	0.03	0.25	0.46	0.45
HopA1	0.01	0.13	0.11	0.04
AvrE	< 0.01	0.01	0.03	0.5
HopM1	0.02	0.1	0.5	0.5

5.2.2.2.1. Comparing Mutant T3SS Effector-CyaA Translocation Relative to WT Reveals Altered Translocation Profiles Unique to Key *hrcN* Mutants

The reporter assay data from Figure 5.4 to Figure 5.8 were compiled and plotted relative to WT for the *G176A*, *E208D*, and *G311A* mutant strains. Based on these following data, *G176A hrcN* was chosen as the mutant of focus for subsequent analyses. The translocation profile of *G176A hrcN* showed the most highly compromised translocation for several effectors. It was hypothesised that these most compromised effectors may be linked to the asymptomatic-like *G176A hrcN* disease phenotype as shown previously.

5.2.2.2.1.1. *G176A hrcN* Relative to WT *hrcN*

The relative effector translocation rates for *G176A hrcN* compared to WT *hrcN Pto* DC3000 is shown in Figure 5.9. Effectors HopAA1-2, HopA1, AvrE, HopY1, HopAM1, HopU1, HopR1, HopQ1, HopI1, HopB1, HopT1-1, HopX1, AvrPtoB, HopG1, HopAF1, HopAA1-1, and HopK1 showed a decrease in translocation rates relative to the respective WT *hrcN* infections for the *G176A hrcN* mutant. HopO1-1 and HopE1 were consistent with the WT. Effectors HopH1, HopF2, AvrPto, and HopM1 showed a slight increase relative to the WT.
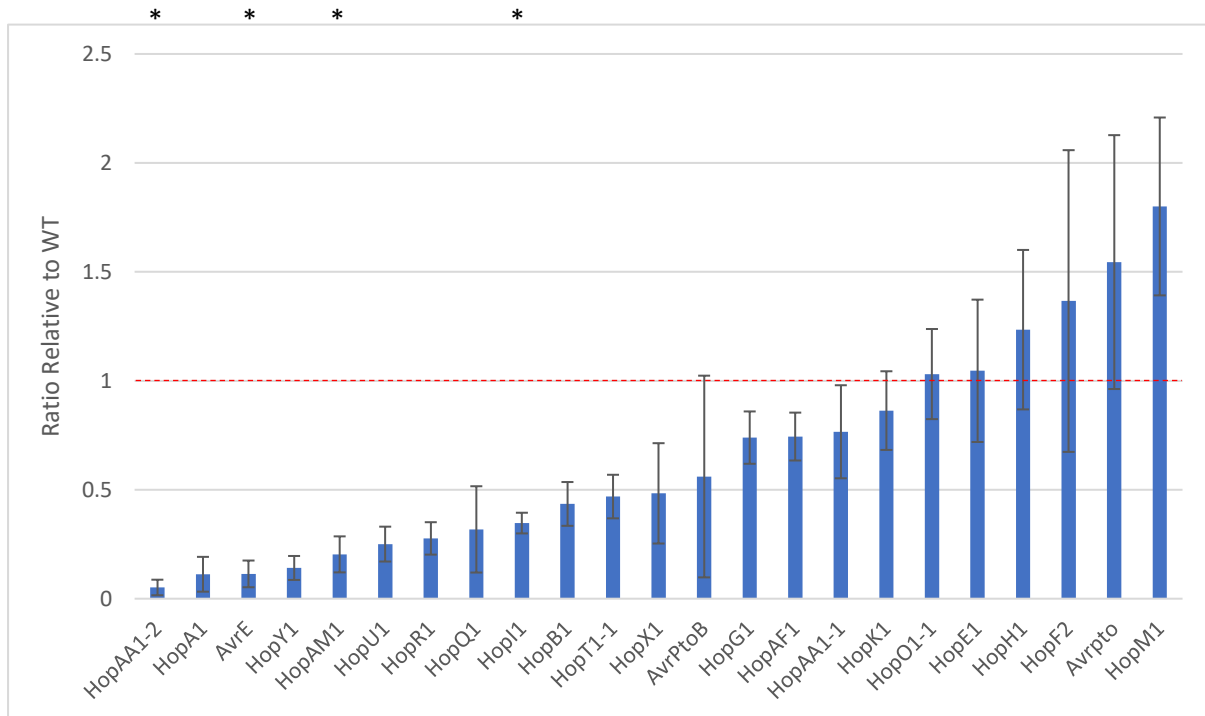
Figure 5.9. *Pto* DC3000 (carrying a mutant *G176A hrcN* allele) effector-CyaA translocation rates shown relative to WT *hrcN*. Values above 1 represent an increase in translocation for a given effector for *G176A hrcN* compared to WT, values below 1 show a decrease (n = 3).

5.2.2.2.1.2. *E208D hrcN* Relative to WT *hrcN*

Shown in Figure 5.10 are the effector translocation rates relative to WT *hrcN* infections for *E208D hrcN*. HopAF1, HopAM1, HopI1, AvrE, HopG1, HopY1, AvrPto, HopAA1-2, HopB1, HopO1-1, and HopAA1-1 had reduced translocation rates compared to the WT. Effectors HopR1, HopH1, HopQ1, AvrPtoB, and HopM1 showed consistent translocation rates relative to the WT. There was an increase in effector translocation compared to the WT for HopX1, HopF2, HopK1, HopU1, HopT1-1, HopA1, and HopE1.
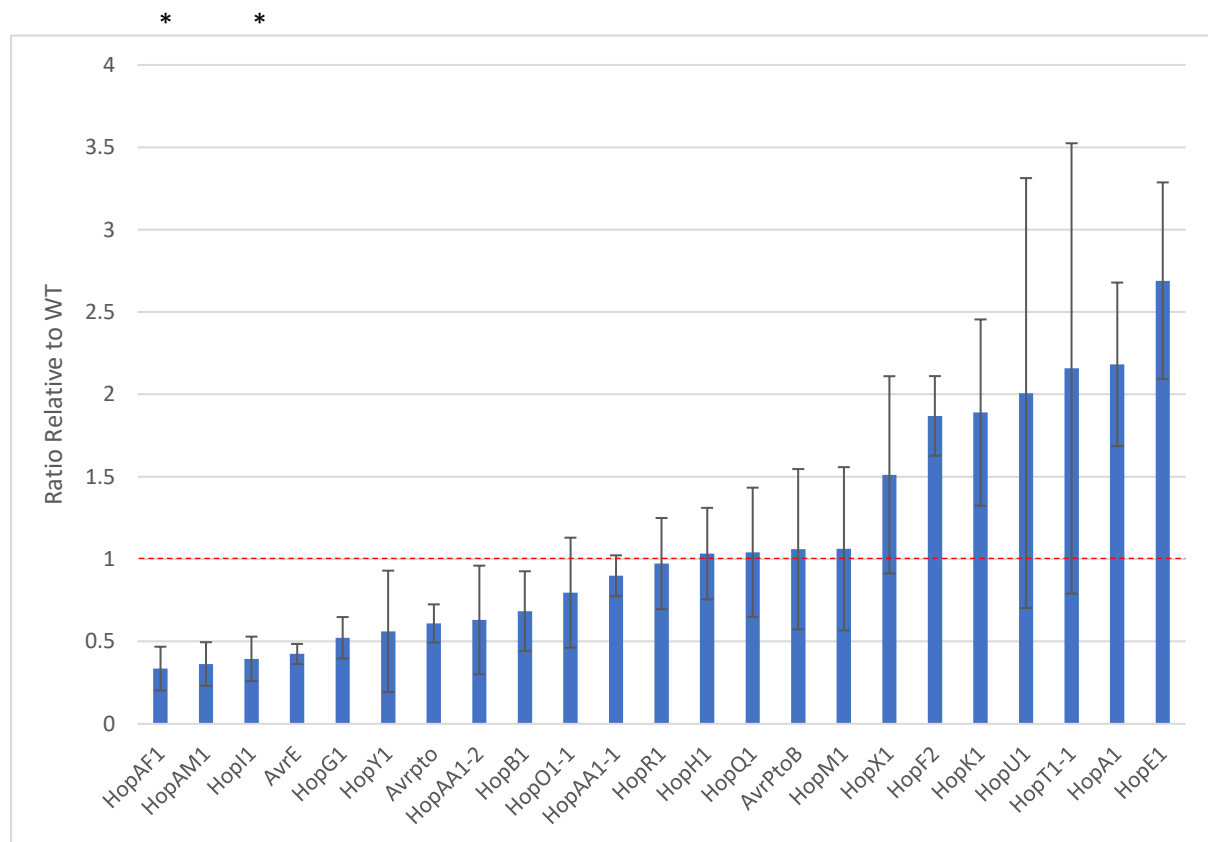
Figure 5.10. *Pto* DC3000 (carrying a mutant *E208D hrcN* allele) effector-CyaA translocation rates shown relative to WT *hrcN*. Values above 1 represent an increase in translocation for a given effector for *E208D hrcN* compared to WT, values below 1 show a decrease (n = 3).

5.2.2.2.1.3.   *G311A* hrcN Relative to WT hrcN

Shown in Figure 5.11 are the effector translocation rates relative to WT *hrcN* infections for *G311A hrcN*. HopAM1, HopY1, HopAF1, AvrPto, HopAA1-2, HopI1, and HopAA1-1 had reduced translocation rates relative to the WT. HopB1, HopR1, HopH1, HopM1, AvrE, AvrPtoB, and HopX1 showed consistent translocation compared to the WT. Effectors HopU1, HopO1-1, HopF2, HopK1, HopE1, HopG1, HopA1, HopQ1, and HopT1-1 have increased translocation rates relative to the respective WT infections.
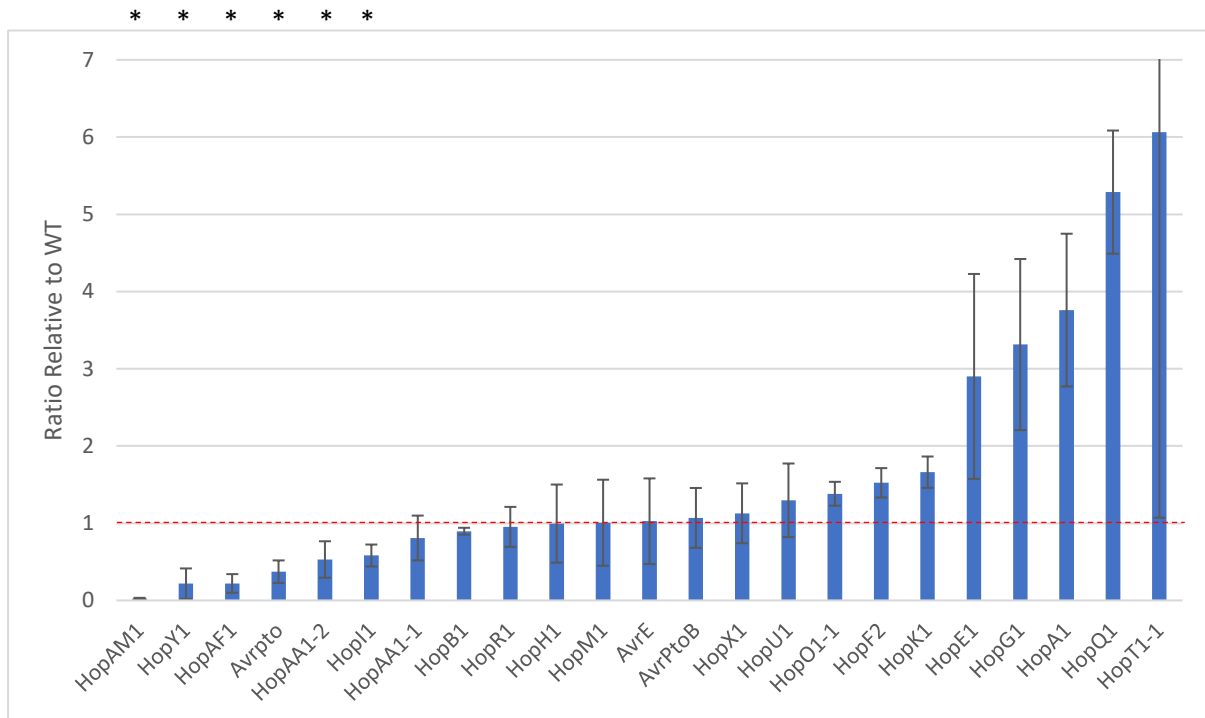
Figure 5.11. *Pto* DC3000 (carrying a mutant *G311A hrcN* allele) effector-CyaA translocation rates shown relative to WT *hrcN*. Values above 1 represent an increase in translocation for a given effector for *G311A hrcN* compared to WT, values below 1 show a decrease (n = 3).

5.2.2.3.   Key Effector Proteins HopAA1-2, HopAM1, and HopAF1 Show Compromised Translocation in *G176A hrcN Pto* Infections, but Not HopH1

As shown in the previous section, there were indications of differential translocation based on a preliminary screen including a large number of effector proteins and *hrcN* mutants. Statistically significant candidates of differential translocation observed in the *G176A hrcN* mutant were repeated with an increased sample size to confirm findings. *G176A hrcN* was chosen as the mutant of focus due to it having many translocation-compromised effector proteins, as well as it previously displaying an asymptomatic visual disease phenotype *in planta.*

HopAA1-2, HopAM1, and HopAF1 were chosen as representative examples of compromised effectors while HopH1 was chosen as a negative control representative of a non-compromised effector protein based on data from the previous effector screen. HopAA1-2, and HopAM1 were chosen as they showed statistically significant decreases in effector translocation for *G176A hrcN* compared to the WT. HopAF1 was chosen due to it being compromised across all tested strains and had statistically significant differences by way of ANOVA. HopH1 showed no statistical difference in translocation across any of the *hrcN* strains screened.

In Figure 5.12 key effector-CyaA fusion translocation reporter repeats, with an increased sample size (for added robustness), are shown for HopAA1-2, HopAM1, and HopAF1 along with HopH1. Effectors were tested in WT *hrcN*, *G176A hrcN*, and Δ*hrcN Pto* DC3000 strains. The cAMP/μg protein values and statistical data are shown in Table 5.6

It was shown that effectors HopAA1-2, HopAM1 and HopAF1 had statistically significant differences in cAMP/μg protein observed for WT *hrcN* compared to *G176A hrcN*. The effector HopH1 showed no such statistically significant differential translocation in *G176A hrcN*. This confirms what was seen in the previous large-scale reporter screen.
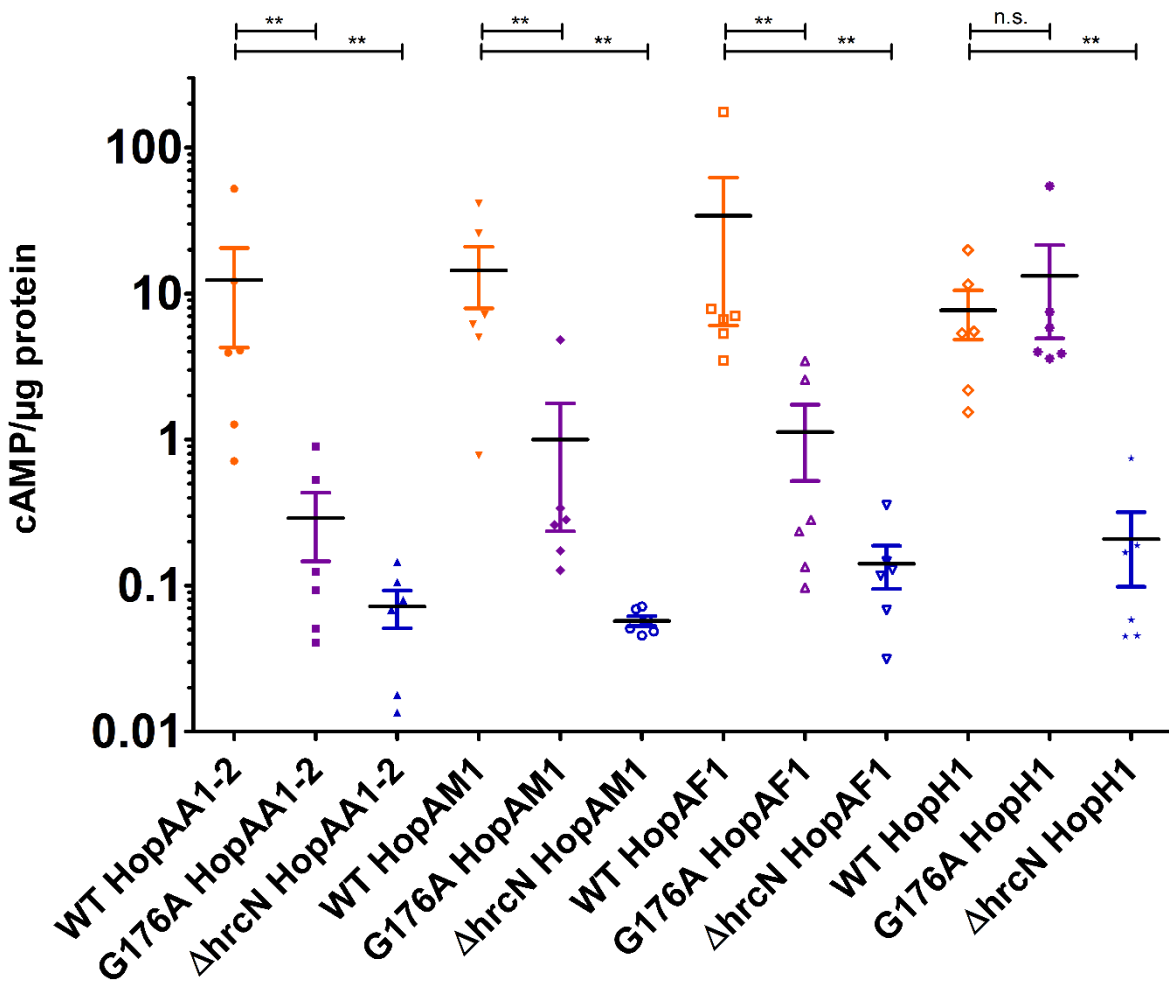
Figure 5.12. T3SS Effector-CyaA protein fusion reporter assay showing key effector translocation for *P. syringae Pto* DC3000 infected *A. thaliana* Col-0 leaves after a 6-hour infection window, where cAMP/µg protein directly correlates with effector translocation. Asterix symbols (*) represent statistical significance (2-sample t test) compared to the mean WT cAMP value where '*' = p ≤ 0.05, and '**' = p ≤ 0.01. 'n.s.' denotes no statistical significance (n = 6).

Table 5.6. Average cAMP/µg protein values at a 6-hour timepoint for *hrcN Pto* DC3000 effector-CyaA fusion strains infected Col-0 *A. thaliana* tissue. p values show significance of a mutant cAMP/µg value compared to WT, calculated using a Mann-Whitney U-test.

	CyaA-fused Effector Protein							
	HopAA1-2		HopAM1		HopAF1		HopH1	
CyaA-fusion *hrcN Pto* DC3000 strain	cAMP/µg protein	p value	cAMP/µg protein	p value	cAMP/µg protein	p value	cAMP/µg protein	p value
WT	12.0	N/A	14.39	N/A	34.16	N/A	7.67	N/A
G176A	0.29	0.0083	1.0	0.0083	1.13	0.0051	13.2	0.81
ΔhrcN	0.07	0.005	0.06	0.005	0.14	0.005	0.25	0.005

5.2.3. Over-expression of Key Effector Genes *hopAA1-2, hopAM1,* and *hopAF1,* but not *hopH1* in the *G176A hrcN* mutant of *Pto* DC3000 Results in Disease Symptom Restoration

HopAA1-2, HopAM1, and HopAF1 showed compromised translocation in *G176A hrcN Pto* infections as previously shown in Figure 5.12. Over-expression of key effector proteins (along with a *hopH1* control which did not previously display compromised translocation in the *G176A hrcN* mutant) during infection was performed to evaluate the possible role of these effectors during infection. HopQ1-1 was also included as this effector previously showed a translocation decrease for *G176A hrcN* in the large effector-CyaA screen.

5.2.3.1. Altered Leaf Phenotypes Were Observed in *G176A hrcN* Upon Key Effector Over-expression

Constitutive over-expression of key compromised effectors in *Pto* DC3000 via a stable pBBR2 vector with *in planta* infection disease phenotype analysis was performed. The day 6 post-infection leaf disease phenotypes are shown in Figure 5.13. As previously shown, WT *hrcN Pto* DC3000 infection shows characteristic chlorosis and necrosis disease symptoms. *Pto* DC3000 carrying a *G176A hrcN* allele shows a compromised disease phenotype with minimal evidence of chlorosis and necrosis symptoms. Similar results are seen when strains are transformed with an empty-pBBR2 expression vector confirming the vector alone does not alter disease phenotypes, and that any subsequent changes in phenotype are due to an over-expressed gene insert.

When effector *hopAA1-2* is over-expressed in the WT *hrcN* background, disease symptoms appear unchanged compared to the standard WT *hrcN* infection with no over-expression. Interestingly, when *hopAA1-2* is over-expressed in the *G176A hrcN* background, there is some evidence of disease symptoms returning where previously, very minimal evidence of any chlorosis or necrosis was present in the standard non-over-expression strain. The same partial return of disease severity for *G176A hrcN* is seen for the other tested effectors: *hopAM1, hopAF1,* and *hopQ1-1*. These effectors were all previously shown to have compromised T3SS translocation in the case of *Pto* DC3000 carrying a mutant *G176A hrcN* allele during plant infection.

In the case of the WT *hrcN* background for *hopAM1, hopAF1, and hopQ1-1*, no visible differences are seen for the over-expression strain infections compared to strains lacking the over-expression plasmid as expected.

HopH1 showed no statistically significant differences in T3SS translocation rates across *G176A Pto* DC3000 infections suggesting that this effector is unaffected by the *G176A* point-mutation. When *hopH1* is over-expressed throughout infection, the WT *hrcN* background developed a standard infection where expected disease symptoms arise. Minimal disease symptoms were observed upon *hopH1* expression in the *G176A hrcN* background, similar to phenotypes observed with the empty pBBR2 over-expression plasmid.

This demonstrates that over-expression of *hopAA1-2*, *hopAM1*, *hopAF1* and *hopQ1-1* are able to partially compensate for the defect in effector translocation and recover the previously lost disease severity phenotype for *Pto* DC3000 carrying a mutant *G176A hrcN* allele, while in the case of *hopH1*, this recovery is not achieved. This may be due to increased effector protein abundance around HrcN and the T3SS. If *G176A hrcN* is less efficient at recruiting a given effector protein due to the point-mutation present, an increase abundance of that effector protein may lessen the impact of this inefficiency. This may be due to an increase chance of that given effector protein being present at the base of the T3SS by HrcN, effectively bypassing the need for efficient effector protein recruitment.

With *hopH1* not causing a return in disease symptoms for *Pto* DC3000 carrying a mutant *G176A hrcN* allele upon over-expression, this suggests that not all effector proteins respond to this mutation in the same way. It suggests that some effector proteins play a role in establishing full disease symptoms and when compromised show an absence of disease severity during infection, while others such as HopH1 are not compromised, and do not show clear evidence of disease symptom establishment. Had a return in disease symptoms been observed for *hopH1* also, it could be argued that expression of any effector protein may cause disease symptoms to return in *G176A*. As shown, this is not the case, indicating that key *G176A hrcN* translocation-compromised effector proteins (HopAA1-2, HopAM1, HopAF1, and HopQ1-1) are important for proper disease symptom establishment and may help to explain why the *G176A hrcN* infection showed the phenotype observed.

WT

G176A

WT Empty pBBR2

G176A **Empty pBBR2**

WT pBBR2-*hopAA1-2*

G176A **pBBR2-*hopAA1-2***

WT pBBR2-*hopAM1*

G176A **pBBR2-*hopAM1***

WT pBBR2-*hopAF1*

G176A **pBBR2-*hopAF1***

WT pBBR2-*hopQ1-1*

G176A **pBBR2-*hopQ1-1***

WT pBBR2-*hopH1*

G176A **pBBR2-*hopH1***

Δ*hrcN*

Uninfected Control
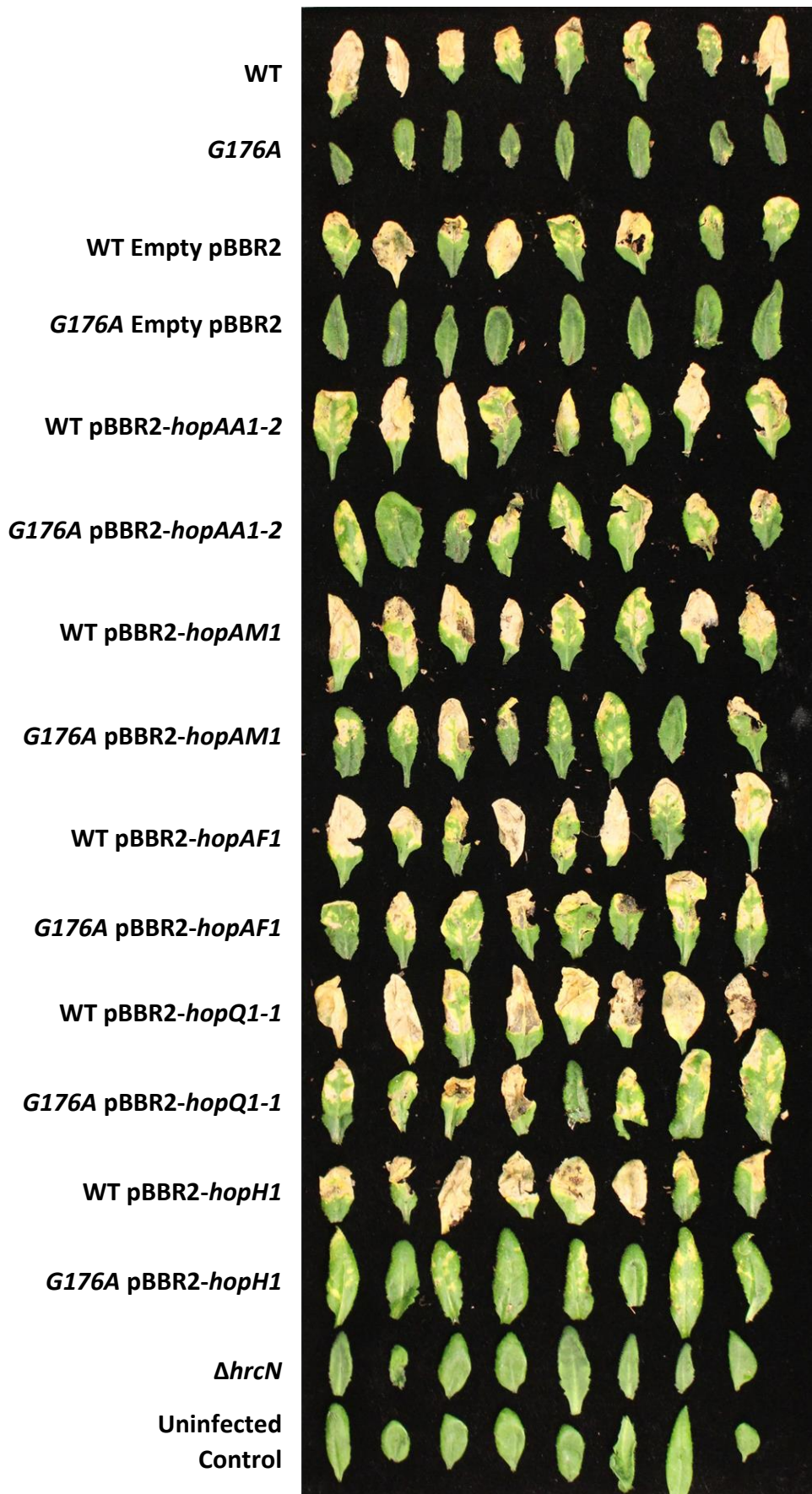
Figure 5.13. Infiltration of *A. thaliana* Col-0 plants with *Pto* DC3000 strains over-expressing key effector proteins in a stable pBBR2 plasmid under the control of a constitutive promoter (derepressed P-lac) (n = 3 plants).

5.2.3.2.   Partial Recovery of Visual Disease Severity Was Observed with *G176A hrcN*
Translocation-compromised Effector Protein Over-expression in *Pto* DC3000, But Not with
Non-translocation-compromised *hopH1*

The infected leaves from Figure 5.13 were analysed using ImageJ to quantify visual disease severity. This was achieved by measuring the average pixel intensity representing the amount of chlorosis present across leaf tissue for each sample. This ImageJ analysis is shown in Figure 5.14.

The *Pto* DC3000 infections (WT and *G176A hrcN*) proceed as previously described. The WT shows a high level of chlorosis represented by a high average pixel intensity of 185.7 across sampled leaves. In comparison, the asymptomatic-like *G176A* shows a statistically significant difference in level of chlorosis represented by a lower average pixel intensity of 126 across sampled leaves. A 2-sample t-test shows this to be a statistically significant difference (p= 0.00001).

A similar result is observed for WT with an empty pBBR2, and *G176A* with an empty pBBR2. WT + empty pBBR2 was measured to have an average pixel intensity of 167 across sampled leaves, while *G176A* + empty pBBR2 had 127.9 average pixel intensity. This difference was statistically significant (p = 0.0004).

Constitutive over-expression of *hopAM1, hopAF1, hopAA1-2,* and *hopQ1-1* see a partial increase in average pixel intensity for their respective *G176A Pto* DC3000 infections (154.7, 153.94, 169.2, and 166.6 respectively). The return of disease symptoms is not a full recovery to WT-levels.

For WT compared to *G176A*, a difference in mean averages of 59.7 is observed (p = 0.00001). For WT + empty pBBR2 compared to *G176A* + empty pBBR2 a difference of 39.2 is present (p = 0.0004). For WT + pBBR2-*hopAM1* compared to *G176A* + pBBR2-*hopAM1* a difference of 30.4 was observed (p = 0.0026). With WT + pBBR2-*hopAF1* compared to *G176A* + pBBR2-*hopAF1* there was a difference of 29.7 (p = 0.0018). WT + pBBR2-*hopAA1-2* compared to *G176A* + pBBR2-*hopAA1-2* had a difference of 21.09 (p = 0.03). WT + pBBR2-*hopQ1-1* compared to *G176A* + pBBR2-*hopQ1-1* had a difference of 28.3 (p = 0.0002). Lastly, WT + pBBR2-*hopH1* compared to *G176A* + pBBR2-*hopH1* saw a difference in mean average pixel intensity of 29.8 (p = 0.0012). In all cases, this difference is statistically significant confirming that any recovery in disease severity observed was not a full recovery, only a partial recovery and that a difference in average pixel intensity between WT and *G176A* still remained, albeit to a lesser extent in most instances. Comparing WT and *G176A* carrying an empty pBBR2 vector with like pBBR2-effector over-expression samples also sees a similar partial restoration of disease severity (indicated by retained significant difference), rather than a full recovery.

When comparing the *G176A* infections without pBBR2 to *G176A* infections over-expressing *hopAM1* (p = 0.0002), *hopAF1* (p = 0.0014), *hopAA1-2* (p = 0.00001), and *hopQ1* (p = 0.0001), a statistically significant difference is observed confirming a difference in average pixel intensity, and thus visual disease severity with effector over-expression during infections.

A small recovery is seen for the *G176A* with *hopH1* over-expression with an average pixel intensity of 153.9 however this is minimal. A statistically significant difference is still observed between WT *hopH1* and *G176A hopH1* confirming no full recovery of disease phenotype was observed (p = 0.0012).

The negative Δ*hrcN* and uninfected controls show lower levels of average pixel intensity of 145.3 and 147.4 respectively.

A standard ANOVA test shows that each of the means are not the same across the sample columns excluding the negative controls (p = 0.0001). This indicates that there is variation present between

columns. By analysing the data further with Dunnett's multiple comparison post-hoc test, columns are compared against a control group to determine whether any differences are present.

When comparing all *G176A* values against the standard *G176A* (with no pBBR2 vector or effector over-expression), a statistically significant result was observed (p = 0.0001) confirming that there is variation across *G176A* group samples. Conversely, no statistically significant variation in means was seen between WT groups.
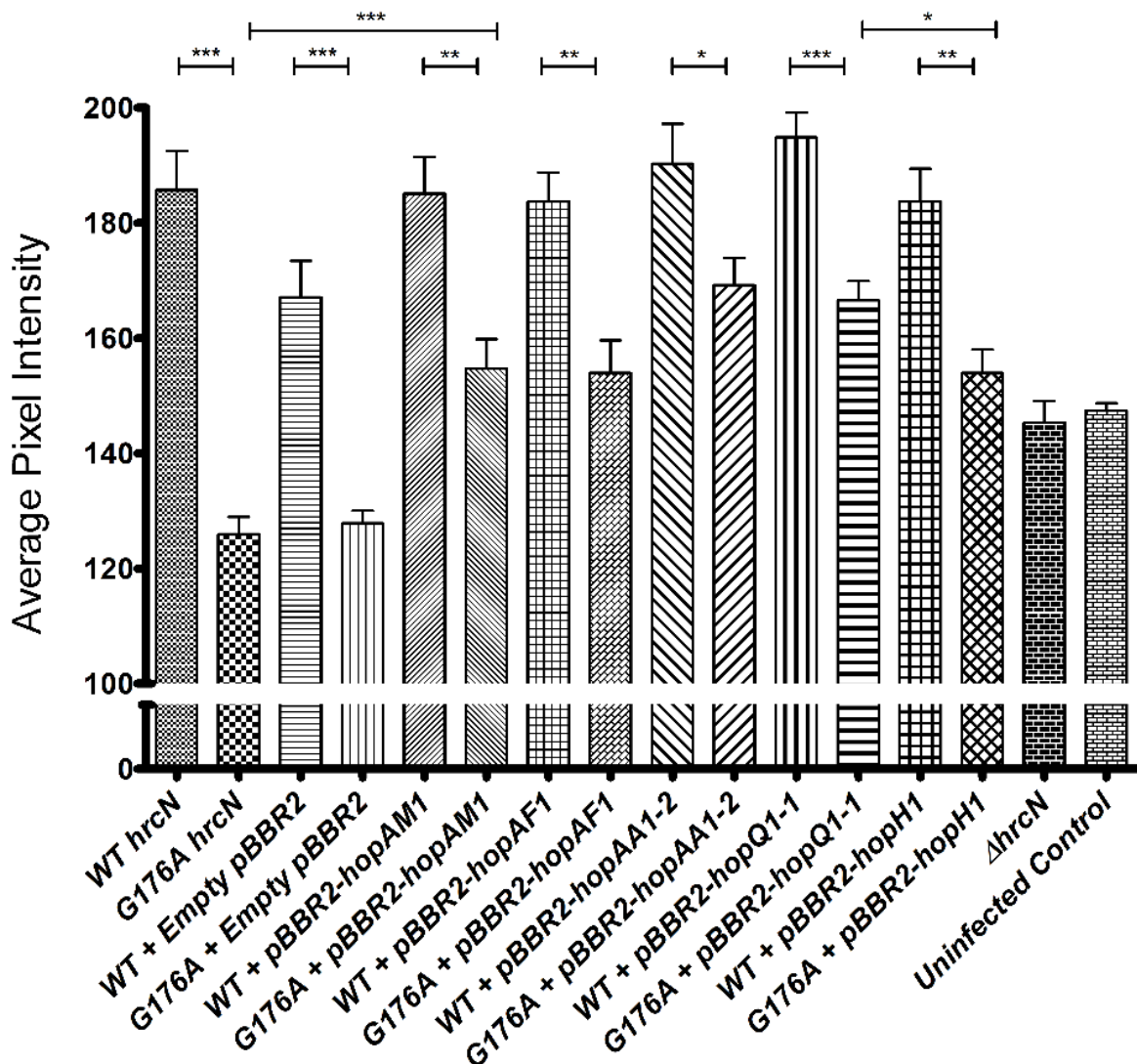
Figure 5.14. Average pixel intensity analysis across representing levels of leaf yellowing for *A thaliana* Col-0 leaves infiltrated with *Pto* DC3000 (carrying mutant *hrcN* alleles) effector over-expression strains 6 days post-infection. Asterix symbols (*) represent statistical significance (2-sample t test) of a given strain compared to WT '*' = p ≤ 0.05, '**' = p ≤ 0.01, and '***' = p ≤ 0.001 (n = 8 leaves)

5.2.3.3. Bacterial Load Remains Unaffected Upon Effector Over-expression

Next, bacterial colonisation of this pBBR2-effector over-expression experiment was investigated (Figure 5.15). Full bacterial colonisation was observed for all samples over a 3 day infection sampling period with exception for the Δ*hrcN* negative control as expected. Infiltrated bacteria appear consistent across day 0 post-infection, with an observed mean log cfu value of approximately 3-4 log

cfu/cm^2. with minimal variation between 5.5 and 7 log cfu/cm^2 then present between day 2 and day 3 post-infection columns.

An ANOVA comparing values all day 2 post-infection values (excluding the negative control) showed no statistically significant difference across samples (p = 0.3). The same is seen with an ANOVA between day 3 post-infection values (p = 0.8).
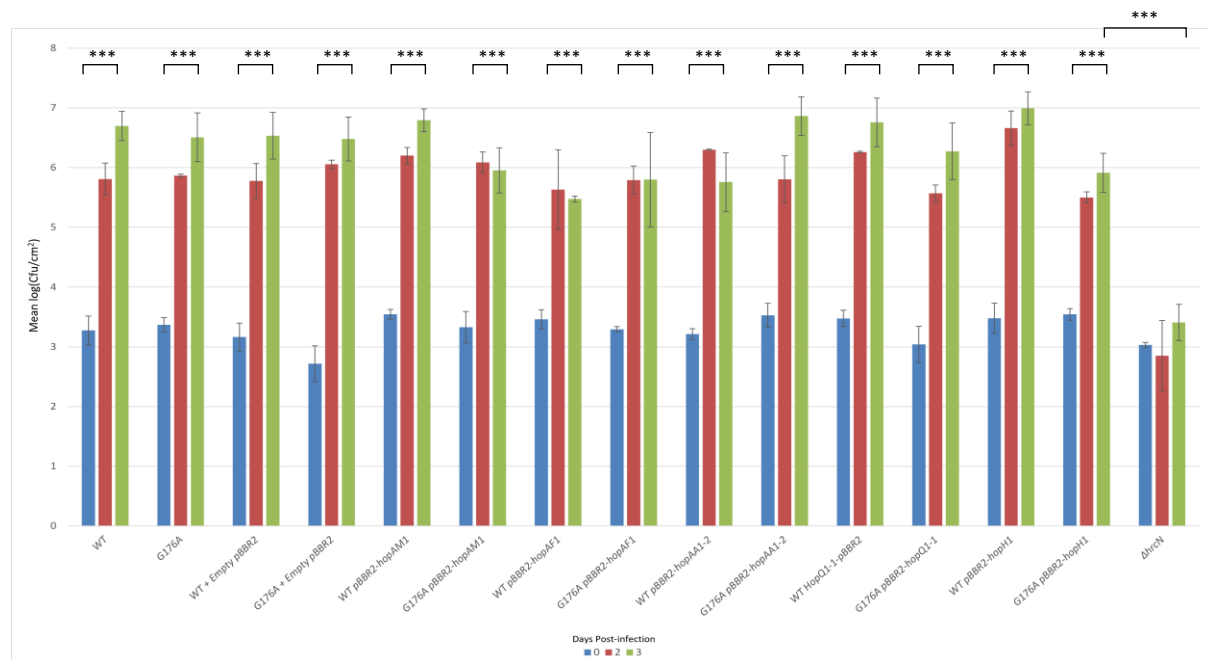
Figure 5.15. Infiltration of *A. thaliana* Col-0 plants with *P. syringae Pto* DC3000 *hrcN* effector over-expression strains. Colony forming units were determined using 4 mm diameter leaf disc sampling across a 3-day infection window. Error bars show standard error. 2-sample t-test analyses were performed where "*" denotes statistical significance. '*' = p ≤ 0.05, '**' = p ≤ 0.01, and '***' = p ≤ 0.001 (n = 3 plants)

5.2.4. Deletion of Key T3SS Effector-encoding Genes in *Pto* DC3000 Sees Disease Symptom Loss with *hopAA1-2* but Not *hopAM1* in a WT *hrcN* background

HopAA1-2 and HopAM1 showed compromised translocation in *Pto* DC3000 strains (carrying a mutant *G176A hrcN* allele) as previously shown in Figure *5.12*. Deletions of key effector-encoding genes were generated in a WT *hrcN* background in order to evaluate their possible role during infection and to help explain the asymptomatic-like visual disease phenotype seen with *G176A hrcN*. These chromosomal deletions were generated via allelic exchange of deletion constructs (500 bp flanking regions upstream and downstream of gene) using pTS-1 sucrose counter selection screening of double-crossover candidates. Successful *Pto* DC3000 chromosomal deletion constructs were verified using colony PCR and sequencing.

5.2.4.1. Altered Leaf Infection Phenotypes Were Observed in WT *hrcN* Upon Key Effector Deletion

Infiltration of *A. thaliana* Col-0 with *Pto* DC3000 strains carrying deletion of key effector-encoding genes is shown in Figure 5.16. Shown are representative leaves at day 6 post-infection.

In the case of WT *hrcN* characteristic chlorosis and necrosis disease symptoms are observed. *G176A hrcN* shows minimal levels of chlorosis and necrosis in most instances as previously seen.

WT Δ*hopAA1-2* infiltrations show a different phenotype than seen in WT *hrcN*. The disease phenotype is closer to *G176A* where minimal chlorosis and necrosis is evident. There are small subtle signs of chlorosis and necrosis being present at the edge of the leaves, but the main central region of the leaves appeared less affected compared to WT.

WT Δ*hopAM1* does not show a large difference compared to the WT. Chlorosis and necrosis symptoms are still present with no indication of deviation from WT-like levels.

The WT Δ*hopAA1-2* Δ*hopAM1* double mutant shows a similar phenotype as observed in the Δ*hopAA1-2* single deletion. Chlorosis and necrosis are not able to fully establish to WT-like levels at day 6 post infection in this experiment.

The Δ*hrcN* and uninfected leaf control show no evidence of disease, indicating that the leaves were healthy throughout the experiment and that the disease response observed was due to type III-mediated virulence.
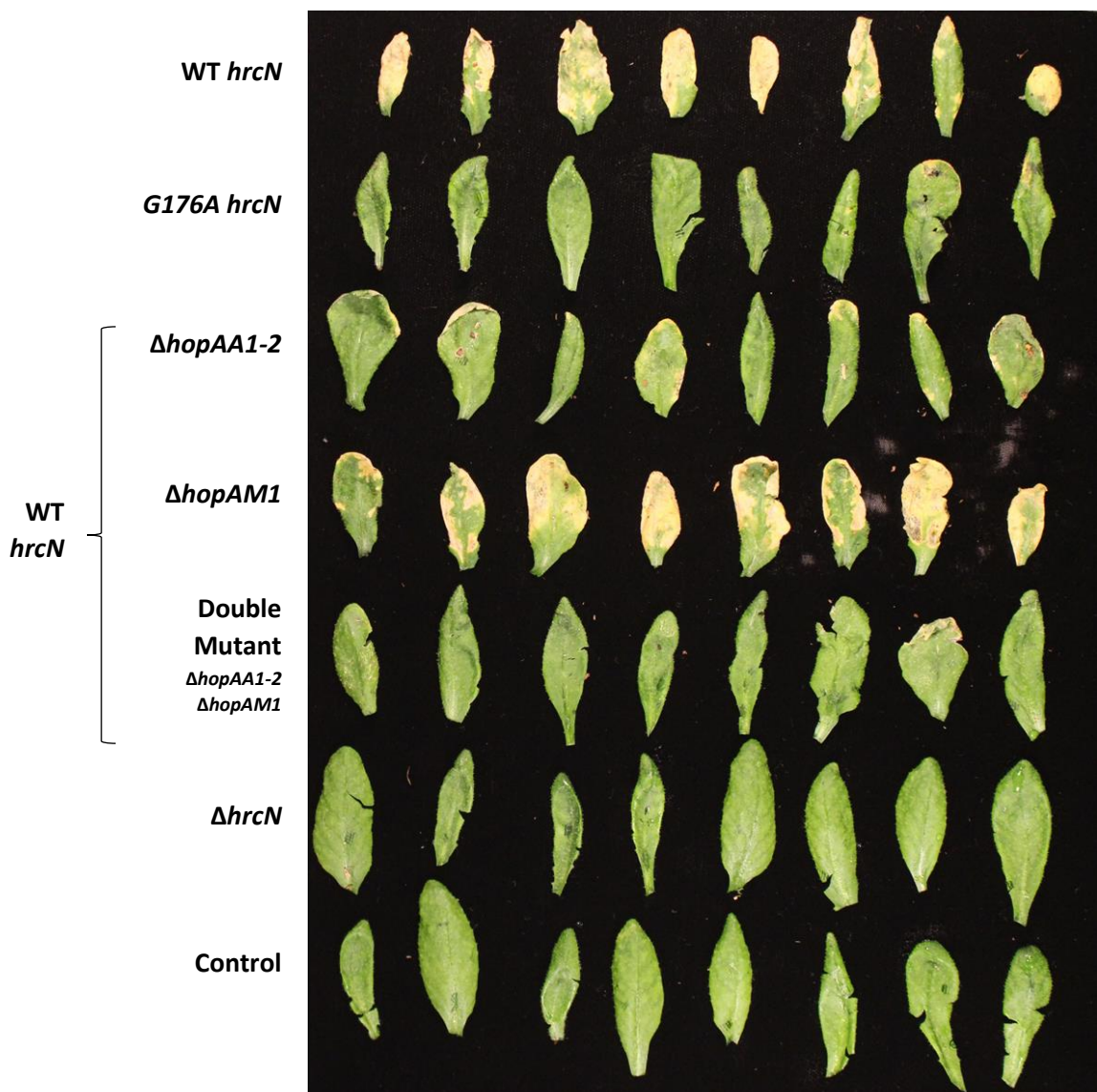
Figure 5.16. Infiltration infection disease phenotypes across *A. thaliana* Col-0 with *P. syringae Pto* DC3000 effector deletions strains in WT *hrcN* background. Leaves photographed 6 days post-infection. (n = 3 plants).

5.2.4.2. Quantified Visual Disease Severity Confirms Loss of Disease Severity for WT *hrcN* Δ*hopAA1-2* but not Δ*hopAM1*

The disease severity in the experiment was quantified by way of ImageJ average pixel intensity analysis, as shown in Figure 5.17.

WT *hrcN* was measured to have an average pixel intensity of 188.5 while *G176A hrcN* had a lower value of 152. This difference was statistically significant (p = 0.00001). The Δ*hopAA1-2* single mutant had a measured average pixel intensity value of 165.1 which was a statistically significant decrease compared to the WT (p = 0.0008). The same is true for the Δ*hopAA1-2* Δ*hopAM1* double mutant which was measured to have an average pixel intensity of 169.74 across sampled leaves. This was a statistically significant decrease compared to the WT (p = 0.004). The Δ*hopAM1* single deletion did not

have a statistically significant decrease however with an average pixel intensity value of 193.4 (p = 0.49).

This difference between samples (excluding the negative controls) was further supported with statistical analysis using ANOVA (p = < 0.0001).

The negative Δ*hrcN* and uninfected leaf controls showed a statistically significant difference compared to the WT as expected, with average pixel intensity values of 160.3 (p = 0.0002) and 156 respectively (p = 0.0002).
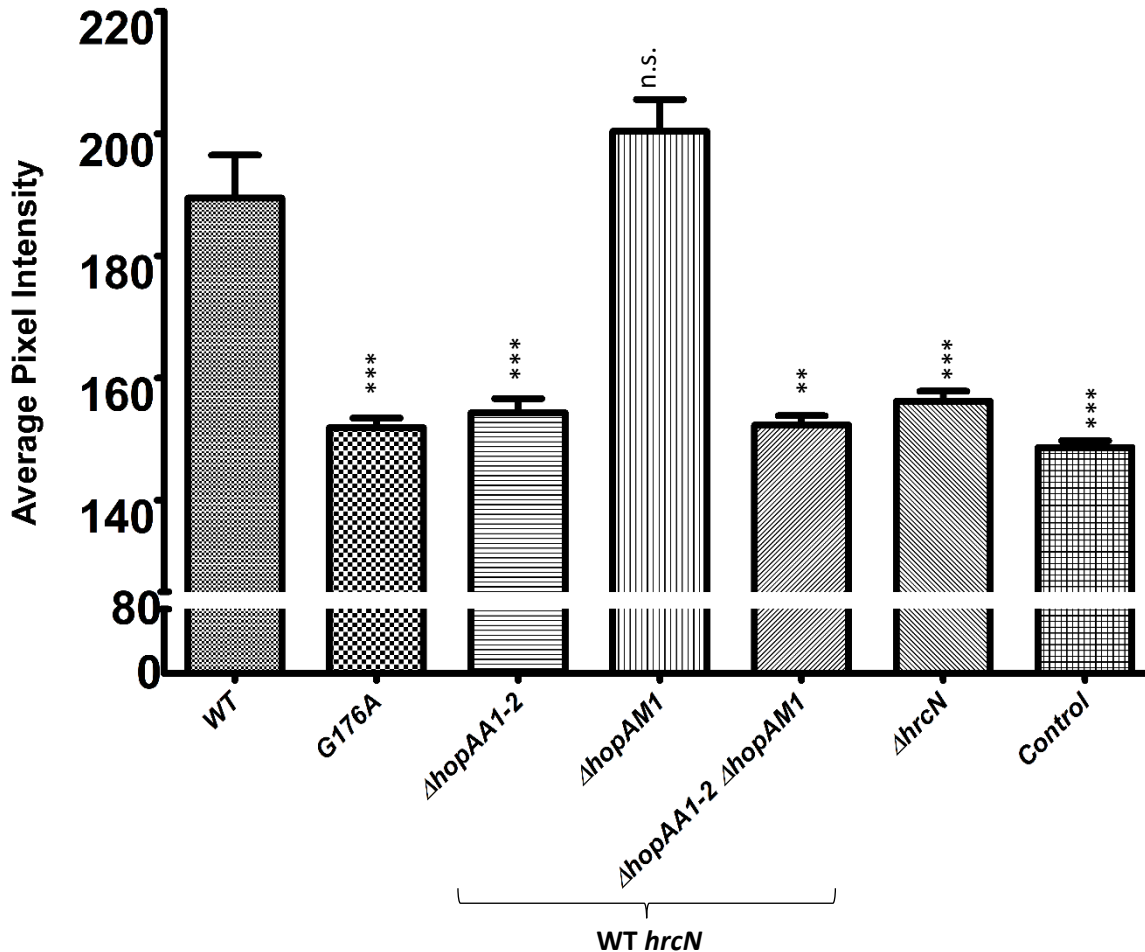
Figure 5.17. Average pixel intensity analysis across representing levels of leaf yellowing for *A. thaliana* Col-0 leaves infiltrated with *Pto* DC3000 effector deletion strains 6 days post-infection. Asterix symbols (*) represent statistical significance (2-sample t test) compared to WT cAMP value of like-timepoint where '*' = $p \leq 0.05$, '**' = $p \leq 0.01$, and '***' = $p \leq 0.001$. 'n.s.' denotes no statistical significance (n = 8 leaves).

5.2.4.3.   Bacterial Load Unaffected with Key Effector Deletions

The bacterial colony forming units have been determined for this infection experiment, as shown in Figure 5.18. Across a 3-day sampling period, all samples saw an increase in bacterial proliferation comparable to the WT, with the exception for the negative Δ*hrcN* control as expected.

At day 0 post-infection, infiltrated values were between 3-4 log cfu/cm^2. This increased to between 5.5 and 7 log cfu/cm^2 for both day 2 and day 3 post-infection for non-Δ*hrcN* samples. There is a

statistically significant increase between day 0 and day 3 post-infection for WT, *G176A*, Δ*hopAA12*, Δ*hopAM1*, and the Δ*hopAA1-2* Δ*hopAM1* double mutant (p = < 0.001 for all).

There is some slight variation seen across day 2 and day 3 between samples, however an ANOVA between day 2 samples (excluding the negative Δ*hrcN* control) shows that there was no statistically significant difference between means (p = 0.47). The same was also true for day 3 post-infection (p = 0.068).
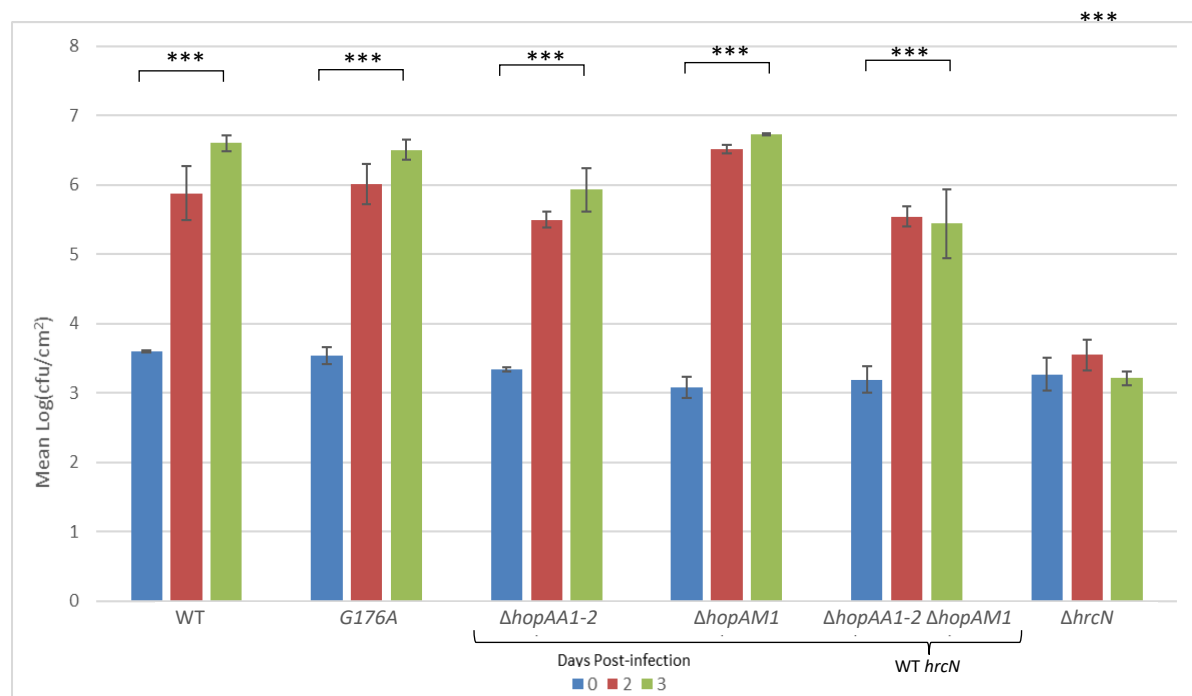
Figure 5.18. Infiltration of *Arabidopsis thaliana* Col-0 plants with *Pseudomonas syringae* DC3000 *hrcN* effector deletion strains. Colony forming units were determined using 4 mm diameter leaf disc sampling across a 3-day infection window. Error bars show standard error of the mean. 2-sample t-test analyses were performed where "*" denotes statistical significance. '*' = P ≤ 0.05, '**' = P ≤ 0.01, and '***' = P ≤ 0.001. (n = 3 plants)

5.2.5.   AlphaFold Structural Prediction of Key Effector Proteins

The structure of key effectors HopAM1, HopAA1-2, and HopAF1 were predicted using AlphaFold (v2.1.0) alongside an MMseqs2 server (Jumper et al., 2021, Mirdita et al., 2019). Predicted structures were visualised and exported using UCSF Chimera version 1.15 software (Pettersen et al., 2004). This structural prediction was performed to identify any structural similarities between these proteins which may explain why these effectors displayed compromised translocation in *G176A hrcN*. From these structural predictions, it was seen that each of these effectors is visually different from one another. As such, it is likely another factor that may explain why these effectors displayed compromised effector translocation in *G176A hrcN*, rather than a shared structural similarity alone.

5.2.5.1.   HopAM1

The predicted AlphaFold structure for HopAM1 is shown in Figure 5.19. In Figure 5.19 A, a ribbon-model representation of HopAM1 is shown with rainbow colouration where blue represents the N-terminus, and red represents the C-terminus. 11 predicted α-helix regions, and 8 β-strand regions interspaced with coiled regions are present in the structure. In Figure 5.19 B, a hydrophobicity space-

fill model of HopAM1 is shown. Shown in red are regions of negative predicted electrostatic potential, and in blue are regions of positive predicted electrostatic potential.
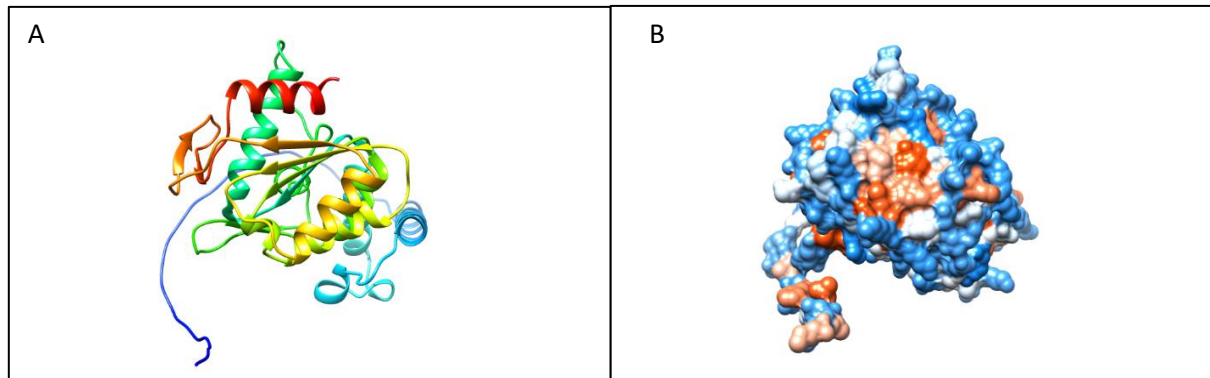
Figure 5.19. Predicted AlphaFold structure for HopAM1 effector protein from *P. syringae* pv. tomato DC3000, visualised via UCSF Chimera. A) shows a ribbon-model representation of secondary structure features with rainbow colouration where blue represents the N-terminus, and red represents the C-terminus. B) shows a Coulombic electrostatic potential space-fill model where red are regions of negative predicted electrostatic potential, and in blue are regions of positive predicted electrostatic potential.

5.2.5.2.   HopAA1-2

The predicted AlphaFold structure for HopAA1-2 is shown in Figure 5.20. In Figure 5.20 A, a ribbon-model representation of HopAA1-2 is shown with rainbow colouration where blue represents the N-terminus, and red represents the C-terminus. 19 predicted α-helix regions interspaced with coiled regions are present in the structure. No β-strand regions are present. In Figure 5.20 B, a hydrophobicity space-fill model of HopAA1-2 is shown. The model is coloured as for HopAM1 above.
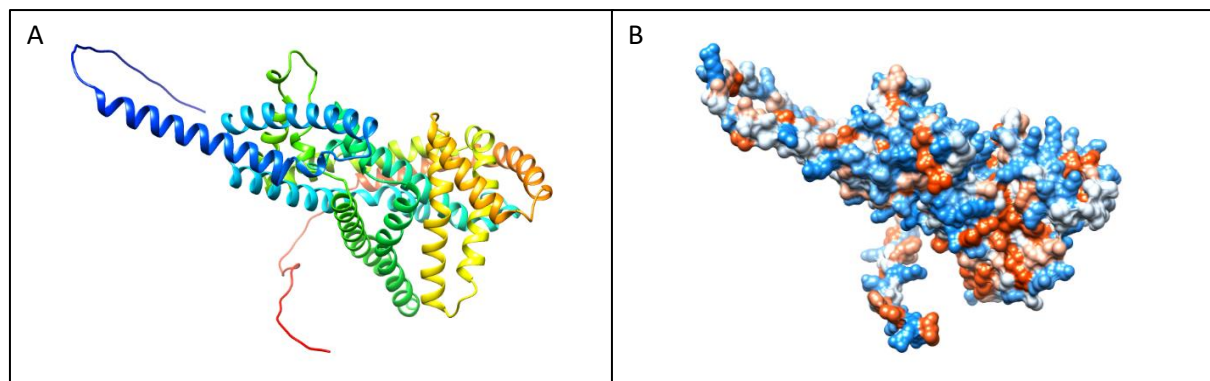
Figure 5.20. Predicted AlphaFold structure for HopAA1-2 effector protein from *P. syringae* pv. tomato DC3000, visualised via UCSF Chimera. A) shows a ribbon-model representation of secondary structure features with rainbow colouration where blue represents the N-terminus, and red represents the C-terminus. B) shows a Coulombic electrostatic potential space-fill model where red are regions of negative predicted electrostatic potential, and in blue are regions of positive predicted electrostatic potential.

5.2.5.3.   HopAF1

The predicted AlphaFold structure for HopAF1 is shown in Figure 5.21. In Figure 5.21 A, a ribbon-model representation of HopAF1 is shown with rainbow colouration where blue represents the N-terminus, and red represents the C-terminus. 6 predicted α-helix regions, and 13 β-strand regions interspaced with coiled regions are present in the structure. In Figure 5.21 B, a hydrophobicity space-fill model of HopAF1 is shown. The model is coloured as above.
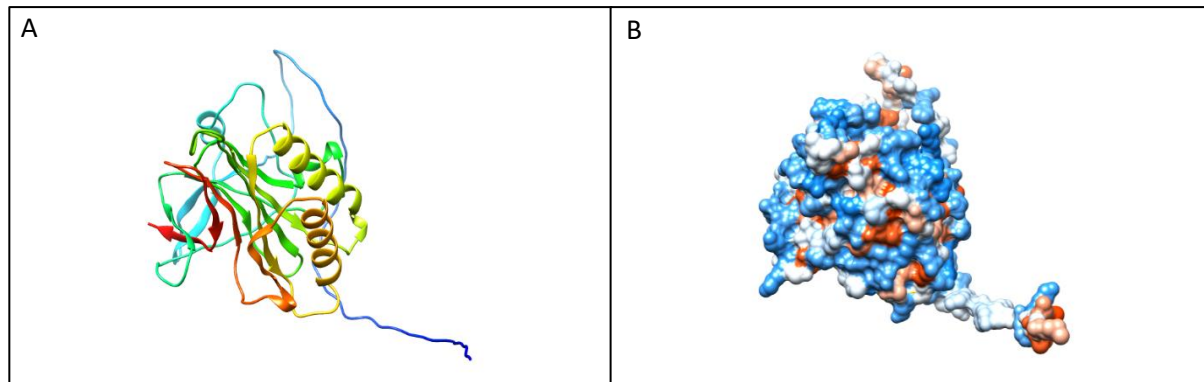
Figure 5.21. Predicted AlphaFold structure for HopAF1 effector protein from *P. syringae* pv. tomato DC3000, visualised via UCSF Chimera. A) shows a ribbon-model representation of secondary structure features with rainbow colouration where blue represents the N-terminus, and red represents the C-terminus. B) shows a Coulombic electrostatic potential space-fill model where red are regions of negative predicted electrostatic potential, and in blue are regions of positive predicted electrostatic potential.

5.2.6.   Co-immunoprecipitation of Key Effectors and Potential Target Proteins in *Pto* DC3000 *A. thaliana* Col-0 Infections

5.2.6.1.   Key Effector Protein *A. thaliana* Co-IP Interaction Candidates Were Identified

Co-immunoprecipitation experiments were performed using HopAM1, HopAA1-2, and HopAF1 effector-CyaA C-terminal fusions bound to protein A Dynabeads as bait for effector targets in *Pto* DC3000-infected Col-0 plants.

Leaf discs from *Pto* DC3000 effector-CyaA infected plants were harvested, lysed, and mixed with protein A Dynabeads bound to an anti-CyaA antibody. Bead washing to remove contaminating proteins and to pull down the effector-CyaA complexes (bound to any interacting plant proteins) followed. The pulled-down samples were subsequently submitted for mass spectrometry analyses to identify candidate interaction partners. This was performed to identify potential effector interaction candidates in the plant to help explain the asymptomatic-like visual disease symptoms with *Pto* DC3000 infection when carrying a mutant *G176A hrcN* allele, and to provide testable targets for future research.

The top five A. thaliana protein pull-down hits are shown in tables for each tested effector protein. Proteins were sorted via an algorithm which factored in SAINT score (probability of true protein-protein interaction), fold change, Bayesian false discovery rate (BFDR), and spectroscopy counts following normalisation against non-CyaA WT Pto DC3000 infected Col-0 A. thaliana control samples. The top 5 denotes the first 5 rows in the sorted list. Non-A. thaliana pull-down results were considered contaminating outliers and were not included. The expanded Co-IP dataset volcano plots from which these candidate proteins were identified from are shown in the appendix section (Figure 8.1 to Figure 8.3).

The top 5 co-immunoprecipitation *Pto* DC3000 *A. thaliana* Col-0 interaction candidates for HopAM1-CyaA are shown in Table 5.7.

Table 5.7. Top five target candidate proteins for HopAM1-CyaA identified via co-immunoprecipitation and mass spectrometry analysis. Raw values subtracted from WT *Pto* DC3000 (no CyaA effector) infected Col-0 *A. thaliana* for normalisation (n=2).

Co-IP Interaction Candidate	Protein Name	Known Function	SAINT score	Fold Change	BFDR	Spectral Counts
AT5G46110.4	ACCLIMATION OF PHOTOSYNTHESIS TO ENVIRONMENT 2	3-phosphoglycerate translocator which transports triose phosphates from Calvin cycle for sucrose synthesis	1	12	0	12
AT2G21660.1	CIRCADIAN RHYTHM, AND RNA BINDING 2	Regulates circadian oscillations and stress tolerance. Known target of HopU1.	1	19	0	19
AT4G39260.1	CIRCADIAN RHYTHM, AND RNA BINDING 1	Regulates circadian oscillations and stress tolerance. Known target of HopU1.	1	9.67	0	29
AT4G30690.1	SVR9-LIKE1	Translational initiation factor	0.99	12	0	12
AT5G03350.1	SA-INDUCED LEGUME LECTIN-LIKE PROTEIN 1	SA35-mediated effector-triggered immunity defence	0.99	10	0	10

The top 5 co-immunoprecipitation *Pto* DC3000 *A. thaliana* Col-0 interaction candidates for HopAA1-2-CyaA are shown in Table *5.8*.

Table 5.8. Top five target candidate proteins for HopAA1-2-CyaA identified via co-immunoprecipitation and mass spectrometry analysis. Raw values subtracted from WT *Pto* DC3000 (no CyaA effector) infected Col-0 *A. thaliana* for normalisation (n=2).

Co-IP Interaction Candidate	Protein Name	Known Function	SAINT score	Fold Change	BFDR	Spectral Counts
AT2G20190.1	CLIP-ASSOCIATED PROTEIN	Microtubule stability-associated protein	0.46	15	0.47	3
AT1G23170.2-DECOY	-	Pathogen-resistance via cell wall modification-association	0.46	15	0.47	3
AT4G30010.1	ATP-dependent RNA helicase	Genetic replication and regulation	0.32	10	0.49	2
AT2G27030.1	CALMODULIN 5	calcium-binding messenger protein	0.32	10	0.49	2
AT2G23670.1	HOMOLOG OF SYNECHOCYSTIS YCF37	Photosynthesis-association	0.32	10	0.49	2

The top 5 co-immunoprecipitation *Pto* DC3000 *A. thaliana* Col-0 interaction candidates for HopAF1-CyaA are shown in Table 5.9.

Table 5.9. Top five target candidate proteins for HopAF1-CyaA identified via co-immunoprecipitation and mass spectrometry analysis. Raw values subtracted from WT *Pto* DC3000 (no CyaA effector) infected Col-0 *A. thaliana* for normalisation (n=2).

Co-IP Interaction Candidate	Protein Name	Known Function	SAINT score	Fold Change	BFDR	Spectral Counts
AT1G73260.1	ARABIDOPSIS THALIANA KUNITZ TRYPSIN INHIBITOR 1	Modulates programmed cell death in plant-pathogen interactions	0.14	10	0.59	2
AT3G16300.1	CASP-LIKE PROTEIN 3A1	Possible stress-tolerance and development role	0.02	2	0.68	4

AT5G42980.1	THIOREDOXIN H-TYPE 3	Biological reaction regulation	0.01	2.33	0.75	5
AT4G27520.1	EARLY NODULIN-LIKE PROTEIN 2	Solute transporter	0	1	0.86	3
AT1G03680.1	THIOREDOXIN M-TYPE 1	Redox regulation	0	1.5	0.86	2

5.2.6.1. Comparison of Effector Protein Physical Attributes Indicates That Hydrophobicity May Be an Important Driver of Differential Translocation

Predicted physical characteristics of *Pto* DC3000 effector proteins were compared to identify any potential trends or patterns which may correlate with translocation behaviours of key effector proteins. This would provide a good starting point for onward research to explore these findings in more detail, and to link with possible causation. This data is shown in Figure 5.22. These data were drawn from the *Pseudomonas* genome database (Winsor et al., 2016).

Subtle trends are present among these effectors. Less negative hydrophobicity values for HopAM1 (-0.543), HopAA1-2 (-0.128) and HopAF1 (-0.346) are present compared to some non-compromised effectors such as HopH1 (-0.802). It could be the case that less negative hydrophobicity is playing a role in compromised translocation of HopAM1, HopAA1-2, and HopAF1 in *G176A hrcN*. Hydrophobicity may be impacting the way in which effectors are able to physically pass through HrcN when structurally altered. The effector proteins travel through the T3SS unfolded and so hydrophobicity may play an important role in this process .This hypothesis would require experimental work to confirm whereby regions of hydrophobicity could me mutated to see what effect this has on effector translocation in WT vs *G176A hrcN*. These data do not explain why there are *G176A hrcN* non-translocation-compromised effector proteins that do not follow the same trend in hydrophobicity This could suggest that while hydrophobicity may play a role with differential translocation of some effector proteins, this may not be universal across all effector proteins. Alternatively, hydrophobicity may play a partial role alongside other factors that were not considered in this analysis. Because of this uncertainty, strong conclusions cannot be drawn from these data alone. Despite this however, hydrophobicity could be a useful starting point for onward exploratory analyses for understanding HopAM1, HopAA1-2, and HopAF1 before expanding onto a wider effector set.
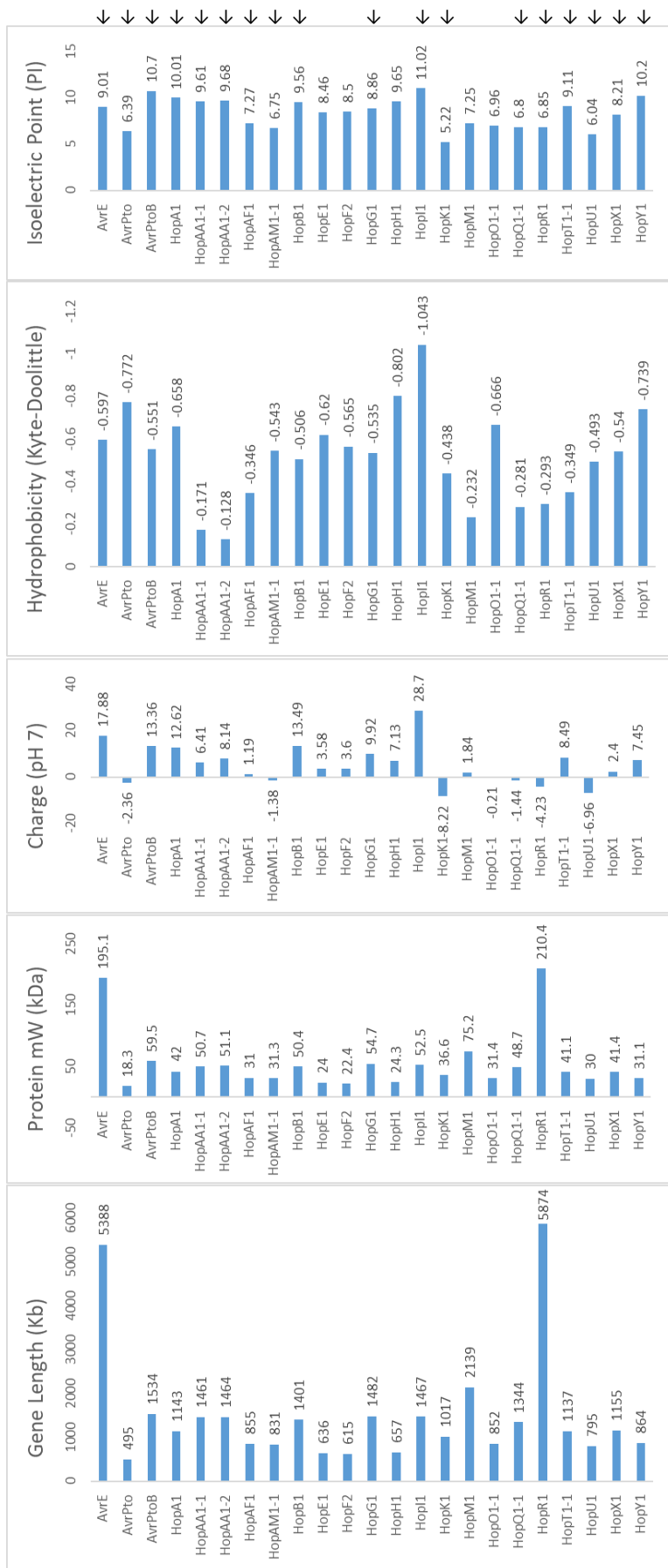
Figure 5.22. Comparison of physical attributes between *Pto* DC3000 effector proteins. Effector proteins which displayed compromised translocation in *G176A hrcN* have been indicated with an arrow symbol. Data drawn from the *Pseudomonas* genome database. (Winsor et al., 2016).

5.3. Discussion

5.3.1. General Overview

In this chapter, the translocation of effector proteins through the *P. syringae Pto* T3SS into *A. thaliana* plant tissue was explored in detail to better understand their potential role in disease establishment and to help explain why a *G176A hrcN* mutant gave rise to a near symptom-less infection despite a comparable bacterial load to WT. Based on results described in the previous chapter, it was hypothesised that effector translocation in the *G176A* mutant may be compromised or altered in some way. An additional component to this hypothesis was that if effector translocation was compromised, only a subset of effectors may be affected, as bacterial colonisation remained unaffected.

In this chapter, a quantitative CyaA-fusion-based cAMP reporter infection assay was used to measure the translocation rate of effector proteins into *A. thaliana* tissue under controlled conditions. Following successful construction and cloning of the effector-CyaA fusions, the reporter infection assay was optimised for *A. thaliana* and the *Pto* DC3000 mutants. No effector translocation was observed for Δ*hrcN* effector CyaA constructs in all cases confirming that cAMP could not increase without T3SS-dependent effector translocation. This confirmed the system to be functional and suitable for screening of effector proteins.

A large subset of effector proteins were then tested using this CyaA system. This large screen indicated that certain effector proteins may show compromised delivery. Effector proteins HopAA1-2, HopAM1, and HopAF1 had statistically significant reduced translocation rates in the *G176A* mutant compared to the WT. Effector HopH1 however showed no such altered effector translocation. From this experiment, it was concluded that *G176A* showed compromised effector translocation of some, but not all effector proteins.

To help further understand the possible link between these key translocation-compromised effector proteins and absence of disease severity in the *G176A hrcN* mutant, additional molecular analyses followed. Key effector proteins were both over-expressed and deleted in *P. syringae Pto* DC3000. It was found that over-expression of key effector proteins *hopAA1-2*, *hopAM1*, and *hopAF1* saw a partial return of visual disease phenotypes in the previously asymptomatic-like *G176A hrcN* mutant, indicating a compensatory effect may be present. No such return of WT-like disease severity was observed upon over-expression of the non-compromised *hopH1* effector. This suggests that these compromised HopAA1-2, HopAM1, and HopAF1 effector proteins are potentially implicated in the onset of disease phenotypes while HopH1 plays less of an obvious role. HopAA1-2 appears to be necessary for full establishment of disease phenotypes, unlike HopAM1, whose deletion mutant retained full WT-like visual disease symptoms. A double mutant containing both deletions phenocopied the single *hopAA1-2* deletion. These data suggest that HopAA1-2 may play an important role in the establishment of chlorosis and/or necrosis.

Next, a co-immunoprecipitation screen was conducted to pull-down potential *A. thaliana* interaction partners for the key effector proteins HopAA1-2, HopAM1, and HopAF1. These potential interaction partners may help to explain why the asymptomatic-like disease phenotype was observed for the *G176A hrcN* mutant, as they may be involved in the suppression of disease symptoms in some way. Going forward, these candidate proteins will be explored in more detail, firstly by verification to confirm any interactions present. This would be achieved by repetition of the Co-IP procedure with additional replicates and increased plant tissue samples to increase confidence, and to reduce the chance of any false-positives. Key plant targets would then be further tested to demonstrate binding and function both *in vivo* and *in vitro*.

CRISPR-based knock-outs or deletions of key plant genes encoding for interaction candidates could be generated and then tested to evaluate what impact this has on plant infection. It could be possible to alter the disease phenotype presented upon deletion of a set of these key interacting proteins, helping to explain their possible roles in disease establishment. Additionally, potential effector interaction partners from *A. thaliana* could be expressed and purified from a suitable expression system for structural and functional analysis. An example would be the use of SPR to show binding of a given purified effector protein to a purified *A. thaliana* plant cell target. Downstream biochemical assays could then be conducted to show what impact this binding interaction has on protein function.

Effector proteins contain a wide variety of sequences, structures, and other physical attributes. Potential clues as to why certain effector proteins displayed more compromised T3SS translocation with the *G176A hrcN* mutant than others compared to the WT were investigated by making comparisons between effector proteins. It is hypothesised that signal sequence and structural differences of the effector proteins may be playing a role in differential translocation. The signal sequences could be explored in more detail with experimental studies going forward. Mutagenesis of signal sequence residues could be carried out to see what effect this has on the translocation of key effector proteins i.e. HopAM1, HopAA1-2, and HopAF1 (with non-translocation-compromised effector proteins as negative controls). Point mutations could be introduced systematically at key regions of interest along the predicted signal sequence region to see what effect this has on *in vivo* T3E translocation. It may be possible to mimic a *G176A hrcN*-like translocation response in a WT *hrcN* background by introducing appropriate mutations to shift the signal sequence more closely towards the signal sequence of a *G176A hrcN* non-translocation-compromised effector protein such as HopH1. Additionally, larger structural changes of the overall effector protein structure could be explored with further mutagenesis work. It does not appear as though these three effectors share any notable conserved predicted domains of interest however this could be explored further to confirm this. From the predicted physical data of effector proteins, it could be possible that hydrophobicity plays an important role in proper effector translocation. As such, some of this mutagenesis work altering the effector structure could focus on altering hydrophobicity in key regions for compromised effectors. Introducing hydrophobicity patterns closer to those found in *G176A hrcN* non-compromised effectors may see some degree of translocation recovery should hydrophobicity be important.

5.3.2. Key *Pto* DC3000 Effector Proteins Implicated in This Research

Secretion of the HopAA1-2, HopAM1, and HopAF1 effector proteins was shown to be significantly compromised in the *G176A hrcN* mutant in comparison to the WT. There has been some limited previous research into these effector proteins, with all three linked to various aspects of plant immunity and disease resistance. However, compared to many other effector proteins in *Pto* DC3000 they remain comparatively understudied. As such, our understanding of their mechanistic function remains incomplete. This study has shown that full translocation of these particular effector proteins was not necessary for bacterial apoplastic colonisation, however full translocation of one or a combination of these effector proteins may be necessary for full chlorosis and necrotic leaf disease symptoms.

5.3.2.1. HopAA1-2

It has been demonstrated that HopAA1-2 interacts with EDS1 and PBS3 by way of a yeast 2-hybrid experiment, which was hypothesised to be linked to salicylic acid-mediated defence subversion (Palmer, 2018). Furthermore, reduced levels of EDS1 and PBS3 were seen when co-expressed with HopAA1-2 (Palmer, 2018). EDS1 or enhanced disease susceptibility 1 forms a heterodimer known to be recruited by toll-interleukin 1-receptor domain NLRs and is involved with transcriptional

mobilisation associated with resistance pathways (Bhandari et al., 2019). PBS3 has been shown to protect EDS1 from proteasome-mediated degradation (Chang et al., 2019). Deletion of a gene cluster containing *hopAA1-2* (along with *hopV1, hopAO1, and hopG1*) showed strongly reduced virulence of *Pto* DC3000 in *N. benthamiana* and *A. thaliana* plants (Wei et al., 2007).

HopAA1-2 remains a highly understudied effector protein with only a few investigative examples. Closely related effector protein HopAA1-1 may also provide an insight into the function of HopAA1-2, however investigative examples of this protein also prove limited. HopAA1-2 is not encoded on the conserved effector locus (CEL) in *P. syringae* unlike paralogue HopAA1-1, however the two proteins do share a high degree of sequence conservation (Munkvold et al., 2009). It was previously shown that HopAA1-1 appeared to show functional redundancy with CmaL chlorosis-promoting factor (PSPTO4723), although fewer necrotic speck lesions were observed with dip-inoculated tomato leaves with a *hopAA1-1* deletion when *cmaL* had also been deleted (Munkvold et al., 2009).

Deletion of *hopAA1-2* led to reduced visual disease severity in *Pto* infection of Col-0, while its over-expression led to a recovery of symptoms in the previously asymptomatic *G176A hrcN* mutant. This demonstrates that HopAA1-2 is important for visual disease establishment, similar to what was previously observed in closely related HopAA1-1 (Munkvold et al., 2009). The work with HopAA1-1 was performed in *S. lycopersicum* plants while the work with HopAA1-2 presented in this thesis was performed in *A. thaliana*. This difference in plant host may be why similar functional redundancy for HopAA1-2 was not observed in this chapter. CmaL may play a different role or may function less efficiently in *A. thaliana* plants due to different cellular architecture and complexity.

Novel interaction candidates for HopAA1-2 were identified in this chapter using co-immunoprecipitation experiments. The candidate proteins have a range of known functions relating to cellular function and disease resistance however none have been identified and linked with HopAA1-2 function previously. As such, these targets offer a selection of new effector targets to investigate with further experimental study. It is possible that HopAA1-2 can interact with multiple host proteins, as seen with many other effector proteins, leading to manipulation and alteration of several host processes. Previously identified EDS1 and PBS3 (Palmer, 2018) were not identified in this screen suggesting that this interaction may only occur under certain defence conditions. It could be possible that EDS1 and PBS3 interactions occur at an earlier or later stage of infection, and so were not pulled down in the screen presented in this thesis as they were not highly active in the plant at the time of sample collection. Additionally, variation in Co-IP protocols may favour a stronger pulldown of certain targets over others. As such, Co-IP experiments can be repeated and optimised using different buffers, incubation times, sample preparation approaches, and different tag and corresponding antibodies to identify the conditions which produce the most accurate results for HopAA1-2.

Identified in the Co-IP screen as the most likely interaction candidate of HopAA1-2 was AT2G20190.1 (CLIP-ASSOCIATED PROTEIN) which is known to be involved with microtubule stability. Many bacterial pathogen effector proteins are known to modulate host microtubule dynamics to aid successful colonisation, typically via GTPase altering effectors (Radhakrishnan and Splitter, 2012). It is not yet clear whether HopAA1-2 has a similar GTPase altering capacity however this would be a good starting point for onward experimental work. HopAA1-2 could be purified and tested *in vitro*, where its effect on purified GTPase proteins could be investigated by way of a GTPase assay. Additionally, microtubule dynamics can be investigated in the cell upon over-expression of *hopAA1-2*. This could be achieved by labelling host microtubules with fluorescent tags and then visualising the response using live fluorescent microscopy.

5.3.2.2.   HopAM1

HopAM1 has previously been shown to play an important role in the effector-triggered immune response in the form of quantifiable cell death (Iakovidis et al., 2016). In this study, *A. thaliana* genetic loci involved in HopAM1-mediated cell death were explored by way of genome-wide association mapping (Iakovidis et al., 2016). EDS1, HSP90.2, and SGT1B affected HopAM1-induced cell death alongside other additional loci (Iakovidis et al., 2016). Additionally, HopAM1 has been demonstrated to play a virulence enhancement role on water-stressed Ws-0 *Arabidopsis* plants, shown with increased hypersensitivity to abscisic acid (Goel et al., 2008). It was shown in another study that HopAM1 suppressed plant immunity, and shared high Toll/interleukin-1 receptor (TIR) domain homology to NB-LRR receptors, which can hydrolyse nicotinamide adenine dinucleotide (NAD$^+$) (Eastman et al., 2021).

In certain strains of *Pseudomonas syringae*, there is evidence that HopAM1 may have a predicted identical second copy (*hopAM1-2*) expressed on a plasmid (pDC3000A) in the form of a mobile genetic element (Landgraf et al., 2006). This may represent an earlier horizontal gene transfer event during the evolution of *P. syringae* (Landgraf et al., 2006). It has been suggested that this identical copy of HopAM1 (formerly called *avrPpiB2$_{Pto}$* in early publications) may provide a site for plasmid integration into the chromosome as seen with certain strains of *P. syringae* (Buell et al., 2003). In this chapter, it was shown that over-expression of *hopAM1* was able to recover disease severity for *G176A hrcN* although the mutant remained asymptomatic upon *hopAM1* deletion. This suggests that while HopAM1 is important for visual disease establishment, it is subject to functional redundancy. This could be by the predicted plasmid-borne HopAM1-2, or by other related proteins. This could be investigated by deleting *hopAM1-2* from *Pto* DC3000, or by generating the chromosomal *hopAM1* deletion in a pDC3000A-null strain, and to then observe what impact this has on the disease phenotype *in planta.*

Due to the recently identified TIR domain in HopAM1 (Eastman et al., 2021), RNA-binding is likely to be an important factor. It was shown that TIR oligomers use DNA and RNA substrates to synthesise noncanonical cyclic nucleotide monophosphate compounds which mediate cell death (Yu et al., 2021). Two RNA binding proteins were identified through Co-IP experiments presented in this chapter: AT2G21660.1 (CIRCADIAN RHYTHM, AND RNA BINDING 2) and AT4G39260.1 (CIRCADIAN RHYTHM, AND RNA BINDING 1). These are both known targets of effector HopU1 (Fu et al., 2007). It would be biologically relevant to test HopAM1 for RNA binding (e.g. using SPR or RNA electrophoretic mobility shift assay) to see whether HopAM1 could mediate cell death using a similar RNA binding mechanism via its TIR domain. Making mutations to this HopAM1 TIR domain could be conducted to see the impact this has on RNA binding and virulence. Both interaction candidates are known regulators of circadian rhythm, and proper regulation of the circadian rhythm is important for disease resistance (Sharma and Bhatt, 2015). Modulating circadian oscillations could leave plant hosts more susceptible to bacterial pathogens because this may lead to gating of defence gene expression, and thus a less effective immune defence response (Sharma and Bhatt, 2015).

While these two RNA binding interaction candidates show promise, the top interaction candidate in the Co-IP screen for HopAM1 was AT5G46110.4 (ACCLIMATION OF PHOTOSYNTHESIS TO ENVIRONMENT 2). This candidate protein is also of interest due to its involvement with photosynthesis and localisation in the chloroplast. Disrupting function of this protein may lead to altered chlorophyll-associated visual disease severity such as chlorosis. Many *P. syringae* phytotoxins and effectors are known to disrupt chloroplast structure and function leading to chlorosis (Lu and Yao, 2018). Deletion of AT5G46110.4 and subsequent infection of the mutant plant with *P. syringae* may be a good first step to verifying this interaction. Alteration of disease phenotypes may give an insight into the role of

this interaction. Functional redundancy may limit phenotypic responses and so multiple techniques should be used including *in vitro* purification and analysis of candidate proteins. As with many other T3SS effector proteins, HopAM1 may interact with several host proteins and so it may be the case that all these Co-IP identified top hits are true targets. Further experimental work is necessary to explore and confirm this.

5.3.2.3.   HopAF1

HopAF1 has been shown to suppress plant immunity by blocking ethylene induction through targeting of methionine recycling (Washington et al., 2016). HopAF1 showed an interaction with Arabidopsis methylthioadenosine nucleosidase (MTN1 and MTN2) via yeast 2-hybrid screens (Washington, 2013, Washington et al., 2016). MTN enzymes are known to be involved in the Yang cycle, a process essential for high levels of cellular ethylene in *A. thaliana* (Washington et al., 2016). It was also shown that HopAF1 suppressed production of reactive oxygen species associated with defence in *Pseudomonas savastonoi*, a plant pathogen closely related to *P. syringae* (Castañeda-Ojeda et al., 2017).

Methionine recycling proteins were previously shown to be targets of HopAF1 (Washington, 2013), however, these particular proteins were not pulled down in the HopAF1 Co-IP screen presented in this chapter. Like with HopAA1-2, MTN1 and MTN2 may have not been highly active at the stage of infection at the time of sample harvesting and as such HopAF1 interactions were low with these proteins. Methionine recycling is a process necessary for metabolic cellular signalling (Washington, 2013). Several of the top Co-IP interaction candidates for HopAF1 presented in this chapter were involved in some form of metabolic regulation. It could be that HopAF1 has a more general effect on manipulating metabolic processes in host cells, and that its interaction is more promiscuous than currently proposed. The most likely candidate identified in the screen was AT1G73260.1 (ARABIDOPSIS THALIANA KUNITZ TRYPSIN INHIBITOR 1) which is involved in modulating programmed cell-death (Arnaiz et al., 2018). The function of this protein has a logical link with the presentation of visual disease severity on *P. syringae* infected leaves and so would be a good candidate to explore further.

5.3.3.   Concluding Remarks

In this chapter, the role of effector proteins in disease establishment was explored. It was demonstrated that asymptomatic *Pto* DC3000 carrying a *G176A hrcN* mutant allele had compromised T3SS effector protein translocation of some, but not all effector proteins. HopAA1-2, HopAM1, and HopAF1 were shown to be significantly compromised, and it was demonstrated that these effectors are important for the full establishment of visual disease severity *in planta*. *A. thaliana* interaction candidates were identified for each of these key effector proteins and provide a good starting point for further research. Overall, it is likely that compromised translocation of these T3SS effector proteins is responsible for the asymptomatic phenotype observed with *Pto* DC3000 carrying a *G176A hrcN* mutant allele. The research presented in this chapter, combined with findings from earlier chapters, highlights the importance of HrcN in mediating efficient T3SS effector translocation and highlights how CdG-dependent oligomerisation of HrcN may be an underlying driver of this process.

Chapter 6: General Discussion

6.1. Summary of Findings

The main aim of this study was to investigate the function of the HrcN ATPase during the type III-mediated bacterial infection process of *Pseudomonas syringae Pto* DC3000, and to elucidate the role of cyclic-di-GMP in regulating this protein. It was found that HrcN binds CdG, and that this process facilitates dodecamerisation of the full ATPase complex. Impeding this multimerization process may impact efficient translocation of effector proteins. It was shown that faithful translocation of key effector proteins is necessary to establish full disease symptoms in plants. Partial or compromised translocation of a subset of effector proteins can allow for bacterial colonisation of plant hosts, however with significantly reduced disease phenotypes. The effectors HopAA1-2, HopAM1, and HopAF1 were identified as key components in the establishment of proper chlorosis and necrosis leaf disease phenotypes.

6.1.1. Visual Representation

Based on the findings presented in this thesis, a representative model has been illustrated in Figure 6.1 showing the differential effector translocation observed between WT *Pto* DC3000 and those carrying a *G176A hrcN* mutant allele. This model serves as a starting point for onward research and for the formation of future testable hypotheses.
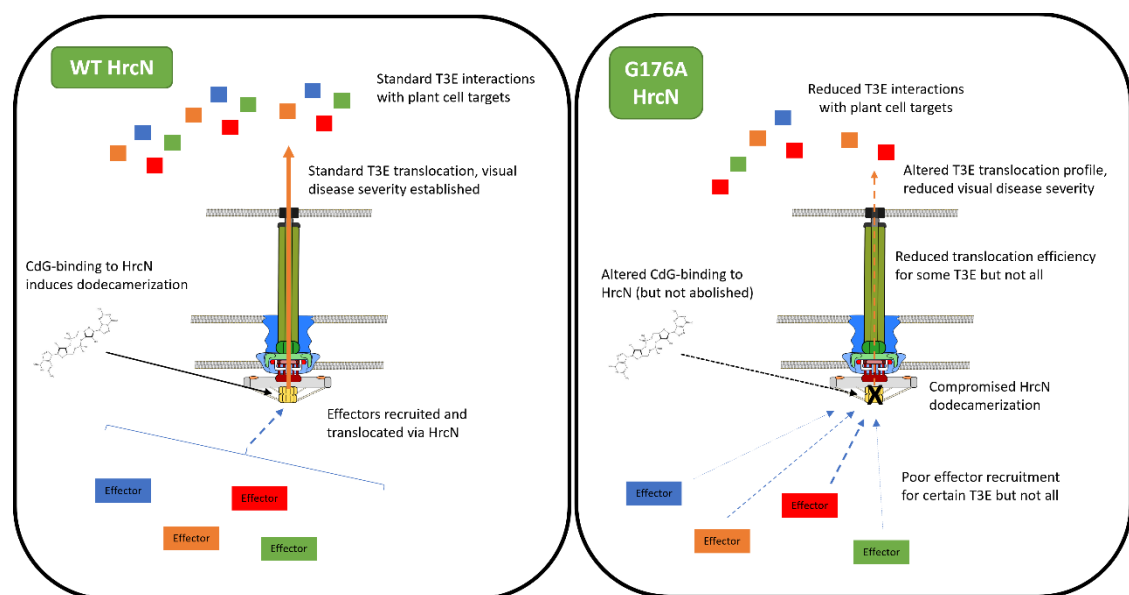
Figure 6.1. A cartoon illustration showing differential type III effector translocation in *WT hrcN* compared to *G176A hrcN*. This model is based on data collected in this thesis. HrcN is shown in yellow.

6.2. Context and Perspective

6.2.1. CdG binding to HrcN

It was shown by way of fluorescent DRaCALA that CdG does bind specifically to purified HrcN as predicted. Interestingly, the G176A point-mutation, which was a key mutant in this study, was able to retain its binding to CdG however the downstream oligomerisation appeared to be altered.

Purified HrcN was highly unstable and would degrade and precipitate rapidly. In the case of some point-mutants, purification was highly challenging due to limited recovery of soluble protein.

Consequently, much of the *in vitro* protein work was limited by the difficult nature of the enzyme. Many experimental assays produced unreliable and non-robust data from which meaningful conclusions could not be drawn. A similar such T3SS-associated ATPase; Spa47 of *Shigella flexneri* (Gao et al., 2018) along with the T3SS-associated PcrG cytoplasmic regulator in *Pseudomonas aeruginosa* (Lee et al., 2014) are two examples of other T3SS-associated proteins that were found to readily precipitate upon attempted purification. This suggests that protein instability may be a frequently encountered problem with such systems, potentially due to the complex and dynamic nature of the T3SS, with each protein having multiple interaction partners and a complex quaternary structure.

Going forward, a useful area of focus would be optimisation of HrcN stability upon purification. Expression using different systems (e.g. yeast or insect cells), usage of optimised cell lines, different purification methods and tags, along with buffer optimisation are all areas that could be further explored to help improve the stability of HrcN. Additionally, purification as part of a larger T3SS complex may also be a sensible approach whereby neighbouring proteins may help to stabilise HrcN.

A more stable HrcN protein would allow for further biochemical and biophysical analyses, particularly with techniques that require extended assay times or require temperature variation. Examples of techniques that would benefit from a more stable protein would be ITC/SPR for additional CdG binding characterisation and structural analysis by crystallography or cryo-EM. Should *in vitro* HrcN stability fail to improve, the research direction could shift to *in vivo* analysis of HrcN using high-resolution live microscopy and fluorescent labelling where possible. Additionally, confirmation of correct protein folding following purification of a more stable HrcN can be explored with circular dichroism or a related technique. This would verify that the secondary structure of HrcN was as expected prior to any assay work to help increase experimental robustness.

There are several examples showing CdG playing an important role in the control of virulence in the published literature. In most cases, CdG acts as a transcriptional regulator by limiting gene expression of key virulence genes, usually by binding to an intermediate protein. A good example of this is with the transcriptional regulator FleQ (a AAA+ ATPase enhancer-binding protein), which controls expression of flagella genes in response to CdG binding (Baraquet and Harwood, 2013). CdG binds directly to FleQ, which suppresses its activity, with enhanced inhibition in the presence of FleN causing down-regulation of flagella gene expression (Baraquet and Harwood, 2013). CdG binding to HrcN appears to be one of the few known examples of CdG exerting virulence control in a post-translational manner by impacting the translocation of effector proteins. This lays the foundation for research to follow looking for related examples of post-translational CdG-dependent control within bacteria.

CdG is implicated in the control of virulence in other secretion systems, suggesting that post-translational regulation by CdG may be prevalent across pathogens more generally. As a relatively recent example of this, CdG plays a role in the inactivation of type VI secretion system (T6SS) and type IV secretion system (T4SS) activity in *Agrobacterium tumefaciens* (McCarthy et al., 2019). Levels of CdG were varied in the cell with over-expression of diguanylate cyclase SadC (elevated CdG), or SadC deletion (lower levels of CdG) (McCarthy et al., 2019). It was shown that high levels of CdG led to reduced T6SS and T4SS activity affecting plant colonisation and plant cell transformation respectively (McCarthy et al., 2019). The molecular mechanism, however, was not elucidated and so it is not clear whether this control of T6SS and T4SS was achieved through a similar direct CdG binding mechanism (as with HrcN) or via a different mechanism. Another example showed CdG binding to ATPases associated with the type II secretion system (T2SS) in *Vibrio cholerae* including MshE, along with other T2SS and type IV pili homologue ATPases (Roelofs et al., 2015). It was shown than CdG binds to the N-terminal of MshE, and that this binding was required for mannose sensitive hemagglutinin function and biofilm formation (Roelofs et al., 2015). Future research could explore the link with CdG and other

secretion systems in similar bacterial pathogens by searching for potential CdG-binding proteins present in secretion system complexes. A CdG capture compound screen followed by protein purification and CdG-binding analysis, similar to previously conducted work could follow for key identified candidate proteins (Trampari et al., 2015).

6.2.2. The Potential Role of Oligomerisation

Through *in vitro* work presented in this thesis, it was shown that oligomerisation may be compromised in the case of G176A HrcN. Previous work showed that T3SS export ATPase oligomerisation is important for efficient translocation of type III effector proteins. A key example illustrating this is the Spa47 T3SS ATPase of *S. flexneri*, where compromised oligomerisation led to a reduction in effector-dependent cellular invasion suggesting reduced effector translocation rates comparable to those seen with HrcN (Burgess et al., 2016b).

The underlying mechanism behind this loss of effector translocation is currently unclear. However, it is feasible that effector protein recruitment and proton motive force may be implicated in some way. While out of scope for this thesis, this underlying molecular mechanism would be an interesting area for future research. It may be the case that accessory proteins and chaperones are more heavily impacted and that the effect of altering HrcN dodecamerisation ability or efficiency is an indirect one on T3E translocation.

A possible route of further experimentation would be to introduce additional HrcN mutants that target oligomerisation in both a CdG-dependant and a CdG-independent way. This could include further point-mutagenesis of the CdG binding site, as well as other structural components away from the binding site important for multimerization (such as the N-terminal multimerization domain or key interface regions). If a range of mutants were produced with different oligomerisation efficiencies or abilities, these could then be tested to evaluate the impact on effector translocation and to confirm the importance of this process on type III function. The translocation of individual effectors could be investigated with these HrcN mutants building upon effector work presented in this thesis. This would help better shape our understanding of effector translocation at a biophysical level, and it would help to identify precisely how CdG controls oligomerisation.

6.2.3. The Effect on Virulence

Mutating certain residues of the predicted HrcN:CdG binding site led to altered visual disease phenotypes in both model *A. thaliana* and native host *S. lycopersicum* plant species compared to the WT HrcN. It was found that this was due to altered effector translocation profiles in key *Pto* DC3000 strains (carrying mutant *hrcN* alleles), whereby secretion of some T3Es were significantly compromised while others were relatively unaffected. Furthermore, the altered symptoms presented by key mutants in both model and native host were different from each other. It was thought that this difference between key mutants across species may be due to different cellular architecture and immunity present in each plant host.

This difference in disease response between plant hosts could be explored further to better understand plant immunity and intracellular targets at a molecular level. Using key *Pto* DC3000 strains (carrying mutant *hrcN* alleles) and knowledge of their T3E translocation profiles, certain groups of effectors could be explored to identify their importance and function in bacterial pathogenesis across these two plant species, and to identify key differences. This will help to build our understanding of the immune systems and response to infection of both *Arabidopsis* and tomato plants. Additional plant species could also be infected and the disease response between different *Pto* DC3000 allelic-

hrcN mutants examined to compare similarities or differences in ETI based on effector translocation profiles.

Infected Col-0 displaying an asymptomatic-like phenotype despite a consistent bacterial load for *G176A* and *G311A hrcN* is rarely seen in the published literature (Klement et al., 1997). The same response was not seen in tomato, where some evidence of visual disease symptoms remained along with a consistent bacterial load. In Col-0, this asymptomatic-like phenotype could be recovered to WT levels upon over-expression of key effector proteins. This suggests that this disease response was caused by compromised translocation of a subset of effectors, which could be overcome or compensated for by increasing effector abundance. If HrcN showed poorer recruitment or translocation efficiency of a given effector upon mutation, increasing the overall abundance of that compromised effector around HrcN will increase the chances of successful translocation. A compromised effector recruitment process will be circumvented due to increased abundance driving the equilibrium towards translocation. The same can be said for a compromised translocation efficiency where slower translocation will be overcome by the fact that more effector is translocated overall, compensating for the deficiency.

It may be the case that there is a threshold of effector translocation needed for bacterial colonisation and for visual disease establishment, which are distinct from one another. In the case of *G176A* (and to a lesser extent *G311A hrcN*) it was shown that compromised effector translocation was significantly reduced but was not completely abolished to Δ*hrcN* negative control levels for any effector. This reduced level of key effector translocation could have been enough to reach the threshold necessary for bacterial colonisation, however not enough for full visual disease severity. This concept of effector translocation thresholds could be explored in more detail by creating and testing other effector translocation mutants that have varying profiles of T3E translocation. The *G176A* and *G311A hrcN* mutants could also be modified through further mutagenesis to see if some recovery of effector translocation or complete abolition of translocation could be possible.

6.2.4.   The Molecular Mechanisms of Effector Translocation

The translocation of effector proteins was believed to have been compromised in some way in the asymptomatic *hrcN* mutants. This was explored using individual effector reporter assays and molecular manipulation of key effector genes. The translocation of certain effector proteins was compromised with certain predicted CdG binding site mutants (notably with *G176A HrcN*). Not all effector proteins showed compromised translocation rates, however, with some showing relatively unaffected translocation despite the *G176A hrcN* mutation. HopAA1-2, HopAM1, and HopAF1 displayed significantly compromised translocation with *G176A hrcN* while most others, such as HopH1 did not.

This suggests is that there may be key differences between effector proteins or between sub-groups of effector proteins that underlie these differing translocation rates. Any patterns or trends could be used to infer T3E mechanistic function and to learn more about the biophysical interaction between effector protein and T3SS apparatus. The complete process of effector protein recruitment and unfolded peptide movement through the type III pilus still has several uncertainties. It is not clear exactly how effectors are recruited and whether each effector is recruited in a different manner. It is known that the N-terminal signal sequence domain of T3Es is important for effector recruitment, and that the T3SS ATPase plays an important role in this recruitment process (Buttner, 2012). However, it is not clear how important a role chaperones and accessory proteins play, although it is likely that they are implicated in some way. There are some examples that implicate a chaperone binding site

downstream of the N-terminal signal sequence, which is presumed to help increase effector recognition to the T3SS (Buttner, 2012).

The order of effector translocation, or an effector hierarchy may explain differential effector translocation. It is not clear whether there exist discrete stages of effector translocation (i.e. early, middle and late) or whether all effectors are translocated consistently throughout infection in the T3SS of *P. syringae*. There is evidence of a hierarchal translocation profile in other systems (such as in *Salmonella typhimurium*), however, no such evidence has so far been collected for *P. syringae* (Winnen et al., 2008, Bergeron et al., 2016, Deane et al., 2010). The CyaA reporter system, along with the generated *Pto* DC3000 mutants (carrying mutant *hrcN* alleles) could be used to explore this unanswered area in more detail to gain a clearer insight into effector timing.

It has been shown that an FlhB protein acts as an export gate in association with other members of the T3SS export apparatus, including the export ATPase (Kuhlen et al., 2020). It could be that the *G176A hrcN* affects proper functioning of this T3SS gating mechanism, and this is limiting the flow of effector proteins through the system. The concept of a gating mechanism is still a relatively new hypothesis. However, this would be an interesting avenue for future research to help explain the compromised translocation of effector proteins with this mutant. Additionally, mutant *hrcN* can be used to probe this potential gating mechanism by investigating the flow of effectors in response to an altered gating response. This will require additional knowledge of this gating process in *P. syringae* in order to better understand the proteins involved. If HrcN is found to be a key component of this gating mechanism, this unlocks a promising new route for understanding control of type III-mediated virulence and for the design of control compounds to artificially regulate this gating process.

6.2.5. T3SS Effector Protein Targets and Mechanisms in Host Plant Cells

Host cell proteins in *A. thaliana* Col-0 were identified to be T3E interaction candidates for HopAA1-2, HopAM1, and HopAF1 from co-immunoprecipitation experiments. A variety of targets were identified and serve as good starting points for future research. These targets may be directly or indirectly involved with the formation of chlorosis and necrosis disease symptoms. By better understanding the molecular targets of T3E-mediated infection, and effector relation to disease symptom establishment, this ultimately gives us a clearer picture into bacterial disease progression *in planta* and of plant defence. This can inform future plant and microbial research at both basic and applied levels.

Immunocompromised *A. thaliana* (fec and bbc) infiltrations showed disease severity returning for previously asymptomatic *Pto* DC3000 allelic-*hrcN* mutants (*G176A* and *G311A*). These experiments suggest that the immune system is implicated in some way with the formation of disease severity in relation to these effector proteins and their targets. It is well known that many *Pto* DC3000 effector proteins can suppress plant immunity (Guo et al., 2009).

It could be that key T3E targets directly or indirectly interact with the immune system. In the case of asymptomatic *G176A hrcN*, these key effector targets likely have relatively undisturbed function due to poorly translocated key T3Es which would otherwise normally interact with a given effector in uncompromised WT *hrcN* infections. This allows the immune system to supress a disease response as immune defence is not compromised or altered by T3E-mediated target manipulation. In the immunocompromised plant lines, this immuno-dependent suppression of disease establishment cannot occur. This would therefore lead to symptoms returning as a functioning immune defence response would be absent.

It is unlikely that the effector proteins are directly triggering chlorosis and necrosis without immune system involvement. Otherwise, the return of disease severity in immunocompromised plant infections would likely have not occurred. It is more likely that interaction with effector targets leads to altered downstream effects in the cell, and this indirectly leads to the formation of chlorosis and necrosis.

HopAA1-2 may play an important role in the formation of visual disease symptoms, with a Δ*hopAA1-2* deletion giving rise to significantly reduced visual disease severity on the leaf surface. It is unusual to see such a clear phenotypic change in response to a single effector deletion. This is because type III effectors are known to have a high degree of functional redundancy and co-interaction; therefore, deletion of one effector is often masked by other effectors with functional overlap. This suggests that HopAA1-2 may work relatively independently from other effectors by interacting with unique plant cell targets not affected by other T3Es. The function of HopAA1-2 could be explored *in planta* by using an effector-free background T3SS strain to examine the effect of this T3E in isolation. A *P. fluorescens* strain with a T3SS lacking effector proteins (a Pf0-1 EtHAn strain: effector-to-host-analyser) exists that can be used to express and translocate HopAA1-2 in isolation, the infected plant tissue could then be investigated in more detail to assess the impact of this effector (Upadhyaya et al., 2014). While this system was originally designed for wheat effectors, it has recently been successfully adapted for *P. syringae* T3Es and so would be a useful tool for exploring the function of HopAA1-2 *in vivo* (Ding et al., 2021).

6.3. Impact and Implications

6.3.1. A Deeper Understanding of the Importance of CdG-dependent Virulence Control and the Bigger Picture

Research presented in this thesis helps to advance our understanding of type III-mediated virulence control by CdG binding to translocation apparatus and lays foundations for future research to build upon. CdG is known to be implicated in various aspects of microbial function across a variety of systems, however a connection with type III-mediated virulence in *P. syringae* has previously been limited. This research project confirms a binding interaction with CdG via the T3SS ATPase HrcN, and this was shown to have implications for effector translocation, potentially through control of ATPase oligomerisation. This helps to advance our understanding of dinucleotide post-translational regulation in *Pseudomonas* bacteria in relation to the T3SS and provides further insight into the role of effector proteins in establishing plant disease.

Addressing key challenges and questions faced in plant health is an important area of focus that has positive implications for food security and sustainable agriculture. By furthering our understanding of plant pathogens such as *P. syringae* with a focus on the molecular complexities, we can use this knowledge as a solid foundation for future translational science and engineering solutions to address current and future agricultural problems. Additionally, the new findings from this plant pathogen may help inform further basic science research endeavours going forward in other bacterial species, and so serves as an important starting point for future projects addressing other biological systems including human pathogens.

6.3.2. Translational Applied Science

The fundamental knowledge gained from this study can be applied to future translational research approaches relating to the type III secretion system. By understanding that CdG does indeed bind to HrcN (and presumably to other closely related T3SS ATPases), and this appears to control virulence by

way of altered effector translocation, this allows future research to manipulate and exploit this regulatory interaction.

Knowledge of HrcN and the CdG binding interaction can be used for the guided engineering of novel antibiotic pharmaceutical reagents to block T3SS-dependent virulence. Chemical compounds can be synthesised that target the key identified residues in the HrcN/ATPase CdG-binding site or associated residues around the binding site to block or enhance CdG binding. Additionally, the T3SS can be used for synthetic biology and biotechnology applications. One such possibility would be to create a controllable secretion system that can translocate chosen substrates, the translocation rates of which could be altered by manipulating CdG levels. This would be a useful tool for biological research and could serve as a useful intracellular delivery mechanism for substrates of interest *in vivo*.

Overall, the T3SS lends itself well to a variety of translational applied projects with downstream societal and commercial benefit. By building upon our knowledge of the fundamentals of type III function, we can inform applied research efforts going forward.

6.4. Future Work

6.4.1. X-ray Crystallography and Cryo-EM Structural Studies Showing CdG Bound to HrcN

This work has advanced our understanding of the CdG:HrcN binding interaction and its role on controlling virulence. We have gained a better appreciation for the complex molecular control systems and inner workings of the type III secretion system as well as a greater understanding of the importance of CdG-dependent regulation within *Pseudomonas* bacteria. Despite this, there are still areas where further research would be beneficial.

As part of this project, preliminary attempts at structural studies via crystallography were performed. Due to poor protein stability and the lack of crystal formation, X-ray crystallography was not completed. Should this work continue, further stability optimisation and extensive crystal trials would need to be undertaken, with the ultimate goal to visualise the HrcN crystal structure showing the CdG binding site bound to a CdG molecule. This structure could be generated alongside mutant HrcN protein structures that display CdG binding variation. Based on current evidence however, HrcN structural work may be better suited to Cryo-EM. This structural technology would allow for an accurate structural prediction with high resolution. As part of the cryofixation process, a flash freezing step in necessary. This may better suit the HrcN protein as it is subject to rapid degradation and aggregation over time. Another advantage of Cryo-EM over X-ray crystallography is that it would allow for the structural visualisation of various oligomeric states with careful experimental planning. This would greatly increase our understanding of the role of CdG in oligomerisation.

There has been previous structural work on other CdG binding ATPase proteins, however this area of study remains limited. A good relevant example of successful structure prediction using X-ray crystallography is of CdG bound to the MshEN binding domain of type IV associated ATPases in *Vibrio cholerae* (Wang et al., 2016). The type IV pilus and its associated ATPase proteins often share many molecular similarities and sequence conservation to the type III secretion system and its ATPases. This suggests that experimental conditions used in this study may be more favourable for HrcN crystallisation once protein stability has been improved.

Another example would be with an N-terminal truncated version of the FliI ATPase of the bacterial flagella of *P. fluorescens* (Trampari, 2016). Truncated FliI was crystallised however CdG could not be localised in the structure due to improper oligomeric conditions (Trampari, 2016). Optimising HrcN for

proper oligomerisation by building upon similar conditions used for FliI may be a good starting point for visualising HrcN bound to CdG.

Furthermore, cryo-EM structural prediction of a type III secretion system ATPase was work performed on the EscN-EscO T3SS ATPase and stalk complex of *Escherichia coli* (Majewski et al., 2019). A 3.3 Å resolution cryo-EM structure was generated, which while not identical to HrcN from *P. syringae*, does lay an experimental groundwork for what is potentially possible. Binding of CdG was not explored in this study. Visualisation of small nucleotide molecules has been shown to be difficult with cryo-EM. Despite this however, one study was able to visualise a similar molecule, cyclic GMP–AMP, in the binding pocket of an endoplasmic-reticulum membrane protein called STING via cryo-EM (Shang et al., 2019).

6.4.2. Mechanism Conservation Among Other Bacterial Species

The T3SS-associated ATPase is notable for its high sequence conservation with a wide variety of other bacterial species. Some published examples of ATPase homologues include Spa47 from *Shigella flexneri*, InvC from *Salmonella gallinarum*, EscN from *Escherichia coli*, SsaN and FliI from *Salmonella typhimurium,* as well as the F1β ATP synthase subunit of *Bos taurus* (Burgess et al., 2016a). It has previously been shown that CdG binding to secretion system and pili-associated ATPases is common across a variety of bacterial species, however, whether the downstream mechanistic responses and impact over function and virulence varies significantly between organisms remains unclear (Trampari et al., 2015, Trampari, 2016, Roelofs et al., 2015). Exploration into the universality of the molecular mechanisms of CdG-dependent ATPase control across different bacterial species would initiate an interesting discussion regarding the evolution of such systems and may give us further insight into the importance of such forms of regulation.

6.4.2.1. *Pseudomonas aeruginosa* (PA01)

Further work may examine conserved homologous T3SS-associated ATPases found in other species of bacteria. My project included some early preliminary work on the opportunistic human pathogen *Pseudomonas aeruginosa* and its T3SS-associated ATPase PscN. Going forward, this strain or a similar organism could be a good starting point for future research. Protein purifications from my early *pscN* constructs could be optimised, and *in vivo* techniques adopted for *Pto* DC3000 (carrying mutant *hrcN* alleles) work could be adapted for *pscN* PA01 to compare type III secretion control between a plant pathogen and a human pathogen. The gene cluster containing *pscN* in *P. aeruginosa* PA01 is shown in Figure 6.2

psc/pcr/pop/exs Gene Cluster
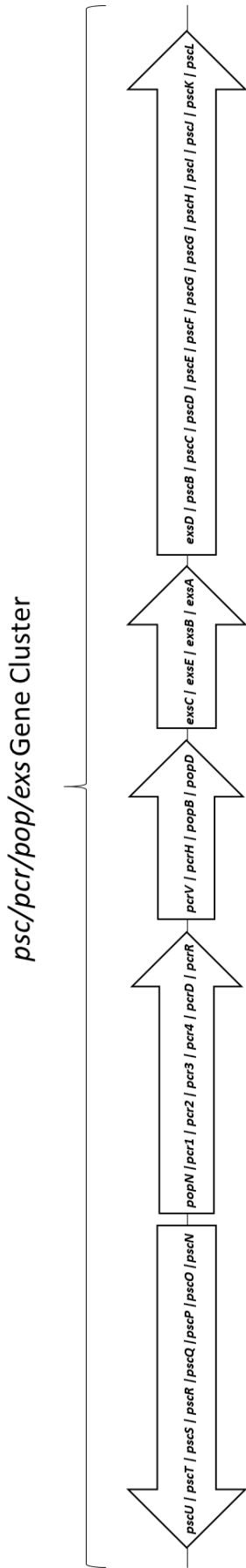
Figure 6.2. Graphical representation depicting the *psc/pop/exs* gene cluster from *Pseudomonas aeruginosa* (Naito et al., 2017).

CdG may play a role in the control of type III and type VI secretion in *Pseudomonas aeruginosa* as shown by wax moth *Galleria mellonella* pathogenicity assays (McCarthy et al., 2017). Additionally, an *ex vivo* pig lung model has been developed, which has been used to study pathogenicity of *Pseudomonas aeruginosa* with a focus on biofilm formation (Harrison et al., 2014, Harrington et al., 2020). Together, these pathogenicity assays could be used to screen for disease phenotypes in *Pseudomonas aeruginosa* with relevant mutations in the predicted CdG binding site of PscN, based on homology modelling comparing HrcN (*P. syringae*) and FliI (*P. fluorescens*). From here, investigative work on effector translocation and PscN *in vitro function* could follow, comparable to the work in this study with HrcN. The effectors in PA01 are considerably different than in *Pto*, however, the underlying T3SS translocation mechanism may share high levels of similarity. The main effector proteins in PA01 are illustrated in Figure 6.3.
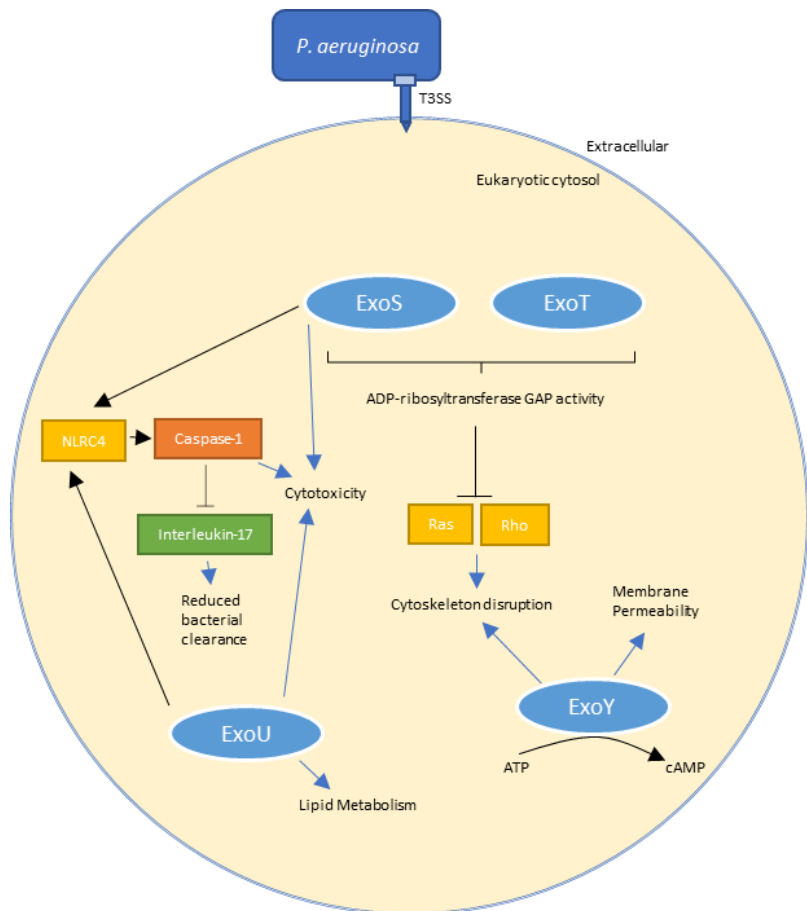
Figure 6.3. Type III effectors of *P. aeruginosa*. Effectors are displayed as blue ovals (adapted from Sawa, 2014, Anantharajah et al., 2016).

6.4.3. Identification and Characterisation of *Pto* DC3000 Key Effector Targets in Plant Hosts

In this study, co-immunoprecipitation was used to identify potential candidate intracellular targets in the *Arabidopsis thaliana* Col-0 model host against key effector proteins involved in chlorosis and necrosis phenotype formation. Three effectors were identified: HopAA1-2, HopAM1, and HopAF1. Going forward, these potential candidate targets should be further investigated to confirm the results of the Co-IP screen. Genetic deletions in key plant target genes could be produced allowing for *in*

planta infection phenotyping with *Pto* DC3000. If key target genes are deleted, and key effectors now lack their intracellular plant target proteins, then altered disease phenotypes may be observed.

Additionally, alternative techniques could be explored to verify observations from the Co-IP screen. Two hybrid screening could be used to confirm interaction between effector proteins and plant intracellular targets. This could then be further verified and analysed by purifying key plant proteins and testing binding kinetics with techniques such as SPR and ITC. RNA-Seq could be used to show expression levels of relevant mRNA transcripts associated with potential targets in the plant cell. If any of the effectors are involved in plant-based mRNA degradation of protein targets, this would enable their detection.

Effector interaction candidates in the plant host can be explored by way of genetic manipulation. CRISPR/Cas9 or a similarly related technique could be used to genetically edit *A. thaliana* and *S. lycopersicum* to knock-out key genes identified in the Co-IP screen, enabling subsequent confirmatory work. Infection with *Pto* on these mutant plant lines may give rise to altered phenotypes. An asymptomatic-like disease phenotype following knock-outs of one or more key plant genes associated with the effector proteins of focus would help to confirm a given target's importance in the establishment of disease severity. Follow-on work could then explore the function of a confirmed target *in vitro* through protein expression, purification, and biochemistry, if the target gene is not already well-understood. Additionally, mutant plant lines may confer, or suggest increased disease resistance traits against *Pto* and other plant pathogens with knock-outs of these plant targets. These may have commercial or societal benefits and may be useful mutant lines for future plant engineering efforts.

6.4.4.   Preliminary Screening of Novel Synthetic CdG:HrcN Control Agents

The findings from this work could lend themselves well to a variety of applied translational research projects. One such project would be to begin screening small molecule libraries to determine if the binding interaction between CdG and HrcN can be blocked or enhanced. This work would use many of the proteins and constructs generated for this project and would lay the foundations for development of a novel potential T3SS control agent. With *P. syringae* being a prominent global plant pathogen, the development of new effective control methods for this pathogen has potential positive implications regarding plant health.

The implications for medical microbiology are potentially even greater. Given that the CdG-binding site of T3SS ATPases is likely to be a universal feature (Trampari et al., 2015), such control compounds could show effectiveness against other bacterial pathogens. This could include other species of *Pseudomonas* such as human pathogen *P. aeruginosa*, along with other T3SS-possesing genera such as *Salmonella*, *Vibrio*, and *Yersinia*. *In vivo* virulence and infection assays can be used to show efficacy of any new control agents across such bacterial species and to evaluate any resistance which may arise. It may be the case that any T3SS ATPase-targeting novel anti-infective compounds may lead to lower levels of antimicrobial resistance forming as it will not directly kill or inhibit bacterial growth, but instead will directly target the virulence system. The direct targeting of virulence systems for future therapeutic discovery against bacterial infections is an emerging strategy that is showing promise (Fleitas Martínez et al., 2019, Heras et al., 2015).

Synthesis of T3SS control agents is not without precedent, with several other T3SS inhibitor molecule discovery studies having already been carried out. Examples include Salicylidene acyl hydrazides blocking T3SS effector proteins in *Yersinia pseudotuberculosis* (Pettersson et al., 1996) and N-hydroxybenzotriazoles inhibiting T3SS LcrF and ExsA transcription factors in pseudotuberculosis

(Gardiner and Procter, 2001). In both cases, molecules were screened for, and then tested via T3SS-activity assays to show efficacy in blocking type III function. Despite these promising examples, specific inhibitory molecules targeting the T3SS via HrcN in *Pseudomonas syringae* remains limited. One of the closest related studies is with the YscN ATPase in *Yersinia pestis* in which screened small-molecules were shown to be able to block YopE effector secretion and showed reduced cellular cytotoxicity (Swietnicki et al., 2011).

6.5. Final Concluding Remarks

In this thesis, CdG-dependent control of T3SS effectors in *Pseudomonas syringae Pto* DC3000 mediated via HrcN was explored. Experimental work explored a link between CdG and HrcN function, and that this function may be important for the integrity of effector translocation. Further investigation revealed that CdG may exert a degree of control over HrcN quaternary structure. The structure of HrcN was shown to be potentially important for proper T3SS effector translocation into plant cells, and necessary for full establishment of visual disease symptoms. This is the first known example of dinucleotide-based T3SS post-translational control of effector protein translocation through direct T3SS-binding.

Chapter 7: References

ABE, A., MATSUZAWA, T. & KUWAE, A. 2005. Type-III effectors: Sophisticated bacterial virulence factors. *Comptes Rendus Biologies,* 328**,** 413-428.

ABRAHAMS, J. P., LESLIE, A. G., LUTTER, R. & WALKER, J. E. 1994. Structure at 2.8 A resolution of F1-ATPase from bovine heart mitochondria. *Nature,* 370**,** 621-8.

ADACHI, H., KAMOUN, S. & MAQBOOL, A. 2019. A resistosome-activated 'death switch'. *Nature Plants,* 5**,** 457-458.

AKEDA, Y. & GALAN, J. E. 2005. Chaperone release and unfolding of substrates in type III secretion. *Nature,* 437**,** 911-915.

ALBERT, M. & FÜRST, U. 2017. Quantitative Detection of Oxidative Burst upon Activation of Plant Receptor Kinases. *In:* AALEN, R. B. (ed.) *Plant Receptor Kinases: Methods and Protocols.* New York, NY: Springer New York.

ALFANO, J. R., CHARKOWSKI, A. O., DENG, W.-L., BADEL, J. L., PETNICKI-OCWIEJA, T., VAN DIJK, K. & COLLMER, A. 2000. The *Pseudomonas syringae* Hrp pathogenicity island has a tripartite mosaic structure composed of a cluster of type III secretion genes bounded by exchangeable effector and conserved effector loci that contribute to parasitic fitness and pathogenicity in plants. *Proceedings of the National Academy of Sciences of the United States of America,* 97**,** 4856-4861.

ALFANO, J. R. & COLLMER, A. 1997. The type III (Hrp) secretion pathway of plant pathogenic bacteria: trafficking harpins, Avr proteins, and death. *Journal of Bacteriology,* 179**,** 5655-5662.

ALFANO, J. R. & COLLMER, A. 2004. Type III Secretion System Effector Proteins: Double Agents in Bacterial Disease and Plant Defense. *Annual Review of Phytopathology,* 42**,** 385-414.

ANANTHARAJAH, A., MINGEOT-LECLERCQ, M.-P. & VAN BAMBEKE, F. 2016. Targeting the Type Three Secretion System in *Pseudomonas aeruginosa*. *Trends in Pharmacological Sciences,* 37**,** 734-749.

ARNAIZ, A., TALAVERA-MATEO, L., GONZALEZ-MELENDI, P., MARTINEZ, M., DIAZ, I. & SANTAMARIA, M. E. 2018. Arabidopsis Kunitz Trypsin Inhibitors in Defense Against Spider Mites. *Frontiers in plant science,* 9**,** 986-986.

ARNOLD, D. L. & PRESTON, G. M. 2019. *Pseudomonas syringae*: enterprising epiphyte and stealthy parasite. *Microbiology,* 165**,** 251-253.

ATKINSON, M. M., HUANG, J. S. & KNOPP, J. A. 1985. The Hypersensitive Reaction of Tobacco to *Pseudomonas syringae* pv. pisi: Activation of a Plasmalemma K/H Exchange Mechanism. *Plant Physiol,* 79**,** 843-7.

AUNG, K., XIN, X., MECEY, C. & HE, S. Y. 2017. Subcellular Localization of *Pseudomonas syringae* pv. tomato Effector Proteins in Plants. *Type 3 Secretion Systems,* 1531**,** 141-153.

BAEK, M., PARK, T., HEO, L., PARK, C. & SEOK, C. 2017. GalaxyHomomer: a web server for protein homo-oligomer structure prediction from a monomer sequence or structure. *Nucleic Acids Research,* 45**,** W320-W324.

BAKER, C. J., ORLANDI, E. W. & MOCK, N. M. 1993. Harpin, An Elicitor of the Hypersensitive Response in Tobacco Caused by *Erwinia amylovora*, Elicits Active Oxygen Production in Suspension Cells. *Plant Physiol,* 102**,** 1341-1344.

BALINT-KURTI, P. 2019. The plant hypersensitive response: concepts, control and consequences. *Molecular plant pathology,* 20**,** 1163-1178.

BALTRUS, D. A., NISHIMURA, M. T., ROMANCHUK, A., CHANG, J. H., MUKHTAR, M. S., CHERKIS, K., ROACH, J., GRANT, S. R., JONES, C. D. & DANGL, J. L. 2011. Dynamic Evolution of Pathogenicity Revealed by Sequencing and Comparative Genomics of 19 *Pseudomonas syringae* Isolates. *PLOS Pathogens,* 7**,** e1002132.

BARAQUET, C. & HARWOOD, C. S. 2013. Cyclic diguanosine monophosphate represses bacterial flagella synthesis by interacting with the Walker A motif of the enhancer-binding protein FleQ. *Proc Natl Acad Sci U S A,* 110**,** 18478-83.

BARENDS, T. R., HARTMANN, E., GRIESE, J. J., BEITLICH, T., KIRIENKO, N. V., RYJENKOV, D. A., REINSTEIN, J., SHOEMAN, R. L., GOMELSKY, M. & SCHLICHTING, I. 2009. Structure and mechanism of a bacterial light-regulated cyclic nucleotide phosphodiesterase. *Nature,* 459**,** 1015-8.

BENACH, J., SWAMINATHAN, S. S., TAMAYO, R., HANDELMAN, S. K., FOLTA-STOGNIEW, E., RAMOS, J. E., FOROUHAR, F., NEELY, H., SEETHARAMAN, J., CAMILLI, A. & HUNT, J. F. 2007. The structural basis of cyclic diguanylate signal transduction by PilZ domains. *The EMBO Journal,* 26**,** 5153-5166.

BENDER, C. L. 1999. Chlorosis-inducing Phytotoxins Produced by *Pseudomonas syringae*. *European Journal of Plant Pathology,* 105**,** 1-12.

BERGERON, J. R., FERNANDEZ, L., WASNEY, G. A., VUCKOVIC, M., REFFUVEILLE, F., HANCOCK, R. E. & STRYNADKA, N. C. 2016. The Structure of a Type 3 Secretion System (T3SS) Ruler Protein Suggests a Molecular Mechanism for Needle Length Sensing. *J Biol Chem,* 291**,** 1676-91.

BERNAL, I., BÖRNICKE, J., HEIDEMANN, J., SVERGUN, D., HORSTMANN, J. A., ERHARDT, M., TUUKKANEN, A., UETRECHT, C. & KOLBE, M. 2019. Molecular Organization of Soluble Type III Secretion System Sorting Platform Complexes. *Journal of Molecular Biology*.

BHANDARI, D. D., LAPIN, D., KRACHER, B., VON BORN, P., BAUTOR, J., NIEFIND, K. & PARKER, J. E. 2019. An EDS1 heterodimer signalling surface enforces timely reprogramming of immunity genes in *Arabidopsis*. *Nature Communications,* 10**,** 772.

BHATTACHARJEE, S., HALANE, M. K., KIM, S. H. & GASSMANN, W. 2011. Pathogen effectors target *Arabidopsis* EDS1 and alter its interactions with immune regulators. *Science,* 334**,** 1405-8.

BLACK, W. P., WANG, L., JING, X., SALDAÑA, R. C., LI, F., SCHARF, B. E., SCHUBOT, F. D. & YANG, Z. 2017. The type IV pilus assembly ATPase PilB functions as a signaling protein to regulate exopolysaccharide production in *Myxococcus xanthus*. *Scientific Reports,* 7**,** 7263.

BLOCK, A. & ALFANO, J. R. 2011. Plant targets for *Pseudomonas syringae* type III effectors: Virulence targets or guarded decoys? *Current opinion in microbiology,* 14**,** 39-46.

BLOCK, A., TORUÑO, T. Y., ELOWSKY, C. G., ZHANG, C., STEINBRENNER, J., BEYNON, J. & ALFANO, J. R. 2014. The *Pseudomonas syringae* type III effector HopD1 suppresses effector-triggered immunity, localizes to the endoplasmic reticulum, and targets the *Arabidopsis* transcription factor NTL9. *New Phytol,* 201**,** 1358-1370.

BOLAND, A., SORY, M. P., IRIARTE, M., KERBOURCH, C., WATTIAU, P. & CORNELIS, G. R. 1996. Status of YopM and YopN in the Yersinia Yop virulon: YopM of *Y.enterocolitica* is internalized inside the cytosol of PU5–1.8 macrophages by the YopB, D, N delivery apparatus. *The EMBO Journal,* 15**,** 5191-5201.

BONARDI, V. & DANGL, J. L. 2012. How complex are intracellular immune receptor signaling complexes? *Frontiers in plant science,* 3**,** 237-237.

BRADFORD, M. M. 1976. A rapid and sensitive method for the quantitation of microgram quantities of protein utilizing the principle of protein-dye binding. *Anal Biochem,* 72**,** 248-54.

BRUTINEL, E. D. & YAHR, T. L. 2008. Control of gene expression by type III secretory activity. *Curr Opin Microbiol,* 11**,** 128-33.

BUCHKO, G. W., NIEMANN, G., BAKER, E. S., BELOV, M. E., SMITH, R. D., HEFFRON, F., ADKINS, J. N. & MCDERMOTT, J. E. 2010. A multi-pronged search for a common structural motif in the secretion signal of *Salmonella enterica* serovar *Typhimurium* type III effector proteins. *Molecular bioSystems,* 6**,** 2448-2458.

BUELL, C. R., JOARDAR, V., LINDEBERG, M., SELENGUT, J., PAULSEN, I. T., GWINN, M. L., DODSON, R. J., DEBOY, R. T., DURKIN, A. S., KOLONAY, J. F., MADUPU, R., DAUGHERTY, S., BRINKAC, L., BEANAN, M. J., HAFT, D. H., NELSON, W. C., DAVIDSEN, T., ZAFAR, N., ZHOU, L. W., LIU, J., YUAN, Q. P., KHOURI, H., FEDOROVA, N., TRAN, B., RUSSELL, D., BERRY, K., UTTERBACK, T., VAN AKEN, S. E., FELDBLYUM, T. V., D'ASCENZO, M., DENG, W. L., RAMOS, A. R., ALFANO, J. R., CARTINHOUR, S., CHATTERJEE, A. K., DELANEY, T. P., LAZAROWITZ, S. G., MARTIN, G. B., SCHNEIDER, D. J., TANG, X. Y., BENDER, C. L., WHITE, O., FRASER, C. M. & COLLMER, A. 2003.

The complete genome sequence of the *Arabidopsis* and tomato pathogen *Pseudomonas syringae* pv. *tomato* DC3000. *Proceedings of the National Academy of Sciences of the United States of America,* 100**,** 10181-10186.

BULL, C. T., DE BOER, S. H., DENNY, T. P., FIRRAO, G., FISCHER-LE SAUX, M., SADDLER, G. S., SCORTICHINI, M., STEAD, D. E. & TAKIKAWA, Y. 2010. Comprehensive List of Names of Plant Pathogenic Bacteria, 1980-2007. *Journal*

of Plant Pathology, 92**,** 551-592.

BURCH, A. Y., SHIMADA, B. K., MULLIN, S. W., DUNLAP, C. A., BOWMAN, M. J. & LINDOW, S. E. 2012. *Pseudomonas syringae* coordinates production of a motility-enabling surfactant with flagellar assembly. *J Bacteriol,* 194**,** 1287-98.

BURGESS, J. L., BURGESS, R. A., MORALES, Y., BOUVANG, J. M., JOHNSON, S. J. & DICKENSON, N. E. 2016a. Structural and Biochemical Characterization of Spa47 Provides Mechanistic Insight into Type III Secretion System ATPase Activation and *Shigella* Virulence Regulation. *The Journal of biological chemistry,* 291**,** 25837-25852.

BURGESS, J. L., JONES, H. B., KUMAR, P., TOTH, R. T. T., MIDDAUGH, C. R., ANTONY, E. & DICKENSON, N. E. 2016b. Spa47 is an oligomerization-activated type three secretion system (T3SS) ATPase from *Shigella flexneri*. *Protein Sci,* 25**,** 1037-48.

BUTLER, M. I., STOCKWELL, P. A., BLACK, M. A., DAY, R. C., LAMONT, I. L. & POULTER, R. T. 2013. *Pseudomonas syringae* pv. *actinidiae* from recent outbreaks of kiwifruit bacterial canker belong to different clones that originated in China. *PLoS One,* 8**,** e57464.

BUTTERWORTH, J. & MCCARTNEY, H. A. 1991. The dispersal of bacteria from leaf surfaces by water splash. *Journal of Applied Bacteriology,* 71**,** 484-496.

BUTTNER, D. 2012. Protein export according to schedule: architecture, assembly, and regulation of type III secretion systems from plant- and animal-pathogenic bacteria. *Microbiol Mol Biol Rev,* 76**,** 262-310.

BÜTTNER, D. 2016. Behind the lines-actions of bacterial type III effector proteins in plant cells. *FEMS Microbiol Rev,* 40**,** 894-937.

BUTTNER, D., NENNSTIEL, D., KLUSENER, B. & BONAS, U. 2002. Functional analysis of HrpF, a putative type III translocon protein from *Xanthomonas campestris* pv. *vesicatoria*. *J Bacteriol,* 184**,** 2389-98.

CAI, R., LEWIS, J., YAN, S., LIU, H., CLARKE, C. R., CAMPANILE, F., ALMEIDA, N. F., STUDHOLME, D. J., LINDEBERG, M., SCHNEIDER, D., ZACCARDELLI, M., SETUBAL, J. C., MORALES-LIZCANO, N. P., BERNAL, A., COAKER, G., BAKER, C., BENDER, C. L., LEMAN, S. & VINATZER, B. A. 2011. The Plant Pathogen *Pseudomonas syringae* pv. *tomato* Is Genetically Monomorphic and under Strong Selection to Evade Tomato Immunity. *PLoS Pathogens,* 7**,** e1002130.

CAMPILONGO, R., FUNG, R. K. Y., LITTLE, R. H., GRENGA, L., TRAMPARI, E., PEPE, S., CHANDRA, G., STEVENSON, C. E. M., RONCARATI, D. & MALONE, J. G. 2017. One ligand, two regulators and three binding sites: How KDPG controls primary carbon metabolism in *Pseudomonas*. *Plos Genetics,* 13.

CASTAÑEDA-OJEDA, M. P., LÓPEZ-SOLANILLA, E. & RAMOS, C. 2017. Differential modulation of plant immune responses by diverse members of the *Pseudomonas savastanoi* pv. *savastanoi* HopAF type III effector family. *Molecular Plant Pathology,* 18**,** 625-634.

CASTRO, M., DEANE, S. M., RUIZ, L., RAWLINGS, D. E. & GUILIANI, N. 2015. Diguanylate Cyclase Null Mutant Reveals That C-Di-GMP Pathway Regulates the Motility and Adherence of the Extremophile Bacterium *Acidithiobacillus caldus*. *PLOS ONE,* 10**,** e0116399.

CESARI, S. 2018. Multiple strategies for pathogen perception by plant immune receptors. *New Phytologist,* 219**,** 17-24.

CHAKRAVARTHY, S., BUTCHER, B. G., LIU, Y., D'AMICO, K., COSTER, M. & FILIATRAULT, M. J. 2017a. Virulence of *Pseudomonas syringae* pv. *tomato* DC3000 Is Influenced by the Catabolite Repression Control Protein Crc. *Mol Plant Microbe Interact,* 30**,** 283-294.

CHAKRAVARTHY, S., HUOT, B. & KVITKO, B. H. 2017b. Effector Translocation: Cya Reporter Assay. *In:* JOURNET, L. & CASCALES, E. (eds.) *Bacterial Protein Secretion Systems: Methods and Protocols.* New York, NY: Springer New York.

CHAKRAVARTHY, S., WORLEY, J. N., MONTES-RODRIGUEZ, A. & COLLMER, A. 2018. *Pseudomonas syringae* pv. *tomato* DC3000 polymutants deploying coronatine and two type III effectors produce quantifiable chlorotic spots from individual bacterial colonies in *Nicotiana benthamiana* leaves. *Mol Plant Pathol,* 19**,** 935-947.

CHAN, C., PAUL, R., SAMORAY, D., AMIOT, N. C., GIESE, B., JENAL, U. & SCHIRMER, T. 2004. Structural basis of activity and allosteric control of diguanylate cyclase. *Proceedings of the National Academy of Sciences of the United States of America,* 101**,** 17084-17089.

CHANG, M., ZHAO, J., CHEN, H., LI, G., CHEN, J., LI, M., PALMER, I. A., SONG, J., ALFANO, J. R., LIU, F. & FU, Z. Q. 2019. PBS3 Protects EDS1 from Proteasome-Mediated Degradation in Plant Immunity. *Mol Plant,* 12**,** 678-688.

CHAROVA, S., GAZI, A., MYLONAS, E., POZIDIS, C., SABARIT, B., ANAGNOSTOU, D., PSATHA, K., AIVALIOTIS, M., BEUZON, C., PANOPOULOS, N., KOKKINIDIS, M. & AUSUBEL, F. 2018. Migration of Type III Secretion System Transcriptional Regulators Links Gene Expression to Secretion. *mBio,* 9**,** e01096-18.

CHARPENTIER, X. & OSWALD, E. 2004. Identification of the secretion and translocation domain of the enteropathogenic and enterohemorrhagic *Escherichia coli* effector Cif, using TEM-1 beta-lactamase as a new fluorescence-based reporter. *J Bacteriol,* 186**,** 5486-95.

CHECKER, V. G., KUSHWAHA, H. R., KUMARI, P. & YADAV, S. 2018. Role of Phytohormones in Plant Defense: Signaling and Cross Talk. *In:* SINGH, A. & SINGH, I. K. (eds.) *Molecular Aspects of Plant-Pathogen Interaction.* Singapore: Springer Singapore.

CHEN, Z.-H. & SCHAAP, P. 2012. The prokaryote messenger c-di-GMP triggers stalk cell differentiation in *Dictyostelium*. *Nature,* 488**,** 680.

CHINCHILLA, D., BAUER, Z., REGENASS, M., BOLLER, T. & FELIX, G. 2006. The *Arabidopsis* receptor kinase FLS2 binds flg22 and determines the specificity of flagellin perception. *The Plant cell,* 18**,** 465-476.

CHINCHILLA, D., ZIPFEL, C., ROBATZEK, S., KEMMERLING, B., NÜRNBERGER, T., JONES, J. D. G., FELIX, G. & BOLLER, T. 2007. A flagellin-induced complex of the receptor FLS2 and BAK1 initiates plant defence. *Nature,* 448**,** 497-500.

CHOI, H., LARSEN, B., LIN, Z.-Y., BREITKREUTZ, A., MELLACHERUVU, D., FERMIN, D., QIN, Z. S., TYERS, M., GINGRAS, A.-C. & NESVIZHSKII, A. I. 2011. SAINT: probabilistic scoring of affinity purification-mass spectrometry data. *Nature methods,* 8**,** 70-73.

CHOI, K. H., GAYNOR, J. B., WHITE, K. G., LOPEZ, C., BOSIO, C. M., KARKHOFF-SCHWEIZER, R. R. & SCHWEIZER, H. P. 2005. A Tn7-based broad-range bacterial cloning and expression system. *Nat Methods,* 2**,** 443-8.

CHOI, S., JAYARAMAN, J., SEGONZAC, C., PARK, H. J., PARK, H., HAN, S. W. & SOHN, K. H. 2017. *Pseudomonas syringae* pv. *actinidiae* Type III Effectors Localized at Multiple Cellular Compartments Activate or Suppress Innate Immune Responses in *Nicotiana benthamiana*. *Front Plant Sci,* 8**,** 2157.

CHOU, S. H. & GALPERIN, M. Y. 2016. Diversity of Cyclic Di-GMP-Binding Proteins and Mechanisms. *J Bacteriol,* 198**,** 32-46.

CHOY, W.-K., ZHOU, L., SYN, C. K.-C., ZHANG, L.-H. & SWARUP, S. 2004. MorA Defines a New Class of Regulators Affecting Flagellar Development and Biofilm Formation in Diverse *Pseudomonas* Species. *Journal of Bacteriology,* 186**,** 7221-7228.

CLARET, L., CALDER, S. R., HIGGINS, M. & HUGHES, C. 2003. Oligomerization and activation of the FliI ATPase central to bacterial flagellum assembly. *Molecular microbiology,* 48**,** 1349-1355.

CLARKE, C. R., CAI, R., STUDHOLME, D. J., GUTTMAN, D. S. & VINATZER, B. A. 2010. *Pseudomonas syringae* strains naturally lacking the classical *P. syringae hrp/hrc* Locus are common leaf

colonizers equipped with an atypical type III secretion system. *Mol Plant Microbe Interact,* 23**,** 198-210.

COBURN, B., SEKIROV, I. & FINLAY, B. B. 2007. Type III Secretion Systems and Disease. *Clinical Microbiology Reviews,* 20**,** 535-549.

COHEN, D., MECHOLD, U., NEVENZAL, H., YARMIYHU, Y., RANDALL, T. E., BAY, D. C., RICH, J. D., PARSEK, M. R., KAEVER, V., HARRISON, J. J. & BANIN, E. 2015. Oligoribonuclease is a central feature of cyclic diguanylate signaling in *Pseudomonas aeruginosa*. *Proc Natl Acad Sci U S A,* 112**,** 11359-64.

COLE, S. J. & LEE, V. T. 2016. Cyclic Di-GMP Signaling Contributes to *Pseudomonas aeruginosa*-Mediated Catheter-Associated Urinary Tract Infection. *Journal of Bacteriology,* 198**,** 91-97.

COLLMER, A., BADEL, J. L., CHARKOWSKI, A. O., DENG, W.-L., FOUTS, D. E., RAMOS, A. R., REHM, A. H., ANDERSON, D. M., SCHNEEWIND, O., VAN DIJK, K. & ALFANO, J. R. 2000. *Pseudomonas syringae* Hrp type III secretion system and effector proteins. *Proceedings of the National Academy of Sciences,* 97**,** 8770.

CORNELIS, G. R. 2002. The *Yersinia* Ysc-Yop virulence apparatus. *Int J Med Microbiol,* 291**,** 455-62.

CRABILL, E., KARPISEK, A. & ALFANO JAMES, R. 2012. The *Pseudomonas syringae* HrpJ protein controls the secretion of type III translocator proteins and has a virulence role inside plant cells. *Molecular Microbiology,* 85**,** 225-238.

CUNNAC, S., CHAKRAVARTHY, S., KVITKO, B. H., RUSSELL, A. B., MARTIN, G. B. & COLLMER, A. 2011. Genetic disassembly and combinatorial reassembly identify a minimal functional repertoire of type III effectors in *Pseudomonas syringae*. *Proceedings of the National Academy of Sciences,* 108**,** 2975-2980.

DANGL, J., HORVATH, D. & STASKAWICZ, B. 2013. Pivoting the Plant Immune System from Dissection to Deployment. *Science,* 341**,** 746-751.

DAY, J. B., FERRACCI, F. & PLANO, G. V. 2003. Translocation of YopE and YopN into eukaryotic cells by *Yersinia pestis yopN, tyeA, sycN, yscB* and *lcrG* deletion mutants measured using a phosphorylatable peptide tag and phosphospecific antibodies. *Mol Microbiol,* 47**,** 807-23.

DEANE, J. E., ABRUSCI, P., JOHNSON, S. & LEA, S. M. 2010. Timing is Everything: The Regulation of Type III Secretion. *Cellular and Molecular Life Sciences,* 67**,** 1065-1075.

DEL POZO, O., PEDLEY, K. F. & MARTIN, G. B. 2004. MAPKKKα is a positive regulator of cell death associated with both plant immunity and disease. *The EMBO Journal,* 23**,** 3072-3082.

DENG, W.-L., PRESTON, G., COLLMER, A., CHANG, C.-J. & HUANG, H.-C. 1998. Characterization of the *hrpC* and *hrpRS* Operons of *Pseudomonas syringae* Pathovars *Syringae, Tomato,* and *Glycinea* and Analysis of the Ability of *hrpF,hrpG, hrcC, hrpT,* and *hrpV* Mutants To Elicit the Hypersensitive Response and Disease in Plants. *Journal of Bacteriology,* 180**,** 4523-4531.

DENG, W., MARSHALL, N. C., ROWLAND, J. L., MCCOY, J. M., WORRALL, L. J., SANTOS, A. S., STRYNADKA, N. C. J. & FINLAY, B. B. 2017. Assembly, structure, function and regulation of type III secretion systems. *Nature Reviews Microbiology,* 15**,** 323-337.

DERKSEN, H., RAMPITSCH, C. & DAAYF, F. 2013. Signaling cross-talk in plant disease resistance. *Plant Sci,* 207**,** 79-87.

DIEPOLD, A. 2020. Assembly and Post-assembly Turnover and Dynamics in the Type III Secretion System. *In:* WAGNER, S. & GALAN, J. E. (eds.) *Bacterial Type III Protein Secretion Systems.* Cham: Springer International Publishing.

DIEPOLD, A. & ARMITAGE, J. P. 2015. Type III secretion systems: the bacterial flagellum and the injectisome. *Philosophical transactions of the Royal Society of London. Series B, Biological sciences,* 370**,** 20150020.

DIEPOLD, A. & WAGNER, S. 2014. Assembly of the bacterial type III secretion machinery. *FEMS Microbiology Reviews,* 38**,** 802-822.

DIJK, K. V., TAM, V. C., RECORDS, A. R., PETNICKI-OCWIEJA, T. & ALFANO, J. R. 2002. The ShcA protein is a molecular chaperone that assists in the secretion of the HopPsyA effector from the type

III (Hrp) protein secretion system of *Pseudomonas syringae*. *Molecular Microbiology,* 44**,** 1469-1481.

DING, P., SAKAI, T., KRISHNA SHRESTHA, R., MANOSALVA PEREZ, N., GUO, W., NGOU, B. P. M., HE, S., LIU, C., FENG, X., ZHANG, R., VANDEPOELE, K., MACLEAN, D. & JONES, J. D. G. 2021. Chromatin accessibility landscapes activated by cell-surface and intracellular immune receptors. *Journal of Experimental Botany,* 72**,** 7927-7941.

DODDS, P. N. & RATHJEN, J. P. 2010. Plant immunity: towards an integrated view of plant–pathogen interactions. *Nature Reviews Genetics,* 11**,** 539-548.

DOHLICH, K., ZUMSTEG, A. B., GOOSMANN, C. & KOLBE, M. 2014. A substrate-fusion protein is trapped inside the Type III Secretion System channel in *Shigella flexneri*. *PLoS pathogens,* 10**,** e1003881-e1003881.

DORTET, L., LOMBARDI, C., CRETIN, F., DESSEN, A. & FILLOUX, A. 2018. Pore-forming activity of the *Pseudomonas aeruginosa* type III secretion system translocon alters the host epigenome. *Nat Microbiol,* 3**,** 378-386.

DUDNIK, A. & DUDLER, R. 2014. Virulence determinants of *Pseudomonas syringae* strains isolated from grasses in the context of a small type III effector repertoire. *BMC microbiology,* 14**,** 304-304.

DÜMMLER, A., LAWRENCE, A. M. & DE MARCO, A. 2005. Simplified screening for the detection of soluble fusion constructs expressed in *E. coli* using a modular set of vectors. *Microb Cell Fact,* 4**,** 34.

EASTMAN, S., SMITH, T., ZAYDMAN, M. A., KIM, P., MARTINEZ, S., DAMARAJU, N., DIANTONIO, A., MILBRANDT, J., CLEMENTE, T. E., ALFANO, J. R. & GUO, M. 2021. A phytobacterial TIR domain effector manipulates NAD+ to promote virulence. *New Phytologist,* n/a.

EDMUNDS, A., CASTIBLANCO, L., SUNDIN, G. & WATERS, C. 2013. Cyclic Di-GMP Modulates the Disease Progression of *Erwinia amylovora*. *Journal of Bacteriology,* 195**,** 2155-2165.

EICHELBERG, K., GINOCCHIO, C. C. & GALAN, J. E. 1994. Molecular And Functional-Characterization Of The *Salmonella Typhimurium* Invasion Genes *invb* And *invc* - Homology Of Invc To The F_0f_1 Atpase Family Of Proteins. *Journal of Bacteriology,* 176**,** 4501-4510.

EL-BANOBY, F. E. & RUDOLPH, K. 1979. Induction of water-soaking in plant leaves by extracellular polysaccharides from phytopathogenic *pseudomonads* and *xanthomonads*. *Physiological Plant Pathology,* 15**,** 341-349.

ENGL, C., WAITE, C. J., MCKENNA, J. F., BENNETT, M. H., HAMANN, T. & BUCK, M. 2014. Chp8, a diguanylate cyclase from *Pseudomonas syringae* pv. *Tomato* DC3000, suppresses the pathogen-associated molecular pattern flagellin, increases extracellular polysaccharides, and promotes plant immune evasion. *mBio,* 5**,** e01168-14.

ERHARDT, M., MERTENS, M. E., FABIANI, F. D. & HUGHES, K. T. 2014. ATPase-independent type-III protein secretion in *Salmonella enterica*. *PLoS Genet,* 10**,** e1004800.

FAN, F. & MACNAB, R. M. 1996. Enzymatic characterization of FliI - An ATPase involved in flagellar assembly in *Salmonella typhimurium*. *Journal of Biological Chemistry,* 271**,** 31981-31988.

FANG, T. 2010. *Pseudomonas syringae type III secretion system: Secretion signals and putative docking stations.* PhD, University of Nebraska - Lincoln.

FELTMAN, H., SCHULERT, G., KHAN, S., JAIN, M., PETERSON, L. & HAUSER, A. R. 2001. Prevalence of type III secretion genes in clinical and environmental isolates of *Pseudomonas aeruginosa*. *Microbiology,* 147**,** 2659-69.

FLEITAS MARTÍNEZ, O., CARDOSO, M. H., RIBEIRO, S. M. & FRANCO, O. L. 2019. Recent Advances in Anti-virulence Therapeutic Strategies With a Focus on Dismantling Bacterial Membrane Microdomains, Toxin Neutralization, Quorum-Sensing Interference and Biofilm Inhibition. *Frontiers in Cellular and Infection Microbiology,* 9.

FLOR, H. H. 1942. Inheritance of pathogenicity of *Melampsora lini*. *Phytopath,* 32**,** 653-669.

FLOR, H. H. 1947. Inheritance of reaction to rust in flax. *Journal of Agricultural Research,* 74**,** 241-262.

FOUTS, D. E., BADEL, J. L., RAMOS, A. R., RAPP, R. A. & COLLMER, A. 2003. A *pseudomonas syringae* pv. *tomato* DC3000 Hrp (Type III secretion) deletion mutant expressing the Hrp system of bean pathogen *P. syringae* pv. *syringae* 61 retains normal host specificity for tomato. *Mol Plant Microbe Interact,* 16**,** 43-52.

FU, Z. Q., GUO, M., JEONG, B. R., TIAN, F., ELTHON, T. E., CERNY, R. L., STAIGER, D. & ALFANO, J. R. 2007. A type III effector ADP-ribosylates RNA-binding proteins and quells plant immunity. *Nature,* 447**,** 284-8.

FURUKAWA, T., INAGAKI, H., TAKAI, R., HIRAI, H. & CHE, F. S. 2014. Two distinct EF-Tu epitopes induce immune responses in rice and *Arabidopsis*. *Mol Plant Microbe Interact,* 27**,** 113-24.

GALAN, J. E. & COLLMER, A. 1999. Type III secretion machines: bacterial devices for protein delivery into host cells. *Science,* 284**,** 1322-8.

GAO, X., MU, Z., YU, X., QIN, B., WOJDYLA, J., WANG, M. & CUI, S. 2018. Structural Insight Into Conformational Changes Induced by ATP Binding in a Type III Secretion-Associated ATPase From *Shigella flexneri*. *Front Microbiol,* 9**,** 1468.

GARCIA, J. T., FERRACCI, F., JACKSON, M. W., JOSEPH, S. S., PATTIS, I., PLANO, L. R., FISCHER, W. & PLANO, G. V. 2006. Measurement of effector protein injection by type III and type IV secretion systems by using a 13-residue phosphorylatable glycogen synthase kinase tag. *Infect Immun,* 74**,** 5645-57.

GARDINER, J. M. & PROCTER, J. 2001. Synthesis of N-alkoxybenzimidazoles with differentiated C2 and O-substituents. *Tetrahedron Letters,* 42**,** 5109-5111.

GAWTHORNE, J. A., AUDRY, L., MCQUITTY, C., DEAN, P., CHRISTIE, J. M., ENNINGA, J. & ROE, A. J. 2016. Visualizing the Translocation and Localization of Bacterial Type III Effector Proteins by Using a Genetically Encoded Reporter System. *Applied and environmental microbiology,* 82**,** 2700-2708.

GHOSH, P. 2004. Process of protein transport by the type III secretion system. *Microbiology and molecular biology reviews : MMBR,* 68**,** 771-795.

GIMENEZ-IBANEZ, S., BOTER, M., FERNÁNDEZ-BARBERO, G., CHINI, A., RATHJEN, J. P. & SOLANO, R. 2014. The Bacterial Effector HopX1 Targets JAZ Transcriptional Repressors to Activate Jasmonate Signaling and Promote Infection in *Arabidopsis*. *PLOS Biology,* 12**,** e1001792.

GIMENEZ-IBANEZ, S., HANN, D. R., CHANG, J. H., SEGONZAC, C., BOLLER, T. & RATHJEN, J. P. 2018. Differential Suppression of *Nicotiana benthamiana* Innate Immune Responses by Transiently Expressed *Pseudomonas syringae* Type III Effectors. *Front Plant Sci,* 9**,** 688.

GOEL, A. K., LUNDBERG, D., TORRES, M. A., MATTHEWS, R., AKIMOTO-TOMIYAMA, C., FARMER, L., DANGL, J. L. & GRANT, S. R. 2008. The *Pseudomonas syringae* Type III Effector HopAM1 Enhances Virulence on Water-Stressed Plants. *Molecular Plant-Microbe Interactions,* 21**,** 361-370.

GÖHRE, V., SPALLEK, T., HÄWEKER, H., MERSMANN, S., MENTZEL, T., BOLLER, T., DE TORRES, M., MANSFIELD, J. W. & ROBATZEK, S. 2008. Plant pattern-recognition receptor FLS2 is directed for degradation by the bacterial ubiquitin ligase AvrPtoB. *Curr Biol,* 18**,** 1824-32.

GRENGA, L., LITTLE, R. H. & MALONE, J. G. 2017. Quick change: post-transcriptional regulation in *Pseudomonas*. *FEMS Microbiology Letters,* 364**,** fnx125.

GUO, M., CHANCEY SCOTT, T., TIAN, F., GE, Z., JAMIR, Y. & ALFANO JAMES, R. 2005. *Pseudomonas syringae* Type III Chaperones ShcO1, ShcS1, and ShcS2 Facilitate Translocation of Their Cognate Effectors and Can Substitute for Each Other in the Secretion of HopO1-1. *Journal of Bacteriology,* 187**,** 4257-4269.

GUO, M., KIM, P., LI, G., ELOWSKY, C. G. & ALFANO, J. R. 2016. A Bacterial Effector Co-opts Calmodulin to Target the Plant Microtubule Network. *Cell Host Microbe,* 19**,** 67-78.

GUO, M., TIAN, F., WAMBOLDT, Y. & ALFANO, J. R. 2009. The majority of the type III effector inventory of *Pseudomonas syringae* pv. *tomato* DC3000 can suppress plant immunity. *Mol Plant Microbe Interact,* 22**,** 1069-80.

GUPTA, K. R., KASETTY, S. & CHATTERJI, D. 2015. Novel Functions of (p)ppGpp and Cyclic di-GMP in *Mycobacterial* Physiology Revealed by Phenotype Microarray Analysis of Wild-Type and Isogenic Strains of *Mycobacterium smegmatis*. *Applied and Environmental Microbiology,* 81**,** 2571-2578.

GURUNG, J. M., AMER, A. A. A., CHEN, S., DIEPOLD, A. & FRANCIS, M. S. 2022. Type III secretion by *Yersinia pseudotuberculosis* is reliant upon an authentic N-terminal YscX secretor domain. *Mol Microbiol,* 117**,** 886-906.

HA, U. H., KIM, J., BADRANE, H., JIA, J., BAKER, H. V., WU, D. & JIN, S. 2004. An in vivo inducible gene of *Pseudomonas aeruginosa* encodes an anti-ExsA to suppress the type III secretion system. *Mol Microbiol,* 54**,** 307-20.

HABYARIMANA, F. & AHMER, B. M. M. 2013. More Evidence for Secretion Signals within the mRNA of Type 3 Secreted Effectors. *Journal of Bacteriology,* 195**,** 2117.

HALL, C. L. & LEE, V. T. 2018. Cyclic-di-GMP regulation of virulence in bacterial pathogens. *Wiley Interdisciplinary Reviews-Rna,* 9**,** 19.

HALTE, M. & ERHARDT, M. 2021. Protein Export via the Type III Secretion System of the Bacterial Flagellum. *Biomolecules,* 11**,** 186.

HANN, D. R. & RATHJEN, J. P. 2007. Early events in the pathogenicity of *Pseudomonas syringae* on *Nicotiana benthamiana*. *Plant Journal,* 49**,** 607-618.

HARRINGTON, N. E., SWEENEY, E. & HARRISON, F. 2020. Building a better biofilm - Formation of in vivo-like biofilm structures by *Pseudomonas aeruginosa* in a porcine model of cystic fibrosis lung infection. *Biofilm,* 2**,** 100024.

HARRISON, F., MURULI, A., HIGGINS, S., DIGGLE, S. P. & MCCORMICK, B. A. 2014. Development of an *Ex Vivo* Porcine Lung Model for Studying Growth, Virulence, and Signaling of *Pseudomonas aeruginosa*. *Infection and Immunity,* 82**,** 3312-3323.

HARVEY, K. L., JAROCKI, V. M., CHARLES, I. G. & DJORDJEVIC, S. P. 2019. The Diverse Functional Roles of Elongation Factor Tu (EF-Tu) in Microbial Pathogenesis. *Frontiers in Microbiology,* 10.

HASSETT, D. J., CUPPOLETTI, J., TRAPNELL, B., LYMAR, S. V., ROWE, J. J., YOON, S. S., HILLIARD, G. M., PARVATIYAR, K., KAMANI, M. C., WOZNIAK, D. J., HWANG, S. H., MCDERMOTT, T. R. & OCHSNER, U. A. 2002. Anaerobic metabolism and quorum sensing by *Pseudomonas aeruginosa* biofilms in chronically infected cystic fibrosis airways: rethinking antibiotic treatment strategies and drug targets. *Advanced Drug Delivery Reviews,* 54**,** 1425-1443.

HENDRICK, W. A., ORR, M. W., MURRAY, S. R., LEE, V. T. & MELVILLE, S. B. 2017. Cyclic Di-GMP Binding by an Assembly ATPase (PilB2) and Control of Type IV Pilin Polymerization in the Gram-Positive Pathogen *Clostridium perfringens*. *J Bacteriol,* 199.

HENTZER, M., TEITZEL GAIL, M., BALZER GRANT, J., HEYDORN, A., MOLIN, S., GIVSKOV, M. & PARSEK MATTHEW, R. 2001. Alginate Overproduction Affects Pseudomonas aeruginosa Biofilm Structure and Function. *Journal of Bacteriology,* 183**,** 5395-5401.

HERAS, B., SCANLON, M. J. & MARTIN, J. L. 2015. Targeting virulence not viability in the search for future antibacterials. *British journal of clinical pharmacology,* 79**,** 208-215.

HICKMAN, J. W. & HARWOOD, C. S. 2008. Identification of FleQ from *Pseudomonas aeruginosa* as a c-di-GMP-responsive transcription factor. *Mol Microbiol,* 69**,** 376-89.

HICKMAN, J. W., TIFREA, D. F. & HARWOOD, C. S. 2005. A chemosensory system that regulates biofilm formation through modulation of cyclic diguanylate levels. *Proceedings of the National Academy of Sciences of the United States of America,* 102**,** 14422-14427.

HOCKETT, K. L., BURCH, A. Y. & LINDOW, S. E. 2013. Thermo-regulation of genes mediating motility and plant interactions in *Pseudomonas syringae*. *PloS one,* 8**,** e59850-e59850.

HU, B., MORADO, D. R., MARGOLIN, W., ROHDE, J. R., ARIZMENDI, O., PICKING, W. L., PICKING, W. D. & LIU, J. 2015. Visualization of the type III secretion sorting platform of *Shigella flexneri*. *Proceedings of the National Academy of Sciences of the United States of America,* 112**,** 1047-1052.

HU, J., WORRALL, L. J., HONG, C., VUCKOVIC, M., ATKINSON, C. E., CAVENEY, N., YU, Z. & STRYNADKA, N. C. J. 2018. Cryo-EM analysis of the T3S injectisome reveals the structure of the needle and open secretin. *Nature Communications,* 9**,** 3840.

HUANG, B., WHITCHURCH, C. B. & MATTICK, J. S. 2003. FimX, a multidomain protein connecting environmental signals to twitching motility in *Pseudomonas aeruginosa*. *J Bacteriol,* 185**,** 7068-76.

IAKOVIDIS, M., TEIXEIRA, P. J. P. L., EXPOSITO-ALONSO, M., COWPER, M. G., LAW, T. F., LIU, Q., VU, M. C., DANG, T. M., CORWIN, J. A., WEIGEL, D., DANGL, J. L. & GRANT, S. R. 2016. Effector-Triggered Immune Response in *Arabidopsis thaliana* Is a Quantitative Trait. *Genetics,* 204**,** 337-353.

ICHIMURA, K., SHINOZAKI, K., TENA, G., SHEEN, J., HENRY, Y., CHAMPION, A., KREIS, M., ZHANG, S., HIRT, H., WILSON, C., HEBERLE-BORS, E., ELLIS, B. E., MORRIS, P. C., INNES, R. W., ECKER, J. R., SCHEEL, D., KLESSIG, D. F., MACHIDA, Y., MUNDY, J., OHASHI, Y. & WALKER, J. C. 2002. Mitogen-activated protein kinase cascades in plants: a new nomenclature. *Trends in Plant Science,* 7**,** 301-308.

ICHINOSE, Y., TAGUCHI, F. & MUKAIHARA, T. 2013. Pathogenicity and virulence factors of *Pseudomonas syringae*. *Journal of General Plant Pathology,* 79**,** 285-296.

JELENSKA, J., VAN HAL, J. A. & GREENBERG, J. T. 2010. *Pseudomonas syringae* hijacks plant stress chaperone machinery for virulence. *Proc Natl Acad Sci U S A,* 107**,** 13177-82.

JIN, L., HAM, J. H., HAGE, R., ZHAO, W., SOTO-HERNÁNDEZ, J., LEE, S. Y., PAEK, S.-M., KIM, M. G., BOONE, C., COPLIN, D. L. & MACKEY, D. 2016. Direct and Indirect Targeting of PP2A by Conserved Bacterial Type-III Effector Proteins. *PLOS Pathogens,* 12**,** e1005609.

JOB, V., MATTEÏ, P.-J., LEMAIRE, D., ATTREE, I. & DESSEN, A. 2010. Structural basis of chaperone recognition of type III secretion system minor translocator proteins. *The Journal of biological chemistry,* 285**,** 23224-23232.

JOHNSON, S., FONG, Y. H., DEME, J. C., FURLONG, E. J., KUHLEN, L. & LEA, S. M. 2020. Symmetry mismatch in the MS-ring of the bacterial flagellar rotor explains the structural coordination of secretion and rotation. *Nature microbiology,* 5**,** 966-975.

JOHNSON, S., KUHLEN, L., DEME JUSTIN, C., ABRUSCI, P., LEA SUSAN, M. & SANSONETTI PHILIPPE, J. 2019. The Structure of an Injectisome Export Gate Demonstrates Conservation of Architecture in the Core Export Gate between Flagellar and Virulence Type III Secretion Systems. *mBio,* 10**,** e00818-19.

JONES, J. D. G. & DANGL, J. L. 2006. The plant immune system. *Nature,* 444**,** 323-329.

JUMPER, J., EVANS, R., PRITZEL, A., GREEN, T., FIGURNOV, M., RONNEBERGER, O., TUNYASUVUNAKOOL, K., BATES, R., ŽÍDEK, A., POTAPENKO, A., BRIDGLAND, A., MEYER, C., KOHL, S. A. A., BALLARD, A. J., COWIE, A., ROMERA-PAREDES, B., NIKOLOV, S., JAIN, R., ADLER, J., BACK, T., PETERSEN, S., REIMAN, D., CLANCY, E., ZIELINSKI, M., STEINEGGER, M., PACHOLSKA, M., BERGHAMMER, T., BODENSTEIN, S., SILVER, D., VINYALS, O., SENIOR, A. W., KAVUKCUOGLU, K., KOHLI, P. & HASSABIS, D. 2021. Highly accurate protein structure prediction with AlphaFold. *Nature,* 596**,** 583-589.

KATO, J., DEY, S., SOTO, J. E., BUTAN, C., WILKINSON, M. C., DE GUZMAN, R. N. & GALAN, J. E. 2018. A protein secreted by the *Salmonella* type III secretion system controls needle filament assembly. *eLife,* 7**,** e35886.

KAWAMOTO, A., MIYATA, T., MAKINO, F., KINOSHITA, M., MINAMINO, T., IMADA, K., KATO, T. & NAMBA, K. 2021. Native flagellar MS ring is formed by 34 subunits with 23-fold and 11-fold subsymmetries. *Nature Communications,* 12**,** 4223.

KIM, M. G., GENG, X., LEE, S. Y. & MACKEY, D. 2009. The *Pseudomonas syringae* type III effector AvrRpm1 induces significant defenses by activating the *Arabidopsis* nucleotide-binding leucine-rich repeat protein RPS2. *Plant J,* 57**,** 645-53.

KLEMENT, Z., BOZSÓ, Z., OTT, P. G. & RUDOLPH, K. 1997. The Mechanism of Symptomless Reaction of Plants Induced by Pathogenic *Pseudomonads*. *In:* RUDOLPH, K., BURR, T. J., MANSFIELD, J.

W., STEAD, D., VIVIAN, A. & VON KIETZELL, J. (eds.) *Pseudomonas Syringae Pathovars and Related Pathogens.* Dordrecht: Springer Netherlands.

KNEPPER, C. & DAY, B. 2010. From perception to activation: the molecular-genetic and biochemical landscape of disease resistance signaling in plants. *The arabidopsis book,* 8**,** e012-e012.

KUHLEN, L., JOHNSON, S., ZEITLER, A., BÄURLE, S., DEME, J. C., CAESAR, J. J. E., DEBO, R., FISHER, J., WAGNER, S. & LEA, S. M. 2020. The substrate specificity switch FlhB assembles onto the export gate to regulate type three secretion. *Nature communications,* 11**,** 1296-1296.

KULASAKARA, H., LEE, V., BRENCIC, A., LIBERATI, N., URBACH, J., MIYATA, S., LEE, D. G., NEELY, A. N., HYODO, M., HAYAKAWA, Y., AUSUBEL, F. M. & LORY, S. 2006. Analysis of *Pseudomonas aeruginosa* diguanylate cyclases and phosphodiesterases reveals a role for bis-(3'-5')-cyclic-GMP in virulence. *Proc Natl Acad Sci U S A,* 103**,** 2839-44.

KUMAR, J., RAMLAL, A., KUMAR, K., RANI, A. & MISHRA, V. 2021. Signaling Pathways and Downstream Effectors of Host Innate Immunity in Plants. *International journal of molecular sciences,* 22**,** 9022.

KUMAR, K. & VERMA, P. 2013. Plant Pathogen Interactions: Crop Improvement Under Adverse Conditions.

KVITKO, B. H., PARK, D. H., VELÁSQUEZ, A. C., WEI, C. F., RUSSELL, A. B., MARTIN, G. B., SCHNEIDER, D. J. & COLLMER, A. 2009. Deletions in the repertoire of *Pseudomonas syringae* pv. *tomato* DC3000 type III secretion effector genes reveal functional overlap among effectors. *PLoS Pathog,* 5**,** e1000388.

LANDGRAF, A., WEINGART, H., TSIAMIS, G. & BOCH, J. 2006. Different versions of *Pseudomonas syringae* pv. *tomato* DC3000 exist due to the activity of an effector transposon. *Molecular Plant Pathology,* 7**,** 355-364.

LARA-TEJERO, M., KATO, J., WAGNER, S., LIU, X. & GALAN, J. E. 2011. A sorting platform determines the order of protein secretion in bacterial type III systems. *Science,* 331**,** 1188-91.

LEBLANC, M.-A., FINK MORGAN, R., PERKINS THOMAS, T. & SOUSA MARCELO, C. 2021. Type III secretion system effector proteins are mechanically labile. *Proceedings of the National Academy of Sciences,* 118**,** e2019566118.

LEDUC, J. L. & ROBERTS, G. P. 2009. Cyclic di-GMP allosterically inhibits the CRP-like protein (Clp) of *Xanthomonas axonopodis* pv. *citri*. *J Bacteriol,* 191**,** 7121-2.

LEE, A. H.-Y., BASTEDO, D. P., YOUN, J.-Y., LO, T., MIDDLETON, M. A., KIREEVA, I., LEE, J. Y., SHARIFPOOR, S., BARYSHNIKOVA, A., ZHANG, J., WANG, P. W., PEISAJOVICH, S. G., CONSTANZO, M., ANDREWS, B. J., BOONE, C. M., DESVEAUX, D. & GUTTMAN, D. S. 2019. Identifying *Pseudomonas syringae* Type III Secreted Effector Function via a Yeast Genomic Screen. *G3: Genes, Genomes, Genetics,* 9**,** 535-547.

LEE, D., LAL, N. K., LIN, Z.-J. D., MA, S., LIU, J., CASTRO, B., TORUÑO, T., DINESH-KUMAR, S. P. & COAKER, G. 2020. Regulation of reactive oxygen species during plant immunity through phosphorylation and ubiquitination of RBOHD. *Nature Communications,* 11**,** 1838.

LEE, P.-C., ZMINA, S. E., STOPFORD, C. M., TOSKA, J. & RIETSCH, A. 2014. Control of type III secretion activity and substrate specificity by the cytoplasmic regulator PcrG. *Proceedings of the National Academy of Sciences,* 111**,** E2027-E2036.

LEE, V. T., MATEWISH, J. M., KESSLER, J. L., HYODO, M., HAYAKAWA, Y. & LORY, S. 2007. A cyclic-di-GMP receptor required for bacterial exopolysaccharide production. *Mol Microbiol,* 65**,** 1474-84.

LI, B., MENG, X., SHAN, L. & HE, P. 2016. Transcriptional Regulation of Pattern-Triggered Immunity in Plants. *Cell host & microbe,* 19**,** 641-650.

LI, J., WEN, J., LEASE, K. A., DOKE, J. T., TAX, F. E. & WALKER, J. C. 2002. BAK1, an *Arabidopsis* LRR receptor-like protein kinase, interacts with BRI1 and modulates brassinosteroid signaling. *Cell,* 110**,** 213-22.

LI, W., YADETA, K. A., ELMORE, J. M. & COAKER, G. 2013. The *Pseudomonas syringae* Effector HopQ1 Promotes Bacterial Virulence and Interacts with Tomato 14-3-3 Proteins in a Phosphorylation-Dependent Manner *Plant Physiology,* 161**,** 2062-2074.

LI, Z., LIU, H., DING, Z., YAN, J., YU, H., PAN, R., HU, J., GUAN, Y. & HUA, J. 2020. Low Temperature Enhances Plant Immunity via Salicylic Acid Pathway Genes That Are Repressed by Ethylene. *Plant Physiol,* 182**,** 626-639.

LIN CHUA, S., LIU, Y., LI, Y., JUN TING, H., KOHLI, G. S., CAI, Z., SUWANCHAIKASEM, P., KAU KIT GOH, K., PIN NG, S., TOLKER-NIELSEN, T., YANG, L. & GIVSKOV, M. 2017. Reduced Intracellular c-di-GMP Content Increases Expression of Quorum Sensing-Regulated Genes in *Pseudomonas aeruginosa*. *Frontiers in Cellular and Infection Microbiology,* 7**,** 451.

LIN, N.-C. & MARTIN, G. B. 2005. An avrPto/avrPtoB Mutant of *Pseudomonas syringae* pv. *tomato* DC3000 Does Not Elicit Pto-Mediated Resistance and Is Less Virulent on Tomato. *Molecular Plant-Microbe Interactions,* 18**,** 43-51.

LINDEBERG, M., STAVRINIDES, J., CHANG, J. H., ALFANO, J. R., COLLMER, A., DANGL, J. L., GREENBERG, J. T., MANSFIELD, J. W. & GUTTMAN, D. S. 2005. Proposed guidelines for a unified nomenclature and phylogenetic analysis of type III Hop effector proteins in the plant pathogen *Pseudomonas syringae*. *Mol Plant Microbe Interact,* 18**,** 275-82.

LINDOW, S. E., ARNY, D. C. & UPPER, C. D. 1982. Bacterial ice nucleation: a factor in frost injury to plants. *Plant physiology,* 70**,** 1084-1089.

LITTLE, R. H., GRENGA, L., SAALBACH, G., HOWAT, A. M., PFEILMEIER, S., TRAMPARI, E. & MALONE, J. G. 2016. Adaptive Remodeling of the Bacterial Proteome by Specific Ribosomal Modification Regulates *Pseudomonas* Infection and Niche Colonisation. *Plos Genetics,* 12.

LIU, L., SONBOL, F.-M., HUOT, B., GU, Y., WITHERS, J., MWIMBA, M., YAO, J., HE, S. Y. & DONG, X. 2016. Salicylic acid receptors activate jasmonic acid signalling through a non-canonical pathway to promote effector-triggered immunity. *Nature Communications,* 7**,** 13099.

LOHOU, D., LONJON, F., GENIN, S. & VAILLEAU, F. 2013. Type III chaperones & Co in bacterial plant pathogens: a set of specialized bodyguards mediating effector delivery. *Frontiers in Plant Science,* 4.

LOMBARDI, C., TOLCHARD, J., BOUILLOT, S., SIGNOR, L., GEBUS, C., LIEBL, D., FENEL, D., TEULON, J.-M., BROCK, J., HABENSTEIN, B., PELLEQUER, J.-L., FAUDRY, E., LOQUET, A., ATTRÉE, I., DESSEN, A. & JOB, V. 2019. Structural and Functional Characterization of the Type Three Secretion System (T3SS) Needle of *Pseudomonas aeruginosa*. *Frontiers in Microbiology,* 10.

LORENZ, C. & BÜTTNER, D. 2009. Functional Characterization of the Type III Secretion ATPase HrcN from the Plant Pathogen *Xanthomonas campestris* pv. *vesicatoria*. *Journal of Bacteriology,* 191**,** 1414-1428.

LU, Y. & YAO, J. 2018. Chloroplasts at the Crossroad of Photosynthesis, Pathogen Infection and Plant Defense. *International journal of molecular sciences,* 19**,** 3900.

MA, K. W., JIANG, S., HAWARA, E., LEE, D., PAN, S., COAKER, G., SONG, J. & MA, W. 2015. Two serine residues in *Pseudomonas syringae* effector HopZ1a are required for acetyltransferase activity and association with the host co-factor. *New Phytol,* 208**,** 1157-68.

MACLEAN, D. & STUDHOLME, D. J. 2010. A Boolean Model of the *Pseudomonas syringae* hrp Regulon Predicts a Tightly Regulated System. *PLOS ONE,* 5**,** e9101.

MAJEWSKI, D. D., WORRALL, L. J., HONG, C., ATKINSON, C. E., VUCKOVIC, M., WATANABE, N., YU, Z. & STRYNADKA, N. C. J. 2019. Cryo-EM structure of the homohexameric T3SS ATPase-central stalk complex reveals rotary ATPase-like asymmetry. *Nature Communications,* 10**,** 626.

MAKI-YONEKURA, S., MATSUOKA, R., YAMASHITA, Y., SHIMIZU, H., TANAKA, M., IWABUKI, F. & YONEKURA, K. 2018. Hexameric and pentameric complexes of the ExbBD energizer in the Ton system. *eLife,* 7**,** e35419.

MAKI, L. R., GALYAN, E. L., CHANGCHI.MM & CALDWELL, D. R. 1974. Ice Nucleation Induced by *Pseudomonas-syringae*. *Applied Microbiology,* 28**,** 456-459.

MALONE, J. G., JAEGER, T., SPANGLER, C., RITZ, D., SPANG, A., ARRIEUMERLOU, C., KAEVER, V., LANDMANN, R. & JENAL, U. 2010. YfiBNR Mediates Cyclic di-GMP Dependent Small Colony Variant Formation and Persistence in *Pseudomonas aeruginosa*. *PLOS Pathogens*, 6**,** e1000804.

MALONE, J. G., WILLIAMS, R., CHRISTEN, M., JENAL, U., SPIERS, A. J. & RAINEY, P. B. 2007. The structure-function relationship of WspR, a *Pseudomonas fluorescens* response regulator with a GGDEF output domain. *Microbiology*, 153**,** 980-94.

MANERA, K., KAMAL, F., BURKINSHAW, B. & DONG, T. G. 2021. Essential functions of chaperones and adaptors of protein secretion systems in Gram-negative bacteria. *The FEBS Journal*, n/a.

MARSDEN, A. E., INTILE, P. J., SCHULMEYER, K. H., SIMMONS-PATTERSON, E. R., URBANOWSKI, M. L., WOLFGANG, M. C. & YAHR, T. L. 2016. Vfr Directly Activates exsA Transcription To Regulate Expression of the *Pseudomonas aeruginosa* Type III Secretion System. *J Bacteriol*, 198**,** 1442-50.

MARTINEZ-GIL, M. & RAMOS, C. 2018. Role of Cyclic di-GMP in the Bacterial Virulence and Evasion of the Plant Immunity. *Curr Issues Mol Biol*, 25**,** 199-222.

MARTÍNEZ-ORTIZ, I. C., AHUMADA-MANUEL, C. L., HSUEH, B. Y., GUZMÁN, J., MORENO, S., COCOTL-YAÑEZ, M., WATERS, C. M., ZAMORANO-SÁNCHEZ, D., ESPÍN, G. & NÚÑEZ, C. 2020. Cyclic di-GMP-Mediated Regulation of Extracellular Mannuronan C-5 Epimerases Is Essential for Cyst Formation in *Azotobacter vinelandii*. *J Bacteriol*, 202.

MATSUYAMA, B. Y., KRASTEVA, P. V., BARAQUET, C., HARWOOD, C. S., SONDERMANN, H. & NAVARRO, M. V. 2016. Mechanistic insights into c-di-GMP-dependent control of the biofilm regulator FleQ from *Pseudomonas aeruginosa*. *Proc Natl Acad Sci U S A*, 113**,** E209-18.

MCCARTHY, R. R., VALENTINI, M. & FILLOUX, A. 2017. Contribution of Cyclic di-GMP in the Control of Type III and Type VI Secretion in *Pseudomonas aeruginosa*. *Methods Mol Biol*, 1657**,** 213-224.

MCCARTHY, R. R., YU, M., EILERS, K., WANG, Y.-C., LAI, E.-M. & FILLOUX, A. 2019. Cyclic di-GMP inactivates T6SS and T4SS activity in *Agrobacterium tumefaciens*. *Molecular Microbiology*, 112**,** 632-648.

MENNA, A., NGUYEN, D., GUTTMAN, D. S. & DESVEAUX, D. 2015. Elevated Temperature Differentially Influences Effector-Triggered Immunity Outputs in *Arabidopsis*. *Frontiers in plant science*, 6**,** 995-995.

MIKICIŃSKI, A., PUŁAWSKA, J., KAŁUŻNA, M., TRZCIŃSKI, P., WĄSIKOWSKI, A. & SOBICZEWSKI, P. 2020. Bacterial etiology of necrotic spots on leaves and shoots of grapevine (*Vitis vinifera L.*) in Poland. *European Journal of Plant Pathology*, 156**,** 913-924.

MILETIC, S., FAHRENKAMP, D., GOESSWEINER-MOHR, N., WALD, J., PANTEL, M., VESPER, O., KOTOV, V. & MARLOVITS, T. C. 2021. Substrate-engaged type III secretion system structures reveal gating mechanism for unfolded protein translocation. *Nature Communications*, 12**,** 1546.

MILLS, E., BARUCH, K., CHARPENTIER, X., KOBI, S. & ROSENSHINE, I. 2008. Real-time analysis of effector translocation by the type III secretion system of enteropathogenic *Escherichia coli*. *Cell Host Microbe*, 3**,** 104-13.

MINAMINO, T., KAZETANI, K., TAHARA, A., SUZUKI, H., FURUKAWA, Y., KIHARA, M. & NAMBA, K. 2006. Oligomerization of the bacterial flagellar ATPase FliI is controlled by its extreme N-terminal region. *J Mol Biol*, 360**,** 510-9.

MINE, A., SEYFFERTH, C., KRACHER, B., BERENS, M. L., BECKER, D. & TSUDA, K. 2018. The Defense Phytohormone Signaling Network Enables Rapid, High-Amplitude Transcriptional Reprogramming during Effector-Triggered Immunity. *The Plant Cell*, 30**,** 1199-1219.

MIRDITA, M., STEINEGGER, M. & SÖDING, J. 2019. MMseqs2 desktop and local web server app for fast, interactive sequence searches. *Bioinformatics*, 35**,** 2856-2858.

MORELLO, J. E. & COLLMER, A. 2009. *Pseudomonas syringae* HrpP Is a type III secretion substrate specificity switch domain protein that is translocated into plant cells but functions atypically for a substrate-switching protein. *J Bacteriol*, 191**,** 3120-31.

MOSCOSO, J. A., JAEGER, T., VALENTINI, M., HUI, K., JENAL, U. & FILLOUX, A. 2014. The diguanylate cyclase SadC is a central player in Gac/Rsm-mediated biofilm formation in *Pseudomonas aeruginosa*. *J Bacteriol,* 196**,** 4081-8.

MOSCOSO, J. A., MIKKELSEN, H., HEEB, S., WILLIAMS, P. & FILLOUX, A. 2011. The *Pseudomonas aeruginosa* sensor RetS switches type III and type VI secretion via c-di-GMP signalling. *Environ Microbiol,* 13**,** 3128-38.

MULLER, S. A., POZIDIS, C., STONE, R., MEESTERS, C., CHAMI, M., ENGEL, A., ECONOMOU, A. & STAHLBERG, H. 2006. Double hexameric ring assembly of the type III protein translocase ATPase HrcN. *Molecular Microbiology,* 61**,** 119-125.

MUNKVOLD, K. R., RUSSELL, A. B., KVITKO, B. H. & COLLMER, A. 2009. *Pseudomonas syringae* pv. *tomato* DC3000 type III effector HopAA1-1 functions redundantly with chlorosis-promoting factor PSPTO4723 to produce bacterial speck lesions in host tomato. *Mol Plant Microbe Interact,* 22**,** 1341-55.

NAITO, Y., MORIYAMA, K. & SAWA, T. 2017. Anti-PcrV Immunization for *Pseudomonas aeruginosa* Pneumonia in Cystic Fibrosis. *In:* SRIRAMULU, D. (ed.) *Progress in Understanding Cystic Fibrosis.* Rijeka: InTech.

NANS, A., KUDRYASHEV, M., SAIBIL, H. R. & HAYWARD, R. D. 2015. Structure of a bacterial type III secretion system in contact with a host membrane in situ. *Nature Communications,* 6.

NAVARRO, M. V. A. S., DE, N., BAE, N., WANG, Q. & SONDERMANN, H. 2009. Structural Analysis of the GGDEF-EAL Domain-Containing c-di-GMP Receptor FimX. *Structure,* 17**,** 1104-1116.

NESPER, J., REINDERS, A., GLATTER, T., SCHMIDT, A. & JENAL, U. 2012. A novel capture compound for the identification and analysis of cyclic di-GMP binding proteins. *J Proteomics,* 75**,** 4874-8.

NGOU, B. P. M., AHN, H.-K., DING, P. & JONES, J. D. G. 2021. Mutual potentiation of plant immunity by cell-surface and intracellular receptors. *Nature,* 592**,** 110-115.

NICAISE, V., JOE, A., JEONG, B.-R., KORNELI, C., BOUTROT, F., WESTEDT, I., STAIGER, D., ALFANO, J. R. & ZIPFEL, C. 2013. *Pseudomonas* HopU1 modulates plant immune receptor levels by blocking the interaction of their mRNAs with GRP7. *The EMBO journal,* 32**,** 701-712.

NICAISE, V., ROUX, M. & ZIPFEL, C. 2009. Recent Advances in PAMP-Triggered Immunity against Bacteria: Pattern Recognition Receptors Watch over and Raise the Alarm. *Plant Physiology,* 150**,** 1638-1647.

NIEMANN, G. S., BROWN, R. N., MUSHAMIRI, I. T., NGUYEN, N. T., TAIWO, R., STUFKENS, A., SMITH, R. D., ADKINS, J. N., MCDERMOTT, J. E. & HEFFRON, F. 2013. RNA Type III Secretion Signals That Require Hfq. *Journal of Bacteriology,* 195**,** 2119.

NIKEL, P. I., MARTINEZ-GARCIA, E. & DE LORENZO, V. 2014. Biotechnological domestication of *pseudomonads* using synthetic biology. *Nature Reviews Microbiology,* 12**,** 368-379.

NOMURA, K., DEBROY, S., LEE, Y. H., PUMPLIN, N., JONES, J. & HE, S. Y. 2006. A bacterial virulence protein suppresses host innate immunity to cause plant disease. *Science,* 313**,** 220-3.

NOMURA, K., MECEY, C., LEE, Y.-N., IMBODEN, L. A., CHANG, J. H. & HE, S. Y. 2011. Effector-triggered immunity blocks pathogen degradation of an immunity-associated vesicle traffic regulator in *Arabidopsis*. *Proceedings of the National Academy of Sciences,* 108**,** 10774.

NOTTI, R. Q. & STEBBINS, C. E. 2016. The Structure and Function of Type III Secretion Systems. *Microbiology spectrum,* 4**,** 10.1128/microbiolspec.VMBF-0004-2015.

O'MALLEY, M. R. & ANDERSON, J. C. 2021. Regulation of the *Pseudomonas syringae* Type III Secretion System by Host Environment Signals. *Microorganisms,* 9**,** 1227.

OH, H. S., KVITKO, B. H., MORELLO, J. E. & COLLMER, A. 2007. *Pseudomonas syringae* lytic transglycosylases coregulated with the type III secretion system contribute to the translocation of effector proteins into plant cells. *J Bacteriol,* 189**,** 8277-89.

ORR, M. W., DONALDSON, G. P., SEVERIN, G. B., WANG, J., SINTIM, H. O., WATERS, C. M. & LEE, V. T. 2015. Oligoribonuclease is the primary degradative enzyme for pGpG in *Pseudomonas*

aeruginosa that is required for cyclic-di-GMP turnover. *Proc Natl Acad Sci U S A,* 112**,** E5048-57.

ORR, M. W. & LEE, V. T. 2017. Differential Radial Capillary Action of Ligand Assay (DRaCALA) for High-Throughput Detection of Protein-Metabolite Interactions in Bacteria. *Methods Mol Biol,* 1535**,** 25-41.

PALMER, I. 2018. *Screening of Novel Active Salicylic Acid Analogs and Identification of a Bacterial Effector Targeting Key Proteins Involved in Salicylic Acid-Mediated Defense.* Master's Thesis, University of South Carolina - Columbia.

PANCHAL, S., ROY, D., CHITRAKAR, R., PRICE, L., BREITBACH, Z. S., ARMSTRONG, D. W. & MELOTTO, M. 2016. Coronatine Facilitates *Pseudomonas syringae* Infection of *Arabidopsis* Leaves at Night. *Frontiers in Plant Science,* 7**,** 880.

PANIJEL, M., CHALUPOWICZ, L., SESSA, G., MANULIS-SASSON, S. & BARASH, I. 2013. Global Regulatory Networks Control the Hrp Regulon of the Gall-Forming Bacterium *Pantoea agglomerans* pv. *gypsophilae*. *Molecular Plant-Microbe Interactions®,* 26**,** 1031-1043.

PASTOR, A., CHABERT, J., LOUWAGIE, M., GARIN, J. & ATTREE, I. 2005. PscF is a major component of the *Pseudomonas aeruginosa* type III secretion needle. *FEMS Microbiol Lett,* 253**,** 95-101.

PÉREZ-MENDOZA, D., ARAGÓN, I. M., PRADA-RAMÍREZ, H. A., ROMERO-JIMÉNEZ, L., RAMOS, C., GALLEGOS, M.-T. & SANJUÁN, J. 2014. Responses to Elevated c-di-GMP Levels in Mutualistic and Pathogenic Plant-Interacting Bacteria. *PLOS ONE,* 9**,** e91645.

PETNICKI-OCWIEJA, T., VAN DIJK, K. & ALFANO, J. R. 2005. The hrpK operon of *Pseudomonas syringae* pv. *tomato* DC3000 encodes two proteins secreted by the type III (Hrp) protein secretion system: HopB1 and HrpK, a putative type III translocator. *Journal of bacteriology,* 187**,** 649-663.

PETTERSEN, E. F., GODDARD, T. D., HUANG, C. C., COUCH, G. S., GREENBLATT, D. M., MENG, E. C. & FERRIN, T. E. 2004. UCSF Chimera--a visualization system for exploratory research and analysis. *J Comput Chem,* 25**,** 1605-12.

PETTERSSON, J., NORDFELTH, R., DUBININA, E., BERGMAN, T., GUSTAFSSON, M., MAGNUSSON, K. E. & WOLF-WATZ, H. 1996. Modulation of Virulence Factor Expression by Pathogen Target Cell Contact. *Science,* 273**,** 1231-1233.

PFEILMEIER, S., SAUR, I. M. L., RATHJEN, J. P., ZIPFEL, C. & MALONE, J. G. 2016. High levels of cyclic-di-GMP in plant-associated *Pseudomonas* correlate with evasion of plant immunity. *Molecular Plant Pathology,* 17**,** 521-531.

PILLA, S. K., WOODCOCK, S. D., PFEILMEIER, S., BORNEMANN, S., ZIPFEL, C. & MALONE, J. G. 2021. *Pseudomonas syringae* addresses distinct environmental challenges during plant infection through the coordinated deployment of polysaccharides. *bioRxiv*, 2021.06.18.449010.

POZIDIS, C., CHALKIADAKI, A., GOMEZ-SERRANO, A., STAHLBERG, H., BROWN, I., TAMPAKAKI, A. P., LUSTIG, A., SIANIDIS, G., POLITOU, A. S., ENGEL, A., PANOPOULOS, N. J., MANSFIELD, J., PUGSLEY, A. P., KARAMANOU, S. & ECONOMOU, A. 2003. Type III protein translocase - HrcN is a peripheral membrane ATPase that is activated by oligomerization. *Journal of Biological Chemistry,* 278**,** 25816-25824.

PRITCHARD, L. & BIRCH, P. R. J. 2014. The zigzag model of plant–microbe interactions: is it time to move on? *Molecular Plant Pathology,* 15**,** 865-870.

PUBCHEM. 2018. *Compound Database; CID=6323195* [Online]. National Center for Biotechnology Information. Available: https://pubchem.ncbi.nlm.nih.gov/compound/6323195 [Accessed 22 March 2018].

PUHAR, A. & SANSONETTI, P. J. 2014. Type III secretion system. *Curr Biol,* 24**,** R784-91.

QUINAUD, M., CHABERT, J., FAUDRY, E., NEUMANN, E., LEMAIRE, D., PASTOR, A., ELSEN, S., DESSEN, A. & ATTREE, I. 2005. The PscE-PscF-PscG complex controls type III secretion needle biogenesis in *Pseudomonas aeruginosa*. *J Biol Chem,* 280**,** 36293-300.

RADHAKRISHNAN, G. K. & SPLITTER, G. A. 2012. Modulation of host microtubule dynamics by pathogenic bacteria. *Biomolecular concepts,* 3**,** 571-580.

RADICS, J., KÖNIGSMAIER, L. & MARLOVITS, T. C. 2013. Structure of a pathogenic type 3 secretion system in action. *Nature Structural &Amp; Molecular Biology,* 21**,** 82.

RAHMATELAHI, H., EL-MATBOULI, M. & MENANTEAU-LEDOUBLE, S. 2021. Delivering the pain: an overview of the type III secretion system with special consideration for aquatic pathogens. *Veterinary Research,* 52**,** 146.

RASMUSSEN, M., ROUX, M., PETERSEN, M. & MUNDY, J. 2012. MAP Kinase Cascades in *Arabidopsis* Innate Immunity. *Frontiers in Plant Science,* 3**,** 169.

RATHINAVELAN, T., ZHANG, L., PICKING, W. L., WEIS, D. D., DE GUZMAN, R. N. & IM, W. 2010. A Repulsive Electrostatic Mechanism for Protein Export through the Type III Secretion Apparatus. *Biophysical Journal,* 98**,** 452-461.

REZZONICO, F., DEFAGO, G. & MOENNE-LOCCOZ, Y. 2004. Comparison of ATPase-encoding type III secretion system hrcN genes in biocontrol fluorescent *pseudomonads* and in phytopathogenic proteobacteria. *Applied and Environmental Microbiology,* 70**,** 5119-5131.

RÍO-ÁLVAREZ, I., RODRÍGUEZ-HERVA, J. J., MARTÍNEZ, P. M., GONZÁLEZ-MELENDI, P., GARCÍA-CASADO, G., RODRÍGUEZ-PALENZUELA, P. & LÓPEZ-SOLANILLA, E. 2014. Light regulates motility, attachment and virulence in the plant pathogen *Pseudomonas syringae* pv *tomato* DC3000. *Environ Microbiol,* 16**,** 2072-85.

RIORDAN, K. E., SORG, J. A., BERUBE, B. J. & SCHNEEWIND, O. 2008. Impassable YscP substrates and their impact on the *Yersinia enterocolitica* type III secretion pathway. *Journal of bacteriology,* 190**,** 6204-6216.

RODRÍGUEZ-HERVA, J. J., GONZÁLEZ-MELENDI, P., CUARTAS-LANZA, R., ANTÚNEZ-LAMAS, M., RÍO-ALVAREZ, I., LI, Z., LÓPEZ-TORREJÓN, G., DÍAZ, I., DEL POZO, J. C., CHAKRAVARTHY, S., COLLMER, A., RODRÍGUEZ-PALENZUELA, P. & LÓPEZ-SOLANILLA, E. 2012. A bacterial cysteine protease effector protein interferes with photosynthesis to suppress plant innate immune responses. *Cell Microbiol,* 14**,** 669-81.

ROELOFS, K. G., JONES, C. J., HELMAN, S. R., SHANG, X., ORR, M. W., GOODSON, J. R., GALPERIN, M. Y., YILDIZ, F. H. & LEE, V. T. 2015. Systematic Identification of Cyclic-di-GMP Binding Proteins in *Vibrio cholerae* Reveals a Novel Class of Cyclic-di-GMP-Binding ATPases Associated with Type II Secretion Systems. *PLoS pathogens,* 11**,** e1005232-e1005232.

ROELOFS, K. G., WANG, J., SINTIM, H. O. & LEE, V. T. 2011. Differential radial capillary action of ligand assay for high-throughput detection of protein-metabolite interactions. *Proc Natl Acad Sci U S A,* 108**,** 15528-33.

ROETERS, S. J., GOLBEK, T. W., BREGNHØJ, M., DRACE, T., ALAMDARI, S., ROSEBOOM, W., KRAMER, G., ŠANTL-TEMKIV, T., FINSTER, K., PFAENDTNER, J., WOUTERSEN, S., BOESEN, T. & WEIDNER, T. 2021. Ice-nucleating proteins are activated by low temperatures to control the structure of interfacial water. *Nature Communications,* 12**,** 1183.

ROINE, E., WEI, W., YUAN, J., NURMIAHO-LASSILA, E. L., KALKKINEN, N., ROMANTSCHUK, M. & HE, S. Y. 1997. Hrp pilus: an hrp-dependent bacterial surface appendage produced by *Pseudomonas syringae* pv. *tomato* DC3000. *Proc Natl Acad Sci U S A,* 94**,** 3459-64.

ROMANTSCHUK, M., ROINE, E. & BJÖRKLÖF, K. 1997. Attachment of *Pseudomonas* syringae to Plant Surfaces. *In:* RUDOLPH, K., BURR, T. J., MANSFIELD, J. W., STEAD, D., VIVIAN, A. & VON KIETZELL, J. (eds.) *Pseudomonas Syringae Pathovars and Related Pathogens.* Dordrecht: Springer Netherlands.

ROMANTSCHUK, M., ROINE, E., OJANEN, T., VAN DOORN, J., LOUHELAINEN, J., NURMIAHO-LASSILA, E.-L. & HAAHTELA, K. 1994. Fimbria (pilus) mediated attachment of *Pseudomonas syringae, Erwinia rhapontici* and *Xanthomonas campestris* to plant surfaces. *In:* KADO, C. I. & CROSA, J. H. (eds.) *Molecular Mechanisms of Bacterial Virulence.* Dordrecht: Springer Netherlands.

RÖMLING, U., GALPERIN, M. Y. & GOMELSKY, M. 2013. Cyclic di-GMP: the first 25 years of a universal bacterial second messenger. *Microbiology and molecular biology reviews : MMBR,* 77**,** 1-52.

ROSS, P., WEINHOUSE, H., ALONI, Y., MICHAELI, D., WEINBERGER-OHANA, P., MAYER, R., BRAUN, S., DE VROOM, E., VAN DER MAREL, G. A., VAN BOOM, J. H. & BENZIMAN, M. 1987. Regulation of cellulose synthesis in *Acetobacter xylinum* by cyclic diguanylic acid. *Nature,* 325**,** 279-81.

SAMUDRALA, R., HEFFRON, F. & MCDERMOTT, J. E. 2009. Accurate prediction of secreted substrates and identification of a conserved putative secretion signal for type III secretion systems. *PLoS pathogens,* 5**,** e1000375-e1000375.

SARENKO, O., KLAUCK, G., WILKE, F. M., PFIFFER, V., RICHTER, A. M., HERBST, S., KAEVER, V. & HENGGE, R. 2017. More than Enzymes That Make or Break Cyclic Di-GMP-Local Signaling in the Interactome of GGDEF/EAL Domain Proteins of *Escherichia coli. MBio,* 8.

SATO, H. & FRANK, D. W. 2011. Multi-Functional Characteristics of the *Pseudomonas aeruginosa* Type III Needle-Tip Protein, PcrV; Comparison to Orthologs in other Gram-negative Bacteria. *Frontiers in Microbiology,* 2**,** 142.

SAWA, T. 2014. The molecular mechanism of acute lung injury caused by *Pseudomonas aeruginosa*: from bacterial pathogenesis to host response. *Journal of Intensive Care,* 2**,** 10.

SCANDALIOS, J. G. 1993. Oxygen Stress and Superoxide Dismutases. *Plant physiology,* 101**,** 7-12.

SCHECHTER, L. M., ROBERTS, K. A., JAMIR, Y., ALFANO, J. R. & COLLMER, A. 2004. *Pseudomonas syringae* type III secretion system targeting signals and novel effectors studied with a Cya translocation reporter. *J Bacteriol,* 186**,** 543-55.

SCHECHTER, L. M., VENCATO, M., JORDAN, K. L., SCHNEIDER, S. E., SCHNEIDER, D. J. & COLLMER, A. 2006. Multiple approaches to a complete inventory of *Pseudomonas syringae* pv. *tomato* DC3000 type III secretion system effector proteins. *Mol Plant Microbe Interact,* 19**,** 1180-92.

SCHMIDT, M. A., BALSANELLI, E., FAORO, H., CRUZ, L. M., WASSEM, R., DE BAURA, V. A., WEISS, V., YATES, M. G., MADEIRA, H. M. F., PEREIRA-FERRARI, L., FUNGARO, M. H. P., DE PAULA, F. M., PEREIRA, L. F. P., VIEIRA, L. G. E., OLIVARES, F. L., PEDROSA, F. O., DE SOUZA, E. M. & MONTEIRO, R. A. 2012. The type III secretion system is necessary for the development of a pathogenic and endophytic interaction between *Herbaspirillum rubrisubalbicans* and *Poaceae*. *BMC Microbiology,* 12**,** 98-98.

SCHOEHN, G., DI GUILMI, A. M., LEMAIRE, D., ATTREE, I., WEISSENHORN, W. & DESSEN, A. 2003. Oligomerization of type III secretion proteins PopB and PopD precedes pore formation in *Pseudomonas*. *The EMBO journal,* 22**,** 4957-4967.

SCHWESSINGER, B., ROUX, M., KADOTA, Y., NTOUKAKIS, V., SKLENAR, J., JONES, A. & ZIPFEL, C. 2011. Phosphorylation-dependent differential regulation of plant growth, cell death, and innate immunity by the regulatory receptor-like kinase BAK1. *PLoS Genet,* 7**,** e1002046.

SHANG, G., ZHANG, C., CHEN, Z. J., BAI, X.-C. & ZHANG, X. 2019. Cryo-EM structures of STING reveal its mechanism of activation by cyclic GMP-AMP. *Nature,* 567**,** 389-393.

SHARMA, M. & BHATT, D. 2015. The circadian clock and defence signalling in plants. *Molecular plant pathology,* 16**,** 210-218.

SHARMA, P., JHA, A. B., DUBEY, R. S. & PESSARAKLI, M. 2012. Reactive Oxygen Species, Oxidative Damage, and Antioxidative Defense Mechanism in Plants under Stressful Conditions. *Journal of Botany,* 2012**,** 217037.

SHAULOV, L., GERSHBERG, J., DENG, W., FINLAY, B. B. & SAL-MAN, N. 2017. The Ruler Protein EscP of the Enteropathogenic *Escherichia coli* Type III Secretion System Is Involved in Calcium Sensing and Secretion Hierarchy Regulation by Interacting with the Gatekeeper Protein SepL. *mBio,* 8**,** e01733-16.

SHIMONO, M., LU, Y.-J., PORTER, K., KVITKO, B. H., HENTY-RIDILLA, J., CREASON, A., HE, S. Y., CHANG, J. H., STAIGER, C. J. & DAY, B. 2016. The *Pseudomonas syringae* Type III Effector HopG1 Induces Actin Remodeling to Promote Symptom Development and Susceptibility during Infection. *Plant physiology,* 171**,** 2239-2255.

SIMM, R., MORR, M., KADER, A., NIMTZ, M. & ROMLING, U. 2004. GGDEF and EAL domains inversely regulate cyclic di-GMP levels and transition from sessility to motility. *Mol Microbiol,* 53**,** 1123-34.

SOLANKI, V., KAPOOR, S. & THAKUR, K. G. 2018. Structural insights into the mechanism of Type IVa pilus extension and retraction ATPase motors. *The FEBS Journal,* 285**,** 3402-3421.

SRIVASTAVA, D., HARRIS, R. C. & WATERS, C. M. 2011. Integration of cyclic di-GMP and quorum sensing in the control of vpsT and aphA in *Vibrio cholerae*. *J Bacteriol,* 193**,** 6331-41.

STUDHOLME, D. J., IBANEZ, S. G., MACLEAN, D., DANGL, J. L., CHANG, J. H. & RATHJEN, J. P. 2009. A draft genome sequence and functional screen reveals the repertoire of type III secreted proteins of *Pseudomonas syringae* pathovar *tabaci* 11528. *BMC Genomics,* 10**,** 395.

SWIETNICKI, W., CARMANY, D., RETFORD, M., GUELTA, M., DORSEY, R., BOZUE, J., LEE, M. S. & OLSON, M. A. 2011. Identification of Small-Molecule Inhibitors of *Yersinia pestis* Type III Secretion System YscN ATPase. *PLOS ONE,* 6**,** e19716.

TACHIYAMA, S., SKAAR, R., CHANG, Y., CARROLL, B. L., MUTHURAMALINGAM, M., WHITTIER, S. K., BARTA, M. L., PICKING, W. L., LIU, J. & PICKING, W. D. 2021. Composition and Biophysical Properties of the Sorting Platform Pods in the *Shigella* Type III Secretion System. *Frontiers in Cellular and Infection Microbiology,* 11.

TAKAYA, A., TAKEDA, H., TASHIRO, S., KAWASHIMA, H. & YAMAMOTO, T. 2019. Chaperone-mediated secretion switching from early to middle substrates in the type III secretion system encoded by *Salmonella* pathogenicity island 2. *Journal of Biological Chemistry,* 294**,** jbc.RA118.005072.

TAMPAKAKI, A. P., FADOULOGLOU, V. E., GAZI, A. D., PANOPOULOS, N. J. & KOKKINIDIS, M. 2004. Conserved features of type III secretion. *Cell Microbiol,* 6**,** 805-16.

TIAN, F. 2010. *Pseudomonas syringae type III secretion system: Secretion signals and putative docking stations.* Ph.D., The University of Nebraska - Lincoln.

TOUM, L., TORRES, P. S., GALLEGO, S. M., BENAVÍDES, M. P., VOJNOV, A. A. & GUDESBLAT, G. E. 2016. Coronatine Inhibits Stomatal Closure through Guard Cell-Specific Inhibition of NADPH Oxidase-Dependent ROS Production. *Frontiers in Plant Science,* 7**,** 1851.

TRAMPARI, E. 2016. *Allosteric control of type III secretion systems by the second message cyclic-di-GMP.* PhD, University of East Anglia.

TRAMPARI, E., STEVENSON, C. E. M., LITTLE, R. H., WILHELM, T., LAWSON, D. M. & MALONE, J. G. 2015. Bacterial Rotary Export ATPases Are Allosterically Regulated by the Nucleotide Second Messenger Cyclic-di-GMP. *Journal of Biological Chemistry,* 290**,** 24470-24483.

UPADHYAYA, N. M., MAGO, R., STASKAWICZ, B. J., AYLIFFE, M. A., ELLIS, J. G. & DODDS, P. N. 2014. A bacterial type III secretion assay for delivery of fungal effector proteins into wheat. *Mol Plant Microbe Interact,* 27**,** 255-64.

UPPALAPATI, S. R., ISHIGA, Y., WANGDI, T., URBANCZYK-WOCHNIAK, E., ISHIGA, T., MYSORE, K. S. & BENDER, C. L. 2008. Pathogenicity of *Pseudomonas syringae* pv. *tomato* on tomato seedlings: phenotypic and gene expression analyses of the virulence function of coronatine. *Mol Plant Microbe Interact,* 21**,** 383-95.

VALENTINI, M. & FILLOUX, A. 2016. Biofilms and Cyclic di-GMP (c-di-GMP) Signaling: Lessons from *Pseudomonas aeruginosa* and Other Bacteria. *J Biol Chem,* 291**,** 12547-55.

VAN DER BIEZEN, E. A. & JONES, J. D. G. 1998. Plant disease-resistance proteins and the gene-for-gene concept. *Trends in Biochemical Sciences,* 23**,** 454-456.

VAN DER WAL, A., TECON, R., KREFT, J.-U., MOOIJ, W. M. & LEVEAU, J. H. J. 2013. Explaining Bacterial Dispersion on Leaf Surfaces with an Individual-Based Model (PHYLLOSIM). *PLOS ONE,* 8**,** e75633.

VANNESTE, J. L. 2017. The Scientific, Economic, and Social Impacts of the New Zealand Outbreak of Bacterial Canker of Kiwifruit (*Pseudomonas syringae* pv. *actinidiae*). *Annu Rev Phytopathol,* 55**,** 377-399.

VINATZER, B. A., TEITZEL, G. M., LEE, M.-W., JELENSKA, J., HOTTON, S., FAIRFAX, K., JENRETTE, J. & GREENBERG, J. T. 2006. The type III effector repertoire of *Pseudomonas syringae* pv. *syringae* B728a and its role in survival and disease on host and non-host plants. *Molecular Microbiology,* 62**,** 26-44.

WAITE, C., SCHUMACHER, J., JOVANOVIC, M., BENNETT, M. & BUCK, M. 2017. Negative Autogenous Control of the Master Type III Secretion System Regulator HrpL in *Pseudomonas syringae*. *mBio,* 8.

WALKER, J. E., SARASTE, M., RUNSWICK, M. J. & GAY, N. J. 1982. Distantly related sequences in the alpha- and beta-subunits of ATP synthase, myosin, kinases and other ATP-requiring enzymes and a common nucleotide binding fold. *The EMBO journal,* 1**,** 945-951.

WANG, J., SHAO, X., ZHANG, Y., ZHU, Y., YANG, P., YUAN, J., WANG, T., YIN, C., WANG, W., CHEN, S., LIANG, H. & DENG, X. 2018. HrpS Is a Global Regulator on Type III Secretion System (T3SS) and Non-T3SS Genes in *Pseudomonas savastanoi* pv. *phaseolicola*. *Molecular Plant-Microbe Interactions,* 31**,** 1232-1243.

WANG, W., LIU, N., GAO, C., RUI, L. & TANG, D. 2019. The *Pseudomonas Syringae* Effector AvrPtoB Associates With and Ubiquitinates Arabidopsis Exocyst Subunit EXO70B1. *Frontiers in Plant Science,* 10**,** 1027.

WANG, Y., LI, J., HOU, S., WANG, X., LI, Y., REN, D., CHEN, S., TANG, X. & ZHOU, J. M. 2010. A *Pseudomonas syringae* ADP-ribosyltransferase inhibits *Arabidopsis* mitogen-activated protein kinase kinases. *Plant Cell,* 22**,** 2033-44.

WANG, Y. C., CHIN, K. H., TU, Z. L., HE, J., JONES, C. J., SANCHEZ, D. Z., YILDIZ, F. H., GALPERIN, M. Y. & CHOU, S. H. 2016. Nucleotide binding by the widespread high-affinity cyclic di-GMP receptor MshEN domain. *Nat Commun,* 7**,** 12481.

WASHINGTON, E. J. 2013. *Characterization of the Role of Pseudomonas syringae Type III Effector HopAF1 in Virulence.* Dissertation, University of North Carolina at Chapel Hill.

WASHINGTON, E. J., MUKHTAR, M. S., FINKEL, O. M., WAN, L., BANFIELD, M. J., KIEBER, J. J. & DANGL, J. L. 2016. *Pseudomonas syringae* type III effector HopAF1 suppresses plant immunity by targeting methionine recycling to block ethylene induction. *Proc Natl Acad Sci U S A,* 113**,** E3577-86.

WEBER, E. & KOEBNIK, R. 2006. Positive selection of the Hrp pilin HrpE of the plant pathogen *Xanthomonas*. *J Bacteriol,* 188**,** 1405-10.

WEI, C.-F., KVITKO, B. H., SHIMIZU, R., CRABILL, E., ALFANO, J. R., LIN, N.-C., MARTIN, G. B., HUANG, H.-C. & COLLMER, A. 2007. A *Pseudomonas syringae* pv. *tomato* DC3000 mutant lacking the type III effector HopQ1-1 is able to cause disease in the model plant *Nicotiana benthamiana*. *The Plant Journal,* 51**,** 32-46.

WEI, H.-L., CHAKRAVARTHY, S., MATHIEU, J., HELMANN, T. C., STODGHILL, P., SWINGLE, B., MARTIN, G. B. & COLLMER, A. 2015. *Pseudomonas syringae* pv. *tomato* DC3000 Type III Secretion Effector Polymutants Reveal an Interplay between HopAD1 and AvrPtoB. *Cell host & microbe,* 17**,** 752-762.

WEI, H.-L. & COLLMER, A. 2018. Defining essential processes in plant pathogenesis with *Pseudomonas syringae* pv. *tomato* DC3000 disarmed polymutants and a subset of key type III effectors. *Molecular plant pathology,* 19**,** 1779-1794.

WEI, H.-L., ZHANG, W. & COLLMER, A. 2018. Modular Study of the Type III Effector Repertoire in *Pseudomonas syringae* pv. *tomato* DC3000 Reveals a Matrix of Effector Interplay in Pathogenesis. *Cell Reports,* 23**,** 1630-1638.

WHALEN, M. C., INNES, R. W., BENT, A. F. & STASKAWICZ, B. J. 1991. Identification of *Pseudomonas Syringae* Pathogens of *Arabidopsis* and A Bacterial Locus Determining Avirulence on Both *Arabidopsis* and Soybean *Plant Cell,* 3**,** 49-59.

WHITNEY, J. C., WHITFIELD, G. B., MARMONT, L. S., YIP, P., NECULAI, A. M., LOBSANOV, Y. D., ROBINSON, H., OHMAN, D. E. & HOWELL, P. L. 2015. Dimeric c-di-GMP is required for post-translational regulation of alginate production in *Pseudomonas aeruginosa*. *J Biol Chem,* 290**,** 12451-62.

WIMMI, S., FLECK, M., HELBIG, C., BRIANCEAU, C., LANGENFELD, K., SZYMANSKI, W., ANGELIDOU, G., GLATTER, T. & DIEPOLD, A. 2022. Pilotins are mobile T3SS components involved in assembly and substrate specificity of the bacterial type III secretion system. bioRxiv.

WINNEN, B., SCHLUMBERGER, M. C., STURM, A., SCHÜPBACH, K., SIEBENMANN, S., JENNY, P. & HARDT, W.-D. 2008. Hierarchical Effector Protein Transport by the *Salmonella Typhimurium* SPI-1 Type III Secretion System. *PLOS ONE,* 3**,** e2178.

WINSOR, G. L., GRIFFITHS, E. J., LO, R., DHILLON, B. K., SHAY, J. A. & BRINKMAN, F. S. 2016. Enhanced annotations and features for comparing thousands of *Pseudomonas genomes* in the *Pseudomonas* genome database. *Nucleic Acids Res,* 44**,** D646-53.

WOLFE, A. & VISICK, K. 2008. Get the Message Out: Cyclic-Di-GMP Regulates Multiple Levels of Flagellum-Based Motility. *Journal of Bacteriology,* 190**,** 463-475.

WU, C.-H., ABD-EL-HALIEM, A., BOZKURT, T. O., BELHAJ, K., TERAUCHI, R., VOSSEN, J. H. & KAMOUN, S. 2017. NLR network mediates immunity to diverse plant pathogens. *Proceedings of the National Academy of Sciences of the United States of America,* 114**,** 8113-8118.

WU, W., BADRANE, H., ARORA, S., BAKER, H. V. & JIN, S. 2004. MucA-Mediated Coordination of Type III Secretion and Alginate Synthesis in *Pseudomonas aeruginosa*. *Journal of Bacteriology,* 186**,** 7575-7585.

WU, W. & JIN, S. 2005. PtrB of *Pseudomonas aeruginosa* Suppresses the Type III Secretion System under the Stress of DNA Damage. *Journal of Bacteriology,* 187**,** 6058-6068.

XIANG, T., ZONG, N., ZOU, Y., WU, Y., ZHANG, J., XING, W., LI, Y., TANG, X., ZHU, L., CHAI, J. & ZHOU, J. M. 2008. *Pseudomonas syringae* effector AvrPto blocks innate immunity by targeting receptor kinases. *Curr Biol,* 18**,** 74-80.

XIN, X.-F., NOMURA, K., AUNG, K., VELÁSQUEZ, A. C., YAO, J., BOUTROT, F., CHANG, J. H., ZIPFEL, C. & HE, S. Y. 2016. Bacteria establish an aqueous living space in plants crucial for virulence. *Nature,* 539**,** 524-529.

XIN, X.-F., NOMURA, K., DING, X., CHEN, X., WANG, K., AUNG, K., URIBE, F., ROSA, B., YAO, J., CHEN, J. & HE, S. Y. 2015. *Pseudomonas syringae* effector AvrE localizes to the host plasma membrane and down-regulates the expression of the NDR/HIN1-like 13 gene required for antibacterial immunity in *Arabidopsis*. *Plant Physiology*.

XIN, X. F. & HE, S. Y. 2013. *Pseudomonas syringae* pv. *tomato* DC3000: a model pathogen for probing disease susceptibility and hormone signaling in plants. *Annu Rev Phytopathol,* 51**,** 473-98.

XIN, X. F., KVITKO, B. & HE, S. Y. 2018. *Pseudomonas syringae*: what it takes to be a pathogen. *Nat Rev Microbiol,* 16**,** 316-328.

XU, L., VENKATARAMANI, P., DING, Y., LIU, Y., DENG, Y., YONG, G. L., XIN, L., YE, R., ZHANG, L., YANG, L. & LIANG, Z. X. 2016. A Cyclic di-GMP-binding Adaptor Protein Interacts with Histidine Kinase to Regulate Two-component Signaling. *J Biol Chem,* 291**,** 16112-23.

YI, X., YAMAZAKI, A., BIDDLE, E., ZENG, Q. & YANG, C.-H. 2010. Genetic analysis of two phosphodiesterases reveals cyclic diguanylate regulation of virulence factors in *Dickeya dadantii*. *Molecular Microbiology,* 77**,** 787-800.

YOSHIDA, Y., MIKI, T., ONO, S., HANEDA, T., ITO, M. & OKADA, N. 2014. Functional Characterization of the Type III Secretion ATPase SsaN Encoded by *Salmonella* Pathogenicity Island 2. *PLOS ONE,* 9**,** e94347.

YU, D., SONG, W., TAN, E. Y. J., LIU, L., CAO, Y., JIRSCHITZKA, J., LI, E., LOGEMANN, E., XU, C., HUANG, S., JIA, A., CHANG, X., HAN, Z., WU, B., SCHULZE-LEFERT, P. & CHAI, J. 2021. TIR domains of plant immune receptors are 2',3'-cAMP/cGMP synthetases mediating cell death. bioRxiv.

YU, J., PEÑALOZA-VÁZQUEZ, A., CHAKRABARTY, A. M. & BENDER, C. L. 1999. Involvement of the exopolysaccharide alginate in the virulence and epiphytic fitness of *Pseudomonas syringae* pv. *syringae*. *Molecular Microbiology,* 33**,** 712-720.

YUAN, J. & HE, S. Y. 1996. The *Pseudomonas syringae* Hrp regulation and secretion system controls the production and secretion of multiple extracellular proteins. *J Bacteriol,* 178**,** 6399-402.

YUAN, M., JIANG, Z., BI, G., NOMURA, K., LIU, M., WANG, Y., CAI, B., ZHOU, J.-M., HE, S. Y. & XIN, X.-F. 2021. Pattern-recognition receptors are required for NLR-mediated plant immunity. *Nature,* 592**,** 105-109.

YUAN, X., KHOKHANI, D., WU, X., YANG, F., BIENER, G., KOESTLER, B. J., RAICU, V., HE, C., WATERS, C. M., SUNDIN, G. W., TIAN, F. & YANG, C. H. 2015. Cross-talk between a regulatory small RNA, cyclic-di-GMP signalling and flagellar regulator FlhDC for virulence and bacterial behaviours. *Environ Microbiol,* 17**,** 4745-63.

YUAN, X., TIAN, F., HE, C., SEVERIN, G. B., WATERS, C. M., ZENG, Q., LIU, F. & YANG, C.-H. 2018. The diguanylate cyclase GcpA inhibits the production of pectate lyases via the H-NS protein and RsmB regulatory RNA in *Dickeya dadantii*. *Molecular Plant Pathology,* 19**,** 1873-1886.

ZARIVACH, R., DENG, W., VUCKOVIC, M., FELISE, H. B., NGUYEN, H. V., MILLER, S. I., FINLAY, B. B. & STRYNADKA, N. C. J. 2008. Structural analysis of the essential self-cleaving type III secretion proteins EscU and SpaS. *Nature,* 453**,** 124.

ZHANG, S. & KLESSIG, D. F. 2001. MAPK cascades in plant defense signaling. *Trends Plant Sci,* 6**,** 520-7.

ZHENG, X. Y., SPIVEY, N. W., ZENG, W., LIU, P. P., FU, Z. Q., KLESSIG, D. F., HE, S. Y. & DONG, X. 2012. Coronatine promotes *Pseudomonas syringae* virulence in plants by activating a signaling cascade that inhibits salicylic acid accumulation. *Cell Host Microbe,* 11**,** 587-96.

ZHOU, H., MORGAN, R. L., GUTTMAN, D. S. & MA, W. 2009. Allelic variants of the *Pseudomonas syringae* type III effector HopZ1 are differentially recognized by plant resistance systems. *Mol Plant Microbe Interact,* 22**,** 176-89.

ZIPFEL, C., KUNZE, G., CHINCHILLA, D., CANIARD, A., JONES, J. D. G., BOLLER, T. & FELIX, G. 2006. Perception of the Bacterial PAMP EF-Tu by the Receptor EFR Restricts *Agrobacterium*-Mediated Transformation. *Cell,* 125**,** 749-760.

Appendix

8.1. Expanded Organism Table

In Table 8.1, a table of organisms used in this study is shown. This expands upon the overview table of parental bacterial strains shown in Table 2.6.

Table 8.1. Expanded organism table showing complete list of organisms used in this study

Name	Organism	Parental Strain	Genotype	Plasmids	Resistance	Purpose	Source/Refence
DH5α	*Escherichia coli*	DH5α	F- Φ80lacZΔM15 Δ(lacZYA-argF) U169 recA1 endA1 hsdR17(rk-, mk+) phoA supE44 thi-1 gyrA96 relA1 λ-	-	-	Molecular cloning	**Invitrogen/ThermoFisher**
DH5α pTS-1	*Escherichia coli*	DH5α	F- Φ80lacZΔM15 Δ(lacZYA-argF) U169 recA1 endA1 hsdR17(rk-, mk+) phoA supE44 thi-1 gyrA96 relA1 λ-	pTS-1	Tetracycline	Plasmid purification	(Campilongo et al., 2017)
DH5α pTS-1-WT *hrcN*	*Escherichia coli*	DH5α	F- Φ80lacZΔM15 Δ(lacZYA-argF) U169 recA1 endA1 hsdR17(rk-, mk+) phoA supE44 thi-1 gyrA96 relA1 λ-	pTS-1- WT *hrcN*	Tetracycline	Plasmid purification	(Trampari et al., 2015)
DH5α pTS-1-*G176A hrcN*	*Escherichia coli*	DH5α	F- Φ80lacZΔM15 Δ(lacZYA-argF) U169 recA1 endA1 hsdR17(rk-, mk+) phoA supE44 thi-1 gyrA96 relA1 λ-	pTS-1-*G176A hrcN*	Tetracycline	Plasmid purification	(Pfeilmeier et al., 2016)
DH5α pTS-1-*E208D hrcN*	*Escherichia coli*	DH5α	F- Φ80lacZΔM15 Δ(lacZYA-argF) U169 recA1 endA1 hsdR17(rk-, mk+) phoA supE44 thi-1 gyrA96 relA1 λ-	pTS-1-*E208D hrcN*	Tetracycline	Plasmid purification	This study
DH5α pTS-1-*R170Q hrcN*	*Escherichia coli*	DH5α	F- Φ80lacZΔM15 Δ(lacZYA-argF) U169 recA1 endA1 hsdR17(rk-, mk+) phoA supE44 thi-1 gyrA96 relA1 λ-	pTS-1-*R170Q hrcN*	Tetracycline	Plasmid purification	This study
DH5α pTS-1-*G311A hrcN*	*Escherichia coli*	DH5α	F- Φ80lacZΔM15 Δ(lacZYA-argF) U169 recA1 endA1 hsdR17(rk-, mk+) phoA supE44 thi-1 gyrA96 relA1 λ-	pTS-1-*G311A hrcN*	Tetracycline	Plasmid purification	This study
DH5α pTS-1-*L338V hrcN*	*Escherichia coli*	DH5α	F- Φ80lacZΔM15 Δ(lacZYA-argF) U169 recA1 endA1 hsdR17(rk-, mk+) phoA supE44 thi-1 gyrA96 relA1 λ-	pTS-1-*L338V hrcN*	Tetracycline	Plasmid purification	This study
DH5α pTS-1-*F174Y hrcN*	*Escherichia coli*	DH5α	F- Φ80lacZΔM15 Δ(lacZYA-argF) U169 recA1 endA1 hsdR17(rk-, mk+) phoA supE44 thi-1 gyrA96 relA1 λ-	pTS-1-*F174Y hrcN*	Tetracycline	Plasmid purification	This study
DH5α pTS-1-*R356H hrcN*	*Escherichia coli*	DH5α	F- Φ80lacZΔM15 Δ(lacZYA-argF) U169 recA1 endA1 hsdR17(rk-, mk+) phoA supE44 thi-1 gyrA96 relA1 λ-	pTS-1-*R356H hrcN*	Tetracycline	Plasmid purification	This study
DH5α pTS-1-*P142G hrcN*	*Escherichia coli*	DH5α	F- Φ80lacZΔM15 Δ(lacZYA-argF) U169 recA1 endA1 hsdR17(rk-, mk+) phoA supE44 thi-1 gyrA96 relA1 λ-	pTS-1-*P142G hrcN*	Tetracycline	Plasmid purification	This study
DH5α pTS1-1-WT *pscN*	*Escherichia coli*	DH5α	F- Φ80lacZΔM15 Δ(lacZYA-argF) U169 recA1 endA1 hsdR17(rk-, mk+) phoA supE44 thi-1 gyrA96 relA1 λ-	pTS1-1-WT *pscN*	Tetracycline	Plasmid purification	This study
DH5α pTS1-1-*P137Q pscN*	*Escherichia coli*	DH5α	F- Φ80lacZΔM15 Δ(lacZYA-argF) U169 recA1 endA1 hsdR17(rk-, mk+) phoA supE44 thi-1 gyrA96 relA1 λ-	pTS1-1-*P137Q pscN*	Tetracycline	Plasmid purification	This study
DH5α pTS1-1-*Q164P pscN*	*Escherichia coli*	DH5α	F- Φ80lacZΔM15 Δ(lacZYA-argF) U169 recA1 endA1 hsdR17(rk-, mk+) phoA supE44 thi-1 gyrA96 relA1 λ-	pTS1-1-*Q164P pscN*	Tetracycline	Plasmid purification	This study
DH5α pTS1-1-E203D *pscN*	*Escherichia coli*	DH5α	F- Φ80lacZΔM15 Δ(lacZYA-argF) U169 recA1 endA1 hsdR17(rk-, mk+) phoA supE44 thi-1 gyrA96 relA1 λ-	pTS1-1-E203D *pscN*	Tetracycline	Plasmid purification	This study
DH5α pTS1-1-*G301D pscN*	*Escherichia coli*	DH5α	F- Φ80lacZΔM15 Δ(lacZYA-argF) U169 recA1 endA1 hsdR17(rk-, mk+) phoA supE44 thi-1 gyrA96 relA1 λ-	pTS1-1-*G301D pscN*	Tetracycline	Plasmid purification	This study

DH5α pTS1-1-*G306D pscN*	*Escherichia coli*	DH5α	F- Φ80lacZΔM15 Δ(lacZYA-argF) U169 recA1 endA1 hsdR17(rk-, mk+) phoA supE44 thi-1 gyrA96 relA1 λ-	pTS1-1-*G306D pscN*	Tetracycline	Plasmid purification	This study
DH5α pTS1-1-*R335Q pscN*	*Escherichia coli*	DH5α	F- Φ80lacZΔM15 Δ(lacZYA-argF) U169 recA1 endA1 hsdR17(rk-, mk+) phoA supE44 thi-1 gyrA96 relA1 λ-	pTS1-1-*R335Q pscN*	Tetracycline	Plasmid purification	This study
DH5α pTS-1-*ΔhrcC*	*Escherichia coli*	DH5α	F- Φ80lacZΔM15 Δ(lacZYA-argF) U169 recA1 endA1 hsdR17(rk-, mk+) phoA supE44 thi-1 gyrA96 relA1 λ-	pTS-1-*ΔhrcC*	Tetracycline	Plasmid purification	This study
DH5α pTS-1-*ΔhrcN*	*Escherichia coli*	DH5α	F- Φ80lacZΔM15 Δ(lacZYA-argF) U169 recA1 endA1 hsdR17(rk-, mk+) phoA supE44 thi-1 gyrA96 relA1 λ-	pTS-1-*ΔhrcN*	Tetracycline	Plasmid purification	This study
DH5α pTS-1-*ΔhopAA1-2*	*Escherichia coli*	DH5α	F- Φ80lacZΔM15 Δ(lacZYA-argF) U169 recA1 endA1 hsdR17(rk-, mk+) phoA supE44 thi-1 gyrA96 relA1 λ-	pTS-1-*ΔhopAA1-2*	Tetracycline	Plasmid purification	This study
DH5α pTS-1-*ΔhopAM1*	*Escherichia coli*	DH5α	F- Φ80lacZΔM15 Δ(lacZYA-argF) U169 recA1 endA1 hsdR17(rk-, mk+) phoA supE44 thi-1 gyrA96 relA1 λ-	pTS-1-*ΔhopAM1*	Tetracycline	Plasmid purification	This study
DH5α pTS-1-*ΔhopAF1*	*Escherichia coli*	DH5α	F- Φ80lacZΔM15 Δ(lacZYA-argF) U169 recA1 endA1 hsdR17(rk-, mk+) phoA supE44 thi-1 gyrA96 relA1 λ-	pTS-1-*ΔhopAF1*	Tetracycline	Plasmid purification	This study
DH5α pETM11	*Escherichia coli*	DH5α	F- Φ80lacZΔM15 Δ(lacZYA-argF) U169 recA1 endA1 hsdR17(rk-, mk+) phoA supE44 thi-1 gyrA96 relA1 λ-	pETM11	Kanamycin	Plasmid purification	
DH5α pETM11-WT *hrcN*	*Escherichia coli*	DH5α	F- Φ80lacZΔM15 Δ(lacZYA-argF) U169 recA1 endA1 hsdR17(rk-, mk+) phoA supE44 thi-1 gyrA96 relA1 λ-	pETM11-WT *hrcN*	Kanamycin	Plasmid purification	This study
DH5α pETM11-*P142Q hrcN*	*Escherichia coli*	DH5α	F- Φ80lacZΔM15 Δ(lacZYA-argF) U169 recA1 endA1 hsdR17(rk-, mk+) phoA supE44 thi-1 gyrA96 relA1 λ-	pETM11-*P142Q hrcN*	Kanamycin	Plasmid purification	This study
DH5α pETM11-*G176A hrcN*	*Escherichia coli*	DH5α	F- Φ80lacZΔM15 Δ(lacZYA-argF) U169 recA1 endA1 hsdR17(rk-, mk+) phoA supE44 thi-1 gyrA96 relA1 λ-	pETM11-*G176A hrcN*	Kanamycin	Plasmid purification	This study
DH5α pETM11-*E208D hrcN*	*Escherichia coli*	DH5α	F- Φ80lacZΔM15 Δ(lacZYA-argF) U169 recA1 endA1 hsdR17(rk-, mk+) phoA supE44 thi-1 gyrA96 relA1 λ-	pETM11-*E208D hrcN*	Kanamycin	Plasmid purification	This study
DH5α pETM11-*G311A-hrcN*	*Escherichia coli*	DH5α	F- Φ80lacZΔM15 Δ(lacZYA-argF) U169 recA1 endA1 hsdR17(rk-, mk+) phoA supE44 thi-1 gyrA96 relA1 λ-	pETM11-*G311A-hrcN*	Kanamycin	Plasmid purification	This study
DH5α pETM11-*R335P-hrcN*	*Escherichia coli*	DH5α	F- Φ80lacZΔM15 Δ(lacZYA-argF) U169 recA1 endA1 hsdR17(rk-, mk+) phoA supE44 thi-1 gyrA96 relA1 λ-	pETM11-*R335P-hrcN*	Kanamycin	Plasmid purification	This study
DH5α pETM11-*L338V-hrcN*	*Escherichia coli*	DH5α	F- Φ80lacZΔM15 Δ(lacZYA-argF) U169 recA1 endA1 hsdR17(rk-, mk+) phoA supE44 thi-1 gyrA96 relA1 λ-	pETM11-*L338V-hrcN*	Kanamycin	Plasmid purification	This study
DH5α pETM11-*L338V-hrcN*	*Escherichia coli*	DH5α	F- Φ80lacZΔM15 Δ(lacZYA-argF) U169 recA1 endA1 hsdR17(rk-, mk+) phoA supE44 thi-1 gyrA96 relA1 λ-	pETM11-*L338V-hrcN*	Kanamycin	Plasmid purification	This study
DH5α pETM11-*P137Q-pscN*	*Escherichia coli*	DH5α	F- Φ80lacZΔM15 Δ(lacZYA-argF) U169 recA1 endA1 hsdR17(rk-, mk+) phoA supE44 thi-1 gyrA96 relA1 λ-	pETM11-*P137Q-pscN*	Kanamycin	Plasmid purification	This study
DH5α pETM11-*E208D-pscN*	*Escherichia coli*	DH5α	F- Φ80lacZΔM15 Δ(lacZYA-argF) U169 recA1 endA1 hsdR17(rk-, mk+) phoA supE44 thi-1 gyrA96 relA1 λ-	pETM11-*E208D-pscN*	Kanamycin	Plasmid purification	This study
DH5α pETM11-*G301D-pscN*	*Escherichia coli*	DH5α	F- Φ80lacZΔM15 Δ(lacZYA-argF) U169 recA1 endA1 hsdR17(rk-, mk+) phoA	pETM11-*G301D-pscN*	Kanamycin	Plasmid purification	This study

			supE44 thi-1 gyrA96 relA1 λ-				
DH5α pETM11-*G306D-pscN*	*Escherichia coli*	DH5α	F- Φ80lacZΔM15 Δ(lacZYA-argF) U169 recA1 endA1 hsdR17(rk-, mk+) phoA supE44 thi-1 gyrA96 relA1 λ-	pETM11-*G306D-pscN*	Kanamycin	Plasmid purification	This study
DH5α pETM11-*R335Q-pscN*	*Escherichia coli*	DH5α	F- Φ80lacZΔM15 Δ(lacZYA-argF) U169 recA1 endA1 hsdR17(rk-, mk+) phoA supE44 thi-1 gyrA96 relA1 λ-	pETM11-*R335Q-pscN*	Kanamycin	Plasmid purification	This study
DH5α pETM11-WT *hrcN* (Δ1-18)	*Escherichia coli*	DH5α	F- Φ80lacZΔM15 Δ(lacZYA-argF) U169 recA1 endA1 hsdR17(rk-, mk+) phoA supE44 thi-1 gyrA96 relA1 λ-	pETM11-WT *hrcN* (Δ1-18)	Kanamycin	Plasmid purification	This study
DH5α pETM11-*G176A hrcN* (Δ1-18)	*Escherichia coli*	DH5α	F- Φ80lacZΔM15 Δ(lacZYA-argF) U169 recA1 endA1 hsdR17(rk-, mk+) phoA supE44 thi-1 gyrA96 relA1 λ-	pETM11-*G176A hrcN* (Δ1-18)	Kanamycin	Plasmid purification	This study
DH5α pETM11-*E208D hrcN* (Δ1-18)	*Escherichia coli*	DH5α	F- Φ80lacZΔM15 Δ(lacZYA-argF) U169 recA1 endA1 hsdR17(rk-, mk+) phoA supE44 thi-1 gyrA96 relA1 λ-	pETM11-*E208D hrcN* (Δ1-18)	Kanamycin	Plasmid purification	This study
DH5α pETM11-*G311A hrcN* (Δ1-18)	*Escherichia coli*	DH5α	F- Φ80lacZΔM15 Δ(lacZYA-argF) U169 recA1 endA1 hsdR17(rk-, mk+) phoA supE44 thi-1 gyrA96 relA1 λ-	pETM11-*G311A hrcN* (Δ1-18)	Kanamycin	Plasmid purification	This study
DH5α pETM11-*L338V hrcN* (Δ1-18)	*Escherichia coli*	DH5α	F- Φ80lacZΔM15 Δ(lacZYA-argF) U169 recA1 endA1 hsdR17(rk-, mk+) phoA supE44 thi-1 gyrA96 relA1 λ-	pETM11-*L338V hrcN* (Δ1-18)	Kanamycin	Plasmid purification	This study
DH5α pETM11-*F174Y hrcN* (Δ1-18)	*Escherichia coli*	DH5α	F- Φ80lacZΔM15 Δ(lacZYA-argF) U169 recA1 endA1 hsdR17(rk-, mk+) phoA supE44 thi-1 gyrA96 relA1 λ-	pETM11-*F174Y hrcN* (Δ1-18)	Kanamycin	Plasmid purification	This study
DH5α pETM11-*P142G hrcN* (Δ1-18)	*Escherichia coli*	DH5α	F- Φ80lacZΔM15 Δ(lacZYA-argF) U169 recA1 endA1 hsdR17(rk-, mk+) phoA supE44 thi-1 gyrA96 relA1 λ-	pETM11-*P142G hrcN* (Δ1-18)	Kanamycin	Plasmid purification	This study
DH5α pBBR4	*Escherichia coli*	DH5α	F- Φ80lacZΔM15 Δ(lacZYA-argF) U169 recA1 endA1 hsdR17(rk-, mk+) phoA supE44 thi-1 gyrA96 relA1 λ-	pBBR4	Carbenicillin	Plasmid purification	(Malone et al., 2010)
DH5α pBBR4-*wspR19*	*Escherichia coli*	DH5α	F- Φ80lacZΔM15 Δ(lacZYA-argF) U169 recA1 endA1 hsdR17(rk-, mk+) phoA supE44 thi-1 gyrA96 relA1 λ-	pBBR4-*wspR19*	Carbenicillin	Plasmid purification	This study
DH5α pBBR4-*bifA*	*Escherichia coli*	DH5α	F- Φ80lacZΔM15 Δ(lacZYA-argF) U169 recA1 endA1 hsdR17(rk-, mk+) phoA supE44 thi-1 gyrA96 relA1 λ-	pBBR4-*bifA*	Carbenicillin	Plasmid purification	This study
DB3.1 pCPP5371 (Empty CyaA backbone)	*Escherichia coli*	DB3.1	F⁻ gyrA462 endA1 Δ(sr1-recA) mcrB mrr hsdS20(rB-, mB-) supE44ara-14 galK2 lacY1 proA2 rpsL20(SmR) xyl-5 λ- leu mtl1	pCPP5371	Gentamycin	Plasmid purification	(Oh et al., 2007)
DB3.1 pENTR-SD/D-TOPO	*Escherichia coli*	DB3.1	F⁻ gyrA462 endA1 Δ(sr1-recA) mcrB mrr hsdS20(rB-, mB-) supE44ara-14 galK2 lacY1 proA2 rpsL20(SmR) xyl-5 λ- leu mtl1	pENTR-SD/D-TOPO	Kanamycin	Plasmid purification	(Schechter et al., 2004)
DB3.1 pENTR-SD/D-TOPO-*shcE-avrE1*	*Escherichia coli*	DB3.1	F⁻ gyrA462 endA1 Δ(sr1-recA) mcrB mrr hsdS20(rB-, mB-) supE44ara-14 galK2 lacY1 proA2 rpsL20(SmR) xyl-5 λ- leu mtl1	pENTR-SD/D-TOPO-*shcE-avrE1*	Kanamycin	Plasmid purification	(Kvitko et al., 2009)
DB3.1 pENTR-SD/D-TOPO-*hopB1*	*Escherichia coli*	DB3.1	F⁻ gyrA462 endA1 Δ(sr1-recA) mcrB mrr hsdS20(rB-, mB-) supE44ara-14 galK2 lacY1 proA2 rpsL20(SmR) xyl-5 λ- leu mtl1	pENTR-SD/D-TOPO-*hopB1*	Kanamycin	Plasmid purification	(Munkvold et al., 2009)
DB3.1 pENTR-SD/D-TOPO -*hopE1*	*Escherichia coli*	DB3.1	F⁻ gyrA462 endA1 Δ(sr1-recA) mcrB mrr hsdS20(rB-, mB-) supE44ara-14 galK2 lacY1 proA2 rpsL20(SmR) xyl-5 λ- leu mtl1	pENTR-SD/D-TOPO -*hopE1*	Kanamycin	Plasmid purification	(Munkvold et al., 2009)
DB3.1 pENTR-SD/D-TOPO-*shcF-hopF2*	*Escherichia coli*	DB3.1	F⁻ gyrA462 endA1 Δ(sr1-recA) mcrB mrr hsdS20(rB-, mB-) supE44ara-14 galK2 lacY1 proA2 rpsL20(SmR) xyl-5 λ- leu mtl1	pENTR-SD/D-TOPO-*shcF-hopF2*	Kanamycin	Plasmid purification	(Wei et al., 2018)

DB3.1 pENTR-SD/D-TOPO-hopG1	*Escherichia coli*	DB3.1	F⁻ gyrA462 endA1 Δ(sr1-recA) mcrB mrr hsdS20(r_B⁻, m_B⁻) supE44ara-14 galK2 lacY1 proA2 rpsL20(Sm^R) xyl-5 λ- leu mtl1	pENTR-SD/D-TOPO-*hopG1*	Kanamycin	Plasmid purification	(Munkvold et al., 2009)
DB3.1 pENTR-SD/D-TOPO-hopH1	*Escherichia coli*	DB3.1	F⁻ gyrA462 endA1 Δ(sr1-recA) mcrB mrr hsdS20(r_B⁻, m_B⁻) supE44ara-14 galK2 lacY1 proA2 rpsL20(Sm^R) xyl-5 λ- leu mtl1	pENTR-SD/D-TOPO-*hopH1*	Kanamycin	Plasmid purification	(Munkvold et al., 2009)
DB3.1 pENTR-SD/D-TOPO-hopI1	*Escherichia coli*	DB3.1	F⁻ gyrA462 endA1 Δ(sr1-recA) mcrB mrr hsdS20(r_B⁻, m_B⁻) supE44ara-14 galK2 lacY1 proA2 rpsL20(Sm^R) xyl-5 λ- leu mtl1	pENTR-SD/D-TOPO-*hopI1*	Kanamycin	Plasmid purification	(Munkvold et al., 2009)
DB3.1 pENTR-SD/D-TOPO-hopK1	*Escherichia coli*	DB3.1	F⁻ gyrA462 endA1 Δ(sr1-recA) mcrB mrr hsdS20(r_B⁻, m_B⁻) supE44ara-14 galK2 lacY1 proA2 rpsL20(Sm^R) xyl-5 λ- leu mtl1	pENTR-SD/D-TOPO-*hopK1*	Kanamycin	Plasmid purification	(Wei et al., 2018)
DB3.1 pENTR-SD/D-TOPO-shcO-hopO1-1	*Escherichia coli*	DB3.1	F⁻ gyrA462 endA1 Δ(sr1-recA) mcrB mrr hsdS20(r_B⁻, m_B⁻) supE44ara-14 galK2 lacY1 proA2 rpsL20(Sm^R) xyl-5 λ- leu mtl1	pENTR-SD/D-TOPO- *shcO-hopO1-1*	Kanamycin	Plasmid purification	(Kvitko et al., 2009)
DB3.1 pENTR-SD/D-TOPO-hopQ1-1	*Escherichia coli*	DB3.1	F⁻ gyrA462 endA1 Δ(sr1-recA) mcrB mrr hsdS20(r_B⁻, m_B⁻) supE44ara-14 galK2 lacY1 proA2 rpsL20(Sm^R) xyl-5 λ- leu mtl1	pENTR-SD/D-TOPO- *hopQ1-1*	Kanamycin	Plasmid purification	(Munkvold et al., 2009)
DB3.1 pENTR-SD/D-TOPO-hopR1	*Escherichia coli*	DB3.1	F⁻ gyrA462 endA1 Δ(sr1-recA) mcrB mrr hsdS20(r_B⁻, m_B⁻) supE44ara-14 galK2 lacY1 proA2 rpsL20(Sm^R) xyl-5 λ- leu mtl1	pENTR-SD/D-TOPO- *hopR1*	Kanamycin	Plasmid purification	(Kvitko et al., 2009)
DB3.1 pENTR-SD/D-TOPO-hopT1-1	*Escherichia coli*	DB3.1	F⁻ gyrA462 endA1 Δ(sr1-recA) mcrB mrr hsdS20(r_B⁻, m_B⁻) supE44ara-14 galK2 lacY1 proA2 rpsL20(Sm^R) xyl-5 λ- leu mtl1	pENTR-SD/D-TOPO- *hopT1-1*	Kanamycin	Plasmid purification	(Munkvold et al., 2009)
DB3.1 pENTR-SD/D-TOPO-hopU1	*Escherichia coli*	DB3.1	F⁻ gyrA462 endA1 Δ(sr1-recA) mcrB mrr hsdS20(r_B⁻, m_B⁻) supE44ara-14 galK2 lacY1 proA2 rpsL20(Sm^R) xyl-5 λ- leu mtl1	pENTR-SD/D-TOPO- *hopU1*	Kanamycin	Plasmid purification	(Munkvold et al., 2009)
DB3.1 pENTR-SD/D-TOPO-hopX1	*Escherichia coli*	DB3.1	F⁻ gyrA462 endA1 Δ(sr1-recA) mcrB mrr hsdS20(r_B⁻, m_B⁻) supE44ara-14 galK2 lacY1 proA2 rpsL20(Sm^R) xyl-5 λ- leu mtl1	pENTR-SD/D-TOPO- *hopX1*	Kanamycin	Plasmid purification	(Munkvold et al., 2009)
DB3.1 pENTR-SD/D-TOPO-hopY1	*Escherichia coli*	DB3.1	F⁻ gyrA462 endA1 Δ(sr1-recA) mcrB mrr hsdS20(r_B⁻, m_B⁻) supE44ara-14 galK2 lacY1 proA2 rpsL20(Sm^R) xyl-5 λ- leu mtl1	pENTR-SD/D-TOPO- *hopY1*	Kanamycin	Plasmid purification	(Munkvold et al., 2009)
DB3.1 pENTR-SD/D-TOPO-hopAA1-1	*Escherichia coli*	DB3.1	F⁻ gyrA462 endA1 Δ(sr1-recA) mcrB mrr hsdS20(r_B⁻, m_B⁻) supE44ara-14 galK2 lacY1 proA2 rpsL20(Sm^R) xyl-5 λ- leu mtl1	pENTR-SD/D-TOPO- *hopAA1-1*	Kanamycin	Plasmid purification	(Munkvold et al., 2009)
DB3.1 pENTR-SD/D-TOPO-hopAA1-2	*Escherichia coli*	DB3.1	F⁻ gyrA462 endA1 Δ(sr1-recA) mcrB mrr hsdS20(r_B⁻, m_B⁻) supE44ara-14 galK2 lacY1 proA2 rpsL20(Sm^R) xyl-5 λ- leu mtl1	pENTR-SD/D-TOPO- *hopAA1-2*	Kanamycin	Plasmid purification	(Munkvold et al., 2009)
DB3.1 pENTR-SD/D-TOPO-hopAF1	*Escherichia coli*	DB3.1	F⁻ gyrA462 endA1 Δ(sr1-recA) mcrB mrr hsdS20(r_B⁻, m_B⁻) supE44ara-14 galK2 lacY1 proA2 rpsL20(Sm^R) xyl-5 λ- leu mtl1	pENTR-SD/D-TOPO- *hopAF1*	Kanamycin	Plasmid purification	(Munkvold et al., 2009)
DB3.1 pENTR-SD/D-TOPO-hopAM1	*Escherichia coli*	DB3.1	F⁻ gyrA462 endA1 Δ(sr1-recA) mcrB mrr hsdS20(r_B⁻, m_B⁻) supE44ara-14 galK2 lacY1 proA2 rpsL20(Sm^R) xyl-5 λ- leu mtl1	pENTR-SD/D-TOPO- *hopAM1*	Kanamycin	Plasmid purification	(Munkvold et al., 2009)
DB3.1 pENTR-SD/D-TOPO-hopA1	*Escherichia coli*	DB3.1	F⁻ gyrA462 endA1 Δ(sr1-recA) mcrB mrr hsdS20(r_B⁻, m_B⁻) supE44ara-14 galK2 lacY1 proA2 rpsL20(Sm^R) xyl-5 λ- leu mtl1	pENTR-SD/D-TOPO- *hopA1*	Kanamycin	Plasmid purification	(Kvitko et al., 2009)
DB3.1 pENTR-SD/D-TOPO-schM-hopM1	*Escherichia coli*	DB3.1	F⁻ gyrA462 endA1 Δ(sr1-recA) mcrB mrr hsdS20(r_B⁻, m_B⁻) supE44ara-14 galK2 lacY1 proA2 rpsL20(Sm^R) xyl-5 λ- leu mtl1	pENTR-SD/D-TOPO- *schM-hopM1*	Kanamycin	Plasmid purification	(Kvitko et al., 2009)
DB3.1 pENTR-SD/D-TOPO-avrPto	*Escherichia coli*	DB3.1	F⁻ gyrA462 endA1 Δ(sr1-recA) mcrB mrr hsdS20(r_B⁻, m_B⁻) supE44ara-14 galK2 lacY1 proA2 rpsL20(Sm^R) xyl-5 λ- leu mtl1	pENTR-SD/D-TOPO- *avrPto*	Kanamycin	Plasmid purification	(Kvitko et al., 2009)
DB3.1 pENTR-	*Escherichia coli*	DB3.1	F⁻ gyrA462 endA1 Δ(sr1-recA) mcrB mrr hsdS20(r_B⁻, m_B⁻) supE44ara-14 galK2	pENTR-SD/D-TOPO- *avrPtoB*	Kanamycin	Plasmid purification	(Kvitko et al., 2009)

SD/D-TOPO-*avrPtoB*			lacY1 proA2 rpsL20(Sm^R) xyl-5 λ- leu mtl1				
pDEST pCPP5371-*shcE-avrE1*-CyaA	*Escherichia coli*	DH5α	F⁻ gyrA462 endA1 Δ(sr1-recA) mcrB mrr hsdS20(r$_B$⁻, m$_B$⁻) supE44ara-14 galK2 lacY1 proA2 rpsL20(Sm^R) xyl-5 λ- leu mtl1	pDEST pCPP5371- *shcE-avrE1*-CyaA	Gentamycin	Plasmid purification	This study
pDEST pCPP5371-*hopB1*-CyaA	*Escherichia coli*	DH5α	F⁻ gyrA462 endA1 Δ(sr1-recA) mcrB hsdS20(r$_B$⁻, m$_B$⁻) supE44ara-14 galK2 lacY1 proA2 rpsL20(Sm^R) xyl-5 λ- leu mtl1	pDEST pCPP5371-*hopB1*-CyaA	Gentamycin	Plasmid purification	This study
pDEST pCPP5371-*hopE1*-CyaA	*Escherichia coli*	DH5α	F⁻ gyrA462 endA1 Δ(sr1-recA) mcrB mrr hsdS20(r$_B$⁻, m$_B$⁻) supE44ara-14 galK2 lacY1 proA2 rpsL20(Sm^R) xyl-5 λ- leu mtl1	pDEST pCPP5371-*hopE1*-CyaA	Gentamycin	Plasmid purification	This study
pDEST pCPP5371-*shcF-hopF2*-CyaA	*Escherichia coli*	DH5α	F⁻ gyrA462 endA1 Δ(sr1-recA) mcrB mrr hsdS20(r$_B$⁻, m$_B$⁻) supE44ara-14 galK2 lacY1 proA2 rpsL20(Sm^R) xyl-5 λ- leu mtl1	pDEST pCPP5371- *shcF-hopF2*-CyaA	Gentamycin	Plasmid purification	This study
pDEST pCPP5371-*hopG1*-CyaA	*Escherichia coli*	DH5α	F⁻ gyrA462 endA1 Δ(sr1-recA) mcrB mrr hsdS20(r$_B$⁻, m$_B$⁻) supE44ara-14 galK2 lacY1 proA2 rpsL20(Sm^R) xyl-5 λ- leu mtl1	pDEST pCPP5371-*hopG1*-CyaA	Gentamycin	Plasmid purification	This study
pDEST pCPP5371-*hopH1*-CyaA	*Escherichia coli*	DH5α	F⁻ gyrA462 endA1 Δ(sr1-recA) mcrB mrr hsdS20(r$_B$⁻, m$_B$⁻) supE44ara-14 galK2 lacY1 proA2 rpsL20(Sm^R) xyl-5 λ- leu mtl1	pDEST pCPP5371-*hopH1*-CyaA	Gentamycin	Plasmid purification	This study
pDEST pCPP5371-*hopI1*-CyaA	*Escherichia coli*	DH5α	F⁻ gyrA462 endA1 Δ(sr1-recA) mcrB mrr hsdS20(r$_B$⁻, m$_B$⁻) supE44ara-14 galK2 lacY1 proA2 rpsL20(Sm^R) xyl-5 λ- leu mtl1	pDEST pCPP5371-*hopI1*-CyaA	Gentamycin	Plasmid purification	This study
pDEST pCPP5371-*hopK1*-CyaA	*Escherichia coli*	DH5α	F⁻ gyrA462 endA1 Δ(sr1-recA) mcrB mrr hsdS20(r$_B$⁻, m$_B$⁻) supE44ara-14 galK2 lacY1 proA2 rpsL20(Sm^R) xyl-5 λ- leu mtl1	pDEST pCPP5371-*hopK1*-CyaA	Gentamycin	Plasmid purification	This study
pDEST pCPP5371-*shcO-hopO1-1*-CyaA	*Escherichia coli*	DH5α	F⁻ gyrA462 endA1 Δ(sr1-recA) mcrB mrr hsdS20(r$_B$⁻, m$_B$⁻) supE44ara-14 galK2 lacY1 proA2 rpsL20(Sm^R) xyl-5 λ- leu mtl1	pDEST pCPP5371-*shcO-hopO1-1*-CyaA	Gentamycin	Plasmid purification	This study
pDEST pCPP5371-*hopQ1-1*-CyaA	*Escherichia coli*	DH5α	F⁻ gyrA462 endA1 Δ(sr1-recA) mcrB mrr hsdS20(r$_B$⁻, m$_B$⁻) supE44ara-14 galK2 lacY1 proA2 rpsL20(Sm^R) xyl-5 λ- leu mtl1	pDEST pCPP5371-*hopQ1-1*-CyaA	Gentamycin	Plasmid purification	This study
pDEST pCPP5371-*hopR1*-CyaA	*Escherichia coli*	DH5α	F⁻ gyrA462 endA1 Δ(sr1-recA) mcrB mrr hsdS20(r$_B$⁻, m$_B$⁻) supE44ara-14 galK2 lacY1 proA2 rpsL20(Sm^R) xyl-5 λ- leu mtl1	pDEST pCPP5371-*hopR1*-CyaA	Gentamycin	Plasmid purification	This study
pDEST pCPP5371-*hopT1-1*-CyaA	*Escherichia coli*	DH5α	F⁻ gyrA462 endA1 Δ(sr1-recA) mcrB mrr hsdS20(r$_B$⁻, m$_B$⁻) supE44ara-14 galK2 lacY1 proA2 rpsL20(Sm^R) xyl-5 λ- leu mtl1	pDEST pCPP5371-*hopT1-1*-CyaA	Gentamycin	Plasmid purification	This study
pDEST pCPP5371-*hopU1*-CyaA	*Escherichia coli*	DH5α	F⁻ gyrA462 endA1 Δ(sr1-recA) mcrB mrr hsdS20(r$_B$⁻, m$_B$⁻) supE44ara-14 galK2 lacY1 proA2 rpsL20(Sm^R) xyl-5 λ- leu mtl1	pDEST pCPP5371-*hopU1*-CyaA	Gentamycin	Plasmid purification	This study
pDEST pCPP5371-*hopX1*-CyaA	*Escherichia coli*	DH5α	F⁻ gyrA462 endA1 Δ(sr1-recA) mcrB mrr hsdS20(r$_B$⁻, m$_B$⁻) supE44ara-14 galK2 lacY1 proA2 rpsL20(Sm^R) xyl-5 λ- leu mtl1	pDEST pCPP5371-*hopX1*-CyaA	Gentamycin	Plasmid purification	This study
pDEST pCPP5371-*hopY1*-CyaA	*Escherichia coli*	DH5α	F⁻ gyrA462 endA1 Δ(sr1-recA) mcrB mrr hsdS20(r$_B$⁻, m$_B$⁻) supE44ara-14 galK2 lacY1 proA2 rpsL20(Sm^R) xyl-5 λ- leu mtl1	pDEST pCPP5371-*hopY1*-CyaA	Gentamycin	Plasmid purification	This study
pDEST pCPP5371-*hopAA1-1*-CyaA	*Escherichia coli*	DH5α	F⁻ gyrA462 endA1 Δ(sr1-recA) mcrB mrr hsdS20(r$_B$⁻, m$_B$⁻) supE44ara-14 galK2 lacY1 proA2 rpsL20(Sm^R) xyl-5 λ- leu mtl1	pDEST pCPP5371-*hopAA1-1*-CyaA	Gentamycin	Plasmid purification	This study
pDEST pCPP5371-*hopAA1-2*-CyaA	*Escherichia coli*	DH5α	F⁻ gyrA462 endA1 Δ(sr1-recA) mcrB mrr hsdS20(r$_B$⁻, m$_B$⁻) supE44ara-14 galK2 lacY1 proA2 rpsL20(Sm^R) xyl-5 λ- leu mtl1	pDEST pCPP5371-*hopAA1-2*-CyaA	Gentamycin	Plasmid purification	This study
pDEST pCPP5371-*hopAF1*-CyaA	*Escherichia coli*	DH5α	F⁻ gyrA462 endA1 Δ(sr1-recA) mcrB mrr hsdS20(r$_B$⁻, m$_B$⁻) supE44ara-14 galK2 lacY1 proA2 rpsL20(Sm^R) xyl-5 λ- leu mtl1	pDEST pCPP5371-*hopAF1*-CyaA	Gentamycin	Plasmid purification	This study

pDEST pCPP5371-*hopAM1*-CyaA	*Escherichia coli*	DH5α	F⁻ gyrA462 endA1 Δ(sr1-recA) mcrB mrr hsdS20(rᵦ-, mᵦ-) supE44ara-14 galK2 lacY1 proA2 rpsL20(Smᴿ) xyl-5 λ- leu mtl1	pDEST pCPP5371-*hopAM1*-CyaA	Gentamycin	Plasmid purification	This study
pDEST pCPP5371-*hopA1*-CyaA	*Escherichia coli*	DH5α	F⁻ gyrA462 endA1 Δ(sr1-recA) mcrB mrr hsdS20(rᵦ-, mᵦ-) supE44ara-14 galK2 lacY1 proA2 rpsL20(Smᴿ) xyl-5 λ- leu mtl1	pDEST pCPP5371-*hopA1*-CyaA	Gentamycin	Plasmid purification	This study
pDEST pCPP5371-*shcM-hopM1*-CyaA	*Escherichia coli*	DH5α	F⁻ gyrA462 endA1 Δ(sr1-recA) mcrB mrr hsdS20(rᵦ-, mᵦ-) supE44ara-14 galK2 lacY1 proA2 rpsL20(Smᴿ) xyl-5 λ- leu mtl1	pDEST pCPP5371-*shcM-hopM1*-CyaA	Gentamycin	Plasmid purification	This study
pDEST pCPP5371-*avrPto*-CyaA	*Escherichia coli*	DH5α	F⁻ gyrA462 endA1 Δ(sr1-recA) mcrB mrr hsdS20(rᵦ-, mᵦ-) supE44ara-14 galK2 lacY1 proA2 rpsL20(Smᴿ) xyl-5 λ- leu mtl1	pDEST pCPP5371-*avrPto*-CyaA	Gentamycin	Plasmid purification	This study
pDEST pCPP5371-*avrPtoB*-CyaA	*Escherichia coli*	DH5α	F⁻ gyrA462 endA1 Δ(sr1-recA) mcrB mrr hsdS20(rᵦ-, mᵦ-) supE44ara-14 galK2 lacY1 proA2 rpsL20(Smᴿ) xyl-5 λ- leu mtl1	pDEST pCPP5371-*avrPtoB*-CyaA	Gentamycin	Plasmid purification	This study
pUC18T-MiniTn7T	*Escherichia coli*	DH5α	F⁻ gyrA462 endA1 Δ(sr1-recA) mcrB mrr hsdS20(rᵦ-, mᵦ-) supE44ara-14 galK2 lacY1 proA2 rpsL20(Smᴿ) xyl-5 λ- leu mtl1	pUC18T-MiniTn7T	Gentamycin	Plasmid purification	(Choi et al., 2005)
pUC18T-MiniTn7T-WT *hrcN*	*Escherichia coli*	DH5α	F⁻ gyrA462 endA1 Δ(sr1-recA) mcrB mrr hsdS20(rᵦ-, mᵦ-) supE44ara-14 galK2 lacY1 proA2 rpsL20(Smᴿ) xyl-5 λ- leu mtl1	pUC18T-MiniTn7T-WT *hrcN*	Gentamycin	Plasmid purification	This study
pUC18T-MiniTn7T-WT *hrcC*	*Escherichia coli*	DH5α	F⁻ gyrA462 endA1 Δ(sr1-recA) mcrB mrr hsdS20(rᵦ-, mᵦ-) supE44ara-14 galK2 lacY1 proA2 rpsL20(Smᴿ) xyl-5 λ- leu mtl1	pUC18T-MiniTn7T-WT *hrcC*	Gentamycin	Plasmid purification	This study
pTNS2	*Escherichia coli*	DH5α	F⁻ gyrA462 endA1 Δ(sr1-recA) mcrB mrr hsdS20(rᵦ-, mᵦ-) supE44ara-14 galK2 lacY1 proA2 rpsL20(Smᴿ) xyl-5 λ- leu mtl1	pTNS2	Gentamycin	Plasmid purification	(Choi et al., 2005)
pBBR2	*Escherichia coli*	DH5α	F⁻ gyrA462 endA1 Δ(sr1-recA) mcrB mrr hsdS20(rᵦ-, mᵦ-) supE44ara-14 galK2 lacY1 proA2 rpsL20(Smᴿ) xyl-5 λ- leu mtl1	pBBR2	Kanamycin	Plasmid purification	(Pfeilmeier et al., 2016)
pBBR2-*HopAA1-2*	*Escherichia coli*	DH5α	F⁻ gyrA462 endA1 Δ(sr1-recA) mcrB mrr hsdS20(rᵦ-, mᵦ-) supE44ara-14 galK2 lacY1 proA2 rpsL20(Smᴿ) xyl-5 λ- leu mtl1	pBBR2-*HopAA1-2*	Gentamycin	Plasmid purification	This study
pBBR2-*HopAM1*	*Escherichia coli*	DH5α	F⁻ gyrA462 endA1 Δ(sr1-recA) mcrB mrr hsdS20(rᵦ-, mᵦ-) supE44ara-14 galK2 lacY1 proA2 rpsL20(Smᴿ) xyl-5 λ- leu mtl1	pBBR2-*HopAM1*	Gentamycin	Plasmid purification	This study
pBBR2-*HopAF1*	*Escherichia coli*	DH5α	F⁻ gyrA462 endA1 Δ(sr1-recA) mcrB mrr hsdS20(rᵦ-, mᵦ-) supE44ara-14 galK2 lacY1 proA2 rpsL20(Smᴿ) xyl-5 λ- leu mtl1	pBBR2-*HopAF1*	Gentamycin	Plasmid purification	This study
BL21 (DE3) pLysS	*Escherichia coli*	BL21 (DE3)	F⁻ompT hsdSB(rᵦ- mᵦ-) gal dcm (DE3) pLysS (Camᴿ)	pLysS	Chloramphenicol	Over-expression	Malone Lab, John Innes Centre
BL21 (DE3) pLysS pETM11	*Escherichia coli*	BL21 (DE3) pLysS	F⁻ompT hsdSB(rᵦ- mᵦ-) gal dcm (DE3) pLysS (Camᴿ)	pETM11	Kanamycin, Chloramphenicol	Over-expression	This study
BL21 (DE3) pLysS pETM11-WT *hrcN*	*Escherichia coli*	BL21 (DE3) pLysS	F⁻ompT hsdSB(rᵦ- mᵦ-) gal dcm (DE3) pLysS (Camᴿ)	pETM11-WT *hrcN*	Kanamycin, Chloramphenicol	Over-expression	This study
BL21 (DE3) pLysS pETM11-*P142Q hrcN*	*Escherichia coli*	BL21 (DE3) pLysS	F⁻ompT hsdSB(rᵦ- mᵦ-) gal dcm (DE3) pLysS (Camᴿ)	pETM11-*P142Q hrcN*	Kanamycin, Chloramphenicol	Over-expression	This study
BL21 (DE3) pLysS pETM11-*G176A hrcN*	*Escherichia coli*	BL21 (DE3) pLysS	F⁻ompT hsdSB(rᵦ- mᵦ-) gal dcm (DE3) pLysS (Camᴿ)	pETM11-*G176A hrcN*	Kanamycin, Chloramphenicol	Over-expression	This study
BL21 (DE3) pLysS pETM11-*E208D hrcN*	*Escherichia coli*	BL21 (DE3) pLysS	F⁻ompT hsdSB(rᵦ- mᵦ-) gal dcm (DE3) pLysS (Camᴿ)	pETM11-*E208D hrcN*	Kanamycin, Chloramphenicol	Over-expression	This study
BL21 (DE3) pLysS pETM11-*G311A-hrcN*	*Escherichia coli*	BL21 (DE3) pLysS	F⁻ompT hsdSB(rᵦ- mᵦ-) gal dcm (DE3) pLysS (Camᴿ)	pETM11-*G311A-hrcN*	Kanamycin, Chloramphenicol	Over-expression	This study
BL21 (DE3) pLysS	*Escherichia coli*	BL21 (DE3) pLysS	F⁻ompT hsdSB(rᵦ- mᵦ-) gal dcm (DE3) pLysS (Camᴿ)	pETM11-*R335P-hrcN*	Kanamycin, Chloramphenicol	Over-expression	This study

pETM11-R335P-hrcN							
BL21 (DE3) pLysS pETM11-L338V-hrcN	*Escherichia coli*	BL21 (DE3) pLysS	F⁻ompT hsdSB(rв- mв-) gal dcm (DE3) pLysS (Cam^R)	pETM11-*L338V-hrcN*	Kanamycin, Chloramphenicol	Over-expression	This study
BL21 (DE3) pLysS pETM11-L338V-hrcN	*Escherichia coli*	BL21 (DE3) pLysS	F⁻ompT hsdSB(rв- mв-) gal dcm (DE3) pLysS (Cam^R)	pETM11-*L338V-hrcN*	Kanamycin, Chloramphenicol	Over-expression	This study
BL21 (DE3) pLysS pETM11-P137Q-pscN	*Escherichia coli*	BL21 (DE3) pLysS	F⁻ompT hsdSB(rв- mв-) gal dcm (DE3) pLysS (Cam^R)	pETM11-*P137Q-pscN*	Kanamycin, Chloramphenicol	Over-expression	This study
BL21 (DE3) pLysS pETM11-E208D-pscN	*Escherichia coli*	BL21 (DE3) pLysS	F⁻ompT hsdSB(rв- mв-) gal dcm (DE3) pLysS (Cam^R)	pETM11-*E208D-pscN*	Kanamycin, Chloramphenicol	Over-expression	This study
BL21 (DE3) pLysS pETM11-G301D-pscN	*Escherichia coli*	BL21 (DE3) pLysS	F⁻ompT hsdSB(rв- mв-) gal dcm (DE3) pLysS (Cam^R)	pETM11-*G301D-pscN*	Kanamycin, Chloramphenicol	Over-expression	This study
BL21 (DE3) pLysS pETM11-G306D-pscN	*Escherichia coli*	BL21 (DE3) pLysS	F⁻ompT hsdSB(rв- mв-) gal dcm (DE3) pLysS (Cam^R)	pETM11-*G306D-pscN*	Kanamycin, Chloramphenicol	Over-expression	This study
BL21 (DE3) pLysS pETM11-R335Q-pscN	*Escherichia coli*	BL21 (DE3) pLysS	F⁻ompT hsdSB(rв- mв-) gal dcm (DE3) pLysS (Cam^R)	pETM11-*R335Q-pscN*	Kanamycin, Chloramphenicol	Over-expression	This study
BL21 (DE3) pLysS pETM11-WT hrcN (Δ1-18)	*Escherichia coli*	BL21 (DE3) pLysS	F⁻ompT hsdSB(rв- mв-) gal dcm (DE3) pLysS (Cam^R)	pETM11-WT *hrcN* (Δ1-18)	Kanamycin, Chloramphenicol	Over-expression	This study
BL21 (DE3) pLysS pETM11-G176A hrcN (Δ1-18)	*Escherichia coli*	BL21 (DE3) pLysS	F⁻ompT hsdSB(rв- mв-) gal dcm (DE3) pLysS (Cam^R)	pETM11-*G176A hrcN* (Δ1-18)	Kanamycin, Chloramphenicol	Over-expression	This study
BL21 (DE3) pLysS pETM11-E208D hrcN (Δ1-18)	*Escherichia coli*	BL21 (DE3) pLysS	F⁻ompT hsdSB(rв- mв-) gal dcm (DE3) pLysS (Cam^R)	pETM11-*E208D hrcN* (Δ1-18)	Kanamycin, Chloramphenicol	Over-expression	This study
BL21 (DE3) pLysS pETM11-G311A hrcN (Δ1-18)	*Escherichia coli*	BL21 (DE3) pLysS	F⁻ompT hsdSB(rв- mв-) gal dcm (DE3) pLysS (Cam^R)	pETM11-*G311A hrcN* (Δ1-18)	Kanamycin, Chloramphenicol	Over-expression	This study
BL21 (DE3) pLysS pETM11-L338V hrcN (Δ1-18)	*Escherichia coli*	BL21 (DE3) pLysS	F⁻ompT hsdSB(rв- mв-) gal dcm (DE3) pLysS (Cam^R)	pETM11-*L338V hrcN* (Δ1-18)	Kanamycin, Chloramphenicol	Over-expression	This study
BL21 (DE3) pLysS pETM11-F174Y hrcN (Δ1-18)	*Escherichia coli*	BL21 (DE3) pLysS	F⁻ompT hsdSB(rв- mв-) gal dcm (DE3) pLysS (Cam^R)	pETM11-*F174Y hrcN* (Δ1-18)	Kanamycin, Chloramphenicol	Over-expression	This study
BL21 (DE3) pLysS pETM11-P142G hrcN (Δ1-18)	*Escherichia coli*	BL21 (DE3) pLysS	F⁻ompT hsdSB(rв- mв-) gal dcm (DE3) pLysS (Cam^R)	pETM11-*P142G hrcN* (Δ1-18)	Kanamycin, Chloramphenicol	Over-expression	This study
Pto DC3000 WT *hrcN*	*Pseudomonas syringae*	*Pto* DC3000	WT *hrcN*	-	Rifampicin	*In vivo* analyses	Malone Lab, John Innes Centre
Pto DC3000 G176A *hrcN*	*Pseudomonas syringae*	*Pto* DC3000	G176A *hrcN*	-	Rifampicin	*In vivo* analyses	(Pfeilmeier et al., 2016)
Pto DC3000 E208D *hrcN*	*Pseudomonas syringae*	*Pto* DC3000	E208D *hrcN*	-	Rifampicin	*In vivo* analyses	This study
Pto DC3000 G311A *hrcN*	*Pseudomonas syringae*	*Pto* DC3000	G311A *hrcN*	-	Rifampicin	*In vivo* analyses	This study
Pto DC3000 L338V *hrcN*	*Pseudomonas syringae*	*Pto* DC3000	L338V *hrcN*	-	Rifampicin	*In vivo* analyses	This study
Pto DC3000 F174Y *hrcN*	*Pseudomonas syringae*	*Pto* DC3000	F174Y *hrcN*	-	Rifampicin	*In vivo* analyses	This study
Pto DC3000 P142G *hrcN*	*Pseudomonas syringae*	*Pto* DC3000	P142G *hrcN*	-	Rifampicin	*In vivo* analyses	This study
Pto DC3000 Δ*hrcC*	*Pseudomonas syringae*	*Pto* DC3000	Δ*hrcC*	-	Rifampicin	*In vivo* analyses	(Pfeilmeier et al., 2016)
Pto DC3000 Δ*hrcN*	*Pseudomonas syringae*	*Pto* DC3000	Δ*hrcN*	-	Rifampicin	*In vivo* analyses	This study
Pto DC3000 Δ*hopAA1-2*	*Pseudomonas syringae*	*Pto* DC3000	Δ*hopAA1-2*	-	Rifampicin	*In vivo* analyses	This study
Pto DC3000 Δ*hopAM1*	*Pseudomonas syringae*	*Pto* DC3000	Δ*hopAM1*	-	Rifampicin	*In vivo* analyses	This study
Pto DC3000 Δ*hopAF1*	*Pseudomonas syringae*	*Pto* DC3000	Δ*hopAF1*	-	Rifampicin	*In vivo* analyses	This study
Pto DC3000 Δ*hopAA1-2* Δ*hopAM1*	*Pseudomonas syringae*	*Pto* DC3000	Δ*hopAA1-2* Δ*hopAM1*	-	Rifampicin	*In vivo* analyses	This study

Pto DC3000 WT *hrcN* pBBR4-*wspr19*	*Pseudomonas syringae*	*Pto* DC3000	WT *hrcN*	pBBR4-*wspr19*	Rifampicin, Carbenicillin	*In vivo* analyses	This study
Pto DC3000 G176A *hrcN* pBBR4-*wspr19*	*Pseudomonas syringae*	*Pto* DC3000	G176A *hrcN*	pBBR4-*wspr19*	Rifampicin, Carbenicillin	DGC over-expression *in vivo* analyses	This study
Pto DC3000 E208D *hrcN* pBBR4-*wspr19*	*Pseudomonas syringae*	*Pto* DC3000	E208D *hrcN*	pBBR4-*wspr19*	Rifampicin, Carbenicillin	DGC over-expression *in vivo* analyses	This study
Pto DC3000 G311A *hrcN* pBBR4-*wspr19*	*Pseudomonas syringae*	*Pto* DC3000	G311A *hrcN*	pBBR4-*wspr19*	Rifampicin, Carbenicillin	DGC over-expression *in vivo* analyses	This study
Pto DC3000 L338V *hrcN* pBBR4-*wspr19*	*Pseudomonas syringae*	*Pto* DC3000	L338V *hrcN*	pBBR4-*wspr19*	Rifampicin, Carbenicillin	DGC over-expression *in vivo* analyses	This study
Pto DC3000 F174Y *hrcN* pBBR4-*wspr19*	*Pseudomonas syringae*	*Pto* DC3000	F174Y *hrcN*	pBBR4-*wspr19*	Rifampicin, Carbenicillin	DGC over-expression *in vivo* analyses	This study
Pto DC3000 P142G *hrcN* pBBR4-*wspr19*	*Pseudomonas syringae*	*Pto* DC3000	P142G *hrcN*	pBBR4-*wspr19*	Rifampicin, Carbenicillin	DGC over-expression *in vivo* analyses	This study
Pto DC3000 WT *hrcN* pBBR4-*bifA*	*Pseudomonas syringae*	*Pto* DC3000	WT *hrcN*	pBBR4-*bifA*	Rifampicin, Carbenicillin	*In vivo* analyses	This study
Pto DC3000 G176A *hrcN* pBBR4-*bifA*	*Pseudomonas syringae*	*Pto* DC3000	G176A *hrcN*	pBBR4-*bifA*	Rifampicin, Carbenicillin	PDE over-expression *in vivo* analyses	This study
Pto DC3000 E208D *hrcN* pBBR4-*bifA*	*Pseudomonas syringae*	*Pto* DC3000	E208D *hrcN*	pBBR4-*bifA*	Rifampicin, Carbenicillin	PDE over-expression *in vivo* analyses	This study
Pto DC3000 G311A *hrcN* pBBR4-*bifA*	*Pseudomonas syringae*	*Pto* DC3000	G311A *hrcN*	pBBR4-*bifA*	Rifampicin, Carbenicillin	PDE over-expression *in vivo* analyses	This study
Pto DC3000 L338V *hrcN* pBBR4-*bifA*	*Pseudomonas syringae*	*Pto* DC3000	L338V *hrcN*	pBBR4-*bifA*	Rifampicin, Carbenicillin	PDE over-expression *in vivo* analyses	This study
Pto DC3000 F174Y *hrcN* pBBR4-*bifA*	*Pseudomonas syringae*	*Pto* DC3000	F174Y *hrcN*	pBBR4-*bifA*	Rifampicin, Carbenicillin	PDE over-expression *in vivo* analyses	This study
Pto DC3000 P142G *hrcN* pBBR4-*bifA*	*Pseudomonas syringae*	*Pto* DC3000	P142G *hrcN*	pBBR4-*bifA*	Rifampicin, Carbenicillin	PDE over-expression *in vivo* analyses	This study
Pto DC3000 WT *hrcN* pBBR2	*Pseudomonas syringae*	*Pto* DC3000	WT *hrcN*	pBBR2	Rifampicin, Kanamycin	T3E over-expression *In vivo* analyses	This study
Pto DC3000 G176A *hrcN* pBBR2	*Pseudomonas syringae*	*Pto* DC3000	G176A *hrcN*	pBBR2	Rifampicin, Kanamycin	T3E over-expression *In vivo* analyses	This study
Pto DC3000 WT *hrcN* pBBR2-*hopAA1-2*	*Pseudomonas syringae*	*Pto* DC3000	WT *hrcN*	pBBR2-*hopAA1-2*	Rifampicin, Kanamycin	T3E over-expression *In vivo* analyses	This study
Pto DC3000 G176A *hrcN* pBBR2-*hopAA1-2*	*Pseudomonas syringae*	*Pto* DC3000	G176A *hrcN*	pBBR2-*hopAA1-2*	Rifampicin, Kanamycin	T3E over-expression *In vivo* analyses	This study
Pto DC3000 WT *hrcN* pBBR2-*hopAM1*	*Pseudomonas syringae*	*Pto* DC3000	WT *hrcN*	pBBR2-*hopAM1*	Rifampicin, Kanamycin	T3E over-expression *In vivo* analyses	This study
Pto DC3000 G176A *hrcN* pBBR2-*hopAM1*	*Pseudomonas syringae*	*Pto* DC3000	G176A *hrcN*	pBBR2-*hopAM1*	Rifampicin, Kanamycin	T3E over-expression *In vivo* analyses	This study
Pto DC3000 WT *hrcN* pBBR2-*hopAF1*	*Pseudomonas syringae*	*Pto* DC3000	WT *hrcN*	pBBR2-*hopAF1*	Rifampicin, Kanamycin	T3E over-expression *In vivo* analyses	This study
Pto DC3000 G176A *hrcN* pBBR2-*hopAF1*	*Pseudomonas syringae*	*Pto* DC3000	G176A *hrcN*	pBBR2-*hopAF1*	Rifampicin, Kanamycin	T3E over-expression *In vivo* analyses	This study
Pto DC3000 WT *hrcN* pBBR2-*hopH1*	*Pseudomonas syringae*	*Pto* DC3000	WT *hrcN*	pBBR2-*hopH1*	Rifampicin, Kanamycin	T3E over-expression *In vivo* analyses	This study
Pto DC3000 G176A *hrcN* pBBR2-*hopH1*	*Pseudomonas syringae*	*Pto* DC3000	G176A *hrcN*	pBBR2-*hopH1*	Rifampicin, Kanamycin	T3E over-expression *In vivo* analyses	This study
Pto DC3000 WT *hrcN* pDEST pCPP5371-*shcE-avrE1*-CyaA	*Pseudomonas syringae*	*Pto* DC3000	WT *hrcN*	pDEST pCPP5371-*shcE-avrE1*-CyaA	Rifampicin, Gentamycin	Effector-CyaA cAMP infection assays	This study

238

Pto DC3000 WT *hrcN* pDEST pCPP5371-*hopB1*-CyaA	*Pseudomonas syringae*	*Pto* DC3000	WT *hrcN*	pDEST pCPP5371-*hopB1*-CyaA	Rifampicin, Gentamycin	Effector-CyaA cAMP infection assays	This study
Pto DC3000 WT *hrcN* pDEST pCPP5371-*hopE1*-CyaA	*Pseudomonas syringae*	*Pto* DC3000	WT *hrcN*	pDEST pCPP5371-*hopE1*-CyaA	Rifampicin, Gentamycin	Effector-CyaA cAMP infection assays	This study
Pto DC3000 WT *hrcN* pDEST pCPP5371-*shcF-hopF2*-CyaA	*Pseudomonas syringae*	*Pto* DC3000	WT *hrcN*	pDEST pCPP5371- *shcF-hopF2*-CyaA	Rifampicin, Gentamycin	Effector-CyaA cAMP infection assays	This study
Pto DC3000 WT *hrcN* pDEST pCPP5371-*hopG1*-CyaA	*Pseudomonas syringae*	*Pto* DC3000	WT *hrcN*	pDEST pCPP5371-*hopG1*-CyaA	Rifampicin, Gentamycin	Effector-CyaA cAMP infection assays	This study
Pto DC3000 WT *hrcN* pDEST pCPP5371-*hopH1*-CyaA	*Pseudomonas syringae*	*Pto* DC3000	WT *hrcN*	pDEST pCPP5371-*hopH1*-CyaA	Rifampicin, Gentamycin	Effector-CyaA cAMP infection assays	This study
Pto DC3000 WT *hrcN* pDEST pCPP5371-*hopI1*-CyaA	*Pseudomonas syringae*	*Pto* DC3000	WT *hrcN*	pDEST pCPP5371-*hopI1*-CyaA	Rifampicin, Gentamycin	Effector-CyaA cAMP infection assays	This study
Pto DC3000 WT *hrcN* pDEST pCPP5371-*hopK1*-CyaA	*Pseudomonas syringae*	*Pto* DC3000	WT *hrcN*	pDEST pCPP5371-*hopK1*-CyaA	Rifampicin, Gentamycin	Effector-CyaA cAMP infection assays	This study
Pto DC3000 WT *hrcN* pDEST pCPP5371-*shcO-hopO1-1*-CyaA	*Pseudomonas syringae*	*Pto* DC3000	WT *hrcN*	pDEST pCPP5371-*shcO-hopO1-1*-CyaA	Rifampicin, Gentamycin	Effector-CyaA cAMP infection assays	This study
Pto DC3000 WT *hrcN* pDEST pCPP5371-*hopQ1-1*-CyaA	*Pseudomonas syringae*	*Pto* DC3000	WT *hrcN*	pDEST pCPP5371-*hopQ1-1*-CyaA	Rifampicin, Gentamycin	Effector-CyaA cAMP infection assays	This study
Pto DC3000 WT *hrcN* pDEST pCPP5371-*hopR1*-CyaA	*Pseudomonas syringae*	*Pto* DC3000	WT *hrcN*	pDEST pCPP5371-*hopR1*-CyaA	Rifampicin, Gentamycin	Effector-CyaA cAMP infection assays	This study
Pto DC3000 WT *hrcN* pDEST pCPP5371-*hopT1-1*-CyaA	*Pseudomonas syringae*	*Pto* DC3000	WT *hrcN*	pDEST pCPP5371-*hopT1-1*-CyaA	Rifampicin, Gentamycin	Effector-CyaA cAMP infection assays	This study
Pto DC3000 WT *hrcN* pDEST pCPP5371-*hopU1*-CyaA	*Pseudomonas syringae*	*Pto* DC3000	WT *hrcN*	pDEST pCPP5371-*hopU1*-CyaA	Rifampicin, Gentamycin	Effector-CyaA cAMP infection assays	This study
Pto DC3000 WT *hrcN* pDEST pCPP5371-*hopX1*-CyaA	*Pseudomonas syringae*	*Pto* DC3000	WT *hrcN*	pDEST pCPP5371-*hopX1*-CyaA	Rifampicin, Gentamycin	Effector-CyaA cAMP infection assays	This study
Pto DC3000 WT *hrcN* pDEST pCPP5371-*hopY1*-CyaA	*Pseudomonas syringae*	*Pto* DC3000	WT *hrcN*	pDEST pCPP5371-*hopY1*-CyaA	Rifampicin, Gentamycin	Effector-CyaA cAMP infection assays	This study
Pto DC3000 WT *hrcN* pDEST pCPP5371-*hopAA1-1*-CyaA	*Pseudomonas syringae*	*Pto* DC3000	WT *hrcN*	pDEST pCPP5371-*hopAA1-1*-CyaA	Rifampicin, Gentamycin	Effector-CyaA cAMP infection assays	This study
Pto DC3000 WT *hrcN* pDEST pCPP5371-*hopAA1-2*-CyaA	*Pseudomonas syringae*	*Pto* DC3000	WT *hrcN*	pDEST pCPP5371-*hopAA1-2*-CyaA	Rifampicin, Gentamycin	Effector-CyaA cAMP infection assays	This study
Pto DC3000 WT *hrcN* pDEST pCPP5371-*hopAF1*-CyaA	*Pseudomonas syringae*	*Pto* DC3000	WT *hrcN*	pDEST pCPP5371-*hopAF1*-CyaA	Rifampicin, Gentamycin	Effector-CyaA cAMP infection assays	This study

Pto DC3000 WT *hrcN* pDEST pCPP5371-*hopAM1*-CyaA	*Pseudomonas syringae*	*Pto* DC3000	WT *hrcN*	pDEST pCPP5371-*hopAM1*-CyaA	Rifampicin, Gentamycin	Effector-CyaA cAMP infection assays	This study
Pto DC3000 WT *hrcN* pDEST pCPP5371-*hopA1*-CyaA	*Pseudomonas syringae*	*Pto* DC3000	WT *hrcN*	pDEST pCPP5371-*hopA1*-CyaA	Rifampicin, Gentamycin	Effector-CyaA cAMP infection assays	This study
Pto DC3000 WT *hrcN* pDEST pCPP5371-*shcM-hopM1*-CyaA	*Pseudomonas syringae*	*Pto* DC3000	WT *hrcN*	pDEST pCPP5371-*shcM-hopM1*-CyaA	Rifampicin, Gentamycin	Effector-CyaA cAMP infection assays	This study
Pto DC3000 WT *hrcN* pDEST pCPP5371-*avrPto*-CyaA	*Pseudomonas syringae*	*Pto* DC3000	WT *hrcN*	pDEST pCPP5371-*avrPto*-CyaA	Rifampicin, Gentamycin	Effector-CyaA cAMP infection assays	This study
Pto DC3000 WT *hrcN* pDEST pCPP5371-*avrPtoB*-CyaA	*Pseudomonas syringae*	*Pto* DC3000	WT *hrcN*	pDEST pCPP5371-*avrPtoB*-CyaA	Rifampicin, Gentamycin	Effector-CyaA cAMP infection assays	This study
Pto DC3000 *G176A hrcN* pDEST pCPP5371-*shcE-avrE1*-CyaA	*Pseudomonas syringae*	*Pto* DC3000	*G176A hrcN*	pDEST pCPP5371- *shcE-avrE1*-CyaA	Rifampicin, Gentamycin	Effector-CyaA cAMP infection assays	This study
Pto DC3000 *G176A hrcN* pDEST pCPP5371-*hopB1*-CyaA	*Pseudomonas syringae*	*Pto* DC3000	*G176A hrcN*	pDEST pCPP5371-*hopB1*-CyaA	Rifampicin, Gentamycin	Effector-CyaA cAMP infection assays	This study
Pto DC3000 *G176A hrcN* pDEST pCPP5371-*hopE1*-CyaA	*Pseudomonas syringae*	*Pto* DC3000	*G176A hrcN*	pDEST pCPP5371-*hopE1*-CyaA	Rifampicin, Gentamycin	Effector-CyaA cAMP infection assays	This study
Pto DC3000 *G176A hrcN* pDEST pCPP5371-*shcF-hopF2*-CyaA	*Pseudomonas syringae*	*Pto* DC3000	*G176A hrcN*	pDEST pCPP5371- *shcF-hopF2*-CyaA	Rifampicin, Gentamycin	Effector-CyaA cAMP infection assays	This study
Pto DC3000 *G176A hrcN* pDEST pCPP5371-*hopG1*-CyaA	*Pseudomonas syringae*	*Pto* DC3000	*G176A hrcN*	pDEST pCPP5371-*hopG1*-CyaA	Rifampicin, Gentamycin	Effector-CyaA cAMP infection assays	This study
Pto DC3000 *G176A hrcN* pDEST pCPP5371-*hopH1*-CyaA	*Pseudomonas syringae*	*Pto* DC3000	*G176A hrcN*	pDEST pCPP5371-*hopH1*-CyaA	Rifampicin, Gentamycin	Effector-CyaA cAMP infection assays	This study
Pto DC3000 *G176A hrcN* pDEST pCPP5371-*hopI1*-CyaA	*Pseudomonas syringae*	*Pto* DC3000	*G176A hrcN*	pDEST pCPP5371-*hopI1*-CyaA	Rifampicin, Gentamycin	Effector-CyaA cAMP infection assays	This study
Pto DC3000 *G176A hrcN* pDEST pCPP5371-*hopK1*-CyaA	*Pseudomonas syringae*	*Pto* DC3000	*G176A hrcN*	pDEST pCPP5371-*hopK1*-CyaA	Rifampicin, Gentamycin	Effector-CyaA cAMP infection assays	This study
Pto DC3000 *G176A hrcN* pDEST pCPP5371-*shcO-hopO1-1*-CyaA	*Pseudomonas syringae*	*Pto* DC3000	*G176A hrcN*	pDEST pCPP5371-*shcO-hopO1-1*-CyaA	Rifampicin, Gentamycin	Effector-CyaA cAMP infection assays	This study
Pto DC3000 *G176A hrcN* pDEST pCPP5371-*hopQ1-1*-CyaA	*Pseudomonas syringae*	*Pto* DC3000	*G176A hrcN*	pDEST pCPP5371-*hopQ1-1*-CyaA	Rifampicin, Gentamycin	Effector-CyaA cAMP infection assays	This study
Pto DC3000 *G176A hrcN* pDEST pCPP5371-*hopR1*-CyaA	*Pseudomonas syringae*	*Pto* DC3000	*G176A hrcN*	pDEST pCPP5371-*hopR1*-CyaA	Rifampicin, Gentamycin	Effector-CyaA cAMP infection assays	This study
Pto DC3000 *G176A hrcN* pDEST pCPP5371-*hopT1-1*-CyaA	*Pseudomonas syringae*	*Pto* DC3000	*G176A hrcN*	pDEST pCPP5371-*hopT1-1*-CyaA	Rifampicin, Gentamycin	Effector-CyaA cAMP infection assays	This study

Pto DC3000 *G176A hrcN* pDEST pCPP5371-*hopU1*-CyaA	*Pseudomonas syringae*	*Pto* DC3000	*G176A hrcN*	pDEST pCPP5371-*hopU1*-CyaA	Rifampicin, Gentamycin	Effector-CyaA cAMP infection assays	This study
Pto DC3000 *G176A hrcN* pDEST pCPP5371-*hopX1*-CyaA	*Pseudomonas syringae*	*Pto* DC3000	*G176A hrcN*	pDEST pCPP5371-*hopX1*-CyaA	Rifampicin, Gentamycin	Effector-CyaA cAMP infection assays	This study
Pto DC3000 *G176A hrcN* pDEST pCPP5371-*hopY1*-CyaA	*Pseudomonas syringae*	*Pto* DC3000	*G176A hrcN*	pDEST pCPP5371-*hopY1*-CyaA	Rifampicin, Gentamycin	Effector-CyaA cAMP infection assays	This study
Pto DC3000 *G176A hrcN* pDEST pCPP5371-*hopAA1-1*-CyaA	*Pseudomonas syringae*	*Pto* DC3000	*G176A hrcN*	pDEST pCPP5371-*hopAA1-1*-CyaA	Rifampicin, Gentamycin	Effector-CyaA cAMP infection assays	This study
Pto DC3000 *G176A hrcN* pDEST pCPP5371-*hopAA1-2*-CyaA	*Pseudomonas syringae*	*Pto* DC3000	*G176A hrcN*	pDEST pCPP5371-*hopAA1-2*-CyaA	Rifampicin, Gentamycin	Effector-CyaA cAMP infection assays	This study
Pto DC3000 *G176A hrcN* pDEST pCPP5371-*hopAF1*-CyaA	*Pseudomonas syringae*	*Pto* DC3000	*G176A hrcN*	pDEST pCPP5371-*hopAF1*-CyaA	Rifampicin, Gentamycin	Effector-CyaA cAMP infection assays	This study
Pto DC3000 *G176A hrcN* pDEST pCPP5371-*hopAM1*-CyaA	*Pseudomonas syringae*	*Pto* DC3000	*G176A hrcN*	pDEST pCPP5371-*hopAM1*-CyaA	Rifampicin, Gentamycin	Effector-CyaA cAMP infection assays	This study
Pto DC3000 *G176A hrcN* pDEST pCPP5371-*hopA1*-CyaA	*Pseudomonas syringae*	*Pto* DC3000	*G176A hrcN*	pDEST pCPP5371-*hopA1*-CyaA	Rifampicin, Gentamycin	Effector-CyaA cAMP infection assays	This study
Pto DC3000 *G176A hrcN* pDEST pCPP5371-*shcM-hopM1*-CyaA	*Pseudomonas syringae*	*Pto* DC3000	*G176A hrcN*	pDEST pCPP5371-*shcM-hopM1*-CyaA	Rifampicin, Gentamycin	Effector-CyaA cAMP infection assays	This study
Pto DC3000 *G176A hrcN* pDEST pCPP5371-*avrPto*-CyaA	*Pseudomonas syringae*	*Pto* DC3000	*G176A hrcN*	pDEST pCPP5371-*avrPto*-CyaA	Rifampicin, Gentamycin	Effector-CyaA cAMP infection assays	This study
Pto DC3000 *G176A hrcN* pDEST pCPP5371-*avrPtoB*-CyaA	*Pseudomonas syringae*	*Pto* DC3000	*G176A hrcN*	pDEST pCPP5371-*avrPtoB*-CyaA	Rifampicin, Gentamycin	Effector-CyaA cAMP infection assays	This study
Pto DC3000 *E208D hrcN* pDEST pCPP5371-*shcE-avrE1*-CyaA	*Pseudomonas syringae*	*Pto* DC3000	*E208D hrcN*	pDEST pCPP5371-*shcE-avrE1*-CyaA	Rifampicin, Gentamycin	Effector-CyaA cAMP infection assays	This study
Pto DC3000 *E208D hrcN* pDEST pCPP5371-*hopB1*-CyaA	*Pseudomonas syringae*	*Pto* DC3000	*E208D hrcN*	pDEST pCPP5371-*hopB1*-CyaA	Rifampicin, Gentamycin	Effector-CyaA cAMP infection assays	This study
Pto DC3000 *E208D hrcN* pDEST pCPP5371-*hopE1*-CyaA	*Pseudomonas syringae*	*Pto* DC3000	*E208D hrcN*	pDEST pCPP5371-*hopE1*-CyaA	Rifampicin, Gentamycin	Effector-CyaA cAMP infection assays	This study
Pto DC3000 *E208D hrcN* pDEST pCPP5371-*shcF-hopF2*-CyaA	*Pseudomonas syringae*	*Pto* DC3000	*E208D hrcN*	pDEST pCPP5371-*shcF-hopF2*-CyaA	Rifampicin, Gentamycin	Effector-CyaA cAMP infection assays	This study
Pto DC3000 *E208D hrcN* pDEST pCPP5371-*hopG1*-CyaA	*Pseudomonas syringae*	*Pto* DC3000	*E208D hrcN*	pDEST pCPP5371-*hopG1*-CyaA	Rifampicin, Gentamycin	Effector-CyaA cAMP infection assays	This study
Pto DC3000 *E208D hrcN* pDEST pCPP5371-*hopH1*-CyaA	*Pseudomonas syringae*	*Pto* DC3000	*E208D hrcN*	pDEST pCPP5371-*hopH1*-CyaA	Rifampicin, Gentamycin	Effector-CyaA cAMP infection assays	This study

Pto DC3000 *E208D hrcN* pDEST pCPP5371-*hopI1*-CyaA	*Pseudomonas syringae*	*Pto* DC3000	*E208D hrcN*	pDEST pCPP5371-*hopI1*-CyaA	Rifampicin, Gentamycin	Effector-CyaA cAMP infection assays	This study
Pto DC3000 *E208D hrcN* pDEST pCPP5371-*hopK1*-CyaA	*Pseudomonas syringae*	*Pto* DC3000	*E208D hrcN*	pDEST pCPP5371-*hopK1*-CyaA	Rifampicin, Gentamycin	Effector-CyaA cAMP infection assays	This study
Pto DC3000 *E208D hrcN* pDEST pCPP5371-*shcO-hopO1-1*-CyaA	*Pseudomonas syringae*	*Pto* DC3000	*E208D hrcN*	pDEST pCPP5371-*shcO-hopO1-1*-CyaA	Rifampicin, Gentamycin	Effector-CyaA cAMP infection assays	This study
Pto DC3000 *E208D hrcN* pDEST pCPP5371-*hopQ1-1*-CyaA	*Pseudomonas syringae*	*Pto* DC3000	*E208D hrcN*	pDEST pCPP5371-*hopQ1-1*-CyaA	Rifampicin, Gentamycin	Effector-CyaA cAMP infection assays	This study
Pto DC3000 *E208D hrcN* pDEST pCPP5371-*hopR1*-CyaA	*Pseudomonas syringae*	*Pto* DC3000	*E208D hrcN*	pDEST pCPP5371-*hopR1*-CyaA	Rifampicin, Gentamycin	Effector-CyaA cAMP infection assays	This study
Pto DC3000 *E208D hrcN* pDEST pCPP5371-*hopT1-1*-CyaA	*Pseudomonas syringae*	*Pto* DC3000	*E208D hrcN*	pDEST pCPP5371-*hopT1-1*-CyaA	Rifampicin, Gentamycin	Effector-CyaA cAMP infection assays	This study
Pto DC3000 *E208D hrcN* pDEST pCPP5371-*hopU1*-CyaA	*Pseudomonas syringae*	*Pto* DC3000	*E208D hrcN*	pDEST pCPP5371-*hopU1*-CyaA	Rifampicin, Gentamycin	Effector-CyaA cAMP infection assays	This study
Pto DC3000 *E208D hrcN* pDEST pCPP5371-*hopX1*-CyaA	*Pseudomonas syringae*	*Pto* DC3000	*E208D hrcN*	pDEST pCPP5371-*hopX1*-CyaA	Rifampicin, Gentamycin	Effector-CyaA cAMP infection assays	This study
Pto DC3000 *E208D hrcN* pDEST pCPP5371-*hopY1*-CyaA	*Pseudomonas syringae*	*Pto* DC3000	*E208D hrcN*	pDEST pCPP5371-*hopY1*-CyaA	Rifampicin, Gentamycin	Effector-CyaA cAMP infection assays	This study
Pto DC3000 *E208D hrcN* pDEST pCPP5371-*hopAA1-1*-CyaA	*Pseudomonas syringae*	*Pto* DC3000	*E208D hrcN*	pDEST pCPP5371-*hopAA1-1*-CyaA	Rifampicin, Gentamycin	Effector-CyaA cAMP infection assays	This study
Pto DC3000 *E208D hrcN* pDEST pCPP5371-*hopAA1-2*-CyaA	*Pseudomonas syringae*	*Pto* DC3000	*E208D hrcN*	pDEST pCPP5371-*hopAA1-2*-CyaA	Rifampicin, Gentamycin	Effector-CyaA cAMP infection assays	This study
Pto DC3000 *E208D hrcN* pDEST pCPP5371-*hopAF1*-CyaA	*Pseudomonas syringae*	*Pto* DC3000	*E208D hrcN*	pDEST pCPP5371-*hopAF1*-CyaA	Rifampicin, Gentamycin	Effector-CyaA cAMP infection assays	This study
Pto DC3000 *E208D hrcN* pDEST pCPP5371-*hopAM1*-CyaA	*Pseudomonas syringae*	*Pto* DC3000	*E208D hrcN*	pDEST pCPP5371-*hopAM1*-CyaA	Rifampicin, Gentamycin	Effector-CyaA cAMP infection assays	This study
Pto DC3000 *E208D hrcN* pDEST pCPP5371-*hopA1*-CyaA	*Pseudomonas syringae*	*Pto* DC3000	*E208D hrcN*	pDEST pCPP5371-*hopA1*-CyaA	Rifampicin, Gentamycin	Effector-CyaA cAMP infection assays	This study
Pto DC3000 *E208D hrcN* pDEST pCPP5371-*shcM-hopM1*-CyaA	*Pseudomonas syringae*	*Pto* DC3000	*E208D hrcN*	pDEST pCPP5371-*shcM-hopM1*-CyaA	Rifampicin, Gentamycin	Effector-CyaA cAMP infection assays	This study
Pto DC3000 *E208D hrcN* pDEST pCPP5371-*avrPto*-CyaA	*Pseudomonas syringae*	*Pto* DC3000	*E208D hrcN*	pDEST pCPP5371-*avrPto*-CyaA	Rifampicin, Gentamycin	Effector-CyaA cAMP infection assays	This study
Pto DC3000 *E208D hrcN* pDEST pCPP5371-*avrPtoB*-CyaA	*Pseudomonas syringae*	*Pto* DC3000	*E208D hrcN*	pDEST pCPP5371-*avrPtoB*-CyaA	Rifampicin, Gentamycin	Effector-CyaA cAMP infection assays	This study

Pto DC3000 *G311A hrcN* pDEST pCPP5371-*shcE-avrE1*-CyaA	*Pseudomonas syringae*	*Pto* DC3000	*G311A hrcN*	pDEST pCPP5371- *shcE-avrE1*-CyaA	Rifampicin, Gentamycin	Effector-CyaA cAMP infection assays	This study
Pto DC3000 *G311A hrcN* pDEST pCPP5371-*hopB1*-CyaA	*Pseudomonas syringae*	*Pto* DC3000	*G311A hrcN*	pDEST pCPP5371-*hopB1*-CyaA	Rifampicin, Gentamycin	Effector-CyaA cAMP infection assays	This study
Pto DC3000 *G311A hrcN* pDEST pCPP5371-*hopE1*-CyaA	*Pseudomonas syringae*	*Pto* DC3000	*G311A hrcN*	pDEST pCPP5371-*hopE1*-CyaA	Rifampicin, Gentamycin	Effector-CyaA cAMP infection assays	This study
Pto DC3000 *G311A hrcN* pDEST pCPP5371-*shcF-hopF2*-CyaA	*Pseudomonas syringae*	*Pto* DC3000	*G311A hrcN*	pDEST pCPP5371- *shcF-hopF2*-CyaA	Rifampicin, Gentamycin	Effector-CyaA cAMP infection assays	This study
Pto DC3000 *G311A hrcN* pDEST pCPP5371-*hopG1*-CyaA	*Pseudomonas syringae*	*Pto* DC3000	*G311A hrcN*	pDEST pCPP5371-*hopG1*-CyaA	Rifampicin, Gentamycin	Effector-CyaA cAMP infection assays	This study
Pto DC3000 *G311A hrcN* pDEST pCPP5371-*hopH1*-CyaA	*Pseudomonas syringae*	*Pto* DC3000	*G311A hrcN*	pDEST pCPP5371-*hopH1*-CyaA	Rifampicin, Gentamycin	Effector-CyaA cAMP infection assays	This study
Pto DC3000 *G311A hrcN* pDEST pCPP5371-*hopI1*-CyaA	*Pseudomonas syringae*	*Pto* DC3000	*G311A hrcN*	pDEST pCPP5371-*hopI1*-CyaA	Rifampicin, Gentamycin	Effector-CyaA cAMP infection assays	This study
Pto DC3000 *G311A hrcN* pDEST pCPP5371-*hopK1*-CyaA	*Pseudomonas syringae*	*Pto* DC3000	*G311A hrcN*	pDEST pCPP5371-*hopK1*-CyaA	Rifampicin, Gentamycin	Effector-CyaA cAMP infection assays	This study
Pto DC3000 *G311A hrcN* pDEST pCPP5371-*shcO-hopO1-1*-CyaA	*Pseudomonas syringae*	*Pto* DC3000	*G311A hrcN*	pDEST pCPP5371-*shcO-hopO1-1*-CyaA	Rifampicin, Gentamycin	Effector-CyaA cAMP infection assays	This study
Pto DC3000 *G311A hrcN* pDEST pCPP5371-*hopQ1-1*-CyaA	*Pseudomonas syringae*	*Pto* DC3000	*G311A hrcN*	pDEST pCPP5371-*hopQ1-1*-CyaA	Rifampicin, Gentamycin	Effector-CyaA cAMP infection assays	This study
Pto DC3000 *G311A hrcN* pDEST pCPP5371-*hopR1*-CyaA	*Pseudomonas syringae*	*Pto* DC3000	*G311A hrcN*	pDEST pCPP5371-*hopR1*-CyaA	Rifampicin, Gentamycin	Effector-CyaA cAMP infection assays	This study
Pto DC3000 *G311A hrcN* pDEST pCPP5371-*hopT1-1*-CyaA	*Pseudomonas syringae*	*Pto* DC3000	*G311A hrcN*	pDEST pCPP5371-*hopT1-1*-CyaA	Rifampicin, Gentamycin	Effector-CyaA cAMP infection assays	This study
Pto DC3000 *G311A hrcN* pDEST pCPP5371-*hopU1*-CyaA	*Pseudomonas syringae*	*Pto* DC3000	*G311A hrcN*	pDEST pCPP5371-*hopU1*-CyaA	Rifampicin, Gentamycin	Effector-CyaA cAMP infection assays	This study
Pto DC3000 *G311A hrcN* pDEST pCPP5371-*hopX1*-CyaA	*Pseudomonas syringae*	*Pto* DC3000	*G311A hrcN*	pDEST pCPP5371-*hopX1*-CyaA	Rifampicin, Gentamycin	Effector-CyaA cAMP infection assays	This study
Pto DC3000 *G311A hrcN* pDEST pCPP5371-*hopY1*-CyaA	*Pseudomonas syringae*	*Pto* DC3000	*G311A hrcN*	pDEST pCPP5371-*hopY1*-CyaA	Rifampicin, Gentamycin	Effector-CyaA cAMP infection assays	This study
Pto DC3000 *G311A hrcN* pDEST pCPP5371-*hopAA1-1*-CyaA	*Pseudomonas syringae*	*Pto* DC3000	*G311A hrcN*	pDEST pCPP5371-*hopAA1-1*-CyaA	Rifampicin, Gentamycin	Effector-CyaA cAMP infection assays	This study
Pto DC3000 *G311A hrcN* pDEST pCPP5371-*hopAA1-2*-CyaA	*Pseudomonas syringae*	*Pto* DC3000	*G311A hrcN*	pDEST pCPP5371-*hopAA1-2*-CyaA	Rifampicin, Gentamycin	Effector-CyaA cAMP infection assays	This study

Pto DC3000 *G311A hrcN* pDEST pCPP5371-*hopAF1*-CyaA	*Pseudomonas syringae*	*Pto* DC3000	*G311A hrcN*	pDEST pCPP5371-*hopAF1*-CyaA	Rifampicin, Gentamycin	Effector-CyaA cAMP infection assays	This study
Pto DC3000 *G311A hrcN* pDEST pCPP5371-*hopAM1*-CyaA	*Pseudomonas syringae*	*Pto* DC3000	*G311A hrcN*	pDEST pCPP5371-*hopAM1*-CyaA	Rifampicin, Gentamycin	Effector-CyaA cAMP infection assays	This study
Pto DC3000 *G311A hrcN* pDEST pCPP5371-*hopA1*-CyaA	*Pseudomonas syringae*	*Pto* DC3000	*G311A hrcN*	pDEST pCPP5371-*hopA1*-CyaA	Rifampicin, Gentamycin	Effector-CyaA cAMP infection assays	This study
Pto DC3000 *G311A hrcN* pDEST pCPP5371-*shcM-hopM1*-CyaA	*Pseudomonas syringae*	*Pto* DC3000	*G311A hrcN*	pDEST pCPP5371-*shcM-hopM1*-CyaA	Rifampicin, Gentamycin	Effector-CyaA cAMP infection assays	This study
Pto DC3000 *G311A hrcN* pDEST pCPP5371-*avrPto*-CyaA	*Pseudomonas syringae*	*Pto* DC3000	*G311A hrcN*	pDEST pCPP5371-*avrPto*-CyaA	Rifampicin, Gentamycin	Effector-CyaA cAMP infection assays	This study
Pto DC3000 *G311A hrcN* pDEST pCPP5371-*avrPtoB*-CyaA	*Pseudomonas syringae*	*Pto* DC3000	*G311A hrcN*	pDEST pCPP5371-*avrPtoB*-CyaA	Rifampicin, Gentamycin	Effector-CyaA cAMP infection assays	This study
Pto DC3000 Δ*hrcN* pDEST pCPP5371-*shcE-avrE1*-CyaA	*Pseudomonas syringae*	*Pto* DC3000	Δ*hrcN*	pDEST pCPP5371- *shcE-avrE1*-CyaA	Rifampicin, Gentamycin	Effector-CyaA cAMP infection assays	This study
Pto DC3000 Δ*hrcN* pDEST pCPP5371-*hopB1*-CyaA	*Pseudomonas syringae*	*Pto* DC3000	Δ*hrcN*	pDEST pCPP5371-*hopB1*-CyaA	Rifampicin, Gentamycin	Effector-CyaA cAMP infection assays	This study
Pto DC3000 Δ*hrcN* pDEST pCPP5371-*hopE1*-CyaA	*Pseudomonas syringae*	*Pto* DC3000	Δ*hrcN*	pDEST pCPP5371-*hopE1*-CyaA	Rifampicin, Gentamycin	Effector-CyaA cAMP infection assays	This study
Pto DC3000 Δ*hrcN* pDEST pCPP5371-*shcF-hopF2*-CyaA	*Pseudomonas syringae*	*Pto* DC3000	Δ*hrcN*	pDEST pCPP5371- *shcF-hopF2*-CyaA	Rifampicin, Gentamycin	Effector-CyaA cAMP infection assays	This study
Pto DC3000 Δ*hrcN* pDEST pCPP5371-*hopG1*-CyaA	*Pseudomonas syringae*	*Pto* DC3000	Δ*hrcN*	pDEST pCPP5371-*hopG1*-CyaA	Rifampicin, Gentamycin	Effector-CyaA cAMP infection assays	This study
Pto DC3000 Δ*hrcN* pDEST pCPP5371-*hopH1*-CyaA	*Pseudomonas syringae*	*Pto* DC3000	Δ*hrcN*	pDEST pCPP5371-*hopH1*-CyaA	Rifampicin, Gentamycin	Effector-CyaA cAMP infection assays	This study
Pto DC3000 Δ*hrcN* pDEST pCPP5371-*hopI1*-CyaA	*Pseudomonas syringae*	*Pto* DC3000	Δ*hrcN*	pDEST pCPP5371-*hopI1*-CyaA	Rifampicin, Gentamycin	Effector-CyaA cAMP infection assays	This study
Pto DC3000 Δ*hrcN* pDEST pCPP5371-*hopK1*-CyaA	*Pseudomonas syringae*	*Pto* DC3000	Δ*hrcN*	pDEST pCPP5371-*hopK1*-CyaA	Rifampicin, Gentamycin	Effector-CyaA cAMP infection assays	This study
Pto DC3000 Δ*hrcN* pDEST pCPP5371-*shcO-hopO1-1*-CyaA	*Pseudomonas syringae*	*Pto* DC3000	Δ*hrcN*	pDEST pCPP5371-*shcO-hopO1-1*-CyaA	Rifampicin, Gentamycin	Effector-CyaA cAMP infection assays	This study
Pto DC3000 Δ*hrcN* pDEST pCPP5371-*hopQ1-1*-CyaA	*Pseudomonas syringae*	*Pto* DC3000	Δ*hrcN*	pDEST pCPP5371-*hopQ1-1*-CyaA	Rifampicin, Gentamycin	Effector-CyaA cAMP infection assays	This study
Pto DC3000 Δ*hrcN* pDEST pCPP5371-*hopR1*-CyaA	*Pseudomonas syringae*	*Pto* DC3000	Δ*hrcN*	pDEST pCPP5371-*hopR1*-CyaA	Rifampicin, Gentamycin	Effector-CyaA cAMP infection assays	This study
Pto DC3000 Δ*hrcN* pDEST pCPP5371-*hopT1-1*-CyaA	*Pseudomonas syringae*	*Pto* DC3000	Δ*hrcN*	pDEST pCPP5371-*hopT1-1*-CyaA	Rifampicin, Gentamycin	Effector-CyaA cAMP infection assays	This study
Pto DC3000 Δ*hrcN* pDEST pCPP5371-*hopU1*-CyaA	*Pseudomonas syringae*	*Pto* DC3000	Δ*hrcN*	pDEST pCPP5371-*hopU1*-CyaA	Rifampicin, Gentamycin	Effector-CyaA cAMP infection assays	This study

Pto DC3000 Δ*hrcN* pDEST pCPP5371-*hopX1*-CyaA	*Pseudomonas syringae*	*Pto* DC3000	Δ*hrcN*	pDEST pCPP5371-*hopX1*-CyaA	Rifampicin, Gentamycin	Effector-CyaA cAMP infection assays	This study
Pto DC3000 Δ*hrcN* pDEST pCPP5371-*hopY1*-CyaA	*Pseudomonas syringae*	*Pto* DC3000	Δ*hrcN*	pDEST pCPP5371-*hopY1*-CyaA	Rifampicin, Gentamycin	Effector-CyaA cAMP infection assays	This study
Pto DC3000 Δ*hrcN* pDEST pCPP5371-*hopAA1-1*-CyaA	*Pseudomonas syringae*	*Pto* DC3000	Δ*hrcN*	pDEST pCPP5371-*hopAA1-1*-CyaA	Rifampicin, Gentamycin	Effector-CyaA cAMP infection assays	This study
Pto DC3000 Δ*hrcN* pDEST pCPP5371-*hopAA1-2*-CyaA	*Pseudomonas syringae*	*Pto* DC3000	Δ*hrcN*	pDEST pCPP5371-*hopAA1-2*-CyaA	Rifampicin, Gentamycin	Effector-CyaA cAMP infection assays	This study
Pto DC3000 Δ*hrcN* pDEST pCPP5371-*hopAF1*-CyaA	*Pseudomonas syringae*	*Pto* DC3000	Δ*hrcN*	pDEST pCPP5371-*hopAF1*-CyaA	Rifampicin, Gentamycin	Effector-CyaA cAMP infection assays	This study
Pto DC3000 Δ*hrcN* pDEST pCPP5371-*hopAM1*-CyaA	*Pseudomonas syringae*	*Pto* DC3000	Δ*hrcN*	pDEST pCPP5371-*hopAM1*-CyaA	Rifampicin, Gentamycin	Effector-CyaA cAMP infection assays	This study
Pto DC3000 Δ*hrcN* pDEST pCPP5371-*hopA1*-CyaA	*Pseudomonas syringae*	*Pto* DC3000	Δ*hrcN*	pDEST pCPP5371-*hopA1*-CyaA	Rifampicin, Gentamycin	Effector-CyaA cAMP infection assays	This study
Pto DC3000 Δ*hrcN* pDEST pCPP5371-*shcM*-*hopM1*-CyaA	*Pseudomonas syringae*	*Pto* DC3000	Δ*hrcN*	pDEST pCPP5371-*shcM*-*hopM1*-CyaA	Rifampicin, Gentamycin	Effector-CyaA cAMP infection assays	This study
Pto DC3000 Δ*hrcN* pDEST pCPP5371-*avrPto*-CyaA	*Pseudomonas syringae*	*Pto* DC3000	Δ*hrcN*	pDEST pCPP5371-*avrPto*-CyaA	Rifampicin, Gentamycin	Effector-CyaA cAMP infection assays	This study
Pto DC3000 Δ*hrcN* pDEST pCPP5371-*avrPtoB*-CyaA	*Pseudomonas syringae*	*Pto* DC3000	Δ*hrcN*	pDEST pCPP5371-*avrPtoB*-CyaA	Rifampicin, Gentamycin	Effector-CyaA cAMP infection assays	This study
Pto DC3000 WT *hrcC* + *hrcC*	*Pseudomonas syringae*	*Pto* DC3000	WT *hrcC*::*hrcC* (GlmS Site Insertion)	-	Rifampicin, Gentamycin	Genetic complementation *in vivo* analyses	This study
Pto DC3000 WT *hrcN* + *hrcN*	*Pseudomonas syringae*	*Pto* DC3000	WT *hrcN*::*hrcN* (GlmS Site Insertion)	-	Rifampicin, Gentamycin	Genetic complementation *in vivo* analyses	This study
Pto DC3000 Δ*hrcC* + *hrcC*	*Pseudomonas syringae*	*Pto* DC3000	Δ*hrcC*::*hrcC* (GlmS Site Insertion)	-	Rifampicin, Gentamycin	Genetic complementation *in vivo* analyses	This study
Pto DC3000 Δ*hrcN* + *hrcN*	*Pseudomonas syringae*	*Pto* DC3000	Δ*hrcN*::*hrcN* (GlmS Site Insertion)	-	Rifampicin, Gentamycin	Genetic complementation *in vivo* analyses	This study
Pto DC3000 G176A *hrcN* + *hrcN*	*Pseudomonas syringae*	*Pto* DC3000	G176A *hrcN*::*hrcN* (GlmS Site Insertion)	-	Rifampicin, Gentamycin	Genetic complementation *in vivo* analyses	This study
Pto DC3000 E208D *hrcN* + *hrcN*	*Pseudomonas syringae*	*Pto* DC3000	E208D *hrcN*::*hrcN* (GlmS Site Insertion)	-	Rifampicin, Gentamycin	Genetic complementation *in vivo* analyses	This study
Pto DC3000 G311A *hrcN* + *hrcN*	*Pseudomonas syringae*	*Pto* DC3000	G311A *hrcN*::*hrcN* (GlmS Site Insertion)	-	Rifampicin, Gentamycin	Genetic complementation *in vivo* analyses	This study
Pto DC3000 L338V *hrcN* + *hrcN*	*Pseudomonas syringae*	*Pto* DC3000	L338V *hrcN*::*hrcN* (GlmS Site Insertion)	-	Rifampicin, Gentamycin	Genetic complementation *in vivo* analyses	This study
Pto DC3000 F174Y *hrcN* + *hrcN*	*Pseudomonas syringae*	*Pto* DC3000	F174Y *hrcN*::*hrcN* (GlmS Site Insertion)	-	Rifampicin, Gentamycin	Genetic complementation *in vivo* analyses	This study
Pto DC3000 P142G *hrcN* + *hrcN*	*Pseudomonas syringae*	*Pto* DC3000	P142G *hrcN*::*hrcN* (GlmS Site Insertion)	-	Rifampicin, Gentamycin	Genetic complementation *in vivo* analyses	This study
PA01 WT *pscN*	*Pseudomonas aeruginosa*	PA01	WT *pscN*	-	-	Preliminary *In vivo* analyses	Malone Lab, John Innes Centre
PA01 *G301D*	*Pseudomonas aeruginosa*	PA01	*G301D pscN*	-	-	Preliminary *In vivo* analyses	This study
PA01 *G306D*	*Pseudomonas aeruginosa*	PA01	*G306D pscN*	-	-	Preliminary *In vivo* analyses	This study
PA01 *R335Q*	*Pseudomonas aeruginosa*	PA01	*R335Q pscN*	-	-	Preliminary *In vivo* analyses	This study

8.2. Expanded Co-IP Pulldown Datasets

The co-immunoprecipitation pull-down datasets for effectors HopAM1, HopAA1-2, and HopAF1 were visualised as volcano plots where the fold-change increase in a given pulldown target was plotted against the adjusted false positive rate. Values closest to the graph origin show values that have a negligible fold change in prey pull-down and a low statistical significance (SAINT score). Values in the top right corner indicate values with a greater fold change in protein pull-down, and higher SAINT score statistical significance. SAINT score (Significance Analysis of INTeractome) is a computer tool which predicts the probability of true protein-protein interactions from potential false positives (Choi et al., 2011). Fold change is relative to a native WT DC3000 Col-0 background processed in the same manner. Non-*A. thaliana* or *Pto* DC3000 proteins (i.e. environmental contaminants) were excluded from top hit selection.

The pulldown success of proteins varies across the different effector protein Co-IP screens with HopAM1 having the greatest candidate pulldown, followed by HopAA1-2, then HopAF1. This difference in signal intensity could be due to differences in abundance of a given effector protein translocated into the plant, weaker protein interactions, or a weaker T3E-CyaA binding to the anti-CyaA antibody (e.g. due to steric hindrance). This could be optimised in future repeats by varying experimental conditions to better suit each effector protein to increase pulldown success. Additionally, it could the case that a given effector interacts with greater or fewer proteins in the host compared to other effectors, therefore pulling down different quantities of protein candidates.

The co-immunoprecipitation *A. thaliana* Col-0 DC3000 interaction pulldown candidates for HopAM1-CyaA represented as a volcano plot are shown in Figure 8.1. Highlighted are the top 5 *A. thaliana* proteins as shown in chapter 5, as selected based on a sorting algorithm sorting for the most probable prey candidates.

The top 5 *A. thaliana* pull-down hits were AT5G46110.1 (SAINT score = 1, fold change = 12, BFDR = 0 (not shown), Spectral counts = 12 (not shown)), AT2G21660.1 (SAINT score = 1, fold change = 19, BFDR = 0 (not shown), Spectral counts = 19 (not shown)), AT4G39260.1 (SAINT score = 1, fold change = 9.67, BFDR = 0 (not shown), Spectral counts = 29 (not shown)), AT4G30690.1 (SAINT score = 0.99, fold change = 12, BFDR = 0 (not shown), Spectral counts = 12 (not shown)), and AT5G03350.1 (SAINT score = 0.99, fold change = 10, BFDR = 0 (not shown), Spectral counts = 10 (not shown)).
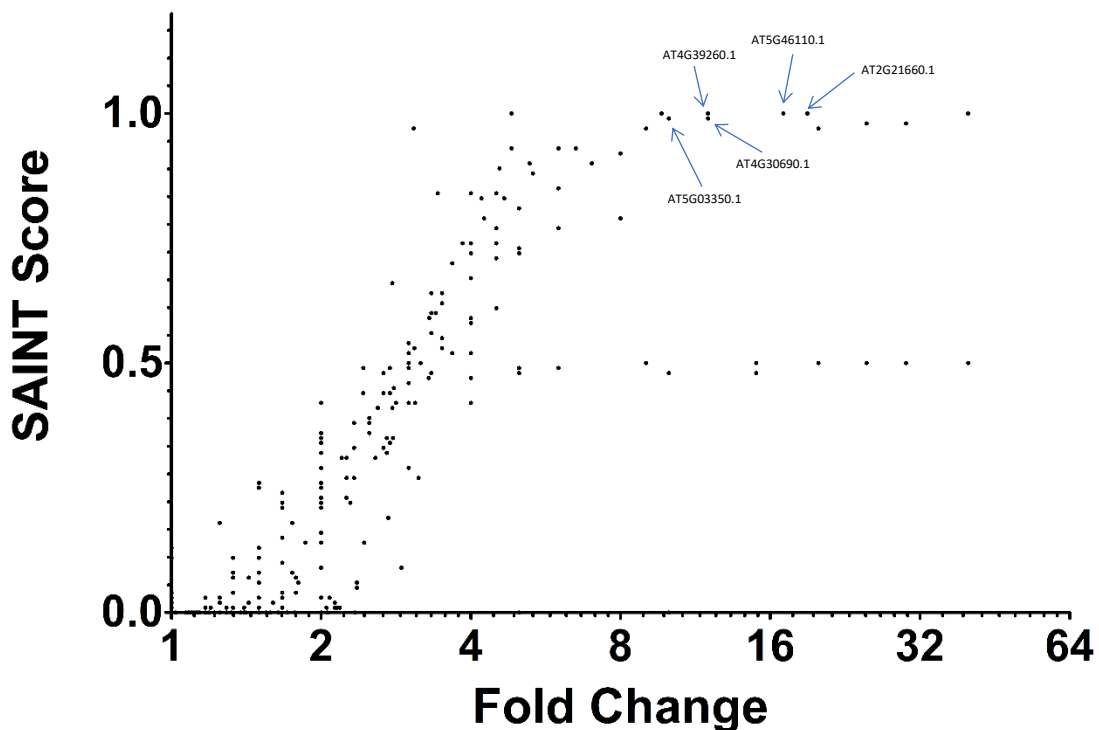
Figure 8.1. Fold change of prey protein interaction candidates for HopAM1-CyaA *Pto* DC3000 infected Col-0 *A. thaliana* in a co-immunoprecipitation and mass spectrometry screen, plotted against the SAINT score representative of true protein-protein interaction probability. Fold change is relative to a native WT DC3000 Col-0 background (non-cyaA like-effectors) processed in the same manner. Highlighted by blue arrows are the top 5 *A. thaliana* most probable protein interaction candidates for HopAM1-CyaA as selected based on a sorting algorithm. (n = 2)

The co-immunoprecipitation *A. thaliana* Col-0 DC3000 interaction pulldown candidates for HopAA1-2-CyaA represented as a volcano plot are shown in Figure 8.2. Highlighted are the top 5 *A. thaliana* proteins as shown in chapter 5, as selected based on a sorting algorithm sorting for the most probable prey candidates.

The top 5 *A. thaliana* pull-down hits were AT2G20190.1 (SAINT score = 0.46, fold change = 15, BFDR = 0.47 (not shown), Spectral counts = 3 (not shown)), AT1G23170.2-DECOY (SAINT score = 0.46, fold change = 15, BFDR = 0.47 (not shown), Spectral counts = 3 (not shown)), AT4G30010.1 (SAINT score = 0.32, fold change = 10, BFDR = 0.49 (not shown), Spectral counts = 2 (not shown)), AT2G27030.1 (SAINT score = 0.32, fold change = 10, BFDR = 0.49 (not shown), Spectral counts = 2 (not shown)), and AT2G23670.1 (SAINT score = 0.32, fold change = 10, BFDR = 0.49 (not shown), Spectral counts = 2 (not shown)).
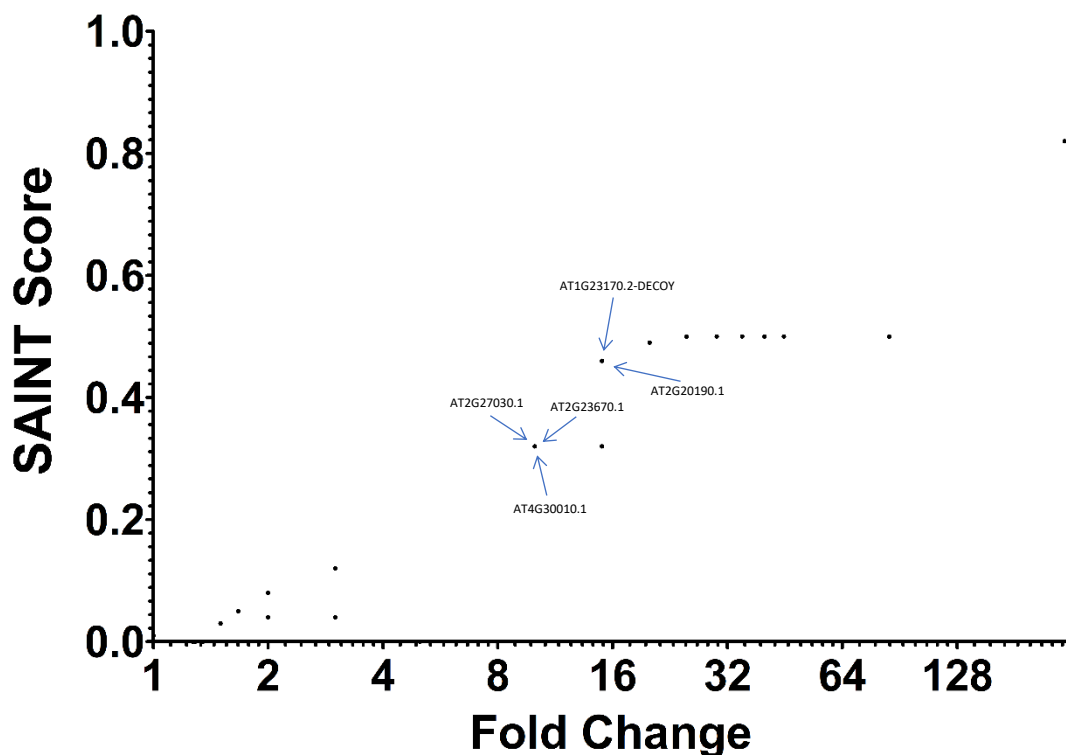
Figure 8.2. Fold change of prey protein interaction candidates for HopAA1-2-CyaA *Pto* DC3000 infected Col-0 *A. thaliana* in a co-immunoprecipitation and mass spectrometry screen, plotted against the SAINT score representative of true protein-protein interaction probability. Fold change is relative to a native WT DC3000 Col-0 background (non-cyaA like-effectors) processed in the same manner. Highlighted by blue arrows are the top 5 *A. thaliana* most probable protein interaction candidates for HopAA1-2-CyaA as selected based on a sorting algorithm. (n = 2)

The co-immunoprecipitation *A. thaliana* Col-0 DC3000 interaction pulldown candidates for HopAF1-CyaA represented as a volcano plot are shown in Figure 8.3. Highlighted are the top 5 *A. thaliana* proteins as shown in chapter 5, as selected based on a sorting algorithm sorting for the most probable prey candidates.

The top 5 *A. thaliana* pull-down hits were AT1G23170.2-DECOY (SAINT score = 0.14, fold change = 10, BFDR = 0.59 (not shown), Spectral counts = 2 (not shown)), AT1G73260.1 (SAINT score = 0.02, fold change = 2, BFDR = 0.68 (not shown), Spectral counts = 4 (not shown)), AT3G16300.1 (SAINT score = 0.01, fold change = 2.33, BFDR = 0.75 (not shown), Spectral counts = 5 (not shown)), AT5G42980.1 (SAINT score = 0, fold change = 1, BFDR = 0.86 (not shown), Spectral counts = 3 (not shown)), and AT4G27520.1 (SAINT score = 0, fold change = 1.5, BFDR = 0.86 (not shown), Spectral counts = 2 (not shown)).
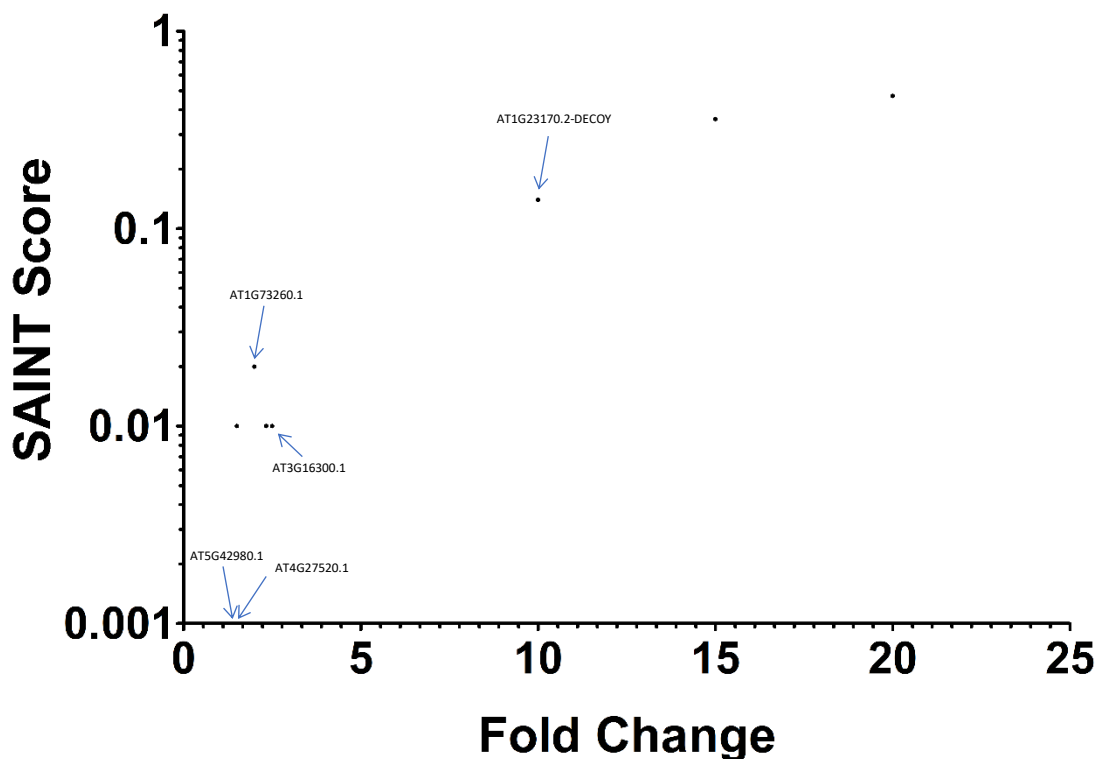
Figure 8.3. Fold change of prey protein interaction candidates for HopAF1-CyaA *Pto* DC3000 infected Col-0 *A. thaliana* in a co-immunoprecipitation and mass spectrometry screen, plotted against the SAINT score representative of true protein-protein interaction probability. Fold change is relative to a native WT DC3000 Col-0 background (non-cyaA like-effectors) processed in the same manner. Highlighted by blue arrows are the top 5 *A. thaliana* most probable protein interaction candidates for HopAF1-CyaA as selected based on a sorting algorithm. (n = 2)

8.3. Full *Pto* DC3000 T3SS Effector Protein Analysis

Shown in Table 8.2 is a full list of *Pto* DC3000 T3SS effector proteins and relevant accompanying information.

Table 8.2. Full *Pto* DC3000 T3SS effector protein analysis data

Effector Protein	Other/former Names	Signal peptide [Sau SignalP 5.0Pipeline]	Isoelectric Point (PI)	Hydrophobicity (Kyte-Doolittle)	Charge (pH 7)	Protein mW (kDa)	Gene Length (Kb)	Chromosome or Plasmid	Part of CyaA assay?	Translocation affected in G176A?	Known Chaperones	Locus Tag	GenBank accession	UniProt accession
AvrE	AvrE1	MQSPSHHNTGSIIGPTVYPDARAATDLQERAEQPIQRDRSHSLSSVGKRALKSVGKLFQKSKAPGQLKAATPP.TAXN.VATPP.PASNVA.TPRN.KARESGFSN	9.01	-0.597	17.88	195.1	5388	Chromosome	Yes	*yes	N/A	PSPTO_1377	AAO4899.1	Q887C9
AvrPto	avrPto1, AvrP, AvrPro	MGNICVGSRMAAHQVNSPDRVSNMSGQEENVVTSSQLLSVRHQLAESAGVPIRQHEFVSNQAPQSLRNVRNVNLVSHTQRTLDMADMQVHRVMTGASGNPGM	6.39	-0.772	-2.36	18.3	495	Chromosome	Yes	*no	N/A	PSPTO_4001	AAO7459.1	Q87Y16
AvrPtoB	avrAB1, avrAB2	MAGINIKAGPSGAYFVGHTDPFPVSGQAHGSGSGAESSNSPQVQPRPSNTPPSNAPAAPPTPIGERRLSRSTALSRQTRENEIEDGIMPTAEDASVRHRRPQVTAD	10.7	-0.551	13.36	59.5	1534	Chromosome	Yes	*yes	N/A	PSPTO_3087	AAL71883.1	Q885Y1
HopA1	hrmA, hopPsyA(Pto), hopPsyA	MNNPICRSFGVQEIRRSNVDIPALKANQLEVDGRRYRBAADDGTISVLRPEQGKSKAKSFFKGASQLIGGSSGQKIADQALNEKVASARTVHQSAMTG	10.01	-0.658	12.62	42	1143	Chromosome	Yes	*yes	N/A	PSPTO_5354	AAO5779.1	Q87UE5
HopAA1-1	hopPtoA1	MHHNRRVQDPPVTATDSFRTASDALSASSVRSVSTDQQRENAIADVLTDHVTAAHKUPADSADGQAAVDVHNAQITAUETRASRLHFEGFPATIA	9.61	-0.171	6.41	50.7	1461	Chromosome	Yes	*yes	N/A	PSPTO_1372	AAO5894.1	G3KDB9
HopAA1-2	hopPtoA2	MHHNQSAQLQPPGVAMESFRTASDALSASSVRSVSTTSCRDLQAITDYLKVHHVFAAHHRSWGSPQERDAALAHHEQIDALVETRANRLYSEGETPATIA	9.68	-0.128	8.14	51.1	1464	Chromosome	Yes	Yes - Stat sig reduction, repeated	N/A	PSPTO_4718	AAO58156.1	Q87W48
HopAE1	hopPtoG, hopPtoI	MUGIHDLHHMRPTAVDSLEPTSATSQTISNTKSRLDPHRVELTFIGVGSSVAVNLENGRFADSGVTTPIGKVSIVGKDDSWAENVRSKGVNHQTE	7.39	-0.389	2.56	69.3	1899	Chromosome	No	N/A	PSPTO_4691	AAO58135.1	Q87W65
HopAF1	hopPtoN, hopPtoI	MGLCDSKHSGGSKYVSDRWQVAPCPPMARSVHSHQTASASDASGDVESERPATSHOLARCGGEYTLSMVSAAAYQAERHHRGINUQDRSQSLPWV	7.27	-0.346	1.19	31	855	Chromosome	Yes	Yes - Stat sig reduction, repeated	N/A	PSPTO_1568	AAO55088.1	Q86L1
HopAG1	hopPsyAG	MNPITHKPSHLGFSNAGQSTSALARKGDKAVPNFVSRGRGGQVVEHFNTADEYRLAROQDEGQVLKSIDGREFMLLQLKYTAAETSDEFADUBAAIPRYSID	9.71	-0.359	4.19	16.7	459	Chromosome	No	N/A	PSPTO_0901	AAO5435.1	Q88BW3
HopAH1	hopPsyAH, hopPtoAH	MSKMNTSVSKNNGPVWSPVSGNNHAPVPDFSGKSSSMAVHEISPESAHHSPSAVSWGKSTFPAATTGNGRAGGAGGGGGGVEALKTLIVALLSVIGNASAHN	7.39	-0.482	1.37	42.9	1269	Chromosome	No	N/A	PSPTO_0905	AAO5439.1	Q88BV1
HopAH2-1	hopPsyAH2	MNINSRSYDLSAMAPFKSAVTNKATLPVNAGNNDAPTTRQSKLDTYTASHKYDSSGRPADAPETAPVYTKALLNRMAQLQXSAAPSDTAPAGQDQVATA	6.65	-0.574	-1.31	42.1	1215	Chromosome	No	N/A	PSPTO_3292	AAO5670.1	Q87ZY0
HopAH2-2	hopPsyAH2	MNIHFARSYDPLMATSEK.PATADRTTRAVDAGATEP.TPEKQAKLDTYTASSRSAETAEGDPVYTRMMLSRNTRSLSEDSSSDTALLASDKALVSQNDT	9.36	-0.557	3.98	44	1251	Chromosome	No	N/A	PSPTO_3293	AAO5671.1	Q87ZY9
HopAI1	hopPtoAI, hopPsyAI	MUALKLNTSVAQAPLKKNAEALRHMNHAEVRAHTPTRFTLNHRAPTYEVACGSAALGENHGWTAVNKFKVTESEVFHHMERSDSRSKGDFAGDKHLSVA	9.3	-0.671	5.61	28.9	786	Chromosome	No	N/A	PSPTO_0906	AAO54440.1	Q88BW0
HopAM1-1	avrPphB, avrPpiB1	MMANPLSSFNRAQHGNLTNVEASQVKSAGTSSTTNIDSKNIEEHVADRLSLGLRPDGGWFFEKSLGTLKNLNEQLAGHHDVLKLTDGVKNIVSFGAREG	6.75	-0.543	-1.38	31.3	831	Chromosome	Yes	Yes - Stat sig reduction, repeated	N/A	PSPTO_1022	AAO54553.1	Q87PR9
HopAM1-2	avrPpiB2	MMANPLSSFNRAQHGNLTNVEASQVKSAGTSSTTNIDSKNIEEHVADRLSLGLRPDGGWFFEKSLGTLKNLNEQLAGHHDVLKLTDGVKNIVSFGAREG	6.75	-0.543	-1.38	31.3	831	Plasmid pDC3000A	.	N/A	N/A	PSPTOA0005	N/A	N/A
HopAO1	avrPphB2	MMPLQPIQDHSITNSQMSGGGGQLDA.EGSQAHNSYSHPDRISLSQLSQLDAHLADLHSTQPNTDHQRVASLVRNAVQDGKFQLLGSSNDTQVTVKTSVCPPAN	7.1	-0.451	0.71	51.4	1407	Chromosome	No	N/A	PSPTO_0722	AAO33450.1	Q79LV0
HopAQ1	hopPtoAA	MMRISTSVSVNSSFKNTAP.TKEA.QNRFASAPDNSPLVV.ATTSTFIGTLVQFGRLDKN.HR1MDSKINFSVAFNLGRTIRSAGGSA	11.5	-0.384	5.22	8.9	252	Chromosome	No	N/A	PSPTO_0703	AAO58143.1	G3K0C7
HopAS1	ORF01152	MTLIRNITKATPVVPLETGSTSQTPPPVTARATEPPVANPAAPASAFGVQDAHGLKTRIAGKALSRRQTNFSLGIPGTGRTLNMPLRSGIPEEGEQVSN	10.05	-0.577	4.93	30.1	840	Chromosome	No	N/A	PSPTO_0474	AAO54018.1	Q88IAB8
HopB1	hopPtoB2, EEL ORF1, hopPsyG	MRPVGGPAPGYYPPTTEAEPTADAAGNDRARSSQASSSPAASVAPETPMQSDLKRFPAGRYPDMK.VENHKLKIEGGEPSGKDGSVKHTRRRKPDAAGSSH	9.56	-0.506	13.49	50.4	1401	Chromosome	Yes	*yes	N/A	PSPTO_1406	AAO54928.1	G3K0C6
HopC1	avrPphC2, hopPtoC	MTVGEHGHHPSLTTVQAGSSASVENQDMPDPADFSGQRMK.KLPTLQSSTDLARFDEDICTNNHGSIQAIAMCFGLSLSVWNMMAGRDHVPYASAEKMR	7.15	-0.131	0.76	29	810	Chromosome	Yes	*yes	N/A	PSPTO_0589	AAO54131.1	Q8L4O8
HopD1	:55.2 hopPtoD1-related	MMPLDSTDHSITTHVLSGGYRLDAVGPDAQCDSHPRKRSPSQLSPGFGHDAVIRDLAQDSTLLEDCQSLSHNDICQTYKAPVC1PADTSTD	8.78	-0.69	4.09	13.5	546	Chromosome	No	N/A	PSPTO_0724	AB9593711	Q87I86
HopE1	hopPtoE	MMPIRSQDHNATPIYSGGPLDAVGPDAQDSHPRKKSPGLSDAHQAELRSANAEHQRLASVRNALQDGITGFDQSNHTQVTVKASLCPADTDTV	6.35	-0.128	-7.24	75	2118	Chromosome	Yes	*no	N/A	PSPTO_0876	AAO54410.1	Q88I78
HopF1	hopPtoE, hopPtoV	MMRVSGSSSATWLDAPVSDLVEQVSERTTLSTTGFVDTAMGRLMPRSDADALMTAMRAQQYTDSAKRTYSETUMNLADLQDRKVRTNSGNLRGAHEMTP	8.46	-0.62	3.58	24	636	Chromosome	Yes	*yes	N/A	PSPTO_4331	AAO57782.1	Q87I57
HopF2	hopPtoF, hopPtoAD	MGNICGTSGRHVYSPSHTQIRTSAPSTSTHVGGDTLTSHGLSHSGIRRDFLRIKRVMHDPMRVMGLDHDTEIRTTDSRYKNDNLAGNPQSMASILMHEELR	8.5	-0.565	3.6	22.4	615	Chromosome	Yes	*no	ShcF	PSPTO_0502	AAO54046.1	Q88A90
HopG1	hopPtoG, hopPsyG	MQKNSHLHVSASRNVCNTTNASPKMEVTNAVAXNNEPAALSATQTACHEGDASGGSSNNSKLFPRAMRYAAYLGYLDKTANNFSLTTSLHDGKG	8.86	-0.535	9.92	54.7	1482	Chromosome	Yes	*yes	N/A	PSPTO_4727	AAO58163.1	Q87W42
HopH1	hopPtoH	MITPSRFPGIYIAPLSNEPTIAAHTFREIQDAEFALDHISAAPSGDXLLRIGSTLASQIDQRKVTLKEEINNQCYTEAAYLSRIQLLRVIPEVNENRHASQL	9.65	-0.802	7.13	24.3	657	Chromosome	Yes	No, repeated	N/A	PSPTO_0588	AAO54130.1	Q88A09
HopI1	hopPtoal	MINLTHIASSLARAALSSTKPKMEBANINVASHAGKVALQVTSLEDQRGILNRDQKGSMILKALSKEPVNNVETHEGGGRFNLARAAFDVASVVW	11.02	-1.043	28.7	52.5	1467	Chromosome	Yes	*yes	N/A	PSPTO_0476	AAO55206.1	Q87W07
HopK1	hopPtoAB, hopProK	MMRISTSVSVNSSFKNTAP.TKEA.QNRFASAPDNSPLVV.ATTSAQASEGQGAIRPGATSMQALDLRQLMGSP.SEQCKRDTMLAKADDAQRINNTQAGSSNS	5.22	-0.438	-8.22	36.6	1017	Chromosome	Yes	*yes	N/A	PSPTO_0044	AAO55399.1	Q88BH0
HopM1	hopPtoM, hopProX, CEL ORF3	MSSRIIGGAQGVELSRVNQHDTVPAQTAHPNAVTAGMNPPLTPDQSGSHATESSAGAARLNVAARHTQLLQFKAEHGTAPVSGAPMSSRIAALLIGS	7.25	-0.232	1.84	75.2	2139	Chromosome	Yes	*no	ShcM	PSPTO_1375	AAO54897.1	Q88I70
HopN1	hopPtoN, hopProT, CEL ORF7	MYIQDSGAQSGVAAKTQHDKFPSLSGLAPGSSDMFARFHFBKAGAFVPLEGHEEVHFDARSFSSVDAADUPSPEQVQFQLHSJRTLLPDLMVSIASLRD	6.8	-0.335	-1.79	38.6	1053	Chromosome	No	N/A	ShcN	PSPTO_1370	AAO54892.1	G3K0C5
HopO1-1	hopPtoO, hopPtoS1	MGNICGTSGNHVYSPPISPQHASEGSTYPVPSASGTMKSLSHEQLSQNYASNKGKVRTNPKGPSPRLSDTLMKQAASSMVQ	6.96	-0.666	-0.21	31.4	852	Plasmid pDC3000A	No	N/A	ShcO1	PSPTOA0018	AAO55043.1	Q88BP8
HopO1-2	hopPtoO2, hopPtoS3	MMNSPVSGAHGSSYPSAGSTASTASKGPSGSFLKQLGSGCFSPCLGLSSTIGAILSPAHEQVLSHTTYSSNJKGKLRTTPPKGPSPRLSDTPMKQALSSMVQ	8.12	-0.611	3.55	32.6	897	Chromosome	No	N/A	N/A	PSPTO_4594	AAO58040.1	Q87WF6
HopO1-3	hopPtoO-premature stop	MMNPLGQAHESAVASPGSDTSKATGKATAAPSFKQLGGGFSPCLGLSSGSFPCLGSHKSSSQQLSASHAQTLSQNVSNIVGQTSRTRAPSPRLSDTPAKQALSSMI	10.17	-0.593	-1.44	18.2	507	Chromosome	No	N/A	N/A	PSPTO_4592	AAO58038.1	Q87WF8
HopQ1	hopPtoQ, ORF19	MMRPTTAQHTTSRGLLQCDSCTQTRPSSSAQSALSQDSEWGRGQAHQATGLFQLDDSWFFTRTAPNAQEBAADMDKNKERSTDDWPAKYTELNVDLLT	6.8	-0.281	-1.44	48.7	1344	Chromosome	Yes	*yes	N/A	PSPTO_0877	AAO54411.1	Q88IP7
HopQ1-2	hopPtoQ2, hopPtoQ-like	MSSPALLEBKSSAPTLLTAQLBEALAHPVDQVLBDVQXSAALGLWEGDAQGLFQLDDSWFFRTAPNAQEBAADMDKNKERSTDDWPAKYTELNVDLLT	5.69	-0.229	-2.29	17.6	483	Chromosome	No	N/A	N/A	PSPTO_4732	AAO58166.1	Q87W41
HopR1	hopPtoR	MKAVTTSSGFTANPTSIHHADSVSRANPPFQLPEPVHVDRVFSHADDESVIMAWLAKRFPVQVSET	6.85	-0.293	-4.23	210.4	5874	Chromosome	Yes	*yes	N/A	PSPTO_0883	AAO54417.1	Q88IP1
HopS1	hopPtoS, hopPtoS4, ORF26	MKKGSSGTQAYALFTAVSYELLPGNYSVAASYELLPGNYSVAASVHGSLVDHHRQPALTRLSNVLFNQAALDLBRFDEGA	10.92	-0.839	10.94	12.4	357	Chromosome	No	N/A	ShcS1	PSPTO_3597	AAO58043.1	Q87WF4
HopS2	hopPtoS2, ORF35	MKVSSGFTANPTSIHHADSVSRANSPFQLPEPVHVDRVFSHADDESVIMAWLAKRFPVQVSET	8.26	-0.201	2.61	18.7	534	Plasmid pDC3000A	No	N/A	ShcS2	PSPTO_4588	AAO58034.1	Q87WG2
HopT1-1	hopPtoU, hopPtoT1	MKTVSNHSIPSTNLVVDAGTESAQKSQPVCSEIQRNSKEKAVEHADHPAAKMTSALVDTLTDVFVRAHGEVKGWAEIVGAVVSRPHDSNRHGSGVL	9.11	-0.349	8.49	41.1	1137	Chromosome	Yes	*yes	N/A	PSPTOA0019	AAO55041.1	Q88BP7
HopT1-2	hopPtoU2	MKTVSDNSIPGTVGIAFTRVDTAQSRPVPSDDLRQNSSEKAVEHADHPAAKVVMSAVEALTGYFVAQGEKGWAEQVAASRPHDSNRKGTGV	7.73	-0.254	3.01	42.1	1170	Chromosome	No	N/A	N/A	PSPTO_4593	AAO58039.1	Q87WF7
HopT2	hopPtoU3 premature stop	MFCHRSCMNQCGRITPARVGSPKTEAASGLQINRKEVVVEHSGSHPAAKITMDSLVGTLAHTFVMAHGEIKGWAEIVDGFSRPHESNRKGGGVFSACVDL	9.65	-0.105	7.03	13.5	384	Chromosome	Yes	*yes	N/A	PSPTO_4590	AAO58036.1	Q87WG0
HopU1	hopPtoS2	MNNNIRDLQPVSGSRRLLTPDVGVSRQACSERHVSTGQDHFVFRFAARLHVDAQCFGLSDDLMDKFSDKHFRAEHPERYPRDVVPFEECSAIVMHTAQDYSN	6.04	-0.493	-6.96	30	795	Chromosome	Yes	*yes	N/A	PSPTO_0501	AAO54045.1	Q88A91
HopV1	hopPtoV	MRFDAARKDQRCPKAPMDAPSLRLRAAEGMPSEEAGTTAPADVNQPPPADVRPEMQVGPVRLEFVKLMVQTLALSTEVRFARYPKGDFAKDPGEGSVWAAINL	9.8	-0.445	12.76	43.1	1173	Chromosome	Yes	N/A	ShcV	PSPTO_4720	AAO58158.1	Q87W46
HopX1	avrPphE, hopPsyE, EEL ORF2, av...	MKHHNAGLTPPLPEGSNVGKAAQSSITDPDSQDLQSFGPPESSETHPDRARAANYPYSSVGTRLPPVASAGPHOQPTPSLPGYLLLRIADRHRPVDGEG	8.21	-0.54	2.4	41.4	1155	Plasmid pDC3000A	Yes	*yes	N/A	PSPTOA0012	AAO55038.1	Q88BO2
HopY1	hopPtoY, hrpA-like	MNLTPLTSAAGKGSSAQSTDKISPTNSTRNIMNAASKWLNKIVRSADSDHRTSEKGKLFEALGSGSNMFGVPALSARPSTLQPVLAFEADPNHDNLVR	10.2	-0.739	7.45	31.1	864	Chromosome	Yes	*yes	N/A	PSPTO_0061	AAO53615.1	Q88BF6